

VOLUME 75

MAY 27, 1971

NUMBER 11

JPCHAx

---

THE JOURNAL OF  
PHYSICAL  
CHEMISTRY

---

PUBLISHED BIWEEKLY BY THE AMERICAN CHEMICAL SOCIETY

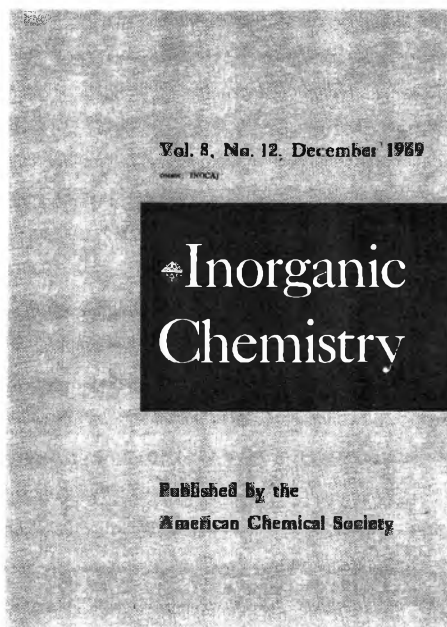
# Inorganic Chemistry is the one...

that publishes both experimental and theoretical fundamental studies in *all phases of inorganic chemistry*.

These studies include synthesis and properties of new compounds, quantitative studies regarding structure, and thermodynamics and kinetics of inorganic reactions. Articles may range from the borders of organic chemistry to the borders of theoretical physics . . . giving you a broad expanse of authoritative information.

Besides the 35 or more papers presented in each monthly issue, you'll also profit from the shorter *Notes* and the *Correspondence* sections, that provide an informal medium of exchange for scientific views and ideas.

**Inorganic Chemistry** is the one . . . to order right now for your own professional interests. Simply complete and return the form below.



**American Chemical Society** / 1155 Sixteenth Street, N.W., Washington, D.C. 20036

Please enter my subscription to **Inorganic Chemistry** at the rates checked below:

ACS Members:  U.S. \$18  Canada, PUAS \$21  Other Nations \$21.50

Nonmembers:  U.S. \$36  Canada, PUAS \$39  Other Nations \$39.50

Bill me  Bill employer  Payment enclosed (Payable to American Chemical Society)

Name \_\_\_\_\_ Title \_\_\_\_\_

Employer \_\_\_\_\_

Address:  Home  Business \_\_\_\_\_

City \_\_\_\_\_ State/Country \_\_\_\_\_ Zip \_\_\_\_\_

Nature of employer's business?

Manufacturing or processing  
 Other

Academic

Government

(Please indicate)

Note: Subscriptions at ACS Member Rates are for personal use only.

I am an ACS member  I am not an ACS member

Payment must be made in U.S. currency, by international money order, UNESCO coupons, U.S. bank draft, or order through your book dealer.

# THE JOURNAL OF PHYSICAL CHEMISTRY

---

**BRYCE CRAWFORD, Jr.**, *Editor*  
STEPHEN PRAGER, *Associate Editor*  
ROBERT W. CARR, Jr., FREDERIC A. VAN CATLEDGE, *Assistant Editors*

**EDITORIAL BOARD:** A. O. ALLEN (1970–1974), R. BERSOHN (1967–1971),  
J. R. BOLTON (1971–1975), S. BRUNAUER (1967–1971), M. FIXMAN (1970–1974),  
H. S. FRANK (1970–1974), J. R. HUIZENGA (1969–1973),  
M. KASHA (1967–1971), W. J. KAUFMANN (1969–1973), W. R. KRIGBAUM (1969–1973),  
R. A. MARCUS (1968–1972), W. J. MOORE (1969–1973), J. A. POPLE (1971–1975),  
B. S. RABINOVITCH (1971–1975), H. REISS (1970–1974), S. A. RICE (1969–1975),  
R. E. RICHARDS (1967–1971), F. S. ROWLAND (1968–1972),  
R. L. SCOTT (1968–1972), R. SEIFERT (1968–1972)

---

CHARLES R. BERTSCH, *Manager, Editorial Production*

---

AMERICAN CHEMICAL SOCIETY, 1155 Sixteenth St., N.W., Washington, D. C. 20036  
FREDERICK T. WALL, *Executive Director*

#### Books and Journals Division

JOHN K. CRUM, *Director (Acting)*  
JOSEPH H. KUNEY, *Head, Business Operations Department*  
RUTH REYNARD, *Assistant to the Director*

©Copyright, 1971, by the American Chemical Society. Published biweekly by the American Chemical Society at 20th and Northampton Sts., Easton, Pa. 18042. Second-class postage paid at Easton, Pa.

All manuscripts should be sent to *The Journal of Physical Chemistry*, Department of Chemistry, University of Minnesota, Minneapolis, Minn. 55455.

*Additions and Corrections* are published once yearly in the final issue. See Volume 74, Number 26 for the proper form.

*Extensive or unusual alterations in an article after it has been set in type are made at the author's expense*, and it is understood that by requesting such alterations the author agrees to defray the cost thereof.

The American Chemical Society and the Editor of *The Journal of Physical Chemistry* assume no responsibility for the statements and opinions advanced by contributors.

Correspondence regarding accepted copy, proofs, and reprints should be directed to Editorial Production Office, American Chemical Society, 20th and Northampton Sts., Easton, Pa. 18042. Manager: CHARLES R. BERTSCH. Assistant Editor: EDWARD A. BORGER. Editorial Assistant: EVELYN J. UHLER.

Advertising Office: Century Communications Corporation, 142 East Avenue, Norwalk, Conn. 06851.

#### Business and Subscription Information

Remittances and orders for subscriptions and for single copies,

notices of changes of address and new professional connections, and claims for missing numbers should be sent to the Subscription Service Department, American Chemical Society, 1155 Sixteenth St., N.W., Washington, D. C. 20036. Allow 4 weeks for changes of address. Please include an old address label with the notification.

Claims for missing numbers will not be allowed (1) if received more than sixty days from date of issue, (2) if loss was due to failure of notice of change of address to be received before the date specified in the preceding paragraph, or (3) if the reason for the claim is "missing from files."

Subscription rates (1971): members of the American Chemical Society, \$20.00 for 1 year; to nonmembers, \$40.00 for 1 year. Those interested in becoming members should write to the Admissions Department, American Chemical Society, 1155 Sixteenth St., N.W., Washington, D. C. 20036. Postage to Canada and countries in the Pan-American Union, \$4.00; all other countries, \$5.00. Single copies for current year: \$2.00. Rates for back issues from Volume 56 to date are available from the Special Issues Sales Department, 1155 Sixteenth St., N.W., Washington, D. C. 20036.

This publication and the other ACS periodical publications are now available on microfilm. For information write to: MICROFILM, Special Issues Sales Department, 1155 Sixteenth St., N.W., Washington, D. C. 20036.

# ISOTOPE EFFECTS IN CHEMICAL PROCESSES

## ADVANCES IN CHEMISTRY SERIES NO. 89

Thirteen papers from a symposium by the Division of Nuclear Chemistry and Technology of the American Chemical Society, chaired by William Spindel. Includes:

- Separating isotopes by chemical exchange, distillation, gas chromatography, electromigration, and photochemical processes
- Methods for fractionating isotopes of hydrogen, lithium, boron, carbon, and nitrogen
- Thermotransport in monatomic and ionic liquids
- Statistical-mechanical theory determining isotope effects

278 pages with index

Clothbound (1969)

\$13.00

Set of L.C. cards free with library orders upon request

Other books in the ADVANCES IN CHEMISTRY SERIES in physical and colloid chemistry include:

- |  |   |
|--|---|
| <p><b>No. 87 Interaction of Liquids at Solid Substrates.</b> Twelve papers survey recent research on solid/liquid interaction, including work on "coupling agents," adhesion of polymers, organic/inorganic interfaces, ultrasonic impedometry. Four more papers are concerned with heparinized surfaces at the blood/material interface.</p> <p style="text-align: right;">212 pages</p> <p>Cloth (1968) <b>\$9.50</b></p>  | <p><b>No. 63 Ordered Fluids and Liquid Crystals.</b> Twenty-two studies on characterization, properties, and occurrence of these phenomena in many substances such as tristearin, p-azoxyanisole, mono- and di-hydric alcohols, phospholipids and polypeptides.</p> <p style="text-align: right;">332 pages</p> <p>Cloth (1967) <b>\$11.50</b></p>                            |
| <p><b>No. 84 Molecular Association in Biological and Related Systems.</b> Nineteen articles survey and report new work on molecular association in fat digestion, in soap systems, in membrane constituents, and in mixed monolayers. Other topics include bile salt micelles, lipid monolayers and membranes, and a definitive review of biological membrane structure.</p> <p style="text-align: right;">308 pages</p> <p>Cloth (1968) <b>\$10.50</b></p>        | <p><b>No. 58 Ion-Molecule Reactions in the Gas Phase.</b> Eighteen papers survey spectrometric and other methods for producing and studying ion-molecule reactions, such as pulsed sources for studying thermal ions, reactions in flames and electrical discharges.</p> <p style="text-align: right;">336 pages</p> <p>Cloth (1966) <b>\$10.50</b></p>                       |
| <p><b>No. 82 Radiation Chemistry—II.</b> Thirty-six papers and 17 abstracts on radiation chemistry in gases, solids, and organic liquids. Includes three plenary lectures.</p> <p style="text-align: right;">558 pages</p> <p>Cloth (1968) <b>\$16.00</b></p>  | <p><b>No. 54 Advanced Propellant Chemistry.</b> Primarily directed to the search for new oxidizers; 26 papers survey oxygen-containing oxidizers, fuels and binders, fluorine systems including oxygen difluoride and difluoramines and liquid systems.</p> <p style="text-align: right;">290 pages</p> <p>Cloth (1966) <b>\$10.50</b></p>                                    |
| <p><b>No. 81 Radiation Chemistry—I.</b> Forty-one papers and 17 abstracts on radiation chemistry in aqueous media, biology, and dosimetry. From the international conference at Argonne National Laboratory.</p> <p style="text-align: right;">616 pages</p> <p>Cloth (1968) <b>\$16.00</b></p>  | <p><b>No. 50 Solvated Electron.</b> Reviews of theory, structure, reactions of solvated and hydrated electrons; detailed papers on electrical transport properties, photochemistry, theory of electron transfer reactions, structure of solvated electrons, hydrated electron research.</p> <p style="text-align: right;">304 pages</p> <p>Cloth (1965) <b>\$10.50</b></p>    |
| <p><b>No. 81 and No. 82 ordered together \$30.00.</b></p>  | <p><b>No. 47 Fuel Cell Systems.</b> Developments in theory, performance, construction, and new systems for the energy converter that is proving itself in military and space uses.</p> <p style="text-align: right;">360 pages</p> <p>Cloth (1965) <b>\$10.50</b></p>   |
| <p><b>No. 79 Adsorption from Aqueous Solution.</b> Fifteen papers discuss thermodynamic and kinetic aspects of adsorption phenomena and the results of studies on a variety of adsorbate-adsorbent systems.</p> <p style="text-align: right;">212 pages</p> <p>Cloth (1968) <b>\$10.00</b></p>   | <p><b>No. 43 Contact Angle, Wettability, and Adhesion.</b> Twenty-six papers on theoretical and practical approaches to wettability and adhesion; with summary of the surface chemical studies of W. A. Zisman, the 1963 Kendall Award winner.</p> <p style="text-align: right;">389 pages</p> <p>Cloth (1964) <b>\$10.50</b></p>   |
| <p><b>No. 68 Mössbauer Effect and its Application in Chemistry.</b> Ten papers that will familiarize chemists with Mössbauer spectroscopy as an analytical tool, for studying chemical bonding, crystal structure, electron density, magnetism, and other properties.</p> <p style="text-align: right;">178 pages</p> <p>Cloth (1967) <b>\$8.00</b></p>  | <p><b>No. 40 Mass Spectral Correlations.</b> By Fred W. McLafferty. Over 4000 spectra listed by mass/charge ratios of fragment ions with the most probable original structures for each.</p> <p style="text-align: right;">117 pages</p> <p>Paper (1963) <b>\$6.00</b></p>  |
| <p><b>No. 67 Equilibrium Concepts in Natural Water Systems.</b> Sixteen papers represent the collaboration of aquatic chemists, analytical chemists, geologists, oceanographers, limnologists, and sanitary engineers, working with simplified models to produce fruitful generalizations and valuable insights into the factors that control the chemistry of natural systems.</p> <p style="text-align: right;">344 pages</p> <p>Cloth (1967) <b>\$11.00</b></p> | <p><b>No. 33 Solid Surfaces and the Gas-Solid Interface.</b> Thirty-seven papers from the Kendall Award Symposium honoring Stephen Brunauer. Theory and techniques for studying surface phenomena.</p> <p style="text-align: right;">389 pages</p> <p>Cloth (1961) <b>\$12.00</b></p>   |
| <p><b>No. 64 Regenerative EMF Cells.</b> Seventeen papers survey current progress and research on regenerative systems for converting and storing electrical energy. Principal emphasis is on thermally regenerative systems, but chemical and photochemical systems are considered.</p> <p style="text-align: right;">309 pages</p> <p>Cloth (1967) <b>\$11.00</b></p>  | <p><b>No. 31 Critical Solution Temperatures.</b> By Alfred W. Francis. CST answers the question, "Do two liquids mix?" and is widely used for screening solvents. Over 6000 systems are included, 70% with a hydrocarbon as one component; nearly 1100 non-hydrocarbon solvents are listed.</p> <p style="text-align: right;">246 pages</p> <p>Cloth (1961) <b>\$8.00</b></p> |

All books postpaid in U.S. and Canada; plus 30 cents in PUAS and elsewhere.

Order from: **SPECIAL ISSUES SALES**  
**AMERICAN CHEMICAL SOCIETY**  
 1155 SIXTEENTH ST., N.W.  
 WASHINGTON, D.C. 20036

# THE JOURNAL OF PHYSICAL CHEMISTRY

Volume 75, Number 11 May 27, 1971

A Shock Tube Study of the $C_2F_4-CF_2$ Equilibrium	Gary A. Carlson	1625
Isomerization of Chemically Activated <i>n</i> -Pentyl Radicals	K. W. Watkins and D. R. Lawson	1632
Energy Partitioning on Photolysis and Pyrolysis of 3-Vinyl-1-pyrazoline	F. H. Dorer, E. Brown, J. Do, and R. Rees	1640
The Radiation Chemistry of Crystalline Glycollic Acid	J. G. Hawke and B. J. Rawson	1648
An Electron Spin Resonance Study of the Rate Constants for Reaction of Hydrogen Atoms with Organic Compounds in Aqueous Solution	P. Neta, Richard W. Fessenden and Robert H. Schuler	1654
Chlorophyll-Poly(vinylpyridine) Complexes. III. Photochemical Activity and Fluorescence Yield	G. R. Seely	1667
The Radiation Chemistry of Polyethylene. XI. The Molten State	M. Budzol and Malcolm Dole	1671
Spectroscopic Investigation of Cyclohexanol and Cyclohexyl Radicals and Their Corresponding Peroxy Radicals	M. Simic and E. Hayon	1677
The Structure of Perchlorocyclopentene	Hans J. Mair and S. H. Bauer	1681
The Molecular Structure of Perfluorocyclopentene and Perchlorocyclopentadiene by Gas Phase Electron Diffraction	C. H. Chang and S. H. Bauer	1685
Electrical Conductivities of Salts of Gum Arabic and Carrageenan in Aqueous Solutions	Roger E. Nelson and Paul Ander	1691
Electrosorption of 5-Chloro-1-pentanol at the Mercury-Solution Interface	Karl Doblhofer and David M. Mohilner	1698
Transport Properties in Hydrogen Bonding Solvents. VI. The Conductance of Electrolytes in 2,2,2-Trifluoroethanol	D. Fennell Evans, John A. Nadas, and Sister Mary A. Matesich	1708
The Conductance of Electrolytes in Acetone and in 1-Propanol-Acetone Mixtures at 25°	D. Fennell Evans, John Thomas, John A. Nadas, and Sister Mary A. Matesich	1714
The Conductance of Tetraalkylammonium Halides in Ethylene Glycol	Robert P. DeSieno, Paul W. Greco, and Ronald C. Mamajek	1722
Transport Behavior in Dimethyl Sulfoxide. II. Viscosity Studies	Neng-Ping Yao and Douglas N. Bennion	1727
Thermochemistry of the Diels-Alder Reaction. I. Enthalpy of Addition of Isoprene to Tetracyanoethylene	F. E. Rogers	1734
Pulse Radiolytic Investigation of $O_{aq}^-$ Radical Ions	Dov Zehavi and Joseph Rabani	1738
Distorted Hydrogen Bonds Formed by Carbonyl Compounds	C. N. R. Rao, Abha Goel, K. Gurudath Rao, and A. S. N. Murthy	1744
On Tunneling Corrections in Chemical Kinetics	S. G. Christov and Z. L. Georgiev	1748

## NOTES

Vibrational Eigenvalues. Sine Basis Sets	David J. Locker	1756
Nitrogen-15 Nuclear Magnetic Resonance Shifts and Coupling Constants for the Methylamine Hydrochlorides in Aqueous Solution	M. Alei, Jr., A. E. Floin, and W. M. Litchman	1758
The Radiation Chemical Yield of $OH^-$ as Determined by Conductometric Pulse Radiolysis	J. Rabani, M. Grätzel, S. A. Chaudhri, G. Beck, and A. Henglein	1759
Mass Spectrometric Determination of the Heats of Formation of $AlOCl(g)$ and $AlOF(g)$	R. D. Srivastava and M. Farber	1760

COMMUNICATIONS TO THE EDITOR

Solvent Effect on the Dimerization of *N*-Methylaniline . . . . . Louis Abello and Guy Pannetier 1763  
 Micellar Effects on the Hydrolysis Rate of Triethylamine-Sulfur Trioxide  
 . . . . Michael D. Bentley, Susan E. Bowie, and Robert D. Limoges 1763

AUTHOR INDEX

Abello, L., 1763	Christov, S. G., 1748	Georgiev, Ž. L., 1748	Mamajek, R. C., 1722	Rawson, B. J., 1648
Alei, M., Jr., 1758	DeSieno, R. P., 1722	Goel, A., 1744	Matesich, M. A., 1708, 1714	Rees, R., 1640
Ander, P., 1691	Do, J., 1640	Grätzel, M., 1759	Mohilner, D. M., 1698	Rogers, F. E., 1734
Bauer, S. H., 1681, 1685	Doblhofer, K., 1698	Greco, P. W., 1722	Murthy, A. S. N., 1744	Schuler, R. H., 1654
Beck, G., 1759	Dole, M., 1671	Hawke, J. G., 1648	Nadas, J. A., 1708, 1714	Seely, G. R., 1667
Bennion, D. N., 1727	Dorer, F. H., 1640	Hayon, E., 1677	Nelson, R. E., 1691	Simic, M., 1677
Bentley, M. D., 1763	Evans, D. F., 1708, 1714	Henglein, A., 1759	Neta, P., 1654	Srivastava, R. D., 1760
Bowie, S. E., 1763	Farber, M., 1760	Lawson, D. R., 1632	Pannetier, G., 1763	Thomas, J., 1714
Brown, E., 1640	Fessenden, R. W., 1654	Limoges, R. D., 1763	Rabani, J., 1738, 1759	Watkins, K. W., 1632
Budzol, M., 1671	Florin, A. E., 1758	Litchman, W. M., 1758	Rao, C. N. R., 1744	Yao, N.-P., 1727
Carlson, G. A., 1625		Locker, D. J., 1756	Rao, K. G., 1744	Zehavi, D., 1738
Chang, C. H., 1685		Mair, H. J., 1681		
Chaudhri, S. A., 1759				

# THE JOURNAL OF PHYSICAL CHEMISTRY

Registered in U. S. Patent Office © Copyright, 1971, by the American Chemical Society

VOLUME 75, NUMBER 11 MAY 27, 1971

## A Shock Tube Study of the $C_2F_4$ - $CF_2$ Equilibrium<sup>1</sup>

by Gary A. Carlson

Sandia Laboratories, Albuquerque, New Mexico 87115 (Received December 10, 1970)

Publication costs assisted by Sandia Laboratories

The decomposition of  $C_2F_4$  in excess argon has been studied in a shock tube at temperatures from 1240 to 1600°K. Over this temperature range, a simple  $C_2F_4 \rightleftharpoons 2CF_2$  equilibrium was found. Second- and third-law treatments of the equilibrium data gave a heat of reaction  $\Delta H_r^{\circ}{}_{298} = 68.4 \pm 0.8$  kcal/mol. From this, the heat of formation of  $CF_2$  was determined to be  $\Delta H_f^{\circ}{}_{298} = -44.5 \pm 0.4$  kcal/mol. Studies of the rate of dissociation of  $C_2F_4$  supported the simple chemical mechanism proposed.

### I. Introduction

The decomposition of  $C_2F_4$  has been studied by Modica and LaGraff (M-L) and by Zmbov, Uy, and Margrave (ZUM). M-L reported kinetics and equilibrium studies of the  $C_2F_4$ - $CF_2$  system from 1165 to 1620°K, shock-heating  $C_2F_4$  in  $Ar^{2a}$  and  $N_2^{2b}$  diluent gases. From a second-law treatment of their equilibrium data, they found  $\Delta H_r^{\circ}{}_{298}(C_2F_4 \rightarrow 2CF_2) = 75.5$  kcal/mol. ZUM<sup>3</sup> studied the  $C_2F_4$ - $CF_2$  equilibrium in a Knudsen cell from 1127 to 1244°K mass spectrometrically, reporting  $\Delta H_r^{\circ}{}_{298} = 76.3 \pm 3.0$  kcal/mol from both second- and third-law treatments. However, the values of  $K_p$  obtained by ZUM are in serious disagreement with those of M-L. In this paper, an independent shock-tube study of  $C_2F_4$  decomposition from 1240 to 1600°K is reported. Experimental evidence is given to support a simple  $C_2F_4$ - $CF_2$  chemical equilibrium. New values of  $\Delta H_r^{\circ}{}_{298}$  and  $\Delta H_f^{\circ}{}_{298}(CF_2)$  are reported. The somewhat unique method of data treatment employed (the  $CF_2$  absorption coefficient used to determine species concentrations was treated as an adjustable parameter) demonstrates potential errors which may result in shock tube chemical equilibrium studies in which reactions approach completion, due to small uncertainties in the determination of species concentrations. Finally, the discrepancies in the earlier equilibrium studies of M-L and ZUM are discussed.

### II. Experimental Section

*Apparatus.* The shock tube used in this study consisted of a 150-cm driver section and a 300-cm driven section, each of 7.6-cm i.d., 0.3-cm wall seamless stainless steel 304 tubing. The inside wall of the driven section was honed to a 0.5- $\mu$  finish. The final 120 cm of the driven section was altered from a circular cross section by pressing 1.9-cm wide flat surfaces on two opposing sides, allowing the use of 1.3-cm diameter flat quartz windows with minimum obstruction to the shocked gas flow. The transition from a circular cross section was accomplished over a length of 10-15 cm. The change in cross-sectional area of the pressed section was calculated to be about 0.1%. Shock-front arrival was monitored by four light-screen schlieren detectors, over a total distance of 75 cm. The signal from the first station activated a 10-MHz counter with nixie tube readout, which recorded the arrival times at the other three detectors with 0.1- $\mu$ sec resolution. The change in shock velocity over the 75-cm distance was

(1) This work was supported by the United States Atomic Energy Commission.

(2) (a) A. P. Modica and J. E. LaGraff, *J. Chem. Phys.*, **43**, 3383 (1965); (b) A. P. Modica and J. E. LaGraff, *ibid.*, **45**, 4729 (1966).

(3) K. F. Zmbov, O. M. Uy, and J. L. Margrave, *J. Amer. Chem. Soc.*, **90**, 5090 (1968).

within the uncertainty in the measured distances between stations ( $\pm 0.2\%$ ).

A 200-W Hg-Xe arc lamp (Hanovia 901 B-1) was used as the light source for the spectroscopic studies. The light was focused and passed through collimating slits on each side of the shock tube before entering a Spex 0.75-m Model 1800 spectrometer. With a 1200 line/mm grating blazed at 3000 Å, and with entrance and exit slit openings of 0.3 and 3 mm, respectively, the resolution of the spectrometer was about 30 Å. The signal was detected with an RCA 1P28 photomultiplier tube, amplified, and displayed on a Tektronix 556 dual-beam oscilloscope. Linearity of detector and amplifier response was confirmed using calibrated neutral density filters.

For kinetics experiments in which fast signal rise-times were expected, 0.8-mm width collimating slits were used, and a detector frequency response of 2.7 MHz ( $-3$  db) was maintained. For other experiments in which signal risetime was not critical, 1.6-mm width collimating slits and a 500-kHz low-pass filter were used to improve signal-to-noise.

Shocks were generated with helium driver gas (hydrogen was used for a few high-temperature experiments), bursting 3- to 7-mil Mylar diaphragms at pressures of 60–105 psia. Crossed concave cutting blades at the inlet to the driven section ensured full opening of the bursting diaphragms.

Both the gas-handling manifold and the shock tube driven section could be evacuated to less than  $10^{-6}$  Torr. Evacuation to the  $10^{-5}$  Torr range was considered adequate for the shock experiments. The gas-handling manifold included two 20-l. stainless steel tanks which were used for storage of the test gas. Test gas pressures from 13 to 60 Torr were measured with a 0–20 Torr absolute pressure gauge (Wallace and Tiernan, Model 160), or with a two-tube mercury manometer (1.3-cm i.d.) read by a cathetometer. Pressure measurements were reproducible within  $\pm 0.1$  Torr.

*Sample Preparation.* Tetrafluorethylene gas was prepared by zinc-debromination of  $C_2F_4Br_2$  in a methanol bath.<sup>4</sup> Very small amounts of  $N_2$  and methanol were collected with the  $C_2F_4$  product in a collection trap at liquid nitrogen temperature. These were excluded by a distillation in which only the center third of the original material was saved. No impurities could be detected in the distilled material by gas chromatographic or mass spectrometric analyses. Matheson ultrahigh purity argon (99.999%) was used without further purification. Mixtures of 0.74–0.78 mol %  $C_2F_4$  in argon were prepared in the storage tanks at 700–800 Torr total pressure and were allowed to equilibrate for a minimum of 24 hr before use to ensure adequate mixing.

### III. Shock Wave Calculations

The calculation procedure used in these studies is

modeled after that of Eberstein.<sup>5</sup> Briefly, the shocked gas parameters are calculated from the shock velocity assuming ideal gas behavior, then modified iteratively to take account of the vibrational and rotational relaxation of the test gas, giving the conditions behind the shock prior to chemical reaction. Chemical reaction is taken into account by numerical integration of a set of coupled first-order differential equations which relate changes in temperature, enthalpy, pressure, particle velocity, and density to the degree of dissociation of the test gas. Shocked gas parameters can be obtained for any degree of chemical reaction up to complete dissociation.

Changes in the shocked gas parameters with chemical reaction are not particularly sensitive to the assumed heat of reaction for mixtures containing a large excess of inert gas. For example, the temperature drop behind the shock front due to complete dissociation of a mixture of 0.75 mol %  $C_2F_4$  in argon is about 80°K, assuming a heat of dissociation of  $C_2F_4$  of about 65 kcal/mol. Thus, uncertainties in the heat of reaction of a few kilocalories per mole would only change calculated temperatures by a few degrees. We have used the heat of reaction determined in this study as input to the calculations.

### IV. Results

Experimental studies were performed in three areas. First, the absorption coefficient of  $CF_2$  was established at temperatures where complete  $C_2F_4$  dissociation occurred (1800–2900°K). Second, the  $C_2F_4$ – $CF_2$  equilibrium was studied in experiments run at lower temperatures (1240–1800°K). Finally, the rate of  $C_2F_4$  dissociation was also studied at the lower temperatures.

*$CF_2$  Absorption Coefficient Determination.* Ultraviolet light absorption by  $CF_2$  was chosen as the diagnostic to be used for determining species concentrations in these studies. The  $CF_2$  radical absorbs light from about 2200 to 2900 Å,<sup>6,7</sup> while  $C_2F_4$  exhibits no absorption in this region. It will be shown in the following section that  $CF_2$  is the only  $C_2F_4$  decomposition product observed up to about 2400°K. Further, it is found that  $C_2F_4$  is essentially completely decomposed above 1800°K. Thus, for shocks at temperatures from 1800 to 2400°K, one can determine the concentration of  $CF_2$  from the initial  $C_2F_4$  concentration and the shocked gas parameters. Assuming Beer's law, which is reasonable with the rather complete overlapping of the  $CF_2$  rotational and vibrational levels at these temperatures, one can then establish an absorption coefficient for  $CF_2$ ,  $\epsilon_{CF_2}$ , over a given wavelength interval and at a given

(4) J. J. Daly, Jr., DuPont Organic Chemical Department, supplied the synthesis procedure as well as the  $C_2F_4Br_2$  reagent.

(5) I. J. Eberstein, "Shock Waves with Chemical Reactions in Shock Tubes," Report No. YU-PPR-SWCR-66/07, Yale University, New Haven, Conn., 1966.

(6) C. W. Mathews, *Can. J. Phys.*, **45**, 2355 (1967).

(7) A. P. Modica, *J. Phys. Chem.*, **72**, 4594 (1968).



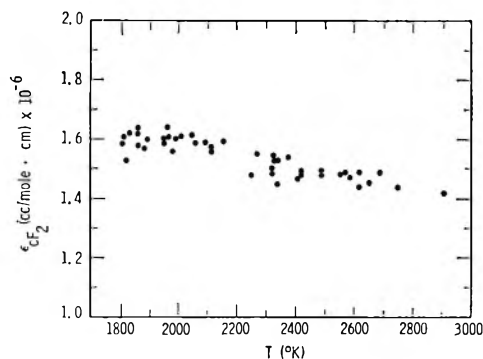


Figure 1. Variation of  $\epsilon_{CF_2}$  with temperature. Wavelength 2620 Å, bandpass 30 Å.

temperature. Finding a wavelength interval over which  $\epsilon_{CF_2}$  is relatively independent of temperature is more difficult. Each CF<sub>2</sub> vibrational level involved in the absorption band has a different temperature-dependent Boltzmann population and, thus, a temperature-dependent absorption coefficient. A temperature-independent absorption would then necessarily involve a particular combination of vibrational levels for which the sum of the absorption coefficients was temperature independent.

In our study,  $\epsilon_{CF_2}$  was found to be constant within experimental error at 2620 Å (30-Å bandwidth) from 1800 to 2100°K, although some temperature dependence was observed at higher temperatures. Figure 1 shows  $\epsilon_{CF_2}$  at 2620 Å as a function of temperature. The values obtained at temperatures above 2400°K were extrapolated back to zero time to allow for the effects of CF<sub>2</sub> dissociation. The use of  $\epsilon_{CF_2}$  in the treatment of data will be discussed more fully in the following section.

**Equilibrium Study.** In their shock tube studies, M-L stated that CF<sub>2</sub> was the only C<sub>2</sub>F<sub>4</sub> decomposition product of any consequence at temperatures below 2600°K, basing their conclusions on time-of-flight mass spectrometric analysis of the shocked gases. Our studies also support a simple C<sub>2</sub>F<sub>4</sub> ⇌ 2CF<sub>2</sub> reaction mechanism. In all experiments run below 2400°K, the CF<sub>2</sub> absorption was constant within experimental error after the initial period of chemical relaxation. Figure 2 shows an experimental trace in which light absorption by CF<sub>2</sub> was monitored following shock-heating of a typical tetrafluoroethylene-argon mixture. Following the shock front passage at  $t = 50 \mu\text{sec}$ , dissociation of C<sub>2</sub>F<sub>4</sub> into CF<sub>2</sub> occurred until equilibrium was reached at about  $t = 100 \mu\text{sec}$ . The constancy of the CF<sub>2</sub> absorption after  $t = 100 \mu\text{sec}$  indicates that no side reactions of either CF<sub>2</sub> or C<sub>2</sub>F<sub>4</sub> occurred later in time. Moreover, kinetics studies which will be discussed later show that no side reactions occurred in these experiments during the initial period of chemical relaxation. Finally, the very good results obtained by analyzing the equilibrium data on the basis of a simple

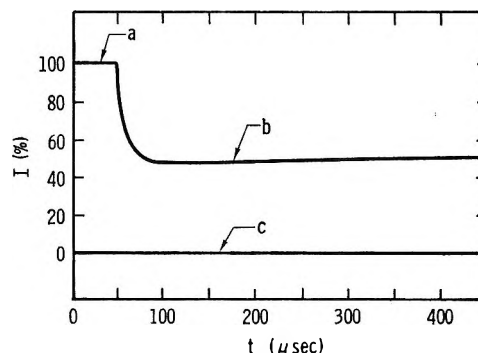


Figure 2. CF<sub>2</sub> absorption at 2620 Å, equilibrium data: a, light intensity before shock arrival; b, equilibrium intensity; c, baseline. At equilibrium, the temperature was 1495°K, and 81% of the C<sub>2</sub>F<sub>4</sub> had dissociated.

dissociation-recombination mechanism confirm the validity of the assumption.<sup>8</sup> The analysis of the equilibrium data is described below.

The equilibrium CF<sub>2</sub> concentration in each experiment was determined from the absorption trace using Beer's law. The equilibrium C<sub>2</sub>F<sub>4</sub> concentration was obtained from the initial C<sub>2</sub>F<sub>4</sub> concentration (taken at the equilibrium temperature and pressure), reduced by half the equilibrium CF<sub>2</sub> concentration. Since the trend of  $\epsilon_{CF_2}$  below 1800°K was not clearly established in the high-temperature studies, a temperature-dependent form of  $\epsilon_{CF_2}$  was used as an adjustable parameter in the Beer's law calculations.

$$\epsilon_{CF_2} = a + b(1800 - T) \text{ cc/mol cm}$$

A number of values of  $a$  close to  $1.60 \times 10^6$ , the approximate value of  $\epsilon_{CF_2}$  at 1800°K, were tested with both positive and negative values of  $b$ . For each combination of  $a$  and  $b$  values tested, equilibrium constants calculated as

$$K_p = (P_{CF_2})^2 / P_{C_2F_4}$$

were used to evaluate  $\Delta H_r^\circ_{298}$  by both second- and third-law methods. The second- and third-law results were then examined separately, and "best" values of  $\Delta H_r^\circ_{298}$  were determined. We shall report the results obtained using  $b = 0$ , giving  $\epsilon_{CF_2} = a$ , although certain other combinations of  $a$  and  $b$ , giving both positive and negative slope to  $\epsilon_{CF_2}$ , gave heats of reaction nearly identical with those reported.

In the second-law treatment, the van't Hoff equation was used.

$$\ln K_p = -\Delta H_r^\circ / RT + \Delta S_r^\circ / R$$

A plot of  $\ln K_p$  vs.  $1/T$  was made for each value of  $\epsilon_{CF_2}$  tested, and the plots were visually investigated

(8) Although thermodynamic data indicate that F, CF<sub>4</sub>, C<sub>2</sub>F<sub>2</sub>, and C<sub>2</sub>F<sub>6</sub> should also be important equilibrium species under these conditions, they are apparently not formed due to the short reaction times in the shock tube.

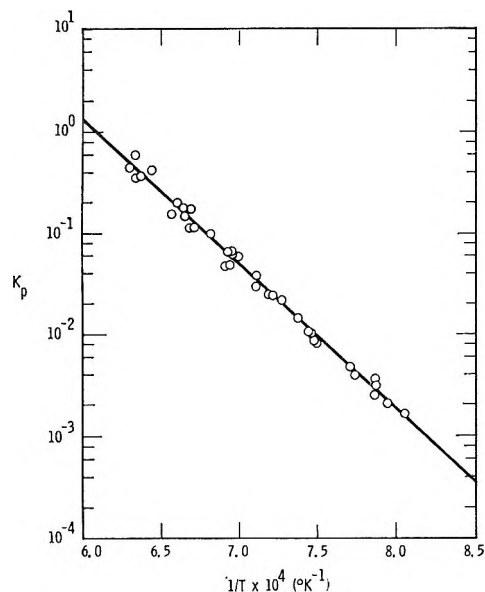


Figure 3. A second-law plot of equilibrium data for the  $C_2F_4-CF_2$  system.

for deviations from linearity. The change in the heat of reaction with temperature is sufficiently small over the experimental temperature range that any noticeable nonlinearity of the plots was an indication that the plotted data were incorrect. Significantly, although the range of values of  $\epsilon_{CF_2}$  tested caused changes of several kilocalories per mole in the calculated heats of reaction, nonlinearity was only observed in data taken above  $1600^\circ K$  where dissociation was 95% or greater, so that small changes in  $\epsilon_{CF_2}$  caused large relative changes in  $P_{C_2F_4}$  and, thus, in  $K_p$ . The implication is that if only data points below  $1600^\circ K$  had been analyzed, there would have been no basis for choosing a "best" straight line data fit. Since the experimental uncertainty was large above  $1600^\circ K$ , nonlinear behavior was judged from the relative numbers of data points falling above and below the least-squares line which fit the lower temperature data. Two plots, obtained with  $\epsilon_{CF_2} = 1.605 \times 10^6$  and  $1.610 \times 10^6$  cc/mol cm, were judged to be relatively linear, while plots obtained with higher and lower values of  $\epsilon_{CF_2}$  were judged to have deviations from linearity outside of the experimental uncertainty. The plot obtained with  $\epsilon_{CF_2} = 1.605 \times 10^6$  cc/mol cm is shown in Figure 3. The experimental data are given in Table I. Results above  $1600^\circ K$ , where scatter was excessive, have been excluded. Results below  $1240^\circ K$  were not obtained because equilibrium was not achieved during the time period of the experiments.

Using the average of the data calculated from the two "linear" plots, we obtain  $\Delta H_r^\circ = 65.1 \pm 1.5$  kcal/mol. The assigned uncertainty just encompasses results obtained from the closest "nonlinear" plots, with  $\epsilon_{CF_2} = 1.600 \times 10^6$  and  $1.615 \times 10^6$  cc/mol cm. The least-squares uncertainty for each plot was much smaller

Table I:  $C_2F_4$  Equilibrium Shock Tube Data ( $P_1$  Is the Initial Test Gas Pressure, and  $\alpha_{equil}$  the Degree of Dissociation at Equilibrium)

Run no.	$P_1$ , Torr	$U_s$ , mm/ $\mu$ sec	$T_{equil}$ , $^\circ K$	$\alpha_{equil}$	$K_p$
1	19.96	1.215	1493	0.9262	$1.706 \times 10^{-1}$
2	17.81	1.255	1577	0.9640	$3.607 \times 10^{-1}$
3	36.20	1.164	1405	0.6940	$3.836 \times 10^{-2}$
4	57.80	1.094	1295	0.3091	$4.706 \times 10^{-3}$
5	40.00	1.081	1269	0.3223	$3.527 \times 10^{-3}$
6	41.80	1.178	1429	0.7375	$5.968 \times 10^{-2}$
7	58.40	1.120	1339	0.4116	$1.041 \times 10^{-2}$
8	19.99	1.256	1579	0.9754	$6.075 \times 10^{-1}$
9	15.03	1.187	1436	0.8752	$6.471 \times 10^{-2}$
10	13.22	1.244	1552	0.9769	$4.220 \times 10^{-1}$
11	60.00	1.116	1333	0.3710	$8.196 \times 10^{-3}$
12	40.20	1.226	1522	0.8552	$1.546 \times 10^{-1}$
13	39.80	1.163	1406	0.6340	$2.983 \times 10^{-2}$
14	30.60	1.156	1391	0.6493	$2.482 \times 10^{-2}$
15	32.60	1.134	1354	0.5536	$1.451 \times 10^{-2}$
16	34.80	1.063	1241	0.2487	$1.616 \times 10^{-3}$
17	35.80	1.121	1336	0.4595	$8.839 \times 10^{-3}$
18	39.20	1.081	1270	0.3040	$3.042 \times 10^{-3}$
19	40.50	1.080	1271	0.2763	$2.491 \times 10^{-3}$
20	41.60	1.092	1291	0.3270	$3.951 \times 10^{-3}$
21	23.40	1.215	1495	0.8814	$1.146 \times 10^{-1}$
22	26.10	1.184	1436	0.8050	$6.161 \times 10^{-2}$
23	24.60	1.201	1467	0.8642	$9.883 \times 10^{-2}$
24	19.80	1.252	1569	0.9611	$3.737 \times 10^{-1}$
25	29.20	1.153	1385	0.6545	$2.433 \times 10^{-2}$
26	32.40	1.126	1343	0.5051	$1.067 \times 10^{-2}$
27	19.20	1.260	1586	0.9688	$4.641 \times 10^{-1}$
28	42.20	1.072	1257	0.2520	$2.056 \times 10^{-3}$
29	24.10	1.186	1446	0.7873	$4.742 \times 10^{-2}$
30	22.00	1.217	1502	0.9129	$1.499 \times 10^{-1}$
31	23.00	1.210	1489	0.8881	$1.141 \times 10^{-1}$
32	21.80	1.223	1514	0.9315	$1.986 \times 10^{-1}$
33	22.60	1.219	1505	0.9222	$1.764 \times 10^{-1}$
34	24.00	1.186	1443	0.8284	$6.487 \times 10^{-2}$
35	25.30	1.184	1441	0.7851	$4.879 \times 10^{-2}$
36	28.00	1.146	1374	0.6533	$2.168 \times 10^{-2}$

( $\pm 0.5$  kcal/mol). Using tabulated values<sup>9</sup> of  $H^\circ_T - H^\circ_{298}$  for  $C_2F_4$  and  $CF_2$  ( $T$  is  $1415^\circ K$ , the mid-range temperature of the experiments), we obtain a second-law  $\Delta H_r^\circ = 67.9 \pm 1.5$  kcal/mol.

In the third-law treatment, free-energy function data<sup>9</sup> were combined with the calculated equilibrium constants to give  $\Delta H_r^\circ$  values for each experiment.

$$\Delta H_r^\circ = -RT \ln K_p - \Delta \left[ \frac{G^\circ_T - H^\circ_{298}}{T} \right] T$$

The results for each value of  $\epsilon_{CF_2}$  tested were plotted as  $\Delta H_r^\circ$  vs.  $T$  to check for temperature dependence (drift). Drift is defined as  $\Delta(\Delta H_r^\circ)/\Delta T$  and is expressed in entropy units (eu = cal/mol deg). If the calculated values of  $\Delta H_r^\circ$  showed a dependence on the experimental temperature outside of the experi-

(9) JANAF Thermochemical Tables and Addenda, D. R. Stull, Ed., Dow Chemical Co., Midland, Mich.

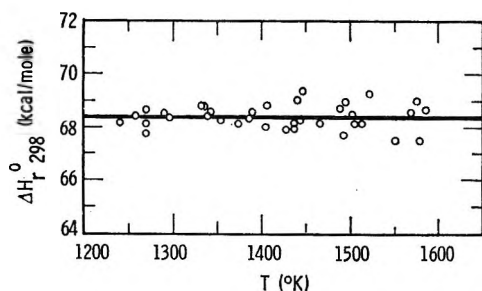


Figure 4. A third-law plot of equilibrium data for the C<sub>2</sub>F<sub>4</sub>-CF<sub>2</sub> system.

mental uncertainty, then either the free-energy function data or the equilibrium constants had to be in error, since  $\Delta H_r^{\circ}{}_{298}$  must obviously be single valued. Since the free-energy functions for both C<sub>2</sub>F<sub>4</sub> and CF<sub>2</sub> are reliably known,<sup>9,10</sup> drift in the third-law data was attributed to incorrect equilibrium constants.

The third-law data plot with minimum drift, obtained with  $\epsilon_{CF_2} = 1.605 \times 10^6$  cc/mol cm, is shown in Figure 4. The third-law  $\Delta H_r^{\circ}{}_{298}$  from this plot is  $68.40 \pm 0.45$  kcal/mol, with a drift of  $-0.1 \pm 0.7$  eu.

The significance of the relatively minor changes in  $\epsilon_{CF_2}$ , which were investigated is shown in Table II, which gives for each  $\epsilon_{CF_2}$  tested the values of  $\Delta H_r^{\circ}{}_{298}$  calculated by second- and third-law methods and the drift in the third-law values. It can be seen that the second-law values vary widely with  $\epsilon_{CF_2}$ , while the third-law values vary only slightly. Since the free-energy functions are well established, the third-law determination is clearly favored. It should be noted that the extreme sensitivity of the second-law values to changes in  $\epsilon_{CF_2}$  is largely due to those experiments giving relatively high conversions, in which a small change in  $\epsilon_{CF_2}$  caused a large change in  $K_p$ . If only reactions giving low conversions were considered, the second-law values would not be particularly sensitive to changes in  $\epsilon_{CF_2}$ .

Citing the above evidence, we assign  $\Delta H_r^{\circ}{}_{298} = 68.4 \pm 0.8$  kcal/mol, based on the third-law determination. The uncertainty given includes the standard deviation of the data ( $\pm 0.45$  kcal/mol) and the estimated uncertainty<sup>10</sup> in the free-energy function data ( $\pm 0.3$  eu). Temperature uncertainties are believed to be sufficiently small to be ignored, due to the precision of the velocity measurements ( $\pm 0.2\%$ ). Uncertainties resulting from systematic errors in species concentration determinations should also be minimal, due to the effective variation of species concentrations through  $\epsilon_{CF_2}$  to obtain a "best" data fit.

**Kinetics Study.** Our primary interest in studying the rate of CF<sub>2</sub> formation was to obtain a check on the C<sub>2</sub>F<sub>4</sub> decomposition mechanism and on the equilibrium results discussed earlier. Since the experiments were run over a limited range of pressures, it was not possible to determine the order of the reaction unambiguously.

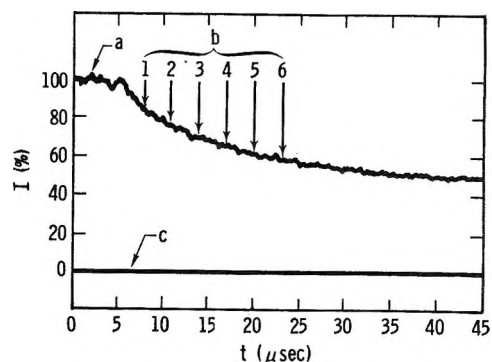
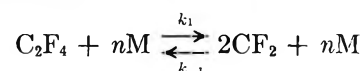


Figure 5. CF<sub>2</sub> absorption at 2620 Å, kinetics data: a, light intensity before shock arrival; b, intensity monitored at 3-μsec intervals for kinetics studies; c, baseline. Temperature over interval monitored ranged from 1483 to 1460°K.

Table II: Values of  $\Delta H_r^{\circ}{}_{298}(C_2F_4 \rightleftharpoons 2CF_2)$  Calculated by Second- and Third-Law Methods Using Different Values of  $\epsilon_{CF_2}$  ("Best" Values Are Italicized)

$\epsilon_{CF_2}$ , cc/mol cm	$\Delta H_r^{\circ}{}_{298}$ , (second law), kcal/mol	$\Delta H_r^{\circ}{}_{298}$ , (third law), kcal/mol	Third-law drift, eu
$1.615 \times 10^6$	$66.64 \pm 0.55$	$68.55 \pm 0.45$	$+1.4 \pm 0.7$
1.610	<i>67.48</i>	68.48	+0.7
1.605	<i>68.39</i>	<i>68.40</i>	-0.1
1.600	69.39	68.33	-0.9
1.595	70.50	68.24	-1.8

The reaction may be assumed to be first order in C<sub>2</sub>F<sub>4</sub>, and from zero to first order ( $n = 0$  to 1) in total gas pressure M (M is primarily argon).



The rate law may then be written

$$d[CF_2]/dt = 2k_1[C_2F_4][M]^n - 2k_{-1}[CF_2]^2[M]^n$$

Using  $k_{-1} = k_1/K_c$ , with  $K_c = K_p/RT$ , the rate constant  $k_1$  is obtained as

$$k_1 = (d[CF_2]/dt)(2[M]^n)([C_2F_4] - [CF_2]^2/K_c)^{-1}$$

Calculations of  $k_1$  were performed as follows for  $n = 0$ ,  $1/2$ , and 1 (total reactor order of 1, 1.5, and 2).

The concentration of CF<sub>2</sub> was determined from the CF<sub>2</sub> absorption traces in 27 experiments at six equally spaced reaction times which represented (approximately) from 20 to 80% of the dissociation at equilibrium. An experimental trace with the data points delineated is shown in Figure 5.<sup>11</sup> A value of  $\epsilon_{CF_2} = 1.605 \times 10^6$  cc/mol cm was used to calculate [CF<sub>2</sub>]. The concentrations [M] and [C<sub>2</sub>F<sub>4</sub>] and the temperature  $T$

(10) H. Prophet, The Dow Chemical Co., JANAF Tables staff, private communication.

(11) Two traces were recorded in most experiments, a faster sweep for equilibrium data and a slower sweep for kinetics data.

were determined from shock wave calculations carried to the point where the observed values of  $\text{CF}_2$  were matched. The values of  $K_e$  were determined at  $T$  from the equilibrium results reported earlier. The rate of change of  $\text{CF}_2$  with time was approximated by the expression

$$(d[\text{CF}_2]/dt)_m = \rho_{31}^{-1}([\text{CF}_2]_{m+1} - [\text{CF}_2]_{m-1})/(t_{m+1} - t_{m-1})$$

where  $m - 1$ ,  $m$ , and  $m + 1$  correspond to successive data points, and  $\rho_{31}$ , the ratio of densities behind and in front of the shock, converts the observed times (laboratory-fixed coordinates) into shocked gas times (particle-fixed coordinates).

Using the above procedure, four values of  $k_1$  (for  $m = 2$  to 5) were obtained for each experiment. The data from all 27 experiments were analyzed using a simple Arrhenius expression

$$k_1 = A \exp(-E_a/RT)$$

The 1.5-order calculations gave the best least-squares fit (plotted as  $\ln k_1$  vs.  $1/T$ ), and also gave the most reasonable preexponential factor  $A$  ( $\sim 10^{14}$ , vs.  $\sim 10^{11}$  and  $\sim 10^{17}$  for the first- and second-order calculations). The activation energies  $E_a$  were all considerably lower than the dissociation energy, varying from 51 kcal/mol for the first-order assumption to 56.5 kcal/mol for the second-order assumption.

A plot of the 1.5-order data is shown in Figure 6. A least-squares fit of the data gives a value of  $k_1 = (6.9 \pm 1.4) \times 10^{14} \exp(-54.30 \pm 0.26)/RT \text{ cm}^3/\text{mol}^{1/2} \text{ sec}$  for dissociation of 0.75%  $\text{C}_2\text{F}_4$  in argon, over a pressure range of 300–800 Torr. The use of this rate constant for other conditions of gas composition and pressure may not be justified.

The kinetic data shown in Figure 6 indicate a single dissociation reaction. Further, when the data taken early in each experiment ( $\sim 30\%$  of the equilibrium dissociation,  $m = 2$ ) were compared to those taken near equilibrium ( $\sim 70\%$  of the equilibrium dissociation,  $m = 5$ ), the least-squares Arrhenius expressions for  $k_1$  for the two cases were the same within experimental error. This not only supports our contention that a single dissociation reaction occurs, but also, since the recombination reaction was important in the case nearing equilibrium, adds further support to the values of  $K_p$  determined in the equilibrium study.

## V. Discussion

In their shock tube study of  $\text{C}_2\text{F}_4$  dissociation at temperatures from 1165 to 1620°K, M-L<sup>2a</sup> reported a second-law  $\Delta H_r^\circ_{1500} = 72.43$  kcal/mol, which gave  $\Delta H_r^\circ_{298} = 75.54$  kcal/mol. A third-law treatment of the same data, however, indicates  $\Delta H_r^\circ_{298} = 66.5$  kcal/mol, with a drift of about  $-6$  eu. Both the inconsistency of the second- and third-law values and the drift in the third-law data suggest that these results are

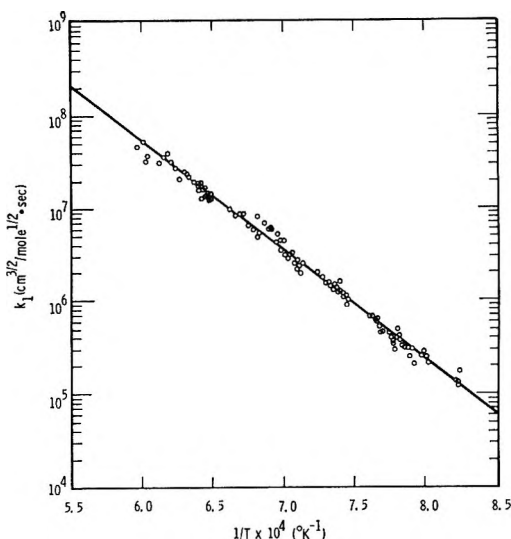


Figure 6. A plot of rate data for  $\text{C}_2\text{F}_4$  dissociation into  $\text{CF}_2$ , using 1.5-order assumption.

not valid. The problem in this work appears to be in the value of  $\epsilon_{\text{CF}_2}$  used. Given the high-temperature  $\epsilon_{\text{CF}_2}$  data reported by M-L, one might reasonably have assigned a higher value to  $\epsilon_{\text{CF}_2}$  below 1800°K. M-L did, in fact, assign a 20% higher value to  $\epsilon_{\text{CF}_2}$  in subsequent studies.<sup>2b,12</sup> Our experience indicates that a higher value of  $\epsilon_{\text{CF}_2}$  would increase the third-law  $\Delta H_r^\circ_{298}$ , reduce its drift, and also reduce the second-law  $\Delta H_r^\circ_{298}$ , so that the results would not only be more self-consistent, but would probably also be in good agreement with the present study.

ZUM,<sup>3</sup> in a Kundsen cell mass spectrometric study of the  $\text{C}_2\text{F}_4$ - $\text{CF}_2$  equilibrium from 1127 to 1244°K, reported consistent second- and third-law  $\Delta H_r^\circ_{298}$  values of  $76.3 \pm 3.0$  kcal/mol. Although the third-law results show excessive drift ( $\sim 8$  eu), this appears to be due to the use of incorrect free-energy function data. If one uses the JANAF free-energy functions for  $\text{C}_2\text{F}_4$  and  $\text{CF}_2$ , the ZUM data indicate a third-law  $\Delta H_r^\circ_{298} = 75.3$  kcal/mol, with little drift.

The higher third-law  $\Delta H_r^\circ_{298}$  in the ZUM study results from values of  $K_p$  that are about an order of magnitude lower than found in the shock tube studies (see Figure 7). Possible reasons for the discrepancy will now be discussed, the shock tube studies being considered first. Since the M-L data have already been considered, the following discussions will be based primarily on the present study. ZUM suggested that nonequilibrium conditions might have been present in the shock tube studies to account for the discrepancy in the third-law  $\Delta H_r^\circ_{298}$  (and reciprocally in the  $K_p$  values). However, our experience has been that a stable equilibrium is definitely achieved in the shock tube studies. In any case, nonequilibrium conditions would cause the

(12) A. P. Modica and J. E. LaGraff, *J. Chem. Phys.*, **44**, 3375 (1966).

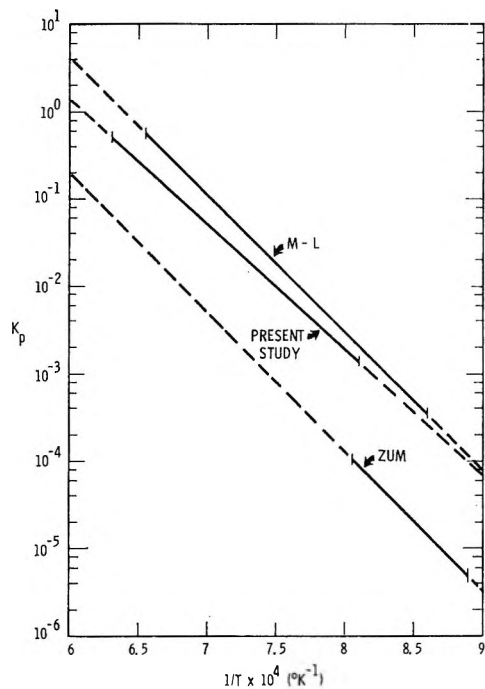


Figure 7. A comparison of reported equilibrium data for the  $C_2F_4$ - $CF_2$  system. Solid lines represent experimental data range.

discrepancy to be the opposite of what is observed. One might also suggest that an incorrect  $\epsilon_{CF_2}$  was used in the present study. After all, if  $\epsilon_{CF_2}$  were truly an arbitrarily adjustable function of temperature, any value of  $\Delta H_r^{\circ 298}$  could be justified. However,  $\epsilon_{CF_2}$  would have to increase by a factor of 4 between 1800 and 1200°K to match the ZUM  $K_p$  values. Since  $\epsilon_{CF_2}$  is relatively constant from 1800 to 2900°K and there is no reason to expect a marked change at lower temperatures, this possibly must be ruled out. In fact, if one assumes that  $\epsilon_{CF_2}$  is known within  $\pm 20\%$  at 1200°K, a reasonable assumption based on the higher-temperature data, then the uncertainty implied in  $\Delta H_r^{\circ 298}$  is less than  $\pm 1$  kcal/mol. Other uncertainties in the shock tube study were discussed earlier and found not to be significant. Thus, it appears that the results of the present study could not be in error by a sufficient amount to match the ZUM data.

Two possible uncertainties in the ZUM study may be suggested. First, the crucible temperature ZUM measured may have been higher than the temperature of the flowing test gas within the crucible. A temperature shift of about 120°K would bring the ZUM data into agreement with the present study. Second, the graph-

ite chips within the Knudsen crucible may have adsorbed  $C_2F_4$  or  $CF_2$ . If  $CF_2$  were adsorbed preferentially, or if it reacted chemically with the graphite chips, the values of  $CF_2$  (hence  $K_p$ ) measured would be too low.

Although the use of an adjustable  $\epsilon_{CF_2}$  in the present study suggests the results to be somewhat empirically determined, we believe that this method of data treatment was not only justified but necessary. As Table II indicates, a minor (1.3%) variation in  $\epsilon_{CF_2}$  was sufficient to cause a significant (5.7%) change in the value of  $\Delta H_r^{\circ 298}$  determined by the second-law method, due to the high conversions involved. The third-law determination, often omitted in studies of this type, was extremely valuable in supplying an independent, and apparently more reliable, value of  $\Delta H_r^{\circ 298}$ . Not only was the third-law value of  $\Delta H_r^{\circ 298}$  much less sensitive to change with  $\epsilon_{CF_2}$ , but also the drift of the third-law values provided a further test of the data. Certainly the use of an adjustable  $\epsilon_{CF_2}$  in our studies is supported by the results obtained. The best second- and third-law data fits, found in independent treatments of the data, not only gave the same value of  $\Delta H_r^{\circ 298}$  within experimental error, but also were obtained with essentially the same value of  $\epsilon_{CF_2}$ . The kinetics studies added further support to the equilibrium results.

The value of  $\Delta H_r^{\circ 298}$  can be used to determine the heat of formation of  $CF_2$ . Using  $\Delta H_f^{\circ 298}(C_2F_4) = -157.4$  kcal/mol,<sup>10</sup> our data support a value of  $\Delta H_f^{\circ 298}(CF_2) = -44.5 \pm 0.4$  kcal/mol. Although this result is somewhat more negative than the presently accepted value ( $\Delta H_f^{\circ 298}(CF_2) = -41 \pm 2$  kcal/mol),<sup>9</sup> we believe that the study of the  $C_2F_4$ - $CF_2$  equilibrium should be the most direct and, in principle, the most accurate means of determining the heat of formation of  $CF_2$ . Since the results of M-L and ZUM are in question, we favor the present value,  $\Delta H_f^{\circ 298}(CF_2) = -44.5 \pm 0.4$  kcal/mol.

*Acknowledgments.* The assistance of G. S. Benson and H. Mayfarth in designing the electronics equipment and conducting many of the experiments in this study is gratefully acknowledged. We thank T. M. Myers for performing infrared and gas chromatographic analyses of several  $C_2F_4$  samples. We also thank Dr. Garry Schott, Los Alamos Scientific Laboratory, for many helpful discussions, and Dr. John Daly, DuPont Organic Chemicals Department, for supplying the procedure for synthesis of  $C_2F_4$  and for supplying a sample of  $C_2F_4Br_2$ .

## Isomerization of Chemically Activated *n*-Pentyl Radicals

by K. W. Watkins\* and D. R. Lawson

Department of Chemistry, Colorado State University, Fort Collins, Colorado 80521 (Received June 24, 1970)

Publication costs borne completely by The Journal of Physical Chemistry

The addition of *n*-propyl radicals to ethylene was found to be a source of chemically activated *n*-pentyl radicals. The average energy of the radicals when first formed was calculated to be  $\sim 35$  kcal mol<sup>-1</sup>. Isomerization of *n*-pentyl *via* 1,4-hydrogen atom migration was the predominant reaction. At 57°, the average rate constant for isomerization was found to be  $3.3 \times 10^6$  sec<sup>-1</sup>. At 100°, it is proposed that the thermal isomerization of previously stabilized *n*-pentyl radicals contributes significantly to the rate of formation of *sec*-pentyl radicals. The experimental data were interpreted using a cyclic activated complex model with specific rate constants calculated according to the RRKM formulation of unimolecular reactions. The best agreement between experimental and theoretical results was found when using a threshold energy of 19 kcal/mol. Other kinetic data reported are: the rate constant for addition of *n*-propyl to ethylene,  $k_4 = 10^{11.15} \exp(-7400/RT)$  cm<sup>3</sup> mol<sup>-1</sup> sec<sup>-1</sup>;  $\Delta(n\text{-Pe}, n\text{-Pe}) = 0.15$ ;  $\Delta(n\text{-Pr}, n\text{-Pe}) = 0.056$ ; and  $\Delta(n\text{-Pr}, sec\text{-Pe}) = 0.11$ . The implication of this work to earlier studies on the isomerization of *n*-pentyl radicals is discussed.

### Introduction

Rate constants for the thermal unimolecular isomerization of *n*-pentyl and *n*-hexyl radicals *via* H-atom migration have been reported.<sup>1,2</sup> The observed rate constants were  $1.4 \times 10^7 \exp(-10.8 \times 10^3/RT)$  and  $2.07 \times 10^7 \exp(-8.3 \times 10^3/RT)$  sec<sup>-1</sup>, respectively. When reasonable entropies of activation are assumed, the observed *A* factors are low by a factor of  $\sim 10^3$ . Both sets of authors agree that these low *A* factors cannot be easily explained. In fact, Frey and Walsh<sup>3</sup> have suggested that the Arrhenius parameters for *n*-pentyl isomerization are in error and have estimated that  $A \sim 10^{10.5}$  sec<sup>-1</sup>. Recently, Hardwidge, *et al.*,<sup>4a</sup> have concluded that the activation energy for isomerization *via* H-atom migration in a five-membered, cyclic activated complex must be  $\sim 15$  kcal mol<sup>-1</sup> to explain their data. The data also suggested an *A* factor of  $\sim 10^{11}$  sec<sup>-1</sup>.

The radicals discussed above were generated by the addition of *n*-propyl and *n*-butyl radicals to ethylene. Since this reaction is exothermic by 22.2 kcal mol<sup>-1</sup> and has an activation energy of 7.4 kcal mol<sup>-1</sup>, the alkyl radicals when first formed will have at least 29.6 kcal mol<sup>-1</sup> of internal energy in excess of the zero-point energy. If the threshold for isomerization is less than 29.6, isomerization of these chemically activated *n*-pentyl and *n*-hexyl radicals can result. Examples of chemically activated isomerization of alkyl and alkenyl radicals have been known for some time.<sup>4</sup> The object of this work was to investigate the system in which *n*-pentyl radicals were produced for evidence of chemically activated isomerization, and to conclude whether the occurrence of chemically activated isomerization could explain the observed low *A* factors.

### Experimental Section

The essential experimental details have been previously described.<sup>5</sup> *n*-Pentyl radicals were produced

by the vapor phase photolysis of azo-*n*-propane in the presence of ethylene. Azopropane [b.p. 108° (640 Torr)] was prepared by the method of Leitch.<sup>6</sup> In several photolyses of pure azopropane at 25°, the average ratio  $R(C_3H_6)/R(C_6H_{14})$  was 0.139. This agrees well with reported values of the disproportionation to combination ratio of *n*-propyl radicals.<sup>7,8</sup>

Reaction vessels of 2, 10, 114, 322, and 1080 cm<sup>3</sup> were used in order to study the effect of pressure upon the product distribution.

The entire reactant-product mixture was analyzed by gas-solid chromatography using a 2-M alumina column (60-80 mesh), and a flame ionization detector. Temperature programming from 50 to 240° was required. An additional 30 min was required for *n*-decane to be eluted. The peaks were well resolved except that *trans*- and *cis*-2-pentene, while well separated, overlapped some with the larger 1-pentene peak which came out between them. Thus, some uncertainty exists in the 2-pentene analyses. The azoalkane appeared to be irreversibly absorbed on the column. Authentic samples were used for identification of the products. To ensure calibration of the system for each run a known amount of ethane (Phillips research grade) was added to the product mixture after photolysis as an internal standard.

- (1) L. Endrenyi and D. J. LeRoy, *J. Phys. Chem.*, **70**, 4081 (1966).
- (2) K. W. Watkins and L. A. Ostreko, *ibid.*, **73**, 2080 (1969).
- (3) H. M. Frey and R. Walsh, *Chem. Rev.*, **69**, 103 (1969).
- (4) (a) E. A. Hardwidge, C. W. Larson, and B. S. Rabinovitch, *J. Amer. Chem. Soc.*, **92**, 3278 (1970); (b) C. W. Larson and B. S. Rabinovitch, *J. Chem. Phys.*, **51**, 2293 (1969); (c) A. F. Trotman-Dickenson, R. R. Getty, and J. A. Kerr, *J. Chem. Soc. A*, 1360 (1967).
- (5) K. W. Watkins and L. A. O'Deen, *J. Phys. Chem.*, **73**, 4094 (1969).
- (6) R. Renaud and L. C. Leitch, *Can. J. Chem.*, **32**, 545 (1954).
- (7) J. O. Terry and J. H. Futrell, *ibid.*, **45**, 2327 (1967).
- (8) J. Grotewold and J. A. Kerr, *J. Chem. Soc.*, 4337 (1963).

**Table I:** Experimental Results at 100°

No.	Reactor <sup>a</sup> volume	Pressure <sup>b</sup> azo- <i>n</i> - propane	Pressure ethylene	Total pressure	<i>T</i> , °K	<i>t</i> , sec	C <sub>3</sub> H <sub>8</sub> <sup>c</sup>	C <sub>3</sub> H <sub>6</sub>	<i>n</i> -C <sub>5</sub> H <sub>12</sub>	1-C <sub>5</sub> H <sub>10</sub>
27	2.01	53.6	218.0	271.7	373.5	180	80.1	26.4	23.7	4.52
28	9.76	9.38	50.4	59.8	373.7	120	24.5	19.1	3.03	1.47
29	9.76	9.71	41.9	51.6	373.4	120	30.6	18.0	2.83	1.23
30	9.76	4.65	25.4	30.1	372.9	150	12.0	10.9	1.40	0.583
31	114.0	0.746	8.70	9.45	372.3	120	1.94	1.61	0.140	0.0807
32	114.0	0.682	2.35	3.03	373.7	120	2.17	1.67	0.0695	0.0277
33	114.0	0.648	7.54	8.19	372.5	120	1.34	1.06	0.0995	0.0564
34	114.0	0.778	4.07	4.85	373.0	120	2.34	2.03	0.120	0.0564
35	322.6	0.357	1.58	1.94	372.7	180	0.921	0.713	0.0303	0.0118
36	322.6	0.348	1.51	1.86	373.8	180	0.782	0.697	0.0364	0.0164
37	322.6	0.246	1.31	1.56	372.7	180	0.841	0.755	0.0358	0.0135
38	1080.0	0.0957	0.449	0.545	371.2	240	0.164	0.179	0.00761	0.00160
39	1080.0	0.111	0.482	0.593	373.3	240	0.188	0.180	0.00712	0.00173
40	1080.0	0.0891	0.463	0.552	373.3	240	0.179	0.169	0.00690	0.00159

	<i>trans</i> - 2-C <sub>5</sub> H <sub>10</sub>	<i>cis</i> - 2-C <sub>5</sub> H <sub>10</sub>	<i>n</i> -C <sub>6</sub> H <sub>14</sub>	3-MHex	<i>n</i> -C <sub>7</sub> H <sub>16</sub>	C <sub>7</sub> H <sub>16</sub>	4-MHept	<i>n</i> -C <sub>8</sub> H <sub>18</sub>	4-MNon	<i>n</i> -C <sub>10</sub> H <sub>22</sub>
27	0.0000	0.0000	156.0	0.0904	4.53	2.46	0.277	58.5	1.29	6.87
28	0.0000	0.0000	139.0	0.00779	0.327	0.222	0.223	23.1		0.709
29	Trace		136.0	0.0156	0.282	0.291	0.240	20.7	0.178	0.882
30	Trace	Trace	78.5	0.00340	0.143	0.149	0.178	10.1	0.0737	0.321
31	0.0040	Trace	11.7	0.000761	0.0102	0.0187	0.0703	1.23	0.00969	0.0588
32	0.0030	Trace	14.2	0.000908	0.0150	0.00530	0.0384	0.399	0.00222	0.0650
33	0.0034	Trace	8.03	0.00128	0.0176	0.0173	0.0550	0.820	0.0129	0.0269
34	0.0042		16.8	0.000704	0.00458	0.00387	0.0661	0.933	0.00715	0.158
35	0.0015	Trace	6.13	0.000347	0.0101	0.00204	0.0241	0.153	0.00113	0.00329
36	0.0026	Trace	5.21	0.000141	0.00146		0.0237	0.184	0.00128	0.00509
37	0.0023	Trace	5.78	0.000239	0.00386	0.00116	0.0246	0.166	0.000558	0.0111
38	0.00044	0.00018	1.43	0.0000877	0.000254	0.000228	0.00618	0.0138	0.000399	0.000749
39	0.00042	0.00026	1.38	0.0000820	0.000246	0.000164	0.00682	0.0173	0.000253	0.000230
40	0.00045	0.00019	1.39	0.0000640	0.000240	0.000032	0.00649	0.0153	0.000207	0.000308

<sup>a</sup> Reactor sizes are given in cubic centimeters. <sup>b</sup> Pressures are expressed in Torr. <sup>c</sup> Products are expressed in terms of their rates of formation in mol cm<sup>-3</sup> sec<sup>-1</sup> × 10<sup>12</sup>.

The pressures of reactants, reaction conditions, and the rates of formation of products are given in Tables I and II.

## Results

*Reactions of Excited *n*-Pentyl Radicals.* The addition of *n*-propyl to ethylene at 57° produces a *n*-pentyl radical with an average of 34.1 kcal mol<sup>-1</sup> (see Discussion section, eq III). When formed at 100°, the average energy is 35.2 kcal mol<sup>-1</sup>. These radicals can either react or be stabilized by collisional energy transfer. The major unimolecular reaction is isomerization to *sec*-pentyl. The presence of 4-methylheptane in the products is evidence for the existence of *sec*-pentyl radicals. Other products assumed to arise from *sec*-pentyl are *cis*- and *trans*-2-pentene, 3-methylhexane, and 4-methylnonane.

Stabilized *n*-pentyl radicals combine most often with *n*-propyl to yield *n*-octane. Cross disproportionation products are *n*-pentane 1-pentene, propane, and propene. Subsequent addition of *n*-pentyl to ethylene results in *n*-heptane, 1-heptene, and *n*-decane products.

*n*-Decane also results from the recombination of *n*-pentyl radicals.

A reaction scheme which can explain the products listed in Table I and their dependence on pressure is given below.

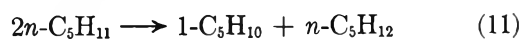
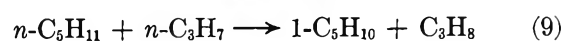
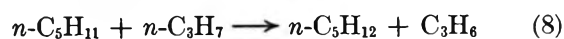
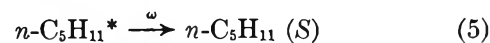
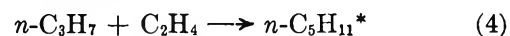
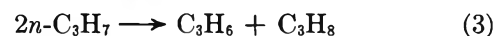
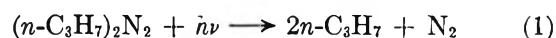
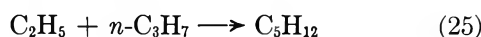
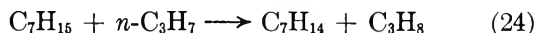
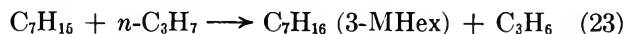
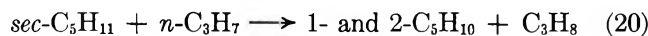
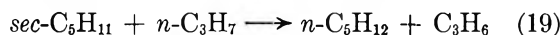
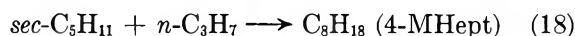
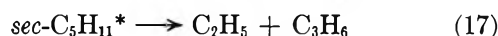
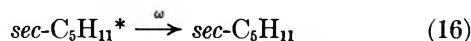
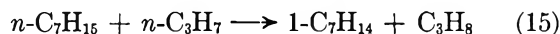
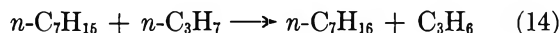
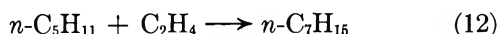


Table II: Experimental Results at 57°<sup>a</sup>

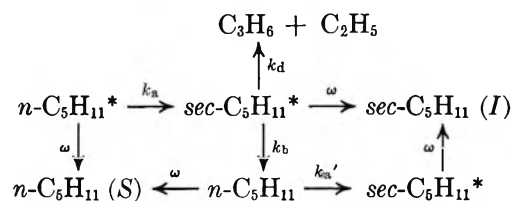
	Reactor volume	Pressure azopropane	Pressure ethylene	Total pressure	T, °K	t, sec	C <sub>3</sub> H <sub>6</sub>	C <sub>2</sub> H <sub>6</sub>	n-C <sub>5</sub> H <sub>12</sub>
41	114.0	0.51	3.79	4.30	329.0	360	0.642	0.642	0.0161
42	9.76	7.7	37.3	45.0	329.7	595	8.34	7.33	0.472
43	114.0	0.82	6.35	7.17	329.3	360	1.06	0.999	0.0259
44	9.76	9.9	55.4	65.3	330.9	606	8.13	6.87	0.612
45	9.76	7.4	43.0	50.4	329.2	600	8.91	8.05	0.543
46	9.76	5.5	24.5	29.9	329.7	600	8.82	7.77	0.319
47	9.76	5.3	17.3	22.6	330.9	600	7.64	6.63	0.227
48	114.0	0.70	7.65	8.35	329.9	720	1.01	0.882	0.0290
49	114.0	0.57	3.57	4.14	330.7	720	0.994	0.930	0.0144
50	114.0	0.76	3.07	3.83	330.3	720	1.04	0.950	0.0137
	1-C <sub>5</sub> H <sub>10</sub>	trans-2-C <sub>5</sub> H <sub>10</sub>	cis-2-C <sub>5</sub> H <sub>10</sub>	n-C <sub>8</sub> H <sub>14</sub>	n-C <sub>7</sub> H <sub>16</sub>	4-MHept	n-C <sub>8</sub> H <sub>18</sub>	4-MNon	n-C <sub>10</sub> H <sub>22</sub>
41	0.00656	0.00051	0.0002	4.98	Trace	0.00504	0.102	0.0000	Trace
42	0.236	Trace		51.6	0.023	0.023	4.11		0.097
43	0.0149	0.0004	0.0003	7.91	0.0016	0.00762	0.236		0.000
44	0.298			49.1	0.039	0.028	5.72	0.020	0.155
45	0.302	Trace	Trace	57.6	0.026	0.030	4.80	0.0000	0.141
46	0.182	Trace	Trace	58.1	0.013	0.023	2.83	0.0000	0.044
47	0.113	0.002		53.0	0.0091	0.016	2.03		
48	0.0196	0.0008	0.0004	8.08	0.0012	0.00860	0.338	0.0008	0.0036
49	0.00917	0.00038	0.0003	7.79	0.00033	0.00698	0.156	0.0000	0.00054
50	0.00790	0.00054	0.0003	7.62	0.00042	0.00629	0.133	0.0000	0.00071

<sup>a</sup> See Table I for units.

#### Chemical Activation Rate Constant for Isomerization.

In chemical activation systems the average rate constant  $k_a$  for a unimolecular reaction is given by  $k_a = \omega(I/S)$ ,<sup>9,10</sup> where  $I$  is the total rate of formation of the isomerization products, and  $S$  is the total rate of formation of stabilization products. The collision frequency of excited pentyl radicals with bath molecules is  $\omega$ . In the case of isomerization reactions, the rate constant is a "practical" rate constant  $k_p$  because of the possibil-

ity of isomerization of the products back to the reactants.<sup>4b</sup> The following scheme illustrates the possible reactions of the *sec*-pentyl radical.



The rate constants for decomposition and isomerization of *sec*-pentyl radicals are given by  $k_d$  and  $k_b$ , respectively. At high pressure, when  $\omega \gg k_b, k_d$ ;  $k_a \equiv k_p$ . The behavior of  $I/S$  over the entire pressure range will not be considered here. It has been described in detail by Larson.<sup>11</sup>

The ratio of steady-state concentrations of stabilized *sec*-pentyl radicals to stabilized *n*-pentyl radicals,  $I/S$ , was obtained from the ratio of the combination products formed when the above radicals react with *n*-propyl radicals. The following expression was used

$$\frac{I}{S} = \theta \frac{R(4\text{-MHept})}{R(n\text{-C}_5\text{H}_{18})}$$

where  $\theta$  is a constant which accounts for the difference

(9) B. S. Rabinovitch and D. W. Setser, *Advan. Photochem.*, **3**, 1 (1964).

(10) B. S. Rabinovitch and M. C. Flowers, *Quart. Rev. Chem. Soc.*, **18**, 122 (1964).

(11) C. W. Larson, Ph.D. Thesis, University of Washington, 1969.



in the disproportionation to combination ratios of the two sets of radicals.

$$\theta = \frac{(k_{18} + k_{19} + k_{20})/k_{18}}{(k_7 + k_8 + k_9)/k_7}$$

The ratio  $(k_7 + k_8 + k_9):k_7$  was estimated to be 1.14 in accord with the known disproportionation to combination ratios for the normal alkyl radicals, and  $(k_{18} + k_{19} + k_{20}):k_{18}$  was estimated to be 1.41 by analogy with  $\Delta(n\text{-C}_3\text{H}_7, i\text{-C}_3\text{H}_7)$  reported by Terry and Futrell.<sup>7</sup> Thus,  $\theta = 1.23$ .

Since  $I/S$  was used to calculate  $k_a$  only from runs at high pressure, it was not necessary to account for decomposition of *sec*-pentyl (reaction 17).

A plot of  $I/S$  vs.  $1/\omega$  is shown in Figure 1. The collision diameters used to calculate the collision frequency of  $n\text{-C}_5\text{H}_{11}^*$ , were  $\sigma_{\text{C}_2\text{H}_4} = 4.40 \text{ \AA}$ ,  $\sigma_{\text{C}_5\text{H}_{11}} = 5.80 \text{ \AA}$ , and  $\sigma_{\text{azo}} = 7.60 \text{ \AA}$ . The last two were chosen by analogy with  $n\text{-C}_5\text{H}_{12}$  and  $n\text{-C}_8\text{H}_{18}$ .<sup>12</sup>

A least-squares treatment of the data gave an intercept of 0.0017, and  $k_a = 8.8 \times 10^6 \text{ sec}^{-1}$  at  $100^\circ$ ; and an intercept of 0.0023, and  $k_a = 3.3 \times 10^6 \text{ sec}^{-1}$  at  $57^\circ$ .

The data taken at lower pressures (runs 32, 35–40) at  $100^\circ$  are not plotted. They show that  $I/S$  begins to level off as  $1/\omega$  increases. This could be due to a loss of *sec*- $\text{C}_5\text{H}_{11}$  by decomposition (reaction 17) or back isomerization. These data are included in Table I for the purpose of establishing the complete reaction mechanism, and for the calculation of other kinetic data.

**Decomposition of the *sec*-Pentyl Radical.** The decomposition of chemically activated *sec*-pentyl radicals produced by the addition of hydrogen atoms to 1-pentene has been studied by Rabinovitch and coworkers.<sup>13</sup> The threshold energy was given as  $30.7 \text{ kcal mol}^{-1}$ , and the average energy of the formed *sec*-pentyl radicals was  $45 \text{ kcal mol}^{-1}$ . The rate constant  $k_a$  was found to be  $1.2 \times 10^7 \text{ sec}^{-1}$ .

In this work, *sec*-pentyl radicals in the  $100^\circ$  runs are formed at an average energy of about  $41 \text{ kcal/mol}$ . We have estimated the  $k_a$  for their decomposition as follows. The reaction mechanism would predict that

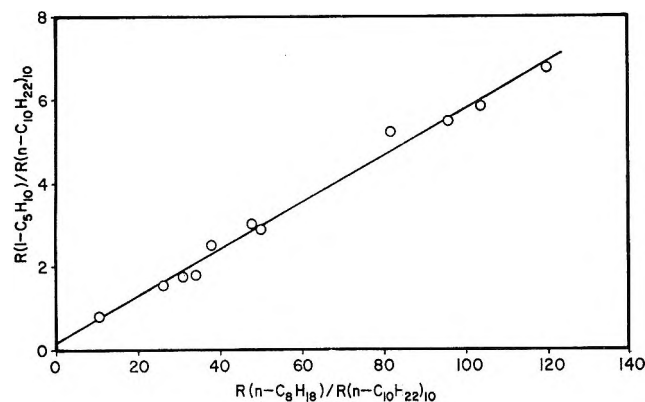


Figure 1. Plot of  $R(1\text{-C}_5\text{H}_{10})/R(n\text{-C}_{10}\text{H}_{22})_{10}$  vs.  $R(n\text{-C}_8\text{H}_{18})/R(n\text{-C}_{10}\text{H}_{22})_{10}$ .

$R(n\text{-C}_5\text{H}_{12})/R(1\text{-C}_5\text{H}_{10}) \simeq 1.0$ . However, in the  $57^\circ$  runs the ratio varies from 1.5 to 2.0, and in the  $100^\circ$  runs the ratio is approximately 2.0 except at the high- and low-pressure extremes where it increases to 5.2 and 4.4, respectively. At high pressure this increase can be reasonably ascribed to hydrogen atom abstraction. The ratio of about 2 in the  $57^\circ$  runs at intermediate pressures should not be ascribed to reaction 25, because the ratio does not increase as the pressure decreases as would be expected. In fact it tends to decrease. Only in the three  $100^\circ$  runs at the lowest pressure (0.5 Torr) can this increase in the ratio of pentane to 1-pentene be reasonably thought to result from reaction 25. The high ratio of about 2 remains unexplained.

If the pentane in runs 38–40 from reaction 25 is given by

$$R(n\text{-C}_5\text{H}_{12})_{25} = R(n\text{-C}_5\text{H}_{12}) - 2R(1\text{-C}_5\text{H}_{10})$$

Then,  $I/S \simeq R(n\text{-C}_5\text{H}_{12})_{25}/1.41R(4\text{MHept})$ , and the average  $k_d$  must be  $3 \times 10^6 \text{ sec}^{-1}$ . From the energy dependence of  $k_E$  as calculated by Rabinovitch and Georgakalos,<sup>14</sup> the value of  $k_d$  corresponds to *sec*-pentyl radicals with an internal energy of  $41.5 \text{ kcal mol}^{-1}$ , which agrees with our estimated energy of  $41 \text{ kcal mol}^{-1}$ . It is unfortunate that our data were not well suited to this type of study because it would be of interest to measure the energy dependence of the rate constant more accurately, and thus test  $k_E$  as calculated from the RRKM theory.

**Rate Constant for Addition of *n*-Propyl to Ethylene.** The rate constant for addition of *n*-propyl radicals to ethylene can be estimated from the expression

$$\frac{k_4}{k_2^{1/2}} = \frac{R(n\text{-pentyl products})}{R^{1/2}(n\text{-hexane})[\text{C}_2\text{H}_4]_0}$$

where  $[\text{C}_2\text{H}_4]_0$  is the initial concentration of ethylene. Less than 1% of the initial ethylene was consumed in a run.  $R(n\text{-pentyl products})$  can be determined from a complete product analysis and is simply the sum of the rates of formation of all the products resulting from *n*-pentyl radicals. From 14 runs at  $100^\circ$ ,  $k_4/k_2^{1/2} = 1.4 \pm 0.3$ , and from 10 runs at  $57^\circ$ ,  $k_4/k_2^{1/2} = 0.38 \pm 0.01$ . In Arrhenius form,  $k_4/k_2^{1/2}$  becomes

$$\log(k_4/k_2^{1/2}) = 4.48 - (7400/2.3RT)$$

Assuming  $k_2$  to equal the rate constant for recombination of methyl radicals,  $2.2 \times 10^{13} \text{ mol}^{-1} \text{ cm}^3 \text{ sec}^{-1}$ , and that  $E_2 = 0$ ; the value found for  $k_4$  was  $\log k_4 = 11.15 - (7400/2.3RT)$ . This result is in excellent agreement

(12) (a) J. O. Hirschfelder, C. F. Curtiss, and R. B. Bird, "Molecular Theory of Gases and Liquids," Wiley, New York, N. Y., 1964; (b) Y. N. Lin, S. C. Chan, and B. S. Rabinovitch, *J. Phys. Chem.*, **72**, 1932 (1968).

(13) (a) M. J. Pearson and B. S. Rabinovitch, *J. Chem. Phys.*, **42**, 1624 (1965); (b) J. H. Georgakalos, B. S. Rabinovitch, and E. J. McAduff, *ibid.*, **52**, 2143 (1970).

(14) B. S. Rabinovitch and J. H. Georgakalos, private communication.

with previous kinetic parameters reported from this laboratory on the addition of ethyl and isopropyl radicals to ethylene.<sup>5</sup> The activation energy is higher than two other values for  $E_A$  of 5.1<sup>15</sup> and 6.5<sup>16</sup> kcal mol<sup>-1</sup>. As stated previously<sup>5</sup> we feel that the higher activation energy results from a more complete product analysis with an accounting of consecutive addition reactions.

**Disproportionation to Combination Ratios.** The ratio of rate constants,  $k_9/k_7$ , gives the cross disproportionation to combination ratio  $\Delta(n\text{-Pr}, n\text{-Pe})$ . This is not given directly by the ratio of  $R(1\text{-C}_5\text{H}_{10})/R(n\text{-C}_8\text{H}_{18})$  because some 1-pentene is produced in reactions 11 and 20 as well as in reaction 9. However, under conditions of relatively high-pressure reaction 20 can be ignored as a source of 1-pentene. Then, the total rate of formation of 1-C<sub>5</sub>H<sub>10</sub> can be written as

$$R(1\text{-C}_5\text{H}_{10}) = \frac{k_9}{k_7}R(n\text{-C}_8\text{H}_{18}) + \frac{k_{11}}{k_{10}}R(n\text{-C}_{10}\text{H}_{22})_{10}$$

where  $R(n\text{-C}_{10}\text{H}_{22})_{10}$  is the rate of formation of  $n$ -decane from reaction 10. Since reaction 13 contributes to the total  $R(n\text{-C}_{10}\text{H}_{22})$ ,  $R(n\text{-C}_{10}\text{H}_{22})_{10}$  was calculated from the  $\phi^2$  relation<sup>7</sup>

$$R(n\text{-C}_{10}\text{H}_{22})_{10} \simeq \frac{0.25R(n\text{-C}_8\text{H}_{18})}{R(n\text{-C}_6\text{H}_{14})}$$

The ratios  $k_9/k_7$  and  $k_{11}/k_{10}$  can be obtained from the slope and intercept of a plot of  $R(1\text{-C}_5\text{H}_{10})/R(n\text{-C}_{10}\text{H}_{22})_{10}$  vs.  $R(n\text{-C}_8\text{H}_{18})/R(n\text{-C}_{10}\text{H}_{22})_{10}$ . A least-squares treatment of the data in Figure 2 (most of the points are from runs carried out at 57°) gave  $k_9/k_7 = \Delta(n\text{-Pr}, n\text{-Pe}) = 0.056$ , and  $k_{11}/k_{10} = \Delta(n\text{-Pe}, n\text{-Pe}) = 0.15$ . The value of  $\Delta(n\text{-Pe}, n\text{-Pe})$  found here agrees well with the ratio 0.14 from a recent study of the photolysis of  $n$ -pentylazomethane.<sup>17</sup>

The cross disproportionation to combination ratio  $\Delta(n\text{-Pr}, sec\text{-Pe})$  was estimated from the ratio  $R(cis\text{-} and \text{trans-}2\text{-C}_5\text{H}_{10})/R(4\text{-MHept})$ . Reaction 20 can be resolved into three reactions

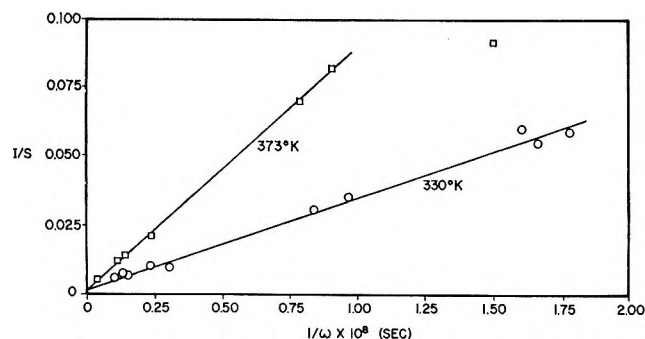
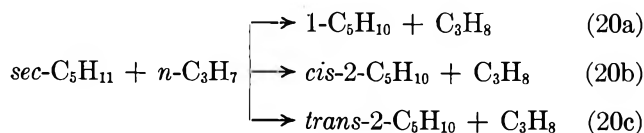


Figure 2. Plots of the function  $I/S$  vs.  $1/\omega$  at 330 and 373°K.

The average of eight runs gave  $R(cis\text{-}2\text{-C}_5\text{H}_{10})/R(4\text{-MHept}) = 0.04$ , and the average of 15 runs gave  $R(trans\text{-}2\text{-C}_5\text{H}_{10})/R(4\text{-MHept}) = 0.074$ . Thus  $\Delta(n\text{-Pr}, sec\text{-Pe}) = 0.11$ . It is interesting to note the ratio of  $trans\text{-}$  to  $cis\text{-}2\text{-C}_5\text{H}_{10}$  is  $\sim 1.8$  which is essentially the equilibrium ratio of 2.02 at 300°K, and 1.40 at 400°K.

## Discussion

**Theoretical Calculation of the Rate Constant.** Rabinovitch and coworkers<sup>9,10</sup> have described equations for the calculation of the average rate constant for reaction of vibrationally excited molecules produced by chemical activation.

$$k_a = \omega(I/S) = \frac{\int_{E_{\min}}^{\infty} \frac{k_E}{k_E + \omega} f(E) dE}{\int_{E_{\min}}^{\infty} \frac{\omega}{k_E + \omega} f(E) dE} \quad (I)$$

In eq I  $\omega$  is the specific deactivation rate constant,  $k_E$  is the rate constant for isomerization at a specific energy  $E$ , and  $f(E)$  is the energy distribution above  $E_{\min}$  of the chemically activated pentyl radical. A schematic potential energy diagram leading from propyl radicals plus ethylene through ethyl plus propene is shown in Figure 3. This figure also serves to define the important quantities,  $E_{\min}$ ,  $E_{\min}^\ddagger$ , and  $E_0$ . These energy differences are estimated in Appendix I.  $k_E$  is given by eq II derived by Marcus<sup>18</sup>

$$k_E = \frac{\sigma Z^\ddagger \sum P(E^\ddagger)}{h Z^* N^*(E)} \quad (II)$$

where  $\sum P(E^\ddagger)$  is the sum of the degeneracies of all possible eigenstates of the active degrees of freedom of the activated complex,  $N^*(E)$  is the density of the active eigenstates in the molecule,  $Z^\ddagger$  and  $Z^*$  are the adiabatic partition functions for the complex and molecule,  $h$  is Planck's constant, and  $\sigma$  is the reaction path degeneracy.

The  $\sum P(E^\ddagger)$  and  $N^*(E)$  were calculated from the Haarhoff approximation.<sup>19</sup> For simple bimolecular combination reactions the distribution function,  $f(E)dE$ , is defined by eq III<sup>20</sup>

$$f(E)dE = \frac{k_E' K(E) dE}{\int_{E_{\min}}^{\infty} k_E' K(E) dE} \quad (III)$$

The rate constant,  $k_E'$ , applies to the dissociation of  $n$ -pentyl radicals into  $n$ -propyl plus ethylene, *i.e.*, the

(15) L. Endrenyi and D. J. LeRoy, *J. Phys. Chem.*, **71**, 1334 (1967).

(16) J. A. Kerr and A. F. Trotman-Dickenson, *Trans. Faraday Soc.*, **55**, 572 (1959).

(17) K. W. Watkins, *J. Amer. Chem. Soc.*, accepted for publication.

(18) R. A. Marcus, *J. Chem. Phys.*, **20**, 359 (1952).

(19) P. C. Haarhoff, *J. Mol. Phys.*, **6**, 337 (1963); **7**, 101 (1963).

(20) B. S. Rabinovitch and R. Diessen, *J. Chem. Phys.*, **30**, 735 (1959).

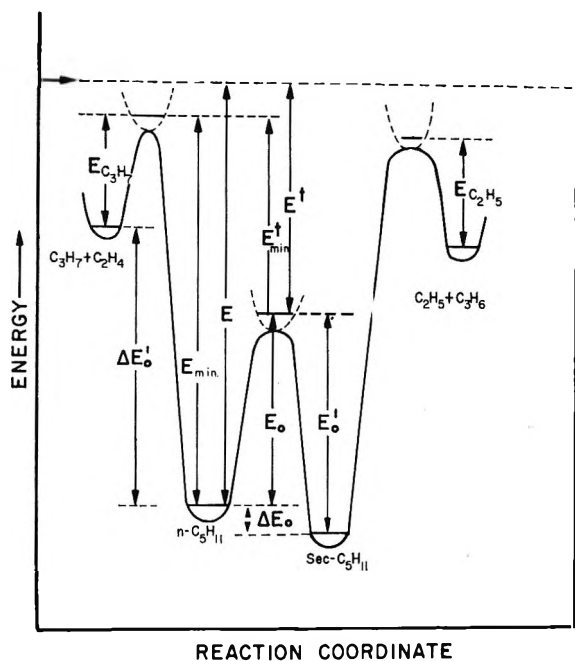
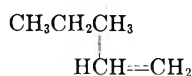


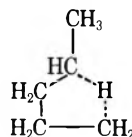
Figure 3. Schematic potential energy diagram.

reverse of the chemical activation formation step, and  $K(E)$  is the Boltzmann distribution.

To evaluate  $k_a$ , models must be specified for the dissociation complex



the isomerization complex



and the *n*-pentyl radical. The models consist of vibration frequencies and moments of inertia. These quantities are used to calculate  $k_E'$  and  $k_E$ .  $k_E'$  is used in the calculation of the distribution function  $f(E)dE$ . In order to compare calculated and experimental rate constants,  $k_E$  must be averaged over the distribution function as in eq I.

The vibration frequencies for the *n*-pentyl radical were taken from frequencies of *n*-pentane calculated by Schnachtschneider and Snyder;<sup>21</sup> it was necessary to remove one primary CH stretch (2960  $\text{cm}^{-1}$ ), two CH bends (1458, 1355  $\text{cm}^{-1}$ ), and to lower one torsion from 215 to 102  $\text{cm}^{-1}$ .

The vibration frequencies for the dissociation complex were based upon those for the radical. Eight modifications were made similar to those described by Rabinovitch<sup>13a</sup> for the decomposition of 2-alkyl radicals. Georgakakos<sup>13b</sup> has described a complex for *n*-pentyl decomposition in which frequencies were lowered by 0.4. All frequency lowerings here were made to correspond to a reduction by a factor of 0.5. Two  $\text{CH}_2$

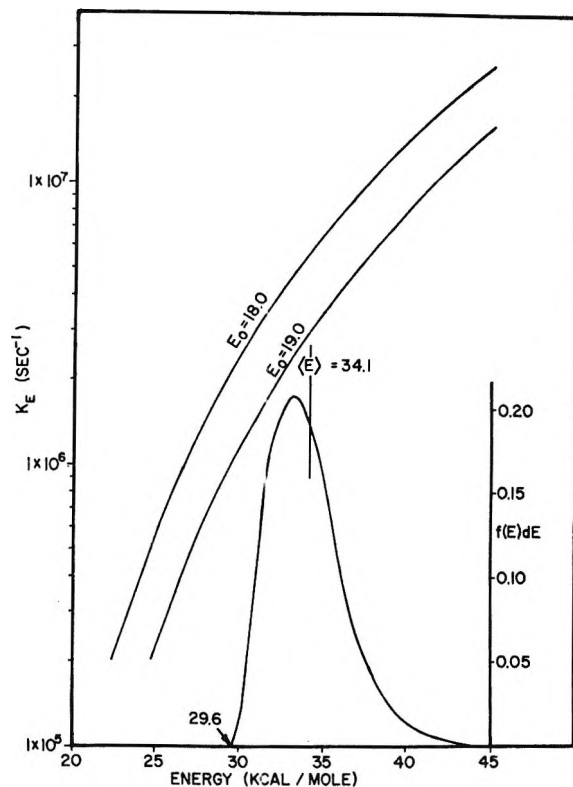


Figure 4. Calculated RRKM rate constants for two values of  $E_0$  and the distribution function at 330°K.

wagging frequencies at 1336 and 1292  $\text{cm}^{-1}$  were lowered to 668 and 646  $\text{cm}^{-1}$  in the complex. Two C-C-C skeletal bendings at 406 and 188  $\text{cm}^{-1}$  were lowered similarly to 203 and 94  $\text{cm}^{-1}$ . The torsional libration frequency of the  $\text{CH}_2$  groups about the breaking bond was reduced from 88 to 44  $\text{cm}^{-1}$ , and the torsional frequency of the forming double bond was raised from 102 to 200  $\text{cm}^{-1}$ . The C-C stretch at 1035  $\text{cm}^{-1}$  associated with the reaction coordinate was taken to be zero. The C-C stretch associated with the forming double bond was raised from 1070 in the radical to 1358  $\text{cm}^{-1}$  in the complex.

This model gives a preexponential factor [ $A = ekT/h \exp(\Delta S^\ddagger/R)$ ] for the dissociation reaction at 100° of  $10^{14.07} \text{ cm}^3 \text{ mol}^{-1} \text{ sec}^{-1}$ , which is somewhat higher than the  $A$  factor for the decomposition of *n*-butyl radicals<sup>22</sup> ( $\log A = 13.57$ ). No experimental data are available on the dissociation of *n*-pentyl radicals. This decomposition complex is used in the calculation of the distribution function  $f(E)dE$  shown in Figure 4. The average energy of the formed radicals at 57° is 34.1 kcal  $\text{mol}^{-1}$ .

The frequency assignment for the isomerization complex were derived from cycloalkane assignments.<sup>23</sup> Here we follow an argument first presented by Larson<sup>11</sup>

(21) J. H. Schnachtschneider and R. G. Snyder, *Spectrochim. Acta*, **19**, 117 (1963).

(22) W. E. Morganroth and J. G. Calvert, *J. Amer. Chem. Soc.*, **88**, 5387 (1966).

for treating the ring normal modes of the activated complex. Cyclic compounds have  $3r - 6$  ring deformation modes, where  $r$  denotes the number of atoms in the ring. These may be grouped into  $r$  modes which are mostly C-C stretch and torsion, and  $2r - 6$  moles which are C-C-C bending plus torsional motions. The frequencies from a recent vibrational assignment for cyclopentane<sup>23a</sup> were used to help assign some of the frequencies on the complex. Since the cyclic complex contains one H atom, three of the ring modes involve motion of H and are assigned a frequency similar to a CCH bend,<sup>4b</sup> *i.e.*,  $1100\text{ cm}^{-1}$ . A value of  $1013\text{ cm}^{-1}$  was used for the four stretching type motions involving C atoms, and  $870$  and  $290\text{ cm}^{-1}$  were assigned to the two bending type, deformation modes. If the ring is to open to yield a *sec*-pentyl radical, one of these deformations must be the reaction coordinate, and thus the ring has eight stable deformation modes.

Examination of frequency assignments of cycloalkanes also reveals that there are  $4m$  methylene motions, where  $m$  is the number of methylene groups. These are  $m$  CH<sub>2</sub> twists,  $m$  CH<sub>2</sub> wags,  $m$  CH<sub>2</sub> scissors, and  $m$  CH<sub>2</sub> rocks. The CH group should have an in-plane and out-of-plane bending modes, and the remaining frequencies are associated with the CH<sub>3</sub> group. The frequencies and moments of inertia for the isomerization complex are given in Table III.

**Table III:** Modes and Frequency Assignments for the Isomerization Complex

Ring deformations (9)	CH stretch (10)	Ring methylene motions (12)
1013 (4)	2966	
870	2965 (2)	CH <sub>2</sub> rock (3)
290	2928	896 (3)
1100 (2)	2922	CH <sub>2</sub> wags (3)
Reaction coordinate	2885 (2)	1298 (2)
CH bend (2)	2859	1254
1150	2856	CH <sub>2</sub> twists (3)
768	2844	1189 (2)
		1041
		CH <sub>2</sub> scissors (3)
		1450 (3)
Modes related to the methyl group (9)		
CH <sub>3</sub> deformations (3)	CCH bend (1)	
1477	1450	
1455 (2)		
CH <sub>3</sub> rock (2)	CCC bend (1)	
1112 (2)	332	
CC stretch (1)	Torsion (1)	
1000	198	
Moments of inertia, 187, 158, 62 amu Å <sup>2</sup>		

The value of the threshold energy for isomerization via H-atom transfer is not accurately known. In the Appendix a minimum value of  $E_0 = 15.3\text{ kcal mol}^{-1}$  is estimated. Calculations using  $E_0 = 18.0$  and  $19.0$

kcal mol<sup>-1</sup> gave the best agreement between the theoretical and experimental rate constants. The calculated specific rate constants  $k_E$  are shown in Figure 4, and the calculated average rate constants are given in Table IV.

*Chemically Activated vs. Thermally Activated Isomerization.* The RRKM calculations do not predict anywhere near as large a temperature dependence for  $k_a$  as was observed. The simplest explanation is that the results at  $100^\circ$  are influenced by the thermal isomerization of previously stabilized *n*-pentyl radicals. If the activation energy for isomerization is  $17\text{ kcal mol}^{-1}$ , lowering the temperature to  $57^\circ$  should decrease the thermal contribution to 0.051 of its  $100^\circ$  contribution. Since the observed  $k_a$  decreases by only 0.38, the thermal contribution at  $57^\circ$  must be decreased almost to where it is negligible. This can be illustrated by taking the difference between the calculated  $k_a$  ( $E_0 = 19.0\text{ kcal}$ ), and the observed  $k_a$  at  $100^\circ$  to be the thermal contribution. This amounts to 59% of the observed  $k_a$ ! At  $57^\circ$ , this thermal contribution would fall to  $0.26 \times 10^6\text{ sec}^{-1}$ , which is only 8% of the observed  $k_a$  at  $57^\circ$ .

Whereas this analysis may put too much emphasis on the validity of the calculated  $k_a$ , the effect of temperature on  $k_a$  is adequately explained by separate contributions from thermally and chemically activated isomerization. We conclude that the  $k_a$  is probably considerably enhanced by a thermal contribution. Evidently, at  $100^\circ$  and at high pressure, where  $I$  is small and  $S$  is large, a small amount of thermal isomerization can add significantly to the ratio  $I/S$ .

*Back Isomerization.* Since the activated complex for the isomerization of *sec*-pentyl to *n*-pentyl is the same as for the forward process, it was of interest to calculate the specific rate constants  $k_E$  for this reaction in order to assess its importance in these systems. The calculation was straightforward because the frequencies for *sec*-pentyl could be obtained from *n*-pentane,<sup>13</sup> and the threshold energy  $E_0'$  should be greater than  $E_0$  for *n*-pentyl isomerization by the difference in zero-point energies of the two radicals. This is  $\sim 4.0\text{ kcal mol}^{-1}$ , the approximate difference in the primary and secondary C-H bond energies. The RRKM calculations were carried out for  $E_0' = 23.0\text{ kcal mol}^{-1}$ , and the  $k_E$  at the appropriate average energy is listed in Table IV as  $k_b$ .

The fraction of *sec*-pentyl radicals returning to *n*-pentyl can be estimated from the relationship  $(k_b/k_b) + k_d + \omega$ . At  $57^\circ$  the pressure in the lowest pressure run was 3.82 Torr, and  $\omega = 55.6 \times 10^6\text{ sec}^{-1}$ . Assuming that  $k_d \simeq 2 \times 10^6\text{ sec}^{-1}$ , taking  $k_b$  from Table IV, the fraction of *sec*-pentyl returning to *n*-pentyl is only

(23) (a) V. Schettino, M. P. Marzocchi, and S. Califaro, *J. Chem. Phys.*, **51**, 5264 (1969); (b) H. Takahashi, T. Shimanouchi, K. Fukushima, and T. Miyazara, *J. Mol. Spectrosc.*, **13**, 43 (1964); (c) G. W. Rathjens, Jr., N. K. Freeman, W. D. Gwinn, and K. S. Pitzer, *J. Amer. Chem. Soc.*, **75**, 5634 (1953).

**Table IV:** Comparison of Calculated with Experimental Results

Temp, °C	$\langle E \rangle^a$	$k_e$ obsd	$k_a$ calcd		$k_b$ calcd <sup>b</sup>	$k_d$ obsd
			$E_0 = 18$	$E_0 = 19^a$		
57	34.1	$3.3 \times 10^6$	$5.3 \times 10^6$	$2.8 \times 10^6$	$1.9 \times 10^6$	
100	35.2	$8.8 \times 10^6$	$6.7 \times 10^6$	$3.6 \times 10^6$	$2.6 \times 10^6$	$3 \times 10^6$

<sup>a</sup> Units, kilocalories per mole. <sup>b</sup> Calculated for  $E_0 = 23$  kcal mol<sup>-1</sup>, the average energy of formed *sec*-pentyl radicals was 39.3 and 40.7 kcal mol<sup>-1</sup> at 57 and 100°, respectively.

0.03. Thus, the high-pressure condition  $k_p \equiv k_a$  is essentially satisfied.

*Low A Factors for Isomerization.* Thermal unimolecular rate constants have been reported for the isomerization of *n*-pentyl<sup>1</sup> and *n*-hexyl<sup>2</sup> radicals. The pressure dependence of  $I/S$  shown in Figure 1 is sufficient evidence that isomerization in these systems at 57° is chemically activated, and not thermal. Endrenyi and LeRoy<sup>1</sup> produced *n*-pentyl radicals in the temperature range 165–230° at pressures of about 105 Torr. We suggest that under their conditions the stabilized *n*-pentyl radicals can isomerize thermally and that this competes favorably with chemically activated isomerization. The temperature dependence therefore involves a combination of the temperature effect on the chemical activation distribution function  $f(E)$  and the thermal Boltzmann distribution  $K(E)$ . Since  $k_a$  does not have as strong a temperature dependence as  $k_{\text{thermal}}$ , and because both chemical activation and thermal activation contribute to the "apparent" unimolecular rate constant, this rate constant has a smaller temperature dependence than if the reaction were completely thermal. This situation would lead to both the low  $A$  factor and low activation energy as reported by Endrenyi and LeRoy. The reader is referred to papers by Rabinovitch, Kubin, and Harrington,<sup>24</sup> and Chang and Setser<sup>25</sup> for discussion of the temperature effect upon chemical activation rate constants.

One of the referees suggested that we make an estimate of the relative importance of the chemically *vs.* thermally activated isomerization in the work of Endrenyi and LeRoy. This would be valuable to the interpretation. However, it requires an accurate knowledge of the energy dependence of  $k_a$ , and since both  $E_0$  and the model of the complex are still somewhat uncertain, the estimation of  $k_a$  in the temperature range 438 to 502°K may not be reliable at this time.

## Appendix I

*Calculation of  $E_{\text{min}}$  and  $E_0$ .* The quantity  $E_{\text{min}}$  is equal to  $E_0'$ , the activation energy at absolute zero for the reverse of the chemical activation step. From the reaction coordinate diagram  $E_{\text{min}} = \Delta E_0' + E_{\text{C}_3\text{H}_7}$ , where  $E_{\text{C}_3\text{H}_7}$  is the activation energy for the addition of *n*-propyl radicals to ethylene.

The following heats of formation,  $\Delta H_f^\circ$  (kcal/mol) at 0°K were used: H, 51.62; *n*-C<sub>5</sub>H<sub>12</sub>, -27.23; C<sub>3</sub>H<sub>8</sub>,

-19.48; and C<sub>2</sub>H<sub>4</sub>, 14.52. The following C-H bond dissociation energies were used:  $D_0^\circ(n\text{-C}_5\text{H}_{11} - \text{H}) = 96.2$ , and  $D_0^\circ(n\text{-C}_3\text{H}_7 - \text{H}) = 96.2$  kcal/mol.<sup>26</sup> Then

$$\Delta H_f^\circ(n\text{-pentyl}) = \Delta H_f^\circ(\text{pentane}) - \Delta H_f^\circ(\text{H}) + D_0^\circ(n\text{-C}_5\text{H}_{11} - \text{H})$$

$$\Delta H_f^\circ(n\text{-pentyl}) = 17.4 \text{ kcal mol}^{-1}$$

and

$$\Delta H_f^\circ(n\text{-propyl}) = \Delta H_f^\circ(\text{propane}) - \Delta H_f^\circ(\text{H}) + D_0^\circ(n\text{-C}_3\text{H}_7 - \text{H})$$

$$\Delta H_f^\circ(n\text{-propyl}) = 25.1 \text{ kcal mol}^{-1}$$

and

$$\Delta E_0' = \Delta H_f^\circ(n\text{-propyl}) + \Delta H_f^\circ(\text{ethylene}) - \Delta H_f^\circ(n\text{-C}_5\text{H}_{11})$$

$$\Delta E_0' = 22.2 \text{ kcal mol}^{-1}$$

The value of  $E_{\text{C}_3\text{H}_7}$  was taken to be 7.4 kcal mol<sup>-1</sup> as was determined in this work. Then  $E_{\text{min}} = E_0' + E_{\text{C}_3\text{H}_7} = 29.6$  kcal/mol, which agrees well with the value for *n*-butyl decomposition reported by Calvert.<sup>22</sup>

$E_0$  for the isomerization of *n*-pentyl radicals has never been measured, and so a method to approximate it was developed. It is assumed that  $E_0 = E_a + E_s$ , where  $E_a$  is the activation energy for a bimolecular H-atom abstraction, and  $E_s$  is the strain energy of a five-membered ring.  $E_a$  was taken as 8.0 kcal/mol by comparison with values tabulated by Calvert.<sup>27</sup>  $E_s = 7.3$  kcal mol<sup>-1</sup>, the strain energy for cyclopentane<sup>28</sup> plus 1 kcal due to additional strain caused by the shorter C-H bonds in the complex compared to C-C bonds in cyclopentane. Because the strain energy could be larger than estimated, the value of  $E_0 = 15.3$  kcal mol<sup>-1</sup>

(24) B. S. Rabinovitch, R. F. Kubin, and R. E. Harrington, *J. Chem. Phys.*, **38**, 405 (1963).

(25) H. W. Chang and D. W. Setser, *J. Amer. Chem. Soc.*, **91**, 7648 (1969).

(26) C. W. Larson and B. S. Rabinovitch, *J. Chem. Phys.*, **52**, 5181 (1970).

(27) D. H. Slater, S. S. Collier, and J. G. Calvert, *J. Amer. Chem. Soc.*, **90**, 268 (1968).

(28) S. W. Benson, "Thermochemical Kinetics," Wiley, New York, N. Y., 1968.

is considered the minimum possible  $E_0$ . For this case  $E_{\min}^\ddagger = E_{\min} - E_0 = 14.3 \text{ kcal mol}^{-1}$ .

*Acknowledgment.* The authors wish to thank Professor D. W. Setser, Kansas State University, for the generous loan of computer programs which were used

in this work. One of us, K. W. W., wishes to thank Dr. D. C. Tardy, University of Iowa, for his helpful conversations concerning this work. We gratefully acknowledge Mr. B. Noordewier for his valuable assistance with the experiments.

## Energy Partitioning on Photolysis and Pyrolysis of 3-Vinyl-1-pyrazoline

by F. H. Dorer,\* E. Brown, J. Do, and R. Rees

*Chemistry Department, California State College, Fullerton, Fullerton, California 92631 (Received November 30, 1970)*

*Publication costs assisted by the National Science Foundation*

The internal vibrational energy distribution function,  $f(E)$ , of the vibrationally excited vinylocyclopropane (VCP\*) produced by photolysis of 3-vinyl-1-pyrazoline has been characterized. By comparison of the experimentally measured unimolecular rate constants for the isomerization of the VCP\* formed in the primary process to cyclopentene and the various diene isomers to rate constants calculated for these reactions using RRKM theory and a Gaussian distribution for  $f(E)$ , we find that the most probable energy of the VCP\* is only  $75 \text{ kcal mol}^{-1}$  when the total available energy is  $132 \text{ kcal mol}^{-1}$ . The product energy distribution observed on photolysis of 3-vinyl-1-pyrazoline is essentially the same as the energy distribution observed when 4-methyl-1-pyrazoline is photolyzed; therefore, even though there is a substantial difference in the activation energy for decomposition of these two 1-pyrazolines in the ground electronic state, this perturbation to the potential energy surface for decomposition has not affected a change in how the available energy is partitioned to the reaction products.

### Introduction

It has been generally accepted that the mechanism for decomposition of 1-pyrazolines to a cyclic hydrocarbon fragment and nitrogen involves a 1,3-diradical intermediate.<sup>1-3</sup> At least for the thermolysis of 1-pyrazolines it appears that the transitory diradical arises by concerted simultaneous rupture of the C-N bonds in the reactant. However, inferences about the nature of the transition state, whether concerted simultaneous bond rupture or stepwise rupturing of the C-N bonds occurs, must necessarily be made from relatively indirect evidence. The probes available for elucidating the details of the dynamics of the bond-rupturing process are even more limited in photolysis reactions.

A kind of information that, in principle, should better reflect the details of the mechanism of the fragmentation reaction is the energy states in which the nascent products are formed.<sup>4</sup> For 1-pyrazoline decomposition the elimination of nitrogen requires a significant change in the N-N bond length on formation of products. Since for concerted simultaneous C-N bond rupture the reaction coordinate should not be appreciably coupled to the N-N vibrational mode, a relatively large fraction of the available energy would be expected to appear as vibrational energy in the nitrogen fragment. For

photolysis of symmetric 1-pyrazolines (symmetric in the sense that the rupturing C-N bonds are equivalent) a relatively small fraction of the available energy is partitioned to the internal degrees of freedom of the hydrocarbon fragment, a result that is consistent with a concerted bond-breaking mechanism.<sup>5-7</sup>

Conceivably, it is possible, by altering the structure of the reactant such that the rupturing C-N bonds are no longer equivalent, to cause the nitrogen elimination reaction to become stepwise, thereby allowing a greater degree of geometric relaxation of the N-N bond and concomitant release of its stored energy to the

(1) (a) R. J. Crawford and A. Mishra, *J. Amer. Chem. Soc.*, **88**, 3963 (1966); (b) R. J. Crawford and G. L. Erickson, *ibid.*, **89**, 3907 (1967); (c) R. J. Crawford and L. H. Ali, *ibid.*, **89**, 3908 (1967); (d) A. Mishra and R. J. Crawford, *Can. J. Chem.*, **47**, 1515 (1969); (e) B. H. Al-Sader and R. J. Crawford, *ibid.*, **46**, 3301 (1968); (f) R. Moore, A. Mishra, and R. J. Crawford, *ibid.*, **46**, 3305 (1968); (g) R. J. Crawford and D. M. Cameron, *ibid.*, **45**, 691 (1967).

(2) E. L. Allred and R. L. Smith, *J. Amer. Chem. Soc.*, **91**, 6766 (1969).

(3) W. R. Roth and M. Martin, *Tetrahedron Lett.*, 4695 (1967).

(4) S. H. Bauer, *J. Amer. Chem. Soc.*, **91**, 3688 (1969).

(5) (a) F. H. Dorer, *J. Phys. Chem.*, **73**, 3109 (1969); (b) F. H. Dorer, *ibid.*, **74**, 1142 (1970).

(6) P. Cadman, H. M. Meunier, and A. F. Trotman-Dickenson, *J. Amer. Chem. Soc.*, **91**, 7640 (1969).

(7) T. F. Thomas, C. I. Sutin, and C. Steel, *ibid.*, **89**, 5107 (1967).

degrees of freedom of the hydrocarbon fragment before their separation. One would then expect that if the lifetime of this chainlike transition state was of the order of several N-N vibrational periods, the energy content of the cyclic hydrocarbon fragment would be much greater than that observed on decomposition of symmetric 1-pyrazolines.

We, therefore, have carried out this study of the partitioning of energy to the vinylcyclopropane fragment produced on photolysis and pyrolysis of 3-vinyl-1-pyrazoline (**1**). Due to allylic resonance stabilization



of the diradical intermediate, the activation energy for decomposition of **1** is 10 kcal mol<sup>-1</sup> less<sup>18</sup> than activation energy for decomposition of 4-methyl-1-pyrazoline (**2**).<sup>1a</sup> Moreover, the entropy of activation for thermolysis of **1** and **2** differ by 5.1 eu at 250°, possibly indicating a change in the ground-state mechanism for decomposition. Although in thermolysis the kinetic isotope effect for decomposition of **1** indicated both bonds are rupturing in the transition state,<sup>15</sup> it seems reasonable to expect that when **1** decomposes the C<sub>3</sub>-N bond order would be substantially less than the C<sub>5</sub>-N bond order. At the very least, decomposition of **1** should involve a much skewed transition state.

### Experimental Section

The 3-vinyl-1-pyrazoline was synthesized by reacting diazomethane with 1,3-butadiene in a manner outlined by Crawford and Cameron.<sup>18</sup> After its purification by vacuum distillation, the ultraviolet spectrum of the product dissolved in methanol displayed a maximum at 320 nm. Identification of the diazomethane-butadiene adduct as 3-vinyl-1-pyrazoline was further substantiated on identification of its pyrolysis and photolysis products.

Matheson instrument grade propane was used as the diluent in the pyrolysis and photolysis runs.

The pyrolysis and photolysis products of 3-vinyl-1-pyrazoline were analyzed on a Hewlett-Packard 5750 chromatograph fitted with a vacuum inlet system for gas analysis. Separation of the reaction products and the propane diluent was achieved by using a 40-ft column packed with 60-80 mesh Chromosorb P coated with 20% by weight of 2,4-dimethylsulfolane. All runs were analyzed using the flame ionization detector. The products, 1,3-butadiene, 1,4-pentadiene, *trans*-1,3-pentadiene, *cis*-1,3-pentadiene, and cyclopentadiene were identified, and their relative detector sensitivities were measured using calibration mixtures made up of authentic samples. Since only one product peak was observed on pyrolysis of the reactant at ~130°, and this

same peak constituted ~90% of the high pressure photolysis products, we concluded that this peak was the vinylcyclopropane. Moreover, since the relative detector sensitivities of the C<sub>5</sub> dienes and cyclopentene on the flame ionization detector were the same, this calibration factor was also used for vinylcyclopropane.

The photolysis runs were carried out by first freezing, using calibrated volumes, a known amount of the reactant and propane into one of three reactors. The partial pressure of the 3-vinyl-1-pyrazoline in any of the runs was no greater than 0.52 Torr, and the propane was always present in at least tenfold excess. Two cylindrical quartz reactors, each 50-mm o.d., having volumes of 172 and 491 cc were used for the runs. For the lowest pressure runs we used a 2000-cc cylindrical Pyrex reactor with a suprasil quartz window blown on its side. This reactor contained a fan for mixing the gases. The contents of the reactors were frozen at liquid nitrogen temperature and pumped to 10<sup>-4</sup> Torr before mixing and irradiation at room temperature for 0.5 to 2 hr. All gas handling was carried out on a greaseless and mercury-free vacuum apparatus fitted with a Pyrex spiral gauge and a Pirani gauge for pressure measurements.

The light source was a Bausch and Lomb high-intensity monochromator (Model No. 5, 7.4 nm/mm dispersion, 22.2-nm band pass) with an Osram HBO 200-W mercury lamp.

The few pyrolysis experiments were carried out much in the same fashion except that the reactants and the propane diluent were frozen into a finger attached to a 1290-cc Pyrex reactor fitted with a greaseless stopcock (Viton A diaphragm). The reactor was embedded in a conventional air bath oven.

### Results

The pressure dependence of the relative amounts of C<sub>4</sub> and C<sub>5</sub> products produced on photolysis of 3-vinyl-1-pyrazoline by 313- and 334-nm radiation are given in Tables I and II.

The 1,3-butadiene is a product of a cleavage reaction characteristic of 1-pyrazoline photolysis.<sup>1f</sup> An alternate mode of cleavage would produce ethylene. However, this peak would have gone undetected in our glpc analysis; consequently, we have no information about its relative importance. It is interesting to note that unlike the cleavage product in 4-methyl-1-pyrazoline photolysis,<sup>5a</sup> the relative amount of the cleavage product produced in this system is neither pressure nor wavelength dependent.

Our chromatographic technique did not provide a good quantitative separation between the *cis*-1,3-pentadiene and the vinylcyclopropane peak. Using an alternate set of glpc columns that separated these two peaks and *trans*-1,3-pentadiene, we found a *cis/trans* ratio for the 1,3-pentadiene isomers of ~0.5 over the pressure range of our measurements; a value that is

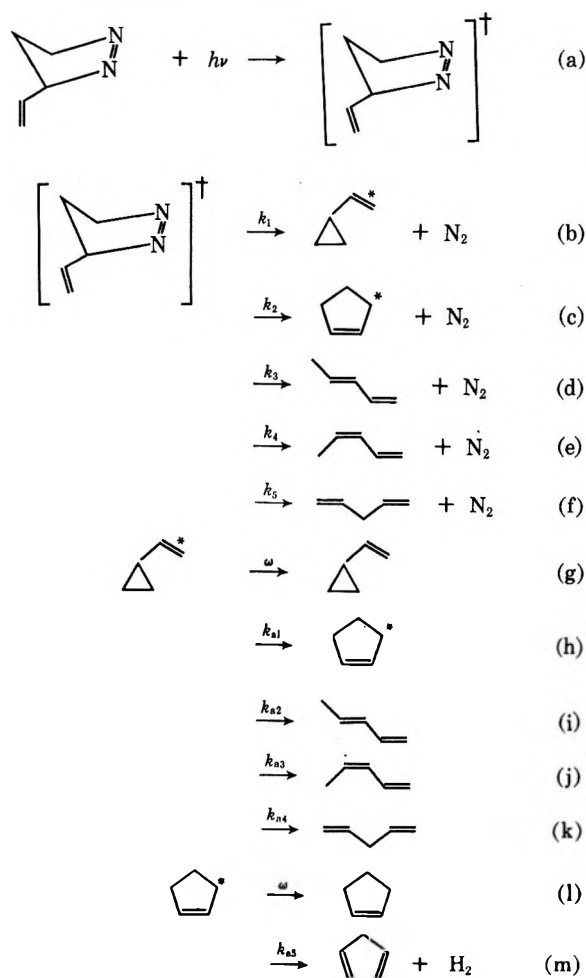
**Table I:** Product Composition As a Function of Pressure: 313-nm Photolysis of 3-Vinyl-1-pyrazoline<sup>a</sup>

Pressure, Torr	Butadiene	1,4-Pentadiene	1,3-Pentadiene	Cyclopentene	Cyclopentadiene	Vinylcyclopropane
0.261	0.055	0.104	0.129	0.135	0.165	0.411
0.311	0.052	0.107	0.117	0.144	0.149	0.430
0.314	0.056	0.110	0.117	0.157	0.150	0.412
1.10	0.052	0.075	0.099	0.152	0.067	0.554
1.11	0.056	0.076	0.087	0.143	0.072	0.566
1.68	0.063	0.072	0.079	0.141	0.063	0.583
3.29	0.056	0.063	0.061	0.137	0.045	0.638
3.37	0.051	0.053	0.057	0.126	0.029	0.685
3.39	0.048	0.054	0.067	0.126	0.029	0.676
5.29	0.057	0.046	0.045	0.109	0.033	0.710
5.38	0.046	0.043	0.046	0.114	0.023	0.728
5.61	0.057	0.044	0.045	0.114	0.017	0.724
333 <sup>b</sup>	0.032	0.007	0.004	0.026	...	0.931
625 <sup>b</sup>	0.055	0.020	0.004	0.043	...	0.879
691 <sup>b</sup>	0.060	0.009	...	0.040	...	0.892
787 <sup>c</sup>	0.060	0.008	0.005	0.037	...	0.891
882 <sup>c</sup>	0.059	0.015	...	0.038	...	0.887

<sup>a</sup> Except where otherwise noted the photolysis mixture contained propane in a greater than tenfold excess relative to the 3-vinyl-1-pyrazoline. <sup>b</sup> Nitrogen was used as the diluent. <sup>c</sup> Methane was used as the diluent.

consistent with the results for chemically activated vinylcyclopropane isomerization.<sup>8</sup>

In photolysis the formation of the vinylcyclopropane and the C<sub>5</sub> dienes can be described by the scheme



In this scheme the dagger denotes an electronically excited species and the asterisk denotes a vibrationally excited ground-state molecule. The  $k_{ai}$  are the unimolecular rate constants for the respective isomerization and decomposition reactions, and  $\omega$  is the collisional deactivation rate of the vibrationally excited species. The data taken at high pressures given in Tables I and II indicate that a small amount of the diene isomers are also formed directly from photolysis of the reactant 1-pyrazoline.

The experimental unimolecular rate constant for isomerization of the VCP\* to cyclopentene and the various diene isomers are given by

$$k_{a1} = \omega \left[ \frac{\text{cyclopentadiene} + \text{cyclopentene}}{\text{vinylcyclopropane}} \right] \quad (1)$$

$$k_{a2} + k_{a3} = \omega \left[ \frac{\text{1,3-pentadiene}}{\text{vinylcyclopropane}} \right] \quad (2)$$

$$k_{a4} = \omega \left[ \frac{\text{1,4-pentadiene}}{\text{vinylcyclopropane}} \right] \quad (3)$$

The unimolecular rate constant for the decomposition of cyclopentene to cyclopentadiene is given by

$$k_{a5} = \omega \left[ \frac{\text{cyclopentadiene}}{\text{cyclopentene}} \right] \quad (4)$$

For eq 1-3 to be correct we must subtract from the measured amounts of cyclopentene + cyclopentadiene, 1,3-pentadiene, and 1,4-pentadiene the relative amounts of these products formed directly from the decomposition of the initially excited 3-vinyl-1-pyrazoline. Assuming that there is no pressure dependence in the rela-

(8) H. M. Frey, *Trans. Faraday Soc.*, **58**, 516 (1962).



**Table II:** Product Composition As a Function of Pressure: 334-nm Photolysis of 3-Vinyl-1-pyrazoline<sup>a</sup>

Pressure, Torr	Butadiene	1,4-Pentadiene	1,3-Pentadiene	Cyclopentene	Cyclopentadiene	Vinylcyclopropane
0.265	0.064	0.099	0.114	0.140	0.143	0.440
0.268	0.057	0.108	0.124	0.149	0.099	0.465
1.09	0.055	0.069	0.073	0.147	0.066	0.590
3.07	0.047	0.044	0.042	0.111	0.023	0.733
3.20	0.054	0.052	0.052	0.120	0.039	0.682
606 <sup>b</sup>	0.050	0.020	0.010	0.034	...	0.885
807 <sup>c</sup>	0.058	0.011	...	0.030	...	0.901

<sup>a</sup> See footnote a, Table I. <sup>b</sup> Nitrogen was used as the diluent. <sup>c</sup> Methane was used as the diluent.

tive rates of production of these isomers to the rate of production of VCP\* in the primary photodecomposition of the 3-vinyl-1-pyrazoline, subtraction of the percentages of the cyclopentene and the diene isomers formed at high pressures (where no VCP\* isomerizes) from their relative amounts measured at lower pressures gives the amounts of these products formed by isomerization of the VCP\*. This is the manner in which values of  $k_{a1}$ ,  $k_{a2} + k_{a3}$ , and  $k_{a4}$  were calculated.

The collision rate of the vibrationally excited vinylcyclopropane and cyclopentene with the bath molecules (propane) was calculated from kinetic theory using the Lennard-Jones force constants obtained from viscosity data and the  $\Omega^{(2,2)}$  integral.<sup>9,10</sup> The Lennard-Jones constants for vinylcyclopropane and cyclopentene were assumed to be the same, and the values were estimated from data available for similar molecules.<sup>9</sup> Making the reasonable assumption of unit collisional deactivation,<sup>10</sup> the vibrational deactivation rate of cyclopentene and vinylcyclopropane by the propane bath molecules at 300°K is

$$\omega/P = 20.6 \times 10^6 \text{ collisions/sec Torr} \quad (5)$$

The experimental rate constants calculated from the

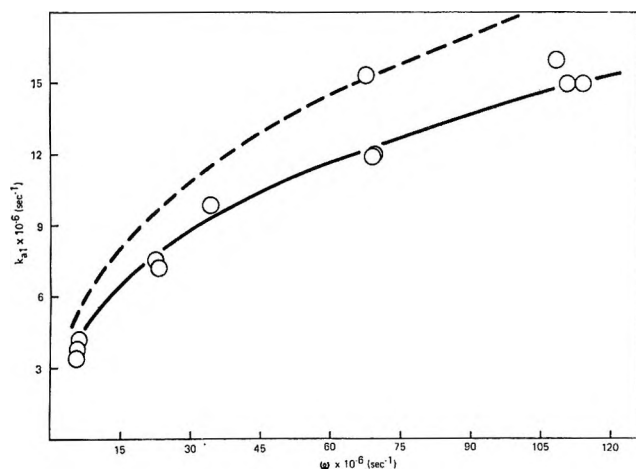


Figure 1. The experimental and calculated values of  $k_{a1}$  as a function of  $\omega$ . The solid line is a calculated curve with  $E_{mp} = 75 \text{ kcal mol}^{-1}$  and  $\sigma = 12 \text{ kcal mol}^{-1}$ . The broken line was calculated with  $E_{mp} = 77 \text{ kcal mol}^{-1}$  and  $\sigma = 12 \text{ kcal mol}^{-1}$ .

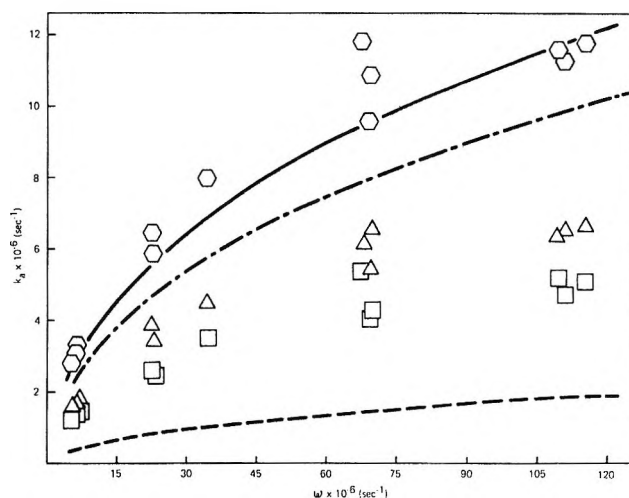


Figure 2. The experimental and calculated values of  $k_{a2} + k_{a3} + k_{a4} = \Delta$ ,  $k_{a4} = \square$ , and  $k_{a2} + k_{a3} + k_{a4} = \circ$ , as a function of  $\omega$ . The solid line is a calculated curve of  $k_{a2} + k_{a3} + k_{a4}$  with  $E_{mp} = 75 \text{ kcal mol}^{-1}$  and  $\sigma = 12 \text{ kcal mol}^{-1}$ . The upper broken line is a calculated curve for  $k_{a2} + k_{a3}$ , and the lower broken line is a calculated curve for  $k_{a4}$  using  $E_{mp} = 75 \text{ kcal mol}^{-1}$  and  $\sigma = 12 \text{ kcal mol}^{-1}$ .

data in Table I using eq 1-5 are illustrated in Figures 1-3. Since only a few experiments were carried out with 334-nm radiation, we have not illustrated the corresponding rate constants calculated from the data in Table II, and we will only mention the qualitative significance of these measurements later in the Discussion.

The product composition observed on pyrolysis of both 1 and 2 at lower pressures is given in Table III.

## Discussion

The experimental unimolecular rate constants,  $k_{ai}$ , are related to the microscopic unimolecular rate constants for isomerization of the vibrationally excited vinylcyclopropane with total energy  $E$  to the appropriate  $C_5$  isomer,  $k_i(E)$ , by

(9) J. O. Hirschfelder, C. F. Curtiss, and R. B. Bird, "Molecular Theory of Gases and Liquids," Wiley, New York, N. Y., 1954.

(10) (a) G. H. Kohlmaier and B. S. Rabinovitch, *J. Chem. Phys.*, **38**, 1962 (1963); (b) G. H. Kohlmaier and B. S. Rabinovitch, *ibid.*, **38**, 1709 (1963).

$$k_{ai} = \omega \frac{\sum_{E_T} \frac{k_i(E)}{k_1(E) + k_2(E) + k_3(E) + k_4(E) + \omega} f(E)}{\sum_{E_T} \frac{\omega}{k_1(E) + k_2(E) + k_3(E) + k_4(E) + \omega} f(E)} \quad (6)$$

In eq 6  $f(E)$  is the internal energy distribution function of the vibrationally excited vinylcyclopropane formed in the primary photodecomposition step. The total energy to which the equation must be summed is equal to the sum of energy of the radiation absorbed by the reactant 3-vinyl-1-pyrazoline, the exothermicity of the reaction at 0°K, and the thermal energy of the reactant.

Assuming that the heat of hydrogenation of vinylcyclopropane at 0°K is the average of the heats of hydrogenation of 3-methyl-1-butene and 1,4-pentadiene,<sup>11</sup> and using the value for  $\Delta H_f^\circ$  of ethylcyclopropane,<sup>12</sup> one concludes that the heat of formation of vinylcyclopropane at 0°K is 39 kcal mol<sup>-1</sup>. This would mean the enthalpy of formation of VCP at 298°K is 33 kcal mol<sup>-1</sup>. Assuming no difference in the enthalpies of hydrogenation of 3-vinyl-1-pyrazoline and vinylcyclopropane, and knowing the exothermicity of 3-methyl-1-pyrazoline decomposition to methylcyclopropane and nitrogen,<sup>5</sup> we estimate the enthalpy of formation of 3-vinyl-1-pyrazoline to be 72 kcal mol<sup>-1</sup> at 25° and 78 kcal mol<sup>-1</sup> at 0°K. Therefore, the decomposition of 3-vinyl-1-pyrazoline to vinylcyclopropane and nitrogen is about 39 kcal mol<sup>-1</sup> exothermic at 0°K, and for 313-nm photolysis, including the thermal energy of the reactant,  $E_T$  is 132 kcal mol<sup>-1</sup>.

Since the decomposition of VCP to cyclopentene is 25 kcal mol<sup>-1</sup> exothermic at 0°K,<sup>11</sup> the rate constant for isomerization of the cyclopentene formed in (h) to cyclopentadiene is given by




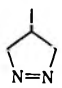

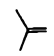
$$k_{a5} = \omega \frac{\sum_{E_T} \frac{k_5(E + 25)}{k_5(E + 25) + \omega} \cdot \frac{k_1(E)}{k_1(E) + k_2(E) + k_3(E) + k_4(E) + \omega} \cdot f(E)}{\sum_{E_T} \frac{\omega}{k_5(E + 25) + \omega} \cdot \frac{k_1(E)}{k_1(E) + k_2(E) + k_3(E) + k_4(E) + \omega} \cdot f(E)} \quad (7)$$

that are available for the decomposition of the symmetric 1-pyrazolines<sup>5-7</sup> we assumed  $f(E)$  to have the form of a Gaussian

$$f(E) = \frac{\exp\left[-\frac{1}{2}\left(\frac{E_{mp} - E_i}{\sigma}\right)^2\right]}{\sum_{E_T} \exp\left[-\frac{1}{2}\left(\frac{E_{mp} - E_i}{\sigma}\right)^2\right]} \quad (8)$$

There are, therefore, only two adjustable parameters in fitting the experimental data to the calculated rate constants;  $E_{mp}$ , the most probable energy of the VCP\* formed in (a), and  $\sigma$ , the dispersion of the internal energy distribution function. The calculated and experimental results are illustrated in Figures 1-3.

**Table III:** Low Pressure Pyrolysis Products of 3-Vinyl-1-pyrazoline and 4-Methyl-1-pyrazoline<sup>a</sup>

Reactant	Pressure, Torr	T, °C	$\omega \times 10^{-6}$ , <sup>b</sup> sec <sup>-1</sup>	Relative amount of C <sub>5</sub> products	
					
	0.55	129	9.6	~1.0	Trace
	0.059 <sup>c</sup>	131	1.1	~1.0	Trace
	0.032 <sup>c</sup>	137	0.57	1.0	
				Relative amount of C <sub>4</sub> products	
					
	0.98	260	16.7	0.574	0.426
	0.20	257	3.4	0.535	0.465
	0.0078	247	0.13	0.556	0.444
	0.0082	297	0.13	0.551	0.449
0.0087	340	0.14	0.535	0.465	
0.0014	345	0.022	0.547	0.453	

<sup>a</sup> Except where otherwise noted all runs were carried out with propane as a diluent in at least sixfold excess relative to the pyrazoline. <sup>b</sup> Calculated from gas kinetic theory assuming the collision cross sections to be temperature independent. <sup>c</sup> No diluent added.

The respective  $k_i(E)$  were calculated by using RRKM theory<sup>13</sup> and allowing all of the internal vibrations of the vinylcyclopropane and cyclopentene to be active degrees of freedom. The molecular vibrational frequency assignments, critical energies, and calculational details are given in the Appendix.

The evaluation of equations were carried out by summing over the appropriate energy range in 1-kcal mol<sup>-1</sup> intervals using a CDC 3150 computer. For purposes of comparison with the energy partitioning data

Within the uncertainty of the exothermicity of reaction h the calculated curves that best fit the 313-nm photolysis results for  $k_{a1}$  and  $k_{a5}$  are the parameters  $E_{mp} = 75$  kcal mol<sup>-1</sup> and  $\sigma = 12$  kcal mol<sup>-1</sup>. However, using these parameters for  $f(E)$ , there appears to be very poor agreement between calculated and experimental results for diene formation from vinylcyclopropane. If the VCP\* contains 75-kcal mol<sup>-1</sup> internal energy, the dienes formed in this system would contain

(11) F. D. Rossini, "Selected Values of Properties of Hydrocarbons," American Petroleum Institute Research Project 44.

(12) F. H. Dorer and B. S. Rabinovitch, *J. Phys. Chem.*, **69**, 1952 (1965).

(13) R. A. Marcus and O. K. Rice, *J. Phys. Colloid Chem.*, **55**, 894 (1951); R. A. Marcus, *J. Chem. Phys.*, **20**, 359 (1952).

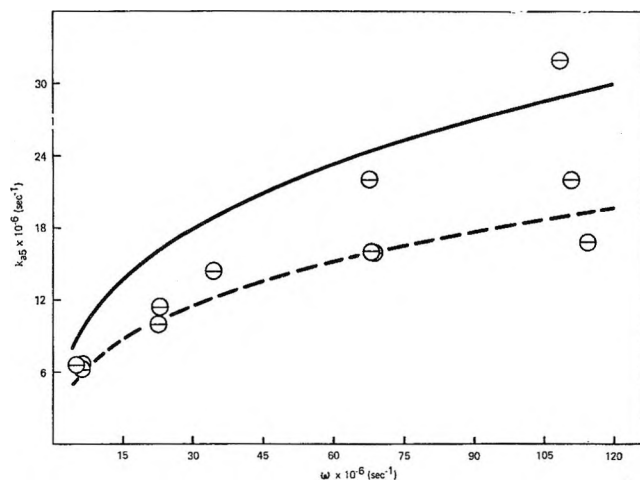


Figure 3. The experimental and calculated values of  $k_{a3}$  as a function of  $\omega$ . The solid line is calculated curve using  $E_{mp} = 75 \text{ kcal mol}^{-1}$ ,  $\sigma = 12 \text{ kcal mol}^{-1}$ , and the exothermicity of reaction h as  $-25 \text{ kcal mol}^{-1}$ . The broken line is a calculated curve using the same Gaussian parameters but with the exothermicity of (h) as  $-21 \text{ kcal mol}^{-1}$ .

$\sim 98 \text{ kcal mol}^{-1}$  (the average energy of the decomposing VCP\* plus the exothermicity of diene formation from VCP), and it is possible that before collisional stabilization the "hot" dienes undergo geometric isomerization to a stoichiometry nearer their equilibrium composition at these high energies.<sup>11</sup> That this may be the case is indicated in Figure 2 by noting that the sum of the rate constants,  $k_{a2} + k_{a3} + k_{a4}$ , is quite well fitted with the Gaussian parameters,  $E_{mp} = 75 \text{ kcal mol}^{-1}$  and  $\sigma = 12 \text{ kcal mol}^{-1}$ . The uncertainty in the choice of these parameters is of the order of  $2 \text{ kcal mol}^{-1}$  for each. The data in Table II indicate that  $E_{mp}$  for the VCP\* formed by 334-nm photolysis of **1** is of the order of  $2 \text{ kcal mol}^{-1}$  less.

It is generally believed that the 1-pyrazolines decompose in the primary process to a trimethyl fragment and nitrogen.<sup>1-3</sup> One model for the decomposition process in photolysis would be that, prior to the fragmentation of the 1-pyrazoline, internal conversion to the ground state occurs, and all of the excess vibrational energy above the critical energy required for fragmentation ( $E^+ = 61 \text{ kcal mol}^{-1}$ )<sup>18</sup> would be randomly distributed between the degrees of freedom of the hydrocarbon and nitrogen fragments. For such a model the internal energy distribution function for the diradical fragment would have the form<sup>14</sup>

$$f(E) = \frac{N(E^+ - E_R) \sum P_R(E_R)}{\sum P^+(E_v^+)} \quad (9)$$

where  $N(E^+ - E_R)$  is the density of energy eigenstates for those degrees of freedom in the activated complex associated with the vibrational degrees of freedom of the diradical product. The  $\sum P_R(E_R)$  term is the sum of energy eigenstates for those degrees of freedom of the activated complex associated with the nitrogen vibra-

tion and the three relative translational and two rotational degrees of freedom of the newly formed products. The normalization term in the denominator of (9) is the sum of energy eigenstates for all of the active degrees of freedom of the activated complex having  $E^+$ .

A calculation of eq 9 was carried out using the approximation of Whitten and Rabinovitch<sup>15</sup> and an exact sum computer program<sup>16</sup> for 3-vinyl-1-pyrazoline decomposition subsequent to its activation by 313-nm radiation. The molecular vibrational frequency assignment of the 3-vinyl-1-pyrazoline activated complex was based on the known assignments for 1-pyrazoline<sup>17</sup> and other related molecules.<sup>18</sup> A statistical model for energy partitioning predicts that the most probable energy of the diradical fragment would be  $49 \text{ kcal mol}^{-1}$ ; therefore, since the ring closure to vinylcyclopropane is  $41 \text{ kcal mol}^{-1}$  exothermic,<sup>19</sup> the vinylcyclopropane would have an  $E_{mp}$  of  $\sim 90 \text{ kcal mol}^{-1}$ . Moreover, the width of the statistical distribution is  $17 \text{ kcal mol}^{-1}$ , whereas the Gaussian that best fits the experimental data has a width ( $2\sigma$ ) of  $24 \text{ kcal mol}^{-1}$ .

In these calculations we have omitted the "reorganization energy," the activation energy of the back reaction of nitrogen and the diradical to form 3-vinyl-1-pyrazoline. This seems plausible since the data in Table III indicates that for neither 3-vinyl-1-pyrazoline or 4-methyl-1-pyrazoline are "hot" cyclopropanes produced on pyrolysis of these compounds at low temperatures and pressures.<sup>19a</sup>

If this reorganization energy ( $\sim 30 \text{ kcal mol}^{-1}$ ) were statistically distributed to the diradical and nitrogen products in 3-vinyl-1-pyrazoline pyrolysis, a calculation using eq 9 indicates that the most probable energy of the formed VCP\* would be  $\sim 64 \text{ kcal mol}^{-1}$ . If this were the case, we would expect to see  $\sim 43\%$  cyclopentene produced by VCP\* isomerization in our lowest pressure measurements. The data of Table III show that this is not the case. Similarly, if there were statistical redistribution of the reorganization energy on pyrolysis of 4-methyl-1-pyrazoline, we would expect  $E_{mp}$  of the formed methylcyclopropane (MCP\*) to be  $76 \text{ kcal mol}^{-1}$ . However, the data on Table III indicate an upper limit to the energy content of the MCP\*

(14) Y. N. Lin and B. S. Rabinovitch, *J. Phys. Chem.*, **74**, 1769 (1970).

(15) G. Z. Whitten and B. S. Rabinovitch, *J. Chem. Phys.*, **38**, 2466 (1963).

(16) Kindly supplied by Professor Rabinovitch.

(17) J. R. Durig, J. M. Karriker, and W. C. Harris, *J. Chem. Phys.*, **52**, 6096 (1970).

(18) F. H. Dorer and B. S. Rabinovitch, *J. Phys. Chem.*, **69**, 1973 (1965).

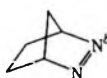
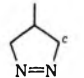
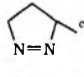

(19) H. E. O'Neal and S. W. Benson, *ibid.*, **72**, 1866 (1968).

(19a) NOTE ADDED IN PROOF. "The unusual results at  $190^\circ$  reported by Crawford and Cameron<sup>18</sup> on the thermolysis of 3-vinyl-1-pyrazoline have been found to be due to surface effects. After several reactions in a static vessel the surface became conditioned and the product distribution was very much like that at  $150^\circ$ ." Private communication from R. J. Crawford.

is 70 kcal mol<sup>-1</sup>.<sup>5a</sup> Therefore, the reorganization energy is nonrandomly distributed to the reaction products during the ground-state decomposition of both of these 1-pyrazolines.

In Table IV we have tabulated the energy partitioning data that are available for the 313-nm photolysis of several symmetric and unsymmetric 1-pyrazolines. It is particularly evident that in the series 4-methyl-, 3-methyl-, and 3-vinyl-1-pyrazoline there is no increase in the vibrational energy content of the hydrocarbon fragment due to this systematic change in the structure of the reactant, even though the ground-state potential energy surface is perturbed to the extent that the activation energy for decomposition in this series decreases from 42 to 32 kcal mol<sup>-1</sup>.

**Table IV:** Energy Partitioning Results for 313-nm Photolysis of Various Substituted 1-Pyrazolines<sup>a</sup>

System	$E_{\max}$	$E_{\text{mp}}$	$\sigma$	$E_{\text{R}}^d$
	106	67.5	6.65	38
	132	83	16	49
	131	81	18	50
	132	75	12	57

<sup>a</sup> Energy units are kcal mol<sup>-1</sup>. <sup>b</sup> Data from ref 7. <sup>c</sup> The data of ref 5 adjusted using Lennard-Jones collision cross sections consistent with the present work. <sup>d</sup> Energy contained in the degrees of freedom other than the internal vibrations of the hydrocarbon fragment.

Since ring closure is 41 kcal mol<sup>-1</sup> exothermic for formation of vinylcyclopropane from the corresponding diradical,<sup>19</sup> the most probable energy actually partitioned to the internal degrees of freedom of this intermediate fragment formed on photolysis of 3-vinyl-1-pyrazoline is 34 kcal mol<sup>-1</sup> from a total of 89 kcal mol<sup>-1</sup> to be distributed between the hydrocarbon and nitrogen fragments. For 4-methyl-1-pyrazoline decomposition, there is only 30 kcal mol<sup>-1</sup> of a total of 79 kcal mol<sup>-1</sup> partitioned to the hydrocarbon fragment. Therefore, there is actually a greater total energy to be distributed between the hydrocarbon and nitrogen fragments on photolysis of 3-vinyl-1-pyrazoline than on photolysis of 4-methyl-1-pyrazoline, and the hydrocarbon fragment receives about half of this "extra" energy in the former system.

The energy content of the remaining degrees of freedom is nearly the same for the series 4-methyl-, 3-methyl-, and 3-vinyl-1-pyrazoline. Since the lifetime

of the excited singlet states of 1-pyrazolines are  $\sim 10^{-8}$  sec,<sup>20</sup> it is reasonable that, prior to fragmentation, the 1-pyrazolines will assume their excited singlet state structure. Since the initial excitation is an  $n\pi^*$  transition at the  $-\text{N}=\text{N}-$  chromophore, the bond order of the  $-\text{N}=\text{N}-$  bond will be decreased by one-half and its length might correspondingly increase from 1.25 to  $\sim 1.35$  Å. Using a Morse potential energy curve for nitrogen<sup>21</sup> one calculates that decreasing the bond length from 1.35 Å in the reactant to 1.09 Å in  $\text{N}_2$  would allow as much as 57 kcal mol<sup>-1</sup> to be stored as vibrational energy in the nitrogen fragment. Since the fluorescence and absorption spectra of 2,3-diazabicyclo-[2.2.1]hept-2-ene do not indicate a large structural change on excitation to the first singlet state,<sup>20</sup> this calculation represents an upper limit to the energy partitioned to the nitrogen vibration.

The experimental results indicate that changing the structure of the 1-pyrazoline from the symmetric 4-methyl-1-pyrazoline to the asymmetric 3-vinyl-1-pyrazoline, thereby causing a substantial perturbation to the ground-state potential energy surface, has caused essentially no alteration of how the total energy is redistributed among the degrees of freedom of the reaction products. It seems, therefore, that such structural changes cause no change in the mechanism of fragmentation of the 1-pyrazolines. If for the symmetric 1-pyrazolines there is simultaneous C-N bond rupture, where both rupturing C-N bonds have equal bond orders during separation of the fragments, it would seem entirely plausible that during the fragmentation of 3-vinyl-1-pyrazoline the C<sub>3</sub>-N bond would be of lower bond order than the C<sub>5</sub>-N bond.<sup>11</sup> It appears, however, that there is complete separation of the fragments before intramolecular energy relaxation from the leaving  $\text{N}_2$  fragment to the hydrocarbon portion of the molecule can occur, which corresponds to a time scale of the order of  $10^{-11}$  sec. This explanation is consistent with the conclusions reached by Crawford and Cameron from kinetic isotope measurements on pyrolysis of 3-vinyl-1-pyrazoline.<sup>18</sup>

*Acknowledgment.* This work has been supported in part by grants from the National Science Foundation and the Research Corporation.

## Appendix. Computational Details

*A. Vinylcyclopropane Isomerization.* The vibrational frequency assignment for vinylcyclopropane was adopted from the available assignment for ethylcyclopropane<sup>18</sup> by deleting the appropriate C-H modes and changing the C-C stretching and torsion modes to frequencies commensurate with the vinyl group (1642 and

(20) B. S. Solomon, T. F. Thomas, and C. Steel, *J. Amer. Chem. Soc.*, **90**, 2249 (1968).

(21) G. Herzberg, "Molecular Spectra and Molecular Structure. I. Spectra of Diatomic Molecules," Van Nostrand, Princeton, N. J., 1950.

995  $\text{cm}^{-1}$ , respectively). The ethyl torsion mode was treated as a 150- $\text{cm}^{-1}$  vibration. The density of states for the molecule was calculated as a function of energy by using the approximation of Whitten and Rabino-vitch.<sup>15</sup>

The reaction coordinate for isomerization of VCP\* to cyclopentene was taken to be a 890- $\text{cm}^{-1}$  ring deformation mode. The activated complex frequency assignment fitted the measured thermal rate data for isomerization of VCP to cyclopentene to within 0.3 log units,<sup>19,22</sup> and the critical energy was calculated to be 48.5 kcal mol<sup>-1</sup>.<sup>23</sup> To calculate the sum of energy eigenstates for the activated complex with an exact sum computer program,<sup>16</sup> the activated complex frequency assignment was grouped into a seven frequency model with the appropriate degeneracies. The grouped frequency model is given in Table V. The reaction path degeneracy is two.

**Table V:** Activated Complex Frequency Assignments<sup>a</sup>

Cyclopentene	VCP isomerization		Cyclopentene decomposition
	1,3-Pentadiene	1,4-Pentadiene	
3029 (8)	3023 (7)	3021 (7)	2986 (6)
1340 (10)	1461 (6)	1467 (6)	2000 (2)
903 (9)	1282 (4)	1283 (4)	1325 (14)
600 (1)	998 (6)	1000 (5)	974 (5)
407 (2)	692 (5)	692 (5)	699 (3)
290 (1)	407 (2)	407 (2)	400 (1)
150 (1)	269 (2)	241 (2)	150 (1)

<sup>a</sup> Frequencies are in units of  $\text{cm}^{-1}$ .

The frequency assignments for isomerization of VCP to 1,3-pentadiene and 1,4-pentadiene were made in a similar fashion, and the grouped activated complex frequency models are also given in Table V. The reaction coordinate for diene formation was assumed to be a C-H stretching mode, and the reaction path degeneracy is four. The activated complex frequency assignments gave fair to good agreement with the thermal rate data.<sup>19,22</sup>

*B. Cyclopentene Decomposition.* The frequency assignment used for cyclopentene was that of Beckett, Freeman, and Pitzer,<sup>24</sup> but with the 76.6- $\text{cm}^{-1}$  ring pucking assignment given by Laane and Lord.<sup>25</sup> It was assumed that hydrogen elimination occurs only from the 3,5 positions, and that the reaction path degeneracy is two. The reaction coordinate was taken to be a methylene twisting mode. The activated complex frequency assignment gave fair agreement (within 0.6 log units) with the thermal rate data.<sup>26</sup> The critical energy was calculated to be 59.9 kcal mol<sup>-1</sup>.

In all of our calculations the ratio of the activated complex and molecule moments of inertia were taken to be unity.

(22) C. A. Wellington, *J. Phys. Chem.*, **66**, 1671 (1962).

(23) S. Glasstone, K. J. Laidler, and H. Eyring, "The Theory of Rate Processes," McGraw-Hill, New York, N. Y., 1941, p 194.

(24) C. W. Beckett, N. K. Freeman, and K. S. Pitzer, *J. Amer. Chem. Soc.*, **70**, 4227 (1948).

(25) J. Laane and R. C. Lord, *J. Chem. Phys.*, **47**, 4941 (1967).

(26) G. I. Mackay and R. E. March, *Can. J. Chem.*, **48**, 913 (1970).

# The Radiation Chemistry of Crystalline Glycollic Acid

by J. G. Hawke\*<sup>1a</sup> and B. J. Rawson<sup>1b</sup>

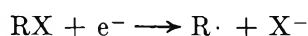
*Physical Chemistry Laboratories, Department of Pharmaceutical Chemistry, University of Sydney, Sydney, Australia*  
(Received January 6, 1971)

*Publication costs borne completely by The Journal of Physical Chemistry*

The radiation chemistry of solid glycollic acid has been examined with a view to establishing a correlation between the chemical products and the electron spin resonance spectra. The major products at room temperatures are carbon dioxide ( $G = 5.45$ ), acetic acid (3.47), methanol (3.33), and tartaric acid (1.65). Formaldehyde, ethylene glycol, malic acid, 2-hydroxypropionic acid, and hydrogen are formed as minor products ( $G < 0.8$ ). Trace amounts of carbon monoxide and methane have been detected. A mechanism is proposed which predicts a substantial  $G(\text{H}_2\text{O})$ . Although water could not be determined at the moderate conversions used, the inclusion of this predicted  $G(\text{H}_2\text{O})$  allows the calculation of a very reasonable mass balance. It was found that the same reaction scheme could be used to explain the yields found when irradiation was carried out at 193°K but that at 77°K it was inadequate, and other modes of decomposition became important.

The radiation chemistry of substituted carboxylic acids in the solid state has been extensively studied by means of the electron paramagnetic resonance (epr) spectra of paramagnetic species produced and trapped in the crystal lattice. It is frequently found that radicals of the general formula  $\text{R}_1\text{R}_2\text{CCOOH}$  are formed by the irradiation of acids  $\text{R}_1\text{R}_2\text{CHCOOH}$  at room temperature. Examples include glycollic acid,<sup>2a,b</sup> malonic acid,<sup>3</sup> glycine,<sup>4</sup> and a large number of dicarboxylic acids.<sup>5</sup>

In several cases, notably glycollic acid,<sup>6</sup> malonic acid,<sup>7</sup> glycine,<sup>8,9</sup> and some other amino acids,<sup>10-12</sup> it has been demonstrated that radicals observed at room temperature are the end products of a series of reactions. Some of the intermediates have been identified on irradiation and examination at reduced temperature. A common primary reaction appears to be dissociative capture of radiolytically produced electrons



a particular example being the deamination of certain amino acids.<sup>12,13</sup>

Gottschall and Tolbert<sup>14</sup> have recently measured the yields of some stable chemical products from the radiolysis of glycine and alanine and have attempted to correlate these with esr data. Despite the interest in such reactions, this type of investigation has been generally neglected. The radiation chemistry of glycollic acid for example has been examined only in aqueous solution.<sup>15,16</sup> The main gaseous product under these conditions is hydrogen, formed by the abstraction reaction



though substantial amounts of carbon dioxide are produced at higher concentrations.<sup>16</sup>

We have examined the chemical products from the

radiolysis of crystalline glycollic acid and report here the yields found.

## Experimental Section

*Materials.* The glycollic acid used ("puriss" grade from A. G. Fluka, Switzerland) was stated to have a purity of 97%, the main contaminant being sodium chloride. The only impurities detected by gas chromatography of an aqueous solution were some very volatile compounds, presumed to be residual solvents from crystallization, which were readily removed in the purification procedures described below. In order to

- (1) (a) School of Chemistry, Macquarie University, Sydney, Australia, 2113; (b) Based on a thesis presented for the degree of Ph.D. at the University of Sydney, 1968.
- (2) (a) P. M. Grant, R. B. Ward, and D. H. Whiffen, *J. Chem. Soc.*, 4635 (1958); (b) N. M. Atherton and D. H. Whiffen, *Mol. Phys.*, 3, 271 (1960).
- (3) H. M. McConnell, C. Heller, T. Cole, and R. W. Fessenden, *J. Amer. Chem. Soc.*, 82, 766 (1960).
- (4) R. F. Weiner and W. S. Koski, *ibid.*, 85, 873 (1963).
- (5) Y. D. Tsvetkov, J. R. Rowlands, and D. H. Whiffen, *J. Chem. Soc.*, 810 (1964).
- (6) J. G. Hawke and B. J. Rawson, *Nature*, 207, 293 (1965).
- (7) (a) A. Horsfield, J. R. Morton, and D. H. Whiffen, *Mol. Phys.*, 4, 327 (1961); (b) A. Horsfield, J. R. Morton, and D. H. Whiffen, *Nature*, 189, 481 (1961).
- (8) M. A. Collins and D. H. Whiffen, *Mol. Phys.*, 10, 317 (1966).
- (9) H. C. Box, H. G. Freund, and E. E. Budzinski, *J. Amer. Chem. Soc.*, 88, 658 (1966).
- (10) J. W. Sinclair and M. W. Hanna, *J. Phys. Chem.*, 71, 84 (1967).
- (11) M. Pujimoto, W. A. Seddon, and D. R. Smith, *J. Chem. Phys.*, 48, 3345 (1968).
- (12) P. B. Ayscough and A. K. Roy, *Trans. Faraday Soc.*, 64, 582 (1968).
- (13) P. B. Ayscough, K. Mach, J. P. Oversby, and A. K. Roy, *Chem. Commun.*, 1084 (1967).
- (14) W. C. Gottschall and B. M. Tolbert, *Advan. Chem. Ser.*, No. 80, 374 (1968).
- (15) (a) P. M. Grant and R. B. Ward, *J. Chem. Soc.*, 2654 (1959); (b) R. M. Grant and R. B. Ward, *ibid.*, 2659 (1959).
- (16) E. Hayon and J. Weiss, *ibid.*, 5091 (1960).

check for the presence of nonvolatile acids, some of the glycollic acid was methylated using acidified methanol solution. Gas chromatography showed a small number of peaks corresponding to 10–1000 ppm in the original acid. No method of purification eliminated these and, since their magnitude increased with the concentration of glycollic acid in the methanol solution during esterification, it was concluded that they were formed only during the methylation procedure.

The acid was sublimed before use, at least twice at pressures below  $10^{-3}$  Torr, after being pumped upon for several hours before each sublimation. The final sublimation was carried out very slowly at  $40^{\circ}$ , with the condensing surface at ambient temperature, in order to eliminate thermal decomposition and condensation of water vapor with the sublimate.

*Preparation of Samples.* Irradiation vessels, approximately 15–20 ml in capacity, were made from 14-mm Pyrex tubing. Those intended for gas analysis were fitted with a break-seal. The tubes were connected to a high-vacuum line via a very fine constriction and were filled by sublimation through a somewhat wider constriction. Both of these were sealed when sublimation was complete. During sublimation both flame-off points were kept at the temperature of the heating bath to prevent condensation of glycollic acid.

The sublimation was carried out very slowly with the condensing surface of the vessel at ambient temperature, and with a surface cooled to liquid air temperature just beyond the capillary connection to the line. Sublimation was complete in about 2 days for the 1-g samples most commonly used, 10–15% of the material being lost into the cold trap. The mass of the sample was determined by weighing the irradiation vessels before and after filling.

*Irradiation and Dosimetry.* The irradiations were carried out using the facilities of the Australian Atomic Energy Commission, Lucas Heights, N. S. W. Conventional underwater  $^{60}\text{Co}$  sources were used having dose rates from 140 to 600 krad  $\text{hr}^{-1}$ .

The Fricke ferrous sulfate dosimeter was used with an appropriate correction for electron density, which implied that 5.5% less energy was absorbed per gram of glycollic acid than per gram of aqueous Fricke solution.

*Identification of Products.* Gases were readily identified by their mass spectra. Most of the other products were identified by gas chromatography. Identical retention volumes of the product (or, in the case of an acid, its ester) with those of the authentic compound on two different stationary phases were taken as proof of identity. Formaldehyde was identified by its characteristic color reaction with chromotropic acid.

*Quantitative Methods.* (i) *Gases.* Gas yields were measured using an A.E.I. Model MS10 mass spectrometer containing a baffle plate fitted between the ion chamber and the diffusion pump in order to reduce the pumping rate to ca. 2 l.  $\text{sec}^{-1}$ .

The mass spectrometer was connected to a conventional gas handling line through a Metrosil Type 278153 leak and the response of the spectrometer was found to be proportional to the pressure in the line up to at least 0.4 Torr. Mass spectrometer readings were stable for 20–30 min under the experimental conditions.

During analysis, the irradiated sample tube was attached to the line, the break-seal was opened, and the crystals were carefully melted thereby releasing the trapped gases into the line. An aliquot of this gas was transferred to a calibrated volume and then introduced into the mass spectrometer. The gas yield was then obtained from calibration graphs in the usual way.

In the analysis of an unirradiated sample using this technique, the amounts of hydrogen and carbon dioxide produced by thermal decomposition were three orders of magnitude lower than the radiation yields measured.

(ii) *Acetic Acid.* The irradiated sample was dissolved in water containing 0.008% pulegone (2-isopropylidene-5-methyl-1-cyclohexanone) which served as the internal standard. A 5-ft column of 10% polyethylene glycol 20M terminated with terephthalic acid on unsilanized acid-washed "Chromosorb W" was used and the temperature was programmed from 80 to  $165^{\circ}$ . Under these conditions the response of the hydrogen flame detector was found to be linear, and the analyses were reliable to  $\pm 3\%$ .

(iii) *Methanol.* Methanol was separated from the irradiated glycollic acid by a microdistillation technique described elsewhere.<sup>17</sup> The resulting aqueous solution (approximately 0.1% in methanol) was chromatographed isothermally at  $75^{\circ}$  on a 9-ft column of 20% polyethylene glycol 20M on silanized "Chromosorb W." Acetone was used as the internal standard and a linear relationship between the ratio of peak areas and the ratio of the weights of methanol and acetone injected allowed an accuracy of  $\pm 2\%$  to be achieved.

(iv) *Tartaric Acid.* Tartaric acid was determined by gas chromatography as the dimethyl ester on a 5-ft column of 10% polyethyleneglycol 20M on "Chromosorb W." Irradiated glycollic acid was esterified in acidified methanol and concentrated to a low volume. By programming the temperature from 100 to  $200^{\circ}$ , separation from the large methyl glycolate peak was effected. Palmitic acid was added before esterification and the methyl palmitate that formed served as the internal standard. The dimethyl tartrate gave rise to an incompletely resolved double peak which was shown to be due to the racemic and meso isomers present in equal proportions. Consequently equal quantities of these isomers were used in the calibration, to produce a linear relationship. The method was found to be accurate to approximately  $\pm 3\%$ .

(v) *Formaldehyde.* The method of Macfadyen,

(17) J. G. Hawke and B. J. Rawson, submitted for publication in *Anal. Chem.*

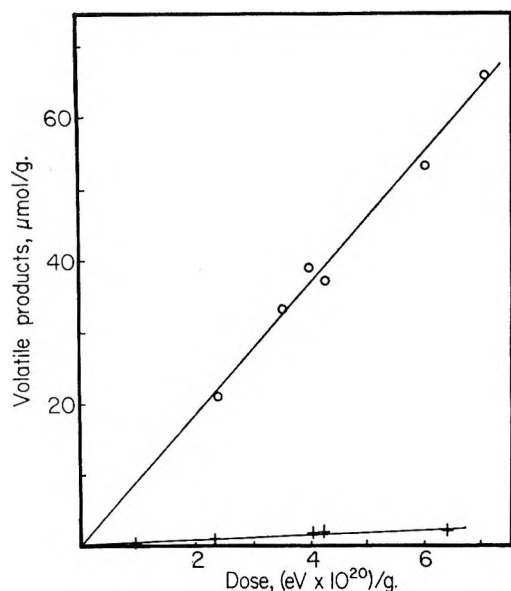


Figure 1. Concentration dependence of the volatile products on dose: carbon dioxide, O; hydrogen, +.

*et al.*,<sup>18</sup> was used without modification. Aqueous solutions of the irradiated glycollic acid were made up and since the acid caused a slight interference, unirradiated glycollic acid was used for the spectrophotometric blank solution.

(vi) *Other Minor Products.* The other minor products, ethylene glycol, 2-hydroxypropionic acid, and malic acid, were estimated by gas chromatography generally using the same chromatograms as those used for the determination of tartaric acid. In these cases measurements of peak heights rather than areas were used, and hence a lower accuracy (*ca.*  $\pm 8\%$ ) was achieved, although this represents a higher absolute accuracy in the smaller  $G$  values than that achieved with the major products.

## Results and Discussion

The major products were identified as carbon dioxide, tartaric acid, acetic acid, and methanol. Figure 1 shows the linear dependence of the yield of carbon dioxide and hydrogen upon dose absorbed over the range examined. Figure 2 shows the same linear dependence for the major nonvolatile products. Table I gives the calculated  $G$  values of both the major and minor products.

Apart from these, several substances were observed to be present in trace amounts.

Two very small peaks corresponding to  $G < 0.005$  were observed in the chromatograms of esterified irradiated glycollic acid. One of these was shown to be dimethyl succinate while the other has not been unequivocally identified owing to the difficulty of separating it from dimethyl malate and the tendency of its retention time to vary. The retention time is very close to that of methyl glycerate, and it is tentatively assigned to this compound.

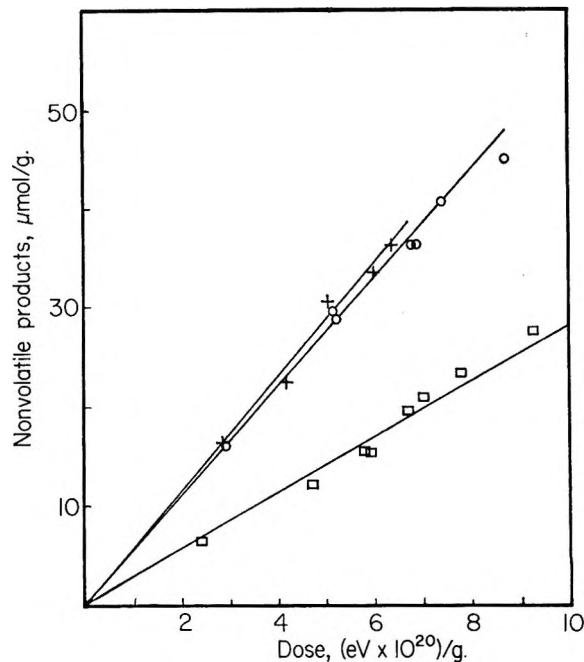


Figure 2. Concentration dependence of the nonvolatile products on dose: acetic acid, +; methanol, O; and tartaric acid, □.

Table I:  $G$  Values (100-eV Yields) for Products at 25°

Compd	Range of doses, Mrads	No. of measurements	$G$ value (mean result)	Est'd uncertainty in $G$ value
Tartaric acid	4-12	8	1.65	$\pm 0.05$
Methanol	4-18	8	3.33	$\pm 0.11$
Acetic acid	4-10	6	3.47	$\pm 0.10$
Carbon dioxide	4-12	6	5.45	$\pm 0.15$
Formaldehyde	8-20	3	0.74	$\pm 0.03$
Ethylene glycol	8-12	5	0.20	$\pm 0.04$
Malic acid	8-12	5	0.13	$\pm 0.03$
2-Hydroxypropionic acid	8-12	5	0.16	$\pm 0.03$
Hydrogen	4-12	5	0.21	$\pm 0.01$

Yields of carbon monoxide and methane could not be determined by the general method for gases described above since the amounts produced by thermal decomposition during melting were of the same order as the radiolytic yield. The values of  $G(\text{CO})$  and  $G(\text{CH}_4)$  were estimated by dissolving irradiated samples in carefully outgassed water on the vacuum line and measuring the proportion of these gases in the uncondensable (77°K) fraction of the gas yield. These were found to be  $17 \pm 1$  and  $2.4 \pm 0.1\%$ , respectively (mean of three measurements). Since  $G(\text{H}_2)$  (Table I) was 0.21 the yields of carbon monoxide and methane were estimated to be 0.045 and 0.006, respectively.

The above method of relaxing the crystals by disso-

(18) D. A. Macfadyen, H. D. Watkins, and P. R. Anderson, *J. Biol. Chem.*, **158**, 107 (1945).



lution was found to be unsatisfactory as a general technique however, since carbon dioxide was removed incompletely by freeze-pump-thaw cycles on the aqueous solution. The technique used for carbon monoxide and methane estimations assumes that these products are removed from the solution with the same efficiency as hydrogen.

**Mass Balance.** A mass balance calculated from all the products at 25° (Table II) shows that the "empiri-

**Table II:** A Mass Balance Calculated for All Products Listed in Table I

Product	Formula	G value	Atom yields		
			C	H	O
Carbon dioxide	CO <sub>2</sub>	5.45	5.45		10.90
Acetic acid	C <sub>2</sub> H <sub>4</sub> O <sub>2</sub>	3.47	6.94	13.88	6.94
Methanol	CH <sub>4</sub> O	3.33	3.33	13.32	3.33
Tartaric acid	C <sub>4</sub> H <sub>6</sub> O <sub>6</sub>	1.65	6.60	9.90	9.90
Formaldehyde	CH <sub>2</sub> O	0.74	0.74	1.48	0.74
Hydrogen	H <sub>2</sub>	0.21		0.42	
Ethylene glycol	C <sub>2</sub> H <sub>6</sub> O <sub>2</sub>	0.20	0.40	1.20	0.40
2-Hydroxypropionic acid	C <sub>3</sub> H <sub>6</sub> O <sub>3</sub>	0.16	0.48	0.96	0.48
Malic acid	C <sub>4</sub> H <sub>6</sub> O <sub>5</sub>	0.13	0.52	0.78	0.65
Total atom yields			24.46	41.94	33.34

cal formula" of the products is C<sub>2</sub>H<sub>3.43</sub>O<sub>2.72</sub> clearly indicating that some major product having a low carbon content remains to be identified.

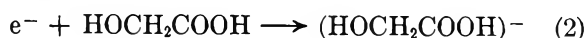
In all probability this compound is water, since, if a yield of  $G(\text{H}_2\text{O}) = 3.33$  is added to Table II a total atom yield of C<sub>2</sub>H<sub>3.97</sub>O<sub>3.00</sub> is achieved with a  $G(-\text{glycollic acid})$  of 12.2. Water is certainly to be expected as a product since it has been identified in irradiated ethanol<sup>19</sup> and acetic acid.<sup>20</sup> Moreover water fits both qualitatively and quantitatively [ $G(\text{H}_2\text{O}) = 3.3$ ] into the proposed reaction scheme so that its inclusion as a probable product is justified.

Water could not be determined in glycollic acid because of its ability to form esters in alcoholic solvents and anhydrides or condensation polymers on heating. If a  $G(\text{H}_2\text{O}) = 3$  and a dose of 10<sup>7</sup> rads were assumed, a moisture content of only 10 ppm in an inert solvent would introduce an uncertainty of  $\pm 20\%$  into the water determination.

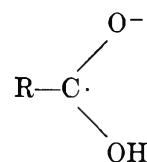
**Suggested Mechanism.** Electron magnetic resonance experiments<sup>6</sup> have shown that the paramagnetic species produced when glycollic acid is irradiated at 77°K undergoes two changes during warming to room temperature. The stable species eventually produced is the same species as that formed when glycollic acid is irradiated at room temperature and has been thoroughly characterized as the radical HO $\dot{\text{C}}\text{HCOOH}$ .<sup>2</sup>

The species produced at 77°K is probably the negative ion formed when the radiolytic electron becomes

attached to a molecule after being reduced to thermal energy

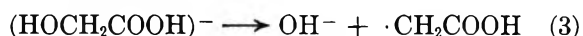


Negative ions of this type have been reported in several systems<sup>10,12</sup> such as the amino acids, which by analogy with the results obtained in aqueous solution would be expected to react much less efficiently with electrons than glycollic acid. Ions of this type are thought to have structures such as

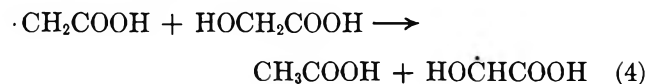


and to explain the doublet splitting observed in the esr spectrum<sup>6,21</sup> it would be necessary to assume that one of the methylene protons lies much closer than the other to the plane of the p orbital containing the unpaired electron.

The two transitions observed are then likely to be a dissociation reaction



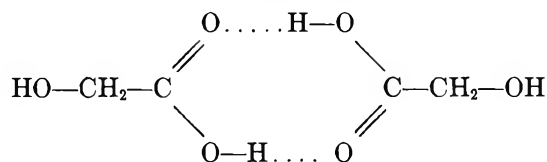
followed by a hydrogen abstraction reaction



Equation 4 accounts for the acetic acid formation and the tartaric acid will be formed when the crystals are relaxed by eq 5



It has been assumed in eq 1 that glycollic acid molecules exist as carboxylic acid dimers



Some spectroscopic evidence exists<sup>22</sup> for this (and for other more extensive hydrogen bonding in the crystal), and the observations of Atherton and Whiffen<sup>2b</sup> regarding the orientation of the radicals in irradiated single crystals require a structure of this type. The positive charge can be presumed located on one of the oxygen atoms of the ring.<sup>23</sup> The positive ion was for-

(19) J. J. Myron and G. R. Freeman, *Can. J. Chem.*, **43**, 381 (1965).

(20) A. S. Newton, *J. Chem. Phys.*, **26**, 1764 (1957).

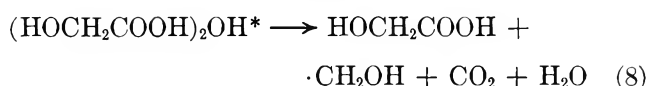
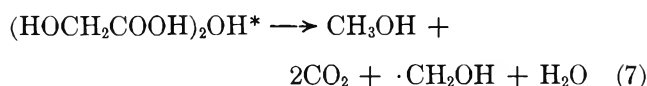
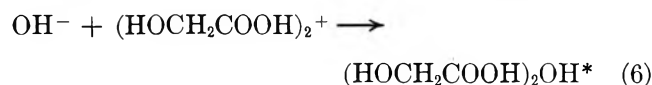
(21) P. M. Gordy, R. B. Ard, and H. Shields, *Proc. U. S. Nat. Acad. Sci.*, **41**, 996 (1955).

(22) J. Bolard, *J. Chim. Phys.*, **62**, 887 (1965).

(23) T. F. Williams, *Nature*, **194**, 348 (1962).

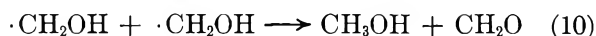
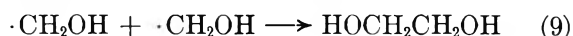
merly<sup>6,21</sup> thought responsible for the low-temperature esr spectrum, but more recent work has shown that such ions, though apparently odd-electron species, rarely give rise to an esr spectrum.<sup>24</sup>

Neutralization of charge followed by decomposition of the excited peroxy radical can be represented by reactions 6-8. The intermediate shown in (6) is prob-



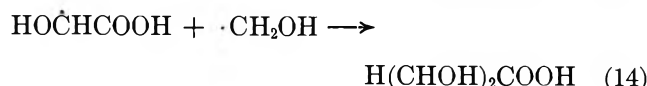
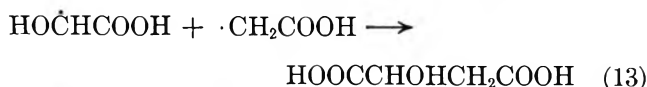
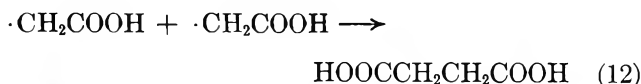
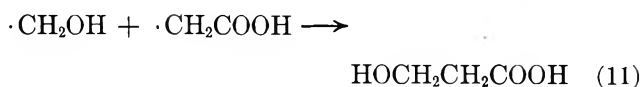
ably no more than a transition state complex in an overall reaction which may result in the decomposition of either or both molecules of the dimer. The energy available for this reaction will be the kinetic energy arising from the electrostatic attraction, which will depend on a number of unknown factors including the mobility of  $\text{OH}^-$  in a crystal lattice and the dielectric constant of the medium. The alternatives (7) and (8) explain the high yield of carbon dioxide compared with other compounds.

An esr signal with a splitting similar to that of the  $\cdot\text{CH}_2\text{OH}$  radical produced in the irradiation of methanol has been observed<sup>6</sup> associated with that of the  $\cdot\text{CH}_2\text{COOH}$  radical, but is very much weaker. The low strength of the signal can be attributed to reactions 9 and 10 occurring in the radiation spur



Both of these are known from methanol radiolysis.<sup>25</sup>

The remainder of the minor products are accounted for by simple radical recombination reactions 11-14.



It is noteworthy that succinic acid, formed in (12) from radicals generated some distance from the ionization site, is produced in much lower yield than ethylene glycol, the dimer of radicals generated at the ionization site, and presumably in greater local concentration.

This reaction scheme, initiated by reaction 1 occurring with  $G \approx 3.3$ , predicts the following relationships between the product yields

$$G(\text{acetic acid}) = 2G(\text{tartaric acid}) = 3.3$$

$$G(\text{methanol}) + 3.3 = G(\text{formaldehyde}) + G(\text{CO}_2)$$

and both hold within experimental error.

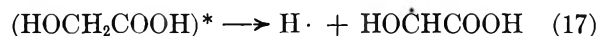
Although this scheme adequately explains the main features of the breakdown pattern, there is insufficient evidence to eliminate the possibility that primary excitation



followed by dissociation, *e.g.*



or



contributes to the products to a small extent.

*Effect of Temperature.* The effect of carrying out the irradiations at reduced temperatures, 77 and 193°K, was investigated and the results are presented in Table III. The yields of products were found to be unaffected

Table III:  $G$  Values of Products at Reduced Temperature

Product	193°K	77°K
Acetic acid	3.2 ± 0.1	1.2 ± 0.1
Methanol	2.5 ± 0.2	0.9 ± 0.1
Tartaric acid	1.45 ± 0.07	1.09 ± 0.04
Formaldehyde	0.78 ± 0.02	0.4 ± 0.15
2-Hydroxypropionic acid	0.12 ± 0.03	Not detected
Ethylene glycol	0.10 ± 0.02	Not detected
Malic acid	0.11 ± 0.02	Trace

by the time at which the sample was held at low temperatures after irradiation.

There are only slight decreases in the yields at 193°K. From the esr evidence,<sup>6</sup> it can be seen that all the reactions of the proposed scheme, except (5) can take place at this temperature and essentially the same processes take place as at room temperature. The only significant difference at this temperature is an increase of (8) over (7) in the competition envisaged between these two reactions. This is reasonable since (7) will have a greater activation energy than (8). This leads to the observed decrease in methanol and carbon dioxide yields; formaldehyde, however, is not affected since

(24) N. Tamura, M. A. Collins, and D. H. Whiffen, *Trans. Faraday Soc.*, **62**, 2434 (1966).

(25) (a) J. Teplý and A. Habersbergerova, *Collect. Czech. Chem. Commun.*, **30**, 785 (1965); J. Teplý and A. Habersbergerova, *ibid.*, **30**, 793 (1965).

the competition does not affect the yield of its precursor, the  $\cdot\text{CH}_2\text{OH}$  radical (10).

Similarly, the yields of products not formed in these reactions, particularly acetic acid and tartaric acids, are unchanged at the lower temperature. A mass balance for the products formed at 193°K was also achieved. The total atom yields were  $\text{C}_{18.9}\text{H}_{32.5}\text{O}_{26.4}$  and again the inclusion of a logical  $G$  (2.8) for water leads to a good mass balance of  $\text{C}_2\text{H}_{4.03}\text{O}_{2.98}$ , and a total decomposition yield of  $G = 9.45$  for glycollic acid.

The yields of all the products are very much more substantially reduced when the irradiation is carried out at 77°K. The esr spectrum shows that at this temperature the  $\cdot\text{CH}_2\text{COOH}$  radicals are not formed, and therefore only reactions 1 and 2 of the proposed reaction scheme can occur during radiolysis. The esr evidence also shows that the subsequent reactions postulated do occur to some extent as the sample is warmed. The lower product yields as well as the absence of others altogether suggest that other processes have to be considered. There is insufficient evidence however

to justify speculation on what these might be, since the total atom yields,  $\text{C}_{10.7}\text{H}_{16.2}\text{O}_{15.5}$ , strongly suggest that some products other than those identified may be formed.

The results support the view that in an appropriate medium electrons may be scavenged immediately after thermalization, eliminating geminate recapture by the positive ion. Also, evidence has been provided that hydrogen abstraction from a methylene carbon by a free radical can take place in the solid phase well below the melting point of the crystal. Finally it is clear that a hydrogen-bonded structure plays an important role in determining the course of the radiolytic decomposition.

*Acknowledgments.* The financial assistance in this work of the Pharmaceutical Society of N. S. W. (S. E. Wright Research Trust) and of the Australian Institute of Nuclear Science and Engineering is gratefully acknowledged as is the cooperation of Dr. J. Clouston and his staff at the Australian Atomic Energy Commission,  $\gamma$ -irradiation facility with the irradiations.

# An Electron Spin Resonance Study of the Rate Constants for Reaction of Hydrogen Atoms with Organic Compounds in Aqueous Solution<sup>1</sup>

by P. Neta, Richard W. Fessenden, and Robert H. Schuler\*

Radiation Research Laboratories and Department of Chemistry, Mellon Institute of Science, Carnegie-Mellon University, Pittsburgh, Pennsylvania 15213 (Received January 4, 1971)

Publication costs assisted by Carnegie-Mellon University and the U. S. Atomic Energy Commission

Hydrogen atoms produced by the electron-proton neutralization reaction in aqueous solution show abnormal esr lines because of an initial nonequilibrium population of the four possible electron-nuclear spin levels. The high-field line is observed in enhanced absorption and the low-field line in emission. At the normal power levels employed in these esr experiments relaxation to an equilibrium distribution occurs with a period  $\sim 50$   $\mu$ sec and chemical reactions will effectively compete with this relaxation if solutes are present at concentrations such that the pseudo-first-order rate constant  $k_s[S]$  is greater than  $10^4$   $\text{sec}^{-1}$ . A steady-state esr method for determining the rate constants for reaction of hydrogen atoms with added solutes has been developed which is based on this competition. A simplified kinetic model, which appears to be adequate for empirical determination of rate constants, is described in the main text and a somewhat more detailed model is discussed in an Appendix. The effect of experimental variables on the observed signal intensity is examined and in particular it is noted that the effect of power on the competitive situation is completely in accord with the proposed model. In cases where comparative data by this and other methods are available relative rate constants are, in most cases, in good agreement. The absolute scale is established by internal comparison with solutes having known rate constants. Observations on more than 60 compounds with second-order rate constants ranging from  $10^5$  to  $10^9$   $M^{-1} \text{sec}^{-1}$  have been carried out. For saturated aliphatic compounds the rate constants are found to increase with molecular size, being  $\sim 10^5$   $M^{-1} \text{sec}^{-1}$  or less only for the simplest of species. A plateau level  $\sim 10^8$   $M^{-1} \text{sec}^{-1}$  is approached for aliphatic derivatives in the  $C_6$  region. As expected, molecules containing reactive features such as double bonds, aromatic rings, or iodine atoms exhibit rate constants in the region near to the diffusion controlled limit.

To date the literature contains relatively little reliable information on the absolute rate constants for the reaction of hydrogen atoms with organic solutes in aqueous systems. The information which was available in 1967 was summarized by Anbar and Neta<sup>2</sup> but in most cases absolute rates had to be inferred from what were frequently rather complex comparisons of relative rates in different systems. Direct measurements of absolute rate constants have been made in only a few instances (*e.g.*, benzoic acid,<sup>3</sup> various other aromatic compounds,<sup>3-6</sup> tetranitromethane,<sup>7</sup> and cyclohexane<sup>8</sup>) in spite of the obvious importance of hydrogen atom reactions in the radiolysis of aqueous systems, particularly those at low pH. This situation exists, of course, because hydrogen atoms do not have a readily accessible absorption that can be followed by kinetic spectrophotometry in the usual type of pulse radiolysis experiment which has provided such a large volume of data on the rates of reaction of other intermediates such as  $e_{aq}^-$ . It has recently been found that esr signals of hydrogen atoms are observable during the irradiation of aqueous systems as a result of their enhancement by spin-polarization effects (*i.e.*, nonequilibrium population of the electron-nuclear spin levels) which are present at times short after formation.<sup>9,10</sup> In steady-state experiments carried out in the absence of reactive solutes these signals are approxi-

mately proportional to the beam current<sup>9</sup> which suggests that the dominant term controlling the size of the signal is the relaxation of this polarization. If so this relaxation should provide, as an internal reference, a first-order decay against which chemical rates can be measured competitively by observing the reduction caused by reactive solutes in the esr signal at steady state. We wish to report here detailed experiments which explore this approach. Relative measurements have been made on a large number of solutes and the results put on the absolute scale by comparison against the known rate for abstraction of deuterium from deuterioisopropyl alcohol. In principle, the absolute scale can

(1) Supported in part by the U. S. Atomic Energy Commission. Presented, in part, at the 161st National Meeting of the American Chemical Society, Los Angeles, Calif., Mar 28-Apr 2, 1971.

(2) M. Anbar and P. Neta, *Int. J. Appl. Radiat. Isotopes*, **18**, 493 (1967).

(3) P. Neta and L. M. Dorfman, *J. Phys. Chem.*, **73**, 413 (1969).

(4) M. C. Sauer, Jr., and B. Ward, *ibid.*, **71**, 3971 (1967).

(5) E. J. Land and M. Ebert, *Trans. Faraday Soc.*, **63**, 1181 (1967).

(6) K.-D. Asmus, B. Cercek, M. Ebert, A. Henglein, and A. Wigger, *ibid.*, **63**, 2435 (1967).

(7) K.-D. Asmus, A. Henglein, M. Ebert, and J. P. Keene, *Ber. Bunsenges. Phys. Chem.*, **68**, 657 (1964).

(8) M. C. Sauer, Jr., and I. Mani, *J. Phys. Chem.*, **72**, 3856 (1968).

(9) K. Eiben and R. W. Fessenden, *ibid.*, **75**, 1186 (1971).

(10) B. Smaller, J. R. Remko, and E. C. Avery, *Proc. Int. Congr. Radiat. Res.* 4th, in press.

also be established from a knowledge of the relaxation period. However, at the present time there is, unfortunately, no direct measurement of this period under the conditions of these steady-state experiments.

Smaller,<sup>10</sup> in recent studies, has taken a more direct approach and measured the time dependence of the hydrogen atom signal in the presence of solutes. Such a technique directly provides absolute rate constants since the experiments can be carried out under conditions where pseudo-first-order kinetics are applicable. It is, however, limited to cases where the period of the chemical reaction is short with respect to the relaxation period of the polarization but long with respect to the time resolution of the spectrometer detector. The steady-state approach used here avoids the requirement of fast spectrometer response and allows one to examine solutes over a somewhat wider concentration range than is possible in pulse experiments.

During the course of the present investigation it appeared desirable to have, for comparison purposes, rate measurements made with a different technique but under chemical conditions comparable to those present in the esr experiments. The reaction rates relative to abstraction of deuterium from deuterioisopropyl alcohol were determined for some 18 solutes<sup>11</sup> and placed on an absolute scale *via* an internal comparison to the addition reaction with benzoic acid. In general the rate constants determined by the esr and chemical approaches agree quite well, as will be discussed below. The results of measurements made by the esr approach described here thus appear to be valid, and because such measurements can be made rapidly and conveniently a large body of information on hydrogen atom rates is readily accessible.

### Experimental Section

The experimental arrangement used was a modification of the original *in situ* radiolysis-esr experiment<sup>12</sup> as described in detail in the recent paper by Eiben and Fessenden.<sup>9</sup> The spectrometer was a conventional X-band ( $9 \times 10^9$  Hz) instrument except for the provision for *in situ* irradiation of the sample. The irradiation was carried out directly in the esr cavity in a flat silica cell of 1 cm width and 0.5 mm internal spacing. The solution flowed through the cell at a rate of 2 cm<sup>3</sup>/sec which corresponds to a residence time of the sample in the irradiation zone of  $\sim 10$  msec. The mean radical lifetime is at least an order of magnitude less in all experiments reported here. The solution was cooled slightly before entering the cell and, except in the one case noted, all measurements pertain to  $\sim 15^\circ$ . Second derivative spectra were recorded by double-modulation techniques employing frequencies of 200 and 100,000 Hz. The electron beam current collected at an electrode in the solution was recorded simultaneously with the esr spectrum and the peak heights (which were found to be approximately propor-

tional to current, see below) normalized to unit current. In most experiments the current to the cell was  $\sim 0.6$   $\mu$ A where the absorbed dose rate was  $\sim 10^{20}$  eV g<sup>-1</sup> sec<sup>-1</sup>. At this dose rate a product concentration of  $\sim 4 \times 10^{-5}$  M is produced in the 10-msec residence period. The accessible current is limited to  $< 2$   $\mu$ A by heating effects. In the absence of solutes, signals could be observed down to  $\sim 0.01$   $\mu$ A.

Most of the organic compounds studied were of the purest grade available commercially (mostly Baker Analyzed Reagents). The amino acids and their derivatives were Grade A Calbiochem or Cyclo Chemical. Hydrocarbons (both liquids and gases) were Phillips Research Grade. The nonhydrocarbon gases were obtained from Matheson. In most experiments, water was doubly distilled and passed with oxygen through a silica tube at  $\sim 600^\circ$  during the second distillation. Some experiments were carried out with water prepared by the basic permanganate-acid dichromate triple distillation procedure frequently used in radiation chemical studies, but no effect was observed on the hydrogen atom signal intensity or competition rates. Solutions were made acid (usually to pH 1) with Baker Analyzed perchloric acid (or sulfuric acid in a few instances) and deoxygenated by bubbling with nitrogen or argon. Oxygen, of course, reacts very rapidly with hydrogen atoms and no signals were observable in a solution saturated with a mixture of 10% O<sub>2</sub> in nitrogen ([O<sub>2</sub>]  $\sim 10^{-4}$  M) at currents below 0.1  $\mu$ A. At higher dose rates the oxygen is partially depleted and small signals are observable.

### Results and Discussion

The esr signals of hydrogen atoms observed during the steady-state irradiation of 0.1 M perchloric acid (containing 0.002 M *tert*-butyl alcohol) are illustrated in Figure 1. The signals are similar to but somewhat more intense than those previously reported<sup>9</sup> (signal-to-noise ratio in Figure 1 is  $\sim 50:1$ ) although the second component previously observed at the low-field line<sup>9</sup> is absent. The hydrogen atom spectrum exhibits strong polarization, *i.e.*, the low-field line appears in emission and the high-field line in enhanced absorption, as previously described.<sup>9</sup> The relative populations of the four spin states for the hydrogen atom which would lead to such a situation are shown in Figure 2. The magnitudes of  $\delta$  and  $\delta'$  must be considerably greater than values appropriate to the Boltzmann equilibrium and in the case of the low-field line the population difference is inverted. The mechanistic source of this nonequilibrium population among the spin levels is only vaguely understood at the moment but is actively being investi-

(11) P. Neta, G. R. Holdren, and R. H. Schuler, *J. Phys. Chem.*, **75**, 449 (1971).

(12) R. W. Fessenden and R. H. Schuler, *J. Chem. Phys.*, **39**, 2147 (1963).

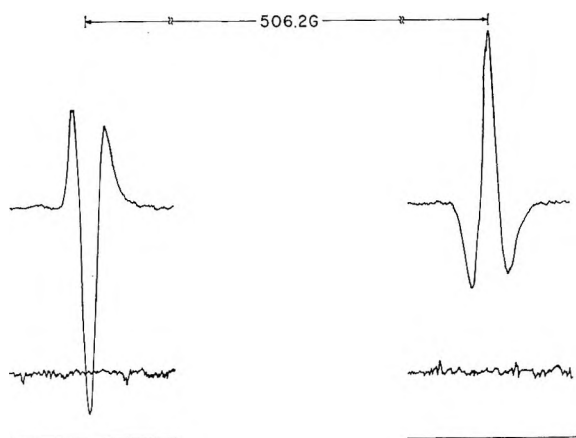


Figure 1. Second derivative esr spectrum of hydrogen atoms observed from a 0.1 *M* perchloric acid solution 0.002 *M* in *tert*-butyl alcohol. The low-field line (at the left) is observed in emission and the high-field line (at the right) in absorption. The electron beam current ( $\sim 0.4 \mu\text{A}$ ) simultaneously recorded is given by the lower traces. The observed spectrum is very similar to but somewhat more intense than that previously reported by Eiben and Fessenden (ref 9). Essentially none of the second low-field component noted in their case is apparent here. The observed line separation corresponds to a hydrogen atom hyperfine constant of 503.0 G.

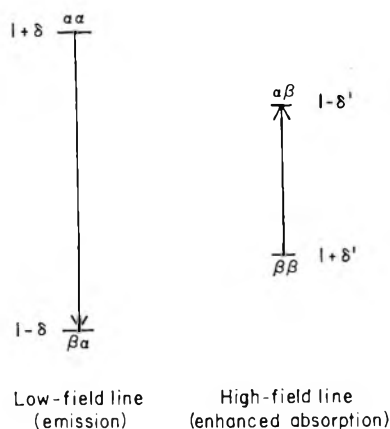


Figure 2. Energy level diagram for the four possible electron-nuclear spin states of the hydrogen atom in a magnetic field. The arrows indicate the two allowed esr transitions. The expressions  $1 + \delta$ , etc. beside the levels show a possible initial population distribution which would give rise to the spectrum observed in Figure 1 with the states  $\alpha\alpha$  and  $\beta\beta$  being overpopulated with respect to  $\beta\alpha$  and  $\alpha\beta$ .

gated by a number of workers.<sup>13-16</sup> It is this polarization which enhances the signals so that they are readily observable. As indicated in the introduction, the relaxation of this initial polarization can serve as an internal timing device with which to measure the rate of reaction with solutes.

At the microwave power normally used in these experiments the signal of either of the H atom lines is very nearly proportional to current over the practical range of currents (as is illustrated for the low-field line by the upper curve in Figure 3 which has an average slope of 0.94 over the current range 0.05 to 0.5  $\mu\text{A}$ ).

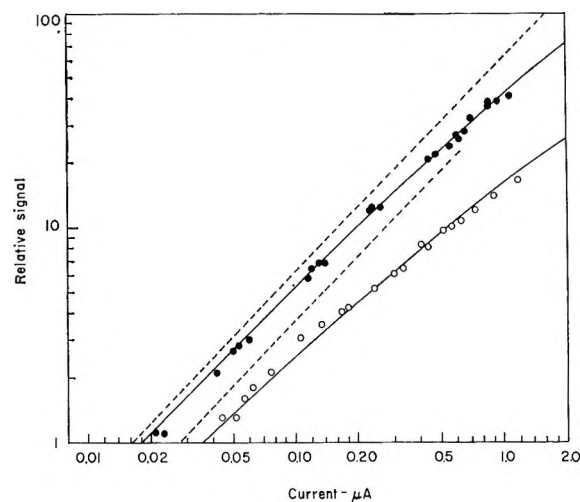


Figure 3. Signal intensity of the low-field hydrogen line as a function of beam current in the presence of 0.002 *M tert*-butyl alcohol at power levels of 3.3 mW (O) and 0.21 mW (●). Solid curves are calculated from eq IX with  $V = 10$ ,  $1/T_1 = 4 \times 10^3 \text{ sec}^{-1}$ ,  $k_r[\text{R}] = 3 \times 10^3 \text{ sec}^{-1}$ ,  $[\text{S}] = 0$ , and the coefficient at the power term =  $1.7 \times 10^3 \text{ sec}^{-1}$ . Dashed lines are of unit slope and represent the limiting dependence at low current if  $[T_1(k_r[\text{R}]))^{-1}$  is small with respect to  $V + 1$ .

This dependence demonstrates that the observed signal is not controlled significantly by the second-order reaction of hydrogen atoms with other radicals (which would give a square root dependence on current as found, for example, for the spectrum of ethyl radicals in liquid ethane; cf. Figure 43 in ref 12). At lower microwave powers or higher currents some deviation from proportionality does occur and the interpretation is treated in the Appendix. As is discussed there, these deviations cannot affect the rate determinations in any direct way provided measurements are made at relatively high concentrations of added solute. The approximate linear dependence on beam current allows small variations in beam current to be taken into account readily and in the kinetic studies all signals were measured at approximately 0.6  $\mu\text{A}$  and normalized to this latter value. The intensity of the signals from water containing 0.1 *M*  $\text{HClO}_4$  and 0.002 *M tert*-butyl alcohol was, in general, quite reproducible. The standard deviation within a set of measurements on a single sample was  $\sim 5\%$ . During any given short period (*i.e.* days) the sample-to-sample reproducibility was usually of this same order of magnitude. Over a longer term, larger variations occurred because of changes within the spectrometer or in the irradiation geometry but were always within the limits of 40–70 units per

(13) R. Kaptein and J. L. Oosterhoff, *Chem. Phys. Lett.*, **4**, 195 (1969).

(14) G. L. Closs, *J. Amer. Chem.*, **91**, 4552 (1969).

(15) H. Fischer, *Chem. Phys. Lett.*, **4**, 611 (1970).

(16) F. J. Adrian, *J. Chem. Phys.*, **53**, 3374 (1970).

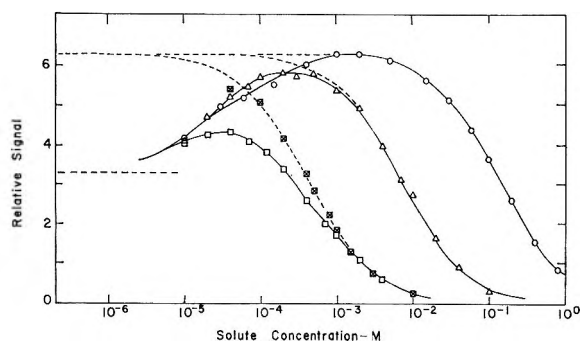


Figure 4. Signal intensity of the low-field hydrogen atom line as a function of solute concentration:  $\circ$ , *tert*-butyl alcohol,  $\Delta$ , methanol;  $\square$ , ethanol;  $\boxtimes$ , ethanol in the presence of 0.002 *M tert*-butyl alcohol. A relative signal of 3.3 units is observed in the absence of added solute as indicated by the dashed line on the left of the figure. The upper dashed curves represent the sigmoidal dependence expected from eq III with  $[H^*]_0$  taken as the value observed in the case of 0.002 *M tert*-butyl alcohol.

$\mu\text{A}$  of beam. No effect of this variation on the kinetics was apparent.

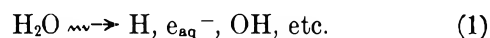
It was observed quite early in preliminary experiments that the addition of a low concentration of compounds such as *tert*-butyl alcohol or methyl chloride, which are relatively unreactive toward hydrogen atoms, results in an increase in the hydrogen atom signal. The effect was the same for both lines of the spectrum, *e.g.*, with 0.002 *M tert*-butyl alcohol the high-field (absorption) line increased in intensity by a factor of 2.0 and the low-field (emission) line by a factor of 1.9. This effect is presumably related, at least in part, to a conversion of OH radicals to other radicals. In the absence of the *tert*-butyl alcohol both the high- and low-field lines depend in the same way on beam current. This common dependence and the similar behavior upon the addition of *tert*-butyl alcohol would seem to rule out any explanation involving chemical reactions of hydrogen atoms at times long after their formation.

The dependence of the low-field signal intensity on methanol, ethanol, and *tert*-butyl alcohol concentrations is given in Figure 4. In all three cases the addition of  $10^{-4}$  *M* or less of solute causes an increase in signal but the effect cannot be treated quantitatively because depletion problems are undoubtedly present at these low concentrations. With the further addition of solute the hydrogen atom signals are observed to decrease again as the result of chemical reactions. At high concentrations the curves of Figure 4 have, in fact, the sigmoidal character expected if there is competition for a fixed number of hydrogen atoms between two reactions, one of which is linearly dependent on the solute concentration. The increase in signal observed at low concentrations causes difficulty in any kinetic treatment and seems likely to be an artifact so that it was decided to saturate this effect as far as possible and carry out further experiments in the presence of 0.002 *M tert*-butyl alcohol. (Of the additives commonly used to

remove OH, *tert*-butyl alcohol has the highest relative ratio for  $k_{\text{OH}}/k_{\text{H}} = 5 \times 10^3$ ).<sup>2</sup> At this concentration the pseudo-first-order rate constant for the reaction of hydrogen atoms with *tert*-butyl alcohol is  $1.6 \times 10^2 \text{ sec}^{-1}$ . This frequency is two orders of magnitude smaller than those for the other competing processes and so the addition of this OH scavenger should have no direct effect on the H atom signal intensity. When *tert*-butyl alcohol is added, the simple competitive situation seems to apply as is illustrated by the dashed curve in Figure 4 for ethanol. The principal problem in the kinetic treatment is in obtaining a reference value for  $H_0$ , the hydrogen atom signal in the absence of the solute of interest. The signal observed in the presence of 0.002 *M tert*-butyl alcohol, where only  $\sim 1\%$  of the hydrogen atoms will be removed by reaction with the solute, is taken as the best available measure of  $H_0$  and accordingly this value was determined in each experiment. Solute was then added at concentration  $[S]$  and the (decreased) intensity  $H$  measured. Additional solute was progressively added to determine the dependence of the relative signal intensity  $H/H_0$  on concentration.

*The Competition Kinetics.* We will disregard the complications here and treat the kinetic problem simply as a competition between chemical reaction and relaxation of the polarization. Such an idealized description, while far from exact as is discussed in the Appendix, appears to be quite adequate for the practical application to the problem of determining H-atom rate constants.

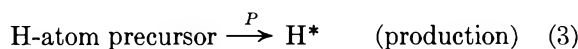
Hydrogen atoms are produced in the irradiation of acid solutions both directly



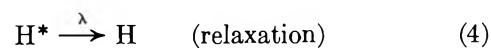
and by reaction of hydrated electrons with hydrogen ions



As far as the esr observations are concerned these reactions can be regarded as producing hydrogen atoms which are "labeled" by virtue of their spin polarization



where  $P$  refers specifically to the production rate of the hydrogen atom component responsible for the abnormal esr absorption. (As is apparent from the treatment in the Appendix this approach does not, in fact, imply two chemically different types of hydrogen atoms.) In the absence of chemical reaction relaxation will occur and the esr signal of the hydrogen atoms produced in reaction 3 will decrease exponentially with a characteristic period defined by the relaxation rate constant  $\lambda$



It is assumed here that the hydrogen atoms produced in reaction 4 do not contribute significantly to the esr signals so that the observed intensity is a direct measure of  $[H^*]$ . (As is discussed in the Appendix, this assumption requires both that the initial polarization be large and that the chemical lifetimes of the hydrogen atoms be of the magnitude of the relaxation period or less. In the practical experiment both criteria appear to be met reasonably well.) In the absence of added solute a steady-state concentration  $[H^*]_0$  will result from the

$$[H^*]_0 = P/\lambda \quad (I)$$

competition between these two reactions and the observed esr signal is expected to be proportional to dose rate. As is illustrated by the upper curve of Figure 3, this behavior is followed reasonably well under the normal conditions of microwave power and dose rate employed. Deviations do, however, occur at lower power, as illustrated in the figure by the lower curve which has a slope of 0.75 in the current region 0.2 to 0.5  $\mu A$ . At the lower power, relaxation is slower and the second-order reactions of hydrogen atoms become competitive with the relaxation process so that a contribution to  $\lambda$ , which is a function of dose rate, exists. Such conditions were avoided as much as possible in the studies comparing the reactivities of different solutes.

When a reactive solute is present, reaction of the hydrogen atoms can occur with a rate constant  $k_s$  which is assumed to be the same for all spin states and equal to the conventional second-order rate constant.



A steady-state treatment of the above competition between production, relaxation and reaction leads directly to

$$[H^*] = \frac{P}{\lambda + k_s[S]} \quad (II)$$

which, incorporating eq I, gives

$$\frac{[H^*]}{[H^*]_0} = \frac{\lambda}{\lambda + k_s[S]} \quad (III)$$

The concentration ratio  $[H^*]/[H^*]_0$  is equated to the experimentally observed ratio of signal intensities  $H/H_0$  and eq III rearranged to the more useful form

$$\frac{H_0}{H} - 1 = \frac{k_s}{\lambda} [S] \quad (IV)$$

which allows logarithmic presentation so that the wide range of concentrations studied can be readily displayed. This form of presentation is illustrated in Figure 5 where the effects of methanol on the high- and low-field signals are compared. It is seen that the

data for both signals exhibit the linear dependence (*i.e.*, the slope is unity) on solute concentration expected from eq IV and that a common dependence is observed for both lines. The signals are reduced by 50% [ $(H_0/H) - 1 = 1$ ] when  $\lambda = k_s[S]_{1/2}$ . Taking  $k_s = 1.6 \times 10^6 M^{-1} \text{sec}^{-1}$  (see below) and  $(CH_3OH)_{1/2} = 0.0070 M$  from Figure 5 in these experiments,  $\lambda$  is determined to be  $1.1 \times 10^4$ , which corresponds to an effective half-period of 62  $\mu\text{sec}$  for the relaxation period of the spin polarization.

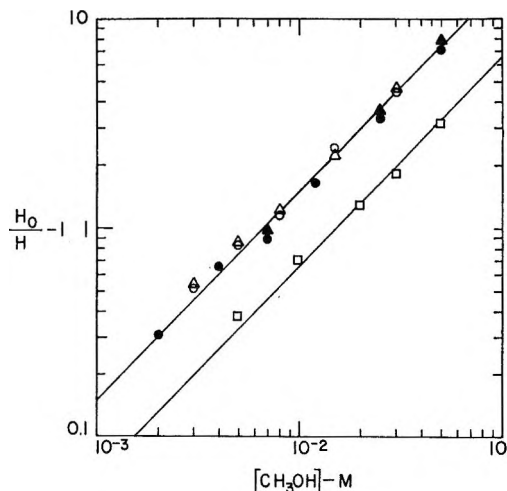


Figure 5. Plot of  $(H_0/H) - 1$  as a function of methanol concentration:  $\Delta$  and  $\blacktriangle$ , low-field line;  $\circ$  and  $\bullet$ , high-field line in two series of experiments in the presence of 0.002  $M$  *tert*-butyl alcohol. The curve on the right ( $\square$ ) represents data obtained for a solution 0.14  $M$  in *tert*-butyl alcohol where the initial signal is reduced by a factor of 2. The lines are of unit slope as indicated by eq IV.

In the limit of low microwave power, the relaxation period is presumably a characteristic of the hydrogen atoms. The experiments performed here were, however, carried out at relatively high power where the signal is partially power-saturated and where the relaxation period can be expected to be reduced because of power-induced transitions between the spin states indicated in Figure 2. The scavenging curves obtained at different power levels but under conditions which were otherwise completely comparable are given in Figure 6. It is seen that the scavenging curve is shifted toward higher concentration, *i.e.*, shorter relaxation periods, at the higher power levels. This demonstration that the period of the process which competes with the chemical reaction is dependent on power level leaves little doubt that it must be dominated by a physical process. The relaxation periods determined at several different power levels are given in Table I. The power level in the cavity will depend on cavity Q and other experimental conditions so that over the long term the scavenging curves can be expected to shift somewhat. Reference experiments with methanol were carried out during



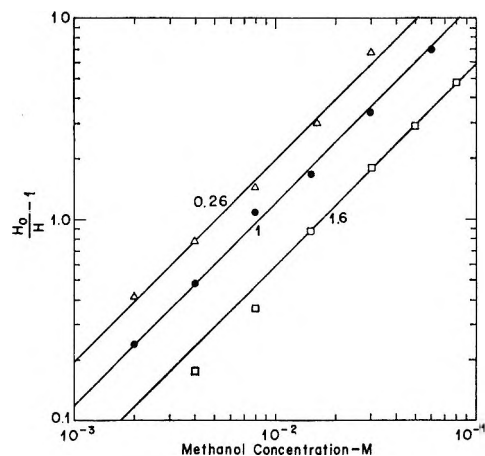


Figure 6. Competition plots for methanol at microwave powers of 0.21 mW ( $\Delta$ ), 3.3 mW ( $\bullet$ ), and 8.1 mW ( $\square$ ). The relative microwave magnetic field intensities ( $\propto P^{1/2}$ ) are indicated in the figure.

each set of measurements and  $[\text{CH}_3\text{OH}]_{1/2}$  was always found to be within the limits 0.0070 and 0.0085 M at a standard power level setting of 3.3 mW.

**Table I:** Effect of Power Level on Relaxation Period

Microwave power level, mW	0.21	3.3	8.1
Relative microwave magnetic field	0.46	1.8	2.85
$[\text{CH}_3\text{OH}]_{1/2}([\text{tert-BuOH}] = 0.002 \text{ M})$	0.0050	0.0085	0.0170
$\tau_{1/2}, \mu\text{sec}^a$	87	51	26
$[\text{CH}_3\text{OH}]_{1/2}([\text{tert-BuOH}] = 0.1 \text{ M})$	0.0085	0.013	0.022
$\tau_{1/2}, \mu\text{sec}^a$	95	52	26

<sup>a</sup> Half-period for relaxation referenced to reaction with methyl alcohol or methyl plus *tert*-butyl alcohol.

The above treatment of the kinetics is rigorous only in the idealized situation where decay of the polarization (reaction 4) can be regarded as purely exponential and where reaction of hydrogen atoms with other radicals is negligible. In the real system neither of these criteria will be obeyed exactly and deviations are expected. An attempt at a somewhat more complete description is given in the Appendix. In spite of potential difficulties, the simple description given above appears to be an excellent approximation as seen by the linearity exhibited in the various plots of  $(H_0/H) - 1$  vs.  $[\text{S}]$ . Since one is mainly interested in the relative concentrations of solutes which produce the same effect on the signal (and therefore have the same  $k_s[\text{S}]$ ) the quantity determined is the concentration required to produce the same effect as in a reference system and small departures from this simplified kinetic model will tend to cancel. At very high solute concentrations, where the scavenging reaction dominates both the re-

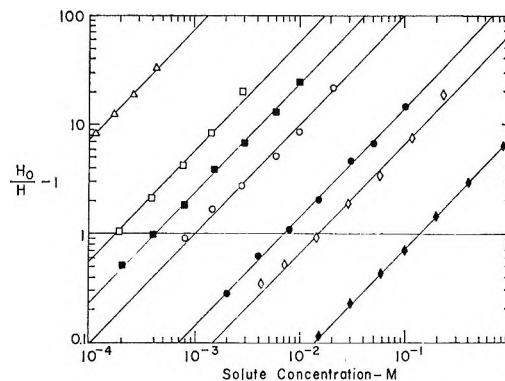


Figure 7. Competition plots for benzoic acid,  $\Delta$ ; isopropyl alcohol,  $\square$ ; ethanol,  $\blacksquare$ ; deuterioisopropyl alcohol,  $\circ$ ; methanol,  $\bullet$ ; formic acid,  $\diamond$ ; and *tert*-butyl alcohol,  $\blacklozenge$ . Fifty per cent scavenging occurs at  $(H_0/H) - 1 = 1$ .

laxation processes and reaction with other radicals so that the steady state is controlled solely by reactions I and V, it should be rigorous that the relative rate constants will be inversely proportional to the concentrations required to reduce the signal to a given level.

**Rate Constants.** Typical plots of representative data obtained with a number of solutes are given in Figure 7. These plots cover the range of reactivities (from *tert*-butyl alcohol to benzoic acid) over which the concentration dependence was studied. In general the data follow eq IV quite well, especially where more than 50% of the hydrogen atoms have been scavenged. It is seen that valid measurements can be made at solute concentrations where the signal is reduced to  $\sim 10\%$  of  $H_0$ . At low concentrations one must effectively examine the small difference in the signal produced by adding solute and accuracy is severely limited. Points obtained where the reduction was  $< 30\%$  (*i.e.*, at an ordinate  $< 0.5$ ) are therefore given very little weight. Taking into account these limitations and the range of concentrations which can be examined ( $10^{-4}$  to  $1 \text{ M}$ ), solutes having rate constants within the range  $1 \times 10^4$  to  $5 \times 10^9 \text{ M}^{-1} \text{ sec}^{-1}$  can be studied as is illustrated in Figure 7.

It can readily be seen from eq IV that the relative rate constants should be inversely proportional to the solute concentration required to give a certain fractional reduction in the signal. The shifts along the concentration axis were determined from the points at which the linear plots cross  $(H_0/H) - 1 = 1$ . The concentration dependence was measured for some 40 compounds in addition to those illustrated in Figure 7 and the relative rate constants were determined from similar plots. The relative rate constants were placed on the absolute scale by reference to parallel measurements on methanol where the rate constant was taken as  $1.6 \times 10^6 \text{ M}^{-1} \text{ sec}^{-1}$ . In the remaining cases studied (mostly hydrocarbons or alkyl halides) only single points were determined on saturated solutions and the rate constants were calculated using solubilities from

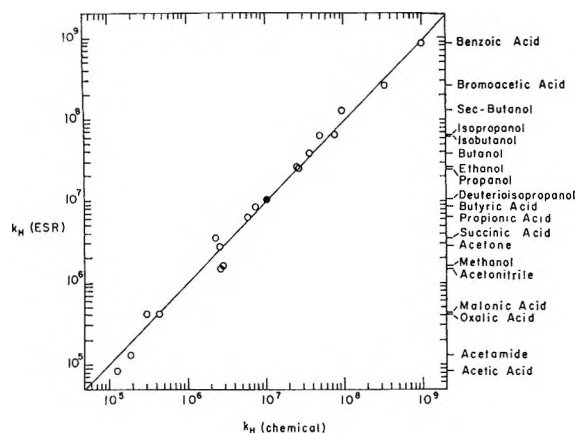


Figure 8. Correlation between rate constants determined in the present esr experiments with those from the chemical experiments reported in ref 11. Absolute rates calculated on the basis of  $k_{H+(CD_3)_2CDOH} = 1.05 \times 10^7 M^{-1} \text{sec}^{-1}$  in both cases. Line is of unit slope through this latter point (●).

the literature, mostly from the Landolt-Bornstein compilation.<sup>17,18</sup>

In most instances, the relative rate constants measured by this esr technique agree quite well with data available from chemical competition studies. A comparison of the present results with the rate constants determined at the same pH by competition with abstraction from deuterioisopropyl alcohol<sup>11</sup> is given for 19 compounds in Figure 8. In the chemical study the absolute rate constant for reaction with deuterioisopropyl alcohol was determined to be  $1.05 \times 10^7 M^{-1} \text{sec}^{-1}$  by comparison with the absolute rate constant for addition to benzoic acid ( $1.00 \pm 0.15 \times 10^9 M^{-1} \text{sec}^{-1}$ ). The latter had been measured directly in pulse radiolysis studies.<sup>3</sup> The absolute values for reaction of hydrogen atoms with the various solutes are given in Table II by reference to this value for deuterioisopropyl alcohol. (Benzoic acid, although a more direct reference, was not used here because it could be studied over only a limited range at very low concentrations where depletion and other secondary chemical problems could be important. If it were used as the reference the rate constants would be 15% higher.)

In 12 out of the 19 comparisons made in Figure 8 the esr and chemical determinations agree to within 20% and in most of the remaining cases to within 50%. It is particularly noted that in all cases where the rate constant determined by the esr method was greater than  $2 \times 10^6 M^{-1} \text{sec}^{-1}$  the two approaches give results that agree within the expected experimental uncertainty ( $\pm 20\%$ ). The particular exception to this general overall agreement is methanol where the rate constant determined by esr is only 55% of that determined chemically. The reason for this discrepancy is, at the moment, unknown. The same materials were used for both the chemical and the esr experiments. The esr measurements were repeated many times on

different samples and completely consistent results were obtained. It will be noted in Table II that the ratio of rate constants for ethanol and methanol is 16. This ratio is considerably higher than ratios between 8 and 12 determined previously by chemical methods<sup>2</sup> and this fact, in part, prompted us to undertake the competition measurements reported in ref 11. A ratio of 8.6 was determined in this latter study in complete accord with previous measurements of this ratio. It was thought that chemical impurities in the ethanol might be responsible but comparison of the scavenging curves using samples obtained from different sources gave similar results. One further esr comparison was made where the sample temperature was increased from 15 to 30°. The rate with methanol increased by 25% and that with ethanol by 15% so that the fact that most of the esr measurements were made at 15° does not contribute significantly to the difference. Since the chemical determination, as in the esr case, also involves the determination of the relative concentrations of two solutes required to produce the same effect with respect to a common competing reaction, the observed difference must reflect some subtle difference between the secondary reactions involved in the methanol and ethanol systems. It is not obvious why these two solutes should be very different and even this one exception from the otherwise excellent agreement is most disturbing. It is presumed that because of the general agreement of the other relative values the difficulty lies with methanol. Until this anomalously low relative value from the esr measurements on methanol is understood, rate constants determined that are less than  $2 \times 10^6$  should be regarded as reliable only to a factor of 2. There is no indication in Figure 8 that any further increase in the discrepancy occurs with the less reactive solutes.

A general summary of all the rate constants measured by this esr method is given in Table II. There does not seem to be a sufficient pattern among these rates that they can be meaningfully treated in a quantitative way in terms of group reactivities. Certain general trends are, however, noted as in Figure 9 where the rate constants are plotted as a function of molecular complexity. In the homologous series of normal alkanes, alcohols, and monocarboxylic acids the rate constants monotonically increase with chain length and appear to approach a plateau in the range of a few times

(17) Landolt-Börnstein Zahlenwerte und Funktionen, II. Band, 2. Teil, Bandteil b, Springer-Verlag, Berlin, 1962.

(18) In the case of pentane and hexane the solubilities given in the earlier literature appear to be high by almost a factor of 10. The use of these solubilities gave apparent rate constants which were inconsistent with the values for propane and butane. Very recently the solubilities have been carefully measured with gas chromatographic techniques [H. D. Nelson and C. L. DeLigny, *Recl. Trav. Chim. Pays-Bas*, 87, 528 (1968)] and these latter values are used in the present work. The solubilities of cyclopentane and cyclohexane were determined in these laboratories (T. Söylemez, private communication) by gas chromatographic techniques to be 0.015 and 0.0017 *M*.

Table II: Rate Constants for the Reactions of Hydrogen Atoms with Organic Compounds in Aqueous Solutions<sup>a</sup>

Compd	Rate constant, $M^{-1} \text{sec}^{-1}$		Compd	Rate constant, $M^{-1} \text{sec}^{-1}$	
	Esr method <sup>b</sup>	Chemical method <sup>c</sup>		Esr method <sup>b</sup>	Chemical method <sup>c</sup>
Urea	$<3 \times 10^4$		Tartaric acid	$1.7 \times 10^7$	
Methyl chloride <sup>d</sup>	$7 \times 10^4$		Ethylene glycol	$1.7 \times 10^7$	
<i>tert</i> -Butyl alcohol	$8 \times 10^4$		Glycolic acid	$1.8 \times 10^7$	
Glycine	$8 \times 10^4$		Lactic acid	$2.2 \times 10^7$	
$\alpha$ -Aminoisobutyric acid	$8 \times 10^4$		Isobutyronitrile	$2.2 \times 10^7$	
Acetic acid	$8.4 \times 10^4$	$13 \times 10^4$	Propane <sup>d</sup>	$2.2 \times 10^7$	
Methane <sup>d</sup>	$<10^6$		Propyl alcohol	$2.5 \times 10^7$	$2.7 \times 10^7$
Acetamide	$1.3 \times 10^6$	$1.9 \times 10^6$	Ethyl alcohol	$2.6 \times 10^7$	$2.5 \times 10^7$
$\alpha$ -Alanine	$2.9 \times 10^6$		Isobutyric acid	$2.6 \times 10^7$	
$\beta$ -Alanine	$3.4 \times 10^6$		Neopentyl alcohol	$2.9 \times 10^7$	
Oxalic acid	$4.1 \times 10^6$	$3 \times 10^6$	Cyclopentane <sup>d</sup>	$3 \times 10^7$	
Malonic acid	$4.2 \times 10^6$	$4.4 \times 10^6$	Cyclohexane <sup>d</sup>	$3 \times 10^7$	
Cyclopropane <sup>d</sup>	$7 \times 10^6$		Acetaldehyde	$3.4 \times 10^7$	
Formic acid	$7.4 \times 10^6$		Butyl alcohol	$3.84 \times 10^7$	$3.7 \times 10^7$
Chlorotrifluoromethane <sup>d</sup>	$<10^6$		Butane <sup>d</sup>	$3.9 \times 10^7$	
Dichlorodifluoromethane <sup>d</sup>	$<10^6$		Nitromethane	$4.4 \times 10^7$	
Acetonitrile	$1.5 \times 10^6$	$2.7 \times 10^6$	Hexanoic acid	$4.6 \times 10^7$	
Methyl alcohol	$1.6 \times 10^6$	$2.9 \times 10^6$	Diethyl ether	$4.7 \times 10^7$	
Trichlorofluoromethane <sup>d</sup>	$1.7 \times 10^6$		Carbon tetrachloride <sup>d</sup>	$4.8 \times 10^7$	
Ethyl chloride <sup>d</sup>	$1.8 \times 10^6$		Isobutyl alcohol	$6.4 \times 10^7$	$5.0 \times 10^7$
Ethane <sup>d</sup>	$2.5 \times 10^6$		Isopropyl alcohol	$6.5 \times 10^7$	$7.8 \times 10^7$
Acetone	$2.8 \times 10^6$	$2.6 \times 10^6$	Pentane <sup>d</sup>	$7 \times 10^7$	
Cyanoacetic acid	$3.2 \times 10^6$		Tetrahydrofuran	$7.8 \times 10^7$	
Succinic acid	$3.5 \times 10^6$	$2.3 \times 10^6$	Hexyl alcohol	$1.04 \times 10^8$	
<i>N</i> -Acetylglycine	$3.8 \times 10^6$		Isobutane <sup>d</sup>	$1.2 \times 10^8$	
Dichloromethane	$4 \times 10^6$		<i>sec</i> -Butyl alcohol	$1.3 \times 10^8$	$0.95 \times 10^8$
Propionic acid	$6.4 \times 10^6$	$5.9 \times 10^6$	Hexane <sup>d</sup>	$1.5 \times 10^8$	
<i>N</i> -Acetylalanine	$8.0 \times 10^6$		Ethyl bromide	$1.7 \times 10^8$	
Butyric acid	$8.6 \times 10^6$	$7.4 \times 10^6$	Bromoacetic acid	$2.6 \times 10^8$	$3.4 \times 10^8$
Propionitrile	$1.06 \times 10^7$		1,3,5-Benzenetricarboxylic acid	$6.5 \times 10^8$	
Deuterioisopropyl alcohol	$(1.05 \times 10^7)^e$	$1.05 \times 10^7$	Benzoic acid	$8.5 \times 10^8$	$(10.0 \times 10^8)^f$
Chloroform	$1.2 \times 10^7$		Methyl iodide	$\geq 2 \times 10^9$	
Dioxane	$1.3 \times 10^7$		Ethylene	$3 \times 10^9$	<sup>g</sup>

<sup>a</sup> Determined at pH 1. <sup>b</sup> At 15°, absolute rate constants calculated assuming  $k_{H+(CD_3)_2CDOH} = 1.05 \times 10^7 M^{-1} \text{sec}^{-1}$ . <sup>c</sup> At 25°, absolute rate constants taken from ref 11. <sup>d</sup> Single measurement made on saturated solution (at 1 atm for gases). <sup>e</sup> Taken from ref 11 and used as a reference to calculate the absolute values for the other compounds. <sup>f</sup> Taken from ref 3 and used in ref 11 to calculate the absolute values for the compounds measured by the chemical method. <sup>g</sup> Determined in solutions saturated (at 1 atm) with different mixtures of ethylene and nitrogen containing between 1 and 17% ethylene.

$10^8 M^{-1} \text{sec}^{-1}$ . The differences between the different series of compounds are very small for  $C_4$  and larger molecules, presumably because the hydrogen atoms adjacent to the functional group do not contribute in a major way to the overall reactivity in these long-chain molecules. For small or branched molecules very large differences are observed. Structural effects are obviously very important, as might be expected. For example, in the butyl alcohol series, *tert*-butyl alcohol is very unreactive, *n*-butyl alcohol some 500 times as reactive, but isobutyl alcohol (which has a tertiary hydrogen atom) only an additional two times as reactive. *sec*-Butyl alcohol, which has a tertiary type hydrogen similar to that in isopropyl alcohol (*i.e.*, on a carbon to which an OH and two alkyl groups are attached) is the most reactive.

The general region expected for compounds without

special features is indicated by the shaded area of Figure 9. It is seen that molecules such as *tert*-butyl alcohol,  $\alpha$ -aminoisobutyric acid,  $\alpha$ - and  $\beta$ -alanine, urea, and cyclopropane are considerably less reactive than other compounds with a similar carbon number. It is clear that methyl groups, by themselves, offer little reactivity toward hydrogen atoms as is seen from the low rate constants for *tert*-butyl alcohol, methyl chloride, and methane. The hydroxyl group, although showing a strong activating effect on the abstraction of hydrogen from the  $\alpha$  position, as in methanol, has little or no effect on the  $\beta$  positions, as in *tert*-butyl alcohol. The positively charged ammonium group very strongly deactivates the adjacent hydrogen atoms, causing the rate constants for the simple amino acids to be only  $\sim 10^5 M^{-1} \text{sec}^{-1}$  in acid solutions. The reactivities of the basic forms of the amino acids are expected to be a

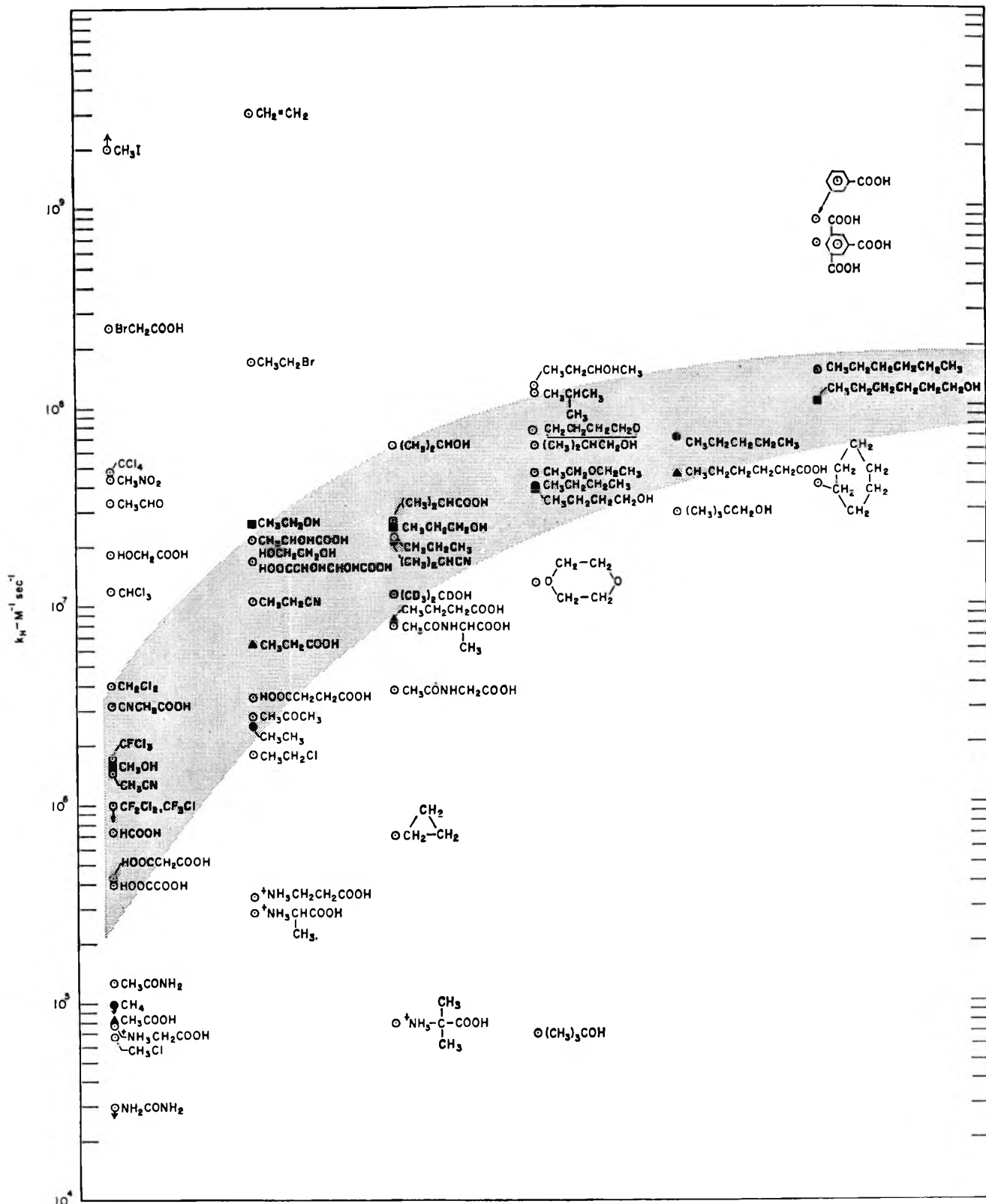


Figure 9. Correlation of hydrogen atom rate constants with molecular complexity. With a few exceptions the abscissa (from 1 to 6) represents the number of carbon atoms which bear abstractable hydrogen atoms. Shaded area represents the region observed for the normal alkanes, acids, and primary alcohols within which compounds without special features can be expected to fall.

few orders of magnitude higher, but have not as yet been measured. *N*-Acetyl substituted glycine and alanine are  $\sim 30$  and  $50$  times as reactive as the acids

themselves showing that the  $\text{CH}_3\text{CONH}$  group has a much weaker effect than the  $\text{NH}_3^+$  group. By comparison with acetamide, the hydrogen abstraction ap-

pears to take place mainly from the amino acid part and not from the acetyl part. Urea shows little or no reactivity toward hydrogen atoms. Abstraction from the  $\text{NH}_2$  groups probably cannot take place, and the addition to the carbonyl group seems, in this case, to be very slow. On the other hand, oxalic acid has a much higher rate constant and the only reaction that can take place is the addition of H (the resulting radical has been observed by esr).<sup>9</sup> In this case the rate constant for addition has also been estimated from chemical studies<sup>11</sup> where, however, measurements had to be carried out at relatively high solute concentrations. At the concentrations employed direct reaction occurred between the oxalic acid and  $e_{\text{aq}}^-$ . The value obtained for the hydrogen atom rate is sensitively dependent on the rate constant assumed for this reaction. In the esr approach one can effectively work at one order of magnitude lower solute concentration so that the scavenging of electrons by the oxalic acid is of lesser importance and in this case the resultant value should be considerably more reliable than that determined chemically. Malonic acid reacts with hydrogen atoms with a rate constant similar to that of oxalic acid, but the mechanism mainly involves abstraction and not addition.<sup>11</sup> This low rate constant compared to that of propionic acid shows the deactivating effect of the second carboxyl group on the abstraction. As in many other of its reactions cyclopropane is quite unreactive and the other cyclic compounds are somewhat less reactive than their normal counterparts. The rate constant obtained for cyclohexane ( $3 \times 10^7 \text{ M}^{-1} \text{ sec}^{-1}$ ) (in good agreement with the absolute determination of  $4 \times 10^7 \text{ M}^{-1} \text{ sec}^{-1}$  by Sauer and Mani<sup>8</sup>) is a factor of 5 less than that for hexane. Cyclopentane, which has a considerably greater solubility than cyclohexane, is about equally reactive.

The order of reactivity of H atoms toward aliphatic compounds generally parallels that of OH radicals.<sup>2,19</sup> The reactivities of the hydrogen atoms at the different positions are in the same order, tertiary > secondary  $\gg$  primary, and the effect of functional groups is similar. However, in the case of H atom reactions many substituents increase the total rate of reaction of the compound by reacting directly with the H atoms. All the compounds above the shaded area in Figure 9 have some especially reactive site. Aromatic rings and double bonds add H atoms with rate constants  $\sim 10^9 \text{ M}^{-1} \text{ sec}^{-1}$ . Abstraction of I and Br from aliphatic iodo and bromo compounds occurs with rate constants of  $\sim 10^9$  and  $10^8 \text{ M}^{-1} \text{ sec}^{-1}$ . Chlorine abstraction, however, is a much slower process (comparable in rate to hydrogen abstraction) and the observed rates for methyl and ethyl chloride are similar to those of their parent hydrocarbons. Multiple chlorination, as in  $\text{CHCl}_3$  and  $\text{CCl}_4$ , results in enhanced reactivity. Addition of H atoms to nitro, aldehyde, cyano, and keto groups also takes place with reactivities decreasing in

that order. Acetonitrile reacts with H atoms mainly by addition<sup>11</sup> as is also clear from the comparison of its rate constant with that of acetic acid. The resulting radical ( $\text{CH}_3\text{CH}=\dot{\text{N}}$ ) has been observed by esr.<sup>20</sup> In the case of cyanoacetic acid, addition and hydrogen abstraction most probably take place at similar rates. It should be noted that, contrary to the case of chloroacetic acid where H abstraction results in the formation of both  $\text{H}_2$  and HCl, no HCN is formed from the reaction of H atoms with cyanoacetic acid.

## Appendix

The purpose of this section is to treat the properties of the esr signals of the hydrogen atom in somewhat greater detail in order to obtain further insight into the nature of the physical process dominating the rate constant  $\lambda$  in eq 4. On several aspects of the problem there is not, at the present, sufficient information for a complete treatment. We will, therefore, only indicate several points which must be considered in any attempt to give an exact description of the real system.

The first problem to be considered is that of the initial nonequilibrium population of the spin levels. Several theories have been advanced<sup>13-15</sup> but little is really known about the source of this phenomenon. The existence of polarization implies a different rate for formation of each of the states which are paired by the allowed transitions indicated in Figure 2. The rates, however, need to be only slightly different because the fractional population difference of the spin levels at equilibrium ( $1 - e^{-h\nu/kT} \sim h\nu/kT = \eta$ ) is typically  $\sim 0.0015$  at room temperature ( $h\nu$  is the transition energy— $4 \times 10^{-5} \text{ eV}$  at X-band,  $k$  the Boltzmann constant, and  $T$  the absolute temperature— $kT = 0.026 \text{ eV}$  at room temperature). In order to get an initial signal enhancement by a factor of 10, the rates need only differ by 1.5%; an amount which is not otherwise chemically significant. Because the H atoms come from two sources, *i.e.*, direct production and from  $e_{\text{aq}}^-$  reaction with  $\text{H}^+$ , the observed effect must be the weighted average from the two if the initial polarizations are different.<sup>21</sup> The inverse situation, differing disappearance reaction rates for the different spin states, is also implied by these various treatments<sup>13-15</sup> and therefore modifications of the level populations during the course of reaction are likely. In fact, the treatment by Adrian<sup>16</sup> achieves nonequilibrium spin populations solely by differing reaction rates for atoms in various spin

(19) M. Anbar, D. Meyerstein, and P. Neta, *J. Chem. Soc. B*, 742 (1966).

(20) P. Neta and R. W. Fessenden, *J. Phys. Chem.*, **74**, 3362 (1970).

(21) A neutral solution containing 0.002 *M* *tert*-butyl alcohol and saturated with  $\text{N}_2\text{O}$  to remove  $e_{\text{aq}}^-$  gave signals similar to those observed in acid but only about 10% of the normal intensity. Presumably these signals represent the hydrogen atoms directly produced in neutral solutions where the total H atom yield should be about  $1/6$  that in acid. These atoms appear to have roughly the same polarization as those produced by the chemical reaction of  $e_{\text{aq}}^-$  with  $\text{H}^+$ .

states. Smaller, in his time-resolved studies, reports<sup>10</sup> both an initial effect and in certain experiments a small post-irradiation increase in the hydrogen atom signal which could result from such differential rates. However, at the present level of understanding this latter effect cannot be adequately treated and will be neglected here. In the treatment to follow, this neglect means taking the chemical disappearance rate constant to be the same for both spin states.

Several observations during the present work which bear on the polarization phenomenon should be reported. Table III gives the H-atom and D-atom signal heights for solutions of H<sub>2</sub> and D<sub>2</sub>. In this case the OH initially produced in the water reacts with H<sub>2</sub> (or D<sub>2</sub>) to produce H atoms (or D atoms). From the inverted low-field line it is seen that formation of D atoms by the reaction OH + D<sub>2</sub> → HDO + D results in initial polarization. The height of the lines is very small reflecting in part the smaller hyperfine constant.<sup>14</sup> However, it is also observed that the H-atom signal grows upon addition of D<sub>2</sub>. This effect appears to be related, at least in part, to the effect produced by solutes like *tert*-butyl alcohol where an increase results from the removal of oxygenated reaction products of OH. The reaction OH + H<sub>2</sub> → H<sub>2</sub>O + H would also partially explain the increase in H atom signal obtained in H<sub>2</sub> saturated solutions because, by analogy with the D<sub>2</sub>-saturated system, the total yield of polarized atoms is expected to be increased.

**Table III:** Low-Field Emission Signals from Solutions Saturated with H<sub>2</sub> and D<sub>2</sub>

Sample	Relative signal intensity	
	H atom	D atom
N <sub>2</sub> saturated	3.9 <sup>a</sup>	
D <sub>2</sub> saturated	5.6	0.2 <sup>b</sup>
H <sub>2</sub> saturated	7.9	

<sup>a</sup> Relative signal intensity is 7.9 in the presence of 0.002 *M tert*-butyl alcohol. <sup>b</sup> This signal, which is observed in emission, is absent in the presence of  $2 \times 10^{-3}$  *M tert*-butyl alcohol. The high-field D-atom line is observed in absorption at approximately twice the signal intensity.

With the reservations expressed in the first paragraph of this Appendix it is possible to calculate the power saturation behavior of the esr lines and also the way in which  $\lambda$  should vary with power. It is assumed that the hydrogen atoms are formed with a certain initial population difference between the levels connected by an allowed transition and that the only important relaxations are between these levels (see Figure 2). Under these assumptions the treatment is similar to that given for the direct observation of the saturation process.<sup>22</sup>

First we will consider the case where hydrogen atoms

are continuously produced at a rate  $P_H$  (in  $M \text{ sec}^{-1}$ ) so that each of the spin states is produced at a rate  $\sim 1/4 P_H$ . The production rate  $P_n = 1/2 P_H(1 + V) \cdot \eta N$  can be considered as applying to the population difference per unit volume,  $n$ , between the states within a pair.  $N$  is Avogadro's number which is included to convert the spins produced to molecular units,  $\eta$  is  $h\nu/kT$  as indicated above, and  $V$  is the enhancement factor  $[(n_0 - n_e)/n_e]$  which describes the excess in the initial population difference,  $n_0 - n_e$ , relative to the difference,  $n_e$ , at equilibrium (in concentration units). Experimentally  $V + 1$  is the ratio of the initial absorption to that which would be observed for the same number of radicals in spin equilibrium.  $V$  may have either positive or negative values and emission corresponds to a negative value for  $V + 1$ . The population of the spin states can be altered either by relaxation processes (which conserve the total number of spins) or by chemical reactions (which destroy spins). The rate of change of the population difference between the paired levels (to which the esr signal is proportional) is given by the kinetic expression

$$\frac{dn}{dt} = -\frac{(n - n_e)}{T_1} - (2W + k_r[R] + k_s[S])n + P_n \quad (\text{V})$$

where  $T_1$  is the spin-lattice relaxation time which describes the thermal approach to equilibrium,  $W$  is the probability per unit time of radiation-induced transitions, and  $k_s[S]$  and  $k_r[R]$  are the pseudo-first-order rate constants for reactions of hydrogen atoms with solutes S and other radicals R. Hydrogen atoms which react with other hydrogen atoms are treated as part of the  $k_r[R]$  term. The steady-state solution ( $dn/dt = 0$ ) is

$$n_{ss} = \frac{P_n + n_e/T_1}{\frac{1}{T_1} + 2W + k_r[R] + k_s[S]} \quad (\text{VI})$$

At steady state  $n_e$  is  $1/2[H]_{ss}\eta N$ , and the hydrogen atom concentration,  $[H]_{ss}$ , is  $P_H/(k_s[S] + k_r[R])$  so that

$$n_e = 1/2 P_H \eta \cdot N / (k_r[R] + k_s[S]) \quad (\text{VII})$$

Taking the value of  $P_n$  given above, the population difference at steady state,  $n_{ss}$ , is

$$n_{ss} = \frac{1}{2} P_H \eta N \left[ \frac{V + 1 + \frac{1}{T_1(k_r[R] + k_s[S])}}{\frac{1}{T_1} + 2W + k_r[R] + k_s[S]} \right] \quad (\text{VIII})$$

At the center of a Lorentzian line  $W = 1/2 \gamma^2 H_1^2 T_1 T_2$  where  $\gamma$  is the magnetogyric ratio for the radical,  $H_1$  is the microwave magnetic field which is proportional to the square root of the power, and  $T_2$  is the spin-spin

(22) G. Bürk and G. Schoffa, *Z. Naturforsch. A*, **21**, 296 (1966).

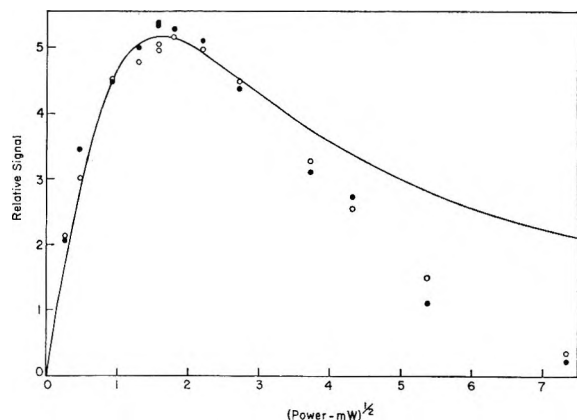


Figure 10. Relative signal intensity of low-field (●) and high-field (○) lines as a function of microwave magnetic field ( $\propto P^{1/2}$ ). Indicated curve represents normal saturation dependence of an absorption line.

relaxation time. The esr signal  $H$  is proportional to  $n_{ss}H_1$  so that at steady state

$$H_{ss} \propto P_H H_1 \left\{ \frac{V + 1 + \frac{1}{T_1(k_r[R] + k_s[S])}}{\frac{1}{T_1} + k_r[R] + k_s[S] + \gamma^2 T_2 H_1^2} \right\} \quad (\text{IX})$$

At constant current this expression is of the same form [ $\propto H_1/(1 + cH_1^2)$ ] as that for normal power saturation. The curve of signal *vs.*  $H_1$  for both the high- and low-field lines is shown in Figure 10. These are reasonably superimposable so that  $T_2$  cannot be far different for the two transitions. It should be recognized that the equation refers to the peak of the absorption curve and that we are taking a second derivative so that the actual form of the observed dependence of signal height will be somewhat different. As a further complication the modulation frequency is greater than the reciprocal of  $T_1$  so that there are certain to be rapid passage effects which can further distort the behavior. All arguments related to the magnitude of  $T_1$  given here are, however, derived from competition studies against chemical reactions so that these complications are not expected to affect the conclusions drawn on this point.

The chemical studies illustrated in Figure 5 show that both lines are equally affected by the addition of methanol so that within experimental error  $(1/T_1) + (\gamma^2 T_2 H_1^2) + k_r[R]$  has the same value for each of the transitions. Given that  $T_2$  is the same for both transitions, as indicated by the power dependence,  $T_1$  must also be similar but small differences could be masked by other effects.

A comparison of eq IX for the cases of the presence and absence of solutes gives

$$\frac{H_0}{H} - F = \frac{k_s[S]}{\lambda} F \quad (\text{X})$$

where  $\lambda$  is  $(1/T_1) + 2W + k_r[R]$  and  $F$  is  $[(V + 1 +$

$(T_1 k_r[R])^{-1}]/[V + 1 + (T_1(k_r[R] + k_s[S]))^{-1}]$ . For the case of emission  $F_e < 1$  and for enhanced absorption  $F_a > 1$ . From Figure 5 it appears that  $|F_e| \sim F_a \sim 1$  so that  $V + 1$  must be large with respect to  $1/T_1 k_r[R]$ . In this case eq X becomes identical with eq IV and  $\lambda$  can be identified with the relaxation constant used empirically in the main text which has a value  $\sim 1.2 \times 10^4 \text{ sec}^{-1}$ . Studies of the current and power dependence indicate that under the normal conditions employed here it can approximately be broken down into the individual terms  $1/T_1 \sim 4 \times 10^3 \text{ sec}^{-1}$ ,  $2W \sim 5 \times 10^3 \text{ sec}^{-1}$ , and  $k_r[R] \sim 3 \times 10^3 \text{ sec}^{-1}$ . The latter term can be rationalized with the production rate if it is assumed that hydrogen atoms and the radicals present react with a rate constant  $\sim 3 \times 10^9 M^{-1} \text{ sec}^{-1}$ . At the power represented by the lower curve in Figure 3, the second term is small and  $k_r[R] \sim 1/T_1$  so that an approximate  $3/4$  power dependence on beam current should be observed, as has been noted above.

For a group of radicals formed at a particular time within a steady-state experiment the time dependence  $n'(t)$  of the corresponding population difference  $n'$  can be given by solving the appropriate modification of eq V which takes into account the fact that the equilibrium population difference of the particular group of radicals under consideration decreases as a result of chemical reactions.

$$\frac{dn'}{dt} = -\frac{n' - (n'_e)_0 e^{-(k_r[R] + k_s[S])t}}{T_1} - (2W + k_r[R] + k_s[S])n' \quad (\text{XI})$$

For a steady-state experiment (but not for a pulsed experiment)  $[R]$  is constant with time and the solution of (XI) is

$$n'(t) = (n'_e)_0 \left\{ \left( 1 + V - \frac{1}{1 + 2WT_1} \right) e^{-(\lambda + k_s[S])t} + \frac{e^{-(k_r[R] + k_s[S])t}}{1 + 2WT_1} \right\} \quad (\text{XII})$$

Plots of  $n'(t)/(n'_e)_0$  are given in Figure 11 for various possible idealized conditions. It is important to recognize, as can be readily seen in the figure, that the long term tail can make a very significant contribution if the hydrogen atoms are not removed from the system by chemical reactions after relaxation has taken place. In the absence of added solute (curves C and C') this removal must occur as a result of reaction with the background of radicals. Under the normal experimental conditions removal by this means is quite effective as can be seen by comparing curves B and C. In the presence of significant concentrations of solute the signals should decay to zero very nearly exponentially, with a time constant equal to  $\lambda + k_s[S]$ . Under these conditions the treatment in the main text becomes the limiting approximation of that given here.

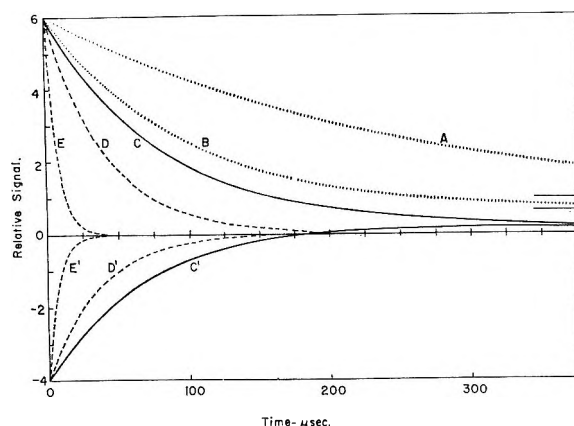


Figure 11. Decay of esr signal of hydrogen lines predicted from eq XII ( $V = 5$ ,  $1/T_1 = 4 \times 10^3 \text{ sec}^{-1}$ ,  $k_s = 1.6 \times 10^6 M^{-1} \text{ sec}^{-1}$ ) for various possible experimental conditions. High-field line starts at +6, low-field line at -4. A: Low current, low power, no solute ( $k_r[\text{R}] = 0$ ,  $2W = 0$ ,  $[\text{S}] = 0$ ), signal decays exponentially from  $V + 1$  to 1 with a time constant  $1/T_1$ . B: Low current, high power, no solute ( $k_r[\text{R}] = 0$ ,  $2W = 6600 \text{ sec}^{-1}$ ,  $[\text{S}] = 0$ ), signal decays exponentially from  $V + 1$  to  $(1)/(1 + 2WT_1)$  with a time constant  $(1/T_1) + 2W$ . Long time limits of A and B are indicated by the lines on the right. C and C': Finite current, high power, no solute, ( $k_r[\text{R}] = 3 \times 10^3 \text{ sec}^{-1}$ ,  $2W = 6600 \text{ sec}^{-1}$ ,  $[\text{S}] = 0$ ) long term tail is suppressed by chemical reaction of hydrogen atoms with background of radicals and goes to zero at very long times. D and D': Same current and power as in C but sufficient solute to reduce the steady state signal by 50%. E and E': Same current and power as in C but sufficient solute to reduce the signal by 90%.

The buildup of the population difference with irradiation is given by summing the contributions from all radicals produced at time  $t'$  during the irradiation period. It can be shown that for long irradiation periods the expression obtained is identical with the steady-state description given in eq VIII. From this it is seen that the term  $[T_1(k_r[\text{R}] + k_s[\text{S}])]^{-1}$  in the numerator of eq VII is the result of a contribution from hydrogen atoms which have attained spin equilibrium but are still present in the background.

The ratio of intensities of the high- and low-field lines is, from eq IX

$$H_H/H_L = \frac{V_H + 1 + \frac{1}{T_1(k_r[\text{R}])}}{V_L + 1 + \frac{1}{T_1(k_r[\text{R}])}} \quad (\text{XIII})$$

Under the conditions of most of the comparisons  $k_r[\text{R}] \sim 1/T_1$  so that

$$\frac{H_H}{H_L} \simeq \frac{V_H + 2}{V_L + 2} \quad (\text{XIV})$$

Since  $V_L$  is negative  $H_H/H_L$  should be  $< -1$  if  $|V_L| = V_H$ . Experimentally the observed ratio is very nearly  $-1$ . Barring gross differences in the enhancement factors of the two lines it is again seen that their magnitudes must be moderately large. Double integration of first derivatives of each of the lines under low modulation conditions gives the ratio of peak intensities as  $\sim -0.8$ . If the departure from the expected value is real it implies that  $V_H < |V_L|$ .

A comparison of the integrated absolute hydrogen atom signal intensities with that of the acetate radical anion produced under similar conditions indicates that  $V$  is  $\sim 4$  if it is assumed that the hydrogen atom yield is  $\sim 3$ . If  $V$  were this small then in the absence of solute the low-field line should be observed in absorption (and not emission) at low currents. All of the chemical arguments given above also indicate that the enhancement factor must be relatively large (*i.e.*,  $\sim 10$  or larger). Thus it is clear that with the treatment given here a question remains as to why the hydrogen atom signal intensities are not even greater than those observed. It is probable that a more rigorous treatment can explain these discrepancies. However, such a treatment seems impractical until more data from direct observations on the time dependence of the hydrogen atom signals become available and until the theoretical aspects of these spin-polarization phenomena become more fully developed.



## Chlorophyll-Poly(vinylpyridine) Complexes. III. Photochemical

## Activity and Fluorescence Yield

by G. R. Seely

*Charles F. Kettering Research Laboratory,<sup>1</sup> Yellow Springs, Ohio 45387 (Received December 16, 1970)**Publication costs assisted by the Charles F. Kettering Research Laboratory*

The fluorescence of denser aggregates of pyrochlorophyll bound to poly(vinylpyridine) is partially quenched, probably by transfer of energy to "quenching centers," consisting of interacting pairs of pigment molecules. The quantum yield for the photoreduction of *p*-dinitrobenzene by hydrazobenzene, sensitized by pyrochlorophyll in these aggregates, is almost directly proportional to the quantum yield of fluorescence. It is concluded that a reactive metastable state, such as the triplet, is not formed in the process of self-quenching of pyrochlorophyll fluorescence in this system.

## Introduction

In the first paper of this series,<sup>2</sup> the formation of complexes between chlorophyll or its derivatives and poly(4-vinylpyridine), and some of their absorption and fluorescence spectral properties, were described. In the second paper,<sup>3</sup> the probability of nonradiative energy transfer was examined as a function of pigment density in the polymer complex.<sup>4</sup> These systems are of interest as a novel approach to the synthesis of artificial aggregates of chlorophyll having properties like those of the natural photosynthetic unit of the green plant.

One of the more notable properties of the poly(vinylpyridine) complexes is the self-quenching of chlorophyll fluorescence when the density of pigment molecules on the polymer is high. Sparsely distributed on the polymer, chlorophyll fluoresces with an intensity normal for true solutions. Densely distributed, the fluorescence is 90–95% quenched. Efficient quenching at chlorophyll coverages well below saturation was attributed to nonradiative transfer of excited state energy to quenching centers consisting of pairs of chlorophyll molecules, associated in some way on the polymer.<sup>2</sup> The energy of interaction between such pairs of chlorophyll molecules was estimated to be about 1 kcal/mol. The quenching would then be a form of concentration quenching of the kind proposed by Perrin,<sup>5</sup> discussed in some detail by Förster,<sup>6</sup> and examined experimentally by Levshin, *et al.*, with several dyes in concentrated solution.<sup>7</sup>

The question examined in this paper is whether singlet excited chlorophyll is quenched by internal conversion to the ground state or by intersystem crossing to a reactive, metastable triplet state. The question is important to photosynthesis. The fluorescence yield of chlorophyll in the chloroplast is of similar magnitude to that in our dense aggregates,<sup>8</sup> yet the photochemical efficiency is quite high. It is not known whether chlorophyll reacts in its singlet excited or triplet excited state in photosynthesis, and it was hoped that the present work with a model system might shed some light on this question.

Our approach is basically quite simple. The quantum yield of fluorescence is compared with the quantum yield of a reaction known to be sensitized by the triplet excited state. If the photoreaction persists at pigment densities great enough to quench fluorescence, it is evident that an appreciable number of singlet excited states are converted into triplets in the process of quenching.

The photoreaction chosen was the sensitized reduction of *p*-dinitrobenzene (DNB) by hydrazobenzene, previously studied in ethanol-pyridine solution.<sup>9</sup> Like many other reactions sensitized by chlorophyll,<sup>10</sup> it is evidently initiated by electron transfer from the photoexcited pigment to DNB. As before,<sup>3,9</sup> we used the more stable pyrochlorophyll (10-decarbomethoxychlorophyll), in place of chlorophyll, with reasonable confi-

duction of *p*-dinitrobenzene (DNB) by hydrazobenzene, previously studied in ethanol-pyridine solution.<sup>9</sup> Like many other reactions sensitized by chlorophyll,<sup>10</sup> it is evidently initiated by electron transfer from the photoexcited pigment to DNB. As before,<sup>3,9</sup> we used the more stable pyrochlorophyll (10-decarbomethoxychlorophyll), in place of chlorophyll, with reasonable confi-

(1) Contribution No. 420.

(2) G. R. Seely, *J. Phys. Chem.*, **71**, 2091 (1967).(3) G. R. Seely, *ibid.*, **74**, 219 (1970).(4) In our discussion of the value of the critical energy transfer distance  $R_0$  in the preceding reference, we failed to cite the values of A. G. Tweet, W. D. Bellamy, and G. L. Gaines, Jr., *J. Chem. Phys.*, **41**, 2068 (1964), of ca. 54 Å for chlorophyll-chlorophyll transfer, and 40 Å for chlorophyll-Cu pheophytin transfer, in dilute monolayers. Although the experimental conditions are somewhat different, these values should be comparable with our value of 42 Å for pyrochlorophyll-pyrochlorophyll transfer.(5) F. Perrin, *C. R. Acad. Sci., Paris*, **192**, 1727 (1931).

(6) T. Förster, "Fluoreszenz Organischer Verbindungen," Vandenhoeck and Ruprecht, Göttingen, 1951, Chapter 11.

(7) V. L. Levshin, *Izv. Akad. Nauk SSSR, Ser. Fiz.*, **20**, 397 (1956); V. L. Levshin and L. V. Krotova, *Opt. Spektrosk.*, **13**, 809 (1962) [*Opt. Spectrosc.*, p 457].(8) P. Latimer, T. T. Bannister, and E. I. Rabinowitch in "Research in Photosynthesis," H. Gaffron, *et al.*, Ed., Interscience Publishers, Inc., New York, N. Y., 1957, p 107.(9) G. R. Seely, *J. Phys. Chem.*, **73**, 117 (1969).(10) G. R. Seely, *ibid.*, **69**, 2779 (1965).

dence that the results with chlorophyll would have been essentially the same.

### Experimental Section

We have previously described the preparation or purification of pyrochlorophyll,<sup>2</sup> poly(4-vinylpyridine),<sup>3</sup> nitromethane,<sup>3</sup> hydrazobenzene,<sup>9</sup> and *p*-dinitrobenzene.<sup>9</sup> The polymer sample was a fraction of molecular weight 440,000.

As in previous work,<sup>3</sup> a portion of a stock solution of pyrochlorophyll in benzene and a small amount (0.005 ml) of purified  $\alpha$ -methyl-naphthalene were introduced into a cuvette, the benzene was evaporated in a stream of  $N_2$ , and the solution of pyrochlorophyll in  $\alpha$ -methyl-naphthalene was diluted with *ca.* 4 ml of nitromethane. The fluorescence intensity was measured to confirm the absence of large amounts of polar impurities.<sup>2</sup> To the cuvette were added about 5 mg of hydrazobenzene and appropriate amounts of stock solutions of poly(vinylpyridine) and DNB in nitromethane, the contents were flushed thoroughly with  $N_2$ , and the fluorescence was determined again. Fluorescence was also determined after the reaction and after the addition of 0.1 ml of pyridine to dissociate pyrochlorophyll from the polymer. Fluorescence intensity after the reaction differed little from that before. Absorption spectra were also recorded on a Cary 14R spectrophotometer at these times.

Fluorescence was measured, and the quantum yield corrected for reabsorption and secondary fluorescence, in apparatus and by procedures described before.<sup>3,11</sup> Fluorescence yields were calculated relative to the value 0.228 already determined for pyrochlorophyll in the presence of excess polymer.<sup>3</sup> Based on this value, the quantum yield of fluorescence in the presence of 0.1 ml of pyridine in nitromethane was 0.197, and this served as an internal standard for the determination of the quantum yield of fluorescence in each run.

Measurements were made at various ratios of the polymer pyridine unit concentration to pyrochlorophyll concentration, (py)/(chl), which is the primary independent variable of the system and which determines the quantum efficiency of fluorescence.<sup>2,3</sup>

The photoreaction was activated by light from a tungsten projector lamp focused through a 670-nm interference filter. The light absorbed was measured by difference with an Eppley thermopile. Changes in the visible absorption spectrum after intervals of illumination were followed with the Cary spectrophotometer.

The quantum yields reported are for the production of azobenzene from hydrazobenzene. The distribution of products of reduction of DNB is not known in detail, but the principal one appears to be *p*-nitrophenylhydroxylamine, which has an absorption band in the violet near the beginning of nitromethane absorption. In reactions that were driven to completion, the

mole ratio of azobenzene produced to DNB initially present was about 2.3 (*cf.* 2.21 in ethanol-pyridine<sup>9</sup>).

Azobenzene in nitromethane has a band centered about 444 nm. To reduce interference from pyrochlorophyll, the appearance of azobenzene is better measured at 470 nm where the absorptivity is  $334 M^{-1} cm^{-1}$ . The absorption increase at 400 nm, due to products of reduction of DNB, is larger than but linearly correlated with the increase at 470 nm. Quantum yields could be calculated with greater precision from the absorbance change at 400 nm and the slope of a plot of that change,  $\Delta\rho_{400}$ , against the absorbance change at 470 nm,  $\Delta\rho_{470}$ . The ratio  $\Delta\rho_{400}/\Delta\rho_{470}$  was determined for each run and ranged from 3.74 at (py)/(chl) = 534 to 2.89 at (py)/(chl) = 9. With 0.23 *M* 4-ethylpyridine in place of polymer, the ratio was 6.50.

The quantum yield declined linearly as the reaction progressed, in such manner as to suggest product inhibition of the later steps in the reduction of the nitro compound. Quantum yields during each run were therefore extrapolated back to their initial values, and only these are reported. In ethanol-pyridine solution, the quantum yield was constant until the DNB was almost consumed.<sup>9</sup>

Measurements were made at room temperature, *ca.* 24°. A low relative humidity is necessary for successful experimentation with this system; during these runs it was  $\leq 35\%$ .

*Association between Components.* Proper interpretation of the data required that unintended associations between the reagents in nitromethane be absent. The attachment of pyrochlorophyll to the polymer was verified by the absorption spectrum<sup>2</sup> and was not affected by the presence of hydrazobenzene and DNB. The interaction, if any, between hydrazobenzene, DNB, and poly(vinylpyridine) was investigated with a Varian A-60 nuclear magnetic resonance spectrometer.

The methyl group of nitromethane absorbs at  $\delta$  4.4 with respect to tetramethylsilane internal standard. One of the  $C_{13}$  peaks flanking this band, at  $\delta$  5.67, affords a convenient reference point for the aromatic proton resonance bands of the solutes.

In 1-2% solutions of poly(4-vinylpyridine) there are two broad, equally intense bands at 63 and 163 Hz below the  $C_{13}$  band. DNB, 0.06 *M*, has a single sharp band 174 Hz below the  $C_{13}$  band. Hydrazobenzene, 0.06 *M*, has a complex group of bands between 72 and 114 Hz below the  $C_{13}$  band and a small band at 36 Hz. None of these bands was appreciably altered in position or shape by the presence of one of the other solutes at these concentrations.

A mixture of solutions concentrated in DNB and in hydrazobenzene has a yellow color owing to increased absorption in the violet. The method of continuous variations, at 0.27 *M* total concentration, indicated

(11) G. R. Seely, *J. Phys. Chem.*, **73**, 125 (1969).

the formation of a 1:1 complex between the two compounds, probably of the charge-transfer type. There was no departure from spectral additivity at  $2.7 \times 10^{-3} M$  total concentration. The nmr spectra at  $0.27 M$  total concentration did not show appreciable deviations from additivity.

In summary, although there is evidence of a small degree of complex formation between DNB and hydrazobenzene at high concentration, there is no evidence of complex formation between any of the solutes at the concentrations used, except of course between pyrochlorophyll and the polymer.

### Results

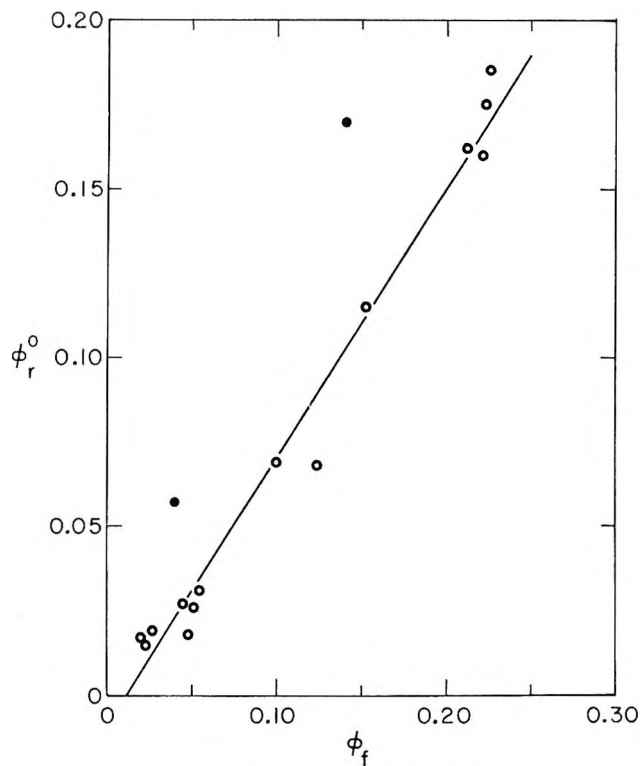
The results listed in Table I include a series in which (py)/(chl) is varied at constant DNB concentration and series in which the DNB concentration is varied at fixed high and low (py)/(chl) ratios. The DNB concentration in the first series is too low to cause appreciable quenching of fluorescence by itself, so that the photoreactions must be sensitized by the triplet state of pyrochlorophyll only. At  $10^{-2} M$  DNB, fluorescence in sparse aggregates is about one third quenched and reaction sensitized by the singlet excited state of pyrochlorophyll is to be expected.

**Table I:** Photoreduction of *p*-Dinitrobenzene by Hydrazobenzene, Sensitized by Pyrochlorophyll-Poly(vinylpyridine) Complexes in Nitromethane. Comparison Initial of Quantum Yield of Reduction,  $\Phi_r^{(0)}$ , with Pyrochlorophyll Fluorescence Yield,  $\Phi_f^a$

$10^3(\text{chl})$ , <i>M</i>	$10^4(\text{DNB})$ , <i>M</i>	(py)/(chl)	$\Phi_r^{(0)}$	$\Phi_f$
1.5	3.8	534	0.185	(0.228)
1.5	4.3	237	0.162	0.213
1.5	4.3	118	0.115	0.154
1.6	4.3	111	0.118	...
1.6	4.4	60	0.068	0.125
1.6	4.3	30	0.031	0.055
1.6	4.8	28	0.026	0.052
1.9	3.6	9	0.018	0.048
2.4	4.3	80	0.069	0.101
2.4	102	334	0.17	0.142
2.4	3.9	365	0.175	0.224
2.5	0.79	324	0.16	0.223
2.1	106	22	0.057	0.040
2.0	55.5	22	0.017	0.020
2.3	16.7	20	0.015	0.023
2.2	8.6	21	0.027	0.045
2.2	4.4	22	0.019	0.027
2.7	4.4	<i>b</i>	0.205	0.197

<sup>a</sup> (chl) = pyrochlorophyll concentration, (DNB) = *p*-dinitrobenzene concentration, (py)/(chl) = ratio of polymer pyridine units to pyrochlorophyll. Hydrazobenzene concentration in the range  $6.1\text{--}7.6 \times 10^{-3} M$ . <sup>b</sup> 4-Ethylpyridine,  $0.23 M$ , in place of polymer.

With the exception of runs in which  $[\text{DNB}] \cong 10^{-2} M$ , the quantum yield data are quite well repre-



**Figure 1.** Plot of initial quantum yield,  $\Phi_r^{(0)}$ , of sensitized photoreduction of DNB by hydrazobenzene against quantum yield of fluorescence of pyrochlorophyll,  $\Phi_f$ , in the same solution. Data of Table I:  $\circ$ ,  $[\text{DNB}] < 10^{-2} M$ ;  $\bullet$ ,  $[\text{DNB}] \cong 10^{-2} M$ . Least-squares line correlates former data points.

sented by the linear correlation in Figure 1. That is, the initial quantum yield of reaction is almost directly proportional to the quantum yield of fluorescence. This clearly argues against the formation of any sort of reactive metastable state<sup>12</sup> as a result of self-quenching of fluorescence, with a lifetime much greater than that of the excited singlet state.

When  $[\text{DNB}] = 10^{-2} M$ , and (py)/(chl) = 334, the quantum yield for reaction is about the same as at lower DNB concentrations, though fluorescence is partly quenched. In previous work,<sup>11</sup> the quantum yield for the reaction of nitro compounds with the singlet excited state of pyrochlorophyll was deduced to be somewhat less than that for reaction with the triplet excited state. The present result is consistent with this.

When  $[\text{DNB}] \cong 10^{-2} M$ , and (py)/(chl) = 22, the quantum yield observed is accounted for if (1) quenching by DNB is competitive with self-quenching, and (2) the quantum yield of reaction initiated by singlet pyrochlorophyll is about 0.17. It is not necessary to suppose that DNB reacts with the product of self-quenching.

(12) The metastable state need not be a triplet; the formation of the ion pair  $\text{Chl}^+ \cdot \text{Chl}^-$  as a result of quenching by two interacting pyrochlorophylls is entirely conceivable, but such an ion pair, if long-lived, should react with both hydrazobenzene and DNB.<sup>11</sup>

Examination of Table I shows that the quantum yield of self-quenched preparations is not tightly correlated with the value of  $(py)/(chl)$ . On the basis of previous experience with the system,<sup>2,3</sup> it is reasonable to conjecture that the actual fluorescence intensity is affected by minute amounts of polar impurities which serve to dissociate quenching pairs of pyrochlorophyll. This does not diminish but rather affirms the significance of the correlation between the two quantum yields.

### Discussion

Induced intersystem crossing to the triplet state is a well-supported mechanism for quenching of fluorescence by foreign molecules containing heavy atoms, such as bromobenzene.<sup>13</sup> Self-quenching through formation of triplet states is indicated in many of the systems studied by Kautsky, *et al.*, in their research on fluorescence, phosphorescence, and reactivity of dyes in solution and in aggregates.<sup>14</sup> Formation of a long-lived excited state has been postulated for the self-quenching of eosin bound to poly(vinylpyrrolidone),<sup>15</sup> but in view of the complexity of the mechanisms of photoreaction of this dye,<sup>16</sup> the long-lived state may not be a triplet.

The yield of triplet states on excitation of chlorophyll in dilute solution is high, but is low or zero in concentrated solutions or solid solutions in which fluorescence is quenched.<sup>17,18</sup> No triplet states could be detected in green leaves.<sup>18,19</sup>

Cellarius and Mauzerall<sup>20</sup> reported that pheophytin adsorbed onto polystyrene particles retained the ability to sensitize the reduction of an azo dye even when the coverage was such that fluorescence was almost entirely quenched. The intervention of a long-lived state is implied. The work of Nekrasov, *et al.*,<sup>21</sup> with chlorophyll adsorbed onto polymer particles points to the

same relationship between fluorescence and photoreactivity.

It is not clear why self-quenching of fluorescence should produce triplet or at least metastable states of chlorophyll and its derivatives in some cases and not in others. Perhaps attachment to a solid support is necessary to induce intersystem crossing or to stabilize a triplet state once formed. The pyrochlorophyll-poly(vinylpyridine) aggregate resembles concentrated solutions and green leaves in that quenching of fluorescence does not result in the formation of observable amounts of metastable states.

*Acknowledgments.* This work was supported in part by National Science Foundation Grant No. GB-7893. We appreciate the assistance of Dr. J. Corbin with the nmr spectroscopy and in the interpretation of the spectra, and the able technical assistance of Mr. T. H. Meyer.

(13) T. Medinger and F. Wilkinson, *Trans. Faraday Soc.*, **61**, 620 (1965); P. G. Bowers and G. Porter, *Proc. Roy. Soc., Ser. A*, **299**, 348 (1967).

(14) H. Kautsky, A. Hirsch, and W. Flesch, *Ber. Deut. Chem. Ges.*, **68**, 152 (1935).

(15) J. S. Bellin and G. Oster, *J. Amer. Chem. Soc.*, **79**, 2461 (1957).

(16) T. Ohno, S. Kato, and M. Koizumi, *Bull. Chem. Soc. Jap.*, **39**, 232 (1966).

(17) P. G. Bowers and G. Porter, *Proc. Roy. Soc., Ser. A*, **296**, 435 (1967).

(18) G. Porter and G. Strauss, *ibid.*, **295**, 1 (1966).

(19) G. T. Rikhireva, L. A. Sibel'dina, Z. P. Gribova, B. S. Marinov, L. P. Kayushin, and A. A. Krasnovskii, *Dokl. Akad. Nauk SSSR*, **181**, 1485 (1968).

(20) R. A. Cellarius and D. Mauzerall, *Biochim. Biophys. Acta*, **112**, 235 (1966).

(21) R. Kapler and L. I. Nekrasov, *Biofizika*, **11**, 420 (1966) (*Biophysics*, p 477); L. I. Nekrasov, A. N. Kiseleva, and N. I. Kobozev, *Biofizika*, **11**, 977 (1966) (*Biophysics*, p 1118).

# The Radiation Chemistry of Polyethylene. XI. The Molten State<sup>1</sup>

by M. Budzoi

*Department of Chemistry and Materials Research Center, Northwestern University, Evanston, Illinois 60201*

and Malcolm Dole\*

*Department of Chemistry, Baylor University, Waco, Texas 76703 (Received August 10, 1970)*

*Publication costs assisted by Baylor University*

Conclusions from the irradiation of a linear polyethylene in the molten state at 155° are the following. (1) There is marked increase of the cross-link yield on passing from the crystalline to the liquid state. (2) At high doses the yield of vinylene double bonds is considerably greater than predicted from the application of the Dole, Milner, and Williams equation to the low-dose data. (3) Material balance is not quite achieved between hydrogen evolution, double bond, and cross-link formation (values extrapolated to zero dose) indicating a small amount of intramolecular cross-linking with a *G* value of *ca.* 0.7. (4) Vinyl group decay is best described by second-order decay kinetics combined with zero-order growth. The latter process is insufficient, however, to account for the small initial *G* value of chain scissions equal to about 0.4. Although conjugated dienes cannot be detected by infrared analysis, the results of the ultraviolet absorption studies indicate a small amount of diene formation, possibly of the *cis-trans* or *cis-cis* configuration.

## Introduction

Some years ago Williams and Dole<sup>2</sup> compared the radiolytic behavior of a high-density polyethylene (PE) at 25 and 142°. They found that the hydrogen, cross-link, and *trans*-vinylene double bond yields all increased with temperature, and that the vinyl group decay was somewhat greater at 142° than at room temperature. Later, Lyons<sup>3</sup> found a much smaller decay of the vinyl group in the molten state during an investigation that covered the range from 30 to 175°. In the case of a high-density PE, Marlex 6002, *G*(-Vi) fell from 5.6 at 125° to 1.8 at 150° (average *G* values over the first megarad of irradiation). He pointed out that the vinyl absorption band at 908 cm<sup>-1</sup> was crystallinity sensitive which was not taken into account by Williams and Dole. In Williams and Dole's experiments<sup>2</sup> the vinyl decay rate at room temperature was essentially equal to that at 142° if the room temperature samples were heated to 142° and then allowed to recrystallize after the irradiation. Dole, Fallgatter, and Katsuura<sup>4</sup> made the pertinent observation that melting and recooling a PE film after about 50% of the vinyl groups had decayed by radiolysis at room temperature restored the vinyl decay constant to its initial value.

Infrared studies by Williams and Dole<sup>2</sup> showed the existence of no absorption band at 990 cm<sup>-1</sup> after irradiation at 142° although one was produced by the irradiation at room temperature. This band had originally<sup>5</sup> been attributed to the formation of cyclic groups or "ringlinks," but later Fallgatter and Dole,<sup>6</sup> on the basis of ultraviolet studies concluded that it was the result of the radiolytic production of diene groups. Slovokhotova, Koritskii, and Buben<sup>7</sup> had earlier made the same suggestion. Silverman and Nielsen,<sup>8</sup> in pulse

radiolysis experiments on a molten high-density polyethylene, found no increase in the uv absorption band in the range 215–243 nm on irradiation. Despite this apparent agreement between the uv and ir results with respect to the lack of diene formation in the molten state, we wished to repeat the ir and uv studies to higher doses, not only to investigate further the possibility of diene or other polyene group formation, but also to reexamine the question of the rate of vinyl decay. At the same time vinylene growth and gel formation could also be reinvestigated.

## Experimental Section

**Materials.** For the uv studies Marlex 6009 PE containing no antioxidant was used in the form of a film 3 mils thick. Its density was 0.951 g cm<sup>-3</sup> as measured in this laboratory; weight and number average molecular weights as supplied by the manufacturer were 133,000 and 11,600, respectively. Its initial unsaturation was all terminal vinyl. For the other studies Marlex 6002 PE, density equal to 0.962, in the form of 10.5-mil thick film was used. Its properties have been described previously.<sup>1</sup>

(1) Paper X of this series: D. C. Waterman and M. Dole, *J. Phys. Chem.*, **74**, 1913 (1970).

(2) F. Williams and M. Dole, *J. Amer. Chem. Soc.*, **81**, 2919 (1959).

(3) B. J. Lyons, *Polym. Prepr., Amer. Chem. Soc.*, **8**, 672 (1967).

(4) M. Dole, M. B. Fallgatter, and K. Katsuura, *J. Phys. Chem.*, **70**, 62 (1966).

(5) M. Dole, D. C. Milner, and F. Williams, *J. Amer. Chem. Soc.*, **79**, 4809 (1957).

(6) M. B. Fallgatter and M. Dole, *J. Phys. Chem.*, **68**, 1988 (1964).

(7) N. A. Slovokhotova, A. T. Koritskii, and N. Y. Buben, *Dokl. Akad. Nauk SSSR*, **129**, 1347 (1959).

(8) J. Silverman and S. O. Nielsen, *Polym. Prepr., Am. Chem. Soc.*, **9**, 296 (1968).

Because of strains induced into the films during their manufacture, on heating to near the melting point severe curling occurred. It was necessary to anneal the films for 30 min *in vacuo* prior to spectroscopic work by heating them above the melting point while they were held flat on a glass plate by weights along all four edges. No curling occurred on subsequent heating after this annealing treatment.

**Radiation Techniques.** During the irradiation with electrons from a General Electric resonant transformer high-voltage accelerator, the polyethylene film was supported on a glass plate on which it had previously been melted. The glass plate was placed into a chamber inside a brass block whose temperature was monitored by thermocouples and held constant either at 155 or 180° by means of electrical heating. The electrical heater consisted of wires wrapped around the brass block and the heating current was automatically controlled by a Leeds and Northrup Speedomax H temperature controller. The latter was situated outside of the radiation room. The radiation cell was continuously evacuated during the irradiation by a fore pump through a stainless steel tube to a pressure of about 0.02 Torr. Electrons entered the cell through thin titanium or aluminum windows. In order to maintain good temperature control it was necessary to protect the radiation cell from the air blast used to cool the window of the electron beam tube. A simple metal container surrounded the cell; it had a window made of 0.5-mil Marlex 6002 through which the electrons passed before reaching the window of the radiation cell. Electron beam dosimetry for irradiations of the thin films was accomplished by measuring at room temperature the rate of decay of vinyl groups whose  $G$  value had previously been determined in a  $^{60}\text{Co}$   $\gamma$ -ray source which had been calibrated by means of a Fricke dosimeter. During the dosimetry experiments the PE film was supported on a glass plate in exactly the same way as during the actual irradiation. The dose rate in the radiation cell was 153 Mrads  $\text{hr}^{-1}$ .

**Analytical Techniques.** To determine the gel content the irradiated polyethylene samples were placed in baskets made of 180 mesh platinum screening and the sol was extracted by immersing the basket with sample in boiling xylene for 24 hr. The samples were then evacuated for 24 hr in a vacuum desiccator and weighed. This whole process was repeated until a constant weight of the residual gel was obtained. For spectroscopic examination of the thin films the following procedure was used. After irradiation the films were removed from the glass plates to which they adhered during the irradiation (the glass-film contact was on one side only; previous results<sup>2</sup> had shown that adherence of a film on one side to a solid support was without influence on the results). For the uv studies the films were fastened to a small stainless steel frame which fitted into the spectrophotometer quartz sample cell. Void space

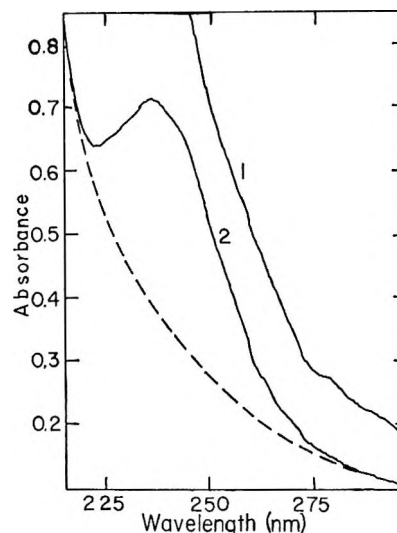


Figure 1. Ultraviolet spectrum of polyethylene irradiated to 76.5 Mrads at 180° before and after post irradiation hexane treatment. Curve 1 before and curve 2 after the treatment. Dotted line indicates assumed background.

in the cell was about 30% and was filled with spectral grade hexane. The thicker films used in the ir studies were merely taped to a standard sample holder and inserted into the ir spectrometer.

In agreement with the observations of Partridge,<sup>9</sup> it was found that the uv absorption in the wavelength range 200–300 nm was considerably reduced by several soakings of the film at room temperature in hexane. The hexane soaking also caused a significant sharpening of the uv absorption band at about 236 nm produced by the electron beam irradiation. Figure 1 illustrates the uv absorbance before and after the hexane treatment of a PE film that had been irradiated to a dose of 76.5 Mrads at 180°. All uv measurements were made with the cell filled with hexane as mentioned above. It is obvious that the intensity of the 236-nm band was much more readily measured after the hexane treatment than before. The dotted line indicates the base line used in estimating the absorbance due to the 236-nm band. We have assumed that this absorbance was due to conjugated diene groups which are believed<sup>10</sup> to have a maximum absorbance in PE at 236 nm.

Densities of the irradiated films were determined by a flotation method and used in the following equation to calculate diene concentrations in units of moles per gram

$$[\text{diene}] = 10^{-3}A/\epsilon\rho t \quad (1)$$

where  $A$  is the measured absorbance,  $\rho$  the density,  $t$  the film thickness as measured with a micrometer, and  $\epsilon$  the extinction coefficient of the diene group taken to be  $2.5 \times 10^4 \text{ l. mol}^{-1} \text{ cm}^{-1}$  at 236 nm.<sup>6</sup> In the calculation of the vinyl and vinylene double-bond concen-

(9) R. H. Partridge, *J. Chem. Phys.*, **45**, 1679 (1966).

(10) D. M. Bodily and M. Dole, *ibid.*, **45**, 1428 (1966).

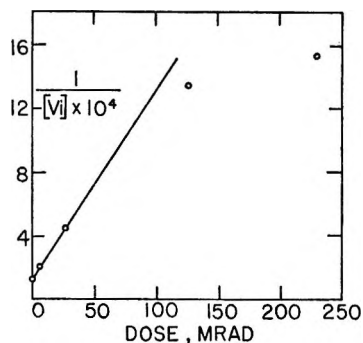


Figure 2. Second-order plot of vinyl double bond decay. Irradiations at 155°.

trations from the absorbances at 910 and 964  $\text{cm}^{-1}$ , 153 and 169  $\text{l. mol}^{-1} \text{cm}^{-1}$ , respectively, were the extinction coefficients used.<sup>5,11</sup> In these calculations  $\rho t$  of eq 1 was replaced by  $m/a$ , where  $m$  and  $a$  are the measured weight and area, respectively, of the film under study in the ir spectrometer.

### Results and Discussion

**Vinyl Decay.** Figure 2 illustrates a second-order plot of the decay of vinyl unsaturation with dose. At high doses the vinyl concentration appears to be leveling off. Williams and Dole<sup>2</sup> observed that a first-order relationship at 142° was valid up to about 16 Mrads, but the data of Figure 2 show that second-order kinetics are valid up to 25 Mrads or higher. The fact that the vinyl group concentration approximately leveled off at high doses very probably means that chain scission reactions occurred, each one of which produced two terminal free radicals,  $-\text{CH}_2\text{CH}_2\cdot$ , which then formed a terminal methyl and a vinyl group by disproportionation. If we assume zero-order kinetics for the chain scission formation of vinyl groups and second-order kinetics for their decay, then the kinetic equation can be written

$$d[\text{Vi}]/dr = \phi - k_2[\text{Vi}]^2 \quad (2)$$

where  $[\text{Vi}]$  is the vinyl concentration in moles  $\text{gram}^{-1}$ ,  $r$  is the dose in Mrads,  $\phi$  is the zero-order vinyl growth constant, and  $k_2$  is the second-order decay constant in  $\text{mol}^{-1} \text{Mrad}^{-1}$ . Integrating between limits of dose  $r$  and zero dose, we obtain

$$\ln \frac{[\text{Vi}] - [\text{Vi}]_\infty}{[\text{Vi}] + [\text{Vi}]_\infty} + \ln \frac{[\text{Vi}]_0 + [\text{Vi}]_\infty}{[\text{Vi}]_0 - [\text{Vi}]_\infty} = -2k_2[\text{Vi}]_\infty r \quad (3)$$

The subscripts 0 and  $\infty$  refer to zero and infinite doses, respectively. To test eq 3 we have plotted  $[\text{Vi}]$  as a function of reciprocal dose and have extrapolated the resulting curve to zero  $r^{-1}$  in order to obtain  $[\text{Vi}]_\infty$ . The latter was found to be  $5.0 \times 10^{-6} \text{ mol g}^{-1}$ . Figure 3 illustrates the vinyl decay data plotted according to the linear relationship of eq 3. The relationship is seen to be valid up to a dose of 126 Mrads, considerably higher than the limiting valid dose of Figure 2. From

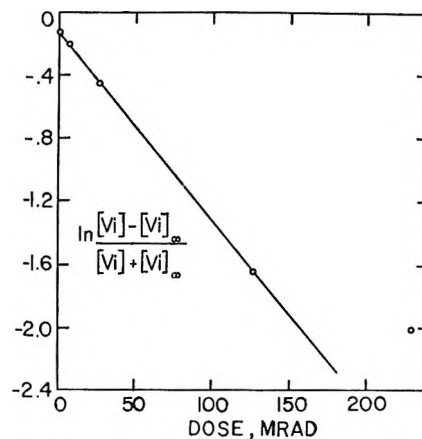


Figure 3. Plot of eq 3 for an assumed zero-order growth and second-order decay of vinyl groups.

the slope of the straight line,  $k_2$ , the second-order decay constant was calculated to be  $1.2 \times 10^3 \text{ g mol}^{-1} \text{ Mrad}^{-1}$ . The second-order decay constant of Figure 2 is  $1.2 \times 10^3 \text{ g mol}^{-1} \text{ Mrad}^{-1}$ , so that the value of  $k_2$  found from eq 3 is consistent with the data at low doses as it should be because at zero dose  $k_2[\text{Vi}]^2$  is 1000-fold greater than  $\phi$ . At infinite dose  $d[\text{Vi}]/dr$  should be zero and  $\phi$  equal to  $k_2[\text{Vi}]_\infty^2$ . With this assumption  $\phi$  is found to be  $3.0 \times 10^{-8} \text{ mol g}^{-1} \text{ Mrad}^{-1}$ . If all of the scissions during the radiolysis produced vinyl groups, then from  $\phi$   $G(\text{S})$  is readily calculated to be 0.03, a very small value. At this point it is necessary to comment on the difference in  $G_0(-\text{Vi})$  as observed by us and by Lyons.<sup>3</sup> Part of the difference is due to the fact that Lyons' value was an average over the first Mrad radiation dose. For example, our average  $G(-\text{Vi})$  from zero to 6.55 Mrads is 4.04 as compared to our estimated  $G_0(-\text{Vi})$  of 6.75 as calculated from the constants found to fit the second-order decay equation. An estimate from the slope of a first-order plot yielded  $G_0(-\text{Vi})$  equal to 5.17. Another difference may be the result of the neglect of the change in crystallinity of the PE due to the irradiation and to the melting and recooling associated with the irradiation. Lyons<sup>3</sup> states that the absorbance at 909  $\text{cm}^{-1}$  could change as much as 13% due to the change in crystallinity over the first 16 Mrads of radiation. If we apply a 13% correction to our  $G_{\text{Av}}(-\text{Vi})$  value of 4.04, given above, we obtain 3.09 which is still greater than the value found by Lyons for Marlex 6002 polyethylene.

Lyons<sup>3</sup> has suggested that the more uniform dispersion of the vinyl groups in the molten state is responsible for the drop in  $G(-\text{Vi})$  values in passing from the semi-crystalline to the molten state. This hypothesis could explain why a simple second-order decay equation agrees with the data to higher doses at 155° than does a simple first-order decay equation. We had previ-

(11) R. J. de Kock, P. A. H. M. Hol, and H. Bos, *Z. Anal. Chem.*, 205, 371 (1964).

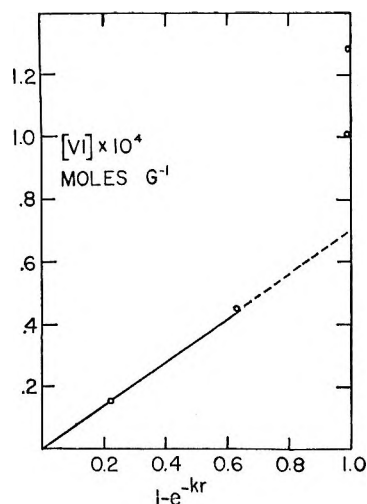


Figure 4. Plot of eq 4 for an assumed zero-order growth and first-order decay of vinylene double bonds. Note the two points close to the abscissa value of unity on the right-hand ordinate. Irradiations at 155°.

ously found that a simple first-order relation<sup>12</sup> was accurately valid at 120°.

*Vinylene Growth and Decay.* According to the zero-order growth and first-order decay equation of Dole, Milner, and Williams<sup>5</sup> for vinylene formation and decay, the vinylene concentration should be given by the equation

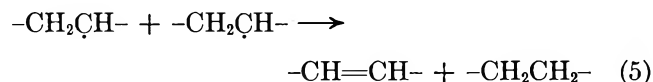
$$[VI] = [VI]_{\infty}[1 - \exp(-k_1r)] \quad (4)$$

where VI stands for trans-vinylene group and  $k_1$  is the first-order vinylene decay constant. Equation 4 is valid when the initial polymer sample contains no vinylene unsaturation as was the case in this work. Figure 4 illustrates this relationship where it can be seen that eq 4 is valid up to at least 25 Mrads, but that the vinylene concentration is considerably greater at high doses than predicted by eq 4. In plotting the data in Figure 4,  $k_1$  was taken to be  $4.0 \times 10^{-2}$  Mrad<sup>-1</sup> which in units of g (eV)<sup>-1</sup> is  $0.64 \times 10^{-21}$ . Williams and Dole<sup>2</sup> found exactly the same value for irradiations at 142°. However, in their work the irradiations were only carried to a dose of about 20 Mrads. Thus, they would not have observed the marked deviations from linearity noted here. If eq 4 remained valid at high doses, the vinylene concentration would level off at a concentration of  $0.7 \times 10^{-4}$  mol g<sup>-1</sup> (where the dotted line intercepts the ordinate at  $\exp(-kr)$  equal to zero). However, at 229 Mrads the vinylene concentration was  $1.3 \times 10^{-4}$  mol g<sup>-1</sup>, nearly twice as great, and still rising with dose.

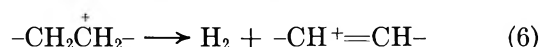
Conversely, if the constants of eq 4 are adjusted to give greater weight to the high-dose vinylene concentrations, better agreement of the theoretical curve with the high-dose points can be obtained, but at the expense of somewhat less good agreement at the low doses. The constants chosen for this calculation were  $1.3 \times$

$10^{-4}$  mol g<sup>-1</sup> for  $[VI]_{\infty}$  and 0.019 Mrad<sup>-1</sup> for  $k_1$ . The latter is about  $1/2$  the value given above. Hence the data can be interpreted in terms of an enhanced vinylene growth rate at the high doses or a decreased vinylene decay rate constant, approximately valid for all doses, in the molten state.

A possible explanation of the enhanced vinylene growth can be given in terms of the disproportionation reaction



which would be enhanced by rise in temperature. The main mechanism for vinylene formation is probably the exothermic temperature-independent reaction<sup>13</sup>



However, the relative importance of reaction 5 as compared with 6 depends on the instantaneous free radical concentration and on the free radical mobility. The former should have been less and the latter greater in the molten state than in the solid; hence, it is difficult to predict the effect of temperature in this case. To explain the results in terms of a decrease in the vinylene decay rate in going from the crystalline to the molten state one would have to postulate increased competition for free radicals from other reactions or an increase in the protective action of one vinylene group on another by the vinylene groups acting as energy sinks as discussed by Dole and Williams.<sup>14</sup>

*Diene Formation.* Since previous infrared studies<sup>2</sup> as well as the pulse radiolysis work of Silverman and Nielsen<sup>8</sup> had shown no diene formation in the molten state we were rather surprised to observe the growth of diene in this work with a rather small initial  $G$  value of 0.073. The production of diene fell off with dose so that this  $G$  value is an estimate obtained from the slope of the diene concentration-dose curve extrapolated to zero dose. At high doses the diene concentration seemed to level off at a concentration of about  $2.4 \times 10^{-6}$  mol g<sup>-1</sup>. In agreement with Williams and Dole,<sup>2</sup> we observed no growth of an infrared absorption band at 988 cm<sup>-1</sup>. Thus, the diene formed in this work was probably not trans-trans diene, but because it was observed by uv spectroscopy it could have been cis-trans or cis-cis diene. Thermodynamically, the higher the temperature the greater the proportion of cis-trans or cis-cis diene is to be expected.<sup>15</sup> Furthermore, the random coil configuration of the polyethylene chain in the molten state should be more conducive to cis-cis

(12) H. Y. Kang, O. Saito, and M. Dole, *J. Amer. Chem. Soc.*, **89**, 1980 (1967).

(13) M. Dole and D. M. Bodily, *Advan. Chem. Ser.*, **No. 66**, 31 (1967).

(14) M. Dole and F. Williams, *Discuss. Faraday Soc.*, **27**, 74 (1959).

(15) C. Doring and H. G. Hauthal, *J. Prakt. Chem.*, **24**, 27 (1964).



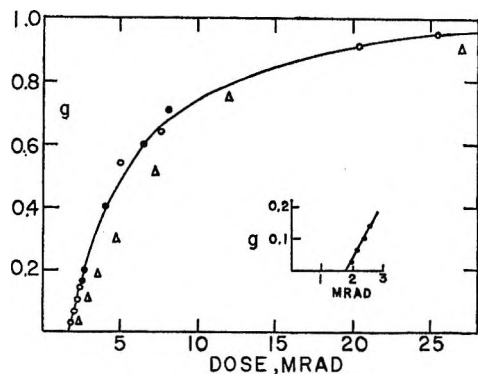


Figure 5. Gel fraction ( $g$ ) dose data. Open circles, irradiations at  $155^\circ$ , this research; closed circles, data of Williams and Dole<sup>2</sup> for irradiations at  $142^\circ$ ; triangles, data of Kang, Saito, and Dole<sup>12</sup> for irradiations at  $120^\circ$ .

diene formation, especially according to the mechanism for diene formation proposed by Partridge.<sup>16</sup>

Although the diene infrared band at  $988\text{ cm}^{-1}$  was not observed, the growth with dose of a small absorption band at  $850\text{ cm}^{-1}$  was seen. This might possibly have been due to a trace of the trialkylethylene double bond  $\text{R}'\text{CH}=\text{CR}''\text{R}'''$ , or to cyclic groups in the polyethylene. The magnitude of the absorption was not great enough, however, to demonstrate a significant yield of either of these species.

**Gel Formation and the Cross-Link Yield.** In Figure 5, gel data obtained in this research for irradiation at  $155^\circ$ , by Williams and Dole<sup>2</sup> at  $142^\circ$ , and by Kang, Saito, and Dole<sup>12</sup> at  $120^\circ$  are compared. Very good agreement is seen to exist except that, as expected, the  $120^\circ$  gel fractions for irradiation of the still largely crystalline material are slightly less than the gel fractions for irradiations in the molten state. The inset is an expanded plot of the data of the present work at very low doses; the dose to the gel point, 1.80 Mrads, was obtained from this plot by extrapolating the gel curve to zero gel. Figure 6 illustrates a plot of the Charlesby-Pinner<sup>17</sup> function,  $s + s^{1/2}$ , where  $s$  is the sol fraction. The abscissa is the dimensionless ratio,  $r_g/r$ , where  $r_g$  is the dose to the gel point. The Charlesby-Pinner equation expressed in dimensionless units is

$$s + s^{1/2} = (1/2)\lambda + \{2 - (1/2)\lambda\}(r_g/r) \quad (7)$$

where  $\lambda$  is the ratio of the  $G$  value for chain scissions,  $G(S)$ , to  $G(X)$ , the cross-linking  $G$  value.

Also plotted in Figure 6 are the data of Kang, Saito, and Dole.<sup>12</sup> The agreement between the two sets of data is probably within the experimental limits of accuracy. This means that the same values of  $\lambda$  from 0.24 to 0.15 used in the previous work<sup>12</sup> can also be used here. The solid line is the theoretical curve calculated from Saito's theory<sup>18</sup> and very good agreement is seen to exist at low doses. The theoretical curve was calculated for  $\lambda$  equal to 0.24 and by using a value of  $\beta$

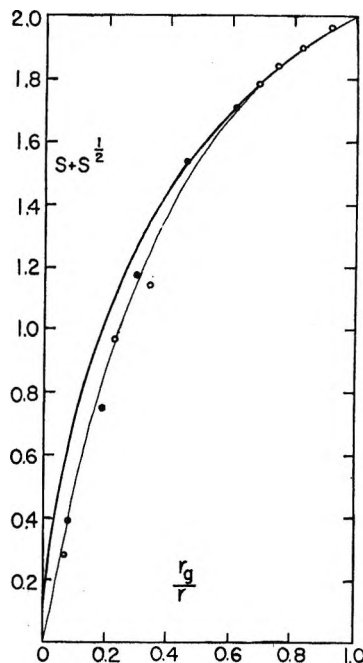


Figure 6. Comparison of Charlesby-Pinner function,  $s + s^{1/2}$ , with Saito theory:<sup>18</sup> open circles, data of this research for irradiations at  $155^\circ$ ; closed circles, data<sup>12</sup> for irradiations at  $120^\circ$ ; solid line, theoretical curve for  $\beta$  equal to 2.21 and  $\lambda$  equal to 0.24; sol fraction,  $s$ , equal to  $1 - g$ .

of the Saito theory equal to 2.21 where  $\beta$  is defined by equation

$$M_{w,0}/M_{n,0} = \exp(\beta^2/2)$$

in which  $M_{w,0}$  and  $M_{n,0}$  are the initial weight and number average molecular weights, respectively.

The cross-linking  $G$  value,  $G(X)$  at  $155^\circ$  and at the gel point, can be estimated from the data of Kang, Saito, and Dole at  $120^\circ$  by means of the ratio  $G(X)_{155^\circ} = G(X)_{120^\circ} r_{g,120^\circ}/r_{g,155^\circ}$ . The value found was 1.38 while from the Saito theory, Figure 6,  $G(X)$  was estimated to be 1.61 for  $\lambda$  equal to 0.24. Hence there is an uncertainty of about 0.2 unit in  $G(X)$ .

From the  $G(X)$  and  $\lambda$  values  $G(S)$  was calculated to be 0.2-0.4. These are an order of magnitude greater than  $G(S)$  estimated above from the rate of vinyl double-bond growth. Any processes producing chain scission without the concomitant formation of vinyl groups would, of course, tend to make  $G(S)$  estimated from the gel data higher than  $G(S)$  estimated from vinyl growth. One such process could be chain scission, followed by chain transfer of the terminal free radical center to another polymer chain leaving methyl groups at the ends of the broken chain.

It is interesting to compare doses to the gel point,  $r_g$ ,

(16) R. H. Partridge, *J. Chem. Phys.*, **52**, 1277 (1970).

(17) A. Charlesby and S. H. Pinner, *Proc. Roy. Soc., Ser. A*, **249**, 367 (1959).

(18) O. Saito, H. Y. Kang, and M. Dole, *J. Chem. Phys.*, **46**, 3607 (1967).

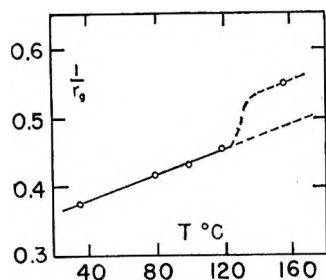


Figure 7. Reciprocal of the dose to the gel point plotted as a function of temperature. Data of Kang, Saito, and Dole<sup>12</sup> at 120° and below.

as obtained at different temperatures. The reciprocal of the dose should be proportional to  $G(X)$  if  $\lambda$  is small and constant. In Figure 7,  $1/r_g$  is plotted as a function of temperature, and it can be seen that up to 120°,  $1/r_g$  is linear with the temperature. Above 120° polyethylene melts, about 90%<sup>19</sup> of Marlex polyethylene of maximum melting point 134° melting in the temperature region above 120°. As can be seen from Figure 7, the melting causes a significant increase in  $G(X)$ , from an extrapolated solid state value of about 1.18 at 155° to 1.4 or 1.6 observed here for the molten state irradiations. This conclusion agrees with the experimental observation of Salovey and Falconer<sup>20</sup> that the  $G$  value for dimer formation in liquid *n*-hexadecane at 19° was greater than that in the solid at 4°, 2.60 as compared with 2.30. Lawton, Balwit, and Powell<sup>21</sup> also concluded that the cross-linking  $G$  value was greater in the amorphous state than in highly crystalline PE, but Kitamaru and Mandelkern<sup>22</sup> observed just the opposite, namely, that the dose to the gel point for a fractionated PE sample of  $M_n$  equal to 182,000 was two-fold greater for a completely amorphous sample at 133° than for a crystalline sample at that temperature. These authors also found that for doses of  $r/r_g$  up to 4 the solubilities of the amorphous and crystalline samples were equal at the same values of  $r/r_g$ . This means that the  $\lambda$  values must have been the same in the two cases; hence, if  $G(X)$  was twice as great for the crystalline sample,  $G(S)$  must also have been twice as great (or zero in both states). We have no explanation for the disagreement in the conclusions of Kitamaru and Mandelkern with those of this paper.

Kang, Saito, and Dole<sup>12</sup> concluded from their gel studies that  $G(X)$  increased with dose, largely as the result of enhanced vinylene group decay. In this work the data of Figure 6 also fall below the theoretical Saito curve; in other words gel formation was greater at high doses than predicted from the data at low doses. It is not possible to obtain agreement between theory and experiment at both low and high doses merely by adjustment of the parameter  $\lambda$ . The agreement that does exist covers the small dose range, 1.80–2.55. Over this dose range the decrease in average  $G(VI)$  from its extrapolated value at zero dose is only 0.10 at 1.80

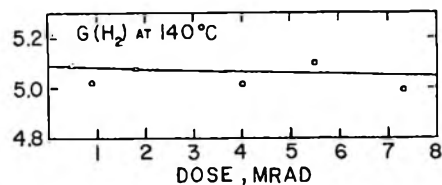


Figure 8.  $G(H_2)$  at 140° as a function of dose. Data of Kang.<sup>23</sup>

Mrads and 0.14 at 2.55 Mrads; these changes in  $G(VI)$  are too small to invalidate the agreement of the experimental data of Figure 6 with the theoretical curve.

**Material Balance.** If extraneous reactions do not interfere, one would expect the material balance equation

$$G(H_2) = G(X) + G(VI) + 2G(\text{diene}) \quad (8)$$

to be valid. In the previous work<sup>12</sup>, this was found to be the case for irradiation in the solid state. Figure 8 illustrates the variation<sup>23</sup> of  $G(H_2)$  with dose up to 7 Mrads at 140°.  $G(H_2)$  decreases slightly with dose; the extrapolated value at zero dose is  $5.08 \pm 0.04$ . Unfortunately, we do not have data taken at 155°; judging from the temperature coefficient of  $G(H_2)$  in the solid state,<sup>12</sup>  $G(H_2)$  would not be expected to increase more than about 0.04 to 0.05  $G$  unit as the temperature is increased from 140 to 155°.  $G(X)$ ,  $G(VI)$ , and  $2G(\text{diene})$  estimated at zero dose at 155° are 1.61, 2.70, and 0.14, respectively, which add to  $4.45 \pm 0.2$ . This is about 0.7  $G$  unit below  $G(H_2)$ , and could be explained by the occurrence of a small amount of intramolecular cross-linking. It is reasonable to expect the formation of more intramolecular cross-links in the molten than in the solid, highly crystalline state. As remarked above, the newly discovered small absorption band at  $850 \text{ cm}^{-1}$  observed in the ir absorption spectrum of polyethylene after irradiation in the molten state may be indicative of intramolecular cross-links.

**Acknowledgments.** This research was supported by the U. S. Atomic Energy Commission, first at Northwestern University and then at Baylor University, and by income from the chair in Chemistry at Baylor University endowed by a gift from The Robert A. Welch Foundation. We are also indebted for support provided by the Advanced Research Projects Agency of the Department of Defense through the Northwestern University Materials Research Center. Dr. J. A. Reid of the Phillips Petroleum Company kindly supplied the polyethylene samples.

(19) B. Wunderlich and M. Dole, *J. Polym. Sci.*, **24**, 201 (1957).

(20) R. Salovey and W. E. Falconer, *J. Phys. Chem.*, **69**, 2345 (1965).

(21) E. J. Lawton, J. S. Balwit, and R. S. Powell, *J. Polym. Sci.*, **32**, 257 (1958).

(22) R. Kitamaru and L. Mandelkern, *J. Amer. Chem. Soc.*, **86**, 3529 (1964).

(23) Data obtained by Dr. H. Y. Kang.

# Spectroscopic Investigation of Cyclohexanol and Cyclohexyl Radicals and Their Corresponding Peroxy Radicals

by M. Simic<sup>1</sup> and E. Hayon\*

*Pioneering Research Laboratory, U. S. Army Natick Laboratories, Natick, Massachusetts 01760  
(Received December 31, 1970)*

*Publication costs assisted by the U. S. Army Natick Laboratories*

The optical absorption spectra of the intermediates produced in the pulse radiolysis of liquid cyclohexanol and cyclohexane at 22° in the presence of 1 atm of Ar, N<sub>2</sub>O, and O<sub>2</sub> have been determined. The ·C<sub>6</sub>H<sub>10</sub>OH radical from cyclohexanol was found to have a structureless absorption spectrum with λ<sub>max</sub> 240 nm, ε<sub>240</sub> 1700 M<sup>-1</sup> cm<sup>-1</sup>, and to decay with 2k = 6.5 × 10<sup>7</sup> M<sup>-1</sup> sec<sup>-1</sup>. The cyclohexane ·C<sub>6</sub>H<sub>11</sub> radical has an absorption maximum at 240 nm, ε<sub>240</sub> 1500 M<sup>-1</sup> cm<sup>-1</sup>, and decays with 2k = 2.4 × 10<sup>9</sup> M<sup>-1</sup> sec<sup>-1</sup>. In the presence of oxygen, structureless absorption bands with λ<sub>max</sub> 246 nm (ε 1600 M<sup>-1</sup> cm<sup>-1</sup>) and 255 nm (ε 1900 M<sup>-1</sup> cm<sup>-1</sup>) for ·O<sub>2</sub>C<sub>6</sub>H<sub>10</sub>OH and ·O<sub>2</sub>C<sub>6</sub>H<sub>11</sub> radicals, respectively, were observed. In the case of the cyclohexyl peroxy radical, following the second-order decay of the radical to form the tetroxide, on the basis of the Russell mechanism, two other transients were observed which decayed by a first-order process with rates of 5 sec<sup>-1</sup> and 1.5 × 10<sup>-1</sup> sec<sup>-1</sup>. A mechanism is tentatively suggested which involves the formation of a trioxide subsequent to the first-order decay of the tetroxide.

## Introduction

Spectroscopic investigation of some alcohol and hydrocarbon radicals in the liquid phase, and their corresponding peroxy radicals, was one of the earliest attempts using the pulse radiolysis technique. It was found,<sup>2</sup> for instance, that the optical absorption spectra of the cyclohexanol radical ·C<sub>6</sub>H<sub>10</sub>OH and the cyclohexyl peroxy radical ·O<sub>2</sub>C<sub>6</sub>H<sub>11</sub> were highly structured in the 290–340- and 260–320-nm regions, respectively. Recent work<sup>3</sup> indicated that the absorption spectra of various aliphatic alcohols, in the pure liquid or in aqueous solution, and their corresponding peroxy radicals were smooth and structureless. As part of a program to study the role of peroxy radicals in autoxidation processes, and in view of the often-quoted<sup>4,5</sup> structured nature of the absorption spectra of peroxy radicals, the pulse radiolysis of liquid cyclohexanol and cyclohexane in the presence and absence of oxygen was reinvestigated. The results obtained are presented below.

## Experimental Section

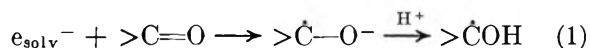
The experimental conditions used have been described.<sup>3,6</sup> In brief, 2.3-MeV electrons, with pulses of ~30-nsec duration, were generated by a Febetron 705 System (Field Emission Corp.). Optical cells of 2-cm light path were used. The output of the analyzing light from a xenon lamp was increased by 20–30 times for ~1.2 msec by pulsing the lamp. Two high-intensity Bausch and Lomb monochromators were used in series to reduce scattered light below 260 nm.

The dose per pulse was determined using KCNS (ε<sub>500</sub> 7600 M<sup>-1</sup> cm<sup>-1</sup>). Appropriate corrections were made for the electron density of the medium. The

best commercially available liquids from Phillips and Matheson Coleman and Bell were used.

## Results

The cyclohexanol used contained ~0.3% of cyclohexanone. Since the solvated electrons (produced from the radiolysis of cyclohexanol) react with cyclohexanone to give α-cyclohexanol radicals,<sup>3</sup> no effort



was made to remove it from the system. The system was, nevertheless, investigated in the presence of 1 atm N<sub>2</sub>O (~0.1 M) to remove the short-lived ·C<sub>6</sub>H<sub>10</sub>O<sup>-</sup> radical, which absorbs<sup>3</sup> predominantly in the 300–450-nm region. Excluding the initial contribution of the anion radical (in 1 atm argon) which disappears fast through protonation, the transient absorption spectrum of the cyclohexanol radicals with λ<sub>max</sub> 240 nm (Figure 1) is identical in Ar and N<sub>2</sub>O solutions. In the presence of oxygen (1 atm), the maximum of the transient optical absorption is only slightly shifted to λ<sub>max</sub> 246 nm; the shape of the spectrum is, however, considerably altered (see Figure 1).

(1) National Academy of Sciences-National Research Council Research Associate at Natick. Present address: Radiation Biology Laboratory, University of Texas, Austin.

(2) R. L. McCarthy and A. MacLachlan, *J. Chem. Phys.*, **35**, 1625 (1961).

(3) M. Simic, P. Neta, and E. Hayon, *J. Phys. Chem.*, **73**, 3794 (1969).

(4) *E.g.*, M. S. Matheson and L. M. Dorfman, "Pulse Radiolysis," MIT Press, Cambridge, Mass., 1969.

(5) K. U. Ingold, *Accounts Chem. Res.*, **2**, 1 (1969).

(6) J. P. Keene, E. D. Black, and E. Hayon, *Rev. Sci. Instrum.*, **40**, 1199 (1969); E. Hayon, *J. Chem. Phys.*, **51**, 4881 (1969).

**Table I:** Absorption Maxima, Extinction Coefficients, and Decay Kinetics of Radicals Produced in the Pulse Radiolysis of Cyclohexanol and Cyclohexane, at 22°, in the Presence of Ar, N<sub>2</sub>O, and O<sub>2</sub> (1 atm)

System	$\lambda_{\max}$ , nm	$\epsilon$ , $M^{-1} \text{ cm}^{-1}$ <sup>a</sup>	Decay kinetics, nm	$2k$ , $M^{-1} \text{ sec}^{-1}$ <sup>a</sup>	Radicals
Cyclohexanol, N <sub>2</sub> O	240	1700	270–320	$6.5 \times 10^7$	$\cdot\text{C}_6\text{H}_{10}\text{OH}$
Cyclohexanol, O <sub>2</sub>	246	1600	250–280	$1.2 \times 10^7$	$\cdot\text{O}_2\text{C}_6\text{H}_{10}\text{OH}$
Cyclohexane, Ar	240	1500	240	$2.4 \times 10^8$	$\cdot\text{C}_6\text{H}_{11}$
Cyclohexane, O <sub>2</sub>	255	1900	240, 270–290	$2.3 \times 10^6$ <sup>b</sup>	$\cdot\text{O}_2\text{C}_6\text{H}_{11}$

<sup>a</sup> Values  $\pm 30\%$ . <sup>b</sup> See text for slow first-order decay of intermediates.

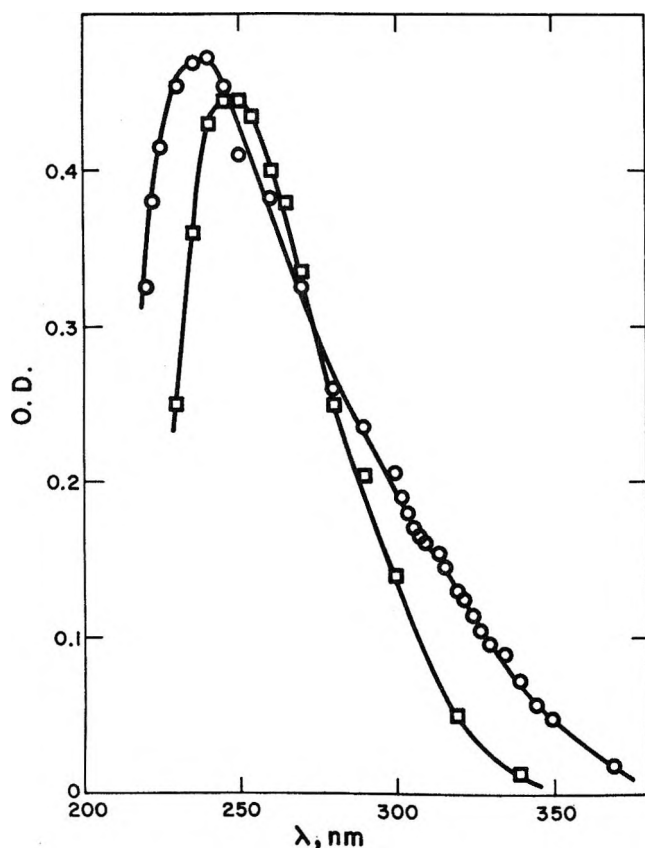


Figure 1. Transient spectra produced in the pulse radiolysis of cyclohexanol at 22° in the presence of 1 atm of N<sub>2</sub>O (○) and of O<sub>2</sub> (□). Dose per pulse  $\sim 19$  krad. Band width of analyzing light  $< 1$  nm between 300 and 350 nm.

On the basis of the yields of products<sup>7</sup> in the radiolysis of cyclohexanol in the presence of O<sub>2</sub>,  $G(\cdot\text{C}_6\text{H}_{10}\text{OH}) = 7.8$  was used in the calculation of the extinction coefficients and decay rates, which are given in Table I.

The spectrum of the cyclohexyl radical  $\cdot\text{C}_6\text{H}_{11}$ , with  $\lambda_{\max}$  240 nm, is presented in Figure 2. This spectrum is essentially the same in Ar- and N<sub>2</sub>O-saturated solutions, although a somewhat higher yield was observed in the presence of N<sub>2</sub>O. A value of  $G(\cdot\text{C}_6\text{H}_{11}) = 5.7^8$  in argon solutions was used for the calculation of the extinction coefficient.

In the presence of O<sub>2</sub>, a much longer-lived transient is formed with  $\lambda_{\max}$  255 nm, and a spectrum consider-

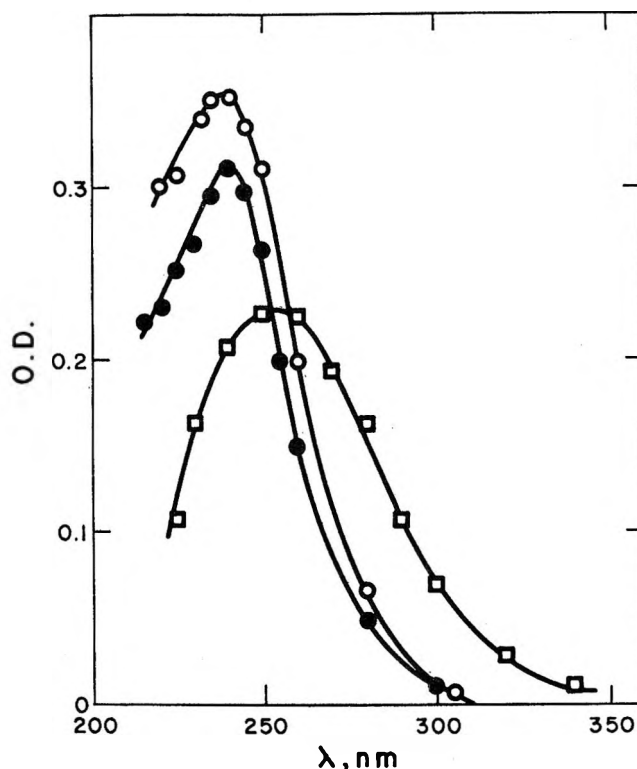


Figure 2. Transient spectra produced in the pulse radiolysis of cyclohexane at 22° in the presence of 1 atm of Ar (●), N<sub>2</sub>O (○), and O<sub>2</sub> (□). Dose per pulse  $\sim 15$  krad.

ably different from that observed in Ar- and N<sub>2</sub>O-saturated solutions of cyclohexane. The total peroxy radical yield  $G_{\text{RO}_2} = 6.0$  was used, based on the product yields obtained<sup>9</sup> in irradiated cyclohexane + O<sub>2</sub> system:  $G(\text{H}_2\text{O}_2) = 0.1$ ,  $G(\text{cyclohexyl hydroperoxide}) = 1.05$ ,  $G(\text{dicyclohexyl peroxide}) = 0.31$ ,  $G(\text{cyclohexanone}) = 2.02$ , and  $G(\text{cyclohexanol}) = 1.55$ .

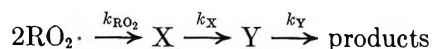
The decay kinetic of the  $\cdot\text{O}_2\text{C}_6\text{H}_{11}$  radical followed good second-order kinetics up to  $\sim 70\%$  decay. Two additional transients were observed at 240 nm; these

(7) R. L. McCarthy and A. MacLachlan, *Trans. Faraday Soc.*, **57**, 1107 (1961).

(8) K. M. Bansal and R. H. Schuler, *J. Phys. Chem.*, **74**, 3924 (1970).

(9) G. Dobson and G. Hughes, *ibid.*, **69**, 1814 (1965).

decayed very slowly and followed first-order kinetics. These events could be represented as

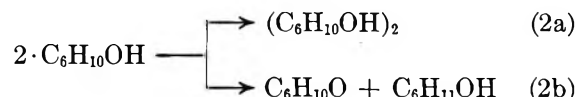


The relative OD of  $\text{RO}_2 \cdot$ , X and Y at 240 nm are 0.23, 0.03, and 0.085, respectively. The decays are  $2k_{\text{RO}_2} = 2.3 \times 10^6 \text{ M}^{-1} \text{ sec}^{-1}$ ,  $k_{\text{X}} = 5 \text{ sec}^{-1}$ , and  $k_{\text{Y}} = 1.5 \times 10^{-1} \text{ sec}^{-1}$ . The spectra of X and Y could not be investigated, owing to the considerable experimental difficulties in the spectral region down to 210 nm.

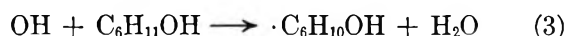
## Discussion

*Cyclohexanol System.* The cyclohexanol radicals  $\cdot\text{C}_6\text{H}_{10}\text{OH}$  are produced on irradiation of cyclohexanol through ionization and excitation processes. In addition, they could be formed in the reactions of solvated electrons with cyclohexanone or in the presence of  $\text{N}_2\text{O}$  via the intermediate OH radical ( $e_{\text{solv}}^- + \text{N}_2\text{O} \xrightarrow{\text{H}^+} \text{N}_2 + \text{OH}$ ). The spectrum of the  $\cdot\text{C}_6\text{H}_{10}\text{OH}$  radical shows neither the well-defined peaks at 302, 314, and 333 nm previously observed<sup>2</sup> nor any signs of fine structure in excess of  $\pm 5\%$  of the recorded absorbances. The spectrum is, in fact, very similar to the spectrum of the  $\cdot\text{C}_6\text{H}_{10}\text{OH}$  radical in aqueous solution,<sup>3</sup> where an overall  $\epsilon_{240} 1400 \text{ M}^{-1} \text{ cm}^{-1}$  was observed.

This radical disappears in a bimolecular process, as previously suggested.<sup>2</sup> The rate of disappearance in

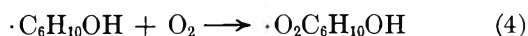


cyclohexanol is about 30 times slower than that in water,<sup>3</sup> which is probably due to the much higher viscosity of cyclohexanol. Since the product of reaction 2a is mainly vicinal diol, it was suggested<sup>2,7</sup> that  $\alpha$ -cyclohexanol radicals,  $>\dot{\text{C}}\text{-OH}$ , are predominantly formed. This is different from the radicals produced from the reaction with OH radicals where it was con-



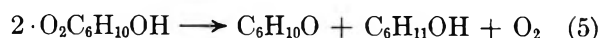
cluded<sup>3</sup> that only  $\sim 20\%$  of the radicals have the unpaired electron in the  $\alpha$  position to the hydroxyl group. On the basis of the similarity of the spectra of  $\cdot\text{C}_6\text{H}_{10}\text{OH}$  radicals in liquid and aqueous<sup>3</sup> cyclohexanol, it would appear that  $\alpha$  as well as  $\beta$  and  $\gamma$  radicals have indistinguishable spectra. It is only the  $\alpha$  radical which dissociates in aqueous alkaline solutions ( $\text{p}K_{\text{a}} = 12.2$ ) to give a significantly different transient spectrum.<sup>3</sup>

Oxygen reacts very fast with the radicals produced in these systems,  $k(\text{R} + \text{O}_2) \geq 10^9 \text{ M}^{-1} \text{ sec}^{-1}$ . The



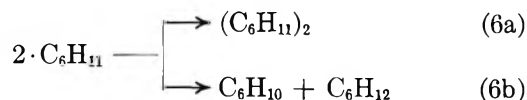
cyclohexanol peroxy radicals have similar spectra in liquid and aqueous<sup>3</sup> cyclohexanol:  $\lambda_{\text{max}}$  246 and 242

nm;  $\epsilon_{\text{max}}$  1600 and  $1500 \text{ M}^{-1} \text{ cm}^{-1}$ , respectively. These radicals disappear in a bimolecular reaction

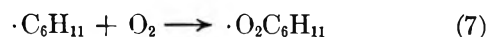


It is not clear in this system whether tetroxides are formed as intermediates (see further below).

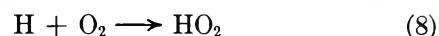
*Cyclohexane System.* The cyclohexyl radical,  $\cdot\text{C}_6\text{H}_{11}$ , is produced on irradiation of cyclohexane via excitation and ionization processes, as well as via free-radical reactions.<sup>10</sup> The spectrum of  $\cdot\text{C}_6\text{H}_{11}$  is in agreement with that obtained by Sauer and Mani,<sup>11</sup> who found  $\lambda_{\text{max}}$  240 nm and  $\epsilon_{240} 2100 \text{ M}^{-1} \text{ cm}^{-1}$ , and above 270 nm with the spectrum originally reported.<sup>12</sup> In the presence of  $\text{N}_2\text{O}$ , only a slight increase in the yield of  $\cdot\text{C}_6\text{H}_{11}$  ( $\sim 15\%$ ) was observed—this is considerably less than that indicated from product analysis<sup>8</sup> ( $\geq 40\%$  increase). No satisfactory explanation can be offered at present. The  $\cdot\text{C}_6\text{H}_{11}$  radicals disappear in a fast bimolecular reaction ( $2k = 2.4 \times 10^9 \text{ M}^{-1} \text{ sec}^{-1}$ ), giving dicyclohexyl and cyclohexene as the product.



In the presence of oxygen (1 atm), reaction 6 is completely suppressed and is replaced by reaction 7. A

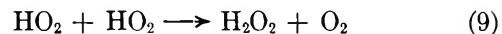


small amount of hydroperoxy radical is also produced

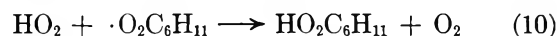


with  $\lambda_{\text{max}} \sim 235 \text{ nm}$ ,<sup>13</sup> and probably contributes only to a small extent to the spectrum attributed to the  $\cdot\text{O}_2\text{-C}_6\text{H}_{11}$  radical. This latter spectrum is very similar to the spectra of some other organic peroxy radicals<sup>3</sup> and quite different from the originally reported<sup>2</sup> spectrum (which exhibited pronounced peaks at 275 and 295 nm).

The  $\text{HO}_2$  and  $\cdot\text{O}_2\text{C}_6\text{H}_{11}$  radicals disappear via two minor reactions



and probably



as indicated by product analysis<sup>9</sup>:  $G(\text{H}_2\text{O}_2) = 0.1$  and  $G(\text{HO}_2\text{C}_6\text{H}_{11}) = 0.3$ . Since the yields of products indicate the absence of a chain reaction, mutual destruction of two peroxy radicals is therefore the predominant mode of disappearance of  $\cdot\text{O}_2\text{C}_6\text{H}_{11}$  radicals. The

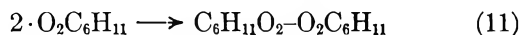
(10) See, for instance, a review by J. M. Warman, R. D. Asmus, and R. H. Schuler, *Advan. Chem. Ser.*, No. 82, 25 (1968).

(11) M. C. Sauer and I. Mani, *J. Phys. Chem.*, 72, 3856 (1968).

(12) M. Ebert, J. P. Keene, E. J. Land, and A. J. Swallow, *Proc. Roy. Soc., Ser. A*, 287, 1 (1965).

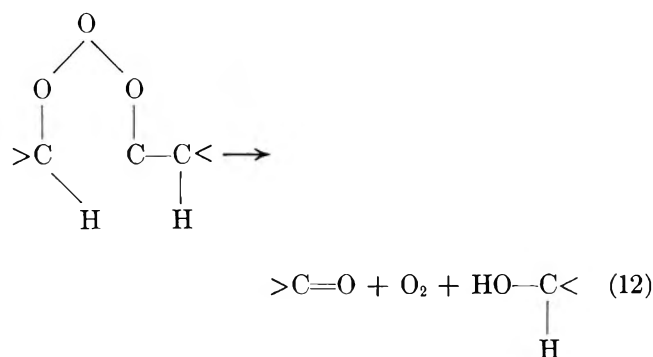
(13) G. Czapski and L. M. Dorfman, *J. Phys. Chem.*, 68, 1169 (1964).

second-order decay kinetics is in accord with this mechanism. This reaction probably involves the initial formation of a tetroxide<sup>5,14</sup>

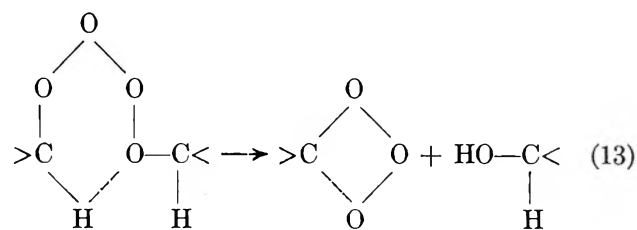


which is commonly accepted as the intermediate in autoxidation reactions.

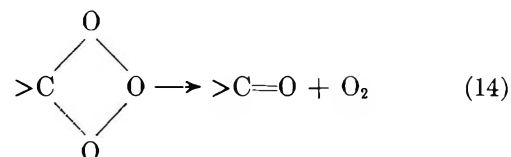
The decomposition of the tetroxide to form two alkoxy radicals and their subsequent rapid disproportionation in the cage is less preferred than the Russell mechanism.<sup>11</sup> This involves decomposition of the tetroxide to form a cyclic transition state in which one of the  $\alpha$ -hydrogen atoms is transferred to give the products ketone, alcohol, and oxygen.



The slow decay of our transient X ( $k_X = 5 \text{ sec}^{-1}$ ) could be identified with this process. However, the decay of X does not lead to products but to another transient, which we designate as Y. On the basis of these observations, a modified mechanism for the decomposition of the tetroxide is tentatively proposed. A trioxide is suggested to be formed



which subsequently decomposes



with  $k_{14} = k_Y = 1.5 \times 10^{-1} \text{ sec}^{-1}$ .

The formation of the organic trioxide as an intermediate is not unreasonable, since other species like  $\text{O}_3^-$  and  $\text{RO}_3$ <sup>15</sup> are well established. Whether it exists in an open radical form or in a cyclic highly strained form is not clear. Further kinetic studies on a number of other primary and secondary peroxy radicals are needed.

The Russell mechanism<sup>5,14</sup> requires that the oxygen evolved in the decomposition of the intermediate tetroxide (reaction 12) be formed in an excited singlet state. It is tempting to speculate that the "residual" molecular oxidation process observed by Dobson and Hughes<sup>9</sup> in the radiation-induced oxidation of organic compounds may be formed by reaction with singlet excited oxygen.

*Acknowledgment.* We thank Dr. P. Neta for his contribution to this work in the preliminary experiments.

(14) G. A. Russell, *J. Amer. Chem. Soc.*, **79**, 3871 (1957).

(15) R. W. Fessenden, *J. Chem. Phys.*, **48**, 3725 (1968).

# The Structure of Perchlorocyclopropene

by Hans J. Mair and S. H. Bauer\*

Department of Chemistry, Cornell University, Ithaca, New York 14850 (Received December 4, 1970)

Publication costs borne completely by The Journal of Physical Chemistry

To ascertain the extent of conjugation which is afforded by perhalosubstitution onto a cyclopropene ring, the gas phase structure of  $C_3Cl_4$  was determined by electron diffraction and compared with the structure of  $C_3H_4$  recently studied by microwave and diffraction techniques. The present diffraction data were recorded over the range of scattering angles  $5 < q < 125 \text{ \AA}^{-1}$ . Because the diffraction pattern "washed out" at the larger angles, several plates were averaged to obtain the optimum signal to noise ratio for the outer rings. Under the assumption that the structure has  $C_{2v}$  symmetry the dimensional parameters were obtained by least-squares analysis of the molecular intensity curve. Corresponding distances ( $r_g$ ) in the perchloro and hydro compounds are:  $C_1=C_2 = 1.320 \pm 0.006$  and  $1.304 \pm 0.003$ ;  $C_2-C_3 = 1.479 \pm 0.010$  and  $1.519 \pm 0.002 \text{ \AA}$  in  $C_3Cl_4$  and  $C_3H_4$ , respectively. Less surprising are the deduced carbon-chlorine bond lengths:  $Cl-C_1 = 1.684 \pm 0.002$  and  $Cl-C_3 = 1.771 \pm 0.002 \text{ \AA}$ . The latter is in the range of  $sp^3$  C-Cl values, and the former corresponds to an internuclear separation intermediate between  $sp^2$  C-Cl (as in tetrachloroethylene:  $1.718 \pm 0.003 \text{ \AA}$ ) and  $sp$  C-Cl (as in chloromethylacetylene:  $1.6371 \pm 0.0002 \text{ \AA}$ ). The  $Cl-C_3-Cl$  bond angle is  $108.8 \pm 1^\circ$  while  $\angle C_1-C_2-Cl = 152.5 \pm 2^\circ$ , intermediate between the values reported for the corresponding angles in cyclopropene.

## Introduction

Perchlorocyclopropene was first prepared by Tobey and West<sup>1</sup> in 1963. Since then several investigations have been reported on its chemical reactions and infrared and Raman spectra.<sup>2-4</sup> The observed frequencies were assigned on the basis of  $C_{2v}$  symmetry, thus distinguishing this molecule from its isomers, perchloroallene and perchloropropyne. To our knowledge this is the first experimental investigation of the internuclear distances present in this molecule. As such this provides data for an interesting comparison with cyclopropene in terms of the effects of electronegative substituents of considerable size and polarizability on the dimensions of a highly strained ring system.

## Experimental Section

The sample used for this study was purchased from Aldrich Chemical Co. The impurities, mostly traces of perchlorocyclopropane, were removed by fractional distillation and condensation, *in vacuo*. Purity levels were checked by the infrared spectra of the initial and final samples. Electron diffraction patterns were taken with the apparatus described by Bauer and Kimura.<sup>5</sup> The sample was kept at  $6^\circ$  during these runs, at which temperature the liquid has approximately 5 Torr of vapor pressure. During the diffraction exposure the ambient pressure in the unit was maintained at  $2.5 \times 10^{-6}$  Torr by a liquid nitrogen cooled cryo-pump located above the gas nozzle. The accelerating voltage was approximately 62 kV; Kodak electron image plates were used to record the diffraction patterns. Two sets of photographs were taken at plate-sample distances of 125 and 253 mm. The sample-plate distance and the wavelength were determined from MgO powder pat-

terns recorded concurrently with the gas diffraction patterns. For each set eight rings were fitted by a method of steepest descent to a sample-plate distance and wavelength. In no case did the standard deviation exceed 0.0008. Selected photographs which covered an optical density range from 0.4 to 2.0 units were microphotometered with a double-beam Jarrell-Ash microdensitometer interfaced with an analog-digital converter. Densities of pairs of plates (with the ratios of  $1/1.5$  to  $1/2$ ) were converted to intensities following the procedure generally used in this laboratory.<sup>6,7</sup>

Since the diffraction patterns appeared to be "washed out" for  $q > 85$  special efforts were made to enhance the resolution by reducing the background.<sup>8</sup> All portions of the sector mount and nozzle and other parts of the apparatus which could reflect scattered X-rays into the photographic plate region were replaced or covered by either magnesium or aluminum. This did considerably reduce the back scattered radiation. Also, a conically shaped diaphragm, of very thin aluminum foil, was inserted into the diffraction chamber with its axis along the electron beam and apex close to the nozzle; this reduced the background due to electrons scattered by the ambient gas along the primary beam on the side of

- (1) S. W. Tobey and R. West, *Tetrahedron Lett.*, (18), 1179 (1963).
- (2) S. W. Tobey and R. West, *J. Amer. Chem. Soc.*, **88**, 2481 (1966).
- (3) M. Ito, *Spectrochim. Acta*, **22**, 1581 (1966).
- (4) G. L. Closs, *Advan. Alicyclic Chem.*, **1**, 53 (1966).
- (5) S. H. Bauer and K. Kimura, *J. Phys. Soc. Jap.*, **17**, 300 (1962).
- (6) J. L. Hencher and S. H. Bauer, *J. Amer. Chem. Soc.*, **89**, 5527 (1967).
- (7) R. Hilderbrandt and S. H. Bauer, *J. Mol. Struct.*, **3**, 325 (1969).
- (8) H. Oberhammer and S. H. Bauer, *J. Amer. Chem. Soc.*, **91**, 10 (1969).

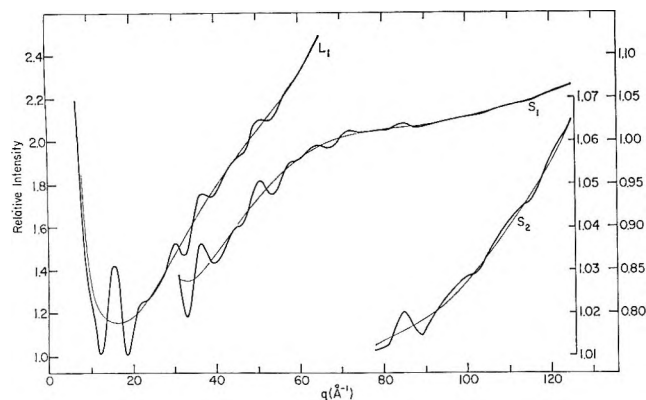


Figure 1. Relative diffracted intensity vs. scattering angle for  $C_3Cl_4$ . Trace  $L_1$  was recorded at the long nozzle-plate distance and  $S_1$  at the short spacing;  $S_2$  is an expanded plot of  $S_1$  for  $80 < q < 125$ .

the nozzle toward the electron gun. Finally, each of the plates was scanned several times and the average taken; then for each region of scattering several plates were analyzed. This greatly improved the reproducibility of the diffraction data. Reference to Figure 1 shows the portion of the diffraction pattern for  $q > 80$  on the usual scale (designated  $S_1$ ) and replotted on the magnified scale of densities as  $S_2$ .

#### Data Reduction and Results

The total experimental intensities as a function of the scattering angle for the two sets of averaged data have been deposited with NAPS. These are also plotted in Figure 1, along with the refined backgrounds. For the long sample-plate distance the  $q$  values covered are from 5 to 65, while for the short sample-plate distance the range is 25–125.

In the following analysis we assumed that the molecule had  $C_{2v}$  symmetry. Geometric parameters were introduced to specify the coordinates of the atoms:  $(C_1=C_2)/2$ , the height of the carbon atom ring,  $C_1-Cl_4$ ,  $C_3-Cl_6$ ,  $\angle C_3-C_1-Cl_4$ , and  $\angle(\text{ring plane})C_3-Cl_7$ . (See Figure 5 for designations). An approximate evaluation of the molecular intensity was obtained by a trial background drawn in for each set of data. This was followed by a series of refinements of the background in the usual manner until a satisfactorily radial distribution curve was obtained, as shown in Figure 2. The curve designated  $d_f$  is the difference between the experimental  $f(r)$  and that calculated for the final model. Figure 3 is a drawing on an expanded scale which shows the resolutions of the first three peaks. From these it is evident that there are several C-C and C-Cl distances in this molecule. Thus, the first shoulder is a superposition of the C=C and C-C distances (1.320 and 1.479 Å) and is followed by the main peak which resolves into two C-Cl separations at 1.684, and 1.771 Å. The second peak is the superposition of three nonbonded C-Cl distances and one nonbonded Cl-Cl distance, while the last peak (not shown on an enlarged scale)

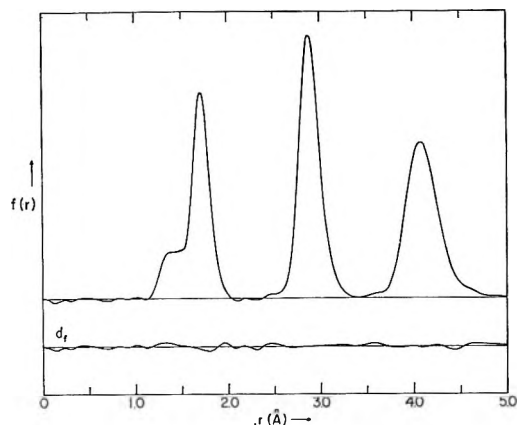


Figure 2. The experimental radial distribution curve from the final cycle of background refinement, for  $C_3Cl_4$ ;  $d_f$  designates the difference between the experimental curve and that calculated for the "best" model.

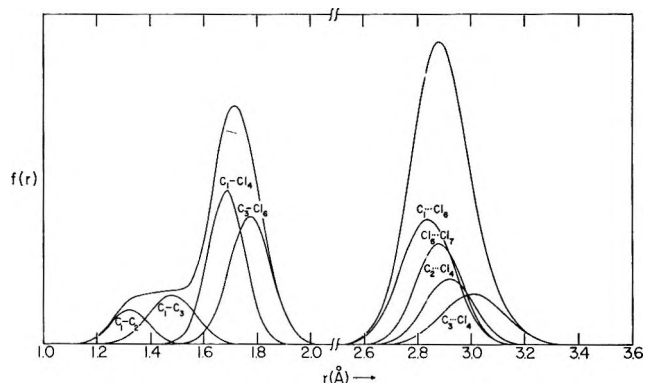


Figure 3. An expanded portion of  $f(r)$  for the region  $1.0 < r < 3.4 \text{ \AA}$ , with the peaks resolved into pair contributions.

consists of the remaining nonbonded Cl-Cl contributions.

The values for the geometrical parameters and the root mean square amplitudes deduced from the radial distribution analysis were then refined in a series of least-squares calculations to match the  $qM(q)$  curve. In the first approximation all the geometrical parameters were allowed to vary while maintaining reasonable values for the  $l_{ij}$ . Then the former was constrained to the optimized magnitudes and the latter allowed to vary. This alternating procedure was continued until the calculations indicated no further changes would be obtained either in the interatomic distances or in the root mean square amplitudes. The reduced experimental molecular intensity curve and that calculated for the best model are shown in Figure 4 along with the difference curve designated  $d_m$ . It is worth noting that, whereas in the least-squares refinement all the  $l_{ij}$  values converged to reasonable values,  $l_{45}$  converged to an unexpectedly high magnitude. Therefore in the final analysis it was constrained to 0.16 Å.

The diagonal elements of the error matrix are the standard deviations for the corresponding parameters



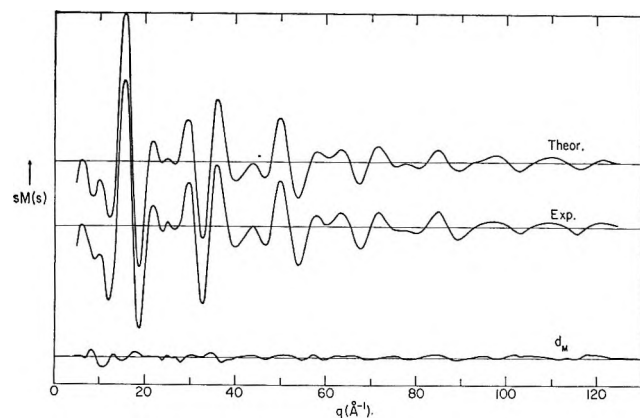


Figure 4. The experimental and calculated  $sM(s)$  curves for  $C_3Cl_4$  and their difference,  $d_m$ .

while the off-diagonal elements measure the correlation between these parameters. In this program we assumed that the correlation between adjacent data points was negligible. The error matrix thus shows that while there was some correlation between the  $l_{ij}$  values, as is expected for a molecule with closely similar distances, there appears to be no significant correlations between the geometric parameters. The error in scale, estimated from fitting of eight rings in the MgO diffraction patterns, corresponds to less than  $\pm 0.002 \text{ \AA}$  in a bonded atom pair separation.<sup>8</sup> We then arbitrarily set the error limits for the interatomic distances at twice their standard deviations, provided these were larger than the geometric scaling error.

### Discussion

The results of the least-squares analysis for structural parameters ( $r_g$  values) and mean-square amplitudes are summarized in Table I. A diagram of the

Table I: Structural Parameters and Mean-Square Amplitudes for  $C_3Cl_4$

Type	$r_{ij}, \text{ \AA}$	$l_{ij}, \text{ \AA}$
$C_1=C_2$	$1.320 \pm 0.010$	$0.042 \pm 0.013$
$C_1-C_3$	$1.479 \pm 0.011$	$0.068 \pm 0.012$
$C_1-Cl_4$	$1.684 \pm 0.004$	$0.043 \pm 0.006$
$C_3-Cl_6$	$1.771 \pm 0.004$	$0.058 \pm 0.006$
$\angle C_2C_1C_3$	$152.5^\circ \pm 0.8^\circ$	
$\angle C_{\text{plane}}-Cl_6$	$125.6^\circ \pm 0.4^\circ$	
Nonbonded Internuclear Distances		
$C_1-Cl_6$	2.838	$0.085 \pm 0.010$
$C_2-Cl_4$	2.919	$0.075 \pm 0.018$
$C_3-Cl_4$	3.009	$0.104 \pm 0.022$
$Cl_6-Cl_7$	2.879	$0.069 \pm 0.013$
$Cl_4-Cl_6$	4.064	$0.138 \pm 0.006$
$Cl_4-Cl_5$	4.308	0.16 (assigned)

molecule is given in Figure 5. Because of the very high ring strain, three-membered carbon rings show unusual

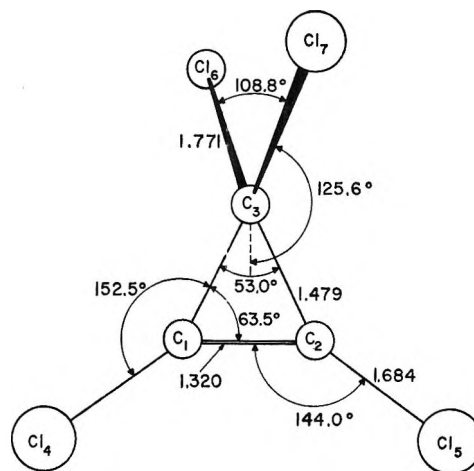


Figure 5. Atom designations for  $C_3Cl_4$  and the "best" values based on the least-squares refinement of the  $sM(s)$  data.

chemical properties as well as characteristic structural features. With respect to the ring dimensions, as shown in Table II, the  $C=C$  distance is  $0.02 \text{ \AA}$  larger and the  $C-C$  is  $\sim 0.04 \text{ \AA}$  smaller in the perchloro compound than in the parent hydrocarbon. Empirically the larger  $C=C$  is consistent with the trend observed in ethylene due to chlorosubstitution. Presumably this is due to a superposition of two factors, the repulsion between the chlorine atoms and a shift of electron density from the region between the carbons to increase the bond order between the carbons and the chlorines. However, the  $(C-C)$  distance is unexpectedly short; it is closer to that present in butadiene ( $1.463 \text{ \AA}$ ) while we expected it to be like that present in the  $C_3H_4$  or in propene.

The two  $C-Cl$  bond distances observed in  $C_3Cl_4$  can be placed on a scale of  $C-Cl$  bond lengths, as shown in Table III. These range in magnitude from  $1.64 \text{ \AA}$  as in  $MeC\equiv CCl$ , to  $1.81 \text{ \AA}$  in *tert*-butyl  $Cl$ , and clearly show that the observed  $C-Cl$  bond lengths are affected by the hybridization on the carbon atoms, which is to some extent determined by the bond angles relative to the other substituents and by conjugation with the rest of the molecule. The relative magnitudes of these bond lengths as present in  $C_3-Cl_4$  correspond to those found in our preliminary studies of perchlorocyclopentadiene. However, in absolute value these are smaller.

The Walsh<sup>9</sup> model for cyclopropane may be extended to cyclopropene to provide some rationale for the observed interatomic distances. Attempts to apply the empirical procedure suggested by Bak and Led<sup>10</sup> have not proved fruitful. With respect to the Walsh model a possible assignment of orbitals is shown in Figure 6, which is a schematic exploded view of the orbitals. The picture emphasizes the highly delocalized nature of

(9) (a) A. D. Walsh, *Nature*, **159**, 165, 712 (1947); (b) W. A. Bennett, *J. Chem. Educ.*, **44**, 16 (1967).

(10) B. Bak and J. J. Led, *J. Mol. Struct.*, **3**, 379 (1969).

Table II: Comparison of C=C and C—C Bond Lengths

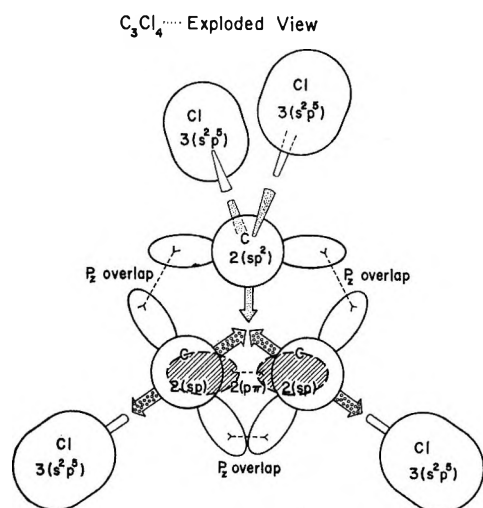
Compd	C=C, Å	C—C, Å	Method	Ref
C <sub>3</sub> H <sub>4</sub>	1.300	1.515	M.W.	a
	1.304 ± 0.003	1.519 ± 0.012	E.D.	b
C <sub>3</sub> Cl <sub>4</sub>	1.320 ± 0.010	1.479 ± 0.011	E.D.	This work
C <sub>3</sub> H <sub>6</sub>	1.336	1.501	E.D.	c
C <sub>3</sub> H <sub>6</sub> (cyclo)		1.5096 ± 0.0015	E.D.	d
C <sub>3</sub> H <sub>3</sub> Cl (cyclo)		1.5131 ± 0.0001	M.W.	e
		1.513 ± 0.004	M.W.	f
C <sub>2</sub> H <sub>4</sub>	1.332 ± 0.002		E.D.	g
C <sub>2</sub> H <sub>2</sub> Cl <sub>2</sub> (1,2)	1.336 ± 0.016 (cis)		E.D.	h
	1.343 ± 0.015 (trans)		E.D.	i
C <sub>2</sub> Cl <sub>4</sub>	1.354 ± 0.003		E.D.	j
C <sub>2</sub> H <sub>6</sub>		1.531 ± 0.002	E.D.; IR	k

<sup>a</sup> P. H. Kasai, R. J. Myers, D. F. Eggers, and K. B. Wiberg, *J. Chem. Phys.*, **29**, 864 (1958). <sup>b</sup> J. F. Chiang, 157th National Meeting of the American Chemical Society, Abstracts, Minneapolis, Minn., 1969; *J. Chin. Chem. Soc. (Taipei)*, **17**, 65 (1970). <sup>c</sup> J. D. Swalen and C. A. Reilly, *J. Chem. Phys.*, **34**, 2122 (1961). <sup>d</sup> O. Bastiansen, F. N. Fritsch, and K. Hedberg, *Acta Crystallogr.*, **17**, 538 (1964). <sup>e</sup> J. P. Friend and B. P. Bailey, *J. Chem. Phys.*, **29**, 577 (1958). <sup>f</sup> R. H. Schwendemann, G. D. Jacobs, and T. M. Krigas, *ibid.*, **40**, 1022 (1964). <sup>g</sup> L. S. Bartell and R. S. Bonham, *ibid.*, **31**, 400 (1959). <sup>h</sup> C. W. W. Hoffman, *Diss. Abstr.*, **18**, 420 (1958). <sup>i</sup> L. H. Kaplan, *ibid.*, **19**, 3130 (1959). <sup>j</sup> T. G. Strand, *Acta Chem. Scand.*, **21**, 1033 (1967). <sup>k</sup> K. Kuchitsu, *J. Chem. Phys.*, **49**, 4456 (1968).

Table III: Comparison of C—Cl Bond Lengths, Å

MeC≡CCl	1.6371	(M.W.) <sup>a</sup>	C <sub>3</sub> H <sub>3</sub> Cl (cyclo)	1.740	(M.W.) <sup>j</sup>
C <sub>6</sub> H <sub>5</sub> Cl	1.706	(M.W.) <sup>b</sup>	C <sub>3</sub> H <sub>7</sub> Cl (spiro)	1.740	(M.W.) <sup>g</sup>
H <sub>2</sub> C=CCl <sub>2</sub>	1.707	(E.D.) <sup>c</sup>	4-Cl-nortricyclene	1.763	(E.D.) <sup>h</sup>
Cl <sub>2</sub> C=CCl <sub>2</sub>	1.718	(E.D.) <sup>d</sup>	MeCCl <sub>3</sub>	1.7712	(M.W.) <sup>i</sup>
H <sub>2</sub> C=CCl	1.726	(M.W.) <sup>e</sup>	H <sub>3</sub> CCl	1.784	(E.D.) <sup>j</sup>
 H			tert-Butyl Cl	1.807	(E.D.) <sup>k</sup>

<sup>a</sup> C. C. Costain, *J. Chem. Phys.*, **23**, 2037 (1955). <sup>b</sup> E. Erlandsson, *Ark. Fys.*, **8**, 341 (1954); see also R. Rudman, *Chem. Commun.*, 536 (1970). <sup>c</sup> L. H. Kaplan, *Diss. Abstr.*, **19**, 3130 (1959). <sup>d</sup> T. G. Strand, *Acta Chem. Scand.*, **21**, 1033 (1967). <sup>e</sup> D. Kivelson, E. B. Wilson, and D. R. Lide, *J. Chem. Phys.*, **32**, 205 (1960). <sup>f</sup> R. H. Schwendemann, G. D. Jacobs, and T. M. Krigas, *ibid.*, **40**, 1022 (1964). <sup>g</sup> L. M. Woerner and M. D. Harmony, *ibid.*, **45**, 2339 (1966). <sup>h</sup> J. F. Chiang, C. F. Wilcox, Jr., and S. H. Bauer, *Tetrahedron*, **25**, 369 (1969). <sup>i</sup> R. Hohn, M. Mitshaff, and H. Hartmann, *Z. Naturforsch. A*, **23**, 307 (1968). <sup>j</sup> L. S. Bartell and L. O. Brockway, *J. Chem. Phys.*, **23**, 1860 (1955). <sup>k</sup> J. Haase, H. D. Kampusmann, and W. Zeil, *Z. Phys. Chem. (Frankfurt am Main)*, **55**, 225 (1967).

Figure 6. An exploded view of the schematic orbitals for C<sub>3</sub>Cl<sub>4</sub>.

frame in cyclopropene may be intermediate between that characteristic of ethylene and of acetylene. Thus the substitution of chlorine atoms for hydrogen at the double bond withdraws electron density from the double-bonded carbon atoms and allows more of an overlap of those p<sub>z</sub> orbitals which involve the third carbon atom. This leads to a longer C=C and a shorter C—C than is present in the parent hydrocarbon. In turn this argument provides a rationale for the observed C—Cl distances. A comparison between this molecule and perchlorocyclopentadiene is made in the accompanying article.

*Acknowledgments.* The authors wish to thank the National Science Foundation for support of this work, under Grant No. GP-7794. We are also grateful to Mr. M. Cardillo for his effort in developing the diaphragms which reduced the background for the electron diffraction photographs and to Mr. R. L. Hilderbrandt for generating the computer programs used in these data reductions.

the electron distribution in this molecule. With respect to conjugation with substituents the carbon atom

# The Molecular Structure of Perfluorocyclopentene and Perchlorocyclopentadiene by Gas Phase Electron Diffraction

by C. H. Chang and S. H. Bauer\*

Department of Chemistry, Cornell University, Ithaca, New York 14850 (Received December 4, 1970)

Publication costs borne completely by The Journal of Physical Chemistry

Gas phase electron diffraction patterns of perfluorocyclopentene and perchlorocyclopentadiene were recorded, with the samples at 25 and 94°, respectively. Least-squares analyses of the intensity data for perfluorocyclopentene revealed that the five-member carbon ring is not planar; the pucker angle is  $21.9 \pm 0.5^\circ$ , and thus 7° smaller than that reported for cyclopentene ( $29.0 \pm 2.5^\circ$ ). The measured bond lengths ( $r_g$ ) are: (C=C) =  $1.342$  [constrained], (=C—C) =  $1.510 \pm 0.028$ , (C—C) =  $1.539 \pm 0.040$ , (=C—F) =  $1.311 \pm 0.016$ , and (C—F) =  $1.351 \pm 0.007$  Å. The ring angles were found to be:  $\angle$ C=C—C =  $113.6 \pm 1.2^\circ$ ,  $\angle$ =C—C—C =  $98.5^\circ$ ,  $\angle$ C—C—C =  $112.2^\circ$ ,  $\angle$ F—C=C =  $128.2 \pm 2.1^\circ$ ,  $\angle$ FC(4)F [C(4) is out of C<sub>4</sub> plane] =  $103.8^\circ$ , and  $\angle$ FCF =  $108.0^\circ$ . Perchlorocyclopentadiene has a planar five-membered carbon ring, with bond lengths ( $r_g$ ): (=C—C=) =  $1.486 \pm 0.015$ , (—C=C—) =  $1.344 \pm 0.020$ , (=C—C—) =  $1.509 \pm 0.034$ , (=C—Cl) =  $1.703 \pm 0.005$ , and (—C—Cl) =  $1.819 \pm 0.017$  Å; the bond angles are:  $\angle$ =C—C=C— =  $107.6 \pm 1.0^\circ$ ,  $\angle$ —C=C—C— =  $112.8^\circ$ ,  $\angle$ =C—C—C= =  $99.2^\circ$ , and  $\angle$ Cl—C—Cl =  $116.8^\circ$ . Comparisons and contrasts with related compounds are presented.

## Introduction

Several investigations have been reported on the molecular structure of unsaturated five-member hydrocarbons. An early electron diffraction study by Schomaker and Pauling<sup>1</sup> revealed that 1,3-cyclopentadiene had a planar carbon ring with bond lengths similar to those found in open-chain compounds. These were later confirmed by microwave<sup>2</sup> and X-ray diffraction<sup>3</sup> data. In contrast, cyclopentene was found to be puckered by 29°, with (C=C) =  $1.343$  Å and (C—C) =  $1.533$  Å, both by microwave<sup>4</sup> and electron diffraction<sup>5</sup> measurements. We have found no data on internuclear distances in the halosubstituted analogs of these ring systems. Therefore, we report here our electron diffraction results for perfluorocyclopentene and perchlorocyclopentadiene.

## Experimental Section

Gaseous electron diffraction patterns of perfluorocyclopentene, C<sub>5</sub>F<sub>8</sub> (sample at room temperature), were recorded on 4 × 5 in. Kodak Electron Image Plates at nozzle-plate distances of 253 mm ( $q = 9\text{--}50$  Å<sup>-1</sup>) and 125 mm ( $q = 42\text{--}124$  Å<sup>-1</sup>). Mass spectrometrically pure C<sub>5</sub>F<sub>8</sub> was obtained from Penninsular ChemResearch. Wavelength and nozzle-to-plate distances were determined from analyses of MgO powder diffraction patterns taken concurrently with the sample photographs.

A sample of perchlorocyclopentadiene, C<sub>5</sub>Cl<sub>6</sub>, was obtained from the Velsicol Chemical Corporation; it had a minimum assay of 97.0%, with perchlorocyclopentene as the primary contaminant. Impurities were removed by vacuum distillation, so that the sample

used in the diffraction experiment had a purity of 99.9%, as checked by its infrared spectrum and a vpc analysis. Since the vapor pressure of C<sub>5</sub>Cl<sub>6</sub> is quite low at room temperature the newly constructed "intermediate temperature" nozzle was used to obtain the diffraction patterns. As shown in Figure 1, the sample container, lead tube, and nozzle are electrically heated. In this case, these were maintained at 94°, at which temperature the liquid has approximately 5 Torr of vapor pressure. Six chromel-alumel thermocouples monitor temperatures along the lead tube, from the sample container to the nozzle tip. Magnesium oxide powder patterns were recorded in order to determine the wavelength of the electron beam (0.045852 Å) and the distance  $L + L'$  (202.54 mm), where  $L$  is the nozzle-to-plate distance and  $L'$  the distance from the MgO mount to the nozzle center. The MgO-nozzle distance  $L'$  (13.31 mm) was measured directly after the photographs were taken. In order to eliminate any systematic error due to the mechanical measurement and a possible discrepancy between the nozzle center at room temperature and the diffraction center at the higher temperature, carbon disulfide (CS<sub>2</sub>) patterns were taken under the same conditions as the sample photographs except that the CS<sub>2</sub> container was not heated. For C<sub>5</sub>Cl<sub>6</sub> useful electron diffraction patterns ranging

(1) V. Schomaker and L. Pauling, *J. Amer. Chem. Soc.*, **61**, 1769 (1939).

(2) L. H. Scharpen and V. W. Laurie, *J. Chem. Phys.*, **43**, 2765 (1965).

(3) G. Liebling and R. E. Marsh, *Acta Crystallogr.*, **19**, 202 (1965).

(4) G. W. Rathjens, Jr., *J. Chem. Phys.*, **36**, 2401 (1962).

(5) M. I. Davis and T. W. Muecke, *J. Phys. Chem.*, **74**, 1104 (1970).

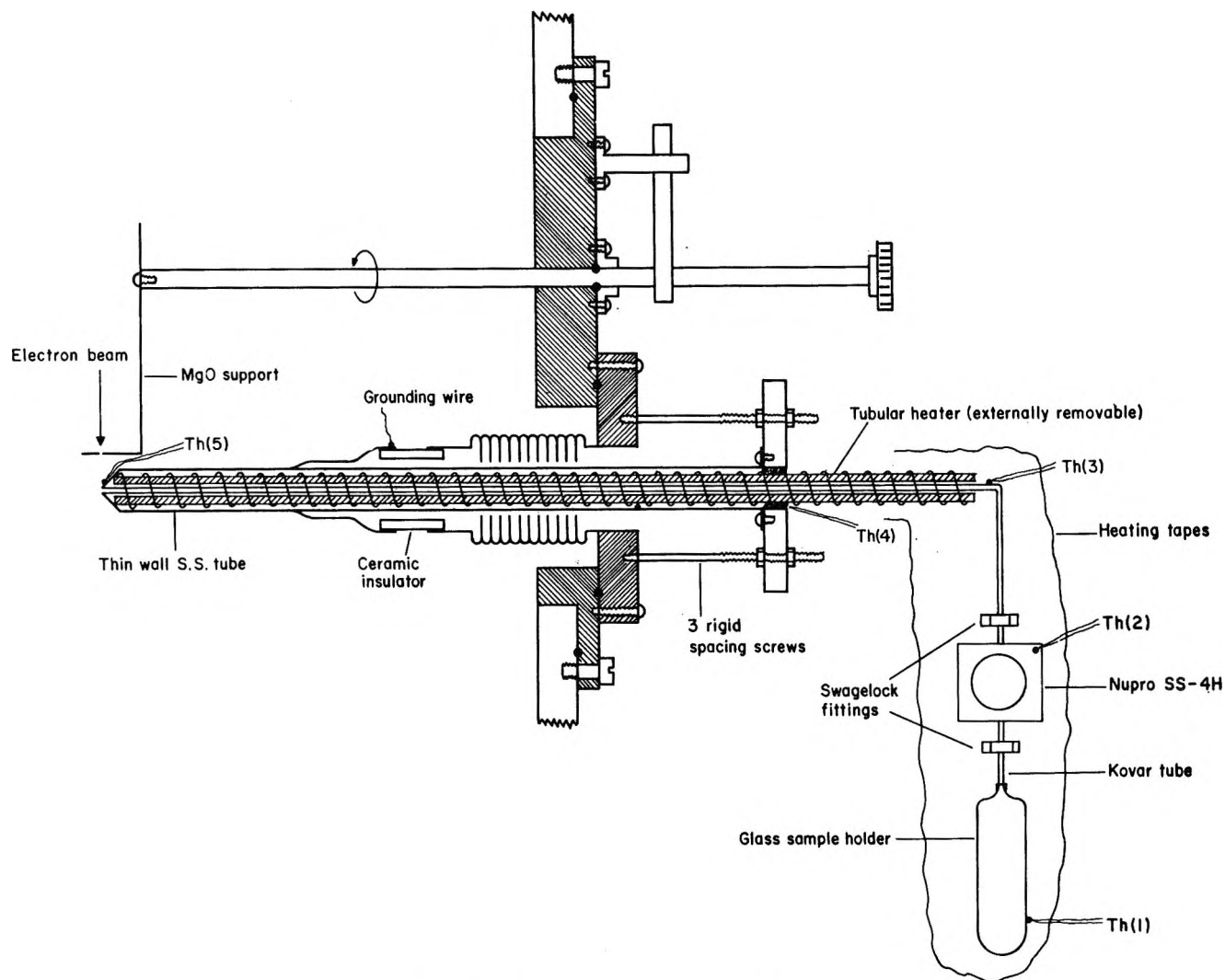


Figure 1. High-temperature nozzle system. Note that the tube heater is at atmospheric pressure.

from  $q = 10$  to  $93 \text{ \AA}^{-1}$  were recorded; from  $q = 8$  to  $49 \text{ \AA}^{-1}$  with a  $0.06248\text{-\AA}$  beam at a nozzle-to-plate distance of  $247.91 \text{ mm}$ , and  $q = 30$  to  $160 \text{ \AA}^{-1}$  with a  $0.04906\text{-\AA}$  beam at a nozzle-to-plate distance of  $89.34 \text{ mm}$ . However, because differences in intensity between maxima and minima were of the order of magnitude of the experimental uncertainty at diffraction angles beyond  $q = 95 \text{ \AA}^{-1}$ , only data at  $q = 10\text{--}93 \text{ \AA}^{-1}$  were used in the structure analysis. All plates were processed to obtain intensity data as described in previous reports from this laboratory.<sup>6</sup>

### Structure Analysis

Reduced experimental data at  $q = 9\text{--}124 \text{ \AA}^{-1}$  for  $\text{C}_5\text{F}_8$  and  $q = 10\text{--}93 \text{ \AA}^{-1}$  for  $\text{C}_5\text{Cl}_6$  have been deposited for reference with NAPS.<sup>7</sup> The patterns were plotted (along with the reduced backgrounds) in Figure 2. Corresponding experimental radial distribution curves are shown in Figure 3, and molecular intensity curves,  $qM(q)$ , in Figure 4. The experimental  $qM(q)$  curves were fitted by least-squares analyses with a nondiagonal

weighting matrix, in the manner described by Murata and Morino.<sup>8</sup>

*Perfluorocyclopentene.* The molecular configuration was assumed to possess a plane of symmetry, in which atoms C(4), F(9), and F(12) are located, as shown in Figure 5a. Five geometric parameters are required to specify the carbon ring. The plane of C(1)C(2)C(3)-C(5) and the symmetry plane were chosen as  $xy$  and  $yz$  planes, respectively. Then (C=C), (=C-C), and  $\angle \text{C}_1\text{C}_2\text{C}_3$  locate the four carbon atoms in the  $xy$  plane. The out-of-plane location of the C(4) atom is specified by two parameters, C(4)-O and  $\angle \text{C}_4\text{O}y$ , where O is the

(6) J. L. Hencher and S. H. Bauer, *J. Amer. Chem. Soc.*, **89**, 5527 (1967); W. Harshbarger, G. Lee, R. F. Porter, and S. H. Bauer, *Inorg. Chem.*, **8**, 1683 (1969); R. L. Hilderbrandt and S. H. Bauer, *J. Mol. Struct.*, **3**, 325 (1969).

(7) Data have been deposited with ASIS-NAPS, c/o CCM Information Corp., 909 3rd Avenue, New York, N. Y. 10022. A copy may be secured by citing the document number and by remitting \$1.00 for microfiche or \$3.00 for photocopies. Advance payment is required. Make checks or money orders payable to: ASIS-NAPS.

(8) Y. Murata and Y. Morino, *Acta Crystallogr.*, **20**, 605 (1966).

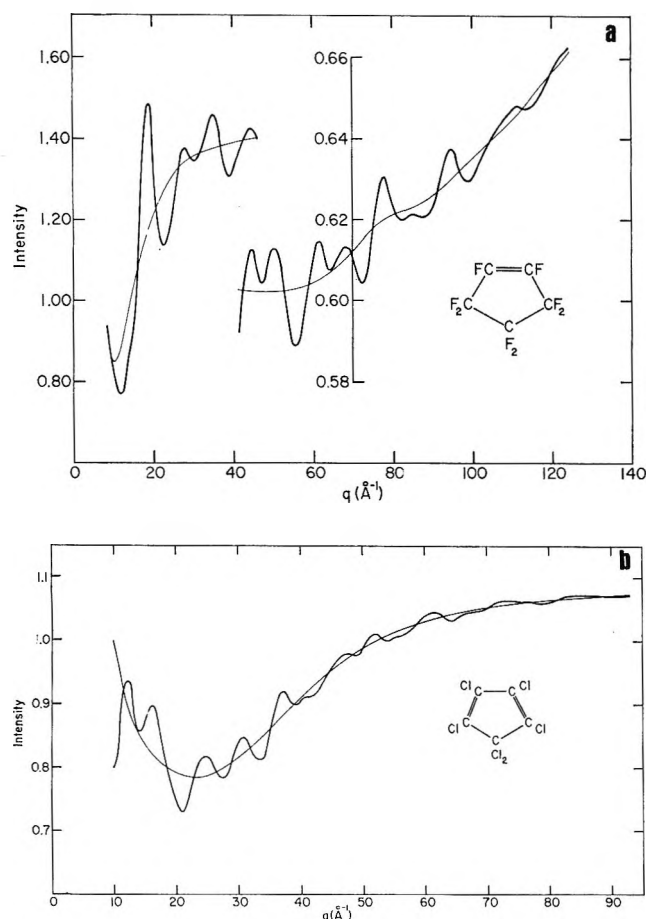


Figure 2. The experimental intensity and background curves for perfluorocyclopentene (a) and perchlorocyclopentadiene (b).

origin of the cartesian coordinates. Two additional assumptions were made with regard to the choice of parameters for locating the fluorine atoms: (i) F(6) and F(7) are in the C(1)C(2)C(3)C(5) plane, and (ii) the other F-atoms are bonded to their respective carbons with equal bond lengths. Thus, the number of parameters required to describe the F positions is reduced to nine; *i.e.*, ( $=\text{C}-\text{F}$ ), ( $\text{C}-\text{F}$ ),  $\angle(\text{F}_6\text{C}_1\text{C}_2)$ ,  $\angle(\text{F}_8\text{C}_3\text{C}_2)$ ,  $\angle(\text{F}_{11}\text{C}_3\text{C}_2)$ ,  $\angle(\text{F}_{11}\text{C}_3\text{F}_8)$ ,  $\angle(\text{F}_9\text{C}_4\text{C}_3)$ ,  $\angle(\text{F}_{12}\text{C}_4\text{C}_3)$ , and  $\angle(\text{F}_8\text{C}_3\text{C}_4)$ .

Thirty-nine vibrational parameters ( $l_{ij}$ ) are needed to describe the atom-pair vibrational motions in the molecule, even when a plane of symmetry is assumed. Since long nonbonded  $l_{ij}$  values are less sensitive to the least-squares refinement of the molecular intensity data, we followed the usual procedures to fix them at reasonable values (selected from a study of the RDR curve) in the final least-squares analysis. Values for ( $\text{C}=\text{C}$ ),  $l(\text{C}=\text{C})$ ,  $l(=\text{C}-\text{C})$ ,  $l(\text{C}-\text{C})$ , and  $l(\text{C}\cdots\text{C})$  were deduced from the RDR curves and preliminary sequential univariant parameter adjustments; these also were constrained in the final least-squares run.

*Perchlorocyclobutadiene.* From the sharpness of the experimental RDR peaks, particularly the peaks assigned to  $\text{C}_1\cdots\text{Cl}_{10}$  and  $\text{Cl}_8\cdots\text{Cl}_{10}$  which center at

3.5  $\text{\AA}$ ,  $\text{C}_1\cdots\text{Cl}_8$  at 3.9  $\text{\AA}$ , and that for the long nonbonding  $\text{Cl}_6\cdots\text{Cl}_{10}$  at 5.1  $\text{\AA}$  and  $\text{Cl}_6\cdots\text{Cl}_8$  at 5.6  $\text{\AA}$ , molecular models in which the carbon skeleton is nonplanar were ruled out during the early stage of the analysis. The molecule was assumed to have the symmetry  $C_{2v}$ . The carbon ring is specified by the parameters: ( $\text{C}_1-\text{C}_2$ ), ( $\text{C}_2=\text{C}_3$ ), ( $\text{C}_4-\text{O}$ ), and  $\angle(\text{C}_1\text{C}_2\text{C}_3)$ ; the chlorine atoms by ( $\text{C}_1-\text{Cl}_6$ ), ( $\text{C}_4-\text{Cl}_{10}$ ),  $\angle(\text{Cl}_6\text{C}_1\text{C}_2)$ ,  $\angle(\text{Cl}_8\text{C}_3\text{C}_2)$ , and  $\angle(\text{Cl}_{10}\text{C}_4\text{C}_3)$ . This gives a total of nine geometric parameters. Of course, Cl(7), Cl(8), Cl(9), Cl(10) were assumed to be in the carbon plane, with equal bond lengths. All geometrical parameters were refined simultaneously along with five  $l_{ij}$  values ( $l_{\text{C}-\text{Cl}}$  and  $l_{\text{C}\cdots\text{Cl}}$ ); the  $l_{ij}$  for carbon atom pairs and for the long nonbonded Cl $\cdots$ Cl pairs were constrained to values deduced from the radial distribution curve and pre-

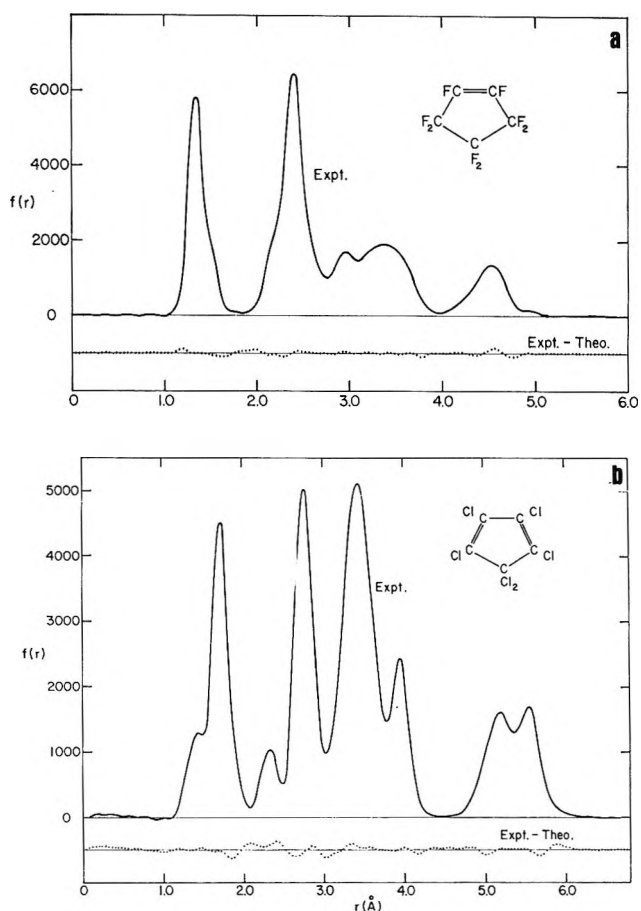


Figure 3. The refined experimental radial distribution curve and the difference curves between the experimental and calculated values for the converged least-squares model: (a)  $\text{C}_5\text{F}_8$ ; (b)  $\text{C}_5\text{Cl}_6$ .

liminary least-squares calculations. The molecular structure of  $\text{CS}_2$  used for calibration was determined by refining ( $\text{C}=\text{S}$ ), ( $\text{S}\cdots\text{S}$ ),  $l(\text{C}-\text{S})$ , and  $l(\text{S}\cdots\text{S})$  simultaneously as per the usual least-squares method. The scale factor deduced from this analysis is unity within  $+0.03\%$  for ( $\text{C}=\text{S}$ ) and  $-0.10\%$  for ( $\text{S}\cdots\text{S}$ ).

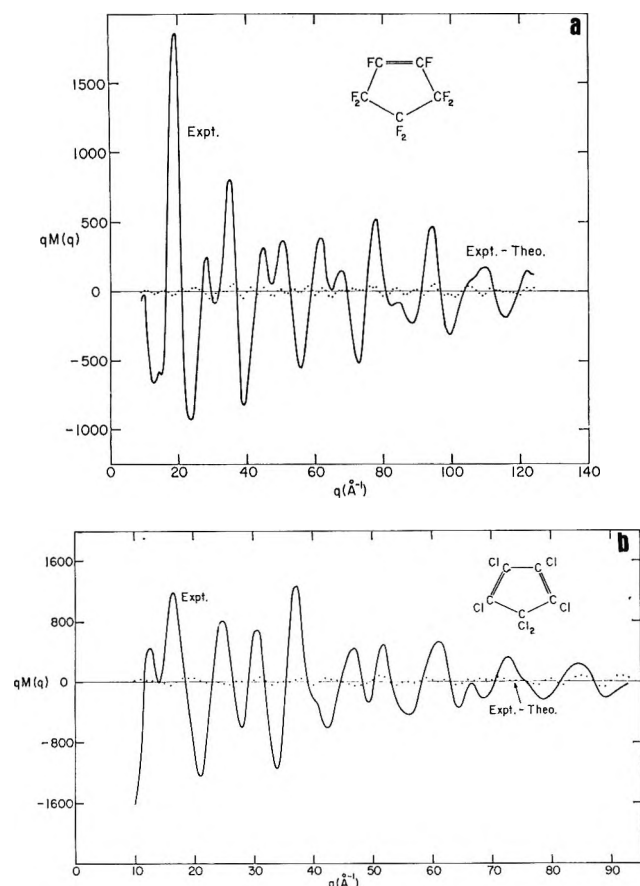


Figure 4. The reduced experimental molecular scattering curves,  $qM(q)$ , and the corresponding difference curves: (a)  $C_5F_8$ ; (b)  $C_5Cl_6$ .

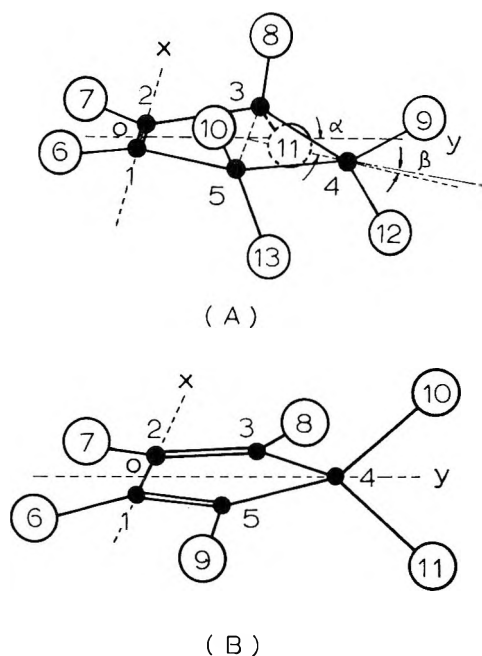


Figure 5. Atom designation for perfluorocyclopentene (A) and perchlorocyclopentadiene (B).

## Results and Discussion

*Perfluorocyclopentene.* The results of this determina-

Table I: Structural Parameters for Cyclopentenes

Parameters	Cyclopentene <sup>a</sup>	Perfluorocyclopentene <sup>b</sup>
(C=C)	1.342 ± 0.010	1.342 <sup>c</sup>
(=C—C)	1.519 ± 0.030	1.510 ± 0.028
(C <sub>4</sub> O)		2.208 ± 0.040
(C—C)	1.546 ± 0.035	1.539 ± 0.040
(=C—X)	1.098 ± 0.006	1.311 ± 0.016
(C—X)	1.098 ± 0.006	1.351 ± 0.007
∠(C <sub>4</sub> Oy)		7.82 ± 1.3
∠(C <sub>1</sub> C <sub>2</sub> C <sub>3</sub> )	111.0 ± 1.2	113.6 ± 1.2
∠(C <sub>2</sub> C <sub>3</sub> C <sub>4</sub> )	[103.0] <sup>d</sup>	[98.5] <sup>d</sup>
∠(C <sub>3</sub> C <sub>4</sub> C <sub>5</sub> )	[104.0] <sup>d</sup>	[112.2] <sup>d</sup>
α	28.8 ± 2.5	[20.5] <sup>d</sup>
β	0.0	[3.5] <sup>d</sup>
∠(X <sub>6</sub> C <sub>1</sub> C <sub>2</sub> ) <sup>e</sup>	121.8 <sup>c</sup>	128.2 ± 2.1
∠(XC <sub>3</sub> X)	101.8 <sup>c</sup>	107.0 ± 2.7
∠(XC <sub>4</sub> X)	104.8 <sup>c</sup>	[104.0] <sup>d</sup>
∠(F <sub>8</sub> C <sub>3</sub> C <sub>2</sub> )		109.9 ± 2.3
∠(F <sub>8</sub> C <sub>3</sub> C <sub>4</sub> )		111.9 ± 2.8
∠(F <sub>11</sub> C <sub>3</sub> C <sub>2</sub> )		113.4 ± 1.8
∠(F <sub>9</sub> C <sub>4</sub> C <sub>3</sub> )		108.4 ± 1.1
∠(F <sub>12</sub> C <sub>4</sub> C <sub>3</sub> )		111.8 ± 1.3
l(C=C) <sup>e</sup>	0.035 ± 0.015	0.038 <sup>c</sup>
l(=C—C)	0.046 ± 0.020	0.050 <sup>c</sup>
l(C—C)	0.046 ± 0.020	0.054 <sup>c</sup>
l(C···C)	0.054 ± 0.020	0.073 <sup>c</sup>
l(C—X)	0.059 ± 0.005	0.048 ± 0.004
l(C <sub>4</sub> ···X <sub>8</sub> )	0.075	0.057 ± 0.007
l(C <sub>1</sub> ···X <sub>8</sub> )	0.076	0.108 ± 0.012
l(X <sub>8</sub> ···X <sub>11</sub> )		0.058 ± 0.013
l(X <sub>8</sub> ···X <sub>9</sub> )		0.073 ± 0.017

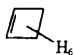
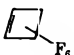





<sup>a</sup> Taken from ref 5. <sup>b</sup> Numbers obtained are  $\tau_R$  values with errors at three times the least-squares standard deviations. <sup>c</sup> Parameters constrained in the final least-squares analysis. <sup>d</sup> Values computed. <sup>e</sup> Bond lengths in ångströms and angles in degrees.

tion of the molecular structure of  $C_5F_8$  are summarized in Table I, along with values reported by Davis and Muecke<sup>5</sup> for  $C_5H_8$ . The carbon-fluorine bond lengths of  $1.311 \pm 0.016$  and  $1.351 \pm 0.007$  Å are within the experimental errors of similar ( $=C-F$ ) and  $>C<F$  parameters observed in other fluorocarbons. Thus,  $1.319 \pm 0.012$  and  $1.336 \pm 0.006$  Å were found in perfluorocyclobutene<sup>9</sup> and  $1.333 \pm 0.002$  Å in perfluorocyclobutane;<sup>9</sup> in open chains,  $1.323 \pm 0.006$  Å was reported for perfluorobutadiene-1,3<sup>10</sup> and  $1.333 \pm 0.003$  Å<sup>10</sup> in perfluorobutynes-2.<sup>10</sup> Since only one simplifying condition was introduced in the model (plane of symmetry), the FCF and FCC bond angles obtained from the least-squares analysis are reliable. The FCF angles are *not* bisected by corresponding CCC planes, so that the F(9)CF(12) group has a tilt angle  $\beta = 3.5^\circ$ , which is comparable with the values of  $4.0$  and  $5.4^\circ$  ob-

(9) C. H. Chang, R. F. Porter, and S. H. Bauer, *J. Mol. Struct.*, **7**, 89 (1971).

(10) C. H. Chang, A. L. Andreassen, and S. H. Bauer, *J. Org. Chem.*, in press.

**Table II:** Bond Lengths and Angles in Cyclobutene and Cyclopentene Rings

								
	Cyclo-butene <sup>a</sup>	Perfluoro-cyclobutene <sup>b</sup>	Cyclo-pentene <sup>c</sup>	Perfluoro-cyclopentene <sup>d</sup>	Norbornadiene		Bicyclo-[2,1,1]hexene <sup>g</sup>	Tricyclo-[3,3,0,0,0]-oct-3-ene <sup>h</sup>
(C=C) <sup>i</sup>	1.342	1.342	1.342	1.342	1.343 <sup>e</sup>	1.357 <sup>f</sup>	1.332	1.345
(=C—C)	1.517	1.508	1.519	1.510	1.535	1.549	1.537	1.503
(C—C)			1.546	1.539	1.573	1.567	1.548	1.580
(C <sub>3</sub> ···C <sub>5</sub> )	1.566	1.595	2.436	2.554				
∠(C <sub>1</sub> C <sub>2</sub> C <sub>3</sub> )	94.2	94.8	111.0	113.6	107.0	108.5	108.4	103.7
∠(C <sub>2</sub> C <sub>3</sub> C <sub>4</sub> )	85.8	85.2	103.0	98.5		96.0	86.4	104.0
∠(C <sub>3</sub> C <sub>4</sub> C <sub>5</sub> )			104.0	112.2	94.1	96.5	96.1	81.3
∠(X <sub>6</sub> C <sub>1</sub> C <sub>2</sub> )	133.5	133.6	121.8	128.2			127.2	131.3
Pucker angle, α			28.8	20.5	57.8	57.3	61.6	58.8

<sup>a</sup> B. Bak, *et al.*, *J. Mol. Struct.*, **3**, 369 (1969). <sup>b</sup> See ref 9. <sup>c</sup> See ref 5. <sup>d</sup> This work. <sup>e</sup> A. Yokozeki and K. Kuchitsu, to be submitted for publication. <sup>f</sup> T. W. Muecke and M. I. Davis, *Trans. Amer. Crystallogr. Ass.*, **2**, 173 (1966). <sup>g</sup> J. F. Chiang and S. H. Bauer, to be submitted for publication. <sup>h</sup> D. L. Zebelman and S. H. Bauer, to be submitted for publication. <sup>i</sup> Bond lengths in Ångstroms and angles in degrees.

served in cyclobutane<sup>11</sup> and perfluorocyclobutane,<sup>9</sup> respectively. The FC<sub>4</sub>F angle is 104° and corresponds closely to that reported for cyclopentene, in which the HCH angle is less accurately determined due to the small scattering by hydrogen. This is the smallest angle reported for (presumably) sp<sup>3</sup> carbon centers.

It is interesting to compare the effect of fluorosubstitution in two unsaturated carbon rings, cyclobutene, and cyclopentene (Table II). Within the precision of our analyses, the C=C bond length is found to be constant (1.342 Å) in all four compounds; however, the =C—C bond is shorter by 0.010 Å due to the fluorine substitution in both rings and the C—C bond in cyclobutene is longer by 0.029 Å. The C—C bond in the C<sub>5</sub>F<sub>8</sub> ring is shorter than in C<sub>5</sub>H<sub>8</sub> by 0.007 Å, but it is more sensitive to compare the nonbonded C<sub>3</sub>···C<sub>5</sub> distances (2.436 in C<sub>5</sub>H<sub>8</sub> and 2.554 in C<sub>5</sub>F<sub>8</sub>); again, the trend toward longer bonds in the C<sub>4</sub> ring is indicated. The pucker angle (α) in C<sub>5</sub>F<sub>8</sub> is less by 8.3° from that in C<sub>5</sub>H<sub>8</sub> and this also corresponds with observations for the cyclobutane ring (27° in C<sub>4</sub>H<sub>8</sub> compare with 17.4° in C<sub>4</sub>F<sub>8</sub>).

Also listed in Table II are bond lengths and valence angles in three fused ring hydrocarbons which have been investigated by electron diffraction. The cyclopentene rings show the same C=C bond length in spite of considerable ring strain since the pucker angle in the polycyclic molecules is twice the corresponding one in C<sub>5</sub>H<sub>8</sub>. It appears that the —C=C, C—C, and CCC angles adjust in different systems in order to distribute the strains throughout the carbon skeletons.

*Perchlorocyclopentadiene.* The converged least-squares results for C<sub>5</sub>Cl<sub>6</sub> are listed in the third column of Table III; data on cyclopentadiene are included for

comparison. The C—Cl bond lengths have been found to range from 1.63 Å, in cyanogen chloride<sup>12</sup> to 1.80 Å in *tert*-butyl chloride.<sup>13</sup> Also, C—Cl interatomic distances in ortho-substituted aromatic compounds<sup>14</sup> are shorter than in other polychlorinated compounds. This suggests that the C—Cl bond length is affected not only by the hybridization of the C atom orbitals but also by van der Waals attractive forces between nonbonded chlorine atoms. The bond length of 1.82 Å found in C<sub>5</sub>Cl<sub>6</sub> is the longest such bond reported to date. The *relative* magnitudes (1.703, 1.819 Å) correspond to similar sets found in perchlorocyclobutene (1.668, 1.780 Å)<sup>15</sup> and perchlorocyclopropene (1.684, 1.771 Å).<sup>16</sup>

The =C—C= and —C=C— bond lengths found in C<sub>5</sub>Cl<sub>6</sub> indicate a conjugated C=C—C=C system as present in butadiene-1,3<sup>17</sup> (1.483 ± 0.010, 1.337 ± 0.005 Å) and cyclopentadiene (1.469 ± 0.002, 1.342 ± 0.003 Å),<sup>18</sup> as compared with perchlorocyclopentadiene (1.486 ± 0.015, 1.345 ± 0.020 Å). The third C—C bond was also found to agree with that in C<sub>5</sub>H<sub>6</sub> in contrast to the cyclopropene system,<sup>16</sup> where the C=C is longer by 0.016 Å and the =C—C shorter by 0.040 Å compared with the hydro compounds.

(11) L. C. Snyder and S. Meiboom, *Science*, **162**, 1337 (1968).

(12) C. H. Townes, A. N. Holden, and F. R. Merritt, *Phys. Rev.*, **74**, 1113 (1948).

(13) O. Bastiansen and L. Smedvik, *Acta Chem. Scand.*, **7**, 652 (1953).

(14) R. Rudman, *Chem. Commun.*, 536 (1970).

(15) C. H. Chang and S. H. Bauer, to be published.

(16) H. Mair and S. H. Bauer, preceding paper.

(17) D. J. Marais, N. Sheppard, and B. P. Stoicheff, *Tetrahedron*, **17**, 163 (1962).

(18) L. H. Scharpen and V. W. Laurie, *J. Chem. Phys.*, **43**, 2765 (1965).

**Table III:** Structural Parameters for Cyclopentadienes

	Cyclopentadiene <sup>a</sup>	Perchlorocyclopentadiene <sup>b</sup>	
		Before calibration	After calibration
(C <sub>1</sub> —C <sub>2</sub> )	1.469 ± 0.002	1.4863 ± 0.015	1.4858 ± 0.015
(C <sub>2</sub> =C <sub>3</sub> )	1.342 ± 0.003	1.3446 ± 0.020	1.3441 ± 0.020
(C <sub>4</sub> —O)	1.509 ± 0.002	2.2595 ± 0.034	
(C <sub>3</sub> —C <sub>4</sub> )	1.509 ± 0.002	1.5096 ± 0.034	1.5091 ± 0.034
(C <sub>1</sub> —Cl <sub>6</sub> )	1.08	1.7033 ± 0.005	1.7027 ± 0.005
(C <sub>4</sub> —Cl <sub>10</sub> )	1.04	1.8199 ± 0.017	1.8193 ± 0.017
∠(C <sub>1</sub> C <sub>2</sub> C <sub>3</sub> )	109°21' ± 10'	107.61 ± 1.0	107.57 ± 1.0
∠(C <sub>2</sub> C <sub>3</sub> C <sub>4</sub> )	109°16' ± 10'	(112.8)	
∠(C <sub>3</sub> C <sub>4</sub> C <sub>5</sub> )	102°46' ± 9'	(99.2)	
∠(Cl <sub>6</sub> C <sub>1</sub> C <sub>2</sub> )	111	127.47 ± 1.0	127.43 ± 1.0
∠(Cl <sub>8</sub> C <sub>3</sub> C <sub>2</sub> )	125	127.58 ± 2.1	127.54 ± 2.1
∠(Cl <sub>10</sub> C <sub>4</sub> C <sub>3</sub> )	99.5	109.87 ± 0.6	109.83 ± 0.6
∠(Cl <sub>10</sub> C <sub>4</sub> Cl <sub>11</sub> )	147	(116.8)	
l(C <sub>1</sub> —C <sub>2</sub> )		0.045	
l(C <sub>2</sub> —C <sub>3</sub> )		0.045	
l(C <sub>3</sub> —C <sub>4</sub> )		0.054	
l(C <sub>1</sub> ···C <sub>3</sub> )		0.050	
l(C <sub>1</sub> —Cl <sub>6</sub> )		0.031 ± 0.010	
l(C <sub>4</sub> —Cl <sub>10</sub> )		0.058	
l(C <sub>1</sub> ···Cl <sub>7</sub> )		0.065 ± 0.010	
l(C <sub>1</sub> ···Cl <sub>8</sub> )		0.065 ± 0.010	
l(C <sub>1</sub> ···Cl <sub>8</sub> )		0.072 ± 0.012	
l(C <sub>1</sub> ···Cl <sub>10</sub> )		0.086 ± 0.024	
l(Cl <sub>10</sub> ···Cl <sub>11</sub> )		0.120	
l(Cl <sub>6</sub> ···Cl <sub>7</sub> )		0.120	
l(Cl <sub>6</sub> ···Cl <sub>8</sub> )		0.100	
l(Cl <sub>6</sub> ···Cl <sub>11</sub> )		0.160	

<sup>a</sup> Bond lengths (in ångströms) and angles (in degrees) in C<sub>5</sub> ring are M.W. values reported by L. H. Scharpen and V. W. Laurie, see ref 18; C—H bonds and other angles are X-ray values from G. Liebling and R. E. Marsh, *Acta Crystallogr.*, **19**, 202 (1965). <sup>b</sup> Bond distances are all  $r_g$  values with error limits at three times the least-squares uncertainties.

*Acknowledgments.* We wish to thank Dr. H. Mair for purifying the perchlorocyclopentadiene used in this investigation. This work was supported by the Ad-

vanced Research Projects Agency through the Material Science Center of Cornell University and the Army Research Office, Durham.



# Electrical Conductivities of Salts of Gum Arabic and Carrageenan

## in Aqueous Solutions<sup>1</sup>

by Roger E. Nelson and Paul Ander\*

Department of Chemistry, Seton Hall University, South Orange, New Jersey 07079 (Received July 25, 1970)

Publication costs assisted by Seton Hall University

The equivalent conductivities of the potassium, sodium, and lithium salts of gum arabic and the potassium and sodium salts of  $\kappa$ - and  $\lambda$ -carrageenan have been measured in water at 0°. From the data the parameter  $\phi$ , defined as the difference in the equivalent conductivities of two salts of the same polyion divided by the difference in the equivalent conductivities of the counterions, has been calculated. Using these data and additional literature data the interpretation of  $\phi$  given by Katchalsky has been extended and interpreted as a conductometric degree of ionization, being both a measure of the unbound counterions and a measure of the conductometric activity of the bound counterions. It has also been shown how the parameter  $\phi$  can be introduced into an extended form of the Onsager equation to yield an equation which is similar to an empirical equation previously found to represent the equivalent conductivities of several polyelectrolytes.

### Introduction

For simple electrolytes it is customary to plot the equivalent conductivity against the square root of the concentration. At low concentrations a linear plot which conforms to the Onsager theory is generally obtained. When a similar plot is made for a polyelectrolyte a linear plot is not obtained, but instead, the equivalent conductivity generally shows a very sharp nonlinear increase with decreasing polyelectrolyte concentration. This type of behavior has been qualitatively ascribed to an elongation of the polyion with dilution and a concomitant increase in the number of free counterions, thus leading to an increase in the number of conducting species in solution.<sup>2,3</sup> However, it has been shown for several polyelectrolytes that the degree of ionization, *i.e.*, the fraction of unassociated counterions, is independent of concentration or shows only a very slight dependence on concentration.<sup>4,5</sup> Thus, some other explanation of the conductometric behavior of polyelectrolytes would be desirable.

At least two empirical equations have been found which represent the concentration dependence of the equivalent conductivity of several polyelectrolytes in water.<sup>6-9</sup> The one which has found the most application is

$$\frac{\sqrt{N}}{\Lambda^0 - \Lambda} = A + B\sqrt{N} \quad (1)$$

where  $\Lambda$  is the equivalent conductivity at normality  $N$ ,  $\Lambda^0$  is the equivalent conductivity at infinite dilution, and  $A$  and  $B$  are empirical constants. This equation is of the same form as the equation first suggested by Lattey<sup>10</sup> for the conductivity of simple electrolytes. The equation is also of the same form as the equation derived by Robinson and Stokes<sup>11</sup> from an extension of

the Onsager theory, which takes into account the finite size of the ions. As pointed out by Gregor and Gold,<sup>8</sup> the values of  $A$  and  $B$  in the case of polyelectrolytes are several orders of magnitude different from the values predicted by the Onsager theory, and thus are not easily interpretable for polyelectrolytes, as expected. Also, it has been found that  $\Lambda^0$  in eq 1 is not unique.<sup>12</sup> Low values chosen for  $\Lambda^0$  do not yield linear plots, while all values above a certain minimum value do yield linear plots. Most workers have taken this minimum value to be the equivalent conductivity at infinite dilution.

Another conductometric relationship has been found to hold in the case of several polyelectrolytes. This relationship, first expressed by Eisenberg,<sup>13</sup> is

$$\phi = \frac{\Lambda_{MP} - \Lambda_{NP}}{\lambda_{M+}^0 - \lambda_{N+}^0} \quad (2)$$

(1) Taken from a portion of the Ph.D. Dissertation of R. E. N., Seton Hall University, 1969.

(2) R. M. Fuoss, *Discuss. Faraday Soc.*, **11**, 125 (1951).

(3) R. M. Fuoss, *J. Polym. Sci.*, **12**, 185 (1954).

(4) J. R. Huizenga, P. F. Grieger, and F. T. Wall, *J. Amer. Chem. Soc.*, **72**, 2636 (1950).

(5) R. L. Darskus, D. O. Jordan, and T. Kurucsev, *Trans. Faraday Soc.*, **62**, 2876 (1966).

(6) A. Oth and P. Doty, *J. Phys. Chem.*, **56**, 43 (1952).

(7) R. A. Mock, C. A. Marshall, and T. E. Slykhouse, *ibid.*, **58**, 498 (1954).

(8) H. P. Gregor and D. H. Gold, *ibid.*, **61**, 1347 (1957).

(9) V. E. Kulshrestha, *J. Polym. Sci.*, **58**, 809 (1962).

(10) R. T. Lattey, *Phil. Mag.*, **4**, 831 (1927).

(11) R. A. Robinson and R. H. Stokes, *J. Amer. Chem. Soc.*, **76**, 1991 (1954).

(12) T. Kurucsev and B. J. Steel, *Rev. Pure Appl. Chem.*, **13**, 149 (1967).

(13) H. Eisenberg, *J. Polym. Sci.*, **30**, 47 (1958).

where  $\Lambda$  is the measured equivalent conductivity at a finite concentration,  $\lambda^0$  is the limiting ionic conductivity of the cations  $M^+$  and  $N^+$ , and  $P$  represents the polyion, anionic in this case. For the alkali metal salts of polyacrylic and polymethacrylic acids, Eisenberg found that  $\phi$  was constant with respect to concentration and furthermore, independent of whether calculated from the differences between the cation pairs K-Na, K-Li, or Na-Li.

Varoqui and Strauss<sup>14</sup> have shown how the parameter  $\phi$  can be equated to the degree of ionization of a polyelectrolyte, provided that the degree of ionization and the mobility of the polyion are independent of the nature of the counterion. With the same provision, Katchalsky, *et al.*,<sup>15</sup> have related  $\phi$  to the osmotic coefficient of a polyelectrolyte solution.

Equivalent conductivity data for the alkali metal salts of gum arabic and carrageenan, two naturally occurring polysaccharides, are presented. The data have been examined according to eq 1 and the parameter  $\phi$  has been calculated. Comparing our results to previously published results for other polyelectrolytes, the constants  $A$  and  $B$  in eq 1 are discussed qualitatively. Also, an interpretation of  $\phi$  is given and it is shown how  $\phi$  can be introduced into eq 1 in order to make it a more general conductivity equation for polyelectrolytes.

### Experimental Section

**Materials. Salts of Gum Arabic.** A batch of crude gum arabic, *Acacia senegal*, a gift from S. B. Penick and Co., New York, N. Y., was used to prepare the salts of gum arabic. The crude gum was dissolved in water to yield a 20% solution. The solution was filtered and then treated with excess HCl. The acid form of the gum was then precipitated by the addition of 95% ethanol. This procedure, acidification and precipitation, was repeated three more times and the final precipitate of arabic acid was washed with 95% ethanol until free of chloride. It was then washed with acetone and dried in a vacuum desiccator for several days. The acid was found by titration to have an equivalent weight of  $1200 \pm 15$ . This value is in excellent agreement with previously published values.<sup>16</sup>

The potassium, sodium, and lithium salts of gum arabic were prepared by titration of the arabic acid with the appropriate alkali hydroxide and then precipitation with 95% ethanol. The salts were also finally washed with acetone and dried in a vacuum desiccator for several days.

**Salts of Carrageenan.** The purified carrageenan samples used, gifts from Marine Colloids, Inc., Rockland, Maine, were the potassium and sodium salts of the  $\kappa$  and  $\lambda$  fractions. Equivalent weights were determined by acid hydrolysis, followed by quantitative determination of the liberated sulfate by precipitation as  $BaSO_4$ . The equivalent weights, on a dry basis, of

K and Na  $\lambda$ -carrageenan are 288 and  $282 \pm 3$ , respectively, and K and Na  $\kappa$ -carrageenan are 369 and  $345 \pm 3$ , respectively.

**Apparatus and Measurements.** All conductivity measurements were made in an oil-filled bath at  $0 \pm 0.01^\circ$ . Temperature control was  $\pm 0.005^\circ$ . Four Pyrex conductivity cells of a modified Shedlovsky design were used. The electrodes were lightly platinized with platinum black.

Cell constants were determined using the conductivity data of Jones and Bradshaw for KCl at  $0^\circ$ .<sup>17</sup> The KCl used was reagent grade material which was further purified by precipitation from an HCl solution, followed by fusion in a platinum crucible, after the method of Lind and Fuoss.<sup>18</sup> The cell constants of the four cells, in  $cm^{-1}$ , were the following:  $A$ ,  $0.5853 \pm 0.0003$ ;  $B$ ,  $1.1375 \pm 0.0005$ ;  $C$ ,  $21.204 \pm 0.008$ ; and  $D$ ,  $44.97 \pm 0.02$ .

The conductivity bridge was after the design of Luder.<sup>19</sup> A Hewlett and Packard variable audio oscillator, Model 701B, was used as the source of the ac signal and a General Radio tuned amplifier and null detector, Type 1232-A, was used as detector. Cell resistances were balanced with either one of two General Radio decade resistance boxes, Type 1432-M or Type 1432-N. When extremely high resistances were measured, for example in the case of conductivity water, a General Radio 100,000 ohm standard resistor, Type 500-U, was inserted into the circuit in parallel with the cell. Resistance measurements were accurate to within  $\pm 0.025\%$ .

Conductivity water was prepared by distilling water which had previously been deionized. It had a specific conductivity of  $0.6$  to  $0.8 \times 10^{-6} \text{ ohm}^{-1} \text{ cm}^{-1}$  at  $0^\circ$ .

Concentrated stock solutions of dry polymer were made up by weight. Aliquots of this were then weighed into 50-ml, Class A, volumetric flasks and then the flasks were filled up to the mark with water. Concentrations were calculated as normality,  $N$ .

Each solution was flushed through a conductivity cell until a constant resistance was reached. This eliminated any possible errors due to absorption of polymer on the electrodes. The resistance of each solution was then measured at 1000, 1500, 2000, and 3000 Hz. These values were then plotted against the inverse of the square root of the frequency to obtain the resistance, or specific conductivity, at infinite frequency. The extrapolated resistances at infinite fre-

(14) R. Varoqui and U. P. Strauss, *J. Phys. Chem.*, **72**, 2507 (1968).

(15) A. Katchalsky, A. Alexandrowicz, and O. Kedem in "Chemical Physics of Ionic Solutions," B. E. Conway and R. G. Banades, Ed., Wiley, New York, N. Y., 1966, Chapter 15.

(16) M. Glicksman and R. E. Schachat in "Industrial Gums," R. L. Whistler, Ed., Academic Press, New York, N. Y., 1959, Chapter X.

(17) G. Jones and B. C. Bradshaw, *J. Amer. Chem. Soc.*, **55**, 1780 (1933).

(18) J. E. Lind and R. M. Fuoss, *J. Phys. Chem.*, **65**, 999 (1961).

(19) W. F. Luder, *J. Amer. Chem. Soc.*, **62**, 89 (1940).

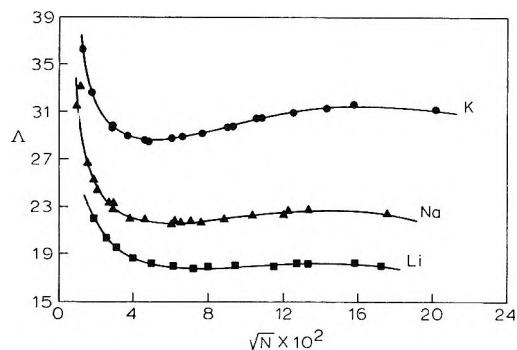


Figure 1. Equivalent conductivities of potassium, sodium, and lithium arabate in water at 0°.

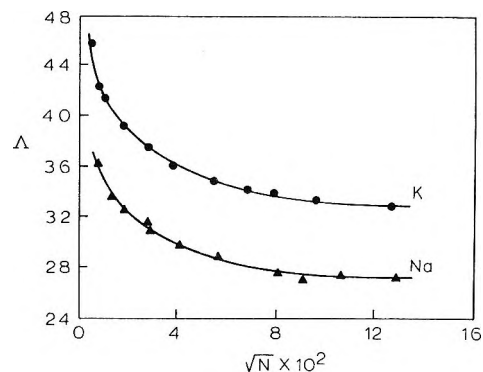


Figure 2. Equivalent conductivities of potassium and sodium λ-carrageenan in water at 0°.

quency were approximately 0.1% lower than those obtained at 1000 Hz.

The equivalent conductivity of each solution was calculated in the conventional manner, after making the appropriate correction for the specific conductivity of the solvent. Due mainly to an uncertainty of approximately 1.5% in the equivalent weights of the polymers, the equivalent conductivities are also uncertain by approximately this amount.

## Results

Figure 1 shows the equivalent conductivities of potassium, sodium, and lithium arabate as a function of the square root of the equivalent concentration. The results are typical of other polyelectrolytes in that the equivalent conductivities show a sharp increase with dilution and thus cannot be extrapolated to infinite dilution. However, the curve for each salt shows a distinct minimum before the sharp increase. The magnitudes of the minima are in the order  $K^+ > Na^+ > Li^+$ . Briggs<sup>20</sup> determined the equivalent conductivities of the alkali metal salts of gum arabic at 25° and found curves very similar to those shown in Figure 1, obtained at 0°. His curves have the same minima at approximately the same concentration and the minima show the same dependence on the counterions.

The equivalent conductivities of the potassium and sodium salts of λ-carrageenan are shown in Figure 2. These curves show more normal polyelectrolyte behavior. That is, they exhibit a continuous increase in conductivity with decreasing concentration, bending up sharply at very low concentrations. In Figure 3 are shown the equivalent conductivities of the potassium and sodium salts of κ-carrageenan. For the potassium salt, measurements could not be made at concentrations any higher than those shown on the graph because the conductivity of this salt at higher concentrations was found to decrease with time. This effect was not investigated further because it is known that κ-carrageenan specifically interacts with potassium ions and can precipitate in the presence of this ion.<sup>21</sup>

The parameter  $\phi$ , given by eq 2, was calculated for

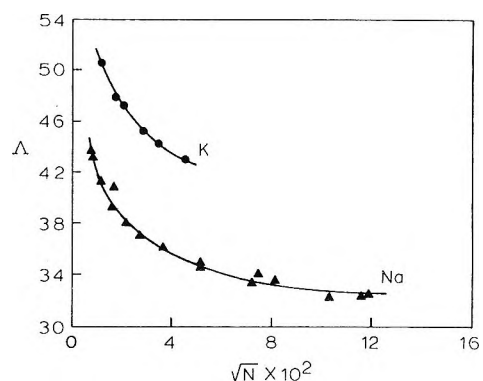


Figure 3. Equivalent conductivities of potassium and sodium κ-carrageenan in water at 0°.

the arabate and carrageenan salts. Values of  $\lambda_{M^+}^0$ , taken from Robinson and Stokes,<sup>22</sup> used were:  $K^+$ , 40.7;  $Na^+$ , 26.5; and  $Li^+$ , 19.4. Figure 4 shows  $\phi$  as a function of  $\sqrt{N}$  for the salts of gum arabic. (The data points in Figure 4 were taken from the smoothed curves of Figure 1, since the conductivities of all of the salts were not determined at exactly the same concentrations.) As can be seen,  $\phi$  is independent of the set of salts used for the calculations and it increases linearly with respect to  $\sqrt{N}$  up to a concentration of approximately 0.01  $N$ . The equation of the limiting linear portions of these curves is

$$\phi = 0.42 + 1.54 \sqrt{N}$$

Values of  $\phi$  were also calculated from the data of Briggs<sup>20</sup> at 25°. These values were identical with the values calculated from the present results obtained at 0°.

Figure 5 shows  $\phi$  as a function of  $\sqrt{N}$  for λ- and κ-carrageenan. For λ-carrageenan,  $\phi$  shows a very slight linear increase with decreasing  $\sqrt{N}$ , while in the case of

(20) D. R. Briggs, *J. Phys. Chem.*, **38**, 867 (1934).

(21) D. B. Smith and W. H. Cook, *Arch. Biochem. Biophys.*, **45**, 232 (1953).

(22) R. A. Robinson and R. H. Stokes, "Electrolyte Solutions," 2nd ed, Butterworths, London, 1965.

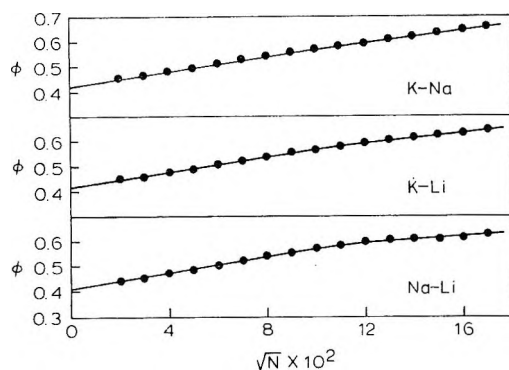


Figure 4.  $\phi$  as a function of  $\sqrt{N}$  for salts of gum arabic at  $0^\circ$ .

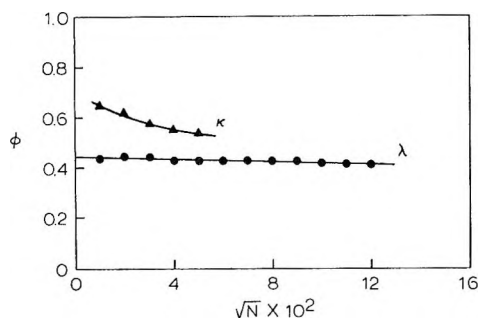


Figure 5.  $\phi$  as a function of  $\sqrt{N}$  for salts of  $\kappa$ - and  $\lambda$ -carrageenan at  $0^\circ$ .

$\kappa$ -carrageenan,  $\phi$  bends slightly upward with decreasing  $\sqrt{N}$ .

### Discussion

Little advance has been made in the understanding of the electric transport properties of dissolved polyelectrolytes because of the complex hydrodynamic and electrostatic interactions involved.<sup>23</sup> In view of this, the approach employed has been to examine the results in terms of the form of the Onsager equation. Robinson and Stokes' extension of Onsager's equation is

$$\Lambda = \Lambda^0 - \frac{(B_1\Lambda^0 + B_2)\sqrt{N}}{(1 + Ba\sqrt{N})} \quad (3)$$

where  $B_1$  and  $B_2$  are the relaxation and electrophoretic terms of the Onsager equation, respectively,  $B$  is a constant which depends on the dielectric constant and the temperature of the solvent, and  $a$  is the distance of closest approach of two ions. To adapt eq 3 to polyelectrolytes, the degree of ionization  $i$  of the polyelectrolyte is included in eq 3 to give

$$\Lambda = i\Lambda^0 - \frac{i(B_1\Lambda^0 + B_2)\sqrt{iN}}{(1 + Ba\sqrt{iN})} \quad (4)$$

Consider the case when  $i$  is independent of the counterion and assume that the law of independent migration holds at infinite dilution in the case of polyelectrolytes, as in the case of simple electrolytes. Under these

conditions, by taking the difference in the conductivities of two salts of the same polyion and dividing by the difference in the limiting single ion conductivities of the counterions, from eq 4, one obtains

$$\phi = \frac{\Lambda_{MP} - \Lambda_{NP}}{\lambda_{M^+}^0 - \lambda_{N^+}^0} = i - \frac{iB_1\sqrt{iN}}{(1 + Ba\sqrt{iN})} \quad (5)$$

If  $Ba \gg B_1$ , it can be seen that this equation reduces to  $\phi = i$ . If the terms have physical significance analogous to those for simple electrolytes, this means that of the factors which affect the conductivity of a polyelectrolyte, the effect of the large size of the polyion is much greater than the effect of relaxation.

Single-ion activity coefficients have been regarded as a measure of the degree of ionization of a polyelectrolyte in salt-free solutions.<sup>24-26</sup> It would be of interest to compare the values of  $\phi$  with single-ion activity coefficients of the counterions  $\gamma_+$  of these polyelectrolytes. The present results were obtained at  $0^\circ$ , but the same values of  $\phi$  were calculated from the data of Briggs,<sup>20</sup> who made his conductivity measurements of the arabate salts at  $25^\circ$ . The values of  $\gamma_+$  were obtained at  $25^\circ$ .<sup>27</sup>

In Figure 6 are shown the values of  $\phi$  and  $\gamma_+$  for  $\kappa$ - and  $\lambda$ -carrageenan and the arabate salts<sup>27</sup> in water. As can be seen in Figure 6, for  $\lambda$ -carrageenan the values of  $\gamma_{K^+}$  and  $\gamma_{Na^+}$  are essentially equal at all concentrations, indicating similar degrees of ionization for both counterions. It is also obvious that  $\phi$  is equivalent to  $\gamma_{K^+}$  and  $\gamma_{Na^+}$ . In the case of  $\kappa$ -carrageenan,  $\gamma_{K^+}$  is significantly higher than  $\gamma_{Na^+}$ , indicating a greater degree of ionization when potassium is the counterion. Clearly,  $\phi$  is not equal to either single-ion activity coefficient. This is to be expected, since the interpretation of  $\phi$  requires equal degrees of ionization of a polyion with different counterions. Therefore, little else can be said about the  $\kappa$ -carrageenan results except that they are not inconsistent with the interpretation of  $\phi$  being equal to  $i$ . For salts of gum arabic, as can be seen,  $\phi$  and  $\gamma_{K^+}$  are very different. However, both show a decrease with decreasing concentration, albeit a very slight decrease in the case of  $\gamma_{K^+}$ .

Katchalsky and coworkers<sup>15</sup> have considered the case where some of the counterions in a polyelectrolyte solution are completely free and the remainder are held within the ionic atmosphere of the polyion. The latter ions are considered to be able to move along the surface of the polyion and contribute to the total conductivity in an electric field. They arrived at an equation which relates  $\phi$  to the osmotic coefficient and found reasonably good agreement for their theoretical equa-

(23) P. J. Napjus and J. J. Hermans, *J. Colloid Sci.*, **14**, 252 (1959).

(24) J. W. Lyons and L. Kotin, *J. Amer. Chem. Soc.*, **87**, 1670 (1965).

(25) T. J. Podlas and P. Ander, *Macromolecules*, **2**, 432 (1969).

(26) T. J. Podlas and P. Ander, *ibid.*, **3**, 154 (1970).

(27) T. J. Podlas, Ph.D. Dissertation, Seton Hall University, 1968.

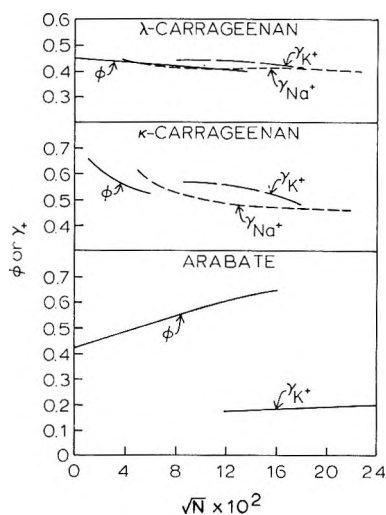


Figure 6. Comparison of  $\phi$  with single-ion activity coefficients  $\gamma_+$  of potassium and sodium  $\kappa$ - and  $\lambda$ -carrageenan and potassium arabate as a function of  $\sqrt{N}$ .

tion upon comparing values of  $\phi$  and osmotic pressure coefficients for polymethacrylic acid. Due to the absence of appropriate thermodynamic data, we replaced the osmotic coefficient in Katchalsky's equation by  $\gamma_+$ .

$$\gamma_+ = \frac{3\phi - 1}{2} \quad (6)$$

For the arabate salts,  $\phi$  has a value of 0.42 at infinite dilution, which when put into eq 6 gives a value of 0.13 for  $\gamma_+$ . This is in very good agreement with the values of  $\gamma_{K^+}$  found by Podlas, which give, on extrapolation to infinite dilution, a value of 0.15. This equation obviously does not hold at higher concentrations because of the large increase in  $\phi$  and the very small increase in  $\gamma_{K^+}$  with increasing concentration. Thus, in the case of the arabate molecule the model of Katchalsky and coworkers would appear to be very appropriate, at least at infinite dilution. The results indicate that approximately 85% of the counterions are bound, but can contribute to the conductivity by movement along the surface of the polyion. If this interpretation of  $\phi$  is correct, then, because of the equality of  $\phi$  and  $\gamma_+$  in the case of  $\lambda$ -carrageenan, one would be forced to conclude that all of the bound counterions in this molecule, approximately 55%, are conductometrically inactive. That is, they are very strongly held by the polyion and do not move under an applied field. The very different conclusion in the case of the arabate molecule may reflect differences in the charge densities of these two polyions. The arabate polyion has one charged group for every 8–10 monosaccharide moieties, whereas the  $\lambda$ -carrageenan polyion has approximately one charged group per moiety. Thus, the higher charge density of  $\lambda$ -carrageenan may prevent the bound counterions from moving freely along the surface of the polyion, while in the case of the arabate polyion, with

its lower charge density, the bound counterions may be much freer to move. If one looks at the calculations of Katchalsky and coworkers,<sup>15</sup> who used experimental values of  $\phi$  and osmotic coefficients for partially neutralized polymethacrylic acid, it is noticed that at very low degrees of neutralization there is virtually 100% agreement of the theoretical and experimental values of  $\phi$ . However, as the degree of neutralization increases the agreement becomes poorer. Since carboxylic acid groups bind hydrogen ions very strongly, a low degree of neutralization corresponds to a low charge density of the polyion. Thus, their results could be interpreted in the same way as the difference between the  $\lambda$ -carrageenan and arabate results. That is, the counterions of a polyion having a low charge density are only very loosely held in the ionic atmosphere and can migrate within the ionic atmosphere under an applied field. In the case of a polyion having a high charge density, however, the counterions, because they are more strongly attracted to the polyion, are less able to migrate within the ionic atmosphere of the polyion.

The model of Katchalsky and coworkers does not take into account the effect of concentration on  $\phi$ . A basic assumption in their derivation is that the bound counterions have a mobility equal to that of free counterions. However, because the bound counterions are restricted to move along the surface of a cylindrical model of a polyelectrolyte the effective contribution of the bound counterions to the total conductivity is only one-third the contribution of a free counterion. This derivation may only be valid at infinite dilution where polyelectrolytes are believed to be represented by rod-like configurations. With increasing concentration the molecules achieve a more spherical shape and in this case the effective contribution of the bound counterions to the total conductivity may become greater than one-third the contribution of the free counterions, and thus  $\phi$  might increase with increasing concentration.

The foregoing interpretation of  $\phi$  leads to a very reasonable explanation of the observed minima in the equivalent conductivity curves of the arabate salts. Thus, the conductivity of a simple electrolyte increases with decreasing concentration, due to a lessening of electrophoretic and relaxation effects. This probably also occurs in the arabate system, although relaxation effects may be very small. At the same time, however, the mobility of the atmospherically bound counterions decreases, thus, causing a decrease in the conductivity. The net result is that these two competing effects give rise to a minimum in the overall conductivity. The minima should then be a function of the conductivities of the individual counterions, being greatest for the counterion having the largest conductivity. The magnitudes of the minima in Figure 1 are in exactly the same order as are the single ion conductivities of the counterions, in agreement with the foregoing argument.

It appears that  $\phi$  should not simply be considered the degree of ionization of the free counterions. It should be regarded as a conductometric degree of ionization, being *both* a measure of the fraction of free ions and a measure of the conductometric activity of the bound counterions. Thus, eq 4 should be rewritten in a more general form by replacing  $i$  with  $\phi$ , and by rearranging one obtains

$$\frac{\phi\sqrt{\phi N}}{\phi\Lambda^0 - \Lambda} = \frac{1}{(B_1\Lambda^0 + B_2)} + \frac{Ba\sqrt{\phi N}}{(B_1\Lambda^0 + B_2)} \quad (7)$$

In cases where the bound ions make no contribution to the conductivity, *i.e.*,  $\phi = i$ , eq 7 would then reduce back to eq 4. It should be noted that eq 7 differs from eq 1 only by the presence of  $\phi$ . Equation 1 has been found empirically to represent the conductivities of several polyelectrolytes in water.<sup>7-9</sup>

It was found that the conductivities of the salts of gum arabic did not yield a linear plot when plotted according to eq 1. However, a linear plot resulted when the more general equation, eq 7, was used. This is because  $\phi$  varies with concentration in the case of the arabate salts. In this equation, as well as in eq 1, there is one unknown constant,  $\Lambda^0$ , the value of the equivalent conductivity at infinite dilution. As was done by Gregor and Gold,<sup>8</sup> different values of  $\Lambda^0$  can be tried until a linear plot is obtained.

Figure 7 shows a plot, according to eq 7, of the conductivity data for potassium, sodium, and lithium arabate at 0°. Instead of varying  $\Lambda^0$ ,  $\lambda_{P^-}^0$  was varied, since at infinite dilution  $\Lambda^0 = \lambda_{M^+}^0 + \lambda_{P^-}^0$ . As will be noticed immediately, the data for all three salts fall on the same curve for a given value of  $\lambda_{P^-}^0$ , despite the fact that  $\Lambda^0$  is different for each salt when  $\lambda_{P^-}^0$  is the same. When  $\lambda_{P^-}^0 = 50$ , a linear plot is not obtained over the entire concentration range. However, as higher values of  $\lambda_{P^-}^0$  are tried, the plot becomes more linear, and at  $\lambda_{P^-}^0 = 80 \pm 10$  the plot is completely linear. Thereafter, larger values of  $\lambda_{P^-}^0$  also yield linear plots. The nonuniqueness of  $\lambda_{P^-}^0$  was also found by Gregor and Gold,<sup>8</sup> who used eq 1. They took the lowest value of  $\lambda_{P^-}^0$  which gave a linear plot as the most appropriate value, and hence the same procedure will be employed here.<sup>28</sup> A similar treatment of the data of Briggs<sup>20</sup> yielded a value of  $\lambda_{P^-}^0$  of  $130 \pm 10$  at 25° for the arabate polyion.

The conductivity data of  $\lambda$ -carrageenan, when plotted according to eq 7, are shown in Figure 8. As for the arabate system, for a given value of  $\lambda_{P^-}^0$ , the data for the potassium and sodium salts fall on the same curve. The minimum value of  $\lambda_{P^-}^0$  to yield a linear plot in this case is  $65 \pm 5$ .

According to eq 7, for a given value of  $\lambda_{P^-}^0$ , the slope and intercept should be different for each polysalt since  $\Lambda^0$  is different in each case. However, for both the  $\lambda$ -carrageenan and arabate polyions the slopes and intercepts were found to be the same for each counter-

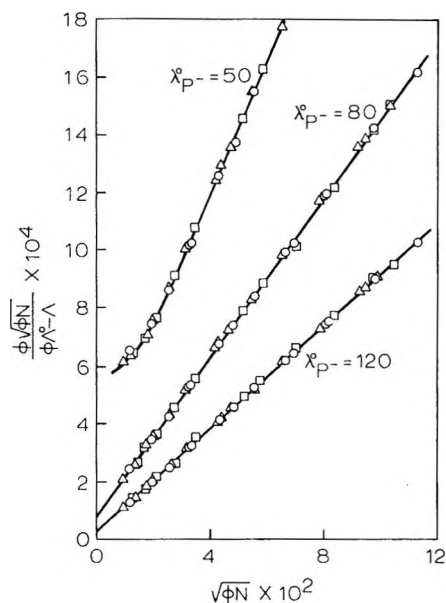


Figure 7.  $\phi\sqrt{\phi N}/(\phi\Lambda^0 - \Lambda)$  as a function of  $\sqrt{\phi N}$  for salts of gum arabic at 0°: O, KAr; □, NaAr; △, LiAr.

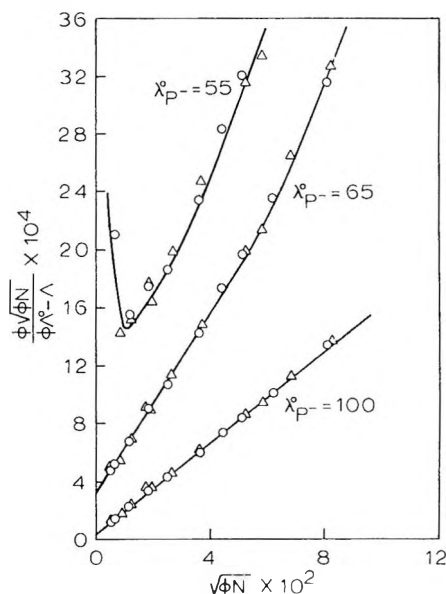


Figure 8.  $\phi\sqrt{\phi N}/(\phi\Lambda^0 - \Lambda)$  as a function of  $\sqrt{\phi N}$  for salts of  $\lambda$ -carrageenan at 0°; O, potassium; △, sodium.

ion for each assumed value of  $\lambda_{P^-}^0$ . Since  $\Lambda^0$  is in the range of 100, the term  $B_1$  must be very small in comparison to the term  $B_2$ . If the experimental fit of the form of the Onsager equation is not merely fortuitous,  $B_1$  and  $B_2$  are considered to be the relaxation and electrophoretic terms, respectively. Thus, this experimentally would indicate the negligibility of relaxation effects in the case of the conductivity of polyelec-

(28) Because of the nonuniqueness of the value of  $\Lambda^0$ , its interpretation as the value of the polyelectrolyte equivalent conductance at infinite dilution is not justified at the present.

trolytes in water and eq 7 can then be approximated by

$$\frac{\phi\sqrt{\phi N}}{\phi\Lambda^0 - \Lambda} = \frac{1}{B_2} + \frac{Ba\sqrt{\phi N}}{B_2} \quad (8)$$

The intercepts in Figures 7 and 8 would then be equal to  $1/B_2$  and the slopes to  $Ba/B_2$ . Thus, the electrophoretic term and the product  $Ba$  can be obtained from these plots. At  $0^\circ$  and  $25^\circ$  in water the constant  $B$  has values of  $0.3248 \times 10^8$  and  $0.3291 \times 10^8 \text{ cm}^{-1} \text{ mol}^{-1/2} \text{ l.}^{1/2}$ , respectively. Thus, from the values of  $Ba$ , determined from the slopes in Figures 7 and 8, one can calculate  $a$ , the distance of closest approach in the polyelectrolyte solutions.

In Table I are summarized the various parameters

**Table I:** Conductivity Parameters for Different Polyions at 0 and  $25^\circ$

Polyion	Temp, $^\circ\text{C}$	$\lambda_{\text{P}^-}$	$B_2 \times 10^{-4}$	$a$ , $\text{\AA}$
Arabate	0	80	1.25	526
Arabate	25	130	2.00	535
$\lambda$ -Carrageenan	0	65	0.32	314
Polymethacrylate	25	200	1.27	237

calculated for the arabate,  $\lambda$ -carrageenan, and polymethacrylate polyions. Mock<sup>7</sup> plotted the conductivity data of Oth and Doty<sup>6</sup> for sodium polymethacrylate at  $25^\circ$  according to eq 1 and obtained a linear plot with a minimum value of  $\Lambda^0$  of 100. However, as noted, this should actually be  $\phi\Lambda^0$ . According to Eisenberg,  $\phi = 0.4$  for this polyion and thus,  $\Lambda^0$  for sodium polymethacrylate should be 250. Since  $\lambda_{\text{Na}^+} = 50.1$  at  $25^\circ$ ,  $\lambda_{\text{P}^-} = 200$  for the polymethacrylate ion. The values of the other parameters listed in Table I for this polyion have also been suitably adjusted with the value of  $\phi$ , so as to conform to eq 7.

The values of  $\lambda_{\text{P}^-}$ , which represent the average conductivity of a single ionic site on a polyion, are larger than the equivalent conductivities of most simple ions. It has been shown that certain ionic dyes can aggregate in solution and when they do, there is an increase in

the equivalent conductivity.<sup>29</sup> This has been shown to be due to the fact that the resistance of the aggregate to movement is less than the sum of the resistances of the individual ions. Thus, the same reasoning may explain the large conductivity in the case of a polyion, which may be considered to be an assemblage of ions.

The values of  $B_2$ , shown in Table I, for the different polyions are all approximately three orders of magnitude greater than the values of the electrophoretic terms for simple electrolytes. In the case of polyions, if some of the bound ions can also move within the ionic atmosphere in the opposite direction, this would tend to increase the electrophoretic drag also. This is qualitatively seen by the fact that  $\lambda$ -carrageenan has a smaller electrophoretic term than does the arabate polyion. It will be recalled that little or no movement of the bound counterions was indicated for the  $\lambda$ -carrageenan polyion. The large values of the "electrophoretic terms" in the case of polyelectrolytes are probably also a consequence of the large size and charge of these ions. This, of course, would depend on the exact shape of the polyion in solution.

The last column in Table I lists the calculated values of  $a$ , the distance of closest approach, for the different polyions. It is interesting that, despite differences in  $\lambda_{\text{P}^-}$  and  $B_2$  for the arabate polyion at 0 and  $25^\circ$ , the calculated values for  $a$  at both temperatures are the same, within experimental error, 530  $\text{\AA}$ . At the present time it is premature to ascribe any physical significance to the values of  $a$  except to state that they are much larger for polyions than for simple ions. It should be noted, however, that the values of  $a$  shown in Table I are directly proportional to the equivalent weights of the polyions and thus might be related to the size of an ionic segment of a polyion.

*Acknowledgment.* We wish to gratefully acknowledge partial support of this work from a Public Health Service Grant.

(29) C. Robinson and H. E. Garrett, *Trans. Faraday Soc.*, **35**, 771, 780 (1939).

## Electrosorption of 5-Chloro-1-pentanol at the Mercury-Solution Interface<sup>1</sup>

by Karl Doblhofer and David M. Mohilner\*

Department of Chemistry, Colorado State University, Fort Collins, Colorado 80521

Publication costs assisted by the Air Force Office of Scientific Research

The electrosorption of 5-chloro-1-pentanol on mercury in the absence of specific ionic adsorption has been studied by means of electrocapillary and differential capacitance measurements. There is a very well defined potential and corresponding charge density of maximum adsorption. The Esin and Markov plot for the charge density of maximum adsorption is precisely linear with zero slope. However, the Esin and Markov plots for all other charge densities are curves and have an approximate S shape. The electrosorption isotherm is congruent neither with respect to electrode potential nor with respect to charge density. A proof is given that the well known necessary conditions for congruence of electrosorption with respect to electrode potential or charge density are also sufficient conditions.

The study of the electrosorption of neutral organic molecules at the mercury-solution interface can provide helpful information for further development of a detailed theory of the inner part of the electrical double layer. In addition to information on the behavior of the organic sorbates themselves, such studies may help illuminate the role of solvent molecules in the inner layer, especially when the experiments are conducted under conditions in which there is no specific ionic adsorption. The present study concerns the adsorption of 5-chloro-1-pentanol on mercury from saturated aqueous solutions of NaF. To our knowledge, this is the first investigation of the electrosorption of this class of substituted aliphatic alcohols to be reported. Both interfacial tension and differential capacitance measurements were made.

### I. Experimental Section

**A. Solutions.** Solutions were prepared using water redistilled from alkaline permanganate in a still equipped with a heated fractionating column packed with glass helices. The saturated NaF base electrolyte was prepared from Mallinckrodt AR sodium fluoride which had been heated at 500° for 1 hr in a platinum dish to destroy any traces of organic matter and then recrystallized. The saturated NaF stock solution (0.916 *M*) was stored in a 1/2-gallon Teflon bottle in order to avoid contamination due to attack on the walls of a glass container by the concentrated fluoride solution. The Teflon bottle was first tested for possible leaching out of surface active materials by ascertaining that no detectable change in the differential capacitance of a salt solution could be observed after the solution had been stored in the bottle for a period of more than 2 weeks. The 5-chloro-1-pentanol was obtained from Pfaltz and Bauer, Research Chemicals, Flushing, N. Y. It was purified by fractional distillation at 6 mm of Hg pressure in a microdistillation apparatus, and the fraction boiling at 79° was taken. Mass spectrometric and infrared tests confirmed the molecular

structure. Solutions were prepared by weighing 5-chloro-1-pentanol and diluting to volume with saturated NaF stock solution.

**B. Electrodes.** Mercury for electrodes was re-purified by vacuum distillation. The mercury was used as a meniscus electrode in the capillary electrometer, as a dropping electrode in differential capacitance measurements, and as the auxiliary electrode in the dc potentiostat circuits for both kinds of measurements. A platinized platinum gauze electrode served as a fourth, ac auxiliary electrode in the differential capacitance measurements. In place of an ordinary reference electrode an Orion fluoride reversible electrode was employed as *indicator electrode* in both the electrocapillary and differential capacitance measurements.<sup>2,3</sup>

**C. Interfacial Tension Measurements.** Interfacial tension was measured with a modified Lippmann capillary electrometer. The fine bore (7- $\mu$  radius) gently tapered capillary was viewed at 120 $\times$  magnification with a Bausch and Lomb stereozoom microscope. The pressure required to bring the meniscus electrode to the reference position in the capillary was adjusted by means of a closed gas pressure system employing two brass bellows, one for coarse, the other for fine adjustment. The gas pressure was measured on a

(1) Taken in part from the thesis of K. Doblhofer submitted to the Department of Chemistry and the Faculty of the Graduate School of Colorado State University in partial fulfillment of the requirements for the degree of Doctor of Philosophy, March 1970.

(2) D. M. Mohilner, *Electroanal. Chem.*, 1, 241 (1966).

(3) *Indicator electrode*, in contrast to an ordinary constant potential reference electrode, denotes an electrode dipping into the same solution used for the electrocapillary measurements which is reversible either to a cation or an anion of that solution. This terminology was introduced and its rationale was given by D. M. Mohilner and N. Hackerman, *Electrochem. Acta*, 11, 1669 (1966). The fluoride reversible electrode was not strictly required for the measurements reported here. However, this electrode was used in order to facilitate future comparisons of these measurements with electrosorption studies of 5-chloro-1-pentanol in NaF solutions of other concentrations. The potential of the Orion fluoride electrode in 0.916 *M* NaF vs. a 0.1 *M* KCl calomel electrode was  $-0.260$  V.



wide-bore mercury manometer which was read with a 1-m cathetometer calibrated to 0.01 mm (Precision Instrument and Tool Co. Ltd., Surrey, England). The same cathetometer was used to measure the head of mercury in the capillary reservoir assembly.

In order to permit the use of the fluoride reversible electrode which has a resistance of about 1 megohm, a solid-state operational amplifier potentiostat was used for potential control. The voltage follower in this potentiostat circuit had FET inputs. The meniscus electrode in the capillary was operated at circuit ground potential and the potential of the fluoride reversible indicator electrode with respect to ground was read at the output of the voltage follower on a Fluke Model 871A differential voltmeter.

The capillary electrometer was calibrated with 0.05 M  $\text{Na}_2\text{SO}_4$  at 25° using as a standard the value of 426.2 dyne/cm at the electrocapillary maximum determined by Smolders from sessile drop measurements.<sup>4</sup> This capillary electrometer had been shown previously<sup>5,6</sup> to be capable of very high precision measurements of interfacial tension. When used with salt solutions such as NaCl or  $\text{Na}_2\text{SO}_4$  the interfacial tension could be determined with a reproducibility of about  $\pm 0.03$  dyn/cm. However, in the case of saturated solutions of NaF the precision of the measurements was worse by more than one order of magnitude. Solutions were deaerated with purified nitrogen bubbling and an atmosphere of nitrogen was maintained over the solutions during measurements.

Electrocapillary curves were measured at 25.0° for the base electrolyte solution (0.916 M NaF) alone and for each of 13 different concentrations of 5-chloro-1-pentanol in this electrolyte. The concentrations of the alcohol ranged from  $4.29 \times 10^{-4}$  to  $4.33 \times 10^{-2}$  M. The experimental data are plotted in Figure 1. The data were taken at 50-mV intervals over a voltage range from +0.30 to -1.40 V vs. the fluoride reversible electrode in each solution. The entire set of data was smoothed and then differentiated with respect to both electrode potential and logarithm of alcohol concentration by digital computer using a modification<sup>7</sup> of the previously published moving fit technique.<sup>8</sup>

*D. Differential Capacitance Measurements.* Differential capacitance at a dropping mercury electrode (DME) was measured with a General Radio Type 1615-A transformer ratio-arm bridge using a Type 1311-A audio oscillator, and a Type 1232-A tuned amplifier and null detector. The dropping electrode was drawn from 0.5-mm bore borosilicate glass capillary tubing. The inner wall of the capillary was dewetted with the vapor of dichlorodimethylsilane,<sup>9</sup> and then the capillary tip was recut.

Solutions were deaerated in the same manner as in the case of the electrocapillary measurements. A four-electrode system was used for the capacitance measurements.<sup>6</sup> The ac voltage (5 mV peak-to-peak)

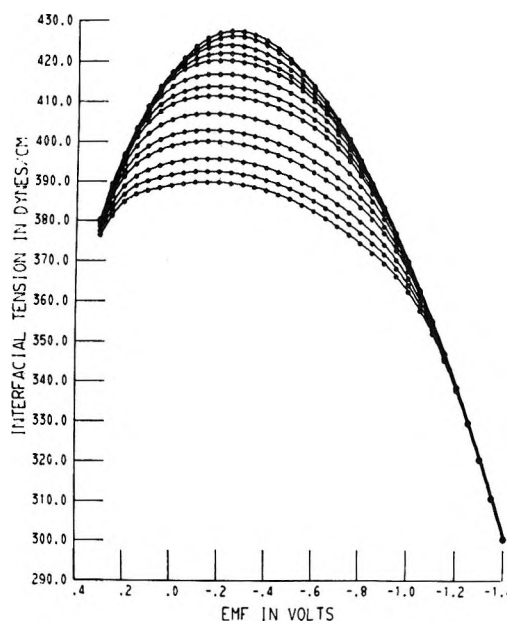


Figure 1. Electrocapillary curves for the electrosorption of 5-chloro-1-pentanol on mercury from 0.916 M NaF at 25°. Reading from upper curve to lower, the concentration of 5-chloro-1-pentanol is: 0.0,  $4.29 \times 10^{-4}$ ,  $1.134 \times 10^{-3}$ ,  $1.716 \times 10^{-3}$ ,  $2.325 \times 10^{-3}$ ,  $3.487 \times 10^{-3}$ ,  $4.65 \times 10^{-3}$ ,  $5.67 \times 10^{-3}$ ,  $8.59 \times 10^{-3}$ ,  $1.290 \times 10^{-2}$ ,  $1.718 \times 10^{-2}$ ,  $2.590 \times 10^{-2}$ ,  $3.436 \times 10^{-2}$ ,  $4.330 \times 10^{-2}$  M.

from the bridge was applied between a platinized platinum gauze electrode and the DME, which was positioned in the center of the gauze. The dc potential of the DME with respect to the fluoride reversible indicator electrode in the same solution was controlled by a solid-state operational amplifier potentiostat. A mercury pool served as auxiliary electrode in this potentiostat circuit. In order to prevent the potentiostat from canceling the ac voltage applied by the bridge, a low pass filter was placed between the output of the potential controlling amplifier and the mercury pool. This filter was effectively isolated from the bridge circuit by a 100-kilohm resistor. The DME was connected to the common ground of the bridge and potentiostat circuits. The potential of the indicator electrode with respect to ground was read at the output of the voltage follower with a Fluke Model 871A differential voltmeter. The method used for determining the bridge balance was a modification of that originated by Grahame.<sup>10</sup> The output of the

(4) C. A. Smolders and E. M. Duyvis, *Recl. Trav. Chim. Pays-Bas*, **80**, 635 (1961).

(5) K. Doblhofer, *J. Electrochem. Soc.*, **116**, 77C (1969).

(6) For detailed design features cf. K. Doblhofer, Ph.D. Thesis, March 1970, Colorado State University. Available from University Microfilms, Inc., Ann Arbor, Mich.

(7) P. R. Mohilner and D. M. Mohilner in "Applications of Computers to Analytical Chemistry," H. B. Mark, Ed., Marcel Dekker, New York, N. Y., in press.

(8) D. M. Mohilner and P. R. Mohilner, *J. Electrochem. Soc.*, **115**, 261 (1968).

(9) R. Payne, *J. Electroanal. Chem.*, **7**, 134 (1964).

(10) D. C. Grahame, *J. Amer. Chem. Soc.*, **71**, 2975 (1949).

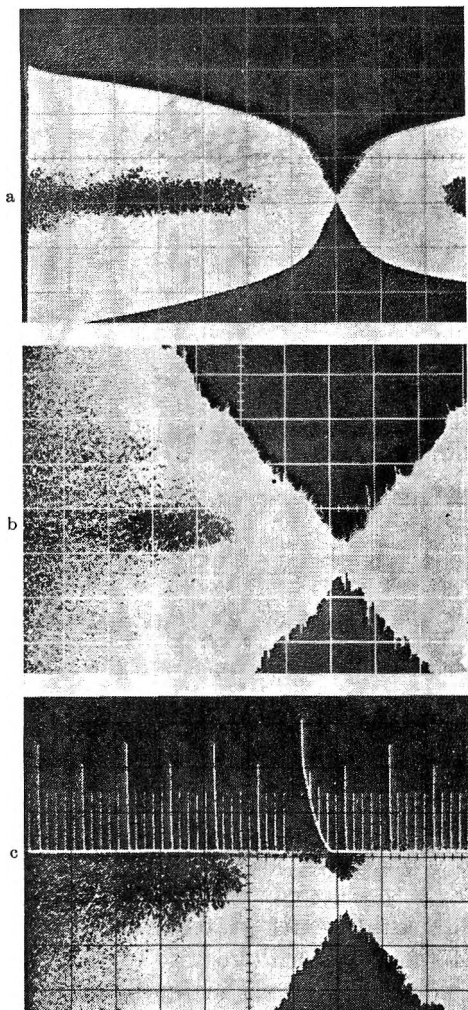


Figure 2. Photographs of oscilloscope screen illustrating method of determining time of bridge balance. (a) Complete picture of null detector output. Horizontal sweep rate = 1 sec/major division. Balance occurs slightly after 7 sec. (b) Same as (a) but using delayed sweep. Sweep rate = 0.05 sec/major division. (c) Same as (b) except upper half of screen has been erased and time marks from Tektronix Type 184 time-mark generator recorded. Small time marks occur every 0.01 sec. Largest time mark showing exponential decay which occurs just before bridge balance is the 7.0 sec mark (*cf.* a above).

bridge null detector which was tuned to the frequency of the applied ac voltage was displayed on the screen of a Tektronix Type 564 storage oscilloscope *via* one channel of a Type 3A1 dual trace preamplifier, and the oscilloscope sweep was controlled by a Type 3B3 dual time base. The delaying sweep of the time base was triggered by a pulse derived by a solid-state operational amplifier differentiator circuit from the very sharp change in output of the null detector which occurred each time a drop fell. The bridge was adjusted to give a minimum output on the null detector at some time late in the drop life (Figure 2a). In practice, null detector output was recorded only in the vicinity of the minimum by storing it in the delayed sweep mode using a delayed sweep rate of 50 msec/cm

(Figure 2b). Then half of the storage screen was erased and a switch was thrown which connected the trigger input of the time base to the trigger output of a Tektronix Type 184 crystal-controlled time-mark generator. The trigger output of the time-mark generator was set to 1.000 sec. Then the first trigger pulse delivered after the switch was thrown triggered the oscilloscope, and time marks were displayed and stored on the screen *via* the other channel of the Type 3A1 vertical preamplifier. The time corresponding to any time mark could be recognized by amplitude and decay time (*cf.* Figure 2c). By this method it was very convenient to determine the time of bridge balance to the nearest 0.01 sec. Moreover, there is the advantage of eliminating any uncertainty in the time of bridge balance due to drift in the time base amplifiers of the oscilloscope. In effect, this method of bridge balance is equivalent to a recalibration of the oscilloscope time base every measurement. The maximum uncertainty in the measurements reported here was less than 2 parts per thousand.

Differential capacitance was measured for the base electrolyte and for 22 different concentrations of 5-chloro-1-pentanol in 0.916 *M* NaF. The alcohol concentration range was  $1.395 \times 10^{-4}$  to  $4.33 \times 10^{-2}$  *M*. In the case of such measurements, in order to arrive at valid thermodynamic capacitances, two different kinds of possible nonequilibrium, dc and ac, must be considered. By dc nonequilibrium it is implied that during the growth of the drop, at fixed dc potential, the surface excess of the organic sorbate has not achieved its equilibrium value due to slow diffusion of the sorbate molecules to the electrode surface. A very sensitive indicator of whether or not dc equilibrium has been achieved is the measured value of the differential capacitance per unit area at fixed ac frequency but at different times in the drop life. If dc equilibrium has not been achieved one will observe, in the potential domain of adsorption, a decrease in the measured capacitance *C* per unit area with increasing time. In the case of the solutions studied here such a decrease was indeed observed early in drop life. However, it was found that even with the most dilute solutions such a change in capacitance was quite negligible (less than 2 parts per thousand) provided the time of bridge balance was delayed by 6 sec, and therefore most of the measurements were taken with the bridge balanced at about 7–8 sec in the drop life. The natural drop time of the capillary was approximately 15 sec.

The second source of nonequilibrium, which results from the inability of the sorbate molecules to follow the small ac voltage imposed by the bridge, is unavoidable. It was found that in this study a plot of measured capacitance *vs.* square root of frequency always gave a very good straight line with negative slope indicating that this frequency dispersion was diffusion

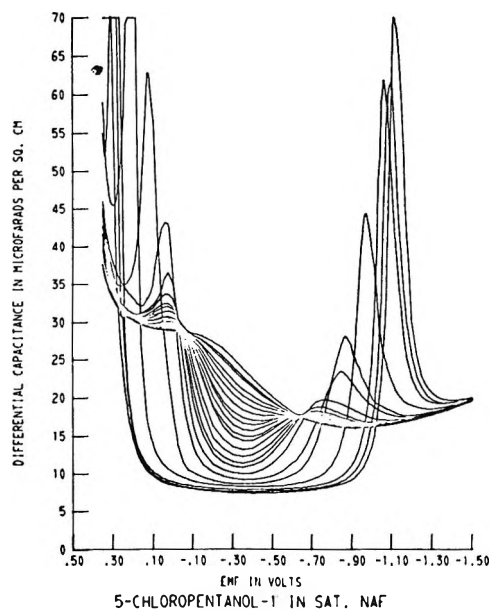


Figure 3. Zero frequency differential capacitance curves for electroadsorption of 5-chloro-1-pentanol from 0.916  $M$  NaF on mercury. Reading from upper curve to lower, in center portion of figure between desorption peaks, the concentration of 5-chloro-1-pentanol is: 0.0,  $1.395 \times 10^{-4}$ ,  $2.145 \times 10^{-4}$ ,  $3.305 \times 10^{-4}$ ,  $4.290 \times 10^{-4}$ ,  $4.572 \times 10^{-4}$ ,  $5.008 \times 10^{-4}$ ,  $5.670 \times 10^{-4}$ ,  $6.610 \times 10^{-4}$ ,  $6.974 \times 10^{-4}$ ,  $7.518 \times 10^{-4}$ ,  $8.580 \times 10^{-4}$ ,  $9.144 \times 10^{-4}$ ,  $1.016 \times 10^{-3}$ ,  $1.134 \times 10^{-3}$ ,  $1.322 \times 10^{-3}$ ,  $1.716 \times 10^{-3}$ ,  $2.662 \times 10^{-3}$ ,  $4.865 \times 10^{-3}$ ,  $1.290 \times 10^{-2}$ ,  $2.950 \times 10^{-2}$ ,  $3.436 \times 10^{-2}$ ,  $4.330 \times 10^{-2} M$ .

controlled.<sup>11</sup> The quality of the straight line was checked numerous times at as many as seven different frequencies ranging from 100 Hz to 10 kHz. The plot found was always so good that it was justifiable for the majority of points to rely on measurements made at only two frequencies, 400 and 1000 Hz.

Figure 3 gives the extrapolated zero frequency differential capacitances per unit area for the base electrolyte and for each of the 22 different concentrations of 5-chloro-1-pentanol. Depending on the amount of structure present in a given capacitance curve, the number of potentials at which measurements were made ranged from 33 to 70 in the potential range from  $-1.50$  to  $+0.30$  V vs. the fluoride reversible electrode in the same solution.

## II. Results and Discussion

*A. Analysis of Interfacial Tension Data.* The chemical potential of the sodium fluoride in each of the solutions studied was always precisely the same due to the fact that each solution was saturated with solid NaF. The temperature was held constant at  $25.00 \pm 0.05^\circ$ , and the external pressure was effectively constant. Thus the complete electrocapillary equation describing the thermodynamic equilibrium for all the solutions studied is<sup>2</sup>

$$d\gamma = -q^M dE - \Gamma_a d\mu_a \quad (1)$$

where  $\gamma$  is the interfacial tension,  $q^M$  is the excess charge density on the metal surface,  $E$  is the potential of the ideal polarized mercury electrode with respect to the fluoride reversible indicator electrode in the same solution,  $\Gamma_a$  is the relative surface excess of the 5-chloro-1-pentanol, and  $\mu_a$  is the chemical potential of the alcohol in the given solution. Activity coefficients are not available for 5-chloro-1-pentanol in saturated NaF solutions, and therefore it was necessary to use concentrations in place of activities in the data analysis as has been done in nearly all previous studies of electroadsorption of organic compounds.<sup>12,13</sup> This approximation appears justifiable in the case of the present study because most of the important conclusions about the nature of the adsorption isotherm are based on data obtained at quite low concentrations ( $<5$  mM). With this approximation eq 1 takes the following form which was actually used as the basis of the data analysis

$$d\gamma = -q^M dE - RT\Gamma_a d \ln c_a \quad (2)$$

In eq 2,  $R$  is the gas constant,  $T$  is the absolute temperature, and  $c_a$  is the molar concentration of the 5-chloro-1-pentanol in the saturated NaF solution.

The Lippmann equation relating the slope of a given electrocapillary curve to the excess charge density is

$$q^M = -\left(\frac{\partial \gamma}{\partial E}\right)_{c_a} \quad (3)$$

The results of the computer differentiation of the smoothed interfacial tension data according to eq 3 are given in Figure 4. The most striking feature of these  $q^M$  vs.  $E$  curves is their point of intersection (crossing point). Since it follows from eq 2 that

$$\left(\frac{\partial q^M}{\partial \ln c_a}\right)_E = RT(\partial \Gamma_a / \partial E)_{c_a} \quad (4)$$

and

$$\left(\frac{\partial E}{\partial \ln c_a}\right)_{q^M} = -RT(\partial \Gamma_a / \partial q^M)_{c_a} \quad (5)$$

one concludes<sup>2</sup> that this point of intersection implies the existence of a single potential, and a corresponding single charge density, of maximum adsorption valid for all concentrations. The potential of the point of intersection was  $-0.295$  V, and the corresponding charge density was  $-1.00 \mu\text{C}/\text{cm}^2$ .

Differentiation of the interfacial tension at constant potential with respect to  $\ln c_a$  yields the relative surface excess of the alcohol

$$\Gamma_a = -RT(\partial \gamma / \partial \ln c_a)_E \quad (6)$$

(11) R. Parsons and P. C. Symons, *Trans. Faraday Soc.*, **64**, 1077 (1968).

(12) Cf., A. N. Frumkin and B. B. Damaskin, "Modern Aspects of Electrochemistry," Vol. 3, J. O'M. Bockris and B. E. Conway, Ed., Butterworths, Washington, D. C., 1964, pp 149-223.

(13) See also, E. Dutkiewicz, J. D. Garnish, and R. Parsons, *J. Electroanal. Chem.*, **16**, 505 (1968).

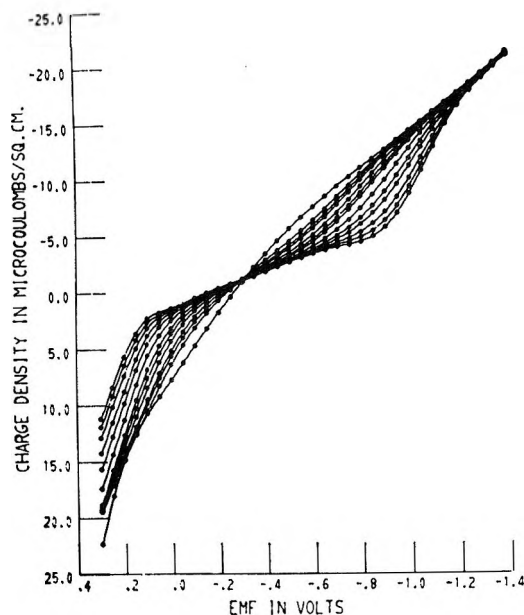


Figure 4.  $q^M$  vs.  $E$  curves obtained by differentiation of electrocapillary curves (cf. Figure 1). Reading from upper curve to lower on the negative side of the crossing point ( $E = 0.295$  V,  $q^M = -1.00 \mu\text{C}/\text{cm}^2$ ) the concentration of the 5-chloro-1-pentanol is:  $0.0$ ,  $1.134 \times 10^{-3}$ ,  $1.716 \times 10^{-3}$ ,  $2.325 \times 10^{-3}$ ,  $3.487 \times 10^{-3}$ ,  $4.65 \times 10^{-3}$ ,  $5.67 \times 10^{-3}$ ,  $8.59 \times 10^{-3}$ ,  $1.290 \times 10^{-2}$ ,  $1.718 \times 10^{-2}$ ,  $2.590 \times 10^{-2}$ ,  $3.436 \times 10^{-2}$ ,  $4.330 \times 10^{-2}$  M.

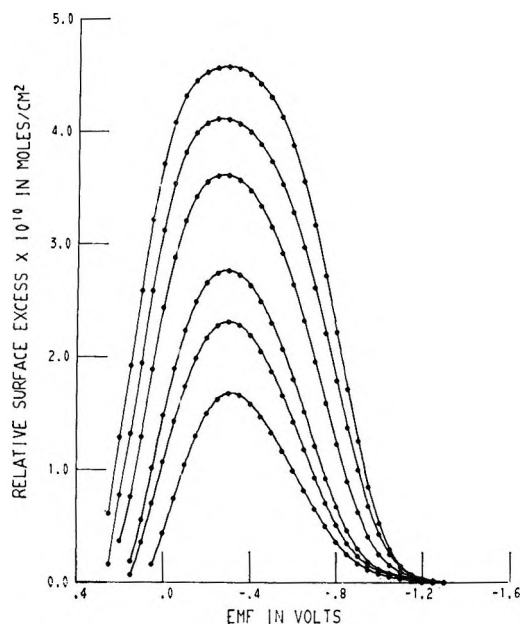


Figure 5. Selected curves showing dependence of relative surface excess of 5-chloro-1-pentanol as a function of electrode potential. Obtained from electrocapillary data. Reading from upper curve to lower, the concentration of 5-chloro-1-pentanol is:  $5.67 \times 10^{-3}$ ,  $4.65 \times 10^{-3}$ ,  $3.48 \times 10^{-3}$ ,  $2.325 \times 10^{-3}$ ,  $1.716 \times 10^{-3}$ ,  $1.134 \times 10^{-3}$  M.

Figure 5 shows plots of  $\Gamma_a$  at several concentrations as a function of the electrode potential, and Figure 6 shows the corresponding plots as a function of charge

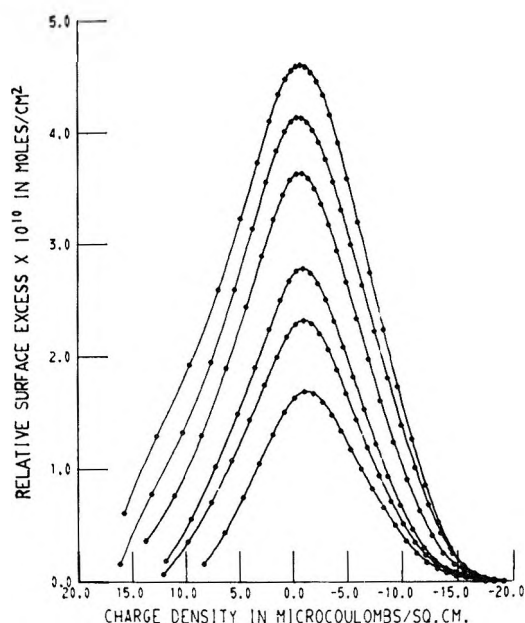


Figure 6. Selected curves showing dependence of relative surface excess of 5-chloro-1-pentanol as a function of  $q^M$ . Obtained from electrocapillary data. Concentrations of 5-chloro-1-pentanol are same as in corresponding curves in Figure 5.

density. It may be seen from these figures that the potential and the charge density of maximum adsorption do correspond with the point of intersection found on the  $q^M$  vs.  $E$  curves. Unfortunately, the precision of the interfacial tension measurements in the saturated NaF solutions was not sufficiently high to permit a more detailed analysis of the adsorption equilibrium. In particular, the  $\Gamma_a$  data were not considered to be accurate enough to permit a distinction to be made between various alternative theoretical adsorption isotherms. On the anodic side of the point of zero charge the measurement of interfacial tension was made difficult by the tendency of the meniscus to "stick" in the capillary, a phenomenon which has been noted by others<sup>14</sup> who have studied NaF solutions. In general, the computer differentiation of interfacial tension as a function of electrode potential at constant concentration was more reliable than the corresponding differentiation as a function of  $\ln c_a$  at constant potential.

*B. Analysis of the Differential Capacitance Data. 1. Basis of the Analysis.* The thermodynamic differential capacitance  $C$  is the first derivative of the excess charge density  $q^M$  or the negative of the second derivative of the interfacial tension  $\gamma$  with respect to electrode potential at constant composition.<sup>2</sup> That is

$$C = (\partial q^M / \partial E)_{c_a} = -(\partial^2 \gamma / \partial E^2)_{c_a} \quad (7)$$

Thus a single integration of a differential capacitance curve from a potential where the value of the charge

(14) J. Lawrence, R. Parsons, and R. Payne, *J. Electroanal. Chem.*, **16**, 193 (1968).

density is known will yield the corresponding  $q^M$  vs.  $E$  curve, and a double integration from a potential where both the value of  $q^M$  and  $\gamma$  are known will yield the corresponding electrocapillary curve. The precision of the electrocapillary data on the far cathodic side of the point of zero charge was much better than on the anodic branch. Therefore, it was planned to carry out a double integration of the zero frequency differential capacitance curves from some potential on the far cathodic branch. It was found that in the case of pure saturated NaF solutions double integration gave practically the same results regardless of the potential on the cathodic branch at which the integration constants were chosen. However, it was also found that the directly measured interfacial tension on the anodic branch was always systematically lower than the interfacial tension resulting from the double integration of the interfacial tension resulting from the double integration of the differential capacitance (cf. Figure 7, upper curve. In more dilute NaF solution this systematic discrepancy on the anodic branch was much worse). Similar results were reported by Lawrence, Parsons and Payne,<sup>14</sup> who suggested that the cause of the phenomenon might be the development of a finite contact angle at the three-phase boundary inside the capillary. The validity of this hypothesis has since been verified by comparison with measurements of the interfacial tension made by the "maximum bubble pressure" method<sup>15,16</sup> and by drop times.<sup>17</sup> This result implies that in saturated NaF solution the values of the interfacial tension and of the charge density derived from them would be systematically in error on the anodic branch of the electrocapillary curve.

Unfortunately, integration of the differential capacitance curves from the far cathodic branch in the presence of the organic sorbate also gave results which were unacceptable. The middle curve in Figure 7 is the doubly integrated differential capacitance for the most concentrated solution used in the study. It was obtained by integrating the differential capacitance from the same potential ( $-1.40$  V) with the same pair of integrating constants ( $q^M = -21.04$  C/cm<sup>2</sup> and  $\gamma = 300.23$  dyn/cm) used to obtain curve 1. The lower curve in Figure 7 is the directly measured electrocapillary curve for the same solution. Clearly, the explanation for the discrepancy between the lower and middle curves in Figure 7 cannot be the finite contact angle because the true electrocapillary curve in the presence of absorbed alcohol should never rise above that for the base electrolyte. The source of the discrepancy is rather to be found in the differential capacitance curve itself, namely: the cathodic desorption peak is too low despite the facts that the capacitance was extrapolated to zero frequency and that the extrapolation vs. square root of frequency had excellent linearity. Similar results have been reported by Cachet, *et al.*<sup>18</sup> Their work and the present study both show that despite ap-

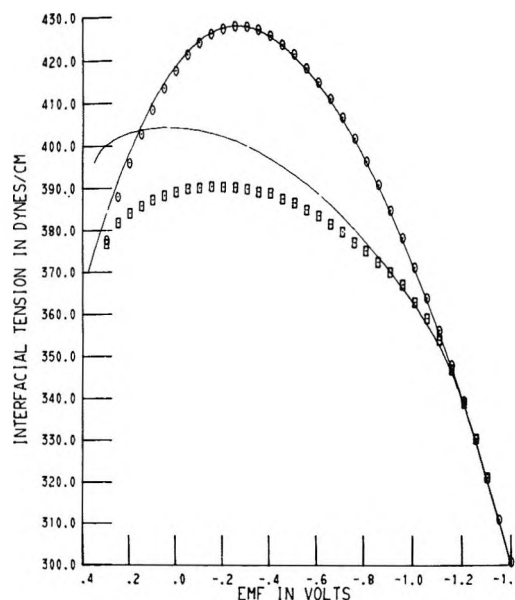


Figure 7. Comparison of electrocapillary curves obtained by direct measurement with capillary electrometer and by double integration of differential capacitance. Upper curves: 0.916 M NaF base electrolyte solution. Solid curve from differential capacitance; points in circles directly measured. Middle solid curve: doubly integrated differential capacitance curve for  $4.330 \times 10^{-2}$  M 5-chloro-1-pentanol in base electrolyte. Lower curve (points inside squares) same solution as middle curve but directly measured with capillary electrometer.

parently good linearity, an extrapolation to zero frequency vs. square root of frequency does not yield the correct value of the differential capacitance in the region of desorption peaks where the frequency dispersion is very pronounced. It was therefore decided in the analysis of the present data to use only those portions of the differential capacitance curves between the peaks where the frequency dispersion is anyway quite low. This required that the integration constant also be selected from the same potential domain. Fortunately, the existence of the crossing point of the  $q^M$  vs.  $E$  curves derived from the electrocapillary measurements made such an integration feasible.

Careful examination of these  $q^M$  vs.  $E$  curves (Figure 3) showed that the maximum uncertainty in the potential of the crossing point ( $-0.295$  V) was less than 5 mV. The comparison illustrated in Figure 7 for the 0.916 M NaF base electrolyte solution indicated no discrepancy at this potential between the directly measured electrocapillary curve and that obtained by double integration of the corresponding differential capacitance curve. However, even if the value of  $q^M$  found at the crossing point ( $-1.00$   $\mu$ C/cm<sup>2</sup>) should be

(15) D. J. Schiffrin, *J. Electroanal. Chem.*, **23**, 168 (1968).

(16) J. Lawrence and D. M. Mohilner, *J. Electrochem. Soc.*, **118**, 259 (1971).

(17) R. Parsons, *Rev. Pure Appl. Chem.*, **18**, 91 (1968).

(18) C. Cachet, I. Epelboin, J. Lestrade, and P. Ravel, *C. R. Acad. Sci., Ser. C*, **264**, 1524 (1967).

somewhat in error due to a nonzero contact angle at this potential, the conclusions reached about the nature of the adsorption isotherm derived from the integration of the differential capacitance curves from the potential of the crossing point will be unaffected because the  $q^M$  values so obtained will all have the same constant error, and only *differences* in charge densities are used in the analysis. Therefore, the 23 zero frequency differential capacitance curves were all integrated from the crossing point, and the corresponding  $q^M$  vs.  $E$  curves were obtained.

2. *Esin and Markov Plots.* Esin and Markov plots, *i.e.*, plots of electrode potential vs.  $RT \ln c_a$  at constant charge density were derived from the integrated differential capacitance curves and are shown in Figure 8. The Esin and Markov plot for  $q^M = -1.00 \mu\text{C}/\text{cm}^2$ , *i.e.*, the charge density of the crossing point, is necessarily a horizontal straight line with ordinate equal to the potential of the crossing point which implies again that there is a single charge density and a single potential of maximum adsorption (*cf.* Figures 4–6). It is worth pointing out, however, that none of the other Esin and Markov plots are linear, but rather are definitely curved and have approximately an “S” shape. This curvature would not have been so clearly defined had the capacitance data not been taken at so many closely spaced concentrations (*cf.* Figure 3). Some previous studies of organic electrosorption<sup>19–21</sup> have indicated that Esin and Markov plots for neutral molecules can exhibit two linear sections with different slopes whose point of intersection might be attributed to a rather abrupt change in orientation of the molecules on the electrode surface with increasing concentration at constant  $q^M$ . The data on which such conclusions have been based were generally obtained for only a relatively low number (*e.g.*, 7) of concentrations of the sorbate over a concentration range of two to three decades. It is evident from Figure 8 that the region of high curvature in the Esin and Markov plots for 5-chloro-1-pentanol occurs over a relatively narrow concentration range from  $4.865 \times 10^{-3}$  to  $4.572 \times 10^{-4} M$  where capacitance data for a total of 14 different concentrations were taken. Had the data in this study not been taken at so many closely spaced concentrations one might plausibly have concluded that for this system also the Esin and Markov plots consist of two or perhaps three straight-line segments. The experimental evidence shows that such a conclusion in this case would have been totally incorrect.

This result does not necessarily invalidate the conclusion based on Esin and Markov plots reached in the previously cited studies.<sup>19,21</sup> It does strongly suggest, however, the importance of taking experimental data on organic electrosorption at many closely spaced concentrations in order to define adequately the nature of the adsorption equilibrium.

3. *Congruence of the Adsorption Isotherm.* A strictly

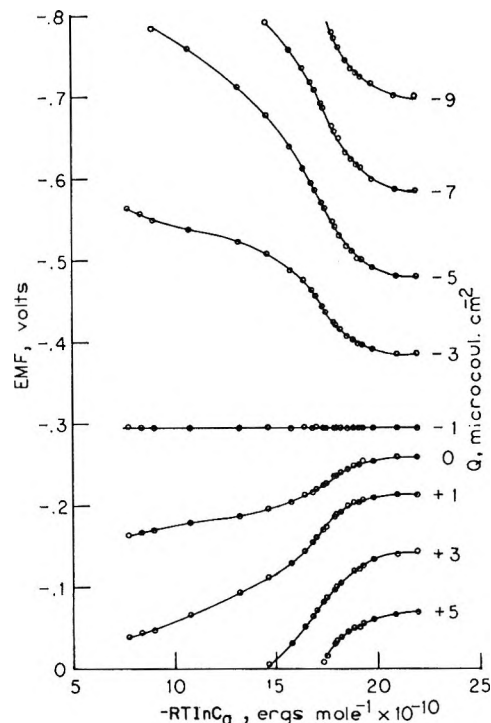


Figure 8. Esin and Markov plots. Constant values of  $q^M$  for each curve indicated in figure (as  $Q$ ).

thermodynamic determination of the adsorption isotherm from differential capacitance data, or rather, from charge density–potential curves obtained by integration of differential capacitance data, is possible only if the adsorption is congruent either with respect to electrode potential or with respect to charge density. The adsorption is said to be congruent with respect to electrode potential if all plots at constant potential of the relative surface excess  $\Gamma_a$  vs.  $\ln c_a$  (strictly speaking, vs.  $\ln a^b$ , where  $a^b$  is the bulk activity of the sorbate in the solution) are of precisely the same size and shape, *i.e.*, are *congruent* in a strictly geometrical sense. Similarly, the adsorption is said to be congruent with respect to charge density if all plots of  $\Gamma_a$  vs.  $\ln c_a$  are superimposable by lateral shifting along the  $\ln c_a$  axis. It is clear that congruence implies that the corresponding plots of the fractional surface coverage,  $\theta = \Gamma_a/\Gamma_s$ , will also have the same property of superimposability by lateral shifting along the  $\ln c_a$  axis. ( $\Gamma_s$  is the value of the relative surface excess on a surface saturated with the sorbate; it is the highest obtainable value of  $\Gamma_a$ .)

If the adsorption isotherm is congruent with respect to potential, it follows, as was first proved thermody-

(19) B. E. Conway and R. G. Barradas, *Electrochim. Acta*, **5**, 319 (1961).

(20) R. G. Barradas and P. G. Hamilton, *Can. J. Chem.*, **43**, 2468 (1965).

(21) R. G. Barradas, P. G. Hamilton, and B. E. Conway, *J. Phys. Chem.*, **69**, 3411 (1965).

namically by Parsons,<sup>22</sup> that at any fixed value of the electrode potential the charge density  $q^M$  in the presence of adsorbed organic molecules is a linear function of the fractional surface coverage, *i.e.*

$$q^M = q_0(1 - \theta) + q'\theta \quad (8)^{23}$$

Here  $q_0$  and  $q'$  denote the values of the charge density at the same electrode potential in the presence of pure supporting electrolyte and when the surface is saturated ( $\theta = 1$ ), respectively. On the other hand, if the adsorption isotherm is congruent with respect to charge density, it follows<sup>22</sup> that at any constant value of  $q^M$  the electrode potential  $E$  in the presence of adsorbed organic molecules is a linear function of  $\theta$ , *i.e.*

$$E = E_0(1 - \theta) + E'\theta \quad (9)$$

Here  $E_0$  and  $E'$  are the values of the electrode potential at the same  $q^M$  in the presence of supporting electrolyte alone and when the surface is saturated ( $\theta = 1$ ), respectively. Equations 8 and 9 are thus the respective necessary conditions for congruence with respect to electrode potential or charge density. It follows that if the adsorption is congruent with respect to  $E$ , the fractional surface coverage may be calculated from  $q^M$  vs.  $E$  data by solving eq 8 for  $\theta$ . Similarly, if the adsorption is congruent with respect to charge density it is possible to calculate the fractional surface coverage from  $q^M$  vs.  $E$  data by solving eq 9 for  $\theta$ . A very sensitive and elegant test for congruence was proposed by Damaskin.<sup>24,25</sup> The idea of this test is to assume that the adsorption is congruent either with respect to electrode potential or with respect to charge density and then to see whether or not this assumption leads to a contradiction. If the adsorption is congruent with respect to electrode potential then by Parsons' proof,<sup>22</sup> of necessity eq 8 will be valid. Therefore, one can use  $q^M$  vs.  $E$  data to calculate  $\theta$  at constant  $E$  by solving eq 8 and one can then test to see if the resulting isotherms have identical geometrical shape. Rather than shifting the curves laterally along the  $\ln c_a$  axis, it is more convenient and completely equivalent to plot  $\theta$  vs. a relative concentration<sup>24</sup> defined as the ratio of the concentration  $c_a$  to that concentration which gives some arbitrarily chosen value of  $\theta$  at the same potential, say  $\theta = 0.3$ . If the assumption of congruence is correct, the plots of  $\theta$  vs. relative concentration for all constant potentials will superimpose. This test for congruence with respect to electrode potential was applied to the  $q^M$  vs.  $E$  data obtained by integration of the differential capacitance data for 5-chloro-1-pentanol. The results are shown in Figure 9. Clearly the curves in this figure are not superimposable. Therefore, the assumption was false; the adsorption of 5-chloro-1-pentanol is not congruent with respect to electrode potential. The test for congruence with respect to charge density is exactly similar. Assume the adsorption is congruent with respect to  $q^M$ . Then eq 9 is valid. Thus, one can calcu-

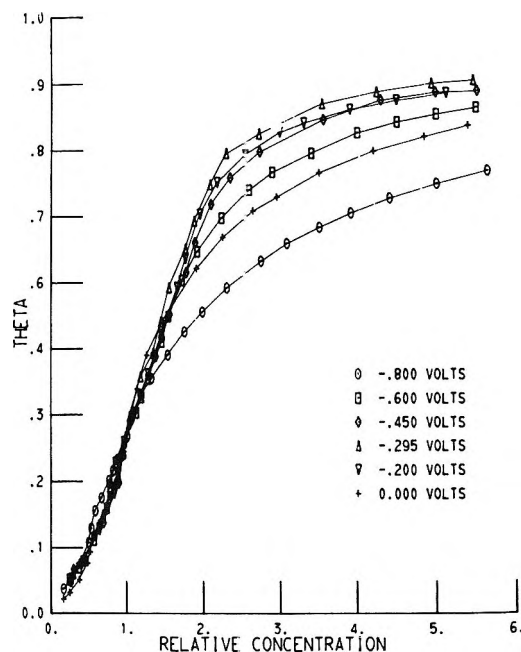


Figure 9. Test of congruence of electroadsorption of 5-chloro-1-pentanol with respect to electrode potential.  $E$  values indicated in figure.

late  $\theta$  from  $q^M$  vs.  $E$  data from eq 9, and all plots of  $\theta$  vs. relative concentration will superimpose. This test was applied to the  $q^M$  vs.  $E$  data obtained by integration of the differential capacitance data and the results are shown in Figure 10. The curves obtained are not identical for the different charge densities. Therefore, the assumption of congruence with respect to charge density was also false. These experimental data prove unequivocally that the true electroadsorption isotherm for 5-chloro-1-pentanol is congruent neither with respect to electrode potential nor with respect to charge density.

Since the adsorption is not congruent it follows<sup>22</sup> that the so-called lateral interaction parameter in the correct isotherm cannot be a constant but rather must be a function of the electrode potential (or charge density). It is worth mentioning that the alternate possibility suggested by Frumkin<sup>26</sup> that eq 8 could be valid but that  $\Gamma_s$  varies with coverage is not an acceptable explanation when the adsorption is not congruent with respect to potential because, as we shall show (*cf.* Appendix), eq 8 and 9 are not only the necessary conditions for congruence as was proved by Parsons,<sup>22</sup> they are also sufficient.<sup>27</sup>

(22) R. Parsons, *Trans. Faraday Soc.*, **55**, 999 (1959).

(23) This equation was originally derived by Frumkin on the basis of a model of the electrical double layer in the presence of adsorbed organic molecules as two capacitors in parallel. A. N. Frumkin, *Z. Phys.*, **35**, 792 (1926).

(24) B. B. Damaskin, *J. Electroanal. Chem.*, **7**, 155 (1964).

(25) A. N. Frumkin, B. B. Damaskin, and A. A. Survilla, *ibid.*, **16**, 493 (1968).

(26) *Cf.* ref 14, pp 159-160, and ref 15.

(27) We are indebted to a reviewer whose comments led us to reconsider this whole question.

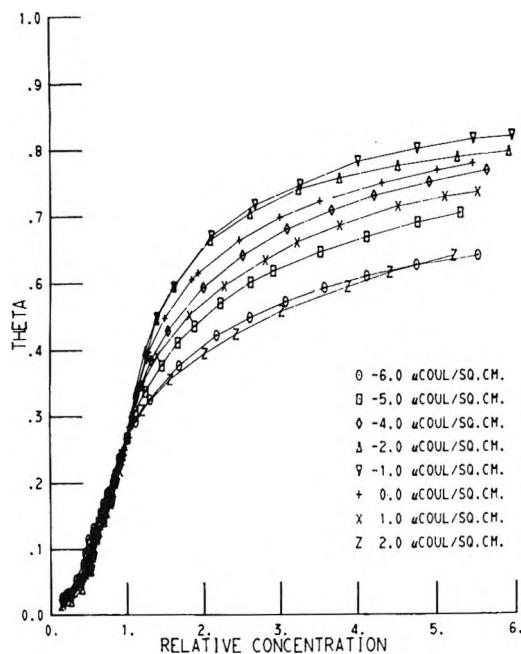


Figure 10. Test of congruence of electroadsorption of 5-chloro-1-pentanol with respect to charge density. The  $q^M$  values are indicated in the figure.

There are instances in the literature<sup>28</sup> in which eq 8 (or a corresponding equation in terms of differential capacitance derived from eq 8) has been used to calculate an adsorption isotherm having a potential dependent lateral interaction parameter, *i.e.*, an isotherm which is not congruent with respect to potential. We have done the same and found that the fit of  $\theta$  calculated by eq 8 to a modified Flory-Huggins isotherm<sup>29</sup> at constant potential is really very good. Figure 11 shows an example of the fit using a linearized plot of the type suggested by Lawrence and Parsons. It would be tempting to try to draw conclusions from this excellent fit about the detailed nature, on a molecular scale, of the adsorption process. However, such an attempt would be without proper foundation. Because eq 8 is both a necessary and a sufficient condition for congruence with respect to electrode potential, and the Damaskin test for congruence shows unequivocally that the isotherm is not congruent with respect to potential, it follows that the quantity denoted by  $\theta$  and calculated by means of eq 8 is not the true fractional surface coverage of the electrode by 5-chloro-1-pentanol. Therefore, the fit of the modified Flory-Huggins isotherm to that quantity is no proof that this same isotherm would fit the true  $\theta$ . Such detailed additional information about the nature of the electroadsorption equilibrium would appear to be accessible only through interfacial tension measurements of considerably higher precision than we have yet been able to achieve with such systems.

A final point to be mentioned is that when, as in this case, the electroadsorption isotherm is congruent neither with respect to electrode potential nor with respect to

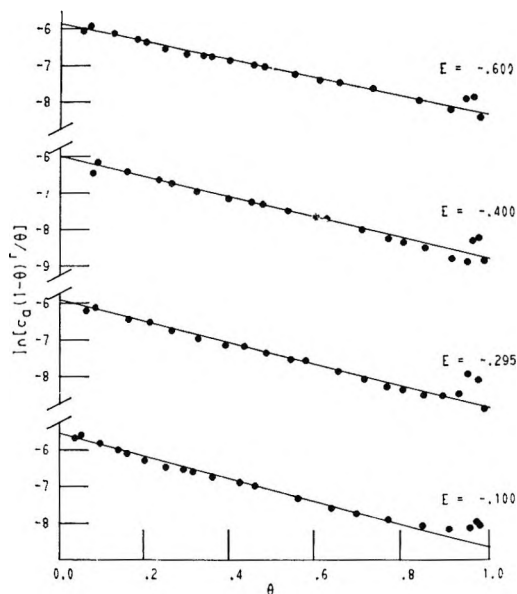


Figure 11. Representative best fits of electroadsorption of 5-chloro-1-pentanol to a modified Flory-Huggins isotherm at constant electrode potential with  $r = 1.2$ .  $E$  values indicated in figure.

charge density, it is no longer profitable to continue the long-standing debate over which of these two electrical variables is the more fundamental.<sup>13,24</sup> The only reason for preferring one electrical variable over the other in such a case would be convenience.

### III. Conclusions

The electroadsorption of 5-chloro-1-pentanol on mercury from saturated NaF has been studied by electrocapillary and differential capacitance measurements. This compound adsorbs at the mercury-solution interface in the absence of specific ionic adsorption<sup>30</sup> with a very well defined potential and charge density of maximum adsorption ( $-0.295$  V *vs.* Orion fluoride reversible electrode in the same solution and  $-1.00$   $\mu\text{C}/\text{cm}^2$ ). The Esin and Markov plot for the charge density of maximum adsorption is precisely linear and horizontal, but for all other charges these plots show distinct curvature with an approximate S shape. The adsorption isotherm is congruent neither with respect to electrode potential nor with respect to charge density. This implies that the parameter usually called a "lateral interaction parameter" in the correct adsorption isotherm must depend upon the electrical variable.

*Acknowledgment.* This research was supported by

(28) B. B. Damaskin and N. B. Grigor'ev, *Dokl. Akad. Nauk SSSR*, **144**, 1073 (1962); ref 14, pp 195-196.

(29) J. Lawrence and R. Parsons, *J. Phys. Chem.*, **73**, 3577 (1969).

(30) The absence of specific adsorption of  $\text{F}^-$  from concentrated alkali metal salt solutions was proven by the work of Grahame. *Cf.* D. C. Grahame and B. A. Soderberg, *J. Chem. Phys.*, **22**, 449 (1954); D. C. Grahame, *J. Amer. Chem. Soc.*, **76**, 4819 (1954). The only possible exception is at extremely anodic potentials far beyond the domain of adsorption of 5-chloro-1-pentanol. *Cf.* R. Payne, ref 11.



the Air Force Office of Scientific Research, AFOSR (AFSC), USAF under Grants AF-AFOSR-68-1451 and AF-AFOSR-70-1887. We thank Dr. Patricia R. Mohilner for helpful discussion and for writing the computer programs used in the analysis of the data. Dr. John Lawrence also made helpful comments.

### Appendix

To our knowledge, no proof has been published that eq 8 and 9 are also sufficient conditions for congruence of electrosorption isotherms with respect to electrode potential or charge density, respectively. Because this fact thereby precludes the use of either of these equations for calculation of the fractional surface coverage whenever the isotherm is characterized by potential or charge dependent lateral interaction parameters, we think it important that a proof of sufficiency be given.

I. Let eq 8 be valid. We shall show that this assumption leads to the conclusion that the isotherm is congruent with respect to  $E$ . From eq 8 and the electrocapillary equation<sup>2</sup> one derives

$$\frac{\left(\frac{\partial\theta}{\partial E}\right)_\mu}{\left(\frac{\partial\theta}{\partial\mu}\right)_E} = \frac{q' - q_0}{\Gamma_s} \quad (\text{A1})$$

However, in general it is true that

$$\frac{\left(\frac{\partial\theta}{\partial E}\right)_\mu}{\left(\frac{\partial\theta}{\partial\mu}\right)_E} = -\left(\frac{\partial\mu}{\partial E}\right)_\theta = -RT\left(\frac{\partial\ln a^b}{\partial E}\right)_\theta \quad (\text{A2})$$

where  $a^b$  is the bulk activity of the sorbate in the solution. Hence, equating the right-hand sides of eq A1 and A2

$$\left(\frac{\partial\ln a^b}{\partial E}\right)_\theta = \frac{-1}{RT\Gamma_s}(q' - q_0) \quad (\text{A3})$$

Note that  $q'$  and  $q_0$  are functions of  $E$  alone. Thus one can integrate eq A3 at any constant  $\theta$  with respect to  $E$  between the limits of  $E$  and  $E_{\max}$ , the potential of maximum adsorption. Therefore

$$\int_E^{E_{\max}} d\ln a_\theta^b = -\frac{1}{RT\Gamma_s} \left[ \int_E^{E_{\max}} q'(E) dE - \int_E^{E_{\max}} q_0(E) dE \right] \quad (\text{A4})$$

In eq A4  $a_\theta^b$  denotes the value of the bulk activity which yields the chosen value of  $\theta$ . Substituting for  $q_0$  and  $q'$  by means of the Lippmann equation one obtains

$$\ln a_\theta^b(E) - \ln a_\theta^b(E_{\max}) = -\frac{1}{RT\Gamma_s} \{ [\gamma_0(E) - \gamma_s(E)] - [\gamma_0(E_{\max}) - \gamma_s(E_{\max})] \} \quad (\text{A5})$$

In eq A5  $a_\theta^b(E)$  is the value of  $a^b$  which gives a fractional surface coverage  $\theta$  at potential  $E$ , and  $a_\theta^b(E_{\max})$  is the value of  $a^b$  which yields the same  $\theta$  at the potential of maximum adsorption.  $\gamma_0$  and  $\gamma_s$  denote the values of the interfacial tension in the presence of the base electrolyte alone and when the surface is saturated at the specified potential, respectively. The second term in brackets inside the braces on the right-hand side of eq A5 is a constant; the first term is a function of potential alone. Thus it follows from eq A5 that the displacement along the  $\ln a^b$  axis of the point on the constant potential isotherm for potential  $E$  from the corresponding point (same value of  $\theta$ ) on the isotherm for  $E_{\max}$  depends only on  $E$ . Since eq A5 is valid for all  $\theta$ , one concludes that the isotherm for  $E$  is exactly parallel (*i.e.*, congruent) to the isotherm for  $E_{\max}$ . Since eq A5 is valid for all  $E$ , it follows that all constant potential isotherms would be superimposable by lateral shifting along the  $\ln a^b$  axis. Thus eq 8 implies that the electrosorption is congruent with respect to potential. Q.E.D.

II. The proof that eq 9 is the sufficient condition for congruence with respect to charge density is similar. Let eq 9 be valid. Then

$$\frac{\left(\frac{\partial\theta}{\partial q^M}\right)_\mu}{\left(\frac{\partial\theta}{\partial\mu}\right)_{q^M}} = -\frac{(E' - E_0)}{\Gamma_s} \quad (\text{A6})$$

However, in general

$$\frac{\left(\frac{\partial\theta}{\partial q^M}\right)_\mu}{\left(\frac{\partial\theta}{\partial\mu}\right)_{q^M}} = -\left(\frac{\partial\mu}{\partial q^M}\right)_\theta = -RT\left(\frac{\partial\ln a^b}{\partial q^M}\right)_\theta \quad (\text{A7})$$

Hence

$$\left(\frac{\partial\ln a^b}{\partial q^M}\right)_\theta = \frac{1}{RT\Gamma_s}(E' - E_0) \quad (\text{A8})$$

$E'$  and  $E_0$  are functions of  $q^M$  alone. Hence integration at constant  $\theta$  between the limits of  $q^M$  and  $q^M_{\max}$ , where  $q^M_{\max}$  denotes the charge density of maximum adsorption yields

$$\int_{q^M}^{q^M_{\max}} d\ln a_\theta^b = \frac{1}{RT\Gamma_s} \left[ \int_{q^M}^{q^M_{\max}} E'(q^M) dq^M - \int_{q^M}^{q^M_{\max}} E_0(q^M) dq^M \right] \quad (\text{A9})$$

Now using the analog of the Lippmann equation for Parson's function  $\xi = \gamma + q^M E$ , *i.e.*,  $E = +(\partial\xi/\partial q^M)_\mu$ , one has

$$\ln a_\theta^b(q^M) = \ln a_\theta^b(q^M_{\max}) = -\frac{1}{RT\Gamma_s} \{ [\xi_0(q^M) - \xi_s(q^M)] - [\xi_0(q^M_{\max}) - \xi_s(q^M_{\max})] \} \quad (\text{A10})$$

where  $\xi_0$  and  $\xi_s$  denote the values of  $\xi$  for the base electrolyte alone and in the presence of the saturated surface at the designated values of  $q^M$ , respectively. Equation A10 shows that all plots of  $\theta$  vs.  $\ln a^b$  at

constant charge density will be exactly superimposable by lateral shifting along the  $\ln a^b$  axis. Hence eq 9 is a sufficient condition that the isotherm be congruent with respect to charge density. Q.E.D.

## Transport Properties in Hydrogen Bonding Solvents. VI. The Conductance of Electrolytes in 2,2,2-Trifluoroethanol<sup>1</sup>

by D. Fennell Evans,\* John A. Nadas,<sup>2</sup>

*Department of Chemistry, Case Western Reserve University, Cleveland, Ohio 44106*

and Sister Mary A. Matesich<sup>3</sup>

*Department of Chemistry, Ohio Dominican College, Columbus, Ohio 43219 (Received August 17, 1970)*

*Publication costs assisted by the Office of Saline Water, U. S. Department of the Interior*

Precise conductance measurements are reported for LiCl, KCl, CsCl, Me<sub>4</sub>NCl, Bu<sub>4</sub>NCl, KBr, Me<sub>4</sub>NBr, Et<sub>4</sub>NBr, Pr<sub>4</sub>NBr, Bu<sub>4</sub>NBr, KI, Me<sub>4</sub>NI, Et<sub>4</sub>NI, Pr<sub>4</sub>NI, Bu<sub>4</sub>NI, *i*-Am<sub>3</sub>BuNI, Hept<sub>4</sub>NI, Me<sub>4</sub>NClO<sub>4</sub>, and Bu<sub>4</sub>NClO<sub>4</sub> in 2,2,2-trifluoroethanol at 25°. The data were analyzed with the Fuoss-Onsager equation and with a modified equation proposed by Justice. Association constants differ from those in the nearly isodielectric solvent ethanol in magnitude, cation dependence, and anion dependence, and appear to agree remarkably well with theoretical predictions. Mobility and association behavior are consistent with enhanced solvation of anions and diminished solvation of cations relative to ethanol.

### Introduction

Fluorinated alcohols are among the most acidic aliphatic alcohols known. This, in addition to their low nucleophilicity and basicity, can be attributed to the electron-withdrawing ability of the adjacent CF<sub>2</sub> and CF<sub>3</sub> groups. Consequently, these solvents would be expected to solvate anions very effectively through hydrogen bonding but interact relatively weakly with cations. Such behavior is in marked contrast to that observed in other hydrogen-bonding solvents where both cation and anion solvation are important or in aprotic solvents where cation solvation predominates.

Therefore we measured the conductance of electrolytes in trifluoroethanol to compare the behavior in this solvent with that observed in the nearly isodielectric solvent ethanol.

### Experimental Section

2,2,2-Trifluoroethanol (Halocarbon Products Corp.) was dried over anhydrous potassium carbonate for 12 hr then distilled from a 2-ft Vigreux column; only the middle fraction was retained. The density was measured in single-neck pycnometers and found to be 1.3826 g/cc. This result is identical with the highest value re-

ported in which 0.03% water was determined by Karl Fischer titration.<sup>4</sup>

Lithium chloride was dried under N<sub>2</sub> atmosphere at 350°; the pH of an aqueous solution was found to be neutral. The rest of the alkali halides were prepared and purified as previously described.<sup>5</sup> The tetraalkylammonium salts were recrystallized from suitable solvents and dried under vacuum.<sup>6</sup>

The electrical equipment, conductance cells, and techniques were the same as previously described.<sup>7,8</sup>

(1) Equivalent conductance data will appear following these pages in the microfilm edition of this volume of the journal. Single copies may be obtained from the Reprint Department, ACS Publications, 1155 Sixteenth St., N. W., Washington, D. C. 20036, by referring to author, title of article, volume, and page number. Remit \$4.00 for photocopy or \$2.00 for microfiche.

(2) Supported by the Undergraduate Research Participation Program of the National Science Foundation.

(3) Supported by the Research Participation for College Teachers Program of the National Science Foundation.

(4) J. Murto and E.-L. Heino, *Suomen Kemistilehti B*, **39**, 263 (1966).

(5) D. P. Ames and P. G. Sears, *J. Phys. Chem.*, **59**, 16 (1955); C. G. Swain and D. F. Evans, *J. Amer. Chem. Soc.*, **88**, 383 (1966).

(6) D. F. Evans and P. Gardam, *J. Phys. Chem.*, **72**, 3281 (1968).

(7) D. F. Evans, C. Zawoyski, and R. L. Kay, *ibid.*, **69**, 3878 (1965).

(8) R. L. Kay, C. Zawoyski, and D. F. Evans, *ibid.*, **69**, 4208 (1965).

The conductance of hygroscopic salts LiCl, Me<sub>4</sub>NCl, and Bu<sub>4</sub>NCl was determined using a weight buret. In all other cases increments of salt were added to the Kraus-type conductance cells using a Hawes-Kay<sup>9</sup> dispensing device.

## Results

The measured equivalent conductance and corresponding electrolyte concentration in moles per liter have been filed with the National Auxiliary Publications Service. The value 26.67<sup>10</sup> was used for the dielectric constant of trifluoroethanol and 1.78 cP<sup>4</sup> for the viscosity.

Conductance data were analyzed both by the Fuoss-Onsager equations<sup>11</sup> (1 and 2)

$$\Lambda = \Lambda_0 - SC^{1/2} + EC \log C + (J - B\Lambda_0)C \quad (1)$$

$$\Lambda = \Lambda_0 - S(C\gamma)^{1/2} + EC\gamma \ln(C\gamma) + (J - B\Lambda_0)C\gamma - K_A f^2 C\gamma\Lambda \quad (2)$$

and the modified equations proposed by Justice<sup>12</sup> (3-5)

$$\Lambda = \gamma(\Lambda_0 - S(C\gamma)^{1/2} + EC\gamma \log C\gamma + J_{(r)}C\gamma + J_{3/2(r)}(C\gamma)^{3/2}) \quad (3)$$

$$K_A = \frac{1 - \gamma}{\gamma^2 C f_{\pm}^2} \quad (4)$$

$$\ln f_{\pm} = \frac{\beta(C\gamma)^{1/2}}{1 + kr\gamma^{1/2}} \quad (5)$$

based on Bjerrum's critical distance  $q$  (6).<sup>13</sup>

$$q = \frac{e^2}{2ekt} \quad (6)$$

In the Justice equations  $r = q = 10.5 \text{ \AA}$  for trifluoroethanol was used to calculate  $J_{(r)}$  and  $f_{\pm}$ . All other terms in the Justice equations are the same as the Fuoss-Onsager terms except that the  $J_{3/2(r)}$  terms are taken from the Fuoss-Hsia analysis<sup>14</sup> and  $E = E_1\Lambda_0 - 2E_2$ .<sup>15</sup>

Conductance parameters in Table I were calculated from eq 1 and 2 using Kay's least-squares programs.<sup>16</sup> Equation 2 for associated electrolytes gave a better fit for all the runs, as would be expected for a three-parameter equation, but resulted in negative association constants ranging from -2 to -18 in extreme cases. For these salts conductance parameters calculated from eq 1 have been listed in Table II, since negative association constants are physically meaningless.

Conductance parameters in Table II were calculated from eq 3-5. Positive association constants were obtained for all the salts. The value of  $r$  calculated from the adjusted  $J_{3/2}$  terms can be compared with  $q$ . Although agreement would not be expected because the  $J_{3/2}$  term is forced to carry uncertainties due to the neglect of higher-order concentration terms in the conductance equation and any other approximations, close agreement is observed.

**Table I:** Conductance Parameters in Trifluoroethanol at 25°, Calculated from Eq 1 and 2

Salt	$\Lambda_0$	$d$	$K_A^a$	$\sigma\Lambda$
LiCl	26.38 ± 0.04	3.2 ± 0.1	130 ± 3	0.01
KCl	33.283 ± 0.008	5.1 ± 0.5	70 ± 4	0.008
CsCl	36.98 ± 0.01	4.3 ± 0.1	43 ± 1	0.008
Me <sub>4</sub> NCl	39.99 ± 0.04	6 ± 1	6 ± 9	0.02
Bu <sub>4</sub> NCl	29.61 ± 0.01	7 ± 1	4 ± 6	0.008
KBr	34.943 ± 0.006	4.1 ± 0.2	48 ± 2	0.004
Me <sub>4</sub> NBr	41.43 ± 0.03	4.08 ± 0.05		0.05
Et <sub>4</sub> NBr	38.58 ± 0.02	4.99 ± 0.05		0.03
Pr <sub>4</sub> NBr	33.57 ± 0.03	5.6 ± 0.1		0.04
Bu <sub>4</sub> NBr	31.00 ± 0.01	5.88 ± 0.06		0.02
KI	36.86 ± 0.02	4.4 ± 0.3	40 ± 3	0.02
Me <sub>4</sub> NI	43.56 ± 0.01	3.91 ± 0.02		0.02
Et <sub>4</sub> NI	40.56 ± 0.01	4.79 ± 0.04		0.02
Pr <sub>4</sub> NI	35.714 ± 0.009	5.21 ± 0.04		0.01
Bu <sub>4</sub> NI	33.10 ± 0.01	5.38 ± 0.05		0.01
<i>i</i> -Am <sub>3</sub> BuNI	32.05 ± 0.02	6.1 ± 0.8	4 ± 6	0.01
<i>i</i> -Am <sub>3</sub> BuNI, Run II	32.32 ± 0.02	6.4 ± 0.9	6 ± 6	0.02
Hept <sub>4</sub> NI	29.818 ± 0.008	6.5 ± 0.6	4 ± 4	0.004
Me <sub>4</sub> NClO <sub>4</sub>	45.37 ± 0.01	3.9 ± 0.1	10 ± 1	0.009
Bu <sub>4</sub> NClO <sub>4</sub>	34.741 ± 0.005	4.98 ± 0.02		0.008

<sup>a</sup> Equation 2 was used where  $K_A$  is given; otherwise eq 1.

As is evident from a comparison of Tables I and II,  $\Lambda_0$  values are very nearly the same in the two treatments except for LiCl. Some indication of the precision of the measurements can be obtained by the constancy of the iodide-bromide difference of  $2.07 \pm 0.11$  for five pairs of salts.

Although transference numbers are not available, the Walden product can be employed for *i*-Am<sub>3</sub>BuN<sup>+</sup> and Hept<sub>4</sub>N<sup>+</sup> in ethanol and trifluoroethanol.<sup>6</sup> This gives an estimated limiting ionic conductance for iodide of  $20.96 \pm 0.15$ . From this value the estimated limiting ionic conductances of Table III have been computed from  $\Lambda_0$  values of Table II.

## Discussion

*Ionic Association in Hydrocarbon Alcohols.* Our investigations of electrolyte behavior in hydrogen-bonding solvents, particularly the hydrocarbon alcohols,<sup>6,9,17-19</sup> have shown that the pattern of ionic asso-

- (9) J. L. Hawes and R. L. Kay, *J. Phys. Chem.*, **69**, 2420 (1965).
- (10) H. C. Eckstrom, J. E. Berger, and L. R. Dawson, *ibid.*, **64**, 1458 (1960).
- (11) R. M. Fuoss and F. Accascina, "Electrolyte Conductance," Interscience, New York, N. Y., 1959.
- (12) R. Bury, M. C. Justice, and J. C. Justice, *C. R. Acad. Sci. Paris*, **268**, 670 (1969).
- (13) N. Bjerrum, *Kgl. Dan. Vidensk. Selsk.*, **7**, 9 (1926).
- (14) R. M. Fuoss and K. L. Hsia, *Proc. Natl. Acad. Sci.*, **57**, 1550 (1967); **58**, 1818 (1967).
- (15) M. S. Chen, Ph.D. Thesis, Yale University, 1969.
- (16) R. L. Kay, *J. Amer. Chem. Soc.*, **82**, 2099 (1960).
- (17) D. F. Evans and P. Gardam, *J. Phys. Chem.*, **73**, 158 (1969).
- (18) M. A. Matesich, J. A. Nadas, and D. F. Evans, *ibid.*, **75**, in press.
- (19) J. A. Thomas and D. F. Evans, *ibid.*, **74**, 3812 (1970).

**Table II:** Conductance Parameters in Trifluoroethanol at 25°, Calculated from Eq 3-5

Salt	$\lambda_0$	$RJ_{3/2}$	$K_A$	$\sigma_A$
LiCl	26.66 ± 0.01	10.21 ± 0.05	192.6 ± 0.7	0.002
KCl	33.19 ± 0.02	6 ± 2	121 ± 3	0.02
CsCl	37.015 ± 0.007	9.7 ± 0.1	76.6 ± 0.5	0.005
Me <sub>4</sub> NCl	40.00 ± 0.04	8.1 ± 1.8	29 ± 4	0.02
Bu <sub>4</sub> NCl	29.61 ± 0.01	6 ± 2	22 ± 2	0.009
KBr	34.95 ± 0.01	11.1 ± 0.6	80.5 ± 1.7	0.005
Me <sub>4</sub> NBr	41.407 ± 0.006	9.74 ± 0.04	32.9 ± 0.2	0.005
Et <sub>4</sub> NBr	38.58 ± 0.03	8.9 ± 0.4	27.8 ± 1.6	0.02
Pr <sub>4</sub> NBr	33.485 ± 0.006	10.1 ± 0.1	17.8 ± 0.4	0.004
Bu <sub>4</sub> NBr	30.97 ± 0.01	9.4 ± 0.4	20 ± 1	0.008
KI	36.87 ± 0.03	9.8 ± 0.5	72 ± 2	0.02
Me <sub>4</sub> NI	43.605 ± 0.004	9.84 ± 0.03	35.7 ± 0.1	0.002
Et <sub>4</sub> NI	40.525 ± 0.008	10.2 ± 0.1	25.6 ± 0.5	0.005
Pr <sub>4</sub> NI	35.688 ± 0.005	10.1 ± 0.2	23.4 ± 0.5	0.004
Bu <sub>4</sub> NI	33.065 ± 0.004	10.1 ± 0.1	22.2 ± 0.4	0.003
<i>i</i> -Am <sub>3</sub> BuNI	32.06 ± 0.02	7.9 ± 1.3	27 ± 2	0.01
<i>i</i> -Am <sub>3</sub> BuNI, Run II	32.33 ± 0.02	7.4 ± 1.5	27 ± 3	0.02
Hept <sub>4</sub> NI	29.87 ± 0.02	$\alpha$	34 ± 5	0.02
Me <sub>4</sub> NClO <sub>4</sub>	45.42 ± 0.02	10.2 ± 0.2	46 ± 1	0.01
Bu <sub>4</sub> NClO <sub>4</sub>	34.744 ± 0.007	9.5 ± 0.2	27.7 ± 0.6	0.006

<sup>a</sup> Concentrations too low.

**Table III:** Estimated Limiting Ionic Conductances in Trifluoroethanol at 25°

Ion	$\lambda_0$	Ion	$\lambda_0$
Li <sup>+</sup>	9.24	Bu <sub>4</sub> N <sup>+</sup>	12.10
K <sup>+</sup>	15.91	<i>i</i> -Am <sub>3</sub> BuN <sup>+</sup>	11.15
C <sub>s</sub> <sup>+</sup>	19.60	Hept <sub>4</sub> N <sup>+</sup>	9.09
Me <sub>4</sub> N <sup>+</sup>	22.64	Cl <sup>-</sup>	17.42
Et <sub>4</sub> N <sup>+</sup>	19.56	Br <sup>-</sup>	18.85
Pr <sub>4</sub> N <sup>+</sup>	14.73	I <sup>-</sup>	20.96
		ClO <sub>4</sub> <sup>-</sup>	22.71

ciation is considerably more complex than in aprotic solvents. The magnitude of the association constants is much greater than that predicted for ions in a continuous dielectric medium using either the Fuoss equation<sup>20</sup>

$$K_A = \frac{4\pi N a_K^3}{3000} \exp\left(\frac{e^2}{a_K \epsilon k T}\right) \quad (7)$$

or the Bjerrum equation<sup>13</sup>

$$K_A = \frac{4\pi N}{1000} \left(\frac{e^2}{\epsilon k T}\right)^3 \int_2^b e^{-t^{-4}} dt \quad (8)$$

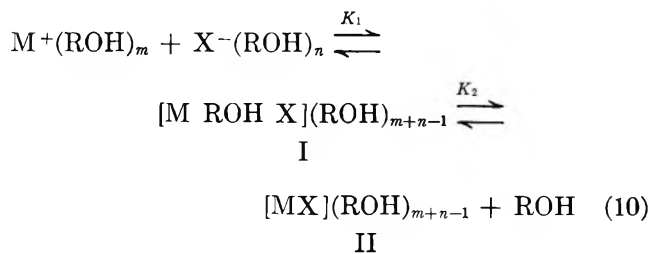
where

$$b = \frac{e^2}{r \epsilon k T} \quad (9)$$

Since the magnitude of the bulk dielectric constant in protic solvents is due in large measure to hydrogen bonding, the effective dielectric constant in the vicinity of an ion pair may be appreciably smaller, due to the

orientation of solvent dipoles by the ions which disrupts intermolecular hydrogen bonding. An estimate of this effect within the context of the Bjerrum approach has been presented and accounts for the magnitude of  $K_A$  satisfactorily.<sup>18</sup> However, this approach does not accommodate two other characteristics of ionic association in the alcohols.

For a given cation the association constant increases with increasing anion radius, contrary to behavior predicted from simple coulombic considerations. This observation is consistent with a multiple-step process<sup>17</sup>



in which the concentration of solvent-separated ion pairs (I) is controlled by diffusion but the concentration of contact ion pairs (II) is determined by the nature of the ion-solvent interaction.

The observed association constant for eq 10 can be shown to be

$$K_{\Sigma} = K_1(1 + K_2/[ROH]) \quad (11)$$

where  $K_1$  can be estimated using eq 7. For the tetra-butylammonium salts in ethanol, values of  $K_2$  calcu-

(20) R. M. Fuoss, *J. Amer. Chem. Soc.*, **80**, 5059 (1948).

lated from the observed  $K_A$  values and  $K_1 = 25$  are 9.5 for  $\text{Cl}^-$ , 34 for  $\text{Br}^-$ , 67 for  $\text{I}^-$ , and 163 for  $\text{ClO}_4^-$ .

The change in association constant with cation for a given anion is also anomalous in hydrogen-bonding solvents.  $K_A$  is small for  $\text{Li}^+$  and  $\text{Bu}_4\text{N}^+$  but increases for cations of intermediate size, passing through a maximum at  $\text{Me}_4\text{N}^+$  or  $\text{Cs}^+$ .

*Solvents.* Some properties of trifluoroethanol and ethanol are compared in Table IV. Both the higher

**Table IV:** Properties of Ethanol and 2,2,2-Trifluoroethanol

	Ethanol	2,2,2-Trifluoroethanol
$\rho^{26}$	0.78511 <sup>a</sup>	1.3826
$\epsilon$	24.33 <sup>a</sup>	26.67 <sup>b</sup>
$D$ , debyes, cyclohexane <sup>c</sup>	1.65	2.03
$n_D^{25}$	1.360 <sup>b</sup>	1.291 <sup>b</sup>
Kirkwood $g$ factor	3.0	3.0
$\eta$ , cP	1.084 <sup>a</sup>	1.78 <sup>d</sup>
$\text{p}K_A$ , water <sup>e</sup>	15.9	12.37
$\Delta H$ form, acetone complex in $\text{CCl}_4$ , kcal/mol <sup>f</sup>	-2.90	-3.72
HCl solubility, mol HCl/mol <sup>g</sup>	0.950	0.063
Boiling point, °C	78.4	73.75 <sup>h</sup>
Entropy of vaporization, eu	26.8	28.0 <sup>i</sup>

<sup>a</sup> Reference 6. <sup>b</sup> Reference 10. <sup>c</sup> A. Kivinen, J. Murto, and M. Lehtonen, *Suomen Kemi. B*, **40**, 336. <sup>d</sup> Reference 4. <sup>e</sup> P. Ballinger and F. A. Long, *J. Amer. Chem. Soc.*, **81**, 1050 (1959); *ibid.*, **92**, 795 (1960). <sup>f</sup> A. Kivinen, J. Murto, and L. Kilpi, *Suomen Kemi. B*, **40**, 301 (1967). <sup>g</sup> W. Gerrard and E. D. Macklen, *J. Appl. Chem.*, **9**, 85 (1959). <sup>h</sup> Reference 30. <sup>i</sup> Pennsalt Chemicals Corp., "Trifluoroethanol," Booklet DC-1254, Philadelphia, Pa., 1956.

acidity of TFE and its more exothermic hydrogen bonding to acetone suggest that it solvates Lewis bases better than ethanol does. Additional evidence is provided by shifts in the OH stretching frequency in the vapor phase as well as in solution,<sup>21</sup> nmr chemical shifts,<sup>22</sup> and shifts in the  $n \rightarrow \pi^*$  bands of unsaturated compounds.<sup>23</sup>

Although this evidence suggests that trifluoroethanol solvates chloride ion better than ethanol, HCl is about 15 times as soluble in the latter. Thus, TFE appears to interact poorly with the proton. Infrared evidence indicates it is a poor hydrogen bond acceptor compared to the other alcohols.<sup>21</sup> This and its low nucleophilicity<sup>24</sup> are consistent with less effective cation solvation by trifluoroethanol.

It is not clear whether trifluoroethanol is more or less self-associated than ethanol. Their boiling points and entropies of vaporization listed in Table IV suggest that intermolecular hydrogen bonding is comparable. The Kirkwood correlation factor  $g$  has been calculated from data in Table IV using the Kirkwood-Frohlich equation<sup>25</sup>

$$\epsilon_0 = \epsilon_\infty + \frac{3\epsilon_0}{2\epsilon_0 + \epsilon_\infty} \left( \frac{\epsilon_\infty + 2}{3} \right)^2 \frac{4\pi N \rho \mu_0^2}{3Mkt} \cdot g \quad (12)$$

Following the practice of Dannhauser and Bahe,<sup>26</sup>  $\epsilon_\infty$  was set equal to  $1.1 (n_D)^2$ . This may not be a good approximation for the fluorinated alcohol. In addition, the dipole moments used are from cyclohexane solution rather than the gas phase, so there is some uncertainty in the calculated  $g$  values. Nevertheless, the fact that both the alcohols give the same  $g$  at 25° shows that they are associated to a similar extent.

On the other hand, infrared<sup>27</sup> and nmr<sup>28</sup> observations of the monomer-dimer equilibrium in dilute solution suggest that ethanol is more associated than trifluoroethanol. The infrared spectrum of pure trifluoroethanol has been interpreted as indicating an appreciable concentration of pure monomer in which the hydroxyl is either "free" or internally hydrogen-bonded to fluorine.<sup>27,29</sup> This is difficult to reconcile with the entropy of vaporization and Kirkwood  $g$  values.

Solutions of trifluoroethanol in ethanol are very non-ideal.<sup>30</sup> Trifluoroethanol-water<sup>4</sup> and trifluoroethanol-methyl isobutyl ketone<sup>10</sup> solutions show markedly different behavior than the corresponding ethanol solutions.<sup>10,31</sup> Thus it is reasonable to expect different conductance behavior in trifluoroethanol than in the hydrocarbon alcohols, in spite of the similarity in structure and dielectric constant.

*Ionic Association in Trifluoroethanol.* Ionic association in trifluoroethanol differs from that in the hydrocarbon alcohols in three respects: the anion dependence; the cation dependence; and the overall magnitude of the association constant.

The anion dependence of  $K_A$  in trifluoroethanol is compared with that in ethanol<sup>6</sup> in Figure 1. In the hydrocarbon alcohols, of which ethanol is a typical example, the order of association is  $\text{ClO}_4^- > \text{I}^- > \text{Br}^- > \text{Cl}^-$ . However, in trifluoroethanol there is little if any anion dependence within experimental uncertainty. In terms

(21) I. H. Reece and R. L. Werner, *Spectrochim. Acta, Part A*, **1271** (1968).

(22) K. F. Purcell and S. T. Wilson, *J. Mol. Spectrosc.*, **24**, 468 (1967).

(23) A. Balasubramanian and C. N. R. Rao, *Spectrochim. Acta*, **18**, 1337 (1962).

(24) F. L. Scott, *Chem. Ind. (London)*, **224** (1959); W. S. Trahanovsky and M. P. Doyle, *Tetrahedron Lett.*, 2155 (1968).

(25) J. G. Kirkwood, *J. Chem. Phys.*, **7**, 911 (1939); H. Frohlich, "Theory of Dielectrics," Oxford University Press, New York, N. Y., 1949.

(26) W. Dannhauser and L. W. Bahe, *ibid.*, **40**, 3058 (1964).

(27) A. Kivinen and J. Murto, *Suomen Kemistilehti B*, **40**, 6 (1967).

(28) B. D. N. Rao, P. Venkateswarlu, A. S. N. Murthy, and C. N. R. Rao, *Can. J. Chem.*, **40**, 387 (1962).

(29) R. N. Haszeldine, *J. Chem. Soc.*, 1757 (1953); C. G. Cannon and B. C. Stace, *Spectrochim. Acta*, **13**, 253 (1958); P. J. Krueger and H. D. Mettee, *Can. J. Chem.*, **42**, 340 (1964).

(30) L. M. Mukherjee and E. Grunwald, *J. Phys. Chem.*, **62**, 1311 (1958).

(31) Ethanol-water solutions are reviewed in F. Franks and D. J. G. Ives, *Quart. Rev. Chem. Soc.*, **20**, 1 (1966).

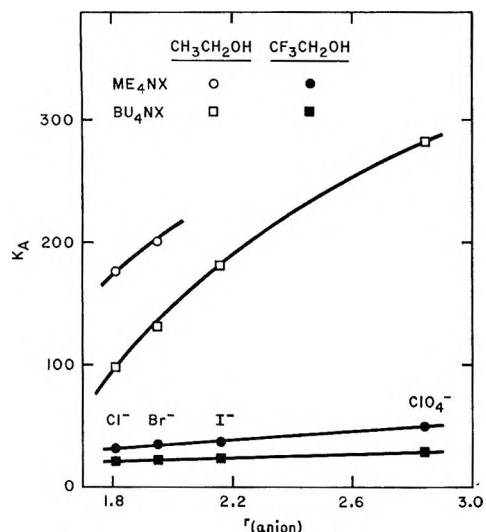


Figure 1. Anion dependence of the association constants of tetraalkylammonium salts in trifluoroethanol and ethanol at 25°. Ethanol data, taken from ref 6 and unpublished results from this laboratory, were analyzed with Justice eq 3-5.

of the postulated multiple-step mechanism, eq 10, this can be explained if only one kind of ion pair predominates. Since anions are more strongly solvated by trifluoroethanol than by ethanol, this enhanced solvation should stabilize the solvent-separated ion pair relative to the contact ion pair. Consequently,  $K_2$  would be smaller in trifluoroethanol and the observed association constant would approach  $K_1$ , which, as calculated from eq 7, is not strongly anion-dependent when the cation radius is large.

The association constants of chlorides in ethanol<sup>6,32</sup> and trifluoroethanol are shown in Figure 2. In trifluoroethanol,  $K_A$  decreases with increasing cation size in accord with the predictions of eq 7 and 8. The complex behavior in ethanol, then, must be caused by solvent-cation interactions which do not occur in the fluorinated alcohol.

This is consistent with the higher cation-solvating ability of ethanol as indicated by HCl solubility and nucleophilicity<sup>24</sup> (Table IV). The small lithium ion appears to be highly solvated in ethanol and sodium and potassium less highly solvated. By the time ionic radius reaches the size of  $\text{Cs}^+$  or  $\text{Me}_4\text{N}^+$  solvation is no longer important in either alcohol and  $K_A$  decreases with further increase in size. Thus, effective electrostatic radii in ethanol may be in the order  $\text{Cs}^+ < \text{Me}_4\text{N}^+ < \text{K}^+_{(\text{solvated})} < \text{Na}^+_{(\text{solvated})} < \text{Bu}_4\text{N}^+ < \text{Li}^+_{(\text{solvated})}$ . Due to the less effective cation solvation in trifluoroethanol, however, the order determined by crystallographic radii,  $\text{Li}^+ < \text{K}^+ < \text{Cs}^+ < \text{Me}_4\text{N}^+ < \text{Bu}_4\text{N}^+$  is observed. It should be noted that this solvation argument does not explain the anion dependence of  $K_A$  discussed above because the crystallographic radii of the halides,  $\text{Cl}^- = 1.81$ ,  $\text{Br}^- = 1.95$ ,  $\text{I}^- = 2.16 \text{ \AA}$ , do not change enough for drastically different degrees of solvation to be expected.

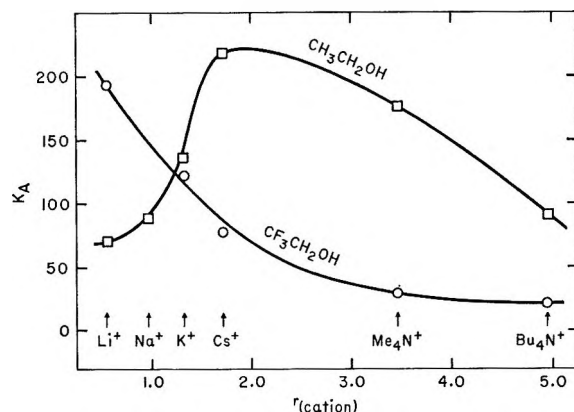


Figure 2. Cation dependence of the association constants of chlorides in trifluoroethanol and ethanol at 25°. Ethanol data for LiCl, NaCl, and KCl (ref 32), CsCl, and  $\text{R}_4\text{NCl}$  (ref 6) were analyzed with Justice eq 3-5.

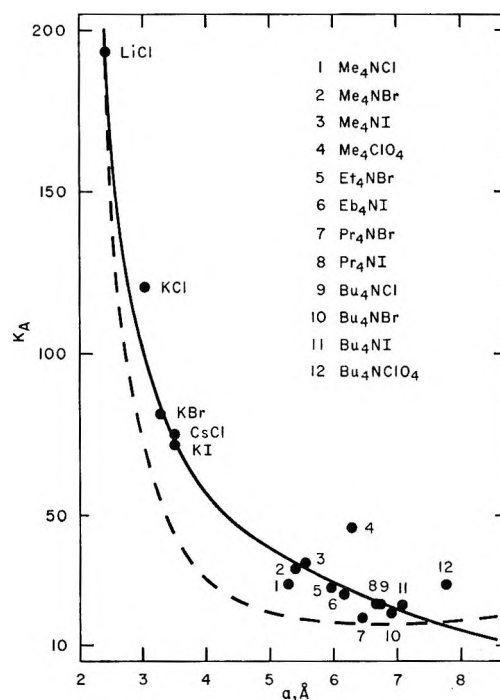


Figure 3. Comparison of observed association constants in trifluoroethanol at 25° (Table III) with predicted behavior from the Fuoss (eq 7, dashed line) and Bjerrum (eq 8, solid line) theories as a function of sum of crystallographic radii.

In the hydrocarbon alcohols, the association constants are generally larger than those predicted by eq 7 or 8. It is the magnitude of  $K_A$  as well as its peculiar dependence on anion size that requires the postulation of a multiple-step association process. Association constants from Table II for trifluoroethanol are plotted in Figure 3 as a function of the sum of the crystallographic radii. Also shown are the predicted values from eq 7, dashed line, and eq 8, solid line, for dielectric

(32) J. R. Graham, G. S. Kell, and A. R. Gordon, *J. Amer. Chem. Soc.*, **79**, 2352 (1957).

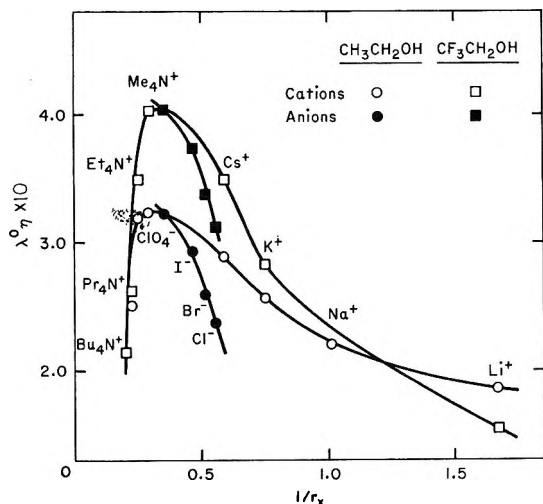


Figure 4. Walden products as a function of inverse crystallographic radii in trifluoroethanol and ethanol at 25°. Ethanol data for  $\text{Li}^+$ ,  $\text{Na}^+$ ,  $\text{K}^+$ , and  $\text{Cl}^-$  from ref 32; for  $\text{Cs}^+$ , this work; for all other ions from ref 6.

constant 26.67, trifluoroethanol. It is doubtful if there is another case where the agreement between experiment and the prediction of eq 8 is as good. This presents a dilemma. If one accepts the significance of  $\delta$  literally, a procedure that has not been notable for its success, the results of Figure 3 argue for contact ion pairs. On the other hand, the comparison between the hydrocarbon alcohols and trifluoroethanol suggests that solvent-separated ion pairs should predominate in the latter. We are not able to resolve this discrepancy at present.

Our initial attempts to obtain additional information from ultrasonic measurements have been unsuccessful owing to another property of trifluoroethanol. It dissolves the epoxy paint which is used as insulation in our apparatus, causing short circuits of the transducers.

*Ionic Mobilities.* Ionic mobilities in trifluoroethanol show the same general pattern as in the other alcohols (Figure 4). The Walden products in trifluoroethanol are higher than those in methanol and ethanol for most ions. A striking exception is lithium for which  $\lambda_{0\eta}$  is 25% lower in trifluoroethanol than in ethanol.

According to the Zwanzig analysis,<sup>33</sup> small ions have decreased mobilities because the high charge densities at their surfaces slow the relaxation of solvent dipoles as they move. This slower relaxation exerts a retarding force on the ion. Solvated lithium ions, having a larger effective radius, would retard dipole relaxation less and hence be more mobile. Thus the low mobility of lithium in trifluoroethanol is consistent with this solvent's low nucleophilicity and basicity and the association pattern of this solvent.

*Conclusion.* 2,2,2-Trifluoroethanol represents an extreme in solvating characteristics of ionizing solvents. On one side of the scale are the aprotic solvents in which cation solvation is important but anion solvation not very effective. In the middle are water, amides, and the hydrocarbon alcohols where both cation and anion solvation are important and complex ionic association patterns result. In trifluoroethanol anion solvation is enhanced while cation solvation decreases, and association behavior is in apparent accord with theoretical predictions.

*Acknowledgment.* We would like to thank Professor J. C. Justice for computing the results given in Table III and for many helpful discussions. This work was supported by Contract No. 14-01-001-1281 and 14-30-2615 with the Office of Saline Water, U. S. Department of the Interior.

(33) R. Zwanzig, *J. Chem. Phys.*, **38**, 1603 (1963).

# The Conductance of Electrolytes in Acetone and in 1-Propanol-Acetone Mixtures at 25°

by D. Fennell Evans,\* John Thomas,<sup>1</sup> John A. Nadas,<sup>2</sup>

Department of Chemistry, Case Western Reserve University, Cleveland, Ohio 44106

and Sister Mary A. Matesich<sup>3</sup>

Department of Chemistry, Ohio Dominican College, Columbus, Ohio 43219

Publication costs assisted by the Office of Saline Water, U. S. Department of the Interior

Conductance measurements are reported for  $\text{Bu}_4\text{NCl}$ ,  $\text{Et}_4\text{NBr}$ ,  $\text{Pr}_4\text{NBr}$ ,  $\text{Bu}_4\text{NBr}$ ,  $\text{Et}_4\text{NI}$ ,  $\text{Pr}_4\text{NI}$ ,  $\text{Bu}_4\text{NI}$ ,  $i\text{-Am}_3\text{BuNI}$ ,  $\text{Me}_4\text{NClO}_4$ ,  $\text{Bu}_4\text{NClO}_4$ ,  $\text{NaBPh}_4$ ,  $\text{KBPh}_4$ ,  $\text{CsBPh}_4$ ,  $\text{Me}_4\text{NBPh}_4$ ,  $\text{Bu}_4\text{NBPh}_4$ , and  $i\text{-Am}_3\text{BuNBPh}_4$  in acetone at 25° and for  $\text{Bu}_4\text{NCl}$ ,  $\text{Bu}_4\text{NBr}$ ,  $\text{Bu}_4\text{NI}$ ,  $\text{Bu}_4\text{NClO}_4$ , and  $\text{LiCl}$  in 20, 40, 60, 80, and 90 mol % acetone in 1-propanol at 25°. Density, viscosity, dielectric constant, and 25-MHz ultrasonic absorption data are also reported for the solvent mixtures. Conductance data were analyzed by the Fuoss-Onsager equation. Limiting equivalent conductance and ionic association in the solvent mixtures are compared with behavior in the two pure solvents. Walden products and association constants can be interpreted in terms of preferential anion solvation by 1-propanol through most of the composition range.

## Introduction

The pattern of ionic association in the two isodielectric solvents acetone and 1-propanol differs dramatically.<sup>4</sup> In acetone  $\text{Bu}_4\text{NCl}$  is almost five times as extensively associated as  $\text{Bu}_4\text{NClO}_4$ . In propanol, on the other hand, the perchlorate is five times more associated than the chloride. Since the dielectric constant in the two solvents is the same, this behavior must arise from specific solvent-ion interactions. In an effort to obtain more information about these effects the conductance of tetrabutylammonium chloride, bromide, iodide, and perchlorate and lithium chloride has been measured throughout the entire composition range 0–100% acetone. Before investigating the variation of  $K_A$  in these mixtures, it was desirable to obtain a complete and precise set of data for acetone, so that behavior in both pure solvents would be well established.

Pistoia and Pecci have recently reported studies of the conductance of several electrolytes in acetone-ethanol mixtures.<sup>5,6</sup> They found complex behavior in the dependence of both the Walden product and the association constant upon solvent composition. However, limited solubility prevented their studying any of the electrolytes throughout the entire composition range. Conductance measurements have also been reported in methanol-nitromethane-acetonitrile mixtures<sup>7</sup> and in methanol-acetonitrile mixtures.<sup>8</sup> Due to their higher dielectric constants, ionic association is much less extensive in these solvents.

## Experimental Section

All experimental equipment, cells, salt cup dispensing device, and general techniques for the conductance measurements were the same as those previously de-

scribed.<sup>9–11</sup> Briefly, the measurements were carried out in Kraus-type conductance cells<sup>12</sup> and increments of salt were added to the cell in small Pyrex cups with the aid of the Hawes-Kay cup-dropping device.<sup>9</sup> The exception to this procedure was for  $\text{LiCl}$  and  $\text{Bu}_4\text{NCl}$ ; a weight buret was used.

The tetraalkylammonium halides were purified by recrystallization. The solvents used in recrystallization and the temperature at which the salts were dried have been given elsewhere.<sup>4,10,11,13</sup> Tetrabutylammonium perchlorate was prepared by the method described by Coetzee.<sup>14</sup> Lithium chloride (reagent grade) from a freshly opened bottle was dried under a nitrogen atmosphere in a platinum boat at 400°, ground in an agate

(1) For further details see J. Thomas, Ph.D. Thesis, Case Western Reserve University, Jan 1970.

(2) Supported by the Undergraduate Research Participation Program of the National Science Foundation.

(3) Supported by the Research Participation for College Teachers Program of the National Science Foundation.

(4) D. F. Evans and P. Gardam, *J. Phys. Chem.*, **72**, 3281 (1968).

(5) G. Pistoia and G. Pecci, *ibid.*, **74**, 1450 (1970).

(6) G. Pistoia, *Ric. Sci.*, **38**, 1250 (1968).

(7) M. A. Coplan and R. M. Fuoss, *J. Phys. Chem.*, **68**, 1181 (1964).

(8) F. Conti and G. Pistoia, *ibid.*, **72**, 2245 (1968).

(9) J. L. Hawes and R. L. Kay, *ibid.*, **69**, 2787 (1964).

(10) D. F. Evans, C. Zawoyski, and R. L. Kay, *ibid.*, **69**, 3878 (1965).

(11) C. G. Swain and D. F. Evans, *J. Amer. Chem. Soc.*, **88**, 388 (1966).

(12) H. M. Daggett, E. J. Bair, and C. A. Kraus, *ibid.*, **73**, 799 (1951).

(13) R. L. Kay, C. Zawoyski, and D. F. Evans, *J. Phys. Chem.*, **69**, 4208 (1965).

(14) J. F. Coetzee and G. P. Cunningham, *J. Amer. Chem. Soc.*, **79**, 870 (1957).



mortar, and redried in a vacuum oven at 100°; all manipulations of this hygroscopic salt were carried out in a drybox. Boride salts were prepared by metathesis of sodium tetraphenyl boride with corresponding halide salts. These salts were recrystallized five times by dissolving in a minimum amount of acetone and reprecipitating by addition of peroxide free dry ether. They were dried at about 50° under vacuum for several days.

Conductivity grade acetone was prepared by distilling Allied Chemical reagent grade acetone from pre-conditioned molecular sieve 3 A, 1/16-in. pellets. These pellets were pretreated by soaking in water for days, washing in a stream of distilled water for a day, and drying first in an oven at 140° for a month and finally in a dry nitrogen stream in a furnace at 360° for 8 hr. The molecular sieves were stored in sealed bottles. The distillations were carried out in a 1.3-m Stedman column and only middle fractions were retained. The whole process was carried out in a closed system with a mercury safety valve. All ground-glass joints were sealed with parafilm layers. Distillations carried out under nitrogen gave a solvent density of  $0.78433 \pm 0.00002$ , identical with that obtained using the closed system. Density measurements made in atmospheric conditions and in dry atmosphere did not differ. Densities of 0.7845 and 0.7840 were reported by Kraus<sup>15,16</sup> and Hughes,<sup>17</sup> respectively.

The results of Hughes<sup>17</sup> made it clear that extreme caution should be exercised at all times to prevent contamination of the acetone by moisture. For the conductance runs involving pure acetone, the following procedure was followed: after cleaning, the cells were dried in a vacuum oven at room temperature for several hours. It has been suspected that drying the cell after cleaning causes a change in the condition of the electrodes which results in an uncertainty in the cell constant. The cell constant was therefore checked after drying and showed less than 0.05% variation. This was deemed preferable to the greater error that would result from moisture contamination of the acetone by the cell. The dried cell was flushed with argon for about 15 min and acetone was transferred directly to it from the distillation flask using an all-glass system. The cup-dropping device was placed on the cell with dry nitrogen being flushed completely through the system. The exception to this careful procedure was for LiCl and Bu<sub>4</sub>NCl. Because of their hygroscopic nature, the conductance runs were done using a weight buret. A concentrated solution was made with all manipulations being carried out in a drybox. Small increments were added from the weight buret to the cell, and in order to prevent atmospheric contamination while the cell was open, solvent saturated nitrogen was passed through the side arm. The runs were made in the shortest time possible.

Conductivity grade 1-propanol was prepared by drying the Fisher reagent grade alcohol over calcium

oxide for several days and then distilling from a fresh batch of calcium oxide.<sup>18</sup> Tests for unsaturated impurities with bromine water were negative.

The solvent mixtures employed in the conductance measurements were individually prepared in the cell just prior to the measurements. The acetone was added from the distillation receiver in an all-glass system. After the weight of acetone in the cell had been determined, the propanol was added under a nitrogen atmosphere until the desired composition was obtained. The mixture concentrations given in the tables are within 0.05%.

The density and viscosity of the solvent mixtures were determined at 20, 40, 60, 80, 90, and 95 mol % acetone. The density measurements were carried out in single-neck capillary tube pycnometers. The viscosity measurements were made in two Cannon Ubbelohde viscometers. The dielectric constants were measured in the all-glass platinum cells described by Kay and Vidulich.<sup>19</sup>

## Results

The measured equivalent conductance and corresponding electrolyte concentrations in moles per liter appears in the microfilm edition of this volume of the journal.<sup>20</sup> Density measurements on the most concentrated solution used in the conductance measurement were used to obtain the volume correction necessary to calculate  $c$ . The density was assumed to follow the relationship  $d = d_0 + A\bar{m}$ , where  $\bar{m}$  is the moles of salt per kilogram of solution. The solvent densities, viscosities, and dielectric constants used in the evaluation of the conductance data are given in Table I. The solvent densities were found to be linear in composition and to be given by the relationship

$$\rho = 0.79974 - 0.01544X_{\text{acetone}} \quad (1)$$

to better than 0.01%. These solvent properties have also been measured by Johari;<sup>21</sup> he obtained a density curve which displayed a slight positive deviation (0.27%) at 50 mol%. In Figure 1 the variation of viscosity and dielectric constant with solvent composition is shown. Our viscosity results agree very well with those of Johari, but are 30% lower than those reported

(15) M. B. Reynolds and C. A. Kraus, *J. Amer. Chem. Soc.*, **70**, 1709 (1948).

(16) M. J. McDowell and C. A. Kraus, *ibid.*, **73**, 3293 (1951).

(17) J. F. J. Dippy and S. R. C. Hughes, *J. Chem. Soc.*, 953 (1954).

(18) W. C. Vosburgh, L. C. Connel, and J. A. V. Butler, *ibid.*, 933 (1933).

(19) G. A. Vidulich and R. L. Kay, *Rev. Sci. Instrum.*, **37**, 1662 (1966).

(20) The measured equivalent conductance and corresponding electrolyte concentrations in moles per liter will appear following these pages in the microfilm edition of this volume of the journal. Single copies may be obtained from the Reprint Department, ACS Publications, 1155 Sixteenth, St., N. W., Washington, D. C. 20036, by referring to the author, title of article, volume, and page number. Remit \$4.00 for photocopy or \$2.00 for microfiche.

(21) G. P. Johari, *J. Chem. Eng. Data*, **13**, 541 (1968).

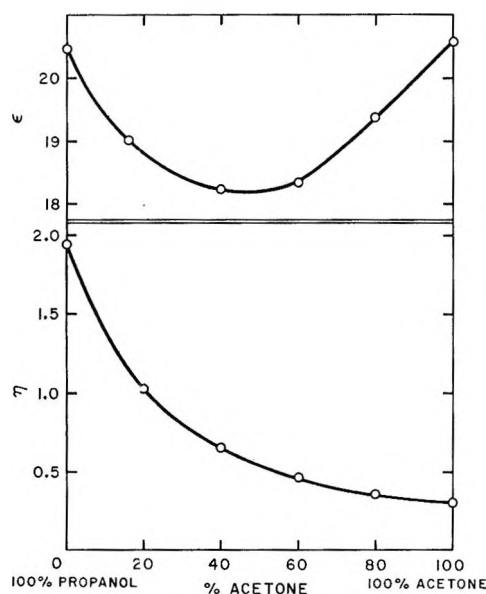


Figure 1. Viscosity and dielectric constant at 25° as a function of mole fraction acetone in 1-propanol.

by Mocharnyuk.<sup>22</sup> The values we obtained for the dielectric constant  $\epsilon$  are consistently 0.1 unit above those determined by Johari. Also shown in Table I is the ultrasonic absorption of the mixtures at 25 MHz.

Table I: Physical Constants for Acetone-Propanol Mixtures at 25°

Mol % acetone	$\epsilon$	$\eta$	$\rho$	$10^{17} \alpha/f^2$ , 25 MHz <sup>a</sup>
0	20.45	0.01952	0.7995	70
20	19.02	0.01026	0.7967	47
40	18.47	0.00647	0.7936	42
60	18.64	0.00463	0.7905	38
80	19.37	0.00361	0.7873	33
90	19.96	0.00332	0.7859	
95	20.27	0.00316	0.7851	
100	20.56	0.00303	0.7843	30

<sup>a</sup> Nepers sec<sup>-2</sup> cm<sup>-1</sup>.

The conductance data were analyzed with the Fuoss-Onsager equation<sup>23</sup> in the form

$$\Lambda = \Lambda_0 - S(C\gamma)^{1/2} + EC\gamma \log C\gamma + (J - B\Lambda_0)C\gamma - K_A f^2 C\gamma \quad (2)$$

The value of  $B$ , which corrects for the effect of the added electrolyte on the viscosity of the solvent was set equal to zero since it makes only a slight change in the  $\bar{\alpha}$ , the ion-size parameter, and has little effect on  $K_A$ .

Shown in Table II for acetone and in Table III for the mixtures are the parameters obtained from eq 2 by a least-squares computer program. Where no association was detected,  $\gamma$  was set equal to 1 and  $K_A$  to zero. Included are the standard deviations in each parameter, and the standard deviations of the individual points.

Also given, for comparison purposes, are the corresponding values in pure propanol. In acetone and acetone-rich mixtures the parameters obtained were found to depend upon the concentration region analyzed if  $\kappa\bar{\alpha} > 0.1$ . Only those points below  $25 \times 10^{-4}C$  were used in the analysis. A number of duplicate conductance determinations which agree to within 0.1% in the parameters can be found in ref 1.

Table II: Conductance Parameters for Acetone Solutions at 25°

	$\Lambda_0$	$\bar{\alpha}$	$K_A$	$\sigma_\Lambda$
Bu <sub>4</sub> NCl	187.6 ± 0.1	5.7 ± 0.1	430 ± 5	0.05
Et <sub>4</sub> NBr	208.81 ± 0.04	5.28 ± 0.07	330 ± 2	0.02
Pr <sub>4</sub> NBr	194.0 ± 0.1	4.8 ± 0.1	335 ± 4	6.06
Bu <sub>4</sub> NBr	185.34 ± 0.09	5.0 ± 0.1	285 ± 5	0.04
Et <sub>4</sub> NI	207.48 ± 0.02	4.82 ± 0.04	155 ± 1	0.02
Pr <sub>4</sub> NI	193.08 ± 0.07	5.1 ± 0.1	174 ± 3	0.04
Bu <sub>4</sub> NI	184.39 ± 0.06	5.1 ± 0.1	155 ± 3	0.03
<i>i</i> -Am <sub>3</sub> BuNI	180.83 ± 0.02	5.18 ± 0.07	155 ± 1	0.01
Me <sub>4</sub> NClO <sub>4</sub>	215.1 ± 0.1	5.3 ± 0.2	186 ± 3	0.03
Bu <sub>4</sub> NClO <sub>4</sub>	184.75 ± 0.04	5.7 ± 0.01	90 ± 2	0.04
NaBPh <sub>4</sub>	140.14 ± 0.07	6.46 ± 0.07		0.08
KBPh <sub>4</sub>	141.39 ± 0.06	6.73 ± 0.08		0.07
CsBPh <sub>4</sub>	146.17 ± 0.09	4.5 ± 0.1		0.09
Me <sub>4</sub> NBPh <sub>4</sub>	159.28 ± 0.03	4.77 ± 0.02		0.04
Bu <sub>4</sub> NBPh <sub>4</sub>	129.05 ± 0.08	5.51 ± 0.06		0.09
<i>i</i> -Am <sub>3</sub> BuNBPh <sub>4</sub>	125.29 ± 0.04	6.1 ± 0.05		0.06
LiCl	181 ± 11		21 × 10 <sup>4</sup> ± 2 × 10 <sup>4</sup>	

## Discussion

**Acetone.** A comparison of Table III with similar data given in the literature shows that the values of  $\Lambda_0$  obtained in the present work are higher by about 2 conductance units. This difference can be ascribed to the lower water content of the acetone as evidenced by the low density of 0.7843 g/cc. With one exception, the densities given in the literature are 0.7845 g/cc or higher.

The lowest density reported is 0.7840 g/cc; however, only the conductance of KI ( $\Lambda_0 = 196.7 \pm 0.5$ ) was reported.<sup>17</sup> Although we did not measure the conductance of this salt, its conductance can be calculated from Table III by combining  $\Lambda_0(i\text{-Am}_3\text{BuNI}) + \Lambda_0(\text{KBPh}_4) - \Lambda_0(i\text{-Am}_3\text{BuNBPh}_4)$  and gives  $\Lambda_0(\text{KI}) = 196.9 \pm 0.1$ . The two results agree within experimental error and suggest that Hughes' acetone and ours are of comparable water content.

Single ion conductances based on the Fuoss-Coplan split,<sup>24</sup>  $\Lambda_0(i\text{-Am}_3\text{BuNBPh}_4)/2 = \lambda_0(i\text{-Am}_3\text{BuN}^+)$ , are

(22) R. F. Mocharnyuk, *Zh. Obshch. Khim.*, **30**, 1081 (1960).

(23) R. M. Fuoss and F. Accascina, "Electrolytic Conductance," Interscience, New York, N. Y., 1959; R. L. Kay, *J. Amer. Chem. Soc.*, **82**, 2099 (1960).

(24) M. A. Coplan and R. M. Fuoss, *J. Phys. Chem.*, **68**, 1177 (1964).

**Table III:** Conductance Parameters for Electrolytes in Acetone-Propanol Mixtures at 25°

% acetone	$\Lambda_0$	$a$	$K_{\Lambda}$	$\sigma_{\Lambda}$
Bu <sub>4</sub> NI				
0	24.60 ± 0.04	4.7 ± 0.1	415 ± 6	0.01
0.20	46.23 ± 0.04	6.5 ± 0.5	260 ± 10	0.04
0.40	70.46 ± 0.08	6.4 ± 0.4	190 ± 10	0.04
0.60	97.49 ± 0.02	5.09 ± 0.07	110 ± 2	0.01
0.80	129.46 ± 0.04	5.1 ± 0.1	105 ± 4	0.03
0.90	149.68 ± 0.08	5.3 ± 0.2	122 ± 4	0.05
Bu <sub>4</sub> NClO <sub>4</sub>				
0	27.13 ± 0.03	4.2 ± 0.1	769 ± 6	0.01
0.20	51.86 ± 0.05	6.1 ± 0.4	370 ± 10	0.03
0.40	80.64 ± 0.06	5.7 ± 0.2	217 ± 7	0.04
0.60	112.25 ± 0.09	6.0 ± 0.3	158 ± 8	0.08
0.80	146.30 ± 0.05	6.0 ± 0.3	114 ± 6	0.06
0.90	165.04 ± 0.08	6.0 ± 0.3	104 ± 6	0.05
LiCl				
0	20.09 ± 0.03	4.8 ± 0.3	210 ± 9	0.03
0.20	36.3 ± 0.1	3.92 ± 0.09	250 ± 10	0.03
0.40	56.4 ± 0.1	4.22 ± 0.09	470 ± 10	0.05
0.60	82.6 ± 0.3	5.1 ± 0.2	990 ± 20	0.03
0.80	112.90 ± 0.05	6.24 ± 0.06	2196 ± 4	0.02
Bu <sub>4</sub> NCl				
0	21.16 ± 0.03	4.4 ± 0.1	149 ± 5	0.02
0.20	40.71 ± 0.03	5.5 ± 0.3	106 ± 7	0.02
0.40	61.72 ± 0.02	4.94 ± 0.09	54 ± 3	0.02
0.60	85.80 ± 0.05	5.3 ± 0.2	68 ± 5	0.03
0.80	113.2 ± 0.1	5.4 ± 0.3	93 ± 8	0.05
0.95	142.1 ± 0.2	5.3 ± 0.6	160 ± 10	0.08
Bu <sub>4</sub> NBr				
0	22.92 ± 0.03	4.6 ± 0.1	266 ± 6	0.01
0.20	42.76 ± 0.05	5.9 ± 0.4	180 ± 10	0.03
0.40	64.76 ± 0.06	5.0 ± 0.1	96 ± 6	0.02
0.60	89.72 ± 0.02	5.11 ± 0.08	88 ± 2	0.02
0.80	118.81 ± 0.03	5.08 ± 0.08	101 ± 2	0.02
0.90	137.55 ± 0.06	5.5 ± 0.2	138 ± 4	0.03

given in Table IV. Where comparisons between values of  $\lambda_0$  are possible, those obtained from transference numbers agree with those from the Fuoss-Coplan split to within at least 1%. The value of the conductance-viscosity product for *i*-Am<sub>3</sub>BuN ion in acetone is 0.190 in good agreement with the value of 0.189 obtained in methyl ethyl ketone,<sup>25</sup> but considerably lower than the values of 0.199 and 0.198 obtained in methanol and acetonitrile, respectively.<sup>26</sup>

**Table IV:** Single Ion Conductances in Acetone at 25° Based on Fuoss-Coplan Split

<i>i</i> -Am <sub>3</sub> BuN <sup>+</sup>	62.65	BPh <sub>4</sub> <sup>-</sup>	62.65
Bu <sub>4</sub> N <sup>+</sup>	66.40	ClO <sub>4</sub> <sup>-</sup>	118.35
Pr <sub>4</sub> N <sup>+</sup>	75.09	I <sup>-</sup>	117.99
Et <sub>4</sub> N <sup>+</sup>	89.49	Br <sup>-</sup>	118.94
Me <sub>4</sub> N <sup>+</sup>	96.63	Cl <sup>-</sup>	121.20
Na <sup>+</sup>	77.49		
K <sup>+</sup>	78.74		
Cs <sup>+</sup>	83.52		

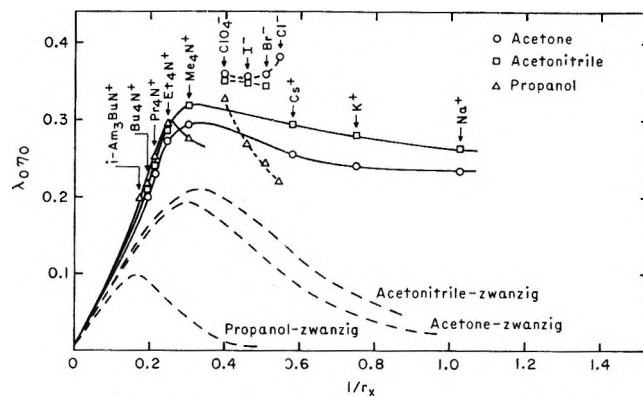


Figure 2. The limiting Walden product for the halide, alkali, and tetraalkylammonium ions as a function of crystallographic size at 25°. Dotted curves show the theoretical predictions.

A decrease in the Walden product with decreasing dielectric constant is the type of behavior detected by Fuoss.<sup>27</sup> It can be attributed to a reduction in the velocity of the moving ion due to interaction with the oriented solvent dipole. This effect which is a correction of Stokes' law has been quantitatively evaluated by Zwanzig.<sup>28</sup>

$$\lambda_0 \eta = \frac{F^2}{N(6\pi r + B/r^3)} \quad (3)$$

where  $F$  is the Faraday and  $N$  is Avogadro's number.  $B$  is a property only of solvent and equals  $(2e^{2/3})(\tau/\eta) \cdot (\epsilon_0 - \epsilon_\infty)/\epsilon_0^2$  where  $\tau$  is the dielectric relaxation time,  $\epsilon_0$  the static permittivity, and  $\epsilon_\infty$  the permittivity at infinite frequency.

Shown in Figure 2 is a plot of  $\lambda_0 \eta$  vs.  $1/r_x$  (the estimated crystallographic radius) for ions in acetonitrile, acetone, and propanol.<sup>29,30</sup> Also shown are the predictions of eq 3 for these solvents. The Zwanzig equation shows a dependence of  $\lambda_0 \eta$  on ionic size that is realistic in the sense that it goes through a maximum at  $r_{\max} = (B/2\pi)^{1/4}$  and then decreases. The position of the maximum for the experimental and calculated curves appears to be almost identical in acetone and acetonitrile, but shows considerable discrepancy in the alcohols<sup>31</sup> of which ProOH is a typical example. The maximum is too small by a factor of 1.5 in acetone and acetonitrile, but by a factor of 3 in hydrogen bonding

(25) S. R. C. Hughes and D. H. Price, *J. Chem. Soc.*, 1093 (1967).

(26) R. L. Kay, D. F. Evans, and G. P. Cunningham, *J. Phys. Chem.*, **73**, 3322 (1969).

(27) R. M. Fuoss, *Proc. Nat. Acad. Sci.*, **45**, 807 (1959).

(28) R. Zwanzig, *J. Chem. Phys.*, **38**, 1603 (1963).

(29) R. L. Kay, G. P. Cunningham, and D. F. Evans in "Hydrogen Bonded Solvents," A. Covington and P. Jones, Ed., Taylor and Francis, London, 1968.

(30) The relaxation time  $\tau$  and dielectric constants  $\epsilon_0$  and  $\epsilon_\infty$  required in eq 2 were taken from F. Buckley and A. A. Maryott, *Nat. Bur. Stand. (U. S.) Circ.* 589 (1958).

(31) D. F. Evans and P. Gardam, *J. Phys. Chem.*, **73**, 158 (1969).

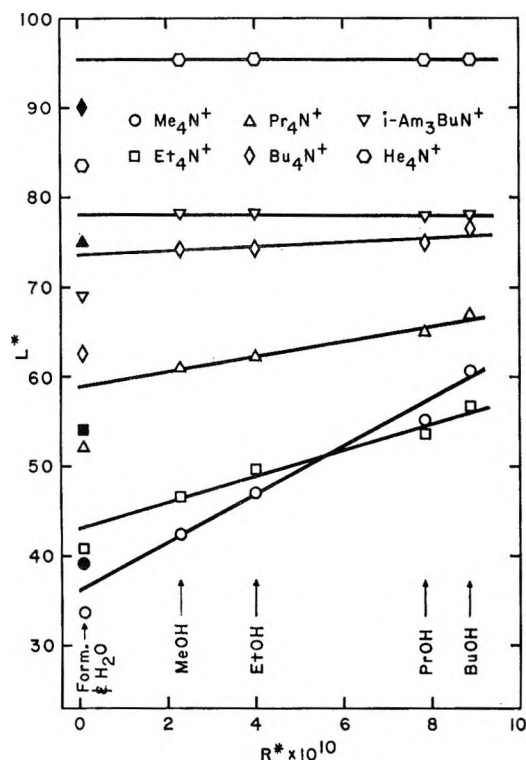


Figure 3. A plot of  $L^*$  vs.  $R^*$  for tetraalkylammonium ions in MeOH, EtOH, PrOH, BuOH, formamide, and water.

solvents. As pointed out by Frank<sup>32</sup> there is no value of  $\bar{r}$  which when substituted into eq 2 will reproduce the magnitude of the measured  $\lambda_{0\eta}$ . If the Zwanzig equation is reevaluated using  $4\pi$  instead of  $6\pi$ , the magnitude of the maximum is increased, but it still lies below the experimental values and the dependence of  $\lambda_{0\eta}$  upon ionic size becomes much more pronounced.

When the behavior in various solvents is to be compared, a more convenient form of the Zwanzig equation is<sup>33</sup>

$$\frac{15.5}{\lambda_{0\eta}} = 18.8r + (15.3 \times 10^{12}/\bar{r}^3) \times [(\tau/n)(\epsilon_0 - \epsilon_\infty)/\epsilon_0^2] \quad (4)$$

This can be expressed in a more succinct manner as  $L^* = 18.8r + (15.3 \times 10^{12}/\bar{r}^3)R^*$  and a plot of  $L^*$  vs.  $R^*$  should be linear. A value of  $\bar{r}$  can be obtained from the slope and the intercept. Shown in Figure 3 is a plot of  $L^*$  vs.  $R^*$  for the tetraalkylammonium ions in the alcohols, methanol, ethanol, propanol, and butanol. The behavior in the alcohols has been discussed in detail elsewhere<sup>29,30</sup> and can be summarized in the following way. Within experimental error, which can for the most part be attributed to the uncertainty in  $\tau$ , a linear relationship between  $R^*$  and  $L^*$  is observed. The values of  $\bar{r}$  calculated from the intercepts are larger than those calculated from the slope by a factor of 3 to 10.

In Figure 4 that portion of the plot between  $R^* = 0$  and  $2.5 \times 10^{-10}$  has been expanded to allow inclusion of

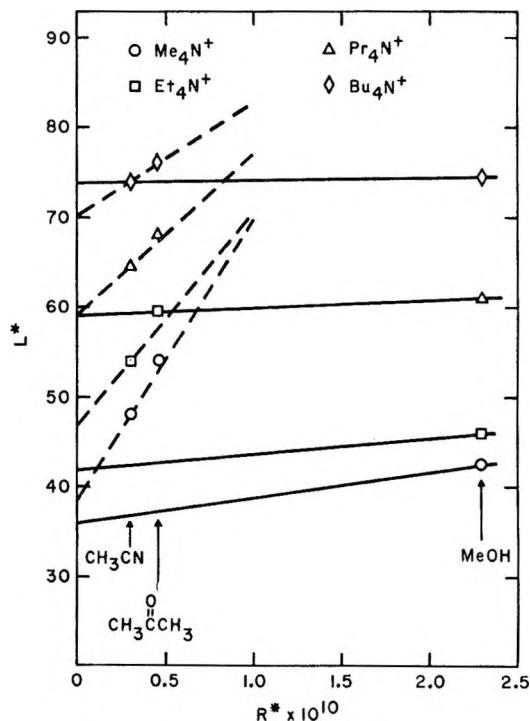


Figure 4. A plot of  $L^*$  vs.  $R^*$  for tetraalkylammonium ions in  $\text{CH}_3\text{CN}$ ,  $\text{CH}_3\text{COCH}_3$  and  $\text{CH}_3\text{COC}_2\text{H}_5$  compared with the plot in alcohols.

points for acetonitrile, acetone, and butanone. The solid lines are extensions of the alcohol lines of Figure 3. The dashed lines for the nonprotic solvents indicate that a different family of curves applies to nonhydrogen bonding solvents. For these the values of  $\bar{r}$  calculated from the slope and the intercept are in closer agreement as can be seen in Table V. Reliable data for  $\tau$  in methyl ethyl ketone, a solvent for which there is a considerable amount of conductance data available, would allow this point to be established with more certainty. It would appear that the Zwanzig equation, the most sophisticated of continuum theories, works best in nonhydrogen bonding solvents.<sup>27</sup>

Table V: Values of  $\bar{r}$  Obtained from  $L^*$  vs.  $R^*$  Plot for  $R_4N^+$  Ion

	$\bar{r}$ from intercept	$\bar{r}$ from slope	Slope/intercept
$\text{Me}_4\text{N}^+$	2.05	3.65	1.7
$\text{Et}_4\text{N}^+$	2.5	4.04	1.6
$\text{Pr}_4\text{N}^+$	3.14	4.4	1.4
$\text{Bu}_4\text{N}^+$	3.72	4.9	1.3

The variation of  $\lambda_{0\eta}$  with ionic size in acetone has been discussed by Adams and Laidler<sup>34</sup> in a different

(32) H. S. Frank, "Chemical Physics of Ionic Solutions," B. E. Conway and R. G. Barradas, Ed., Wiley, New York, N. Y., 1966, p 61.

(33) G. Atkinson and Y. Mori, *ibid.*, 71, 3523 (1967).

(34) W. A. Adams and K. L. Laidler, *Can. J. Chem.*, 46, 1989 (1968).

context. They postulate the existence of a critical size,  $r^* = 2.3$ , below which the conductance decreases with decreasing ionic size as a result of solvation. Above this critical size, the conductance decreases with increasing size due to hydrodynamic effects. There appear to be at least two ways of accounting for the reduction in mobility of the smaller ions; one is based on a static picture involving solvation and the other a dynamic picture, described by the Zwanzig effect. There is some evidence in other liquids, for example water, that both mechanisms can be operative depending on the charge on the ion.<sup>32</sup> To what extent this is true in acetone remains an unanswered question.

*Alcohol-Acetone Mixtures.* Alcohols are good hydrogen bond donors and acceptors. Consequently, the liquids are extensively self-associated, forming hydrogen-bonded chains. Acetone is a good hydrogen bond acceptor but has no donor hydrogens, so is unassociated as the pure liquid. In alcohol-acetone mixtures, both alcohol-alcohol and alcohol-ketone hydrogen bonding can occur. This should affect the properties of the solvent mixtures.

The density of propanol-acetone mixtures is a linear function of mole fraction according to our data. Mixtures of ethanol, 1-propanol, and 1-pentanol with methyl isobutyl ketone also show ideal volumes of mixing.<sup>35</sup> The ethanol-acetone system shows a positive deviation from linearity, however.<sup>7</sup>

Heats of mixing are large and positive. Although the 1-propanol-acetone system has not been reported, the data of Murakami for the closely related systems 1-butanol-acetone<sup>36</sup> and 2-propanol-acetone<sup>37</sup> show that 330 and 390 cal/mol of heat, respectively, are absorbed in forming an equimolar mixture of the two components. This indicates that the heat evolved on forming acetone-alcohol hydrogen bonds does not compensate for the heats absorbed on breaking the alcohol-alcohol hydrogen bonds. Both the relative strength of the two interactions and the number of bonds of each kind formed are reflected in this. In the pure alcohol a molecule can form two or more hydrogen bonds at the same time. Acetone, however can only bond to one alcohol at a time and steric requirements for this interaction may prevent the alcohol molecule from simultaneously acting as an acceptor for another hydrogen bond.

The strengths of alcohol-alcohol and alcohol-ketone hydrogen bonds can be estimated from thermal and infrared measurements. From heat of mixing data extrapolated to infinite dilution, enthalpies can be calculated for the 2-propanol-2-propanol and 2-propanol-acetone interactions of  $-5.90$  and  $-3.79$  kcal/mol, respectively.<sup>37</sup> Corresponding numbers for the 1-butanol-acetone system are  $-5.50$  and  $-3.72$  kcal/mol.<sup>36</sup> From infrared measurements as a function of temperature enthalpies for ethanol-ethanol and ethanol-acetone complexes in  $\text{CCl}_4$  were found to be  $-7.2$ <sup>38</sup> and

$-3.46$ <sup>39</sup> kcal/mol. The ethanol interaction was interpreted as formation of a cyclic dimer with each hydrogen bond  $-3.6$  kcal. A calorimetric measurement of the ethanol-acetone interaction in  $\text{CCl}_4$  gives  $-3.44$  kcal/mol.<sup>40</sup> Thus the indication from experimental work is that the alcohol-alcohol hydrogen bond is somewhat stronger than the alcohol-acetone hydrogen bond. Barker and Smith<sup>41</sup> were able to calculate the heats of mixing of acetone and ethanol reasonably well using a statistical thermodynamics treatment with estimated enthalpies of  $-6.74$  kcal/mol for ethanol-ethanol, and  $-5.72$  kcal/mol for ethanol-acetone.

The viscosity of 1-propanol drops sharply as acetone is added (Figure 1). This indicates that the formation of alcohol-acetone hydrogen bonds destroys the alcohol chains. Similar behavior is observed in ethanol-acetone.<sup>7</sup> The ultrasonic absorption of acetone-propanol solutions at 25 MHz parallels the viscosity, a plot of  $\alpha/f^2$  vs.  $\eta$  being linear within experimental uncertainty.

The dielectric constants of propanol-acetone mixtures deviate from ideal behavior in a manner that also reflects the disruption of alcohol self-association by acetone. The dipole moment of acetone is 2.89, whereas that of propanol is only 1.69. The fact that the two pure liquids are isodielectric is due to the extensive association of the alcohol. The Kirkwood  $g$  factor for 1-propanol at 25° is 3.1,<sup>42</sup> whereas that for acetone is only 1.1.<sup>21</sup> As the propanol association is disrupted by the addition of acetone the dielectric constant drops. At higher mole fractions of acetone the increasing concentration of acetone molecules with their higher dipole moment causes the dielectric constant to increase again. Similar behavior has been observed in several other systems involving alcohols or amines and hydrogen bond acceptors.<sup>43, 44</sup>

The thermodynamics of transfer of electrolytes from aprotic solvents to alcohols gives some indication of ion-solvent interactions. Heats of solution of electrolytes have been measured in several nonaqueous solvents of high dielectric constant where ionic association is minimal. Patterns observed in these solvents should persist in similar solvents of lower dielectric constant. In Table VI are listed heats of transfer of tetraethyl-

(35) H. C. Eckstrom, J. E. Berger, and L. R. Dawson, *J. Phys. Chem.*, **64**, 1458 (1960).

(36) S. Murakami and R. Fujishiro, *Bull. Chem. Soc. Jap.*, **39**, 720 (1966).

(37) S. Murakami, K. Amaya, and R. Fujishiro, *ibid.*, **37**, 1776 (1964).

(38) U. Lidell and E. D. Becker, *Spectrochim. Acta*, **10**, 70 (1957).

(39) E. D. Becker, *ibid.*, **17**, 436 (1961).

(40) L. Lamberts, *J. Chim. Phys.*, **62**, 1404 (1965).

(41) J. A. Barker and F. Smith, *J. Chem. Phys.*, **22**, 375 (1954).

(42) W. Dannhauser and L. W. Bahe, *ibid.*, **40**, 3058 (1964).

(43) O. A. Osipov, M. A. Panina, O. E. Kashirenov, G. V. Nemirov, and I. K. Shelomov, *Zh. Obshch. Khim.*, **31**, 3153 (1961).

(44) A. V. Celiano, P. S. Gentile, and M. Cefola, *J. Chem. Eng. Data*, **7**, 391 (1962).

ammonium salts from sulfolane, dimethyl sulfoxide, and dimethylformamide to methanol, taken from the compilation of heats of solution of Choux and Benoit.<sup>45</sup> Less complete data for alkali halides in these solvents show the same pattern of anion dependence. The transfer of chloride to a hydrogen-bonding solvent is clearly accompanied by a much greater stabilization than perchlorate. Entropies of transfer of ions for a number of solvent pairs have been shown to be relatively independent of the nature of the ionic species.<sup>46</sup> The  $T\Delta S$  terms are typically all of the same sign and about the same magnitude for a given pair of solvents. Thus, the free energies of transfer reflect the pattern observed for heats of transfer. This is apparent in solvent activity coefficients calculated from solubility products in nonaqueous solvents.<sup>47</sup> The fact that in hydrogen bonding solvents chloride has a significantly lower free energy relative to perchlorate than in aprotic solvents must be considered in analyzing ionic association in these systems.

**Table VI:** Heats of Transfer of Tetraethylammonium Salts from Aprotic Solvents to Methanol (kcal/mol)<sup>a</sup>

	$E_t\text{NCl}$	$E_t\text{NBr}$	$E_t\text{NI}$	$E_t\text{NClO}_4$
DMSO $\rightarrow$ MeOH	-5.44	-1.89	+1.97	+4.20
Sulfolane $\rightarrow$ MeOH	-4.25	-0.61	+2.46	+4.61
DMF $\rightarrow$ MeOH	-1.65		+5.04	+6.44

<sup>a</sup> Calculated from heats of solution compiled in ref 45.

**Mobilities.** The conductance viscosity product for salts in the acetone-propanol mixtures is shown in Figure 5. In pure propanol the mobilities of the tetrabutylammonium salts are in the order  $\text{ClO}_4^- > \text{I}^- > \text{Br}^- > \text{Cl}^-$ . Heat of transfer data reveal that chloride receives much greater additional stabilization in alcohols than perchlorate,<sup>45</sup> a result attributable to more effective hydrogen bonding to the smaller anion. This is compatible with chloride having the largest hydrodynamic radius of the anions studied, due to increased solvation. In pure acetone, on the other hand, there is virtually no difference in the anionic mobilities. Acetone is a typical aprotic solvent in that it solvates cations strongly but anions only weakly.

The mobility order for the tetrabutylammonium salts observed in pure propanol persists until the mole fraction of acetone reaches approximately 80%. This suggests that the same hydrodynamic entities present in pure propanol exist through this composition range. The salts show nearly parallel behavior in the small variations in Walden product up to 80% acetone, suggesting a common origin. The most likely explanation is a variation in the Zwanzig effect which results in a retardation in mobility at about 50% acetone. The 10% decrease in dielectric constant at this composition is in

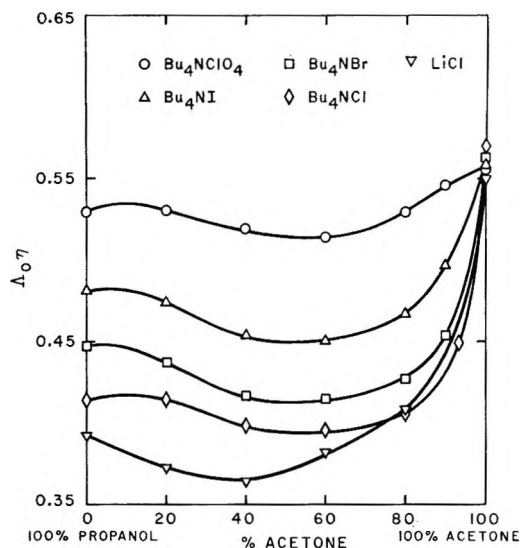


Figure 5. Walden product at 25° as a function of mole fraction of acetone in 1-propanol.

the right direction for such an effect. However, the lack of reliable dielectric relaxation times for this system prevents quantitative calculations.

As the mole fraction of acetone exceeds 80%, the mobilities increase rapidly. Preferential solvation by propanol diminishes in these acetone-rich solutions and the mobilities approach the values characteristic of pure acetone.

The Walden products for lithium chloride show the same general behavior as those for the other salts. It might be expected that the larger dipole moment of acetone would result in its preferential solvation of the lithium ion. However, the mobility data by themselves do not allow this conclusion to be drawn.

**Association Constants.** Simple coulombic theory predicts that for isodielectric solvents such as propanol and acetone the association constants for a given electrolyte should be identical. Two such equations are<sup>48</sup>

$$K_A = \frac{4\pi N a_K^3}{3000} \exp\left(\frac{e^2}{a_K \epsilon k T}\right) \quad (5)$$

and<sup>49</sup>

$$K_A = \frac{4\pi N}{1000} \left(\frac{e^2}{\epsilon k T}\right)^3 \int_2^b e^{-t^{-4}} dt \quad (6)$$

where

$$b = \frac{e^2}{r \epsilon k T} \quad (7)$$

(45) G. Choux and R. L. Benoit, *J. Amer. Chem. Soc.*, **91**, 6221 (1969).

(46) C. M. Criss, R. P. Held, and E. Lukshaz, *J. Phys. Chem.*, **72**, 2970 (1968).

(47) R. Alexander, E. C. F. Ko, A. J. Parker, and T. J. Broxton, *J. Amer. Chem. Soc.*, **90**, 5049 (1968).

(48) R. M. Fuoss, *ibid.*, **80**, 5059 (1958).

(49) N. Bjerrum, *Kgl. Dan. Vidensk. Selsk.*, **7**, 9 (1926).

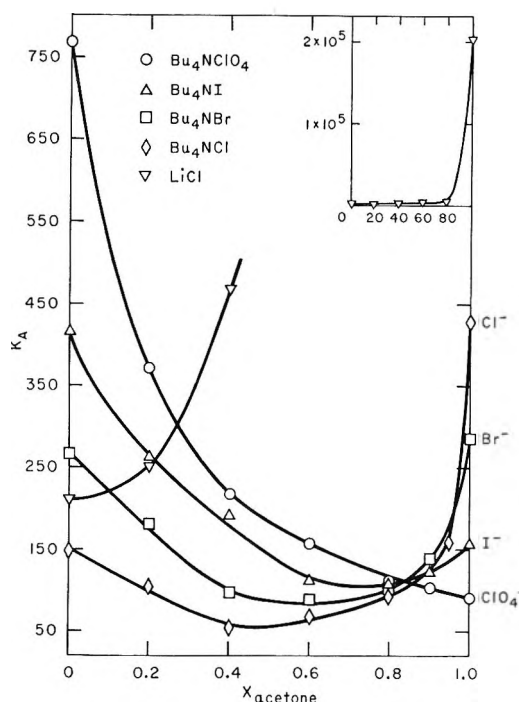
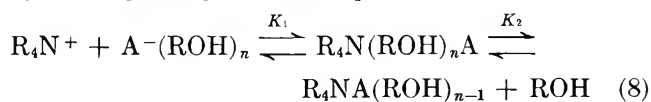


Figure 6. Association constant at 25° as a function of mole fraction of acetone in 1-propanol.

In both pure solvents the values of  $K_A$  for the salts are much larger than those predicted by either eq 5 or 6. For example, eq 5 gives an average value of  $K_A = 40$  for  $a = 6$  to  $12 \text{ \AA}$  in a solvent of dielectric constant 20.5. Furthermore, the dependence of  $K_A$  upon anion size in these two solvents is opposite as can be seen in Figure 6. In acetone  $K_A$  decreases with anion size in qualitative agreement with theory, whereas the opposite dependence is observed in propanol.

The large values of  $K_A$  and the peculiar dependence upon anion size observed in propanol can be attributed to two factors: (1) a diminution in the dielectric constant in the vicinity of an ion pair and (2) a multiple-step association process. The magnitude of the bulk dielectric constant in hydrogen bonding solvents is due in large measure to the structures arising from hydrogen bonding. However, in the vicinity of an ion pair, extensive hydrogen bonding between the alcohol molecules is unlikely because of the orientation of the alcohol dipoles by the ions. This results in a decreased local dielectric constant, thereby enhancing the coulomb attraction between ions and increasing ionic association. In fact by treating  $\epsilon$  as an adjustable parameter it is possible to obtain a value which predicts the correct magnitude of  $K_A$ .<sup>50</sup> However, it is impossible within such a continuum framework to account for the perchlorate being five times as associated as the corresponding chloride. This behavior is best accounted for by a multiple-step association process such as



in which the concentration of solvent-separated ion pairs is controlled by diffusion, but the concentration of contact ion pairs is determined by the nature of the anion-solvent interaction.<sup>51</sup> The observed association constant can be shown to be equal to

$$K_A = K_2 = K_1 \{1 + K_2/[ROH]\} \quad (9)$$

Preliminary evidence for such an association mechanism in the alcohols has been obtained from ultrasonic measurements in our laboratory.

The association process of tetraalkylammonium salts in acetone has been studied by Petrucci and Darbari using ultrasonics.<sup>52</sup> Although they found only one relaxation time in the frequency range studied, they concluded that ionic association is a multiple-step process and that the data are consistent with the Eigen-Tamm-type mechanism<sup>53</sup> of eq 8. It is difficult to see on this basis why  $K_A$  changes so radically with size in acetone since variations in  $K_2$  would be expected to be small when anion-solvent interactions are weak.

Furthermore, neither eq 5 or 6 satisfactorily explains the association in pure acetone, since it is impossible to account for a fourfold variation in association constant when the sum of the ionic radii changes only from a value near  $7 \text{ \AA}$  for  $Bu_4NCl$  to about  $8 \text{ \AA}$  for  $Bu_4NClO_4$ . The low value of the Kirkwood  $g$  factor for acetone, indicating little enhancement of dielectric constant by cooperative behavior, makes a lowering of dielectric constant in the region of ion pairs unlikely.

Lithium chloride has an association constant comparable to that of tetrabutylammonium chloride in pure propanol. A lithium ion tightly solvated by propanol should resemble a tetrabutylammonium ion. In these terms the similarity in both mobility and association constant for the two chlorides in propanol is understandable. In acetone, however, lithium chloride is enormously associated,  $K_A$  being near 200,000. This behavior has been observed in several aprotic solvents and has been discussed in terms of dielectric saturation by Fernandez-Prini and Prue.<sup>54</sup>

Although the pure solvents are isodielectric the mixtures are not. As a result of the observed 10% decrease in dielectric constant at 50% acetone  $K_A$  would be predicted to increase by a factor of 2. As shown in Figure 6,  $K_A$  for the tetrabutylammonium salts actually passes through a minimum at this point. The mobility data suggest that anion solvation remains relatively unchanged up to about 80% acetone. If this is the case the decrease in  $K_A$  in the propanol-rich region can only be attributed to an increase in dielec-

(50) M. A. Matesich, J. A. Nadas, and D. F. Evans, *J. Phys. Chem.*, **74**, 4568 (1970).

(51) D. F. Evans and P. Gardam, *ibid.*, **73**, 158 (1969).

(52) G. S. Darbari and S. Petrucci, *ibid.*, **74**, 268 (1970).

(53) M. Eigen and K. Tamm, *Z. Elektrochem.*, **66**, 93 (1962).

(54) R. Fernandez-Prini and J. E. Prue, *Trans. Faraday Soc.*, **62**, 1257 (1966).

tric constant near an ion pair. Such an effect should parallel increase in acetone content since the higher dipole moment of acetone should result in an effectively higher local dielectric constant. This remains the dominant factor until the propanol concentration is so small that anion solvation by hydrogen bonding disappears. At this point the  $K_A$  values rapidly approach those observed in pure acetone. A comparison of Figures 5 and 6 shows that this explanation is consistent with both mobility and association behavior.

For lithium chloride the association behavior is dominated by extremely high ionic association in pure acetone. Between 0 and 80% acetone, a region in which chloride is solvated predominantly by alcohol,  $K_A$  increases by a factor of 10. However, between 80 and 100% acetone, where alcohol solvation is replaced by acetone,  $K_A$  increases by a factor of 100. The inset in Figure 6 shows this dramatic increase. Ap-

parently up to 80% acetone the small but constantly increasing fraction of acetone-solvated chloride ions form very stable ion pairs with lithium. In going from 80 to 100% acetone all chlorides lose their alcohol solvation. The major part of the increase in  $K_A$  occurs in these acetone-rich solutions, just as it does with  $\text{Bu}_4\text{NCl}$ , but the extent of association is much greater with  $\text{LiCl}$ .

The results presented here indicate that some insight into ion-solvent interactions can be obtained from studies in solvent mixtures, but that a careful consideration of the properties of the mixed solvents themselves is a prerequisite for a meaningful discussion of the solutions.

*Acknowledgment.* This work was supported by Contract No. 14-01-001-1281 and 14-30-2615 with the Office of Saline Water, U. S. Department of the Interior.

## The Conductance of Tetraalkylammonium Halides in Ethylene Glycol

by Robert P. DeSieno,\* Paul W. Greco, and Ronald C. Mamajek<sup>1</sup>

Chemistry Department, Westminster College, New Wilmington, Pennsylvania 16142. (Received June 25, 1970)

Publication costs borne completely by The Journal of Physical Chemistry

We have studied, individually, the conductance of  $(\text{CH}_3)_4\text{NBr}$ ,  $(\text{CH}_3)_4\text{NI}$ ,  $(\text{C}_2\text{H}_5)_4\text{NBr}$ ,  $(\text{C}_2\text{H}_5)_4\text{NI}$ ,  $(\text{C}_3\text{H}_7)_4\text{NBr}$ ,  $(\text{C}_3\text{H}_7)_4\text{NI}$ ,  $(\text{C}_4\text{H}_9)_4\text{NBr}$ , and  $(\text{C}_4\text{H}_9)_4\text{NI}$  dissolved in ethylene glycol and analyzed the data with the Fuoss-Onsager equation. We found no evidence of association by the tetraalkylammonium and halide ions in ethylene glycol. For pairs of salts with a common tetraalkylammonium ion, bromides exhibit larger values of the ion-size parameters in ethylene glycol than do iodides. All the salts exhibited values of the ion-size parameter which were smaller than the crystallographic radii of the salts. The values of the Walden products, for the tetraalkylammonium halides in ethylene glycol, are the largest values reported to date for these salts in solution and are nearly three times as large as the corresponding values of  $\Lambda_{07}$  predicted by the Boyd-Zwanzig equation.

### Introduction

Ethylene glycol, a difunctional alcohol with a relatively large density (1.1095 g/cc) and viscosity (0.16190 P) at 25° is an interesting substance in which to study the interaction between ions and solvent. For example, Crickard and Skinner in studying the viscosities of cesium iodide-ethylene glycol solutions observed cesium iodide to act as a breaker of structure in ethylene glycol, and calculated negative values for the  $B$  term in the Jones-Dole equation describing the viscosities of these solutions.<sup>2a,b</sup> Because of this unusual behavior, we have started a program to measure the conductance of cesium halides and tetraalkylammonium halides in ethylene glycol and thereby gain another experimental

view of the interaction between relatively large ions and ethylene glycol.

Several investigators have measured the conductance of various tetraalkylammonium halides and perchlorates in methanol, ethanol, propanol, and water.<sup>3-5</sup> In these solvents, for salts with a common tetraalkyl-

(1) This work evolved from an independent study project by P. W. G. and R. C. M.

(2) (a) K. Crickard and J. F. Skinner, *J. Phys. Chem.*, **73**, 2060 (1969); (b) G. Jones and M. Dole, *J. Amer. Chem. Soc.*, **51**, 2950 (1929).

(3) R. L. Kay, C. Zawoyski, and D. F. Evans, *J. Phys. Chem.*, **69**, 4208 (1965).

(4) D. F. Evans and P. Gardam, *ibid.*, **72**, 3281 (1968).

(5) D. F. Evans and R. L. Kay, *ibid.*, **70**, 366 (1966).



ammonium cation, the degree of ion pairing increases as the size of the accompanying anion increases. This behavior contrasts with that for ions in nonhydrogen-bonding solvents where the degree of ion pairing increases as the radii of the ions in solution decrease.<sup>6</sup>

This paper reports measurements of the conductance of several tetraalkylammonium halides in ethylene glycol and contrasts these data with the measurements of conductance for the same salts in monohydroxy alcohols.

### Experimental Section

We obtained all of our tetraalkylammonium salts from Professor D. F. Evans (Case Western Reserve University). These salts (Eastman Kodak) had been recrystallized from mixtures of methanol and ether, or acetone and ether, and then dried for 12 hr in a vacuum oven at 65°. We dried the salts in a vacuum oven for an additional 12 hr at 65° before we used them.

We added magnesium turnings to ethylene glycol (Fisher Certified), distilled the solvent under dry nitrogen at 10 Torr, and collected solvent at a head temperature of 55 to 56°. We transferred the distillate, under nitrogen, to large Pyrex storage vessels and drained the solvent directly into a mixed bed ion-exchange column (4 ft) that had been conditioned with several liters of ethylene glycol. We transferred solvent to the conductance cell through a system that permitted us to maintain dry nitrogen over the solvent at all times.

With the aid of a Hawes-Kay cup-dropping device,<sup>7</sup> we studied changes in solution conductance with changes in electrolyte concentration. We added 60–70-mg increments of salt directly to 500 g of ethylene glycol contained in an erlenmeyer conductance cell immersed in an oil bath at 25 ± 0.005°.

We measured the cell constant of our cell to be 0.4659 ± 0.0001. By measuring the conductance of several tetraalkylammonium halides in methanol and comparing our values with values in the literature, we tested the reliability of our cell constant and found it to be satisfactory.

We measured the resistance of the solutions with an audiofrequency Wheatstone bridge. The bridge consisted of a Shackelton Ratio box equipped with a Wagner earthing device and two matched 1-kohm resistors. The cell and a precision decade resistance box (111,111 ohms in 0.1-ohm steps) composed the other two arms of the bridge. An oscillator tuned to 1600 or 3100 Hz energized the bridge through an isolation transformer. Two cascaded operational amplifiers, tuned by an adjustable twin-T filter and isolated from the bridge, amplified any signal imbalance in the bridge. An oscilloscope used as an  $x$ - $y$  plotter detected balance in the bridge.

When we measured the resistance of ethylene glycol solutions, we shunted the cell with a 50-kohm resistor. We measured the resistances of the solutions at two fre-

quencies (1600 and 3100 Hz) and found no significant change of resistance with change of frequency. Between each measurement of resistance, we checked the calibration of the bridge by inserting a precision 10-kohm resistor into the experimental arm of the bridge and observed, at balance, a satisfactory agreement (±0.01%) between the values of resistance from the decade box and the 10-kohm resistor.

We measured the viscosity of ethylene glycol (0.16190 P at 25°) with a calibrated Cannon-Ubbelohde dilution viscometer and protected the solvent from moisture during the measurement (435 sec). We measured the density (1.1095 g/cc at 25°) of ethylene glycol with a pycnometer (Gay-Lussac) capped to prevent absorption of moisture by the solvent. In our calculations, we used the value of the dielectric constant for ethylene glycol (37.70 at 25°) reported in the literature.<sup>8</sup>

### Results

To analyze our data (Table I), we used the Fuoss-Onsager equation in the form

$$\Lambda = \Lambda_0 - Sc^{1/2} + Ec \log c + (J(a) - \theta)c$$

[for unassociated electrolytes]

and in the form

$$\Lambda = \Lambda_0 - S(c)^{1/2} + Ec\gamma \log c\gamma + (J(a) - \theta)c\gamma - K_{AC}\gamma\Lambda f^2$$

[for associated electrolytes]<sup>9</sup>

In the Fuoss-Onsager equation,  $E = E_1\Lambda_0 - E_2$ ,  $S = \alpha\Lambda_0 + \beta_1$ ,  $J = \sigma_1\Lambda_0 + \sigma_2$ ,  $\gamma$  is the degree of dissociation, and  $f$  is the activity coefficient.  $\sigma_1$ ,  $\sigma_2$ ,  $\gamma$ ,  $\beta$ ,  $E_1$ , and  $E_2$  have been defined by Fuoss<sup>9</sup> and  $\sigma$ ,  $\beta$ ,  $E_1$ , and  $E_2$  are constants of a given experimental system and for our system have values of 0.6884, 4.602, 4.770, and 4.669, respectively. We set  $\theta = B\Lambda_0$ , where  $B$  is the viscosity coefficient.

Since we had no data describing the viscosity of solutions of tetraalkylammonium halides in ethylene glycol, we set  $B$  equal to zero. Other investigators<sup>4</sup> have shown that this does not alter the value of  $K_A$  or  $\Lambda_0$ , and changes the value of  $\bar{a}$ , by 0.2 Å.

We used a computer program<sup>10</sup> that linearizes the Fuoss-Onsager equation in  $\Lambda_0$ ,  $\bar{a}$  (ion size parameter), and when required  $K_A$ . It then provides a least-squares fit of the experimental data to the equation. Through a comparison of the precision of  $\Lambda_0$ ,  $\bar{a}$  (and  $K_A$ ) derived from the two modes of calculation we concluded that the mode of the Fuoss-Onsager equation

(6) D. F. Evans, C. Zawoyski, and R. L. Kay, *J. Phys. Chem.*, **69**, 3878 (1965).

(7) J. L. Hawes and R. L. Kay, *ibid.*, **69**, 2420 (1965).

(8) A. A. Maryott and E. F. Smith, *Nat. Bur. Stand. (U. S.) Circular*, No. 514 (1951).

(9) R. Fuoss, *J. Amer. Chem. Soc.*, **81**, 2659 (1959).

(10) R. L. Kay, *ibid.*, **82**, 2099 (1960).

**Table I:** Equivalent Conductances in Ethylene Glycol at 25°

10 <sup>4</sup> c Me <sub>4</sub> NBr κ <sub>0</sub> × 10 <sup>8</sup> = 1.4		A		10 <sup>4</sup> c Et <sub>4</sub> NBr κ <sub>0</sub> × 10 <sup>8</sup> = 0.94		A		10 <sup>4</sup> c Pr <sub>4</sub> NBr κ <sub>0</sub> × 10 <sup>8</sup> = 0.94		A		10 <sup>4</sup> c Bu <sub>4</sub> NBr κ <sub>0</sub> × 10 <sup>8</sup> = 1.0		A	
8.576	7.626	3.620	6.982	4.297	6.515	6.124	6.251								
16.507	7.487	9.534	6.848	8.914	6.411	11.665	6.153								
25.848	7.368	13.797	6.792	14.223	6.335	16.981	6.081								
35.025	7.276	17.840	6.745	19.580	6.265	22.922	6.023								
43.133	7.209	22.488	6.695	24.940	6.212	28.637	5.971								
52.148	7.141	27.173	6.651	30.311	6.164	34.425	5.925								
60.055	7.089	31.834	6.607	35.241	6.122	40.667	5.877								
68.810	7.032	36.434	6.571	40.114	6.085	45.955	5.852								
78.072	6.969	41.210	6.537	45.414	6.050	51.256	5.816								
86.335	6.927	45.975	6.506	50.561	6.016	56.412	5.783								
10 <sup>4</sup> c Me <sub>4</sub> NI κ <sub>0</sub> × 10 <sup>8</sup> = 1.0		A		10 <sup>4</sup> c Et <sub>4</sub> NI κ <sub>0</sub> × 10 <sup>8</sup> = 0.94		A		10 <sup>4</sup> c Pr <sub>4</sub> NI κ <sub>0</sub> × 10 <sup>8</sup> = 0.94		A		10 <sup>4</sup> c Bu <sub>4</sub> NI κ <sub>0</sub> × 10 <sup>8</sup> = 1.0		A	
6.790	7.285	3.710	6.605	3.895	6.141	3.947	5.866								
13.595	7.174	10.131	6.476	7.988	6.063	7.749	5.792								
19.672	7.074	14.067	6.426	11.993	5.990	11.771	5.728								
25.629	7.002	18.130	6.372	16.399	5.921	15.800	5.675								
31.826	6.947	22.220	6.324	20.511	5.870	20.008	5.617								
38.590	6.882	26.809	6.274	24.855	5.821	23.781	5.511								
45.124	6.829	30.496	6.239	28.912	5.773	29.112	5.514								
51.319	6.779	34.357	6.203	33.198	5.731	33.528	5.472								
57.407	6.734	38.331	6.167	37.252	5.695	38.845	5.422								
64.140	6.685	43.115	6.130	41.057	5.664	42.918	5.391								

which describes unassociated electrolytes yielded the only consistent results (Table II).

**Table II:** Conductance Parameters at 25° for Tetraalkylammonium Halides in Ethylene Glycol

	Λ <sub>0</sub>	<i>d</i>	σΛ	<i>J</i>
Me <sub>4</sub> NBr	7.956 ± 0.003	2.86 ± 0.03	0.005	58.387
Me <sub>4</sub> NI	7.577 ± 0.004	2.71 ± 0.05	0.005	53.230
Et <sub>4</sub> NBr	7.174 ± 0.003	3.63 ± 0.06	0.004	64.847
Et <sub>4</sub> NI	6.808 ± 0.004	2.89 ± 0.08	0.005	50.934
Pr <sub>4</sub> NBr	6.716 ± 0.002	3.12 ± 0.04	0.003	53.797
Pr <sub>4</sub> NI	6.345 ± 0.003	2.06 ± 0.06	0.004	34.664
Bu <sub>4</sub> NBr	6.489 ± 0.002	3.34 ± 0.05	0.003	55.144
Bu <sub>4</sub> NI	6.069 ± 0.003	2.08 ± 0.08	0.005	33.694

By applying Kohlrausch's law to the Λ<sub>0</sub> values in Table II, we note that the quantity (λ°Br<sup>-</sup> - λ°I<sup>-</sup>) for the four pairs of salts is reproducible to within ±0.05 conductance unit. This suggests our reagents were of adequate purity and that our data are internally consistent. To calculate *c*(*M*/1), we obtained values of *A* (Table III) for each salt by inserting the value of the

**Table III:** Density Constants [*A*] at 25°

	Br <sup>-</sup>	I <sup>-</sup>
Me <sub>4</sub> N <sup>+</sup>	0.121	0.134
Et <sub>4</sub> N <sup>+</sup>	0.114	0.159
Pr <sub>4</sub> N <sup>+</sup>	0.083	0.142
Bu <sub>4</sub> N <sup>+</sup>	0.058	0.118

density for ethylene glycol (*d*<sub>0</sub>) and the density (*d*) of the most concentrated solution from each conductance run into the equation

$$d = d_0 + Am$$

where *m* is the moles of solute/kilogram of solution.<sup>11</sup>

## Discussion

Predictably (based on considerations of viscosity), the limiting equivalent conductances of these salts are relatively small in ethylene glycol. However, the absence of evidence for association by the ions of these salts in ethylene glycol is surprising. In acetonitrile, dimethylformamide, or ethanolamine, solvents with comparable dielectric constants and/or similar viscosities, there is evidence for small but calculable amounts of ionic association by the tetraalkylammonium halides.<sup>6,12-16</sup> The tetraalkylammonium halides exhibit no observable association in only one other solvent (dimethylacetamide) of dielectric constant 37-38.<sup>17</sup>

For the various pairs (common cation) of tetraalkylammonium bromides and iodides, the bromides exhibit

(11) H. S. Harned and B. B. Owen, "The Physical Chemistry of Electrolytic Solutions," 3rd ed, Reinhold, New York, N. Y., 1958.

(12) G. Sears, E. D. Wilhoit, and L. R. Dawson, *J. Phys. Chem.*, **59**, 373 (1955).

(13) P. W. Brewster, F. C. Schmidt, and W. B. Schaap, *J. Amer. Chem. Soc.*, **81**, 5532 (1959).

(14) R. Fuoss, *ibid.*, **80**, 5059 (1958).

(15) W. R. Gilkerson, *J. Chem. Phys.*, **25**, 1199 (1956).

(16) F. Franks and D. J. G. Ives, *Quart. Rev. Chem. Soc.*, **20** (1966).

(17) G. R. Lester, T. A. Grover, and P. G. Sears, *J. Phys. Chem.*, **60**, 1076 (1966).

**Table IV:** Walden Products for Various Tetraalkylammonium Halides in Ethylene Glycol, Water, Methanol, Ethanol, Propanol, and Acetonitrile

	Ethylene glycol, $\Lambda_{07}$	Water <sup>5</sup>	Methanol <sup>3</sup>	Ethanol <sup>4</sup> $\Lambda_{070}$	Propanol <sup>4</sup>	Aceto- nitrile <sup>6</sup>
Me <sub>4</sub> NBr	1.346	1.092	0.682	0.587	0.525	0.673
Me <sub>4</sub> NI	1.281	1.081	0.715			0.678
Et <sub>4</sub> NBr	1.213	0.983	0.637	0.574	0.531	
Et <sub>4</sub> NI	1.151			0.608	0.566	
Pr <sub>4</sub> NBr	1.136	0.903	0.558	0.506	0.477	0.590
Pr <sub>4</sub> NI	1.073	0.892	0.594	0.539	0.509	0.596
Bu <sub>4</sub> NBr	1.097	0.868	0.519	0.470	0.447	0.559
Bu <sub>4</sub> NI	1.026	0.856	0.554	0.504	0.480	0.566

larger values of  $\bar{a}$ . This evidence suggests that if these salts do associate slightly in ethylene glycol, the degree of ion pairing is greater for the iodides than it is for the bromides. Such behavior would be consistent with the behavior of the tetraalkylammonium halides in other hydrogen bonding solvents.<sup>4</sup> An intercomparison of  $\bar{a}$  values for all the salts dissolved in ethylene glycol provides no useful correlation and the trend in  $\bar{a}$  values fails to follow the trend in ionic radii for the salts we studied.

As an additional test for evidence of association by the ions, we prepared a series of plots of  $\Lambda'$  against  $c$ . By rearrangement of the Fuoss-Onsager equation for nonassociated electrolytes, we obtain

$$\Lambda' \equiv \Lambda - \Lambda_0 + Sc^{1/2} - Ec \log c = J(a)c$$

If significant association by ions occurred in ethylene glycol, a plot of  $\Lambda'$  against  $c$  should exhibit considerable curvature. At most, these curves (Figure 1) exhibited only slight curvature and they support our conclusion that ionic association is minimal for the tetraalkylammonium halides in ethylene glycol. The slopes of the plots are consistently larger in the instance of the bromides as compared with the iodide salts. This result is consistent with the behavior of the tetraalkylammonium halides in water.<sup>5</sup> This behavior diverges from prediction since the slopes of these plots are  $J(a)$ , and according to Fuoss-Onsager theory the value of  $J(a)$  should increase<sup>18</sup> with increasing crystallographic radii of the tetraalkylammonium halides.

The tetraalkylammonium halides, dissolved in ethylene glycol, exhibit values of the Walden product that are larger than those reported for the salts in any other solvent (Table IV).

In order to compare our experimentally determined values of the Walden product with those predicted by a continuum model for the solvent, we used the Boyd-Zwanzig equation to compute Walden products for the various tetraalkylammonium halides in ethylene glycol.<sup>19</sup> We used the equation in the form

$$\lambda_{07} = F^2/N(6\pi r + B/r^3)$$

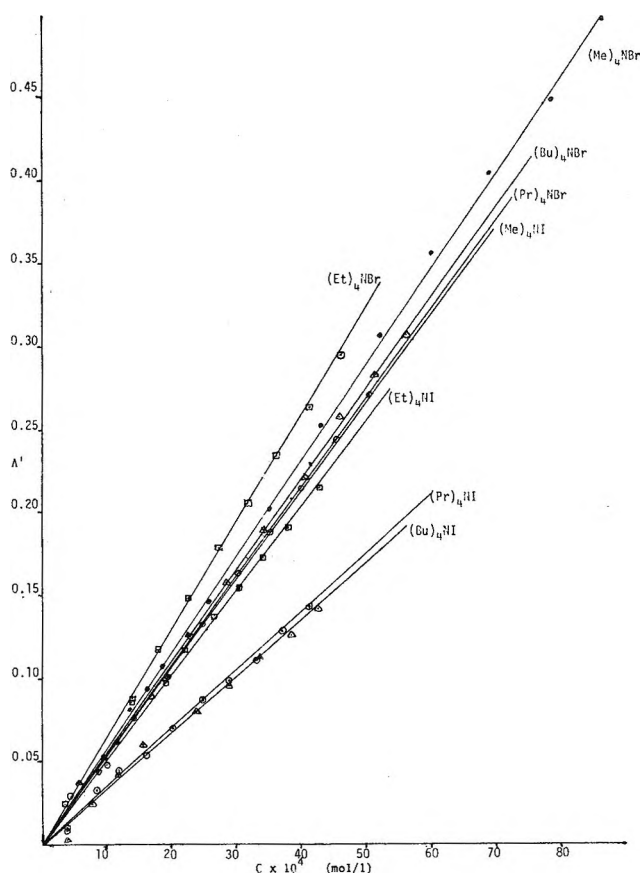


Figure 1.  $\Lambda'$  vs. concentration plots for tetraalkylammonium halides in ethylene glycol at 25°.

where  $B$  is a function only of solvent properties and is given by

$$B = (2e^2/3)(\tau/\eta)[(e_0 - e_\infty)/e_0^2]$$

We obtained values of  $\tau$ , the relaxation time of the solvent,  $e_0$ , the static dielectric constant of ethylene glycol, and  $e_\infty$ , the dielectric constant of ethylene glycol at infinite frequency from the compilation of Buckley

(18) R. M. Fuoss and F. Accascina, "Electrolytic Conductance," Interscience, New York, N. Y., 1959.

(19) R. Zwanzig, *J. Chem. Phys.*, **38**, 1603 (1963).

and Maryott.<sup>20</sup> The calculated values of the Walden products are summarized in Table V.

**Table V:** Walden Products for Tetraalkylammonium Halides in Ethylene Glycol Calculated with Boyd-Zwanzig Equation

Salt	$\frac{\Lambda_{0\eta}}{(\lambda_{0^+} + \lambda_{0^-})}$
Me <sub>4</sub> NBr	0.449
Me <sub>4</sub> NI	0.464
Et <sub>4</sub> NBr	0.427
Et <sub>4</sub> NI	0.442
Pr <sub>4</sub> NBr	0.407
Pr <sub>4</sub> NI	0.422
Bu <sub>4</sub> NBr	0.394
Bu <sub>4</sub> NI	0.409

The calculated values ( $\Lambda_{0\eta}$ ) account for  $\sim 35\%$  of the experimentally determined Walden products. This result is consistent with the predictions of Frank,<sup>21</sup> who shows that the Boyd-Zwanzig equation cannot account for the relatively large values of the Walden product exhibited by ions in water. The discrepancy between our experimental and calculated values of the Walden product agrees qualitatively with the discrepancies between these values for salts dissolved in methanol, ethanol, and propanol.<sup>22</sup>

In summary, the behavior of tetraalkylammonium halides in ethylene glycol bears an interesting resemblance to the behavior of these salts in water. The tetraalkylammonium and halide ions do not appear to associate in either solvent, and the behavior of  $J(a)$

as a function of ionic radii for salts dissolved in ethylene glycol resembles that for salts dissolved in water. The tetraalkylammonium halides exhibit large values of the Walden product ( $\Lambda_{0\eta}$  data) when they are dissolved in ethylene glycol or in water. Finally, the Boyd-Zwanzig equation predicts a maximum for  $\lambda_{0\eta}$  at an ionic radius for  $r = (B/2\pi)^{1/4}$ . For ethylene glycol  $r = 2.5 \text{ \AA}$ , for water  $r = 2.3 \text{ \AA}$ , and for methanol  $r = 5.7 \text{ \AA}$ . Because we do not have values for single ion conductances in ethylene glycol, we are unable to show the relationship between the calculated values for  $r$  and the values of  $r$  determined by experiment. Evans and Gardam<sup>22</sup> have shown the experimental values of  $r$  for ions in methanol and butanol are considerably smaller than corresponding values of  $r$  calculated from the Boyd-Zwanzig equation.

These data coupled with the findings of Crickard and Skinner suggest some interesting qualities for ionic solutions of ethylene glycol. We are continuing this study by measuring conductance of the alkali halides in ethylene glycol and measuring the variation of this conductance as a function of temperature.

*Acknowledgment.* We wish to thank Professor D. F. Evans of Case Western Reserve University for loaning us equipment. We also wish to thank the Mack Foundation for providing financial support.

(20) F. Buckley and A. A. Maryott, *Nat. Bur. Stand. (U. S.) Circular*, No. 589 (1958).

(21) H. S. Frank, "Chemical Physics of Ionic Solutions," B. G. Conway and R. G. Barradas, Ed., Wiley, New York, N. Y., 1966, p 61.

(22) D. F. Evans and P. Gardam, *J. Phys. Chem.*, **73**, 158 (1969).

## Transport Behavior in Dimethyl Sulfoxide. II. Viscosity Studies

by Neng-Ping Yao and Douglas N. Bennion\*

*Energy and Kinetics Department, School of Engineering and Applied Science,  
University of California, Los Angeles 90024 (Received May 11, 1970)*

*Publication costs borne completely by The Journal of Physical Chemistry*

Viscosities of  $\text{NaClO}_4$ ,  $\text{NaSCN}$ ,  $\text{NaB(Ph)}_4$ ,  $(i\text{-amyl})_3\text{BuNB(Ph)}_4$ , and  $\text{CF}_3\text{SO}_3\text{Na}$  in DMSO were determined over a concentration range  $10^{-3}$  M to near saturation and the temperature range 25–55°. The viscosity data were analyzed with the Jones-Dole equation up to approximately 0.1 M. Ionic viscosity  $B_{\pm}$  coefficients, based on equal  $B_{\pm}$  coefficients for  $(i\text{-amyl})_3\text{BuN}^+$  and  $\text{B(Ph)}_4^-$  ions, were interpreted by the Einstein equation.  $(i\text{-amyl})_3\text{BuN}^+$ ,  $\text{B(Ph)}_4^-$ , and  $\text{Na}^+$  ions have spherical kinetic entities with effective radii of 4.90, 4.90, and 3.83 Å, respectively, in viscous flow.  $\text{Na}^+$  ion is solvated.  $\text{CF}_3\text{SO}_3^-$ ,  $\text{SCN}^-$ , and  $\text{ClO}_4^-$  are unsolvated in DMSO and have nonspherical kinetic entities in viscous flow. Effective ionic radii obtained from the  $B_{\pm}$  coefficients are insensitive to temperature for the ions. The activation energy for viscous flow for the electrolyte solutions was interpreted by the activated rate process. The results show that  $(i\text{-amyl})_3\text{BuN}^+$ ,  $\text{B(Ph)}_4^-$ , and the  $\text{Na}^+$  ions present obstruction while  $\text{CF}_3\text{SO}_3^-$  and  $\text{SCN}^-$  ions present little or no influence on the viscous flow. The  $\text{ClO}_4^-$  ion appears to be a structure breaker in DMSO and tends to lower the activation energy for viscous flow in the dilute concentration range. The ionic activation energy for viscous flow decreases in the order of  $(i\text{-amyl})_3\text{BuN}^+ = \text{B(Ph)}_4^- > \text{Na}^+ > \text{SCN}^- \simeq \text{CF}_3\text{SO}_3^- > \text{ClO}_4^-$ .

### Introduction

Dimethyl sulfoxide (DMSO) is an aprotic solvent which has useful properties for application in organic syntheses<sup>1,2</sup> and in electrochemical systems.<sup>3</sup> The dipolar character of the DMSO molecules makes the solvent a good nucleophilic agent and tends to enhance reaction rates and yields of many organic syntheses by stabilizing charged intermediates in the reactions.<sup>1</sup> The good dipolar and physical properties of DMSO coupled with the stability of some potentially useful electrode materials in DMSO make the solvent theoretically promising for high-energy density battery application. Transport behavior of ions in DMSO as applied to battery application and the function of DMSO solvent molecules in organic reactions both require the understanding of the nature of ion-solvent interaction. Transport parameters of electrolyte solutions such as ionic conductance and viscosity can provide information concerning the nature of the kinetic entities from which the ion-solvent interaction can be inferred.

In a previous paper, ionic conductance studies in DMSO were reported.<sup>4</sup> In this paper the results of viscosity measurements on solutions of sodium perchlorate, sodium thiocyanate, sodium tetraphenylboride, sodium trifluoromethanesulfonate, and triisooamylbutylammonium tetraphenylboride in DMSO are reported. Concentrations over the range  $10^{-3}$  M to near saturation and temperatures from 25 to 55° were studied. Single ionic viscosity  $B$  coefficients are calculated based on equal ionic viscosity  $B$  coefficients assigned to the triisooamylbutylammonium and tetraphenylboride ions.<sup>5</sup> These ions are large, centrally symmetric, and have been shown to have the same ionic

mobility in methanol.<sup>6</sup> The ionic size is inferred by applying the Einstein viscosity expression for colloidal suspensions to the ionic particles.<sup>7,8</sup> The ionic viscosity  $B$  coefficients and their temperature variation are qualitatively interpreted in terms of their effective ionic radii. The viscous flow is interpreted as an activated rate process. The activation energies and entropies for viscous flow are calculated, and the significance of the effect of various ions on these quantities discussed.

### Experimental Section

Solvent purification and the preparation and purification of the salts have been described elsewhere.<sup>4</sup> The DMSO purified by vacuum distillation contained less than 30 ppm of water determined by Karl Fischer potentiometric titration. No organic impurity was detected by nmr analysis. Melting points and ir spectra of the purified salts were identical to the previously reported values in the literature.<sup>4</sup>

All solutions were prepared by weight (corrected to vacuum) in a nitrogen atmosphere drybox. The volume concentration was obtained from the weight concentration and the density.

Kinematic viscosity measurements were made with modified Cannon-Ubbelohde viscometers in an appa-

- (1) W. C. Kuryla, *J. Appl. Polym. Sci.*, **9**, 1019 (1965).
- (2) A. J. Parker, *Quart. Rev. Chem. Soc.*, **16**, 163 (1962).
- (3) J. N. Butler, *J. Electroanal. Chem.*, **14**, 89 (1967).
- (4) Part I: N. P. Yao and D. N. Bennion, *J. Electrochem. Soc.*, in press.
- (5) D. F. T. Tuan and R. M. Fuoss, *J. Phys. Chem.*, **67**, 1343 (1963).
- (6) M. A. Coplan and R. M. Fuoss, *ibid.*, **68**, 1177 (1964).
- (7) A. Einstein, *Ann. Phys.*, **19**, 289 (1906).
- (8) T. F. Ford, *J. Phys. Chem.*, **64**, 1168 (1960).

ratus manipulated under a nitrogen atmosphere.<sup>9</sup> Four semimicro viscometers with calibrated cell constants of respectively 0.001836, 0.003910, 0.00774, and 0.01469 cSt/sec were supplied by Cannon Instrument Co., State College, Pa. The cell constants were independent of temperature. An appropriate viscometer was selected for a particular run to give an efflux time between 500 and 900 sec. The kinetic energy correction, the surface tension correction, and the error due to viscometer misalignment were calculated to be approximately 0.00018, 0, and <0.1%, respectively. The individual readings for the three or four measurements at a set temperature agreed with each other to within 0.2 sec, *i.e.*,  $\pm 0.04\%$  for a 500-sec efflux time, and  $\pm 0.02\%$  for a 900-sec efflux time. Overall accuracy of the viscosity measurements was estimated to be better than 0.1%.

Density measurements were made with a two-capillary relative method which is similar to that described by McAuley, *et al.*<sup>10</sup> Dibutyl phthalate served as the reference fluid, and its density has been reported by Kempinen and Gokcen.<sup>11</sup> Three or four measurements at each temperature were taken and the average value is reported. Overall accuracy of the density measurements was estimated to be  $\pm 0.1\%$ .

Both viscosity and density measurements were made in a double-wall viscosimeter oil temperature bath (E. H. Sargent and Co.), and constant temperature was maintained to  $\pm 0.03^\circ$  as checked with a Beckmann differential thermometer. Equilibrium temperature of the oil bath was read on an Anschutz-type mercury thermometer with accuracy  $\pm 0.1^\circ$ .

## Results

Density and viscosity of distilled DMSO at 25, 35, 45, and 55° are given in Table I.<sup>12</sup> As can be seen from Table II,<sup>12</sup> the maximum relative viscosity,  $\eta/\eta_0$ , for the electrolyte solutions did not exceed 1.25. The NaClO<sub>4</sub> solution has a maximum  $\eta/\eta_0$  value of approximately 4.6 at a concentration of 1.5 M at 25°. The low values of  $\eta/\eta_0$  for most of the solutions, except for NaClO<sub>4</sub> solutions, were due to the low solubility of the salts in DMSO. The  $\eta/\eta_0$  vs.  $C$  plots for the electrolyte solutions exhibit approximately linear dependence of  $\eta/\eta_0$  on concentration within the concentration range.

The viscosity data were fitted with the empirical Jones and Dole<sup>13</sup> equation.

$$\frac{\eta}{\eta_0} = 1 + AC^{1/2} + BC \quad (1)$$

where  $\eta$  and  $\eta_0$  are solution and solvent viscosities,  $C$  is molar concentration, and  $A$ ,  $B$  are constants specific to the ion and solvent. Viscosity  $A$  and  $B$  coefficients for the electrolytes were obtained from plots,  $[(\eta/\eta_0) - 1]/C^{1/2}$  vs.  $C^{1/2}$ , such as those shown in Figure 1. The linear lines in Figure 1 give the viscosity  $A$  coefficient at the intercept to the ordinate and the viscosity  $B$

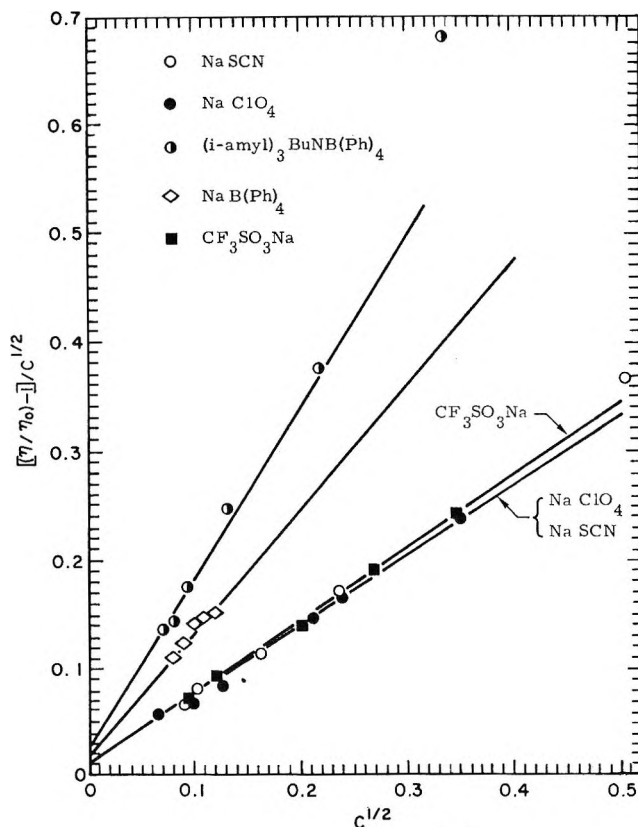


Figure 1.  $(\eta/\eta_0 - 1)/C^{1/2}$  vs.  $C^{1/2}$  for electrolyte solutions at 25°.

coefficient from the slope for each electrolyte solution in accordance with eq 1.

The viscosity  $A$  coefficient could not be determined unambiguously because  $(\eta/\eta_0 - 1)/C^{1/2}$  values at extremely low concentrations scattered due to the experimental inaccuracies at these concentrations. A least-squares fitting yielded, in some cases, negative viscosity  $A$  coefficients. Such a result appears to be without physical significance.<sup>14</sup> A similar difficulty was encountered by Kay, *et al.*,<sup>15</sup> who had to correct their viscosity data for some tetraalkylammonium salts in aqueous solutions at low concentrations. They attributed the error to a surface tension effect resulting from a minute trace of surface active impurity in the

(9) N. P. Yao, "Transport Behavior in Dimethyl Sulfoxide," Ph.D. Thesis, University of California, Los Angeles, Calif., June 1969.

(10) W. T. McAuley, E. Rhodes, and A. R. Ubbelohde, *Proc. Roy. Soc., Ser. A*, **289**, 151 (1966).

(11) A. I. Kempinen and N. A. Gokcen, *J. Phys. Chem.*, **60**, 126 (1956).

(12) Tables I and II will appear immediately following this article in the microfilm edition of this volume of the journal. Single copies may be obtained from the Reprint Department, ACS Publications, 1155 Sixteenth St., N.W., Washington, D. C. 20036. Remit \$3.00 for photocopy or \$2.00 for microfilm.

(13) G. Jones and M. Dole, *J. Amer. Chem. Soc.*, **51**, 2950 (1929).

(14) H. S. Harned and B. B. Owen, "The Physical Chemistry of Electrolytic Solutions," 3rd ed, Reinhold, New York, N. Y., 1958.

(15) R. L. Kay, T. Vituccio, C. Zawoyski, and D. F. Evans, *J. Phys. Chem.*, **70**, 2336 (1966).

salts. However, the viscosity  $A$  coefficients can be calculated from the mobility data and solvent properties based on the theoretical consideration of ion-ion interaction<sup>16</sup> in viscous flow. The limiting theoretical  $A$  coefficient, designated by  $S_{(\eta)}$ , for uni-univalent electrolytes is of the form

$$S_{(\eta)} = \frac{\beta^*}{320} \frac{\Lambda_0}{\lambda_+^{\circ} \lambda_-^{\circ}} \left[ 1 - 0.6863 \left( \frac{\lambda_+^{\circ} - \lambda_-^{\circ}}{\Lambda_0} \right)^2 \right] \quad (2)$$

where

$$\beta^* = \left( \frac{28.98 \times 2\sqrt{2}}{\eta_0(\epsilon_0 T)^{1/2}} \right) \left( \frac{|z_+| + |z_-|}{2} \right) \left( \frac{\nu|z_+z_-|}{2} \right)^{1/2} \quad (3)$$

$\lambda_i^{\circ}$  is the limiting ionic equivalent conductance of  $i$  ion,  $z_i$  is the valence of  $i$  ion,  $\nu = \nu_+ + \nu_-$  is the number of ions produced by dissociation of one molecule of electrolyte,  $\Lambda_0$  is the limiting equivalent conductance of the electrolyte,  $T$  is absolute temperature, and  $\eta_0, \epsilon_0$  are solvent viscosity and dielectric constant, respectively. The limiting form of eq 2 for the special case of  $\lambda_+^{\circ} = \lambda_-^{\circ}$  was in fact derived earlier by Falkenhagen, *et al.*<sup>17</sup> Comparison of the experimental  $A$  coefficient with the limiting theoretical  $S_{(\eta)}$  coefficient for many aqueous strong electrolytes showed good agreement.<sup>14</sup> Theoretical extension of the limiting eq 2 was made from statistical consideration by Falkenhagen, *et al.*,<sup>18</sup> and more recently by Kraeft,<sup>19</sup> who accounted for the finite ion size and the short-range repulsive forces between the ions. As they noted, however, the ion size consideration in the extended theory does not reproduce the characteristic variations of the viscosity coefficient, the same conclusion reached by Pitts.<sup>20</sup> Any significant success in viscosity theory over an extended concentration range will have to come from specific consideration of the ion-solvent and higher-order interactions, all of which become more important in a concentrated electrolyte.

The limiting theoretical  $S_{(\eta)}$  coefficients for the electrolyte solutions have been summarized in Table III as a function of temperature. The values vary between  $1 \times 10^{-2}$  and  $2 \times 10^{-2}$  and decrease in the order  $(i\text{-amyl})_3\text{BuNB(Ph)}_4 > \text{NaB(Ph)}_4 > \text{NaSCN} \simeq \text{CF}_3\text{SO}_3\text{Na} \simeq \text{NaClO}_4$ . The theoretical  $S_{(\eta)}$  coefficients for the electrolytes have been calculated using the limiting equivalent conductance values and the limiting ionic equivalent conductance values for each electrolyte which have been reported elsewhere.<sup>4</sup>  $\beta^*$  values, defined in eq 3, were 35.10, 42.54, 50.44, and 49.02 at 25, 35, 45, and 55°, respectively, for the electrolytes in DMSO.

In Figure 1 the intercepts were forced close to  $S_{(\eta)}$  while still retaining a minimum standard deviation with the experimental points. The data can be approximated by a straight line for each electrolyte solution up to concentrations of approximately 0.16  $M$ ; *i.e.*,  $C^{1/2} = 0.4$  although  $(i\text{-amyl})_3\text{BuNB(Ph)}_4$  solutions showed

**Table III:** Theoretical  $S_{(\eta)}$  Coefficients for the Electrolytes in DMSO

Salt	$S_{(\eta)}$ coefficient $\times 10^2$			
	25°	35°	45°	55°
$(i\text{-amyl})_3\text{BuNB(Ph)}_4$	1.985	1.987	1.969	1.968
$\text{NaB(Ph)}_4$	1.737	1.735	1.728	1.721
$\text{NaSCN}$	1.038	1.045	1.052	1.062
$\text{CF}_3\text{SO}_3\text{Na}$	1.210	1.216	1.223	1.230
$\text{NaClO}_4$	1.158	1.163	1.176	1.164

positive deviation to the linear line at a concentration of approximately 0.04  $M$ .

Viscosity  $B$  coefficients for the electrolytes were obtained from the slopes of  $(\eta/\eta_0 - 1)/C^{1/2}$  vs.  $C^{1/2}$  plots. The values are summarized in Table IV. The viscosity  $B$  coefficients show only a slight decrease with increasing temperature. The weak temperature dependence of  $B$  coefficients in nonaqueous solvents such as in DMSO of the present work and in methanol or acetonitrile<sup>16</sup> is in contrast to the stronger temperature dependence of  $B$  coefficients of some electrolytes in aqueous solutions.<sup>15,21</sup>

**Table IV:** Viscosity  $B$  Coefficients for the Electrolytes in DMSO

Salt	$B$ coefficients			
	25°	35°	45°	55°
$(i\text{-amyl})_3\text{BuNB(Ph)}_4$	1.57	1.47	1.44	1.44
$\text{NaB(Ph)}_4$	1.14	1.07	1.01	1.00
$\text{NaSCN}$	0.62	0.60	0.56	0.58
$\text{CF}_3\text{SO}_3\text{Na}$	0.64	0.61	0.59	0.58
$\text{NaClO}_4$	0.62	0.60	0.56	0.55

The viscosity  $B$  coefficients have been found to be approximately additive properties of the respective ionic components: *i.e.*,  $B = B_+ + B_-$ , for many aqueous electrolyte solutions.<sup>22,23</sup> Separation of the observed  $B$  coefficient into its ionic  $B_{\pm}$  coefficients has been an arbitrary process<sup>22-24</sup> because a quantity analogous to transference number in mobility assignments does not exist in viscous flow. Tuan and Fuoss<sup>5</sup> studied the viscosities of many quaternary ammonium salts in ace-

(16) L. Onsager and R. M. Fuoss, *J. Phys. Chem.*, **36**, 2689 (1932).

(17) H. Falkenhagen and M. Dole, *Phys. Z.*, **30**, 611 (1929); H. Falkenhagen and E. L. Vernon, *ibid.*, **33**, 140 (1932).

(18) H. Falkenhagen and G. Kelbg, *Z. Elektrochem.*, **56**, 834 (1952); H. Falkenhagen and G. Kelbg, *Discuss. Faraday Soc.*, **24**, 20 (1957).

(19) W. D. Kraeft, *Z. Phys. Chem.*, **233**, 266 (1966).

(20) E. Pitts, *Proc. Roy. Soc., Ser. A*, **217**, 43 (1953).

(21) D. F. Evans, G. P. Cunningham, and R. L. Kay, *J. Phys. Chem.*, **70**, 2974 (1966).

(22) W. M. Cox and J. H. Wolfenden, *Proc. Roy. Soc., Ser. A*, **145**, 475 (1934).

(23) M. Kaminsky, *Discuss. Faraday Soc.*, **24**, 171 (1957).

(24) R. W. Gurney, "Ionic Processes in Solution," McGraw-Hill, New York, N. Y., 1953.

tonitrile and several other nonaqueous solvents at 25° and equal ionic  $B_{\pm}$  coefficients were assigned to  $\text{Bu}_4\text{N}^+$  and  $\text{B}(\text{Ph})_4^-$  ions on the basis of equal size and equal mobility.

Assuming equal ionic viscosity  $B_{\pm}$  coefficients for  $(i\text{-amyl})_3\text{BuN}^+$  and  $\text{B}(\text{Ph})_4^-$  ions in DMSO because of their equal, spherical size and low surface charge density, the viscosity  $B$  coefficients for other electrolytes can be separated into their respective ionic viscosity  $B_{\pm}$  coefficients. The ionic  $B_{\pm}$  coefficients are summarized in Table V as a function of temperature.

As can be seen from Table V, the ionic  $B_{\pm}$  coefficient for the  $\text{Na}^+$  ion decreases while the  $B_{\pm}$  coefficients for  $\text{ClO}_4^-$ ,  $\text{SCN}^-$ , and  $\text{CF}_3\text{SO}_3^-$  ions increase with increasing temperature. The  $B_{\pm}$  coefficient for the  $(i\text{-amyl})_3\text{BuN}^+$  ion decreases slightly with increasing temperature and remains practically constant above 35°.

Table V: Ionic Viscosity  $B_{\pm}$  Coefficients in DMSO

Ion	Temperature			
	25°	35°	45°	55°
$(i\text{-amyl})_3\text{BuN}^+$	0.79	0.74	0.72	0.72
$\text{B}(\text{Ph})_4^-$	0.79	0.74	0.72	0.72
$\text{Na}^+$	0.35	0.33	0.29	0.28
$\text{SCN}^-$	0.26	0.27	0.27	0.30
$\text{CF}_3\text{SO}_3^-$	0.28	0.28	0.29	0.31
$\text{ClO}_4^-$	0.26	0.26	0.27	0.27

The viscosity  $B$  coefficient is approximately related to the volume fraction of the solute particles according to the Einstein equation,<sup>7</sup> *i.e.*

$$B = 2.5 \frac{\phi}{C} = 2.5 \frac{4}{3} \frac{\pi(r_+^3 + r_-^3)N}{1000} \quad (4)$$

where 2.5 is the shape factor for a sphere,  $\phi$  is the volume fraction of the solute particles in cubic centimeters of solute/cubic centimeters of solution,  $r_{\pm}$  is the effective radius for a spherical ion, and  $N$  is Avogadro's number. The effective ionic radii can, therefore, be obtained from the ionic viscosity  $B_{\pm}$  coefficient using eq 4. The values are shown in Table VI. In the sixth column of Table VI the "corrected" Stokes' radii at 25° which were obtained from conductance studies<sup>4</sup> are listed. The estimated crystallographic radii for the ions<sup>4</sup> are given in the last column of the table. Comparison of the "corrected" Stokes' radii from the conductance studies with the effective ionic radii at 25° from the viscosity studies show that agreement is reasonably good for  $(i\text{-amyl})_3\text{BuN}^+$ ,  $\text{B}(\text{Ph})_4^-$ , and  $\text{Na}^+$  ions, but the ionic radii for  $\text{SCN}^-$ ,  $\text{CF}_3\text{SO}_3^-$ , and  $\text{ClO}_4^-$  ions obtained from  $B_{\pm}$  coefficients are significantly larger than the corresponding  $r_{\text{cor}}$  from conductance data. A possible explanation for the discrepancy is that eq 4 assumes a shape factor of 2.5 which implies the effective ionic entity is spherical. The results, there-

fore, appear to indicate that  $(i\text{-amyl})_3\text{BuN}^+$ ,  $\text{B}(\text{Ph})_4^-$ , and  $\text{Na}^+$  ions are effectively spherical as expected, while  $\text{SCN}^-$ ,  $\text{CF}_3\text{SO}_3^-$ , and  $\text{ClO}_4^-$  ions assume other shapes in viscous flow. The average value of 4.90 Å obtained for the effective radius of  $\text{B}(\text{Ph})_4^-$  ion in the present work compares favorably with the 4.81-Å value obtained for the same ion in acetonitrile<sup>5</sup> from viscosity data.

Table VI: Effective Ionic Radii in Ångströms as Calculated from Ionic Viscosity  $B_{\pm}$  Coefficients

Ion	Temperature				$r_{\text{cor}}$ (25°)	Esti- mated $r_c$
	25°	35°	45°	55°		
$(i\text{-amyl})_3\text{BuN}^+$	5.01	4.90	4.85	4.85	5.12	4.94
$\text{B}(\text{Ph})_4^-$	5.01	4.90	4.85	4.85	5.12	4.94
$\text{Na}^+$	3.83	3.74	3.59	3.54	4.32	0.95
$\text{SCN}^-$	3.46	3.50	3.50	3.62	2.37	2.27
$\text{CF}_3\text{SO}_3^-$	3.54	3.54	3.59	3.67	3.03	2.96
$\text{ClO}_4^-$	3.46	3.46	3.50	3.50	2.82	2.40

Arrhenius-type activation energies for viscous flow,  $\Delta E_{\eta}^{\dagger}$ , have been calculated for the electrolyte solutions as a function of concentration. The values are plotted in Figure 2 as a function of concentration with a  $\pm 0.03$ -kcal/mol confidence level. As can be seen in Figure 2, the activation energies for viscous flow increase almost linearly with increasing concentration.  $\Delta E_{\eta}^{\dagger}$  for  $\text{NaClO}_4$  solution increases rapidly above 0.2  $M$ . In the dilute concentration range  $\Delta E_{\eta}^{\dagger}$  decreases in the order of  $(i\text{-amyl})_3\text{BuNB}(\text{Ph})_4 \cong \text{NaB}(\text{Ph})_4 > \text{NaSCN} \cong \text{CF}_3\text{SO}_3\text{Na} > \text{NaClO}_4$ .

According to the concept of rate processes,<sup>25</sup> the free energy of activation,  $\Delta G_{\eta}^{\dagger}$ , for viscous flow is given by

$$\Delta G_{\eta}^{\dagger} = RT \ln \frac{\eta V}{hN} \quad (5)$$

where  $h$  is the Planck constant,  $N$  is Avogadro's number,  $R$  is the gas constant, and  $V$  is the volume of 1 mol of solution particles. The values of  $\Delta G_{\eta}^{\dagger}$  have been calculated for the electrolytes as a function of concentration and are summarized in Table VII.

If the logarithmic Jones-Dole equation, eq 1, is differentiated with respect to  $1/T$  neglecting the small ion-ion interaction term,  $AC^{1/2}$ , the following equation is obtained

$$R \frac{d \ln \eta}{d\left(\frac{1}{T}\right)} = R \frac{d \ln \eta_0}{d\left(\frac{1}{T}\right)} + \frac{R}{1 + BC} \frac{d(1 + BC)}{d\left(\frac{1}{T}\right)} \quad (6)$$

where  $R(d \ln \eta/d(1/T))$  and  $R(d \ln \eta_0/d(1/T))$  in eq 6 can be identified as the activation energies for

(25) S. Glasstone, K. J. Laidler, and H. Eyring, "The Theory of Rate Processes," McGraw-Hill, New York, N. Y., 1941.



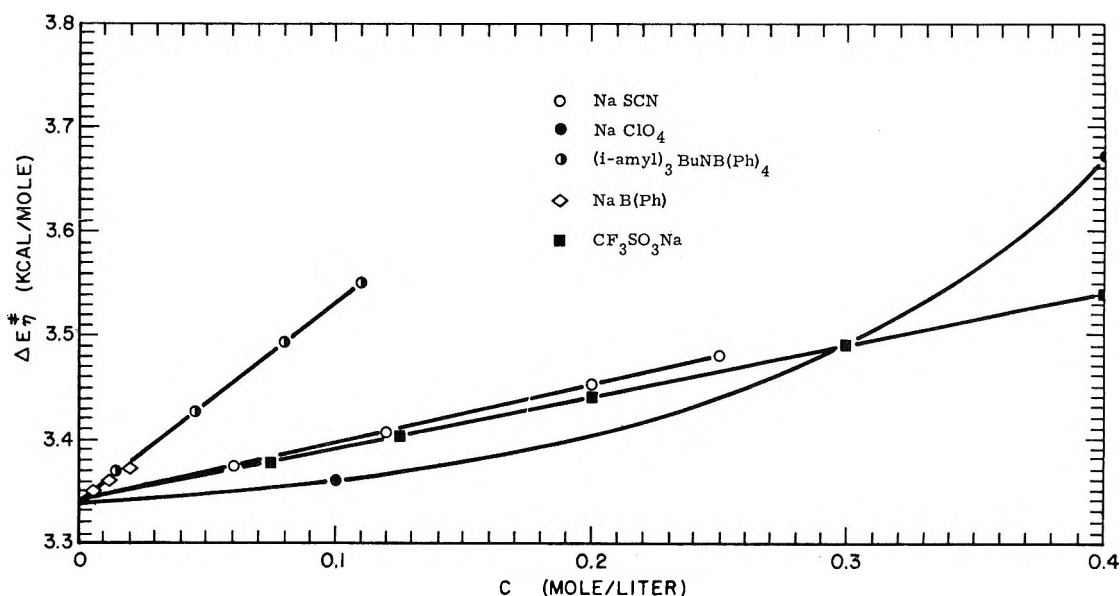


Figure 2. Activation energies for viscous flow as a function of concentration for electrolytes in DMSO.

**Table VII:** Free Energy of Activation,  $\Delta G_{\eta}^{\ddagger}$ , in Kilocalories/Mole, for Viscous Flow in DMSO at 25°

NaClO <sub>4</sub>		NaSCN		NaB(Ph) <sub>4</sub>		(i-amyl) <sub>3</sub> BuNB(Ph) <sub>4</sub>		CF <sub>3</sub> SO <sub>3</sub> Na	
C	$\Delta G_{\eta}^{\ddagger}$	C	$\Delta G_{\eta}^{\ddagger}$	C	$\Delta G_{\eta}^{\ddagger}$	C	$\Delta G_{\eta}^{\ddagger}$	C	$\Delta G_{\eta}^{\ddagger}$
0.01006	3.48	0.00582	3.49	0.00668	3.49	0.0089	3.49	0.0152	3.48
0.04563	3.50	0.0108	3.49	0.0102	3.49	0.0167	3.50	0.0420	3.50
0.1230	3.53	0.0267	3.49	0.0149	3.49	0.0470	3.54	0.0727	3.51
0.3807	3.62	0.0561	3.50	0.0210	3.50	0.1046	3.62	0.122	3.52
1.250	4.30	0.2551	3.56					0.417	3.56

solution,  $\Delta E_{\eta}^{\ddagger}$ , and for solvent,  $\Delta E_{\eta_0}^{\ddagger}$ , respectively. Equation 6 can now be written in a formal way, as

$$\Delta E_{\eta}^{\ddagger} = \Delta E_{\eta_0}^{\ddagger} + \Delta E_s^{\ddagger} \quad (7)$$

where  $\Delta E_s^{\ddagger} = [R/(1 + BC)][d(1 + BC)/d(1/T)]$  and may be interpreted as the increase or decrease of the activation energy for viscous flow for the pure solvent due to the presence of the ions. This view is reasonable in that at the maximum concentration, *i.e.*, 0.1 M, where the Jones-Dole equation is valid, each ion is surrounded by approximately 70 or more solvent molecules in DMSO solution and that  $\Delta E_s^{\ddagger}$  is only a small fraction of  $\Delta E_{\eta}^{\ddagger}$  or  $\Delta E_{\eta_0}^{\ddagger}$ . Thus it is convenient to interpret  $\Delta E_s^{\ddagger}$  as the effective influence of ions upon the viscous flow of the solvent molecules rather than relating  $\Delta E_s^{\ddagger}$  to the activation energy associated with the ion movements themselves.

Inasmuch as the viscosity *B* coefficients are additive properties of the ions, one may assume that  $\Delta E_s^{\ddagger}$  is associated with the separate contributions by the respective ions to the solvent viscosity. Equation 7 is now written in the form

$$\Delta E_{\eta}^{\ddagger} = \Delta E_{\eta_0}^{\ddagger} + \nu_+ \Delta E_+^{\ddagger} + \nu_- \Delta E_-^{\ddagger} \quad (8)$$

where  $\Delta E_{\eta_0}^{\ddagger}$  is the activation energy for pure solvent

( $\Delta E_{\eta_0}^{\ddagger} = 3.34$  kcal/mol in DMSO) and  $\Delta E_+^{\ddagger}$ ,  $\Delta E_-^{\ddagger}$ , are the change of activation energies of the solvent caused by the cation and anion.  $\Delta E_+^{\ddagger}$  and  $\Delta E_-^{\ddagger}$  will hereafter be termed ionic activation energies, but should not be confused with the activation energies for ions. By these definitions ionic activation energies are interpreted as the change in activation energy for movement of the solvent molecules due to the presence of the ions. The activation energy for an ion is that activation energy for an ion itself to make a "jump" into a neighboring "hole." The latter is assumed to make a negligible contribution to the total observed activation energy at low concentrations for this model. A similar type of equation to eq 8 may be written for the free energy of activation,  $\Delta G_{\eta}^{\ddagger}$ , for viscous flow with  $\Delta G_{\eta_0}^{\ddagger} = 3.477$  kcal/mol in DMSO. Equation 8 is similar to that proposed by Nightingale and Benck<sup>26</sup> for aqueous solutions. With the assumptions that  $\Delta E_+^{\ddagger} = \Delta E_-^{\ddagger}$  and  $\Delta G_+^{\ddagger} = \Delta G_-^{\ddagger}$  for (i-amyl)<sub>3</sub>BuN<sup>+</sup> and B(Ph)<sub>4</sub><sup>-</sup> ions, the ionic activation energy,  $\Delta E_{\pm}^{\ddagger}$ , and ionic free energy of activation,  $\Delta G_{\pm}^{\ddagger}$ , for other ions can be calculated.

(26) E. R. Nightingale, Jr. and R. F. Benck, *J. Phys. Chem.*, **63**, 1777 (1959).

The values of ionic activation energy,  $\Delta E_{\pm}^{\ddagger}$ , and ionic free energy of activation,  $\Delta G_{\pm}^{\ddagger}$ , are given in Table VIII at concentration 0.02 *M* and 25°.

**Table VIII:** Ionic Energies and Entropies of Activation for Viscous Flow in DMSO at 25° and *C* = 0.02 *M*

Ion	$\Delta E_{\pm}^{\ddagger}$ , cal/mol	$\Delta G_{\pm}^{\ddagger}$ , cal/mol	$\Delta S_{\pm}^{\ddagger}$ , eu
( <i>i</i> -amyl) <sub>3</sub> BuN <sup>+</sup>	+20	+13.5	+0.022
B(Ph) <sub>4</sub> <sup>-</sup>	+20	+13.5	+0.022
Na <sup>+</sup>	+10	+6.5	+0.012
SCN <sup>-</sup>	+2	+0.5	+0.005
CF <sub>3</sub> SO <sub>3</sub> <sup>-</sup>	0	-1.5	+0.005
ClO <sub>4</sub> <sup>-</sup>	-8	-1.5	-0.022

Assuming that the ionic activation enthalpy does not differ appreciably from the ionic activation energy,  $\Delta E_{\pm}^{\ddagger}$ , the ionic entropy of activation  $\Delta S_{\pm}^{\ddagger}$  may also be calculated as

$$\Delta S_{\pm}^{\ddagger} = (\Delta E_{\pm}^{\ddagger} - \Delta G_{\pm}^{\ddagger})/T$$

The values of  $\Delta S_{\pm}^{\ddagger}$  at *C* = 0.02 *M* and 25° are also shown in Table VIII. It is interesting to note that the values of  $\Delta E_{-}^{\ddagger}$  and  $\Delta S_{-}^{\ddagger}$  for ClO<sub>4</sub><sup>-</sup> ion are negative. The ionic activation energy decreases in the order of (*i*-amyl)<sub>3</sub>BuN<sup>+</sup> = B(Ph)<sub>4</sub><sup>-</sup> > Na<sup>+</sup> > SCN<sup>-</sup> ≅ CF<sub>3</sub>SO<sub>3</sub><sup>-</sup> > ClO<sub>4</sub><sup>-</sup>, and the corresponding ionic entropy of activation decreases in the same order.

## Discussion

The viscosity *B* coefficients for the electrolyte solutions have been given in Table IV as a function of temperature. The *B* coefficients are all positive in DMSO indicating that the viscosity of the solutions increases with increasing concentration of the electrolytes. The effect of the temperature on the *B* coefficients is weak in DMSO which appears to be general in most of the nonaqueous solvents in which the solvent structures are not as highly associated as that of H<sub>2</sub>O.

The ionic *B*<sub>±</sub> coefficients for (*i*-amyl)<sub>3</sub>BuN<sup>+</sup> and B(Ph)<sub>4</sub><sup>-</sup> ions show some decrease with increasing temperature between 25 and 35° in Table V. But the limiting Walden product, λ<sub>070</sub>, for the two ions has been found to be independent of temperature from the conductance studies.<sup>4</sup> The discrepancy is likely due to the error in obtaining the viscosity *B* coefficients for (*i*-amyl)<sub>3</sub>BuNB(Ph)<sub>4</sub> electrolytes from the Jones and Dole plots. The data for (*i*-amyl)<sub>3</sub>BuNB(Ph)<sub>4</sub> electrolytes were more scattered and showed positive deviation from the straight lines at comparatively low concentration; *i.e.*, approximately 0.02 *M* in Figure 1. The limiting Walden product is believed to be more reliable. Adjusting the value of ionic *B*<sub>±</sub> coefficient for (*i*-amyl)<sub>3</sub>BuN<sup>+</sup> or B(Ph)<sub>4</sub><sup>-</sup> ions at 25° from 0.79 to 0.72 in order to be consistent with the limiting Walden

product does not alter the temperature dependence of ionic *B*<sub>±</sub> coefficients for other ions. In fact this discrepancy, *i.e.*, Δ*B*<sub>±</sub> = 0.07, corresponds only to a difference of 3% in the effective ionic radii of (*i*-amyl)<sub>3</sub>BuN<sup>+</sup> or B(Ph)<sub>4</sub><sup>-</sup> ions shown in Table VI.

The effective ionic radii for the ions have been given in Table VI. They were calculated using Einstein's equation, eq 4, for a sphere. The effective radii for (*i*-amyl)<sub>3</sub>BuN<sup>+</sup> or B(Ph)<sub>4</sub><sup>-</sup> and Na<sup>+</sup> ions are, respectively, 5.01 and 3.83 Å at 25° which are in fair agreement with the values of 5.12 and 4.32 Å obtained for (*i*-amyl)<sub>3</sub>BuN<sup>+</sup> and Na<sup>+</sup> ions by conductance studies. This implies that the kinetic entities for the two ions can be approximated by spheres and the Na<sup>+</sup> ion is solvated in DMSO solution, the same result as suggested by the conductance studies.<sup>4</sup>

The effective ionic radii for SCN<sup>-</sup>, CF<sub>3</sub>SO<sub>3</sub><sup>-</sup>, and ClO<sub>4</sub><sup>-</sup> ions are, respectively 3.46, 3.54, and 3.46 Å at 25° as determined from the *B*<sub>±</sub> coefficients using Einstein's equation for a sphere. These values are significantly larger than the respective ionic radii; *i.e.*, 2.37, 3.03, and 2.82 Å for SCN<sup>-</sup>, CF<sub>3</sub>SO<sub>3</sub><sup>-</sup>, and ClO<sub>4</sub><sup>-</sup> ions, respectively, as obtained from the conductance studies. This is expected because the Einstein equation used in calculating the effective ionic radii has a shape factor of 2.5 which is valid only for a sphere. The intrinsic ionic structures for the ions and the conductance results that these ions are unsolvated in DMSO clearly point out that a shape factor other than 2.5 must be used in calculating the effective ionic radii for these ions. For example, Jeffery<sup>27</sup> and Simha<sup>28</sup> have derived the shape factor for ellipsoidal particles immersed in a viscous medium as a function of the axial ratio of an ellipsoid. The result is that the shape factor reaches a minimum value of 2.5 at axial ratios equal to unity; *i.e.*, a sphere, and the shape factor increases with increasing axial ratio for both prolate and oblate ellipsoidal particles. Assuming CF<sub>3</sub>SO<sub>3</sub><sup>-</sup> and SCN<sup>-</sup> ions are both prolate ellipsoidal particles with approximate axial ratios (axial ratio = major axes/minor axes) of 2 and 3.7, respectively, as estimated from the crystallographic radii,<sup>29</sup> the shape factors of about 3 and 4.2 are obtained for CF<sub>3</sub>SO<sub>3</sub><sup>-</sup> and SCN<sup>-</sup> ions. With these shape factors the ionic radii for CF<sub>3</sub>SO<sub>3</sub><sup>-</sup> and SCN<sup>-</sup> ions were calculated to be 3.33 and 2.91 Å, respectively. These radii are still larger than the effective radii for the ions as calculated from the conductance studies. The assumption of ellipsoidal shape for the ions and the fact that the ions are approximately the same size as a DMSO solvent molecule as opposed to the Einstein continuum assumption for eq 4 make such calculations questionable. It is, however, valid to say that CF<sub>3</sub>SO<sub>3</sub><sup>-</sup> and SCN<sup>-</sup> ions are not spherical kinetic entities in DMSO.

(27) G. B. Jeffery, *Proc. Roy. Soc., Ser. A*, **102**, 161 (1922).

(28) R. Simha, *J. Phys. Chem.*, **44**, 25 (1940).

(29) L. Pauling, "The Nature of the Chemical Bond," 2nd ed, Cornell University Press, New York, N. Y., 1940.

According to the concept of an activated rate process,<sup>25</sup> the activation energy for viscous flow in a pure liquid can be interpreted as the energy required to occupy the volume of the hole into which the molecule jumps plus that required to break the bond with other molecules if the liquid is associated. The activation energy for viscous flow,  $\Delta E_{\eta_0}^\ddagger$ , for pure DMSO solvent is 3.34 kcal/mol, see Figure 2. The energy required to form a hole of molecular size in DMSO is approximately  $12.64/N$  kcal/hole as estimated from the molar heat of vaporization of DMSO at 25°; *i.e.*, 12.64 kcal/mol.<sup>30</sup> Therefore, the activation energy for viscous flow in pure DMSO solvent represents some  $1/4$  of the energy required to form a hole of molecular size. This value is in the range  $\Delta E_{\eta_0}^\ddagger/L_v = 1/3^{-1/4}$ , where  $L_v$  is heat of vaporization, found for many nonpolar and polar liquids. In particular,  $\Delta E_{\eta_0}^\ddagger/L_v \cong 1/4$  was found for polar liquids<sup>25</sup> as is verified by that for DMSO in the present work.  $\Delta E_{\eta_0}^\ddagger/L_v \cong 1/2.4$  has been found<sup>25</sup> for water at 25°. The comparatively higher ratio found for H<sub>2</sub>O reflects, in part, the associated state of liquid water.  $\Delta E_{\eta_0}^\ddagger/L_v \approx 1/3.8$  found for DMSO at 25° appears to indicate that DMSO is not as highly associated as H<sub>2</sub>O. The view is consistent with the Trouton constants found for the two liquids; *i.e.*, 22.3 for DMSO and 26.0 for water.

The difference between the activation energy for the electrolyte solution and the pure solvent up to approximately 0.1 *M* has been attributed to the presence of the respective ions and is a measure of the effect of the ions upon the solvent viscous flow. At 0.1 *M* each ion is surrounded by 70 or more DMSO solvent molecules, and therefore, the viscous flow of most DMSO molecules except a few surrounding the ions is practically unaffected by the ions. This is why the difference in the activation energies, *i.e.*,  $\Delta E_{\eta}^\ddagger - \Delta E_{\eta_0}^\ddagger$ , is only about 2–3% of the total activation energy at *C* = 0.1 *M*.

Ionic energies and entropies of activation for viscous flow at 25° and *C* = 0.2 *M* are summarized in Table VIII. The values have been obtained based on the assumption that the effect of (*i*-amyl)<sub>3</sub>BuN<sup>+</sup> and B(Ph)<sub>4</sub><sup>-</sup> ions upon the solvent viscous flow is the same. This assumption is reasonable because the two ions are of equal size and have only a weak surface charge density.<sup>5,6</sup> The two ions present a simple obstruction to the solvent viscous flow.

Viscous flow of pure DMSO solvent may be thought of as consisting of many parallel planes of molecular size moving relative to each other. Each plane is approximately 5 Å thick; *i.e.*, the effective diameter of a DMSO molecule, and contains DMSO molecules and a small fraction of holes. For a DMSO molecule jumping into a neighboring hole, the molecule must possess enough energy to break the bond with an adjacent DMSO molecule and to capture the hole. This energy has been identified as the activation energy for pure

DMSO solvent. Upon introduction of an ion in the neighborhood of the molecule, the liquid structure and orientation of the molecules surrounding the ion will be altered. The degree to which the presence of an ion alters the neighboring solvent structure, thus the viscosity, depends on the charge, size, and shape of the ion.

The following classifications are made for the ions and the resultant effects of the ions upon the neighboring DMSO molecules are described in order to explain the observed results in Table VIII.

(1) *Spherically Symmetrical Ions with Weak Surface Charge.* Interaction between this type of ion and DMSO dipole is weak and the ions present only a hydrodynamic obstruction to the solvent flow plane. The larger the ion size, the larger the interference on the viscous flow of solvent. (*i*-amyl)<sub>3</sub>BuN<sup>+</sup> and B(Ph)<sub>4</sub><sup>-</sup> ions are examples of this type. The effective diameter of the ions is about 10 Å which is twice the thickness of the DMSO plane. Such obstruction increases the viscosity with a "concomitant" positive increase of entropy.

(2) *Ions of Small Size with Strong Surface Charge Density.* An example of this is a small alkali ion which interacts with the solvent dipole strongly to form a solvation sheath. The interaction energy between the Na<sup>+</sup> ion and the DMSO dipole is at least six times as great as the DMSO–DMSO bond strength.<sup>9</sup> This strong interaction immobilizes the neighboring DMSO molecules and in effect presents a large obstruction similar to type (1) ions.

(3) *Ions of the Same Size as the Solvent Molecules but with Dissimilar Shapes and Weak Permanent Dipole Moments.* SCN<sup>-</sup> and CF<sub>3</sub>SO<sub>3</sub><sup>-</sup> ions are examples of this type which interact with DMSO dipoles only weakly and do not present much interference to the solvent flow.

(4) *Ions with Approximately the Same Size and Geometry of Solvent Molecules with or without Weak Dipole Moments.* The ClO<sub>4</sub><sup>-</sup> ion has a tetrahedral structure with an effective diameter of about 5 Å which may be fitted quite well into the pyramidal DMSO structure. Because of the induced dipole–dipole interaction, the solvent molecules in the immediate vicinity of the ions compete in establishing bond angles and separation between the ion and the neighboring solvent molecules. The net effect is to loosen or to break the surrounding solvent bonds. This in effect decreases the local viscosity and the activation energy necessary for the solvent jumping into a hole. This view is similar to the concept of negative hydration by Samoilov<sup>31</sup> and the structure breaking concept by Frank and Wen<sup>32</sup> in

(30) T. B. Douglas, *J. Amer. Chem. Soc.*, **70**, 2001 (1948).

(31) O. Ya. Samoilov, "Structure of Aqueous Electrolyte Solutions and the Hydration of Ions," Consultants Bureau, New York, N. Y., 1965.

(32) H. S. Frank and W. Y. Wen, *Discuss. Faraday Soc.*, **24**, 133 (1957).

aqueous solutions. However, the temperature dependence of the ionic  $B_{\pm}$  coefficients is slightly positive for the  $\text{ClO}_4^-$  ion (Table V) which implies that the structure broken DMSO is now more susceptible to the electrical field of the  $\text{ClO}_4^-$  ion. It therefore appears that the perchlorate ion has two effects on DMSO structure. One is to create structure in the formation of a solvation sheath. The other is to break structure by loosening adjacent solvent-solvent bonds. The net effect, as suggested by  $\Delta E_{-}^{\ddagger} = -8$  cal/mol for  $\text{ClO}_4^-$  in Table VIII, seems to favor structure breaking at  $25^\circ$  and  $C = 0.02$  M. The DMSO structure is increasingly broken with increasing  $\text{ClO}_4^-$  concentration and at some concentration it is to be expected that the structure making due to solvation around the ions becomes predominant. This would mean a large increase of activation energy for viscous flow at that concentration. The rapid increase in activation energy for  $\text{NaClO}_4$  above 0.2 M, Figure 2, is therefore explained.

In conclusion, the present results of viscosity studies support the general conclusion reached in the previous conductance studies that ionic transport in DMSO is strongly governed by the ion-solvent dipole interaction. The ionic solvation, as a result of the ion-solvent dipole interaction, determines the effective ionic radii and the mobilities of the ions in the highly associated DMSO solvent. Although positive viscosity  $B$  coefficients were obtained for all electrolytes investigated, the perchlorate ion appears to be a structure breaker in dilute DMSO solution. The weak temperature dependence of viscosity  $B$  coefficients in DMSO solvent, in contrast to many aqueous electrolyte solutions, appears to be typical for most electrolytes in nonaqueous solvents.

*Acknowledgment.* This work was supported by the U. S. Army Mobility Equipment Research and Development Center, Fort Belvoir, Virginia, under Contract No. DA-44-009-AMC-1661(T).

## Thermochemistry of the Diels-Alder Reaction. I. Enthalpy of

### Addition of Isoprene to Tetracyanoethylene<sup>1</sup>

by F. E. Rogers

Department of Chemistry, University of Dayton, Dayton, Ohio 45409 (Received May 19, 1970)

Publication costs assisted by the University of Dayton

The enthalpy for the Diels-Alder addition of tetracyanoethylene to isoprene has been determined calorimetrically. Corrections for heats of solution and vaporization gave  $-43.8$  kcal/mol for the enthalpy of the gas phase reaction at  $25^\circ$ . Comparison is made with the analogous ethylene reactions.

The Diels-Alder reaction is of uncommon synthetic utility for the preparation of carbocyclic and heterocyclic intermediates. Numerous investigations have been made into details of its mechanism and stereochemistry.<sup>2</sup> This investigation is concerned with the thermochemical aspects of the Diels-Alder reaction as studied by reaction calorimetry. Solution calorimetry is ideally suited for those reactions that are clean, fast, and essentially quantitative at room temperature; tetracyanoethylene (TCNE) addition reactions<sup>3</sup> meet these requirements. We investigated the heat of addition of this dienophile to isoprene in dichloromethane. The enthalpy for the vapor phase reaction was obtained after corrections were made for the heats of solution and heats of vaporization of the compounds.

### Discussion

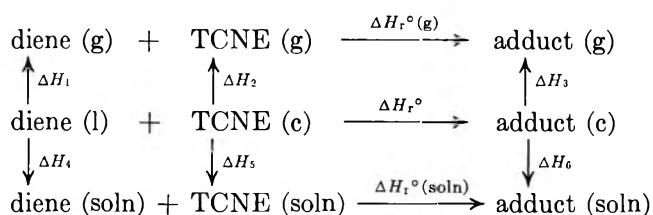
The enthalpies for the Diels-Alder reaction in the

(1) This investigation was supported by the University of Dayton Research Council.

(2) The following reviews summarize our knowledge of the Diels-Alder reaction: (a) A. Wasserman, "Diels Alder Reaction," Elsevier, New York, N. Y., 1965; (b) J. Hamer, "1,4-Cycloaddition Reactions: the Diels-Alder Reaction in Heterocyclic Syntheses," Academic Press, New York, N. Y., 1967; (c) J. Sauer *Angew. Chem., Int. Ed. Engl.*, **5**, 211 (1966); **6**, 16 (1967).

(3) The chemistry of TCNE has been reported in a series of publications: (a) T. L. Cairns, R. A. Carboni, D. D. Coffman, V. A. Engelhardt, R. E. Heckert, E. L. Little, E. G. McGeer, B. C. McKusick, W. J. Middleton, R. M. Scribner, C. W. Theobald, and H. E. Winberg, *J. Amer. Chem. Soc.*, **80**, 2775 (1958); (b) R. E. Merrifield and W. D. Phillips, *ibid.*, **80**, 2778 (1958); (c) W. J. Middleton, R. E. Heckert, E. L. Little, and C. G. Krespan, *ibid.*, **80**, 2783 (1958).

solution, condensed and vapor phases were determined by the use of the following cycle.



Since TCNE was added to the reaction solution  $\Delta H^\circ_{\text{exptl}} = \Delta H_r^\circ(\text{soln}) + \Delta H_5$  and  $\Delta H_r^\circ(\text{g}) = \Delta H^\circ_{\text{exptl}} + \Delta H_4 - \Delta H_2 - \Delta H_1 - \Delta H_6 + \Delta H_3$ . The values of the various  $\Delta H$  values determined are listed in Table I.

**Table I:** Enthalpies at 25°C

	Isoprene	TCNE	Adduct
$\Delta H^\circ_{\text{soln}}$	$0.246 \pm 0.012$	$5.60 \pm 0.12$	$3.78 \pm 0.21$
$\Delta H^\circ_{\text{vap}}$	$6.40 \pm 0.06^c$	$19.4 \pm 1^c$	$19.6 \pm 0.5^b$
$\Delta H_{\text{exptl}} = -34.06 \pm 0.55$			

<sup>a</sup> In kilocalories per mole. <sup>b</sup>  $\Delta H_v$  values at 350°K uncorrected to 298°. <sup>c</sup> Values taken from ref 5.

The McLeod gauge method was used for vapor pressure determinations. Although this method has not gained wide acceptance since its inception by Menzies in 1920, it is simple and capable of good precision.<sup>4</sup> The present version of the apparatus was checked against anthracene. Anthracene (a) is stable and readily available in a high state of purity, (b) has a heat of sublimation which falls in a useful range, and (c) has already received attention in precision work. For these reasons it is a useful standard for heat of sublimation studies. The vapor pressure of anthracene was determined in the range of 100–130° at 5° intervals. The data treated by the method of least squares gave the equation  $\log P(\mu) = -5236.3/T(^{\circ}\text{K}) + 15.2290$  and  $\Delta H_v(373^{\circ}\text{K}) = 24.0 \pm 0.4$  kcal/mol. This is in excellent agreement with the "selected value" of  $24.3 \pm 1.0$  kcal/mol reported by Cox and Pilcher.<sup>5</sup>

For the tetracyanocyclohexene adduct 15 vapor pressure measurements were made in the range 70–105°. A least-squares treatment of the data gave the equation  $\log P(\mu) = -4275.1/T(^{\circ}\text{K}) + 13.4696$  with a correlation coefficient of 0.9946 and  $\Delta H_v = 19.6$  kcal/mol. From these data the calculated heats for the Diels-Alder reaction are:  $\Delta H_r^\circ(\text{soln})$ ,  $-39.7 \pm 0.7$ ;  $\Delta H_r^\circ$ ,  $-37.6 \pm 0.8$ ;  $\Delta H_r^\circ(\text{g})$ ,  $-43.8 \pm 2.8$  kcal/mol.

Transferring the reaction from the vapor phase to solution requires 4 kcal/mol. By comparison the dimerization of cyclopentadiene in the gas or solution phase differ only by 0.7 kcal/mol. From the enthalpy cycle and the data of Table I the heat of solvation of

the gaseous components,  $\Delta H_{\text{soln}}$ , is given by  $\Delta H_{\text{soln}} - \Delta H_{\text{vap}}$ . The calculated  $\Delta H_{\text{soln}}$  are: TCNE,  $-13.8$ ; diene,  $-6.15$ ; adduct,  $-15.8$  kcal/mol. Thus the heat of solvation of the gaseous reactants is more exothermic by 4.1 kcal/mol than the products. Part of this difference is attributed to the ability of TCNE to form strong complexes with a wide variety of solvents<sup>3b</sup> and recent X-ray studies give evidence for complex formation between TCNE and dichloromethane.<sup>6</sup>

The gas phase heats of formation at 25° of isoprene and TCNE are 18.1 and 168.5 kcal/mol, respectively.<sup>5</sup> Combining these values with the enthalpy of the gas phase reaction,  $\Delta H_r^\circ(\text{g})$ , gave 142.8 kcal/mol as the heat of formation of the adduct (g). Strain energy is generally assigned as the difference between the experimental and estimated heats of formation. We adopted the group increment scheme of Benson<sup>7</sup> and assigned 68.4 kcal/mol as the enthalpy contribution of the  $>\text{C}(\text{CN})_2$  group.<sup>8</sup> Since this value is based on malononitrile it contains the geminal interaction of two cyano groups. This repulsive interaction has been calculated as 9 kcal/mol<sup>9</sup> although the disproportionation of acetonitrile to malononitrile and methane indicates a value of 3.6 kcal/mol. The estimated heat of formation, 136.1 kcal/mol, is about 7 kcal lower than the experimental value. The difference is taken as the repulsive interaction of two adjacent  $>\text{C}(\text{CN})_2$  groups. The interaction energy of the cyano groups in succinonitrile as a function of the torsional angle has been calculated by Lewis and Smyth.<sup>10</sup> Using these values and a cyclohexene-like structure<sup>11</sup> for the adduct we calculate the repulsive interaction of adjacent dicyanomethylene groups as 10 kcal which agrees closely with the experimental quantity.

Since the cyano group is often referred to as a pseudohalogen it is instructive to compare the thermochemical behavior of TCNE with polyhaloalkenes. Using the heats of formation from a recent critical compilation<sup>5</sup> and the data of this work we constructed the following disproportionation reactions. The corresponding ethylene reaction is built in as the reference reaction.

(4) G. W. Thomson in *A. Weissberger, "Technique in Organic Chemistry, Physical Methods,"* 3rd ed, Interscience, New York, N. Y., Part I, p 457.

(5) J. D. Cox and G. Pilcher, "Thermochemistry of Organic and Organometallic Compounds," Academic Press, New York, N. Y., 1970.

(6) I. L. Karle and A. V. Fratini, *Acta Crystallogr., Sect. B*, **26**, 596 (1970).

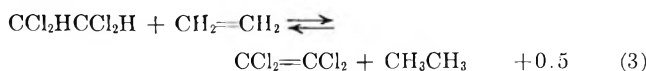
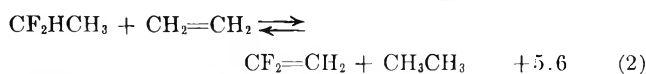
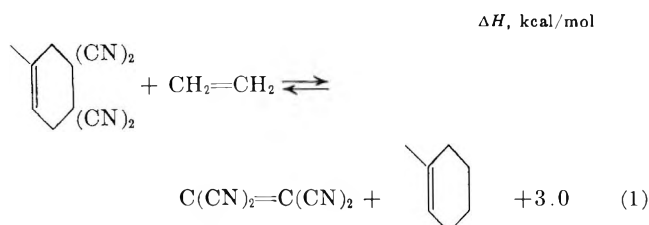
(7) S. W. Benson, "Thermochemical Kinetics," Wiley, New York, N. Y., 1968.

(8) Calculated by the formula  $\Delta H[>\text{C}(\text{CN})_2] = \Delta H_f[\text{CH}_2(\text{CN})_2] - \Delta H[\text{C}-(\text{H})_2(\text{C})_2]$ , where  $\Delta H_f[\text{CH}_2(\text{CN})_2]$  is 63.5 and  $\Delta H[\text{C}-(\text{H})_2(\text{C})_2]$  is  $-4.95$  kcal/mol.

(9) R. H. Boyd, K. Ranjan, and R. Wuthrich, *J. Phys. Chem.*, **71**, 2187 (1967).

(10) G. L. Lewis and C. P. Smyth, *J. Chem. Phys.*, **7**, 1085 (1939).

(11) J. F. Chiang and S. H. Bauer, *J. Amer. Chem. Soc.*, **91**, 1898 (1969).



Transferring two pairs of chlorine atoms from tetrahedral to trigonal carbon (reaction 3) is essentially a thermoneutral reaction. A similar process (reaction 1) for the cyano group is slightly endothermic. While it is known that a cluster of cyano groups on tetrahedral carbon has a destabilizing effect<sup>12</sup> it would appear that this destabilization is slightly greater on trigonal carbon. Reaction 2 indicates that two fluorines are more stable on tetrahedral carbon. This latter effect has been dealt with at length in other work.<sup>13</sup> The behavior of the cyano group thus falls between that of chlorine and fluorine. From reaction 1 it appears that the heat of any Diels-Alder reaction of TCNE can be estimated from the analogous reaction with ethylene. This conclusion is currently being explored.

### Experimental Section

**Reagents.** Isoprene (Aldrich Chemical Co., puriss grade) and dichloromethane (Matheson Coleman and Bell) showed only one peak on glpc analysis and were used without further purification. The tetracyanoethylene (TCNE) (Eastman Organic Chemicals) was sublimed and stored in amber bottles under nitrogen. The Diels-Alder adduct, 1-methyl-4,4,5,5-tetracyanocyclohexene, was prepared in quantitative yield from the addition of an excess of isoprene to a solution of TCNE in dichloromethane at room temperature. Sublimation gave the adduct, mp 113–114.3°. *Anal.* Calcd for C<sub>11</sub>H<sub>8</sub>N<sub>4</sub>: C, 67.33; H, 4.11; N, 28.59. Found: C, 67.03; H, 4.10; N, 28.42.

**Calorimeter.** The twin dewar calorimeter was based on the original design of Arnett<sup>14</sup> except that a second reference dewar was used in place of the base line compensator. The two half-pint dewars were mounted side by side at the end of a 8.5 × 11 in. aluminum plate and driven through a gear train by a single Fisher jumbo stirrer. The stirrer and gears were mounted on another 8.5 × 11 in. aluminum plate supported by two stainless steel rods directly above the dewars (Figure 1). To ensure equal stirring, nonslip gears and belt (PIC Design Corp., East Rockaway, N. Y.) were used and their ratios chosen to provide stirrer speed of 200 or 400 rpm. The 2000-ohm thermistor from each dewar was connected to opposed legs of a wheatstone bridge, the third leg was a 2000-ohm 1% resistor, and the fourth

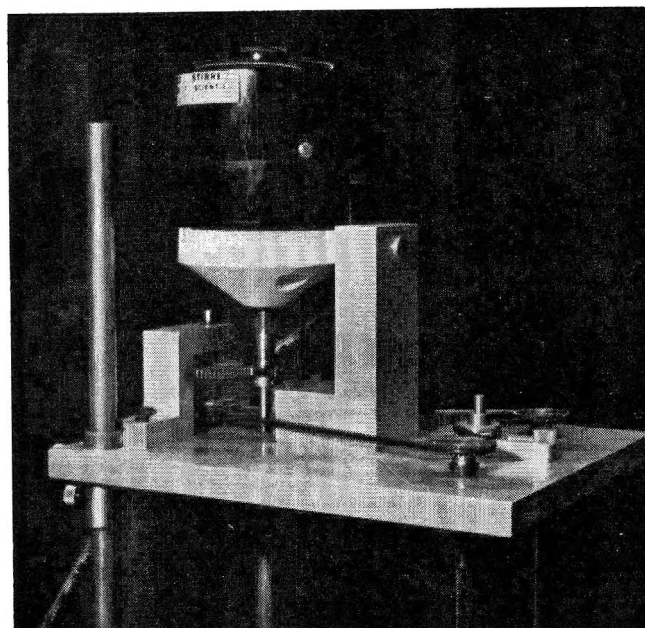


Figure 1.

a 1500-ohm 1% resistor in series with a 10-turn 1000-ohm potentiometer. The signal from the bridge was fed to a Sargent SR recorder. At equilibrium the recorder trace was perfectly flat.

The construction and geometry of the heaters, stirrer, and thermistor well in each dewar were identical so that they could be used consecutively, the reaction dewar serving as the reference in the next reaction. Power to the manganin heaters was supplied by a regulated dc source (Model ABC 18-0.5M, Kepco, Flushing, N. Y.). The voltage was measured by a James G. Biddle Potentiometer (Model 604004, Plymouth Meeting, Pa.). The calorimeter was checked against two standards, the heat of solution of [2-amino-2-(hydroxymethyl)-1,3-propanediol (THAM) in 0.1 N hydrochloric acid and the heat of solution of potassium chloride; of the two THAM is developing as the most reliable primary standard for solution calorimetry. Our average value for the heat of solution of THAM (Eastman Organic Chemicals) in 0.1 N hydrochloric acid is  $-7.15 \pm 0.01$  kcal/mol. Hill, Öjelund, and Wadsö<sup>15</sup> have recently reported  $-7.109 \pm (0.001)$  kcal/mol for this reaction.<sup>16</sup> The heat of solution of KCl (Baker and Adamson Reagent Special) in water corrected for the heat of concentration and the temperature coefficient of the heat

(12) M. B. Frankel, A. B. Amster, E. R. Wilson, M. McCormick, and M. McEachern, Jr., *Advan. Chem. Ser.*, No. 54 (1969).

(13) J. Hine, *J. Amer. Chem. Soc.*, **85**, 3239 (1963).

(14) E. M. Arnett, W. G. Bertrude, J. J. Burke, and P. Duggleby, *ibid.*, **87**, 1951 (1965).

(15) J. O. Hill, G. Öjelund, and I. Wadsö, *J. Chem. Thermodyn.*, **1**, 111 (1969).

(16) The U. S. Calorimetry Conference Standards Committee recommends initial concentration of 5 g of THAM per liter of 0.1 N HCl solution. Since the differential heat of solution is very low, significant differences in  $\Delta H$  values do not appear even with 2 g of THAM.

of solution<sup>17</sup> is  $+4.20 \pm 0.06$  kcal/mol compared to the accepted value of  $+4.194 \pm 0.003$  kcal/mol.<sup>18</sup>

*Vapor Pressure Apparatus.* The Method of Menzies was adopted for the determination of vapor pressures. After several designs, the apparatus was constructed in the following manner. A vacuum stopcock is attached to one end of a 19-cm length of 3-mm capillary tubing and a "dosing" stopcock to the other. (For the dosing stopcock the passage in a vacuum stopcock was filled with sufficient epoxy resin so that a small quantity of inert gas—ca.  $50 \mu$ —was admitted at each turn.) Two female spherical joints were attached 14.5 cm apart on the capillary tubing; one for the 100-ml, cylindrical bulb, fitted with a side arm for a thermometer; the other for the multirange McLeod gauge (Kontes Glass Company, Catalog No. K-922400). The bulb was heated by a constant temperature oil bath. An 800-ml beaker insulated with a layer of foam rubber and asbestos was filled with heavy mineral oil, heated by a 100-ohm 35-W resistor, and stirred magnetically. Power was supplied from a calibrated Variac. The volume of the McLeod gauge (allowing for the mercury), the capillary, and the vaporizing bulb were measured with water. The ratio ( $V_r$ ) of the "hot" volume (up to the oil level) to the "cold" volume (from the oil level to the gauge) calculated in this manner was 4.28.

The apparatus was calibrated with anthracene (Aldrich Chemical Co. puriss grade) over the range 100–130°. Two successive runs gave a heat of sublimation of 23.56 and 24.36 kcal/mol (lit.<sup>5</sup>  $\Delta H_v = 24.3 \pm 1.0$  kcal/mol).

*Vapor Pressure of 1-Methyl-4,4,5,5-tetracyanocyclohexene.* A sufficient amount of the Diels–Alder adduct (0.1–0.2 g) was placed in the bulb and the system evacuated. The system was washed with nitrogen by means of five turns of the dosing stopcock (ca.  $300 \mu$ ), then reevacuated. This sequence was repeated several times. The bulb was filled with sufficient nitrogen *via* the dosing stopcock to give an initial pressure of about  $400 \mu$ . The temperature of the oil bath was slowly adjusted to the uppermost temperature and raised up to cover the bulb. When the system comes to thermal equilibrium (about 30 min) pressure readings were taken. The capillary arm of the McLeod gauge must be scrupulously clean to prevent a sticking mercury column. At least three pressure readings were made at each temperature. The oil bath temperature was

lowered about 5–10° and the pressure again measured after equilibrium was established. Successive readings made in this manner were checked by a repetition of the entire process.

*Enthalpy of Addition: Isoprene and Tetracyanoethylene.* In these studies a special plastic syringe was used to inject solids into the calorimeter. The syringe was based on the original design of Arnett.<sup>14</sup> The needle end of a 2-ml disposable syringe (B-D Plasticpak) was cut off, the rubber plunger replaced with a machined polyethylene piston. The sample is weighed into the syringe and the end capped with a tight fitting polyethylene plug. The plug is attached to the end of the syringe with a short length of Teflon or polyethylene wire.

To make a run, 200 ml of dichloromethane and 3 ml of isoprene were added to each dewar. The cap, stirrer, and syringe were set in place and equilibrated to  $25 \pm 0.5^\circ$ . To initiate the reaction about 0.07873 g of TCNE was injected into the solution. Within 10 min the recorder trace begins to level out. The integral heats of solution of the reactants and product were determined at concentrations similar to those of the actual Diels–Alder reaction. However, in the case of isoprene, the heat of the solution is so low that higher molar ratios of diene to solvent were used.

The Diels–Alder reaction followed on a Coleman-Hatashi 124 uv spectrophotometer shows that the TCNE absorption (275 nm,  $\epsilon \sim 10^4$ ) is completely gone within 5 min at room temperature. The nmr spectrum of the isolated products is consistent with the adduct 1-methyl-4,4,5,5-tetracyanocyclohexene:  $\tau$  8.10 (s, CH<sub>3</sub>, 3 H), 6.90 (m, CF<sub>2</sub>, 4 H), 4.18 (m, =CH, 1 H).

The heat of solution of the adduct was determined by injection of about 0.102 g into 200-ml of dichloromethane. About 0.13 g of TCNE and 200 ml of dichloromethane were used for the heat of solution of TCNE. The isoprene (about 0.478 g) was weighed into a small bulb blown on the end of 3-mm tubing. A length of stiff wire inserted through a small serum stopper at the other end served to break the bulb to initiate the reaction.

(17) E. Lange and J. Monheim, *Z. Phys. Chem., Abt. A*, **150**, 349 (1930).

(18) R. J. Irving and I. Wadsö, *Acta Chem. Scand.*, **18**, 195 (1964).

# Pulse Radiolytic Investigation of $O_{aq}^-$ Radical Ions

by Dov Zehavi and Joseph Rabani\*

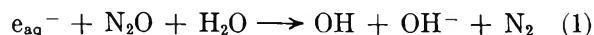
Department of Physical Chemistry, Hebrew University of Jerusalem, Jerusalem, Israel (Received June 25, 1970)

Publication costs borne completely by The Journal of Physical Chemistry

The reactivity of the oxidizing radicals in  $N_2O$  saturated aqueous solutions was measured by pulse radiolysis. Competition experiments between methanol, ethanol, and other solutes such as ferrocyanide, iodide, bromide, thiocyanate, ferrous, and cerous ions were carried out. Comparison with results in the alkaline pH range indicates that  $O^-$  is formed as an intermediate in the reaction of  $e_{aq}^-$  with  $N_2O$ .  $O^-$  reacts quickly with water,  $k_{(O^-+H_2O)} = 9.6 \times 10^7 \text{ sec}^{-1}$ . At high solute concentrations, competition for  $O^-$  (generated from  $N_2O$ ) was carried out. The following reaction rate constants (in  $M^{-1} \text{ sec}^{-1}$ ) were determined:  $k_{(O^-+I^-)} = 2.2 \times 10^9$ ;  $k_{(O^-+CNS^-)} = 1.4 \times 10^9$ ;  $k_{(O^-+methanol)} = 5.3 \times 10^8$ ;  $k_{(O^-+ethanol)} = 9.8 \times 10^8$ ;  $k_{(O^-+ferrocyanide)} \leq 3 \times 10^7$ ;  $k_{(O^-+Br^-)} = 1.8 \times 10^8$ ;  $k_{(O^-+ferrous)} = 3.1 \times 10^9$ ;  $k_{(O^-+cerous)} = 5.9 \times 10^8$ . The reactivity of  $O^-$  as compared with that of  $OH$  is discussed. An upper limit ( $\sim 10^7 \text{ sec}^{-1}$ ) is estimated for  $k_{(N_2O^- \rightarrow N_2+O^-)}$ .

## Introduction

The use of nitrous oxide in radiation chemistry of aqueous solutions was introduced by Proskurnin and Kolotyrykin.<sup>1</sup> Dainton and Peterson<sup>2</sup> have shown that  $N_2O$  converts hydrated electrons into hydroxyl radicals according to eq 1



There is a controversy regarding the mechanism of process 1. A negative ion,  $N_2O^-$ , has been proposed as an intermediate capable of reacting with solutes.<sup>3-6</sup> In several systems<sup>7-12</sup> there was evidence that  $N_2O^-$  is converted quickly<sup>7</sup> into  $OH$  radicals; several papers indicated half-lives less than 0.2–0.3  $\mu\text{sec}$ .<sup>8-12</sup> Adams<sup>13</sup> has put an even lower limit on the lifetime of  $N_2O^-$ . His limit is based on competition between methanol and  $CNS^-$  for  $OH$  radicals. From the deviations in the relative reactivity of  $CNS^-$  and methanol, Adams' semiquantitative treatment resulted in an upper limit for the  $N_2O^-$  lifetime of  $\sim 1 \text{ nsec}$ . Czapski<sup>14</sup> pointed out that  $O^-$ , and not  $N_2O^-$ , may be the reactive species in some aqueous systems in which high solute concentrations were used. He concluded, from the  $pK$  of  $OH$  radicals (assuming that  $k_{(OH+OH^-)} = 10^{10} M^{-1} \text{ sec}^{-1}$ ), that  $O^-$  may live as long as  $10^{-8}$  to  $10^{-9} \text{ sec}$  at  $pH > 2$ .

The purpose of this work is to investigate the mechanism according to which  $N_2O$  converts hydrated electrons into  $OH$  radicals and to obtain information on the nature, lifetime, and reactivities of the intermediates ( $O^-$ ,  $N_2O^-$ ).

## Experimental Section

The pulse radiolysis apparatus and syringe technique were essentially the same as described elsewhere.<sup>15-17</sup> The linear accelerator at the Hebrew University was used as an electron pulse source at 5 MeV and 200 mA. A rectangular silica cell ( $1 \times 2 \times 4 \text{ cm}$ ) with a light

path of 12.2 cm was used (3 passes) unless otherwise stated. The electron beam was perpendicular to the light beam, and was absorbed in the 1-cm thick water medium after passing through 0.5-mm thick quartz windows. The cell filling method was based on the method developed previously at Risö,<sup>18</sup> except that magnetic valves with photodiode relays were used for both filling and emptying the irradiation cell.

(1) M. A. Proskurnin and V. M. Kolotyrykin, *Proc. U. N. Int. Conf. Peaceful Uses At. Energy*, 2nd, 29, 52 (1958).

(2) F. S. Dainton and D. B. Peterson, *Proc. Roy. Soc. Ser. A*, 267, 443 (1962).

(3) M. Anbar, R. A. Munoz, and P. Rona, *J. Phys. Chem.*, 67, 2708 (1963).

(4) J. H. Baxendale, E. M. Fielden, and J. P. Keene, "Pulse Radiolysis," M. Ebert, *et al.*, Ed., Academic Press, London, 1965, p 207.

(5) (a) K. F. Nakken and A. Pihl, *Radiat. Res.*, 26, 519 (1965); (b) K. F. Nakken, T. Brustad, and A. K. Hansen, *Advan. Chem. Ser.*, 81, 251 (1968).

(6) K. D. Asmus, A. Henglein, and G. Beck, *Ber. Bunsenges. Phys. Chem.*, 70, 459 (1966).

(7) (a) B. L. Gall and L. M. Dorfman, *J. Amer. Chem. Soc.*, 91, 2199 (1969); (b) R. Wander, B. L. Gall, and L. M. Dorfman, *J. Phys. Chem.*, 74, 1819 (1970).

(8) J. Rabani and M. S. Matheson, *ibid.*, 70, 761 (1966).

(9) J. L. Weeks and J. Rabani, *ibid.*, 70, 2100 (1966).

(10) M. S. Matheson, W. A. Mulac, J. L. Weeks, and J. Rabani, *ibid.*, 70, 2092 (1966).

(11) J. Rabani, "Radiation Chemistry of Aqueous Systems," G. Stein, Ed., The Weizmann Science Press, Jerusalem, 1968, p 229.

(12) K. H. Schmidt and S. M. Ander, *J. Phys. Chem.*, 73, 2846 (1969).

(13) G. E. Adams, "Radiation Research," G. Silini, Ed., North-Holland Publishing Co., Amsterdam, 1967, p 195.

(14) G. Czapski, "Radiation Chemistry of Aqueous Systems," G. Stein, Ed., The Weizmann Science Press, Jerusalem, 1968, p 211.

(15) M. S. Matheson and L. M. Dorfman, *J. Chem. Phys.*, 32, 1870 (1960).

(16) L. M. Dorfman, I. A. Taub, and R. E. Bühler, *ibid.*, 36, 3051 (1962).

(17) (a) S. Gordon, E. J. Hart, M. S. Matheson, J. Rabani, and J. K. Thomas, *Discuss. Faraday Soc.*, 36, 193 (1963); (b) E. J. Hart, S. Gordon, and J. K. Thomas, *J. Phys. Chem.*, 68, 1271 (1964).

(18) H. Christensen, G. Nilsson, P. Pagsberg, and S. O. Nielsen, *Rev. Sci. Instrum.*, 40, 786 (1969).



The electron pulse intensity was constant within  $\pm 5\%$ . We used the inductive current obtained by the electron beam in a coil to monitor the pulse intensity. Whenever comparison of optical densities was needed they were first corrected for the differences in pulse intensity as measured by the monitor. The reproducibility of corrected optical densities was better than 3%.

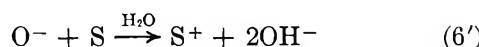
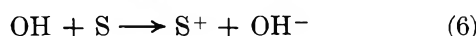
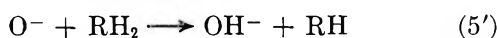
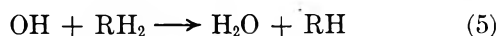
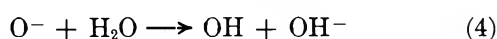
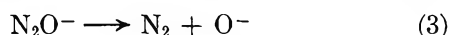
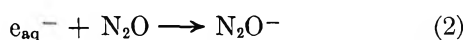
An IP28 photomultiplier, a Bausch and Lomb high intensity monochromator, and Tektronix 556 double beam and 454 single beam oscilloscopes were used in all the experiments. An Osram xenon 150-W lamp with water cooling was used as a light source. Appropriate light filters were employed in order to avoid second-order light signals through the monochromator, as well as to minimize photochemistry of the solutions (especially when ferrocyanide was used as a solute). To minimize photochemistry of the solutions and to protect the photomultiplier system from excess illumination, a shutter operated mechanically by air pressure was used between the irradiation cell and the light source.

Ultrahigh purity argon and  $O_2$  (Matheson Co.) were used for the preparation of the solutions.  $N_2O$  (Matheson Co.) was purified by the procedure described before.<sup>8</sup> Triple distilled water was used in all the experiments; 20 M NaOH (Merck analytical reagent) was used as a stock solution for the preparation of alkaline solutions.  $K_4Fe(CN)_6 \cdot 3H_2O$  and methanol (Mallinckrodt AR), KI and KBr (Baker analyzed reagent), KCNS and  $CCl_4$  (Hopkin and Williams, Analar), ethanol (Merck reagent),  $(NH_4)_2Fe(SO_4)_2 \cdot 6H_2O$  (Riedel-de Haën analytical reagent), and  $Ce_2(SO_4)_3 \cdot 8H_2O$  (Fluka puriss reagent) were used without further purification. The temperature was  $23 \pm 2^\circ$ .

## Results

We carried out competition experiments in which two solutes,  $RH_2$  and S, competed for OH radicals and their equivalents, in the presence of  $N_2O$ . As  $RH_2$  we used ethanol and methanol, which are known to undergo dehydrogenation by OH radicals, forming free radicals of the type RH which have optical absorptions in the uv region.<sup>19</sup> As S, we chose ferrocyanide, iodide, bromide, thiocyanate, ferrous or cerous salts.

Let us assume the following mechanism ( $3.5 < pH < 10$ )



In all the systems investigated,  $S^+$  was a relatively stable product, compared with the radical species taking part in reactions 2–6. Usually,  $S^+$  could further react with another  $S^+$  radical, with H atoms, or with RH radicals. However, under our conditions these reactions were slow enough to enable the determination of "initial" (extrapolated to the middle of the pulse) optical densities of  $S^+$ . The reaction of H atoms with  $N_2O$  was neglected ( $k < 3 \times 10^5 M^{-1} sec^{-1}$ ).<sup>20</sup> These optical densities could be a measure of the total amount of oxidizing radicals which reacted with S in competition with their reactions with  $RH_2$ .

Let us define the following:  $G_X$ , the "primary" yield of X;  $G_{(Y)}$ , the experimental yield of Y;  $R_i$ , the rate of reaction i;  $G_{(i)}$ , the yield of reaction (i).

From the above mechanism (reactions 2–6') it is evident that  $G_{(S^+)} = G_{(6)} + G_{(6')}$ .  $RH_2$  and S compete for the OH radicals. Such a competition can be described by the relation

$$G_{(6)} = G_{(OH)} / (1 + R_5/R_6)$$

where  $G_{(OH)}$  represents the total yield of OH formed both primarily and *via* reaction 4.

$$G_{(OH)} = G_{OH} + G_{(4)}$$

Similarly

$$G_{(4)} = G_e / (1 + (R_{5'} + R_{6'})/R_4)$$

and

$$G_{(6')} = G_e / (1 + (R_1 + R_{5'})/R_{6'})$$

(the last two equations are based on the assumption that all the hydrated electrons are converted into  $O^-$  radical ions due to reactions 2 and 3). Combining the above relations leads to formula I

$$G_{(S^+)} = \frac{G_{OH} + G_e / [1 + (R_{5'} + R_{6'})/R_4]}{1 - R_5/R_6} + \frac{G_e}{1 + (R_4 + R_{5'})/R_{6'}} \quad (I)$$

Equation I can be modified into (II)

$$D/D_0 = \frac{1 - G_R / [1 + R_4 / (R_{5'} + R_{6'})]}{1 + R_5/R_6} + \frac{G_R}{1 + (R_4 + R_{5'})/R_{6'}} \quad (II)$$

where  $D$  and  $D_0$  are the extrapolated optical densities of  $S^+$ , in the presence and in the absence of  $RH_2$ , respectively, and  $G_R$  is defined as the ratio  $G_e / (G_e + G_{OH})$ . Equation II can be used to determine relative rate constants, as will be seen later.

(19) (a) M. Simić, P. Neta, and E. Hayon, *J. Phys. Chem.*, **73**, 3794 (1969); (b) I. A. Taub and L. M. Dorfman, *J. Amer. Chem. Soc.*, **84**, 4053 (1962).

(20) M. Anbar and P. Neta, *Int. J. Appl. Radiat. Isotopes*, **18**, 493 (1967).

**Determination of  $G_R$ .** Primary  $G$  values are known to depend on the nature of the solutes and on their concentrations. In Table I we demonstrate the effect of [ferrocyanide] on  $D_0$ . The ratio  $D_0$  ( $O_2$ , 1 atm)/ $D_0$  ( $N_2O$ , 0.1 atm) = 0.50  $\approx$  (1 -  $G_R$ ) is practically independent of the ferrocyanide concentration. In similar experiments, carried out with negative ions other than ferrocyanide, values of  $G_R$  ranging from 0.50 to 0.48 were obtained. The value  $G_R = 0.50$  was used whenever eq II has been applied in all the systems containing negative ions S.  $G_R$  was assumed to be independent of  $[N_2O]$  and  $[RH_2]$ .

**Table I:** Calculation of  $G_R$  for Ferrocyanide<sup>a</sup>

$[K_4Fe(CN)_6]$ , $M$	$D_0$ ( $O_2$ , 1 atm)	$D_0$ ( $N_2O$ , 0.1 atm)	$\frac{D_0(O_2, 1 \text{ atm})}{D_0(N_2O, 0.1 \text{ atm})}$
$1 \times 10^{-3}$	0.076	0.148	0.51
$1 \times 10^{-2}$	0.083	0.168	0.49
$1 \times 10^{-1}$	0.097	0.192	0.51

<sup>a</sup> Results measured at 1.5- $\mu$ sec pulses.

**Determination of  $k_5/k_6$ .** Both  $k_5$  and  $k_6$  have been measured before.<sup>8,10,21,22</sup> We measured directly the ratio  $k_5/k_6$ , using solutions of S-ethanol and S-methanol. Two sets of experiments were carried out for each solute S. (a) In one set,  $O_2$  saturated solutions of relatively high S concentrations were used. The concentrations of S were chosen so that they were about equal to those used later in the competition experiments for  $O_{aq}^-$  radical ions. (b)  $N_2O$ -saturated  $O_2$ -free solutions with relatively low solute concentrations were used, so that  $R_4 \gg (R_5 + R_6)$ . In both cases, eq II reduces to (III)

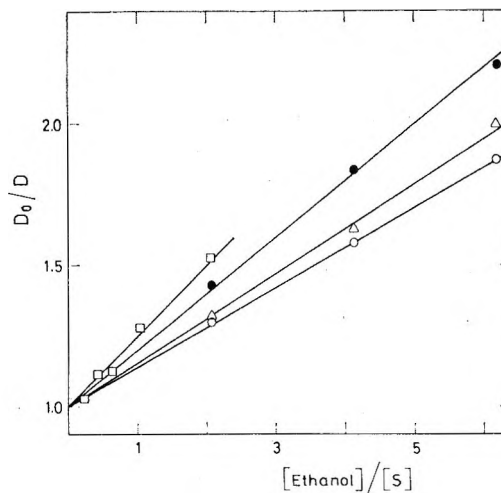
$$D_0/D = 1 + R_5/R_6 \quad (III)$$

From eq III,  $k_5/k_6$  can be obtained using appropriate plots. Such plots are presented in Figure 1. The  $k_5/k_6$  ratios are summarized in Table II.

**Table II:**  $k_5/k_6$  for Negative Ions<sup>a</sup>

S	[S], M	$D_0$	Pulse duration, $\mu$ sec	$k_5/k_6$	
				Ethanol	Methanol
$K_4Fe(CN)_6$	0.05 <sup>a</sup>	0.0752	0.5	0.199	0.087 <sup>c</sup>
$K_4Fe(CN)_6$	$2 \times 10^{-4}$ <sup>b</sup>	0.0612	0.35	0.186	0.081
$CNS^-$	0.2 <sup>a</sup>	0.0762	0.075	0.157	0.075 <sup>c</sup>
$CNS^-$	$3 \times 10^{-4}$ <sup>a</sup>	0.164	0.1	0.181	0.086
$I^-$	0.1 <sup>a</sup>	0.102	0.075	0.141	
$I^-$	$1 \times 10^{-4}$ <sup>b</sup>	0.217	0.1	0.181	
$Br^-$	1.0 <sup>a</sup>	0.188	0.13	0.250	
$Br^-$	$1 \times 10^{-3}$ <sup>b</sup>	0.186	0.1	1.57	

<sup>a</sup> Saturated with oxygen. <sup>b</sup> Saturated with  $N_2O$ . <sup>c</sup> Based on the ethanol results assuming  $k_5$  is independent of solute concentrations. <sup>d</sup> Ferricyanide ions,  $(CNS)_2^-$ ,  $I_2^-$ , and  $Br_2^-$  were detected at 4200, 4750, 3800, and 3600 Å, respectively.



**Figure 1.** Determination of  $k_5/k_6$  in oxygenated solutions of negative ions: ●,  $K_4Fe(CN)_6$  (0.05 M); Δ, KCNS (0.2 M); ○, KI (0.1 M); □, KBr (1.0 M).

The results obtained in the  $N_2O$  saturated solutions agree with the known absolute reaction rate constants.<sup>8,10,21,22</sup> At the relatively high solute concentrations ( $O_2$  saturated), the ratios  $k_5/k_6$  are not identical with the ratios obtained at low solute concentrations. In the case of ferrocyanide, the small difference, if real, may be due to ion association. We have no explanation for the small (but definitely outside experimental error) concentration effects in the thiocyanate and iodide systems. The discrepancy in the case of bromide is especially large. It is probably connected with the particular oxidation mechanism of  $Br^-$  by OH radicals.<sup>10</sup> In our experiments, the overall reaction rate of  $Br^-$  with OH is measured. If the intermediate<sup>10</sup>  $BrOH^-$  is capable of reacting with  $Br^-$  to yield  $OH^-$  and  $Br_2^-$ , an effect of  $[Br^-]$  on the competition is expected.

Reaction of  $Br^-$  with  $H_2O^+$  can also account for our observations. However, there is no conclusive evidence for reactions of  $H_2O^+$  with solute in irradiated aqueous solutions, and we believe that the observed effect is specific to the intermediates of the solute.

**Determination of  $k_4$ .** The ferrocyanide system has the advantage that it has been studied extensively.<sup>8,21</sup> It is known that ferrocyanide is not reactive towards  $O^-$  radical ions.<sup>8</sup>

We extended this work<sup>8</sup> and studied the rate of oxidation of ferrocyanide in solutions containing  $[NaOH] = 0.366$  and  $1.11 M$ . The apparent reaction rate constants of hydroxyl radicals with ferrocyanide ( $10^{-3} M$ ) were  $2.57 \times 10^8$  and  $1.06 \times 10^8 M^{-1} sec^{-1}$ , respectively. From this, an upper limit  $k_6 \leq 3 \times 10^7 M^{-1}$

(21) (a) J. Rabani and M. S. Matheson, *J. Amer. Chem. Soc.*, **86**, 3175 (1964); (b) G. E. Adams, J. W. Boag, and B. D. Michael, *Trans. Faraday Soc.*, **61**, 492 (1965).

(22) (a) J. K. Thomas, *ibid.*, **61**, 702 (1965); (b) G. E. Adams, J. W. Boag, J. Currant, and B. D. Michael, "Pulse Radiolysis," M. Ebert, *et al.*, Ed., Academic Press, London, 1965, p 117; (c) J. H. Baxendale, P. L. T. Bevan, and D. A. Stott, *Trans. Faraday Soc.*, **64**, 2389 (1968); (d) G. V. Buxton, *ibid.*, **65**, 2150 (1969).

$\text{sec}^{-1}$  was obtained. This justifies the neglect of  $R_{6'}$  in eq II, in both ferrocyanide-ethanol and ferrocyanide-methanol experiments under our conditions. Equation II is then modified into (IV)

$$D/D_0 = \frac{1 - G_{\text{R}}/(1 + R_4/R_{5'})}{1 + R_5/R_6} \quad (\text{IV})$$

Measurements of  $D/D_0$ , under conditions where  $R_4$  is equal to  $R_{6'}$  (within a factor of 2-3), make it possible to obtain the ratio  $k_4/k_{5'}$ , from which  $k_4$  can be calculated if  $k_{5'}$  is known. Using competition experiments we found (Table VI)  $k_{5'} = 5.3 \times 10^8$  and  $9.8 \times 10^8 M^{-1} \text{sec}^{-1}$  for methanol and ethanol, respectively, in good agreement with Gall and Dorfman<sup>7a</sup> and Wander, Gall, and Dorfman.<sup>7b</sup> In Table III we present  $k_4$ , calculated from eq IV, using our values of  $G_{\text{R}}$ ,  $k_5/k_6$ ,  $k_{5'}$ , and neglecting  $k_{6'}$ . Table III shows that results based on the ethanol system are practically identical with those based on the methanol system, yielding  $k_4 = (9.6 \pm 2.3) \times 10^7 \text{sec}^{-1}$ . (The value  $2.3 \times 10^7$  is the standard deviation.)

**Table III:** Determination of the  $O^- + H_2O$  Rate Constant ( $k_4$ ) (pH 8-8.8)

[ $K_4\text{Fe}(\text{CN})_6$ ], M	[ $\text{RH}_2$ ], M	$D^a$	$k_4 \times 10^{-8}$ $\text{sec}^{-1}$
0.01		0.174 (4)	
0.01	0.025 <sup>b</sup>	0.104 (6)	0.90
0.01	0.05 <sup>b</sup>	0.075 (5)	1.30
0.025		0.184 (10)	
0.025	0.05 <sup>b</sup>	0.111 (9)	1.08
0.025	0.10 <sup>b</sup>	0.077 (6)	0.98
0.025	0.0495 <sup>c</sup>	0.134 (3)	0.61
0.025	0.099 <sup>c</sup>	0.114 (9)	1.05
0.05		0.194 (10)	
0.05	0.05 <sup>b</sup>	0.134 (5)	0.92
0.05	0.10 <sup>b</sup>	0.098 (7)	0.68
0.05	0.099 <sup>c</sup>	0.134 (8)	0.86
0.05	0.198 <sup>c</sup>	0.115 (7)	1.54
0.10		0.199 (6)	
0.10	0.05 <sup>b</sup>	0.146 (4)	0.76
0.10	0.25 <sup>b</sup>	0.084 (6)	0.85
0.10	0.0495 <sup>c</sup>	0.169 (4)	0.87
0.10	0.099 <sup>c</sup>	0.151 (10)	0.97
0.10	0.198 <sup>c</sup>	0.128 (5)	1.10

<sup>a</sup> Average optical density extrapolated to the middle of the pulse duration. Numbers in parentheses represent the number of parallel determinations from which the average optical density was calculated. <sup>b</sup> Ethanol. <sup>c</sup> Methanol.

In Table IV we present data on the sensitivity of the calculated  $k_4$  (average values) to errors in optical densities, solute concentrations, and various parameters ( $G_{\text{R}}$ ,  $k_5/k_6$ ,  $k_{5'}$ , and  $k_{6'}$ ).

From Table IV it is evident that the results are most sensitive to the accuracy of the optical densities. Other parameters have a relatively small effect.

**Table IV:** Sensitivity of the Calculated  $k$  to Errors

Parameter	Error in parameter, %	Deviation in $k$ , %			
		$K_4\text{Fe}(\text{CN})_6$	$\text{CNS}^-$	$\text{I}^-$	$\text{Br}^-$
$D_0$	+3	-18	-20	-20	-28
$D$	+3	+24	+20	+30	+30
[S]	+3	-4	-5	-5	-5
[ $\text{RH}_2$ ]	+3	+11	+5	+5	+5
$G_{\text{R}}$	+4	+7	+6	+5	+16
$k_5/k_6$	+10	+14	+15	+11	+11
$k_4$	+30		-5	-5	-16
$k_{5'}$	-10	-7	-10	-10	-17
$k_{6'}$	$5 \times 10^7$ <sup>a</sup>	-4			

<sup>a</sup> Absolute reaction rate constant in units of  $M^{-1} \text{sec}^{-1}$ .

*Reaction Rate Constants for  $O^-$  Radical Ions. (a) Neutral pH (6-7 before Pulse).* Equation II was used to obtain ratios of  $R_5/R_{6'}$ , at high solute concentration, where the contribution of reaction 4 may be neglected. In Table V we present reaction rate constants for  $O^-$  radical ions in neutral solutions. The  $k_5/k_6$  values obtained at high solute concentrations (Table II) were used for the calculations of the  $O^-$  reaction rate constants.

From Table V,  $k_{6'} = (1.5 \pm 0.5) \times 10^9$ ,  $(2.3 \pm 0.4) \times 10^9$ , and  $(1.8 \pm 0.2) \times 10^8 M^{-1} \text{sec}^{-1}$  for  $\text{CNS}^-$ ,  $\text{I}^-$ , and  $\text{Br}^-$ , respectively.

The effect of errors on the calculation of  $k_{6'}$  is demonstrated in Table IV.

The significance of  $k_{5'}$  in the case of bromide is not clear in the light of the complications discussed in connection with the reactivity of  $\text{Br}^-$  towards OH radicals. If  $\text{Br}^-$  reacts with  $\text{H}_2\text{O}^+$  (presumably the precursor of OH), the net result is an apparent increase in the scavenging efficiency of OH by  $\text{Br}^-$  at high concentration. Such an effect was taken into account by using the results at the high  $\text{Br}^-$  concentration for the calculations of  $k_{6'}$ . However, the apparent effect of  $[\text{Br}^-]$  on  $k_6$  may indicate complications due to the intermediate  $\text{BrOH}^-$  as discussed above. It is likely that such an intermediate is formed also when  $\text{Br}^-$  reacts with  $O^-$  radical ions. In this case, the apparent reaction rate constant of  $O^-$  may also depend on  $[\text{Br}^-]$ . At present we can only conclude that  $O^-$  seems to be less reactive than OH towards  $\text{Br}^-$ . Further work is in progress in order to elucidate the reaction mechanism of OH with  $\text{Br}^-$ .

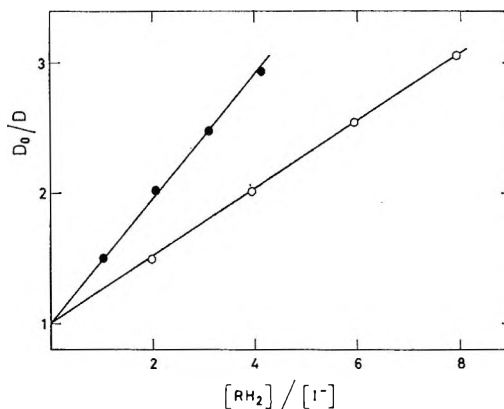
(b) *Alkaline Solutions.* In the alkaline medium, rate constants were measured either directly, following the formation of the product  $\text{S}^+$  by its optical absorption, or by competition with other solutes. In the case of iodide, thiocyanate, and ferrocyanide, the formation of the product  $\text{S}^+$  [ $\text{I}_2^-$ ,  $(\text{CNS})_2^-$ , and  $\text{Fe}(\text{CN})_6^{3-}$ , respectively] could be followed directly. In the case of iodide and thiocyanate, it is known that the oxidation of these ions is followed by a reaction to form the  $\text{X}_2^-$

**Table V:** Reaction Rate Constants for O<sup>-</sup> Radical Ions in Neutral Solutions Saturated with N<sub>2</sub>O<sup>a</sup>

[S], M	[RH <sub>2</sub> ], <sup>b</sup> M	D <sup>c</sup>	k × 10 <sup>-9</sup> , M <sup>-1</sup> sec <sup>-1</sup>
CNS <sup>-</sup>			
0.049		0.280 (3)	
0.049	0.05	0.213 (3)	0.7
0.049	0.10	0.178 (3)	1.1
0.196		0.182 (12)	
0.196	0.5	0.108 (13)	2.0
0.196	1.0	0.0735 (9)	1.5
0.196	0.99 <sup>d</sup>	0.111 (6)	2.6
0.196	1.98 <sup>d</sup>	0.073 (6)	1.5
0.49		0.192 (10)	
0.49	0.5	0.141 (9)	1.4
0.49	1.0	0.114 (11)	1.4
0.49	0.99 <sup>d</sup>	0.140 (9)	1.5
0.49	1.98 <sup>d</sup>	0.109 (7)	1.2
I <sup>-</sup>			
0.1		0.279 (7)	
0.1	0.103	0.230 (6)	3.0
0.1	0.206	0.185 (7)	2.0
0.1	0.412	0.143 (7)	2.2
0.2		0.282 (6)	
0.2	0.103	0.248 (6)	2.1
0.2	0.206	0.222 (7)	2.1
0.2	0.412	0.189 (6)	2.4
Br <sup>-</sup>			
0.5		0.303 (12)	
0.5	0.103	0.242 (10)	0.20
0.5	0.515	0.155 (10)	0.15
0.5	1.03	0.119 (7)	0.17
1.0		0.314 (9)	
1.0	0.103	0.264 (9)	0.15
1.0	0.515	0.195 (7)	0.19
1.0	1.03	0.158 (8)	0.19
2.0		0.335 (9)	
2.0	0.103	0.302 (7)	0.18
2.0	0.515	0.240 (10)	0.20
2.0	1.03	0.202 (8)	0.20

<sup>a</sup> (CNS)<sub>2</sub><sup>-</sup>, I<sub>2</sub><sup>-</sup>, and Br<sub>2</sub><sup>-</sup> were detected at 4750, 3800, and 3600 Å, respectively. <sup>b</sup> Ethanol, except if marked d. <sup>c</sup> The pulse intensity was constant in all the experiments of any particular solute S, except for the results with 0.049 M thiocyanate which were carried out with a pulse intensity different from the other thiocyanate experiments. The numbers in parentheses represent the number of parallel measurements, from which an average value was calculated. <sup>d</sup> Methanol.

radical ion.<sup>22</sup> The rate of formation of X<sub>2</sub><sup>-</sup> can be used to determine k<sub>6</sub> at neutral pH's and k<sub>6</sub>' in alkaline solutions provided that reaction 6 or 6' is rate determining. In earlier work this point has been disregarded both in the iodide<sup>22a</sup> and in the thiocyanate<sup>22b</sup> systems. Baxendale, Bevan, and Stott<sup>22c</sup> pointed out that in both the iodide and the thiocyanate systems, the formation of X<sub>2</sub><sup>-</sup> from X and X<sup>-</sup>, and not reaction 6, was actually the rate determining step. However, in alkaline solutions the formation of CNS and I radicals is much slower and the rate of X<sub>2</sub><sup>-</sup> formation is determined by reaction 6'.



**Figure 2.** Determination of  $k_5'/k_6'$  in N<sub>2</sub>O saturated alkaline iodide solutions: [NaOH] = 0.58 M; [I<sup>-</sup>] = 5 × 10<sup>-4</sup> M; D<sub>0</sub> = 0.263; 0.1-μsec pulse; ●, ethanol solutions; ○, methanol solutions.

In the alkaline range, plots of log (D<sub>∞</sub> - D) vs. t for both I<sub>2</sub><sup>-</sup> and (CNS)<sub>2</sub><sup>-</sup> are linear. D<sub>∞</sub> is the optical density measured after all the oxidizing radicals react, and before [X<sub>2</sub><sup>-</sup>] decreases due to recombination. The reaction rate constant of O<sup>-</sup> with Br<sup>-</sup> could not be determined in the alkaline pH range because of the reverse reaction<sup>23</sup> and the complications in the oxidation of Br<sup>-</sup> in alkaline solutions.<sup>10</sup>

The reactivity of O<sup>-</sup> towards methanol and ethanol in alkaline solutions has been determined by competition with iodide in N<sub>2</sub>O saturated alkaline solutions (Figure 2). In Table VI the results in the alkaline pH range are summarized.

**Table VI:** The Reactivity of O<sup>-</sup> in Alkaline Solutions

S	[S], M	[NaOH], M	"k" <sub>(OH+S)</sub> × 10 <sup>-9</sup> , <sup>a</sup> M <sup>-1</sup> sec <sup>-1</sup>	k <sub>(O<sup>-</sup>+S)</sub> × 10 <sup>-9</sup> , M <sup>-1</sup> sec <sup>-1</sup>
I <sup>-</sup>	5 × 10 <sup>-4</sup>	0.58	2.1	2.0
I <sup>-</sup>	1 × 10 <sup>-4</sup>	0.11	2.4	1.9
CNS <sup>-</sup>	1 × 10 <sup>-3</sup>	0.36	1.3	1.1
CNS <sup>-</sup>	1 × 10 <sup>-3</sup>	1.08	1.4	1.3
Ethanol		0.58	0.99 <sup>b</sup>	0.98
Methanol		0.58	0.54 <sup>b</sup>	0.53

<sup>a</sup> Apparent rate constant for the oxidation of the solute by (OH + O<sup>-</sup>) radicals. <sup>b</sup> From competition with iodide ions.

**Positive Ions. Ferrous and Cerous Ions (as Sulfates).** The identification of O<sup>-</sup> as an intermediate in the reaction of N<sub>2</sub>O with e<sub>aq</sub><sup>-</sup> was used to investigate the reactivity of O<sup>-</sup> with positive ions which are usually unstable in alkaline media. Again, as with negative ions, high solute concentrations have been employed to suppress reaction 4.

**The Ratio k<sub>5</sub>/k<sub>6</sub>.** The ratio k<sub>5</sub>/k<sub>6</sub> was measured in

(23) V. J. Linnenbom, C. H. Cheek, and J. W. Swinnerton, *NRL Quarterly on Nuclear Science and Technology*, April 1962, p 46.

both dilute solutions saturated with  $N_2O$  and relatively concentrated (0.1 M) deaerated solutions, in a way similar to that described before. The products of the oxidation of S,  $S^+$ , are ferric and ceric ions. Initial optical absorptions of these products were measured at 3050 and 3200 Å, respectively. Ferrocyanide saturated  $N_2O$  solutions ( $1 \times 10^{-3}$  M) were used for the determination of the pulse doses. As the optical absorptions were relatively small, we could not neglect the optical absorptions of ethanol radicals (only ethanol was used as  $RH_2$ ). The correction for the ethanol radical absorption was made by successive approximations, using extinction coefficients of 170 and 110  $M^{-1} \text{ cm}^{-1}$  at 3050 and 3200 Å, respectively. These values, measured in  $N_2O$  solutions containing no S, are in agreement with those previously reported.<sup>19a</sup> The formation of reduction products,  $S^-$ , by the reaction of the hydrated electrons with S was considered. The extinction coefficient of  $S^-$  was determined in Ar saturated 1 M ethanol solutions containing  $5 \times 10^{-3}$  M ferrous sulfate or cerous sulfate. The extinction coefficients  $\sim 500$  and  $\sim 40 M^{-1} \text{ cm}^{-1}$  were found for  $Fe^+$  at 3050 and  $Ce^{2+}$  at 3200 Å, respectively. Rate constants for  $e_{aq}^- + S$  reactions were taken from previous work.<sup>24</sup>

In Figure 3 we present the competition data for OH radicals. We obtained  $k_5/k_6$  values of 5.45 and 6.5 for ferrous and cerous ions, respectively, in agreement with previous results.<sup>25,26</sup>

**Reactivity of  $O^-$  Radical Ions.** To obtain the reactivity of  $O^-$  radical ions towards ferrous and cerous ions,  $G_{R'}$ , defined as the ratio  $G_{O^-}/(G_{OH} + G_{O^-})$  had to be determined. Unlike the negative ions, here the solutes S reacted with  $e_{aq}^-$  in competition with  $N_2O$ . In addition, a fraction of the  $e_{aq}^-$  reacted with  $H^+$ , which was present as a result of partial hydrolysis of S. We assumed  $G_{R'} = D_{CCl_4}/D_{N_2O}$ ;  $D_{CCl_4}$  and  $D_{N_2O}$  are the corrected optical densities obtained in solutions saturated with  $CCl_4$  and  $N_2O$ , respectively.  $CCl_4$  has a high reaction rate constant with  $e_{aq}^-$ .<sup>20</sup> The  $CCl_3$  radicals formed did not oxidize the positive ions used. (We determined the extinction coefficients of  $CCl_3$  as 130 and 115 at 3050 and 3200 Å, respectively.) The reactivity of  $O^-$  towards ferrous and cerous ions was calculated from initial corrected optical densities using a modified eq II, in which  $G_R$  was substituted by  $G_{R'}$ . The results are presented in Table VII.

From Table VII,  $k_6 = (3.1 \pm 1.2) \times 10^9$  and  $(5.9 \pm 2.2) \times 10^8 M^{-1} \text{ sec}^{-1}$  for ferrous and cerous ions. The value of  $k_6 = 7.6 \times 10^8 M^{-1} \text{ sec}^{-1}$  was calculated for cerous ions if  $k_4$  was  $3 \times 10^8 \text{ sec}^{-1}$  instead of  $1 \times 10^8 \text{ sec}^{-1}$  (in order to account for the possibility of the reaction  $O^- + H^+$ ).

## Discussion

(a)  $O^-$  as an Intermediate in Process 1. Reaction rate constants for  $O^-$  radical ions from two sources were compared and found identical within experimental

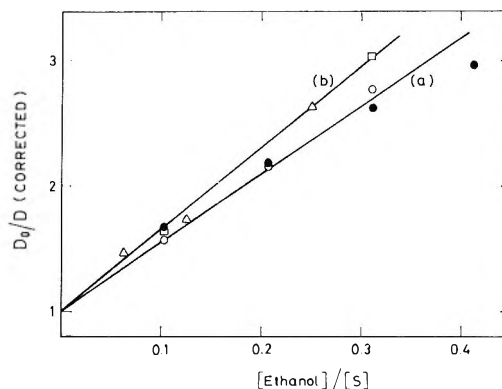


Figure 3. Determination of  $k_5/k_6$  for ferrous and cerous ions: (a) S =  $FeSO_4$ , 0.5- $\mu$ sec pulse;  $\bullet$ ,  $[Fe^{2+}] = 5 \times 10^{-3}$  M,  $N_2O$  saturated, pH 6.2,  $D_0 = 0.167$ ;  $\circ$ ,  $[Fe^{2+}] = 0.1$  M, Ar saturated, pH 4.5,  $D_0 = 0.097$ ; (b) S =  $Ce_2(SO_4)_3$ ,  $\Delta$ ,  $[Ce^{3+}] = 4 \times 10^{-3}$  M,  $N_2O$  saturated, pH 2.95 ( $H_2SO_4$  was added),  $D_0 = 0.0387$ , 0.3- $\mu$ sec pulse;  $\square$ ,  $[Ce^{3+}] = 0.1$  M, Ar saturated, pH 2.6,  $D_0 = 0.130$ , 0.6- $\mu$ sec pulse.

Table VII: Reactivity of  $O^-$  Radical Ions toward Ferrous and Cerous Ions

[S], M	[Ethanol], M	pH	$G_{R'}$	$D^a$ (cor)	$k \times 10^{-8}$ , $M^{-1} \text{ sec}^{-1}$
			<b><math>Fe^{2+}</math></b>		
0.05		4.8	0.52	0.176 (7)	
0.05	0.515			0.022 (6)	35
0.05	1.03			0.018 (5)	51
0.1		4.6	0.50	0.174 (5)	
0.1	0.515			0.028 (5)	24
0.1	1.03			0.0225 (6)	35
0.2		4.4	0.47	0.169 (5)	
0.2	0.515			0.033 (5)	15
0.2	1.03			0.030 (3)	28
			<b><math>Ce^{3+}</math></b>		
0.1		2.6	0.47	0.173 (5)	
0.1	0.25			0.0164 (8)	4.8
0.1	0.5			0.0133 (6)	8.5
0.2		2.3	0.42	0.229 (6)	
0.2	0.25			0.0332 (8)	3.5
0.2	0.5			0.0264 (6)	6.8

<sup>a</sup> See footnote a in Table III.

error: (a)  $O^-$  radical ions obtained *via* process 1; (b)  $O^-$  radical ions obtained by the ionic dissociation of OH radicals. This strongly indicates the identity of the two species as tentatively suggested by Czapski<sup>14</sup> on the basis of the results of Adams.<sup>13</sup> Moreover, our results in the ferrocyanide system give  $k_{(O^-+H_2O)} = 9.6 \times 10^7 \text{ sec}^{-1}$ . Combining this with  $pK_{OH} = 11.85$ <sup>8,9</sup> gives  $k_{(OH+OH^-)} = 1.3 \times 10^{10} M^{-1} \text{ sec}^{-1}$ . Adams,

(24) (a) J. H. Baxendale, *et al.*, *Nature*, **201**, 468 (1964); (b) J. H. Baxendale, E. M. Fielden, and J. P. Keene, *Proc. Roy. Soc. Ser. A*, **286**, 320 (1965).

(25) W. G. Rothschild and A. O. Allen, *Radiat. Res.*, **8**, 101 (1958).

(26) (a) T. J. Sworski, *ibid.*, **6**, 645 (1957); (b) Oak Ridge National Laboratory Annual Report, ORNL-3832 (1965).

Boag, and Michael<sup>21</sup> reported  $k_{(\text{OH}+\text{OH}^-)} = 3 \times 10^9 M^{-1} \text{ sec}^{-1}$ , based on  $k_{(\text{OH}+\text{ferrocyanide})} = 5 \times 10^9 M^{-1} \text{ sec}^{-1}$ . If the directly<sup>8</sup> measured value of  $k_{(\text{OH}+\text{ferrocyanide})} = 1.07 \times 10^{10} M^{-1} \text{ sec}^{-1}$  is used,  $k_{(\text{OH}+\text{OH}^-)} = 6.4 \times 10^9 M^{-1} \text{ sec}^{-1}$  results. Since  $k_{(\text{OH}+\text{OH}^-)}$  was obtained indirectly, using several rate constant ratios for the cross examination, we consider the results as being in agreement. This provides further support for the identification of  $\text{O}^-$  as an intermediate in process 1.

(b) *The Reactivity of  $\text{O}^-$  Radical Ions.* The appearance of  $\text{O}^-$  as an intermediate in process 1 may be used to investigate the reactivity of  $\text{O}^-$  in neutral and even in moderately acid solutions including solutes such as positive metal ions that are not stable in alkaline solutions. The ratio  $k_{(\text{O}^-+\text{reactant})}/k_{(\text{OH}+\text{reactant})}$  increases with the increase in the amount of positive charge of the reactant. The ferrous and cerous positive ions react with  $\text{O}^-$  faster than with  $\text{OH}$ . *While negative ions react faster with  $\text{OH}$ , the relative reactivity towards  $\text{OH}$  increases with the amount of negative charge.*

(c) *The Lifetime of  $\text{N}_2\text{O}^-$ .* In previous publications,<sup>8-12</sup> 0.2–0.3  $\mu\text{sec}$  has been set as an upper limit

for the lifetime of  $\text{N}_2\text{O}^-$ . We have assumed in all the calculations that  $\text{N}_2\text{O}^-$  does not react with any of the solutes, but forms exclusively  $\text{O}^-$  by reaction 3. The consistency of the rate constant ratios obtained in different systems supports this assumption. In order to determine the lifetime of  $\text{N}_2\text{O}^-$ , we carried out experiments at relatively high  $[\text{S}]$  ( $\text{I}^-$  or ferrocyanide ions were used as  $\text{S}$ ). Under our conditions,  $\text{e}_{\text{aq}}^-$  reacted with  $\text{N}_2\text{O}$  with a half-life of less than 10 nsec,  $\text{O}^-$  was converted into  $\text{OH}$  with a half-life of 7 nsec, and  $\text{OH}$  reacted with the solute (half-lives were calculated as 2–20 nsec depending on the solute concentrations). The time resolution in these experiments was about 50 nsec. Optical absorption was formed within 50 nsec and increased by 10–20% with a half-life of 50–100 nsec. If this increase is due to the conversion of  $\text{N}_2\text{O}^-$  into  $\text{O}^-$  radical ions, our results suggest that  $k_3 \simeq 10^7 \text{ sec}^{-1}$ .

*Acknowledgment.* The authors are indebted to Mr. Jechiel Ogdan for the operation of the linear accelerator and for invaluable support in maintenance and improvements in the system.

## Distorted Hydrogen Bonds Formed by Carbonyl Compounds

by C. N. R. Rao,\* Abha Goel, K. Gurudath Rao, and A. S. N. Murthy

Department of Chemistry, Indian Institute of Technology, Kanpur-16, India (Received June 2, 1970)

Publication costs borne completely by The Journal of Physical Chemistry

Molecular orbital calculations have been carried out on the open formamide dimer and the formaldehyde-water system to examine the effects of deviations from the lone-pair approach and from the linearity of the hydrogen bond. While deviations from the lone-pair approach do not markedly affect the properties of the hydrogen bonds formed by these carbonyl donors, bending the hydrogen bond beyond  $\sim 20^\circ$  causes a large decrease in the dissociation energy.

It is generally believed that hydrogen bonds formed by carbonyl compounds should be along the  $\text{sp}^2$  lone-pair direction of the carbonyl group.<sup>1,2</sup> Thus, the angle between an  $\text{X-H}$  bond and the axis of the carbonyl bond would be expected to be  $60^\circ$ . However, experimental molecular structure studies indicate that the angle,  $\phi$ , between the  $\text{X-H}$  bond and the lone-pair direction of the carbonyl oxygen (Figure 1) varies anywhere between 0 and  $60^\circ$  in amides, amino acids, and other systems.<sup>1,3,4</sup> Further, hydrogen bonds in most of these systems are bent,<sup>1,3,4</sup> the angle of bending,  $\theta$ , (Figure 1) being as large as 20 or  $25^\circ$ . We considered it interesting to investigate the effect of  $\phi$  and  $\theta$  on the

properties of the hydrogen bonded systems involving carbonyl donors. For this purpose, we have carried out semiempirical molecular orbital calculations on the formaldehyde-water system and the open trans dimer of formamide. In the case of formaldehyde-water, we

(1) G. C. Pimentel and A. L. McClellan, "The Hydrogen Bond," W. H. Freeman, San Francisco, Calif., 1960.

(2) A. S. N. Murthy and C. N. R. Rao, *J. Mol. Struct.*, **6**, 453 (1970).

(3) J. Donohue in "Structural Chemistry and Molecular Biology," (dedicated to Linus Pauling), A. Rich and N. Davidson, Ed., W. H. Freeman, San Francisco, Calif., 1968.

(4) G. N. Ramachandran and C. Ramakrishnan, "Symposium on Fibrous Proteins," Butterworths, Australia, 1967.

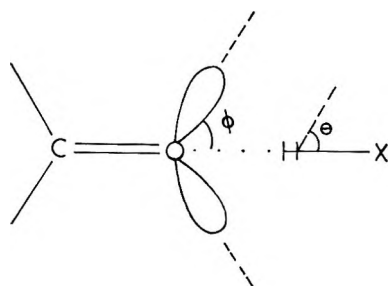


Figure 1. Angles  $\phi$  and  $\theta$  in the hydrogen bonds formed by carbonyl donors. When  $\phi = 0^\circ$ , the hydrogen bond ( $O \cdots X$ ) is along the lone-pair direction and when  $\phi = 60^\circ$ ,  $C=O$  and  $H-X$  are collinear.  $\theta$  is a measure of the deviation of the  $OH \cdots X$  bond from linearity. When  $\theta = 0^\circ$ ,  $X-H$  and  $O$  are collinear (*i.e.*,  $\angle XHO = 180^\circ$ ).

have employed both the CNDO/2<sup>5</sup> and the extended Hückel<sup>6</sup> (EHT) methods. A comparison of the properties calculated by the CNDO/2 and EHT methods enables us to have greater confidence in the conclusions from these calculations. As pointed out by Scheraga and coworkers,<sup>7</sup> such a comparative study provides a narrow bracketing range of results that we might obtain from more exact quantum mechanical calculations. In the case of the formamide dimer, we have employed only the CNDO/2 method since the EHT method does not predict a minimum energy configuration for the dimer.<sup>8,9</sup>

### Methods of Calculation

The EHT and CNDO/2 methods have been described in detail in the literature.<sup>5,6</sup> We have successfully employed these methods in this laboratory for the study of hydrogen bonds.<sup>8,10,11</sup> In EHT calculations, we employed the following  $H_{ii}$  values (eV):  $H_{ii}(C, 2s)$ ,  $-21.43$ ;  $(C, 2p)$ ,  $-11.42$ ;  $(O, 2s)$ ,  $-35.50$ ;  $(O, 2p)$ ,  $-17.76$ ;  $(N, 2s)$ ,  $-26.00$ ;  $(N, 2p)$ ,  $-13.40$ ; and  $(H, 1s)$ ,  $-13.60$ . The Slater orbital exponents were: H, 1.000; C, 1.625; N, 1.950; and O, 2.275. The Wolfsberg-Helmholz factor was taken to be 1.75. The values of the orbital exponents and Coulomb integrals employed in the CNDO/2 calculations were the same as those reported by Yan and others.<sup>7</sup> The orbital exponent of hydrogen in the CNDO/2 method was 1.2 which makes a strict comparison of the CNDO results with the EHT results difficult. The structural parameters of formamide and formaldehyde were taken from the literature.<sup>8,12</sup>

In the CNDO/2 calculations on the formaldehyde-water system, we have employed the minimized distances of 1.03 and 1.04 Å for the free and bonded O-H bonds<sup>13</sup> and an HOH angle of  $107^\circ$ . In the EHT calculations also we have employed these structural parameters since this method does not predict any minimum energy configuration for water; EHT calculations with the experimental geometry of  $H_2O$  also gave similar results. The magnitudes of hydrogen bond dissociation energies in the formaldehyde-water system by the CNDO/2 and the EHT methods would, however, differ

not only because of the inherent differences between the two methods,<sup>3,11</sup> but also because we have employed the CNDO minimized O-H distances in the EHT calculations as well; hydrogen bond energies are known to be quite sensitive to the O-H distance employed.<sup>14</sup> This should not seriously matter to us since we are mainly interested in examining the trends in the variation of  $D_e$  with  $\phi$  and  $\theta$ .

The energies of both the hydrogen bonded systems were calculated as functions of the  $X \cdots O$  distance,<sup>15</sup>  $R$ , for various values of  $\phi$  and  $\theta$ . From the potential energy curves (see Figure 2 for typical curves) thus calculated, we could get the dissociation energies ( $D_e$ ) of the hydrogen bonds. The charges (to be discussed later) are all for the minimum energy configurations. The computer programs for the CNDO/2 and EHT calculations were obtained from the Quantum Chemistry Program Exchange (QCPE 30 and 91). An IBM 7044/1401 computer was used for the calculations.

### Results and Discussion

CNDO/2 calculations on the formamide dimer clearly show that the dissociation energy of the hydrogen bond,  $D_e$ , increases slightly as  $\phi$  increases from  $0$  to  $60^\circ$  (Table I). In the formaldehyde-water system (Table I), the CNDO/2 method predicts the most stable configuration to be one with the O-H bond along the lone-pair direction ( $\phi = 0^\circ$ ); the EHT method, however, predicts that  $\phi = 60^\circ$  is the most stable configuration (Table II). The variations of the  $E_T$  and  $D_e$  with  $\phi$  are slightly more marked in the EHT results (Table II). These differences between the EHT and CNDO/2 results are not entirely unexpected. The EHT method generally overemphasizes charge separations.

In the case of the linear water dimer, CNDO/2 calculations predict the most stable configuration to be one where an O-H bond is directed in between the lone-

(5) J. A. Pople, *et al.*, *J. Chem. Phys.*, **43**, 129, 136 (1965); *ibid.*, **44**, 3289 (1966).

(6) R. Hoffmann, *ibid.*, **39**, 1397 (1963).

(7) J. F. Yan, F. A. Momany, R. Hoffmann, and H. A. Scheraga, *J. Phys. Chem.*, **74**, 420 (1970).

(8) A. S. N. Murthy, K. G. Rao, and C. N. R. Rao, *J. Amer. Chem. Soc.*, **92**, 3544 (1970).

(9) F. A. Momany, R. F. McGuire, J. F. Yan, and H. A. Scheraga, *J. Phys. Chem.*, **74**, 2424 (1970).

(10) A. S. N. Murthy and C. N. R. Rao, *Chem. Phys. Lett.*, **2**, 123 (1968).

(11) (a) A. S. N. Murthy, R. E. Davis, and C. N. R. Rao, *Theor. Chim. Acta*, **13**, 81 (1969); (b) A. S. N. Murthy, S. N. Bhat, and C. N. R. Rao, *J. Chem. Soc. A*, 1251 (1970).

(12) L. E. Sutton, Ed., "Tables of Interatomic Distances and Configurations in Molecules and Ions," Chemical Society, London, 1958, 1965.

(13) The bonded O-H distance was obtained from the first minimum in the proton potential curve.<sup>10,11a,b</sup>

(14) (a) P. A. Kollman and L. C. Allen, *J. Amer. Chem. Soc.*, **92**, 753 (1970); (b) A. Goel, A. S. N. Murthy, and C. N. R. Rao, *Indian J. Chem.*, **9**, 56 (1971); (c) C. N. R. Rao in "Water—A Treatise," F. Franks, Ed., Plenum Press, New York, N. Y., 1971.

(15) X is oxygen in formaldehyde-water and nitrogen in formamide dimer.

**Table I:** CNDO/2 Calculations on the Effect of  $\phi$  on Linear Hydrogen Bonds

$\phi$ , deg	$R_e$ , Å	$E_T$ , eV	$D_e$ , kcal mol <sup>-1</sup>	Charges <sup>a</sup>				
				O <sub>D</sub>	C <sup>b</sup>	H <sup>c</sup>	X <sub>A</sub> <sup>d</sup>	$\mu$ (D)
Formaldehyde-Water ( $\theta = 0^\circ$ )								
0°	2.6	-1271.74	7.5	$\sigma$ 4.997 (5.027) $\pi$ 1.190 (1.165)	2.966 (2.955) 0.811 (0.835)	0.831 (0.865) 0.0 (0.0)	4.314 (4.270) 2.00 (2.00)	4.50
30	2.6	-1271.73	7.3	$\sigma$ 4.998 $\pi$ 1.190	2.967 0.810	0.830 0.0	4.312 2.00	4.50
60	2.6	-1271.72	7.2	$\sigma$ 5.001 $\pi$ 1.190	2.996 0.810	0.831 0.0	4.311 2.00	4.20
Formamide Open Dimer ( $\theta = 0^\circ$ )								
0	2.6	-2138.92	5.0	$\sigma$ 4.994 (4.964) $\pi$ 1.371 (1.343)	2.863 (2.857) 0.779 (0.798)	0.835 (0.880) 0.0 (0.0)	3.445 (3.402) 1.853 (1.859)	7.30
30°	2.6	-2138.93	5.3	$\sigma$ 4.946 $\pi$ 1.371	2.864 0.778	0.834 0.0	3.443 1.852	7.50
60	2.6	-2138.93	5.3	$\sigma$ 4.948 $\pi$ 1.371	2.864 0.778	0.834 0.0	3.442 0.852	7.30

<sup>a</sup> Charges on the atoms in the parent electron donors (D) and acceptors (A) are shown in parentheses. <sup>b</sup> Carbon of the donor carbonyl group. <sup>c</sup> Hydrogen taking part in hydrogen bonding. <sup>d</sup> X is the acceptor atom. <sup>e</sup> When  $\phi = 20^\circ$ , the  $R_e$ ,  $E_T$ ,  $D_e$ ,  $\mu$ , etc., are nearly the same.

**Table II:** EHT Calculations on the Effect of  $\phi$  on the Formaldehyde-Water System ( $\theta = 0^\circ$ )

$\phi$ , deg	$R_e$ , Å	$E_T$ , eV	$D_e$ , kcal mol <sup>-1</sup>	Charges <sup>a</sup>				Overlap populations		
				O <sub>D</sub>	C <sup>b</sup>	H <sup>c</sup>	X <sub>A</sub> <sup>d</sup>	O—H	O...H	C=O
0	2.6	-436.95	3.2	$\sigma$ 5.438 (5.519) $\pi$ 1.821 (1.821)	2.695 (2.690) 0.179 (0.179)	0.380 (0.372) 0.0 (0.0)	5.326 (5.257) 0.0 (0.0)	0.3959 (0.4527)	0.1017 (0.0)	0.7609 (0.7573)
30	2.6	-436.98	3.9	$\sigma$ 5.429 $\pi$ 1.821	2.697 0.179	0.385 0.0	5.329 0.0	0.3901	0.1080	0.7619
60	2.6	-436.99	4.1	$\sigma$ 5.428 $\pi$ 1.821	2.697 0.179	0.386 0.0	5.330 0.0	0.3893	0.1082	0.7616

<sup>a</sup> Charges on the atoms in the parent electron donors (D) and acceptors (A). <sup>b</sup> Carbon of the donor carbonyl group. <sup>c</sup> Hydrogen taking part in hydrogen bonding. <sup>d</sup> X is the acceptor oxygen atom.

pair orbitals of the donor oxygen;<sup>16</sup> *ab initio* calculations predict a variation of  $\phi$  between 0 and 30°. <sup>17,18</sup> It appears that in all the systems investigated until now,  $D_e$  of the hydrogen bond does not vary very much with  $\phi$ . It appears that the lone-pair approach is not a rule as generally assumed; the lone-pair orbital of the oxygen can be distorted by electronic interactions in such a way that the most stable configuration is not dictated by the direction of the pure hybrid orbital.

CNDO/2 calculations on bent hydrogen bonds show that the hydrogen bond dissociation energy decreases with increase in the angle of bend,  $\theta$ , the decrease becoming more marked when  $\theta$  is more than  $\sim 20^\circ$  (Table III). In Figure 2, we have plotted the change in energy,  $\Delta E$ , when the monomers are brought together, as a

function of  $\theta$ . The decrease in  $D_e$  is accompanied by an increase in the total molecular energy of the system as well as in  $R_e$ . The decrease in  $D_e$  beyond a  $\theta$  of  $\sim 20^\circ$  is between 80 and 130 cal deg<sup>-1</sup> bend. A decrease in  $D_e$  with increase in  $\theta$  has also been noted by Scheraga and coworkers,<sup>9</sup> but the tolerable limit of  $\theta$  mentioned here is worth noting. EHT calculations on the formaldehyde-water system (Table IV) also show that  $D_e$  decreases markedly when  $\theta > 20^\circ$ . It appears as though that with carbonyl donors, a  $\theta$  of  $\sim 20^\circ$  can be

(16) A. Geol, A. S. N. Murthy, and C. N. R. Rao, *J. Chem. Soc. A*, 190 (1971).

(17) J. Del Bene and J. A. Pople, *J. Chem. Phys.*, **52**, 4858 (1970).

(18) P. A. Kollman and L. C. Allen, *ibid.*, **51**, 3286 (1970).



**Table III:** CNDO/2 Calculations of the Effect of Bending Hydrogen Bonds

$\theta$ , deg	$R_{\text{OH}}$ , Å	$E_{\text{T}}$ , eV	$D_e$ , kcal mol <sup>-1</sup>	Charges <sup>a</sup>				
				O <sub>D</sub>	C <sup>b</sup>	H <sup>c</sup>	X <sub>A</sub> <sup>d</sup>	$\mu$ (D)
Formaldehyde-Water ( $\phi = 0^\circ$ )								
0	2.6	-1271.74	7.5	$\sigma$ 4.997 (5.027) $\pi$ 1.190 (1.165)	2.966 (2.955) 0.811 (0.835)	0.831 (0.865) 0.0 (0.0)	4.314 (4.270) 2.00 (2.00)	4.50
20	2.6	-1271.71	6.9	$\sigma$ 4.998 $\pi$ 1.190	2.965 0.810	0.829 0.0	4.315 2.00	4.40
30	2.7	-1271.69	6.3	$\sigma$ 4.999 $\pi$ 1.190	2.965 0.810	0.828 0.0	4.315 2.00	4.30
60	2.8	-1271.57	3.4	$\sigma$ 5.014 $\pi$ 1.179	2.962 0.821	0.849 0.0	4.295 2.00	3.90
Formamide Open Dimer ( $\phi = 0^\circ$ )								
0	2.6	-2138.92	5.0	$\sigma$ 4.944 (4.964) $\pi$ 1.371 (1.343)	2.863 (2.857) 0.779 (0.798)	0.835 (0.880) 0.0 (0.0)	3.445 (3.402) 1.853 (1.859)	7.30
20	2.6	-2138.88	4.4	$\sigma$ 4.945 $\pi$ 1.370	2.863 0.779	0.834 0.0	3.446 1.853	6.85
30	2.7	-2138.86	3.8	$\sigma$ 4.951 $\pi$ 1.364	2.861 0.783	0.842 0.0	3.435 1.854	6.40
60	2.9	-2138.75	1.3	$\sigma$ 4.960 $\pi$ 1.355	2.858 0.790	0.854 0.0	3.420 1.855	5.07

<sup>a</sup> Charges on the atoms in the parent electron donors (D) and acceptors (A) are shown in the parentheses. <sup>b</sup> Carbon of the donor carbonyl group. <sup>c</sup> Hydrogen taking part in hydrogen bonding. <sup>d</sup> X is the acceptor atom.

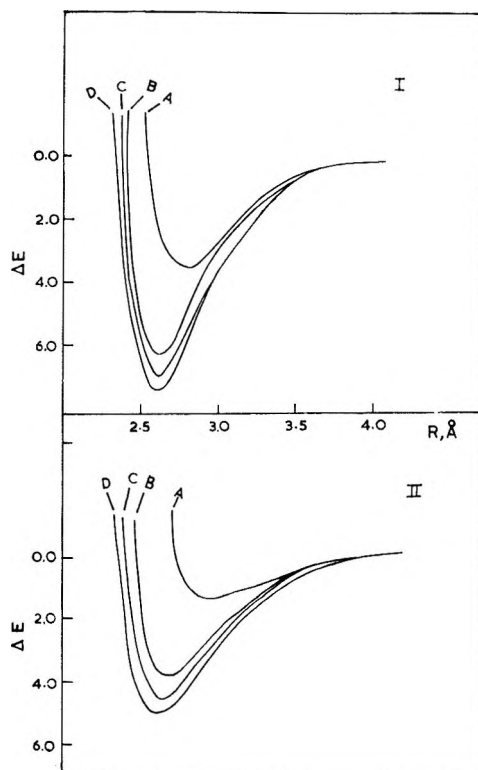


Figure 2. Variation of  $\Delta E$  (kcal/mol) with  $\theta$  in formaldehyde-water (I) and formamide trans dimer (II). Angle of bending,  $\theta$ , is  $60^\circ$ ,  $30^\circ$ ,  $20^\circ$ , and  $0^\circ$  in curves A, B, C, and D, respectively. The  $\Delta E$  values were obtained from CNDO/2 calculations.

accommodated without much gain in the energy of the system (Figure 2). In the case of the water dimer, Rao and coworkers<sup>16</sup> find that the decrease in  $D_e$  becomes marked when  $\theta$  is greater than  $\sim 20^\circ$ . These results of molecular orbital calculations on bent hydrogen bonds are consistent with experimental observations.<sup>1,3,4</sup>

From the CNDO/2 results (Tables I and III), we see that hydrogen bonding in formamide dimer causes  $\sigma$  gain and a small  $\pi$  loss in both nitrogen and carbon,  $\sigma$  loss and  $\pi$  gain in oxygen, and  $\sigma$  loss in hydrogen; the direction of transfer of negative charge is from the C=O group to the H-N group. The changes in the charges of the formaldehyde-water system are very similar. Variation of  $\phi$  does not significantly alter the charges or the dipole moments of the hydrogen bonded systems; increase in  $\theta$ , however, markedly affects both the charges and the dipole moments, particularly beyond a  $\theta$  of  $20^\circ$ . As  $\theta$  increases, we see that charges approach those in the isolated monomers as expected.

As mentioned earlier, the EHT method exaggerates charge separation particularly in the case of the C=O bond. We see that the changes in the EHT charges are essentially due to  $\sigma$  contributions (Table II and IV). Although the CNDO charges are likely to be more reasonable, we see that the Mulliken overlap populations as well as the EHT charges listed in Table IV show the expected variations with  $\theta$ .

**Table IV:** EHT Calculations on the Effects of Bending the Hydrogen Bond in Formaldehyde-Water System ( $\phi = 0^\circ$ )

$\theta$ , deg	$R_e$ , Å	$E_T$ , eV	$D_{e_1}$ , kcal mol <sup>-1</sup>	Charges <sup>a</sup>				Overlap populations		
				O <sub>D</sub>	C <sup>b</sup>	H <sup>c</sup>	X <sub>A</sub> <sup>d</sup>	O—H	O...H	C=O
0	2.6	-436.95	3.2	$\sigma$ 5.438	2.695	0.380	5.326	0.3959	0.1017	0.7609
				(5.519)	(2.690)	(0.372)	(5.257)	(0.4527)	(0.0)	(0.7573)
				$\pi$ 1.821	0.179	0.0	2.0			
20	2.6	-436.94	3.0	$\sigma$ 5.438	2.694	0.380	5.326	0.3963	0.1016	0.7626
				$\pi$ 1.821	0.179	0.0	2.0			
				(1.821)	(0.179)	(0.0)	(2.0)			
30	2.7	-436.93	2.8	$\sigma$ 5.456	2.692	0.379	5.311	0.4089	0.0790	0.7623
				$\pi$ 1.821	0.179	0.0	2.0			
				$\sigma$ 5.506	2.692	0.373	5.268	0.4408	0.0151	0.7568
60	3.2	-436.83	0.5	$\pi$ 1.821	0.179	0.0	2.0			

<sup>a</sup> Charges on the atoms in the parent electron donors (D) and acceptors (A) are shown in the parentheses. <sup>b</sup> Carbon of the donor carbonyl group. <sup>c</sup> Hydrogen taking part in hydrogen bonding. <sup>d</sup> X is the acceptor oxygen atom.

*Acknowledgment.* The authors are thankful to the Council of Scientific and Industrial Research, India, for

the support of this research and the staff of the IITK Computer Centre for the facilities.

## On Tunneling Corrections in Chemical Kinetics

by S. G. Christov\*

*Institute of Physical Chemistry, Bulgarian Academy of Sciences, Sofia, Bulgaria*

and Ž. L. Georgiev

*Department of Physical Chemistry, Higher Chemico-Technological Institute, Sofia, Bulgaria (Received August 5, 1970)*

*Publication costs borne completely by The Journal of Physical Chemistry*

A comparison is made between the results of one-dimensional and two-dimensional procedures of calculating tunneling corrections for reactions of the type  $AH + B \rightarrow A + HB$  (via a linear activated complex  $A-H-B$ ), where A and B are heavy atoms. An improvement of the method of Johnston and Rapp for estimation of two-dimensional tunneling corrections for these reactions is proposed. Computations show that the one-dimensional treatment of the (extended) reaction path overestimates tunneling, but not too much, but underestimates it if the mass transferred is taken to be equal to the proton mass.

### I. Introduction

The role of the tunnel effect in the kinetics of chemical reactions of hydrogen and its isotopes has been discussed many times in recent years.<sup>1-10</sup> There exist both theoretical reasons and experimental facts which clearly show that it is necessary to introduce a correcting factor to the classical reaction rate in order to account for the tunneling of protons or hydrogen atoms through the potential energy barrier.

An exact solution of the tunneling problem is possible in the usual one-dimensional approximation. Johnston<sup>5</sup> has posed the question whether this approximation is justified if one wishes to connect it with an ap-

plication of the activated complex method for a complete evaluation of the reaction rate. He has stressed

- (1) R. P. Bell, *Trans. Faraday Soc.*, **55**, 1 (1959).
- (2) R. E. Weston, *J. Chem. Phys.*, **31**, 892 (1959).
- (3) S. G. Christov, *Z. Elektrochem.*, **62**, 567 (1958).
- (4) S. G. Christov, *Dokl. Akad. Nauk SSSR*, **136**, 663 (1960).
- (5) H. S. Johnston, *Advan. Chem. Phys.*, **3**, 131 (1960).
- (6) T. E. Sharp and H. S. Johnston, *J. Chem. Phys.*, **37**, 1541 (1960).
- (7) H. S. Johnston and D. Rapp, *J. Amer. Chem. Soc.*, **83**, 1 (1961).
- (8) E. F. Caldin, *Discussions Faraday Soc.*, **39**, 2 (1965).
- (9) S. G. Christov, *J. Res. Inst. Catalysis, Hokkaido Univ.*, **16**, 169 (1968).
- (10) E. M. Mortensen, *J. Chem. Phys.*, **48**, 4029 (1968); **49**, 3526 (1968).

that the motion of the system along the reaction path could be treated as a one-dimensional tunneling problem only in the vicinity of the transition state, which practically means a restriction for the application of the usual method to reactions at relatively high temperatures.

Johnston and Rapp<sup>7</sup> have suggested an approximate method which, under certain conditions, allows a consideration of the problem for motion with two degrees of freedom. In this way they have found that at low temperatures the tunneling correction may be considerably smaller in comparison to that obtained in treating the movement of the system in one dimension along the entire classical reaction path.

These results have been already discussed in a previous paper.<sup>9</sup> It has been shown, using the numerical data of Sharp and Johnston,<sup>6</sup> that the one-dimensional treatment of the reaction path gives a lower limit of the tunneling correction provided that the mass transferred through the barrier is equal to the proton mass,  $m_H$ <sup>9</sup> (see Conclusions).

Recently Mortensen<sup>10</sup> has treated quantum-mechanically the isotopic reactions of the type  $H_2 + H = H + H_2$  as a two-dimensional problem. He has found that the tunneling corrections are greater than the one-dimensional ones although they do not differ largely from them.

In view of the importance of the problem, in the present work an investigation on the conditions of applicability of one- and two-dimensional approach for evaluation of the tunneling corrections is carried out, and a comparison of their results is made. For this purpose, an improved modification of the procedure of Johnston and Rapp<sup>7</sup> is used which is based on a better approximation of the potential barrier. A simplified approximate method for calculation of the tunneling corrections is also proposed, which permits one to replace a large part of the numerical calculations by means of analytical expressions.

To verify the conclusions of Johnston and Rapp<sup>7</sup> we use the same potential energy surface; however, we refer it to a hypothetical reacting system for which the procedure of calculation employed is much more justifiable than in the case studied by those authors.<sup>7</sup> This is permissible as our purpose is to compare one-dimensional and two-dimensional tunneling corrections under the same conditions.

## II. General Considerations

Let us consider the reaction



where H is a hydrogen atom or proton, and A and B are atoms or radicals treated as mass points. In particular,  $A = H$  (D or T) and  $B = H$  (D or T). We assume that energetically the most favorable reaction path corresponds to a linear complex  $A \cdots H \cdots B$ , so

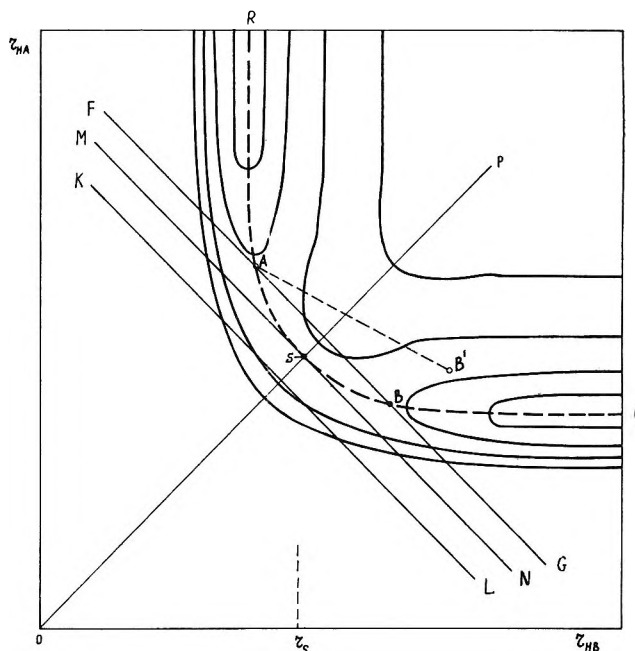


Figure 1. Potential energy map of the complex A-H-B ( $A = H$  and  $B = H$ ); S, saddlepoint;  $r_s$ , saddlepoint coordinate; OP, bisecting line; RSC, reaction coordinate; KL, MN, and FG, cross sections with a slope of  $-45^\circ$ .

that the potential energy of the system  $V(r_{AH}, r_{HB})$  is a function of two distances  $r_{AH}$  and  $r_{HB}$ .

The topographic map of the potential energy surface for the system H-H-H has been constructed by Weston,<sup>2</sup> using Sato's method<sup>11</sup> in a coordinate system with an angle between the axes of  $60^\circ$ . Following Johnston and Rapp<sup>7</sup> we shall use Weston's data in a rectangular coordinate system (Figure 1) at conditions which will be specified below.<sup>12</sup>

The reaction is described classically in the plane  $r_{AH}, r_{HB}$  by the translational motion of a representative point, with an effective mass  $\mu$ ,<sup>13</sup> along the reaction coordinate RC, passing through the saddlepoint S of the potential energy surface  $V(r_{AH}, r_{HB})$ . In the vicinity of that point the movement of the system may be also treated as an unstable harmonic vibration  $\vec{A} \cdots \vec{H} \cdots \vec{B}$  with an imaginary frequency  $\nu_s^* = 1/2\pi \sqrt{f^*/\mu^*}$ , where the force constant  $f^* < 0$  and the effective mass is given by the expression

$$\mu^* = 1/2 m_H \frac{m_A + m_B}{m_H + m_A + m_B} \quad (2)$$

(11) S. Sato, *J. Chem. Phys.*, 23, 59, 2465 (1955).

(12) It should be stressed once more that for the purpose of comparing the one- and two-dimensional approach for tunneling calculation it is permissible to use a somewhat arbitrary potential energy surface. The conclusions drawn from such comparison will probably not change essentially if Weston's energy surface is replaced by a more accurate one (see, for example, the work of Shavitt [J. Shavitt, *ibid.*, 48, 2700 (1968)] which shows, however, that the Weston surface is qualitatively correct).

(13) The effective mass varies during the movement along the reaction path because of the change in its direction (*cf.* eq 5).

$m_H$ ,  $m_A$ , and  $m_B$  being the masses of H, A, and B, respectively.

If A and B are heavy atoms or radicals, so that  $m_H \ll m_A$  and  $m_H \ll m_B$ , one obtains  $\mu^* = 1/2 m_H$  from eq 2. In this case reaction 1 proceeds in the critical region in such a way that A and B remain stationary at a fixed distance during the transfer of H from A to B, i.e.,  $r_{AB} = r_{AH} + r_{HB} = \text{constant}$  ( $dr_{AH} = -dr_{HB}$ ), whereas a small motion of A-B assures the conservation of the mass center.<sup>7</sup> This means that in a rectangular coordinate system  $r_{AH}$ ,  $r_{HB}$  the reaction path will pass through the saddlepoint with a slope  $dr_{AH}/dr_{HB} = \arctan(-45^\circ)$ . These conditions are obviously not fulfilled for the linear complex H-H-H for which, according to eq 2,  $\mu^* = 1/3 m_H$ . A somewhat better approximation to the conditions of heavy end atoms is achieved if the end atoms A and B are replaced by the hydrogen isotopes D or T. Then one obtains  $\mu^* = 2/3 m_H$  and  $\mu^* = 3/7 m_H$ , for the systems D-H-D and T-H-T, respectively. If a hypothetical super heavy hydrogen isotope X is considered, with atomic mass considerably larger than  $m_H$ , we could obtain  $\mu^* = 1/2 m_H$  for the complex X-H-X. For that hypothetical complex it will be justified to use Weston's data to calculate the tunneling correction. These data are represented in a rectangular coordinate system such as in Figure 1.

The reaction coordinate is the most probable path for a classical transfer of the system from the initial to the final state. The reaction will undoubtedly occur along that path at sufficiently high temperatures. At these conditions, it is possible to account for a small degree of tunneling in the transition state, as shown by Wigner,<sup>14</sup> if the movement along the reaction coordinate is considered as an unstable harmonic vibration around the saddlepoint, separable from the real vibrations of the activated complex. This means that the problem is reduced to one-dimensional tunneling of a mass point with an effective mass  $\mu^*$  given by eq 2, through a parabolic barrier, which adequately describes the profile of the potential energy surface in a region  $\Delta$  around the saddlepoint. According to Johnston,<sup>5</sup> this treatment is justified only under the condition  $\lambda \ll \Delta$  where  $\lambda = h/\sqrt{2\pi\mu^*kT}$  is the De Broglie wavelength which is connected with the motion along the reaction path. In this case the reaction coordinate in the region  $\Delta$  can be separated from the real vibrations, and the tunneling problem may be considered in one dimension. Another criterion is suggested by Christov,<sup>3,4,15</sup> who has introduced a characteristic temperature  $T_K$ , at which the probability of the system to overcome the barrier or to penetrate through it by tunneling is one and the same. For a truncated parabolic barrier, this temperature is defined by the expression<sup>4,15</sup>

$$T_K = \frac{h}{2\pi^2k} \sqrt{\frac{L_m}{\mu}}, \quad L_m = -\left(\frac{\partial^2 V}{\partial x^2}\right)_{x=x_m} \quad (3)$$

where  $L_m$  is the barrier curvature. This equation<sup>16</sup>

applies to any one-dimensional barrier<sup>4,15</sup>  $V(x)$ , with curvature at top ( $x = x_m$ ) equal to  $L_m$ . It also applies as a good approximation to a two-dimensional barrier<sup>9</sup>  $V(r_{AH}, r_{HB})$ , if  $L_m$  is expressed by means of the curvature of the barrier profile along the reaction coordinate at the saddlepoint, since at  $T = T_K$ , by definition, half of the systems should pass over the barrier profile and the other half tunnel through it—mainly in the region  $\Delta$ , where the reaction coordinate is separable. Hence, at  $T \gtrsim T_K$  the tunneling correction could be always calculated by the formula<sup>17</sup>

$$\mathcal{K} = \frac{(\pi/2)(T_K/T)}{\sin[(\pi/2)(T_K/T)]} \quad (4)$$

which is identical with the Bell expression<sup>1</sup> for a parabolic barrier. Sometimes this formula could also apply to a certain extent, at temperatures  $T < T_K$ , if the range  $\Delta$  around the saddlepoint is comparatively wide.<sup>9</sup>

However, at temperatures considerably lower than  $T_K$ , nonseparable quantum-mechanical penetration through the barrier could deviate the reaction sensibly from its classical path. In general, a tunnel transfer is possible from any point of the reaction coordinate to any point, corresponding to the same energy level at the other side of the barrier. The most favorable "tunneling direction" will have a slope of  $-45^\circ$ , since "the tunneling path" is the shortest and the effective mass is the smallest one. Indeed, it is seen in Figure 1 that the line segment AB (with a slope of  $-45^\circ$ ) is shorter than the line segment AB'—along which a tunneling may also occur from point A. Further, from the general expression for the effective mass of the linear complex A-H-B<sup>18</sup>

$$\mu = \frac{m_A m_B (1+c)^2 + m_H m_B c^2 + m_H m_A}{(m_A + m_B + m_H)(1+c^2)}, \quad c = \frac{dr_{AH}}{dr_{HB}} \quad (5)$$

it follows that  $\mu$  has a minimum value at  $c = -1$  (slope of  $-45^\circ$ ). Then, eq 5 reduces to eq 2.<sup>19</sup> One should note that the effective mass depends only on the slope  $c$  of the line along the plane  $r_{AH}$ ,  $r_{HB}$ .

These considerations are the basis of the Johnston-Rapp method<sup>7</sup> for calculation of the tunneling corrections at  $T \ll T_K$ , when the reaction coordinate is nonseparable from the other coordinates of the system

(14) E. Wigner, *Z. Phys. Chem. (A)*, **19**, 203 (1932).

(15) S. G. Christov, *Ann. Phys.*, **12**, 20 (1963).

(16) Johnston and Rapp, using numerical methods, have come to an equivalent result (ref 7, Figures 6-8), but no conclusion has been drawn from it.

(17) S. G. Christov, *Ann. Phys.*, **15**, 87 (1965).

(18) H. S. Johnston, "Gas Phase Reaction Rate Theory," Ronald Press, New York, N. Y., 1966.

(19) The general expression (5), recently derived by Johnston,<sup>18</sup> applies equally well both for a stable molecule and for an activated complex. It contains, as particular cases, the well-known expressions for the effective masses of the symmetrical and asymmetrical stretching vibrations of a stable molecule of the type A-x-B at  $c = 1$  and  $c = -1$ , respectively (eq 2 applies for the latter case).

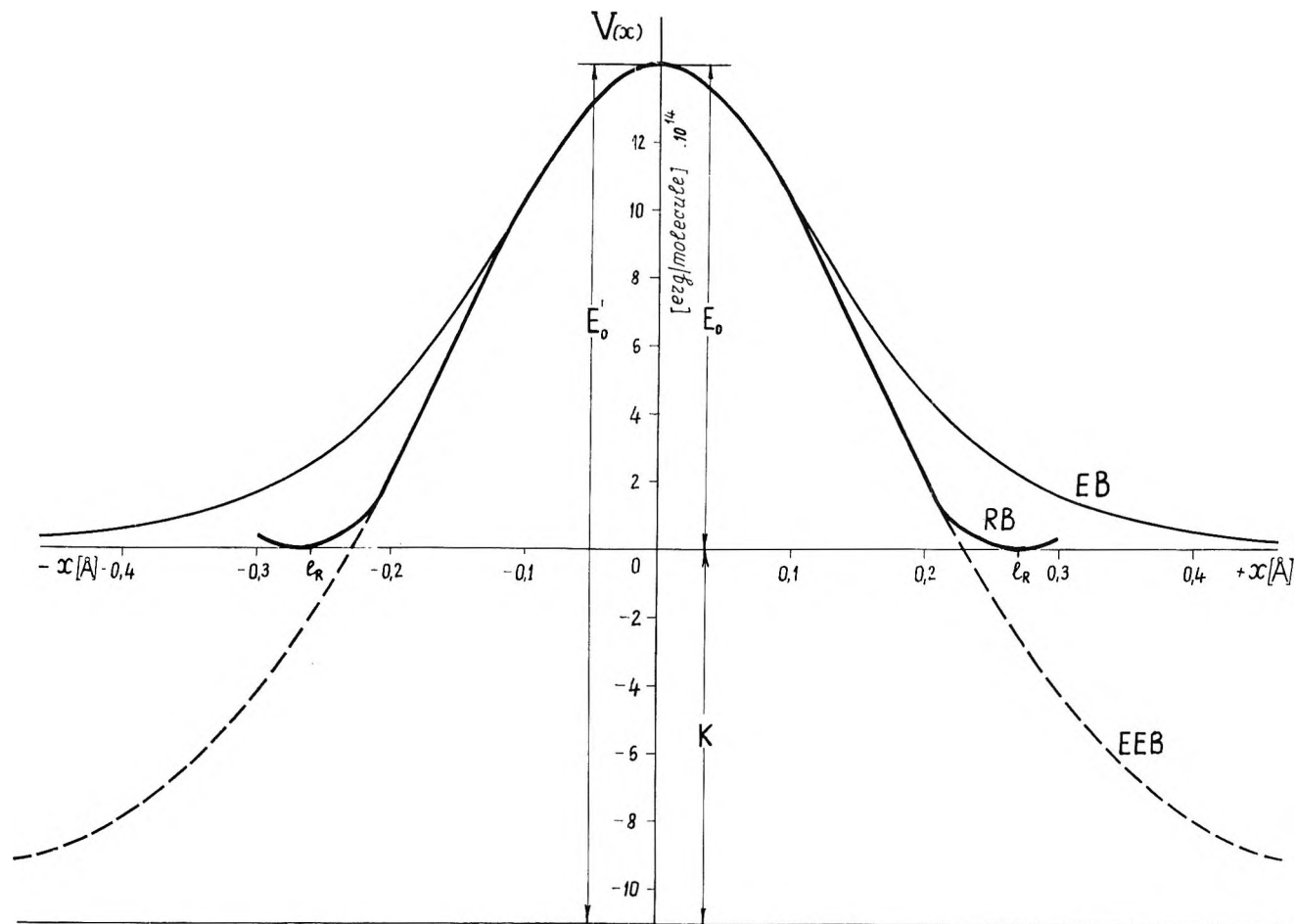


Figure 2. An example of two different approximations of potential profiles of a section through the two-dimensional barrier: RB, real barrier (a profile of the barrier in the section with coordinates of its crossing point with OP,  $r_{AH} = r_{HB} = 0.955 \text{ \AA}$ ); EB, Eckart barrier; EEB, equivalent Eckart barrier, corresponding to the generalized Eckart barrier (GEB) expressed by eq 15;  $E_0$ , height of RB, EB, and GEB;  $E_0' = E_0 + K$ , height of EEB;  $l_R = 0.261 \text{ \AA}$ ,  $l = 0.230 \text{ \AA}$ ,  $l_E = 0.537 \text{ \AA}$ ,  $l' = 0.741 \text{ \AA}$  ( $a = 0.974$ ); cf. eq 15.

( $\lambda \gg \Delta$ ). One assumes that all transfers from the initial to the final state occur in the most favorable "tunneling directions," *i.e.*, along a set of parallel lines (with a slope of  $-45^\circ$ ), determined by the intersection points with the bisecting line OP of the coordinate axes. Any transfer along a given line is treated as a one-dimensional tunneling problem. The corresponding one-dimensional barrier  $V_r(x)$  is the profile of a cross section through the potential energy surface  $V(r_{AH}, r_{HB})$  along that line (Figure 2). The reaction rate can be expressed by a sum over the transitions along all parallel cross sections.

This approach implies that at any arbitrary distance between A and B, the transfer of H from A to B occurs so rapidly that the distance  $r_{AB} = r_{AH} + r_{HB}$  remains unchanged during the transfer ( $\Delta r_{AH} = -\Delta r_{HB}$ ). This assumption is certainly not true for large distances  $r_{AB}$ ; in this case, however, the transfer probability is small because of the large dimensions (width and height) of the barrier profile at the corresponding sections. In any case, the Johnston-Rapp method seems

to be justified enough if the most probable path intersects the line OP not too far from the saddlepoint so that the distance  $r_{AB}$  is not so much larger than the length of the "classical" activated complex.

### III. Method of Calculation

Let us denote as  $r$  the distance between the intersection point of a given cut with the bisecting line OP from the zero point  $O$  of the coordinate system (Figure 1). The total probability for a system to pass through or over the barrier profile  $V_r(x)$  in a given cross section is expressed by

$$P'(r) = \frac{1}{kT} \int_0^\infty W_r(U_r) e^{-U_r/kT} dU_r \quad (6)$$

where  $U_r$  is the energy of the system measured from the minimum  $V_0(r)$  of the corresponding profile (Figure 2) (on the left side of the barrier  $V_r(x)$ ), and  $W_r(U_r)$  is the corresponding "tunneling probability" (permeability of the barrier). The classical probability for the transfer in consideration is  $P_{cl}'(r) = e^{-E_0(r)/kT}$ , where

$E_0(r)$  is the height of the one-dimensional barrier, while the ratio

$$\mathcal{C}_r = \frac{P'(r)}{P_{cl}'(r)} = \frac{e^{E_0(r)/kT}}{kT} \int_0^\infty W_r(U_r) e^{-U_r/kT} dU_r \quad (7)$$

is the tunneling correction factor for a given cross-cut.

For a system in the initial state ( $r_{HB} = \infty$ ) there is a probability to reach the energy level  $V_0(r)$  along the reaction path given by  $e^{-V_0(r)/kT}$ . Thus

$$P(r) = P'(r) e^{-V_0(r)/kT} \quad (8)$$

represents the probability of the system to pass along the corresponding cross section, while

$$P = \int_0^\infty P(r) dr \quad (9)$$

is the total probability of a transfer from the initial to the final state along any cross-cut of the barrier  $V(r_{AH}, r_{HB})$ . From eq 6-9 one obtains

$$P = \frac{1}{kT} \int_0^\infty e^{-V_0(r)/kT} dr \int_0^\infty W_r(U_r) e^{-U_r/kT} dU_r = \int_0^\infty e^{-E(r)/kT} \mathcal{C}_r dr \quad (10)$$

where  $E(r) = V_0(r) + E_0(r)$ . The total probability for a classical transfer ( $\mathcal{C}_r = 1$ ) is

$$P_{cl} = \int_0^\infty e^{-E(r)/kT} dr \quad (11)$$

The ratio

$$\mathcal{C} = \frac{P}{P_{cl}} = \frac{\int_0^\infty e^{-E(r)/kT} \mathcal{C}_r dr}{\int_0^\infty e^{-E(r)/kT} dr} \quad (12)$$

represents the tunneling correction factor for a two-dimensional barrier  $V(r_{AH}, r_{HB})$ . It obviously defines a mean value of the tunneling corrections  $\mathcal{C}_r$  for the various cross sections of the barrier. Equation 12 is essentially the expression used by Johnston and Rapp.<sup>7</sup> The above derivation is only a somewhat different, more clear formulation of their procedure of calculation.

The one-dimensional "tunneling probability"  $W_r(U_r)$  depends on the shape of the barrier profile  $V_r(x)$  in the corresponding cross section. Johnston and Rapp<sup>7</sup> have used the Eckart<sup>20</sup> symmetrical potential

$$V(x) = 4E_0 \frac{e^{2\pi x/l}}{(1 + e^{2\pi x/l})^2} = \frac{E_0}{\cosh^2(2\pi x/l)} \quad (13)$$

for all cross sections, setting the height  $E_0$  and the top curvature  $L_m$  of this barrier to be equal to those ( $E_0(r)$  and  $L_m(r)$ ) of the real profile. However, the Eckart barrier width  $2l_E$  proves to be larger than the real barrier width  $2l_R$  for all cross-cuts of the potential energy surface (Figure 2).

A considerably better approximation in any cross section could be obtained by means of the generalized (symmetrical) Eckart potential<sup>15</sup>

$$V(x) = B \left( \frac{e^{2ax/l}}{(1 + e^{2ax/l})^2} - C \right) \quad (14)$$

where

$$B = 4E_0 \left( \frac{e^{2a} + 1}{e^{2a} - 1} \right)^2; \quad C = \frac{e^{2a}}{(1 + e^{2a})^2}$$

and the parameter  $a$  can vary from 0 to  $\infty$ . For  $a = \pi$  this expression practically coincides with the Eckart potential (eq 13) (then  $B \approx 4E_0$ ,  $C \approx 0$ ), while as  $a \rightarrow 0$  it turns into a parabolic potential.<sup>15</sup>

The function 14 can be expressed as well as

$$V(x) = \frac{E_0'}{\cosh^2(\pi x/l')} - K \quad (15)$$

where

$$E_0' = E_0 \coth^2 a; \quad l' = \frac{\pi l}{a}; \quad K = E_0' - E_0 = \frac{E_0}{\sinh^2 a}$$

This expression is identical with the equation of an Eckart barrier with a height  $E_0'$  and width  $2l'$  truncated at the level  $K$  above its base.<sup>21</sup> This is illustrated in Figure 2, which shows that by means of a proper choice of the parameters  $E_0'$  and  $l'$  (or  $a$  and  $l$ ) it is possible to obtain a very good approximation to the profile in every section of the barrier  $V(r_{AH}, r_{HB})$ .

The permeability of the Eckart barrier (13) is given exactly by the expression<sup>20</sup>

$$W(U) = \frac{\cosh 4\pi\alpha - 1}{\cosh 4\pi\alpha + \cosh 2\pi\sigma} \quad (16)$$

where

$$\alpha = \frac{l}{h} \sqrt{2\mu U}; \quad \sigma = \frac{1}{2} \sqrt{(32\mu l^2 E_0/h) - 1}$$

(at the condition that  $32\mu l^2 E_0/h^2 > 1$ ). Unfortunately, an analytical calculation of the one-dimensional tunneling correction  $\mathcal{C}_r$  by means of that expression seems impossible. Johnston and Rapp<sup>7</sup> have tabulated the  $\mathcal{C}$  values for the Eckart barrier obtained through a numerical integration.

The expression 16 could be also used for an approximation calculation of the permeability of the generalized Eckart barrier (eq 15) for any value of  $a > 0$ , if  $U$ ,  $l$ , and  $E_0$  are replaced by  $U + K$ ,  $l'$ , and  $E_0'$ , correspondingly, for the conditions<sup>15,21</sup>

$$\frac{4\pi l'}{h} \sqrt{2\mu K} \gtrsim 2\pi; \quad \delta' \left( 1 - \sqrt{\frac{K}{E_0'}} \right) \gtrsim 1. \quad (17)$$

(20) C. Eckart, *Phys. Rev.*, **25**, 1303 (1930).

(21) S. G. Christov, *Commun. Dept. Chem., Bulg. Acad. Sci.*, **4**, 19 (1971).

Thus, eq 16 is simplified as<sup>16,21</sup>

$$W(U) = \frac{1}{1 + e^{2\delta'(1 - \sqrt{(U+K)/E})}} \quad (18)$$

where

$$\delta' = \frac{2\pi l' \sqrt{2\mu E_0'}}{h}$$

Recently, using eq 14-18, approximate formulas for  $\mathcal{Z}$ , have been derived<sup>17,21</sup>

$$\mathcal{Z} = \mathcal{Z}' + \mathcal{Z}'' \quad (19)$$

where  $\mathcal{Z}'$  is determined by the expression

$$\mathcal{Z}' = \delta' \sqrt{\frac{\pi}{\gamma'}} (\Phi(y_1) + \Phi(y_2)) \gamma'^{-2\delta'} \left(1 - \frac{\delta'}{\gamma'}\right) \quad (20)$$

in which

$$\Phi(y) = \frac{2}{\sqrt{2\pi}} \int_0^y e^{-t^2/2} dt, \quad y_1 = \frac{\gamma'}{\delta'} \sqrt{\frac{\gamma'}{2}} \left( \frac{\delta'^2}{\gamma'^2} - \frac{K}{E_0'} \right),$$

$$y_2 = \frac{\gamma'}{\delta'} \sqrt{\frac{\gamma'}{2}} \left( 1 - \frac{2}{\delta'} - \frac{\delta'^2}{\gamma'^2} \right), \quad \gamma' = E_0'/kT$$

and  $\mathcal{Z}''$  can be calculated using the equations

$$\mathcal{Z}'' = \frac{\pi\gamma'/\delta'}{\sin(\pi\gamma'/\delta')} - \frac{\gamma'}{\delta' - \gamma'} e^{-(\delta' - \gamma')\theta'} \quad (\delta' > \gamma') \quad (21a)$$

$$\mathcal{Z}'' = \delta'\theta' \left[ 1 + \frac{1}{2}(\gamma' - \delta')\theta' - \frac{\delta'}{6}(\gamma' - \delta')^2\theta'^3 + \dots \right] \quad (\gamma' \approx \delta') \quad (21b)$$

$$\mathcal{Z}'' = \frac{e^{\gamma'\theta'}}{\gamma' - \delta'} (\gamma' e^{-\delta'\theta'} - \delta' e^{-\gamma'\theta'}) \quad (\gamma' > \delta') \quad (21c)$$

where  $\theta' = 2/\delta'$ .

Setting  $\theta' = 1$  in eq 21a-c gives the corresponding expressions for the total correcting factor  $\mathcal{Z} = \mathcal{Z}' + \mathcal{Z}''$  of a symmetrical parabolic barrier.<sup>1,22</sup> These expressions should be applied in the case of barrier profiles for which  $a \ll 1$  ( $a < 0.2$ ) for the conditions in (17).<sup>15</sup> They could be also used as approximations when  $\mathcal{Z}' < 0$ .

#### IV. Results

The tunneling corrections have been calculated, using the method described in the present paper, for the linear complexes X-H-X ( $\mu = m_H/2$ ) and X-D-X ( $\mu = m_H$ ). For our purposes, 13 sections in the energy diagram (Figure 1) in the region from  $r_{AH} = r_{HB} = 0.883 \text{ \AA}$  to  $r_{AH} = r_{HB} = 1.001 \text{ \AA}$  (which includes the saddlepoint  $r_{AH} = r_{HB} = r_s = 0.93$ ) have been made. The profile of one of these cross sections with  $r_{AH} = r_{HB} = 0.955 \text{ \AA}$  is shown in Figure 2.

From the profile of the cross-cut passing through the saddlepoint ( $r_{AH} = r_{HB} = r_s$ ), the characteristic tem-

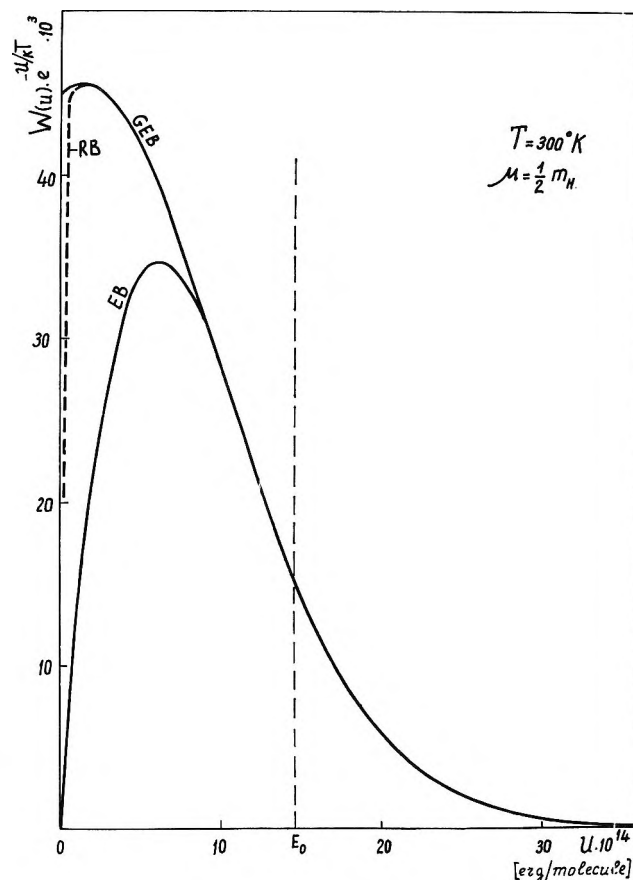


Figure 3. The integrand in eq 6 for the tunneling path which passes through the point  $r_{AH} = r_{HB} = 0.955 \text{ \AA}$  (cf. Figure 2). The energy dependence of the integrand is shown for two different approximations of the barrier profile: EB, Eckart barrier with height  $E_{0,r}$ ; GEB, generalized Eckart barrier. An expected energy dependence of the integrand for the exact barrier shapes is also traced (RB).

perature has been first obtained, using eq 3 which could be written as

$$T_K = \frac{h\sqrt{E_0}}{\pi^2 k d \sqrt{2\mu}} \quad (3a)$$

where  $E_0$  and  $2d$  are the height and the width of a truncated parabola of the same curvature at the top,  $L_m(r_s) = 2E_0/d^2$ . Thus, it has been found

$$T_K = 640^\circ \text{K for } \mu = m_H/2$$

$$T_K = 445^\circ \text{K for } \mu = m_H$$

which means that the tunneling correction for X-H-X as well for X-D-X should be significant at ordinary temperatures. Hence the calculations for the two cases have been carried out at  $T = 300^\circ \text{K}$ . To make comparison with formula 4, the tunneling correction for  $\mu = m_H/2$  has been calculated also at  $T = 512^\circ \text{K}$ .

The potential energy profiles have been well approximated with the potential energy function (eq 15), while the Eckart potential (eq 13) allows a good approximation

(22) S. G. Christov, *Z. Elektrochem.*, **64**, 84 (1960).

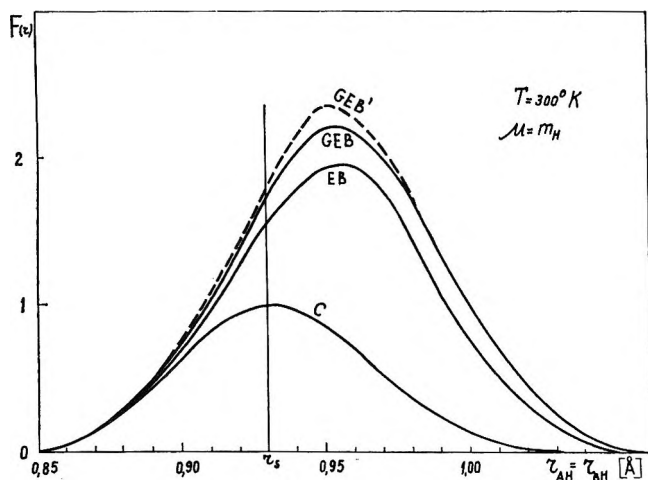


Figure 4. The integrands in eq 22,  $F(r) = A(r)$ ,  $\kappa(r)$ , for curve C,  $F(r) = A(r)$ ; EB, approximation by an Eckart barrier; GEB, approximation by a generalized Eckart barrier; GEB', according to eq 19 and 20.

in the upper part of the profiles only (cf. Figure 2). Since the permeability in the lower profile part is considerable, an improved approximation leads to an increase of the  $\mathcal{K}_T$  values from 20 to 60% (and more) in comparison to those obtained by the Eckart barrier.<sup>23</sup>

The one-dimensional tunneling corrections  $\mathcal{K}_T$  for various cross sections have been calculated using expression 16 for  $W(U_T + K)$  or (18) for  $W(U_T)$  in two ways: exactly by graphical integration of eq 7 and approximately by using eq 19 and 20. The two methods give results which differ not more than 10%. Hence, the approximate method should be used with an advantage because of its greater simplicity.

The calculation of the two-dimensional tunneling correction can be carried out conveniently if eq 12 is presented in the form

$$\mathcal{K} = \frac{\int_0^\infty A(r)\mathcal{K}_T dr}{\int_0^\infty A(r) dr}, \quad A(r) = e^{-(E(r) - V_s)/kT} \quad (22)$$

where  $V_s$  is the height of the saddlepoint. The numerator and the denominator of this expression may be calculated by graphical integration (cf. Figures 4-6).

The results obtained for the two-dimensional tunneling correction are presented in Table I, where a comparison is made with the corresponding results of the approximation by the Eckart potential. The exact calculation of  $\mathcal{K}_T$  by means of the improved approximation of the barrier profiles leads to an increase of the  $\mathcal{K}$  values from 3.5 to 4.9 (about 40%) for  $\mu = m_H/2$  and from 2.25 to 2.46 (about 10%) for  $\mu = m_H$  (at  $T = 300^\circ\text{K}$ ). Nearly the same results for  $\mathcal{K}$  are obtained using the approximate formulas (eq 19):  $\mathcal{K} = 5.4$  for  $\mu = m_H/2$  and  $\mathcal{K} = 2.50$  for  $\mu = m_H$  ( $T = 300^\circ\text{K}$ ).

Instead of  $\mathcal{K}$ , *i.e.*, the mean value of  $\mathcal{K}_T$ , it is much easier to calculate (cf. eq 22) the maximum value of

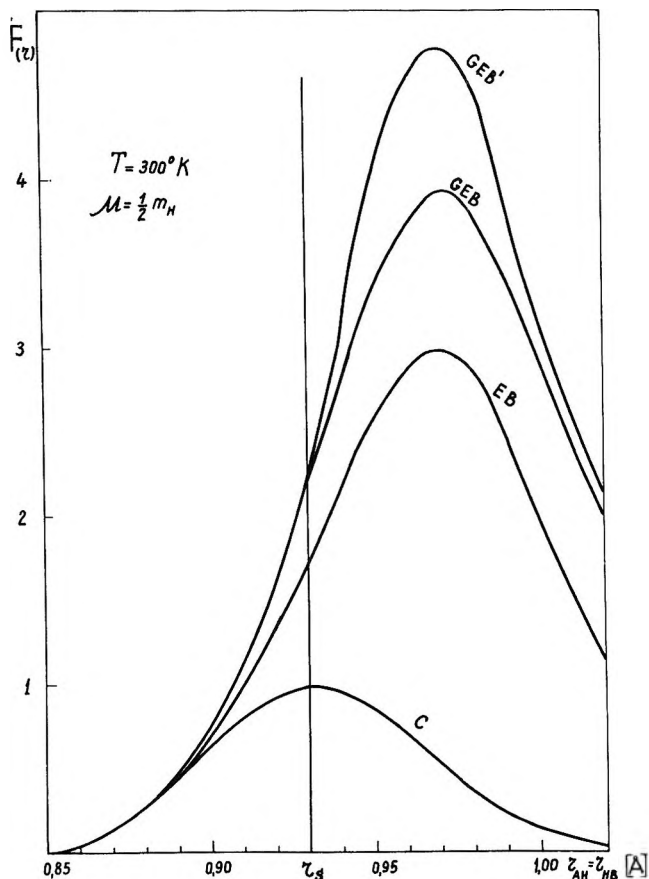


Figure 5. Same notation as Figure 4.

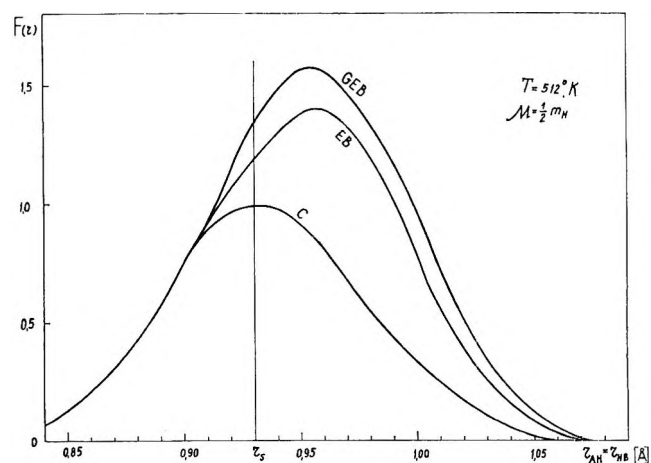


Figure 6. Same notation as Figure 4.

$F(r) = A(r)\mathcal{K}_T$ , which corresponds to the most probable reaction path. This path is determined by  $r_{AH} = r_{HB} = r_{mp} = 0.970$  for  $\mu = m_H/2$  and  $r_{mp} = 0.955$  for  $\mu = m_H$

(23) These values are somewhat overestimated because the expression 16 for  $U = 0$  gives  $W(U + K) > 0$  instead of  $W(U + K) = 0$  as required from an exact solution. However, this overestimation is not significant since the conditions (eq 17) are fulfilled for almost all cross sections. This is seen in Figure 3, which represents the integrand of expression 6 calculated using the approximations by an Eckart barrier (eq 13) and by a generalized Eckart barrier (eq 14, 15) compared with that for the real barrier.



Table I

Barrier	Method of approximation of the sections	$T = 300^\circ\text{K}$ $\mu = m_{\text{H}}$	$T = 300^\circ\text{K}$ $\mu = 1/2m_{\text{H}}$	$T = 512^\circ\text{K}$ $\mu = 1/2m_{\text{H}}$
One-dimensional barrier $V(x)$ along the extended reaction coordinate (RC)	Parabola (according to eq 4)	3.2	...	1.78
	EB <sup>a</sup>	2.52	6.81	1.79
	GEB <sup>b</sup>	...	6.74	...
	According to eq 19	3.20	6.5	...
Two-dimensional barrier $V(r_{\text{AH}}, r_{\text{HB}})$	EB	2.25	3.5	1.45
	GEB	2.45	4.9	1.67
	According to eq 19	2.50	5.4	...
Section along the most probable path	EB	1.96	3.0	1.41
	GEB	2.22	3.9	1.58
	According to eq 19	2.30	4.8	...

<sup>a</sup> EB, Eckart barrier. <sup>b</sup> GEB, generalized Eckart barrier.

(cf. Figure 2). A comparison between the maximum  $F(r)$  values (cf. Figures 4 and 5) shows that an exact calculation, using the improved barrier profile approximation, increases these values from 3.0 to 3.9 for  $\mu = m_{\text{H}}/2$  and from 1.96 to 2.22 for  $\mu = m_{\text{H}}$ . It is also seen that the maximum  $F(r)$  value is close to the mean value  $\bar{\mathcal{K}}_r = \mathcal{K}$  as already noted by Johnston and Rapp.<sup>7</sup> The calculation of  $F(r)$  by means of the formulas (eq 19 and 20) is very simple and gives satisfactory results for  $\mathcal{K}$ : 4.8 for  $\mu = m_{\text{H}}/2$  and 2.30 for  $\mu = m_{\text{H}}$  instead of the exact values 4.9 and 2.45.

The tunneling corrections for a one-dimensional barrier, referring to the (extended) reaction coordinate, are also shown in Table I. The values of these corrections ( $\mathcal{K} = 6.8$  for  $\mu = m_{\text{H}}/2$  and  $\mathcal{K} = 2.52$  for  $\mu = m_{\text{H}}$ ) are larger than the corresponding values for a two-dimensional barrier (4.9 and 2.45) as found first by Johnston and Rapp.<sup>7</sup> However the differences are not very large (about 40% for  $\mu = m_{\text{H}}/2$  and 5% for  $\mu = m_{\text{H}}$ ).

## V. Conclusions

The conclusions of Johnston and Rapp<sup>7</sup> that the one-dimensional treatment of the (extended) reaction path leads to a *large* overestimation of the tunneling is based on their calculations for the linear complex H-H-H for which  $\mu = m_{\text{H}}/3$ .<sup>24</sup> However, the condition that the distance between the end atoms remains constant during the transfer is not fulfilled for that complex. Hence, the application of Johnston-Rapp method is not justified in this case. If we assume that the end atoms A and B of the linear complex A-H-B are much heavier than H so that  $\mu = m_{\text{H}}/2$ , then we find the one-dimensional tunneling corrections for the (extended) reaction path do not overestimate the two-dimensional corrections calculated using the Johnston-Rapp method too much.

A similar conclusion can be drawn also from the data of Mortensen,<sup>10</sup> who calculated two-dimensional and one-dimensional tunneling corrections for various isotopic reactions of the type  $\text{H}_2 + \text{H} = \text{H} + \text{H}_2$  using an appropriate quantum-mechanical approach. However, his results cannot be compared directly with those reported here because both the systems studied and the procedure of calculation differ essentially in the two cases. Mortensen has investigated a system A-H-B (with A and B light atoms) for which the method of Johnston-Rapp is not correct.<sup>25</sup> In the present work a system A-H-B (with A and B heavy atoms) is studied for which this method is much more justified. However, we may conclude that a correct treatment in each of the two cases leads independently to the same essential result, namely, that the one-dimensional tunneling corrections do not overestimate largely the two-dimensional ones.

The data in Table I also confirm our previous conclusion<sup>9</sup> that the treatment of the reaction path in one dimension gives a lower limit for the tunneling correction, if we assume that  $\mu = m_{\text{H}}$ . The value ( $\mathcal{K} = 2.52$ ) thus obtained is considerably smaller than the value ( $\mathcal{K} = 4.9$ ) of the two-dimensional tunneling correction computed with  $\mu = m_{\text{H}}/2$ .

Finally, the results of the calculations at 300°K (with  $\mu = m_{\text{H}}$ ) and at 512°K (with  $\mu = m_{\text{H}}/2$ ) (Figure 6) show that the formula (eq 4) for the tunneling correction of a parabolic barrier is applicable with a good approximation not only at temperatures higher than  $T_{\text{K}}$ , but also at tem-

(24) Our calculations for  $\mu = m_{\text{H}}/3$  are in agreement with Johnston-Rapp data.<sup>7</sup> The tunneling correction for the extended reaction path is about three times larger than the two-dimensional tunneling correction calculated by Johnston-Rapp method.

(25) This is evident also from a comparison of the data of Johnston and Rapp<sup>7</sup> with the much more accurate results of Mortensen<sup>10</sup> referring to the same system H-H-H.

peratures somewhat lower than  $T_K$  ( $T \simeq 0.7T_K$ ). These results confirm once again the previous conclusion<sup>9</sup> that the characteristic temperature  $T_K$ , defined by eq 3,

could be always used as a criterion for determination of the relative role of the tunneling both in one-dimensional and many-dimensional treatment of chemical reactions.

## NOTES

### Vibrational Eigenvalues. Sine Basis Sets<sup>1</sup>

by David J. Locker

Department of Chemistry, Vanderbilt University,  
Nashville, Tennessee 37203 (Received November 9, 1970)

Publication costs assisted by the National Science Foundation

In the present work the energy eigenvalues of Fues and Morse oscillators are numerically computed. For these two models exact energy eigenvalues are known. Thus the Fues and Morse oscillators are useful models for the verification of numerical energy level calculations. The Fues potential energy has the form

$$V(x) = 2D\{r_e/(x + r_e) - r_e^2/2(x + r_e)^2\}$$

where there is a second-order pole at  $x = -r_e$  and the potential energy minimum occurs at  $x = 0$ . The vibrational energy levels for the nonrotating Fues oscillator are given in ref 2.

The vibrational energy levels for the two models are computed using sine basis sets and standard linear variation. Although the sine basis functions do not span the complete coordinate space of the Fues and Morse wave functions, only a small error in energy eigenvalues results for well-chosen basis set parameters. The kinetic energy matrix elements may be readily determined in the sine basis set. For the computation of the potential energy matrix elements the method of Harris, Engerholm, and Gwinn<sup>3</sup> is used.

Founded on the techniques of matrix transformation theory and the matrix formulation of quantum mechanics, the HEG method is readily adaptable to computer calculations. The HEG method necessitates the representation of a function by a finite number of basis functions instead of by the complete infinite set. This constraint thereby introduces errors into the calculation of eigenvalues and in turn eigenkets. In Endres' work<sup>4</sup> the HEG method was employed to calcu-

late vibrational energy eigenvalues of a Morse oscillator; with 40 harmonic oscillator basis functions he obtained eigenvalues accurate to four figures for the first seven energy levels. Endres also discovered that the accuracy of the eigenvalues can be improved by displacement of the basis set origin. In particular, eigenvalues for the Morse oscillator are improved by shifting the origin of the basis set toward the attractive region of the Morse potential.

Lesk<sup>5</sup> has examined the factors governing optimal choice of basis set parameters. Dickenson and Certain<sup>6</sup> have discussed the equivalence of the HEG method to Gaussian quadratures. And by using sets of equally spaced normalized Gaussian functions Chesick<sup>7</sup> has been able to compute accurate eigenvalues for the Morse oscillator.

The  $m$ th sine basis function has the form

$$\phi_m(x) = (2/l)^{1/2} \sin \{m\pi(x - \Delta x)/l\}$$

where  $\Delta x$  and  $l$  are basis set parameters. For the Fues oscillator it is found in the present work that the sine basis set affords eigenvalues similar to those obtained by employing the harmonic oscillator basis set for the five lowest energy levels. For the higher energy levels the eigenvalues calculated by using the sine basis set are in much better agreement with the exact values than are the results calculated by using a harmonic oscillator basis set centered around the potential minimum. Furthermore, increasing the parameter  $l$  im-

(1) The calculations presented in this work were performed while the author was in the Chemistry Department at the University of Rochester, Rochester, N. Y.

(2) R. Dubrow, D. Hatzenbuehler, W. Marx, E. Zahorian, and D. J. Wilson, *J. Phys. Chem.*, **72**, 2489 (1968).

(3) D. Harris, G. Engerholm, and W. Gwinn, *J. Chem. Phys.*, **43**, 1515 (1965); hereafter referred to as the HEG method.

(4) P. F. Endres, *ibid.*, **47**, 798 (1967); here harmonic oscillator basis sets were employed:  $\phi_m(\alpha x) = (\alpha/\pi^{1/2}2^m m!)^{1/2} H_m(\alpha x) \exp(-\alpha^2 x^2/2)$ , where  $\alpha = (\mu\omega/\hbar)^{1/2}$  and  $\omega = (2D/\mu r_e^2)^{1/2}$ .

(5) A. M. Lesk, *J. Chem. Phys.*, **49**, 3898 (1968).

(6) A. S. Dickenson and P. R. Certain, *ibid.*, **49**, 4209 (1968).

(7) J. P. Chesick, *ibid.*, **49**, 3772 (1968).

**Table I:** Eigenvalues for the Fues Oscillator<sup>a</sup>

Exact energy	JWKB	Potential expansion harmonic oscillator basis	Energy $\times 10^{11}$ , ergs							
			30 sine basis functions $\Delta x = 0.2 \text{ \AA}$ $l = 2.5 \text{ \AA}$	30 sine functions			Harmonic oscillator			
				$\Delta x = 0$ , $l = 2.5 \text{ \AA}$	$\Delta x = 0$ , $l = 3.3 \text{ \AA}$	40 functions	30 functions	15 functions	10 functions	
-0.683389	-0.683328	-0.683071	-0.683096	-0.683096	-0.683096	-0.683096	-0.683096	-0.683096	-0.683093	-0.683096
-0.631109	-0.631091	-0.630510	-0.630838	-0.630838	-0.630838	-0.630838	-0.630838	-0.630837	-0.630769	-0.630804
-0.584600	-0.584579	-0.580883	-0.584354	-0.584354	-0.584354	-0.584355	-0.584356	-0.584385	-0.584385	-0.583445
-0.543053	-0.543026	-0.526483	-0.542826	-0.542826	-0.542821	-0.542825	-0.542813	-0.541285	-0.541285	-0.534120
-0.505790	-0.505751	-0.462627	-0.505572	-0.505572	-0.505552	-0.505584	-0.505586	-0.497506	-0.497506	-0.476601
-0.472223	-0.472186	-0.308343	-0.472026	-0.472026	-0.471979	-0.471896	-0.470705	-0.442589	-0.442589	-0.399496
-0.441900	-0.441855	-0.389505	-0.441711	-0.441710	-0.441639	-0.441072	-0.435839	-0.381017	-0.381017	-0.318398
-0.414403	-0.414355	-0.219938	-0.414225	-0.414199	-0.414153	-0.408610	-0.393714	-0.303960	-0.303960	-0.260967
-0.389394	-0.389345	-0.123958	-0.389209	-0.388818	-0.389213	-0.373467	-0.347666	-0.222957	-0.222957	-0.222957
-0.366583	-0.366533	-0.018130	-0.366124	-0.363676	-0.366553	-0.330956	-0.299644	-0.111564	-0.111564	-0.111564

<sup>a</sup> Data given for H<sub>2</sub>:  $r_e = 0.74 \text{ \AA}$ ,  $D = 0.7120 \times 10^{-11} \text{ erg/molecule}$ ,  $\mu = 0.83 \times 10^{-24} \text{ g}$ . Columns 1-3 are from Table II of ref 8.

proves the calculated energies for the higher vibrational levels. The eigenvalues for the H<sub>2</sub> molecule and the basis set parameters are given in Table I.

Eigenvalues for the Morse oscillator also were calculated using the sine basis set and were compared with Endres' results which were computed using the harmonic oscillator basis set. See Table II. As in the case of the Fues oscillator, for the Morse oscillator the

In the "potential expansion" method the Hamiltonian matrix elements  $H_{mn}$  are generated by expanding the potential energy in a power series in  $x/r_e$  and then integrating  $H_{mn} = \int \phi_m (\hat{T} + \hat{V}) \phi_n dx$ . The "potential expansion" eigenvalues are then obtained by the linear variation method. The discrepancy between column 3 and columns 4-10 of Table I is due to the second-order pole in  $V_{\text{Fues}}$  at  $x = -r_e$ . This forces a limited radius of convergence for the series expansion.

The reasons for the accurate eigenvalues at the higher levels obtained by employing either the sine basis or Chesick's Gaussian nonorthogonal sets are readily seen. Consider the use of sine *vs.* harmonic oscillator basis sets for the representation of the Fues oscillator eigenfunctions. Harmonic oscillator functions approach zero rapidly for values of the coordinate in the classically forbidden region. The Fues potential increases slowly in the attractive region and hence the probability of finding an oscillator with a coordinate value far into the attractive region is high especially for high-energy oscillators. Representation of these probabilities becomes hopeless in the harmonic oscillator basis set, since as we move an appreciable distance into the attractive region for the Fues oscillator at a given high energy we are moving into the classically forbidden region for the harmonic oscillator. This accounts for Endres' observation that displacement of the origin of the harmonic oscillator functions into the attractive region improves the Morse eigenvalues corresponding to the higher energy levels (above the fourth excited state). Sine functions on the other hand can be chosen to span all of the relevant coordinate space merely by changing the  $l$  parameter which represents the width of the infinite square well defining the sine basis set.

*Acknowledgment.* The author wishes to thank Professors D. J. Wilson and P. F. Endres for their interest and comments.

**Table II:** Eigenvalues of the Morse Oscillator<sup>a</sup>

Exact energy	Energy $\times 10^{11}$ , ergs	
	HEG method harmonic oscillator basis 40 functions	HEG method sine basis set, 30 functions $\Delta x = 0$ , $l = 2.5 \text{ \AA}$
0.0428775	0.0428760	0.0428766
0.1248979	0.1248916	0.1248925
0.2019387	0.2019306	0.2019290
0.2739999	0.2739906	0.2739895
0.3410814	0.3410708	0.3410732
0.4031834	0.4031713	0.4031764
0.4603058	0.4603011	0.4602710
0.5124486	0.5126280	0.5123390
0.5596117	0.5617329	0.5594541
0.6017953	0.6124088	0.6017368

<sup>a</sup> H<sub>2</sub> molecule:  $\hbar\omega = 0.87 \times 10^{-12} \text{ erg}$ ,  $D = 0.76 \times 10^{-11} \text{ erg}$ .

sine basis yields more accurate eigenvalues in the high energy region of the vibrational spectrum. And for the lower energy levels sine and harmonic oscillator basis set results are comparable.

The linear variation eigenvalues of the Fues oscillator for which the Hamiltonian matrix is computed by the HEG method are given in columns 4-10 of Table I. The JWKB and "potential expansion" eigenvalues<sup>2</sup> are presented in columns 2 and 3 of Table I, respectively.

## Nitrogen-15 Nuclear Magnetic Resonance Shifts and Coupling Constants for the Methylamine Hydrochlorides in Aqueous Solution<sup>1</sup>

by M. Alei, Jr.,\* A. E. Florin,

*Los Alamos Scientific Laboratory, University of California,  
Los Alamos, New Mexico 87544*

and W. M. Litchman<sup>2</sup>

*Department of Chemistry,  
University of New Mexico, Albuquerque, New Mexico 87106  
(Received November 23, 1970)*

*Publication costs assisted by the Los Alamos Scientific Laboratory*

In the course of studies of the <sup>15</sup>N shifts in ammonia and the methylamines,<sup>3</sup> we became interested in the <sup>15</sup>N shifts for the protonated forms of these compounds. Although both <sup>14</sup>N and <sup>15</sup>N shifts for these species have been reported in the literature,<sup>4-8</sup> there are large discrepancies between values reported by different workers. We have therefore measured the <sup>15</sup>N shifts for <sup>15</sup>NH<sub>4</sub><sup>+</sup> and all the methylammonium species including Me<sub>4</sub>-<sup>15</sup>N<sup>+</sup> in an effort to obtain a reliable set of values. In the course of this investigation, we also obtained values for *J*<sub>15NH</sub> over the series from <sup>15</sup>NH<sub>4</sub><sup>+</sup> to Me<sub>3</sub><sup>15</sup>NH<sup>+</sup>.

ready comparison. Since temperature and solution composition were not always specified in the earlier work, we were interested in possible effects of these variables on the <sup>15</sup>N shifts. For a given Me<sub>*x*</sub><sup>15</sup>NH<sub>4-*x*</sub><sup>+</sup> species at constant solution composition we found no measurable change of <sup>15</sup>N shift with temperature over ranges of the order of 50°. With regard to solution composition, we found that the <sup>15</sup>N shift was essentially independent of Me<sub>*x*</sub><sup>15</sup>NH<sub>4-*x*</sub><sup>+</sup> concentration at constant total [Cl<sup>-</sup>] but did vary significantly with total [Cl<sup>-</sup>] as shown in Figure 1. Substituting LiCl or NaCl for HCl as the source of additional [Cl<sup>-</sup>] had a negligible effect and susceptibility corrections were insignificant.

The dependence of the <sup>15</sup>N shift upon [Cl<sup>-</sup>] clearly indicates a significant change in the immediate environment of the Me<sub>*x*</sub><sup>15</sup>NH<sub>4-*x*</sub><sup>+</sup> species with increasing total [Cl<sup>-</sup>]. The effect diminishes with increasing methyl substitution in accord with the expectation that methyl groups would be more effective than protons in shielding the nitrogen from effects of liquid phase interactions. A small amount of ion-pair formation could reasonably account for the data and observations but other interpretations are possible. Whatever the origin of the change in shift with [Cl<sup>-</sup>], the larger discrepancies in Table I cannot be attributed to this cause. Thus, *e.g.*, shifts of -27 ppm (Ogg and Ray<sup>4</sup>) or -49 ppm (Witanowski and Januszewski<sup>8</sup>) for Me<sub>3</sub><sup>15</sup>NH<sup>+</sup> lie far

**Table I:** <sup>15</sup>N Shifts<sup>a</sup> and Coupling Constants for Me<sub>*x*</sub><sup>15</sup>NH<sub>4-*x*</sub><sup>+</sup> in Aqueous Solution<sup>b</sup>

	Ref 4 <sup>14</sup> N shifts <sup>c</sup>	Ref 5 <sup>14</sup> N shifts	Ref 6 <sup>15</sup> N shifts	Ref 7 <sup>14</sup> N shifts	Ref 8 <sup>14</sup> N shifts <sup>g</sup>	Our results	
						<sup>15</sup> N shifts <sup>h</sup>	<i>J</i> <sub>15NH</sub> <sup>i</sup>
<sup>15</sup> NH <sub>4</sub> <sup>+</sup>	-25	-21	-24	-23 <sup>e</sup>	-28.5	-26.1	73.3
Me <sup>15</sup> NH <sub>3</sub> <sup>+</sup>	-35		-28		-32	-24.5	75.4
Me <sub>2</sub> <sup>15</sup> NH <sub>2</sub> <sup>+</sup>	-40				-35	-26.6	76.1
Me <sub>3</sub> <sup>15</sup> NH <sup>+</sup>	-27				-49	-33.8	76.7
Me <sub>4</sub> <sup>15</sup> N <sup>+</sup>	-53 <sup>d</sup>	-41		-44 <sup>f</sup>	-49.5	-44.7	

<sup>a</sup> All shifts are in ppm relative to <sup>15</sup>NH<sub>3</sub>(liq) at 30°. <sup>b</sup> The anion is Cl<sup>-</sup> except as otherwise noted. <sup>c</sup> These were derived from published, calibrated spectra. Values are probably uncertain to ±2 or 3 ppm. <sup>d</sup> Anion is OH<sup>-</sup>. <sup>e</sup> Anion is NO<sub>3</sub><sup>-</sup>. <sup>f</sup> Anion is Br<sup>-</sup>. <sup>g</sup> Uncertainty = ±0.5-1 ppm. <sup>h</sup> Values measured at 30° in aqueous solutions 5 *M* in amine hydrochloride and 1 *M* in HCl. Uncertainty = ±0.3 ppm. <sup>i</sup> Units are Hertz. Uncertainty = ±0.3 Hz.

In all cases, the shifts were measured by locking the magnetic field and sweeping the frequency. The stability and reproducibility of the system was such that the <sup>15</sup>N shift for a given sample could be reproduced to within ±1 Hz (at ~6 MHz) over periods of several days even with repeated removal and replacement of the sample in the probe. The various amine hydrochlorides were prepared by standard techniques and their identification and purity confirmed by proton as well as <sup>15</sup>N nmr spectra.

Table I lists the <sup>15</sup>N shifts and coupling constants which we measured at 30° in aqueous solutions 5 *M* in amine hydrochloride and 1 *M* in HCl. Shifts previously reported in the literature are also included for

outside the range (roughly -32 to -36 ppm) of values which we measured over a wide range of solution com-

- (1) Work supported by the U. S. Atomic Energy Commission.
- (2) AWU Faculty Participant at Los Alamos Scientific Laboratory.
- (3) M. Alei, Jr., A. E. Florin, and W. M. Litchman, *J. F. O'Brien, J. Phys. Chem.*, **75**, 932 (1971).
- (4) R. A. Ogg and J. D. Ray, *J. Chem. Phys.*, **26**, 1339 (1957).
- (5) B. M. Schmidt, L. C. Brown, and D. Williams, *J. Mol. Spectrosc.*, **2**, 539 (1958).
- (6) J. C. Lambert, G. Binsch, and J. D. Roberts, *Proc. Nat. Acad. Sci. U. S.*, **51**, 735 (1964).
- (7) D. Herbison-Evans and R. E. Richards, *Mol. Phys.*, **8**, 19 (1964).
- (8) M. Witanowski and H. Januszewski, *Can. J. Chem.*, **47**, 1321 (1969).

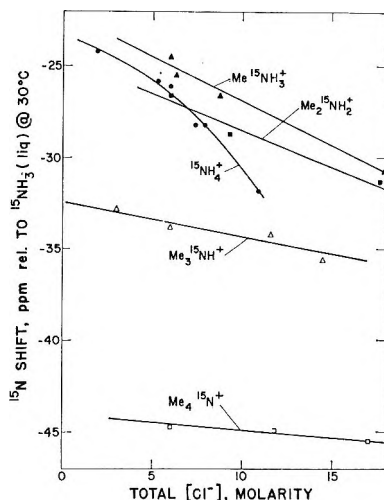


Figure 1. Variation of  $^{15}\text{N}$  shift with total chloride concentration in aqueous solutions of amine hydrochlorides at  $30^\circ\text{C}$ .

position. We conclude that the discrepancies must arise either from unreliable referencing or improper identification of the  $\text{Me}_x^{15}\text{NH}_{4-x}^+$  species.

With regard to the  $^{15}\text{NH}$  coupling constants, our values for  $^{15}\text{NH}_4^+$  and  $\text{CH}_3^{15}\text{NH}_3^+$  are in good agreement with those reported by Binsch, Lambert, Roberts, and Roberts.<sup>9</sup> Values for  $(\text{CH}_3)_2^{15}\text{NH}_2^+$  and  $(\text{CH}_3)_3^{15}\text{NH}^+$  have not, to our knowledge, been previously reported. It appears that the trend to higher values of  $J_{^{15}\text{NH}}$  with increasing methyl substitution persists throughout the series from  $^{15}\text{NH}_4^+$  to  $(\text{CH}_3)_3^{15}\text{NH}^+$ . A similar trend was previously reported<sup>3</sup> for the free amines from  $^{15}\text{NH}_3$  to  $(\text{CH}_3)^{15}\text{NH}$  but the increase in  $J_{^{15}\text{NH}}$  per methyl group for the amines was about three times as great as for the protonated species.

(9) G. Binsch, J. B. Lambert, B. W. Roberts, and J. D. Roberts, *J. Amer. Chem. Soc.*, **86**, 5564 (1964).

## The Radiation Chemical Yield of $\text{OH}^-$ as Determined by Conductometric Pulse Radiolysis

by J. Rabani,<sup>1</sup> M. Grätzel, S. A. Chaudhri,<sup>2</sup> G. Beck, and A. Henglein\*

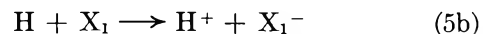
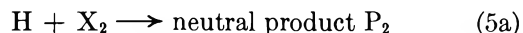
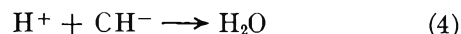
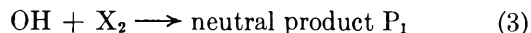
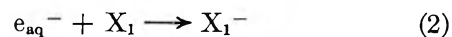
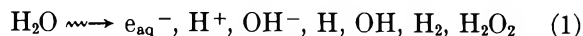
Hahn-Meitner-Institut für Kernforschung Berlin, Sektor Strahlenchemie, Berlin-Wannsee (Received December 22, 1970)

Publication costs assisted by the Hahn-Meitner-Institut

Although the formation of  $\text{OH}^-$  ions due to the reaction of  $\text{OH} + e_{\text{aq}}^-$  in spurs had been considered several years ago,<sup>3</sup> attempts to measure their yield have only recently been made. A total yield of 2.1 per 100 eV in the spurs can be derived from Schwarz' diffusion model.<sup>4</sup> For the yield of  $\text{OH}^-$  that escape the spurs, two

conductivity measurements have given quite different values, *i.e.*,  $G(\text{OH}^-) = 0.1^5$  and  $0.8.^6$  In the conductometric pulse radiolysis work carried out in this laboratory for several years,<sup>7</sup> a number of systems have been encountered which are suitable for the measurement of  $G(\text{OH}^-)$ . In view of the difference between published values for  $G(\text{OH}^-)$ , we would like to report some of our observations.

A suitable system consists of a dilute aqueous solution of a scavenger  $\text{X}_1$  for the hydrated electron and  $\text{X}_2$  for the  $\text{OH}$  radical



After the pulse, an initial increase in conductivity  $\kappa_i$  is observed which is caused by  $(\text{H}^+ + \text{OH}^-)$  and  $(\text{H}^+ + \text{X}_1^-)$ . (The concentrations of  $\text{X}_1$  and  $\text{X}_2$  are high enough to assure completion of reactions 2, 3, and 5 during the pulse.)  $\kappa$  decreases after the pulse until a final value  $\kappa_f$  is reached. The decrease, which under our conditions occurs with a half-life of 10–30  $\mu\text{sec}$ , is due to the neutralization of  $\text{H}^+ + \text{OH}^-$ .  $\kappa_f$  is therefore the conductivity caused by  $\text{H}^+ + \text{X}_1^-$ . ( $\text{X}_1^-$  should be long lived and the products  $\text{P}_1$  and  $\text{P}_2$  should not react with  $\text{X}_1^-$ .) The ratio  $G(\text{OH}^-)/G(e_{\text{aq}}^-)$  can readily be calculated from  $\kappa_i$  and  $\kappa_f$ .

$$\frac{G(\text{OH}^-)}{G(e_{\text{aq}}^-)} = \frac{\kappa_i - \kappa_f \Lambda_{(\text{H}^+)} + \Lambda_{(\text{X}_1^-)}}{\kappa_f \Lambda_{(\text{H}^+)} + \Lambda_{(\text{OH}^-)}} \quad (6)$$

If  $\text{H}$  reacts according to (5b),  $G(e_{\text{aq}}^-)$  in eq 6 has to be substituted by  $G(e_{\text{aq}}^-) + G(\text{H})$ . The  $\Lambda$  values are molar conductivities. This method has also been used by Barker, *et al.*<sup>6</sup> Their scavengers  $\text{X}_1$  were ions such as  $\text{Cd}^{2+}$  and  $\text{NO}_2^-$  that cause a rather high base-line conductivity of the solutions. In our case, nitrobenzene and  $\text{O}_2$  were used as electron scavengers. Both

(1) Visiting professor from the Physical Chemistry Department, Hebrew University, Jerusalem, Israel.

(2) Postdoctoral Fellow from the Atomic Energy Commission, Karachi, Pakistan, with a grant from the Alexander v. Humboldt-Stiftung, Bad Godesberg.

(3) (a) M. S. Matheson, *Radiat. Res. Suppl.*, **4**, 1 (1964); (b) J. Rabani, *ibid.*, **4**, 71 (1964).

(4) H. A. Schwarz, *J. Phys. Chem.*, **73**, 1928 (1969).

(5) K. H. Schmidt and S. M. Ander, *ibid.*, **73**, 2846 (1969).

(6) (a) G. C. Barker, P. Fowles, D. C. Sammon, and B. Stringer, *Trans. Faraday Soc.*, **66**, 1498 (1970); (b) G. C. Barker, P. Fowles, and B. Stringer, *ibid.*, **66**, 1509 (1970); (c) G. C. Barker and P. Fowles, *ibid.*, **66**, 1661 (1970).

(7) G. Beck, *Int. J. Radiat. Phys. Chem.*, **1**, 361 (1969).

substances give long-lived negative ions.<sup>8,9</sup> The molar conductivity of  $O_2^-$  is  $65 \text{ ohm}^{-1} \text{ cm}^2 \text{ mol}^{-1}$ ; a plausible value of  $30 \text{ ohm}^{-1} \text{ cm}^2 \text{ mol}^{-1}$  was used for  $C_6H_5NO_2^-$ . Nitrobenzene also acts as scavenger  $X_2$  for OH and H according to eq 3 and 5a.<sup>10</sup> In the case of  $O_2$ , isopropyl alcohol was added as OH scavenger. The peroxy radical  $(CH_3)_2C(OH)(O_2^-)$  that is formed in isopropyl alcohol- $O_2$  solutions does not ionize in slightly acid solutions. It finally gives conducting tetroxides in a comparatively slow reaction which can be neglected on the time scale of our present experiments.<sup>11</sup>

The electron pulse always lasted  $0.3 \mu\text{sec}$ ; the dose was 40–200 rads per pulse. The  $H^+$  concentration as measured by conductometry before the pulse amounted to more than  $4 \times 10^{-7} M$  in most of the experiments (range,  $2 \times 10^{-7}$  to  $8 \times 10^{-7} M$ ). Since  $OH^-$  is formed in concentrations of only  $0.2\text{--}1.5 \times 10^{-7} M$ , the neutralization after the pulse leads to a pseudo-first-order decrease in conductivity. Knowing the total  $H^+$  concentration after the pulse, the rate constant for the reaction of  $H^+$  with  $OH^-$  could be calculated from the measured half-life of the decrease in  $\kappa$ . A value of  $1.1 \pm 0.2 \times 10^{11} M^{-1} \text{ sec}^{-1}$  was obtained in sufficient agreement with Eigen's measurements which shows that the initial drop in conductivity is really due to the neutralization  $H^+ + OH^- \rightarrow H_2O$ . For several microseconds after the pulse, the conductivity signal is distorted. By extrapolating the first-order decay of the conductivity back to time zero, the increase in conductivity  $\kappa_i$  immediately after the pulse was obtained.  $\kappa_f$  was obtained from the conductivity change of the solution after  $100 \mu\text{sec}$ . Figure 1 shows a typical oscillogram and a semilogarithmic plot of  $(\kappa - \kappa_f)/\kappa_f$  vs. time.

The average of the ratio  $G(OH^-)/G(e_{aq}^-)$  obtained from 40 experiments amounted to  $0.28 \pm 0.02$  in solutions containing nitrobenzene at  $1 \times 10^{-4} M$  and decreased to  $0.23 \pm 0.02$  with increasing nitrobenzene concentrations up to  $1 \times 10^{-2} M$ . It would indeed be expected that nitrobenzene scavenges electrons in the spurs at higher concentrations which would increase  $G(e_{aq}^-)$ . An average value for  $G(OH^-)/G(e_{aq}^-)$  of  $0.26 \pm 0.02$  was obtained for the isopropyl alcohol-saturated  $O_2$  system (isopropyl alcohol,  $1 \times 10^{-3}$  to  $1.4 \times 10^{-2} M$ ). Taking  $G(e_{aq}^-) = 2.7$ , we obtain  $G(OH^-) = 0.73 \pm 0.1$  from the average value of the measured ratios  $G(OH^-)/G(e_{aq}^-)$  in agreement with Barker, *et al.*<sup>6</sup>

A few remarks should be made about some minor corrections to the measurements. Since the initial  $H^+$  concentration of the solution was rather low, a slight decrease in pH resulted from the production of  $H^+ + X_1^-$ . Some of the  $OH^-$  ions initially present in the solution were therefore neutralized. The correction due to this effect generally was less than 12%. The conductivity of the water used amounted to 40–80% above the theoretical value at  $25^\circ$ . The worst im-

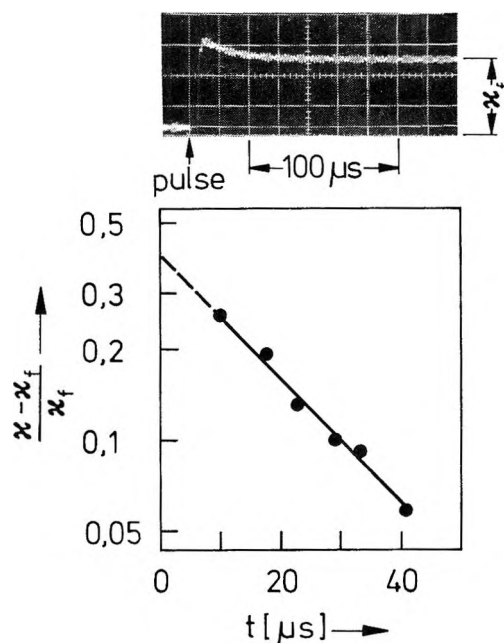


Figure 1. Upper part, oscillogram for the change in conductivity as a function of time;  $[H^+] = 2.9 \times 10^{-7} M$  before the pulse. Additional  $[H^+]$  produced by the pulse was  $0.95 \times 10^{-7} M$ ; nitrobenzene concentration,  $1.7 \times 10^{-3} M$ . Ordinate scale, 2 mV per major division. Lower part, semilogarithmic plot of  $(\kappa - \kappa_f)/\kappa_f$ . The extrapolation to  $t = 0$  yields  $(\kappa_i - \kappa_f)/\kappa_f = 0.41$ .

purity that can influence the measurements is bicarbonate. Even if one assumes that bicarbonate is responsible for all the excess conductivity the results are not changed.

(8) K.-D. Asmus, A. Wigger, and A. Henglein, *Ber. Bunsenges. Phys. Chem.*, **70**, 862 (1966).

(9) (a) J. Rabani and S. O. Nielsen, *J. Phys. Chem.*, **73**, 3736 (1969); (b) D. Behar, G. Czapski, J. Rabani, L. M. Dorfman, and H. A. Schwarz, *ibid.*, **74**, 3209 (1970).

(10) K.-D. Asmus, B. Cercek, M. Ebert, A. Henglein, and A. Wigger, *Trans. Faraday Soc.*, **63**, 2435 (1967).

(11) K. Stockhausen, A. Fojtik, and A. Henglein, *Ber. Bunsenges. Phys. Chem.*, **74**, 34 (1970).

### Mass Spectrometric Determination of the Heats of Formation of $AlOCl(g)$ and $AlOF(g)$ <sup>1</sup>

by R. D. Srivastava and M. Farber\*

Space Sciences, Inc., Monrovia, California 91016  
(Received November 24, 1970)

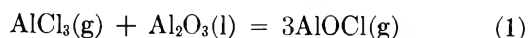
Publication costs assisted by Space Sciences, Inc.

The possible existence of the  $AlOCl$  molecule was first reported by Fischer and Gewehr.<sup>2</sup> Schafer,

(1) This work was sponsored by the Air Force Rocket Propulsion Laboratory, Air Force Systems Command, United States Air Force, Edwards, Calif.

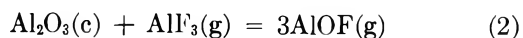
(2) W. Fischer and R. Gewehr, *Z. Anorg. All. Chem.*, **209**, 17 (1932).

*et al.*,<sup>3,4</sup> obtained a value of  $-190$  kcal/mol for the  $\Delta H_f$  of crystalline AlOCl based on calorimetric measurements of the heat of solution of AlOCl(c) in aqueous HCl. Employing the molecular flow effusion method, Farber, *et al.*,<sup>5</sup> studied the heat of formation of AlOCl(g) at  $2400^\circ\text{K}$  by means of a study of the reaction



and reported a value of  $-83.2 \pm 5$  kcal/mol for  $\Delta H_{f298}$  for AlOCl(g).

The only reported values for the AlOF molecule are the results of Farber and Petersen<sup>6</sup> using the molecular flow effusion method. For the reaction



third law studies at  $2200^\circ\text{K}$  yielded a value of  $-140.2 \pm 2.6$  kcal/mol for  $\Delta H_{f298}$  of AlOF(g). Since none of the previous work directly identified AlOCl(g) and AlOF(g), the present work involved a mass spectrometric study to identify the AlOCl(g) and AlOF(g) species in the temperature ranges  $1473$  to  $1600^\circ\text{K}$  and  $1483$  to  $1923^\circ\text{K}$ , respectively. The results are compared with the published data.

### Experimental Section

The mass spectrometer, vacuum systems, and furnace apparatus employed for these studies have been described previously.<sup>7</sup> The effusion cell was fabricated of alumina (inside diameter 6.8 mm, length 25.4 mm) with an orifice diameter and thickness of 0.986 and 6.6 mm, respectively. An alumina connecting tube with an inside diameter of 1 mm was used both as a reservoir for the AlF<sub>3</sub> and as a flow tube for the Cl<sub>2</sub>.

The gaseous chlorine was contained in a low-pressure vessel and was metered directly into the effusion cell for the studies involving AlOCl(g). For the AlOF(g) investigation the alumina tube acted as a reservoir and contained AlF<sub>3</sub> crystals. The AlF<sub>3</sub> reservoir was heated with a tungsten heater to a temperature which produced the desired vapor pressure of AlF<sub>3</sub> in the reaction cell.

The ion intensities were identified by their masses, isotopic distribution, and appearance potentials. The shutterable, or chopped, portion only of the ion intensities was directly recorded. In order to minimize contributions due to fragmentation, ionizing electron energies of 3 eV above the appearance potentials were used to ensure that the species were the parent ions. The previously reported ion appearance potentials<sup>8</sup> used in these studies were for Al, 6 eV, for AlF,  $9 \pm 1$  eV, for Al<sub>2</sub>O,  $7.7 \pm 0.5$  eV, and for Cl,  $13 \pm 1$  eV.

### Results and Discussion

**AlOCl Molecule.** A mass spectrometric determination was made of the reaction of Al<sub>2</sub>O<sub>3</sub> with gaseous chlorine in the temperature range  $1473$  to  $1600^\circ\text{K}$ . Mass spectrometer intensities were obtained for the species involved in the isomolecular reaction



The equilibrium constants in terms of ion intensities for reaction 3 are given by

$$K_1 = \frac{I_{\text{AlOCl}}I_{\text{Al}}}{I_{\text{Al}_2\text{O}}I_{\text{Cl}}} \quad (4)$$

The appearance potential for AlOCl(g) was found to be  $12 \pm 1$  eV. The intensities and thermodynamic data for the third-law calculations based on JANAF thermochemical data<sup>9</sup> for the species Al<sub>2</sub>O(g), Cl(g), and Al(g) are presented in Table I. The second-law  $\Delta H_f$  at an average temperature of  $1540^\circ\text{K}$  is  $-6.4 \pm 1$  kcal. This yields a  $\Delta H_{f298}$  of  $-86.4 \pm 2$  kcal/mol. The average third-law value for  $\Delta H_{f298}$  of AlOCl(g) is  $-82.5 \pm 1$  kcal/mol, which is nearly identical with the value of  $-83.2$  kcal/mol obtained from the effusion experiments.<sup>5</sup>

**Table I:** Ion Intensities and Thermodynamic Data for the Reaction  $\text{Cl}(\text{g}) + \text{Al}_2\text{O}(\text{g}) = \text{AlOCl}(\text{g}) + \text{Al}(\text{g})$

T, °K	Relative intensities				log K <sub>1</sub>	ΔF, kcal	TΔS <sub>T</sub> , kcal/ mol
	Al	AlOCl	Al <sub>2</sub> O	Cl			
1473	120	4	18	36	-0.120	-0.808	-2.044
1528	320	6	62	40	-0.110	-0.770	-2.076
1543	9000	40	500	1000	-0.056	-0.722	-2.085
1553	2000	18	120	340	-0.053	-0.426	-2.089
1600	500	50	60	450	-0.034	-0.293	-2.112

**AlOF Molecule.** A mass spectrometric study of the reaction between Al<sub>2</sub>O<sub>3</sub>(c) and gaseous AlF<sub>3</sub> has been

**Table II:** Ion Intensities and Thermodynamic Data for the Reaction  $\text{AlF}(\text{g}) + \text{Al}_2\text{O}(\text{g}) = 2\text{Al}(\text{g}) + \text{AlOF}(\text{g})$

T, °K	Relative intensities				log K <sub>2</sub>
	Al	AlOF	AlF	Al <sub>2</sub> O	
1540	140	11	180	100	4.26
1560	180	12	180	100	4.53
1640	1000	8	260	300	5.23
1700	2300	5	200	500	5.65
1723	2000	10	120	620	5.96
1773	3000	6	360	1720	6.22
1800	3000	1	160	260	6.64
1923	3800	26	12	280	7.26

(3) H. Schafer, G. Goser, and L. Bayer, *Z. Anorg. Allg. Chem.*, **263**, 87 (1950).

(4) H. Schafer, F. E. Wittig, and W. Wilborn, *ibid.*, **297**, 48 (1958).

(5) M. A. Greenbaum, J. A. Blauer, M. R. Arshadi, and M. Farber, *Trans. Faraday Soc.*, **60**, 1592 (1964).

(6) M. Farber and H. L. Petersen, *ibid.*, **59**, 836 (1963).

(7) M. Farber, M. A. Frisch, and H. C. Ko, *ibid.*, **65**, 3202 (1969).

(8) "Ionization Potentials, Appearance Potentials, and Heats of Formation of Gaseous Positive Ions," National Bureau of Standards Publication NSRDS-NBS 26, Washington, D. C., June 1969.

(9) "JANAF Thermochemical Tables," The Dow Chemical Company, Midland, Mich., 1961, 1965.

performed in the temperature range 1483 to 1923°K to identify the AlOF species. In this temperature range an appearance potential of  $10.5 \pm 1$  eV was obtained for the AlOF(g) species. The mass spectrometer intensities for the reaction



are presented in Table II.

A second-law least-squares plot of  $\log K_2$  vs.  $1/T$ , where

$$K_2 = \frac{I_{\text{AlOF}}(I_{\text{Al}})^2}{I_{\text{AlF}}I_{\text{Al}_2\text{O}}} T \quad (6)$$

yielded a value of  $109 \pm 1.8$  kcal for  $\Delta H_r$  at an average temperature of 1700°K. This yields a value of  $-148 \pm 1$  kcal/mol for  $\Delta H_f$  of AlOF(g). Reduction of these data to 298°K using the heat content data in the current JANAF Thermochemical Tables gives  $-143.8 \pm 1$  kcal/mol for  $\Delta H_{f298}$ , which is in close agreement with the previously published third-law effusion studies at the single temperature of 2200°K, which yielded a value of  $-140.2 \pm 2.6$  kcal/mol for  $\Delta H_{f298}$  of AlOF(g).<sup>6</sup>



# COMMUNICATIONS TO THE EDITOR

## Solvent Effect on the Dimerization of *N*-Methylaniline

Publication cost borne completely by The Journal of Physical Chemistry

*Sir:* Ellison and Meyer<sup>1</sup> have recently determined the dimerization constant  $K_D$  of *N*-methylaniline (NMA) in cyclohexane, at 25°, using a dielectric method based upon Onsager's theory. While the value obtained compared well with that found by Lady and Whetsel,<sup>2</sup> in the same solvent, using the infrared technique, an important difference (by approximately a factor of 2) was noted between their value and the value which we had calculated from thermodynamic activity coefficients as determined by an isothermal liquid-vapor equilibrium study of NMA-carbon tetrachloride mixtures.<sup>3</sup> According to Ellison and Meyer the discrepancy lies either in our theory, or in our data. In our opinion, however, this discrepancy lies simply in that association constants are solvent dependent and that the comparison has been made with our  $K_D$  value as measured in carbon tetrachloride. Fortunately, we had performed a similar analysis of vapor-liquid equilibrium data for the NMA-cyclohexane mixture,<sup>4</sup> which seems to have escaped the attention of Ellison and Meyer. Table I gives  $K_D$  values in the same solvent, cyclohexane, obtained by three different techniques and it may be seen that they are in reasonable agreement.

Table I: Dimerization of *N*-Methylaniline in Cyclohexane at 25°

Technique	$K_D$ , l. mol <sup>-1</sup>	Ref
Ir	0.434 ± 0.025	2
Dielectric	0.422 ± 0.085	1
Thermodynamic	0.36 ± 0.02	4

The somewhat smaller dimerization constant, inferred from the thermodynamic data, may be due to the fact that in our treatment the formation of higher NMA associates has also been taken into account. This is in fact necessary when one wishes to explain the behavior of the system at higher concentrations.

The smaller dimerization constant of NMA in carbon tetrachloride should be ascribed to the competition between N-H···N bond formation and a direct Cl···N interaction. This explanation is identical with that given by Kehiaian<sup>5</sup> for the self-association constant of diethylamine, smaller in carbon tetrachloride than in cyclohexane, and bases on a comparison of the

enthalpies of mixing tertiary amines with carbon tetrachloride or cyclohexane.

In our previous publication<sup>4</sup> we had investigated the self-association of aniline and NMA in cyclohexane, carbon tetrachloride, and benzene and had refound the classification of solvents according to their "degree of inertia" with respect to molecular interactions.<sup>6-10</sup>

- (1) H. R. Ellison and B. W. Meyer, *J. Phys. Chem.*, **74**, 3861 (1970).
- (2) J. H. Lady and K. B. Whetsel, *ibid.*, **71**, 1421 (1967).
- (3) G. Pannetier and L. Abello, *Bull. Soc. Chim. Fr.*, 1645 (1968).
- (4) L. Abello, B. Servais, M. Kern, and G. Pannetier, *ibid.*, 4360 (1969).
- (5) K. Sosnkowska-Kehiaian, K. Orzel, and H. Kehiaian, *Bull. Acad. Polon. Sci., Ser. Sci. Chim.*, **14**, 711 (1966).
- (6) M. L. Josien, *J. Chim. Phys.*, **61**, 24 (1964).
- (7) P. V. Huong and J. C. Lassegues, *Spectrochim. Acta, Part A*, **26**, 269 (1970).
- (8) J. C. Lassegues and P. V. Huong, *Method. Phys. Anal.*, **5**, 69 (1969).
- (9) H. Buchowski, J. Devaure, P. V. Huong, and J. Lascombe, *Bull. Soc. Chim. Fr.*, 2532 (1966).
- (10) Professor Ellison has informed the Editors that he is in agreement with the authors' comments on ref 1.

LABORATOIRE DE CINÉTIQUE CHIMIQUE  
FACULTÉ DES SCIENCES DE PARIS  
1, RUE GUY DE LA BROSSE  
75-PARIS V° FRANCE

LOUIS ABELLO\*  
GUY PANNETIER

RECEIVED DECEMBER 29, 1970

## Micellar Effects on the Hydrolysis Rate of Triethylamine-Sulfur Trioxide

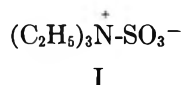
Publication costs assisted by the University of Maine

*Sir:* It is well established that the rates of certain organic reactions are markedly altered in the presence of micellar solutions.<sup>1</sup> Electrostatic as well as hydrophobic interactions are thought to be the principal causes of these rate effects.<sup>1,2</sup> Generally it is found that reactions catalyzed by cationic surfactants are unaffected or inhibited by anionic surfactants and *vice versa*.<sup>3-6</sup> We reasoned that reaction of a zwitterionic

- (1) For reviews see (a) E. H. Cordes and R. B. Dunlap, *Accounts Chem. Res.*, **2**, 329 (1969); (b) E. J. Fendler and J. H. Fendler, *Advan. Phys. Org. Chem.*, **8**, 271 (1970).
- (2) C. Gittler and A. Ochoa-Solano, *J. Amer. Chem. Soc.*, **90**, 5004 (1968).
- (3) C. A. Bunton and M. J. Minch, *Tetrahedron Lett.*, **44**, 3881 (1970).
- (4) E. J. Fendler, R. R. Liechti, and J. H. Fendler, *J. Org. Chem.*, **35**, 1658 (1970).
- (5) G. J. Buist, C. A. Bunton, L. Robinson, L. Sepulveda, and M. Stam, *J. Amer. Chem. Soc.*, **92**, 4072 (1970).
- (6) C. R. Cramer and J. L. Berg, *J. Phys. Chem.*, **72**, 3686 (1968).

substance, where the possibility of binding with either type of charged micelle exists, might prove to be an exception to this general rule. In the present communication, we wish to report the preliminary results of our studies of such a system.

Hydrolysis of triethylamine-sulfur trioxide (I) is



believed<sup>7</sup> to occur *via* a nucleophilic attack on sulfur by water and thus results in the ejection of triethylamine with concomitant formation of the bisulfate ion. Rate data for this reaction were obtained by pH titration of the liberated acid contained in aliquots of the reaction mixture using dilute sodium hydroxide solution. In Table I are listed pseudo-first-order rate

**Table I:** Pseudo-First-Order Rate Constants for Hydrolysis of 0.01 M Triethylamine-Sulfur Trioxide at 77.9° in the Presence of Surfactants at Varying Concentrations

Surfactant	Concentration, M	10 <sup>4</sup> k, sec <sup>-1</sup>
None	...	1.00 <sup>a</sup>
ETAB	1 × 10 <sup>-2</sup>	5.04
ETAB	2 × 10 <sup>-2</sup>	9.88
DTAB	2 × 10 <sup>-2</sup>	3.17
SHS	9.7 × 10 <sup>-3</sup>	2.30
SHS	2 × 10 <sup>-2</sup>	3.35

<sup>a</sup> See ref 7, value 1.10 × 10<sup>-4</sup> sec<sup>-1</sup>.

constants for the hydrolysis of I alone and in the presence of the cationic surfactants, eicosyltrimethylammonium bromide (ETAB) and dodecyltrimethylammonium bromide (DTAB), and the anionic surfactant, sodium hexadecylsulfonate (SHS).

There clearly exists in this reaction a rate acceleration effect for *both* anionic and cationic surfactants. The smooth increase in rate upon addition of the cationic surfactant ETAB is shown in Figure 1. At higher concentrations of ETAB, the typical dampening of the effect occurs, signalling the approaching saturation of the micellar pseudophase.

It is likely that hydrophobic interactions are superimposed on the electrostatic effects which bring the

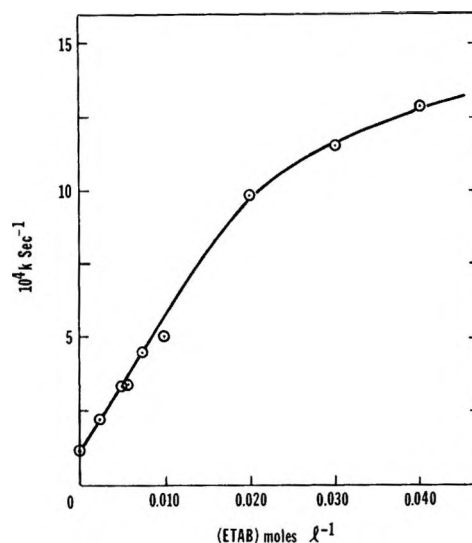


Figure 1. The effect of added ETAB on the hydrolysis rate of triethylamine-sulfur trioxide at 77.9°.

substrate into the micellar region for more facile hydrolysis. Some interactions could well aid in departure of the triethylamine moiety with its lessening positive charge. A manifestation of the hydrophobic assistance may be the smaller catalytic effect observed with shorter surfactant chain length as illustrated in Table I with ETAB and DTAB. This idea is further supported by some kinetic measurements on the methyl analog, trimethylamine-sulfur trioxide. The rate of hydrolysis of trimethylamine-sulfur trioxide in the presence of 0.02 M ETAB at 77.9° relative to that in water at the same temperature is 1.72; the corresponding ratio for triethylamine-sulfur trioxide is 9.33. Our investigation of this reaction is continuing with emphasis on experiments designed to test the importance of hydrophobic interactions.

*Acknowledgment.* The authors gratefully acknowledge support in part by a Frederick Gardner Cottrell Grant-In-Aid from The Research Corporation.

(7) B. E. Fleischfresser and I. Lauder, *Aust. J. Chem.*, **15**, 251 (1962).

DEPARTMENT OF CHEMISTRY  
UNIVERSITY OF MAINE  
ORONO, MAINE 04473

MICHAEL D. BENTLEY\*  
SUSAN E. BOWIE  
ROBERT D. LIMOGES

RECEIVED FEBRUARY 1, 1971

# Platinum Group Metals and Compounds

ADVANCES IN CHEMISTRY SERIES  
NO. 98



Eleven papers from a symposium by the Division of Inorganic Chemistry of the American Chemical Society chaired by U. V. Rao.

What new complexes of the platinum group metals have been synthesized? Here is a collection of papers presenting data on chalcogenides, oxides, nitrido and hydrido complexes, as well as the catalytic properties of these metals and their alloys. Information is included on

- synthesis
- structure
- magnetic susceptibility
- double bond migration

The platinum group metals are considered from the viewpoints of both industry and research. Their magnetic and thermodynamic properties are explored, as well as recent chemistry of  $\sigma$ - and  $\pi$ -bonded complexes. Crystal structure is discussed by several authors, with data presented in the form of

- x-ray scattering data
- absorption spectra
- crystal spectra
- infrared spectra
- Mossbauer spectra
- vibrational spectra

165 pages with index. Cloth bound (1971) \$9.00  
Postpaid in U.S. and Canada; plus 35 cents elsewhere.

Set of L. C. cards with library orders upon request.

Other books in the ADVANCES IN CHEMISTRY SERIES of interest to inorganic chemists include:

<b>No. 89</b>	<b>Isotope Effects in Chemical Processes</b>	278 pages	Cloth bound	(1969)	\$13.00
<b>No. 82</b>	<b>Radiation Chemistry — II</b>	558 pages	Cloth bound	(1968)	\$16.00
<b>No. 81</b>	<b>Radiation Chemistry — I</b>	616 pages	Cloth bound	(1968)	\$16.00
<b>No. 81 and No. 82 ordered together \$30.00</b>					
<b>No. 78</b>	<b>Literature of Chemical Technology</b>	732 pages	Cloth bound	(1968)	\$17.50
<b>No. 73</b>	<b>Trace Inorganics in Water</b>	396 pages	Cloth bound	(1968)	\$12.50
<b>No. 72</b>	<b>Mass Spectrometry in Inorganic Chemistry</b>	329 pages	Cloth bound	(1968)	\$12.00

Order from:  
**Special Issues Sales**  
**American Chemical Society**  
1155 16th St., N. W.  
Washington, D. C. 20036

# LOS ALAMOS SCIENTIFIC LABORATORY

The 1972 fiscal year budget for the Los Alamos Scientific Laboratory will require a reduction in our staff. We will be releasing a number of Physicists, Chemists, Metallurgists, Mathematicians and Engineers at all degree levels as well as talented technicians engaged in basic and applied research in the physical sciences and all phases of engineering.

If you are in need of experienced personnel advise us of your interest. The individuals we must release are uniquely qualified and would be an asset to any organization.

AN EQUAL  
OPPORTUNITY  
EMPLOYER



R. Lynn Wilson  
Recruiting Supervisor  
Los Alamos Scientific  
Laboratory  
Dept. 4 P.O. Box 1663  
Los Alamos, New Mexico  
87544  
Area Code 505 667-4243

**los  
alamos**  
SCIENTIFIC LABORATORY  
OF THE UNIVERSITY OF CALIFORNIA  
LOS ALAMOS, NEW MEXICO

## INTERACTION OF LIQUIDS AT SOLID SUBSTRATES

ADVANCES IN CHEMISTRY SERIES NO. 87

Papers from two symposia by the Division of Organic Coatings and Plastics Chemistry of the American Chemical Society.

This volume includes twelve papers comprising the symposium on "The Interaction of Liquids at Solid Substrates," chaired by Allen L. Alexander. These papers include work on "coupling agents," adhesion of polymers, organic/inorganic interfaces, and ultrasonic impedometry. Also included are four papers concerned with heparinized surfaces at the blood/material interface which were part of the symposium on "The Medical Applications of Plastics," chaired by R. I. Leininger.

212 pages with index      Clothbound      (1968)      \$9.50

Postpaid in U.S. and Canada; plus 30 cents elsewhere.

Free set of L. C. cards with library orders upon request.

Order from:

SPECIAL ISSUES SALES  
AMERICAN CHEMICAL SOCIETY  
1155 SIXTEENTH ST., N.W.  
WASHINGTON, D.C. 20036

# Directory of Graduate Research 1969

*Biennial publication of the  
ACS Committee on Professional Training*

Covers the universities and colleges in the United States and Canada known to offer an organized curriculum leading to the doctoral degree in chemistry, biochemistry, chemical engineering, and pharmaceutical or medicinal chemistry.

The guide to graduate schools, research, and personnel in these areas.

201 Departments of Chemistry  
165 Departments offering Biochemistry  
106 Departments of Chemical Engineering  
29 Departments of Pharmaceutical or Medicinal Chemistry

Lists 2807 full- and part-time staff members, each with outline of career, teaching and research specialties, and list of publications for the past two or five years.

Statistical data on departments include number of Ph.D. degrees conferred during the previous two years, number of staff members, and number of post-doctoral appointments.

Other listings include interdisciplinary programs and doctoral theses accepted during previous two years.

1213 pp. with index of names paper bound (1970)  
\$10.00 postpaid in U.S., plus 50 cents Canada and Pan America, plus 75 cents foreign.

Order from: Special Issue Sales  
American Chemical Society  
1155 Sixteenth St., N.W.  
Washington, D. C. 20036